Final Technical Report
Report Number 15323R15
(October 1, 2002 – September 30, 2006)

DEVELOPMENT AND OPTIMIZATION OF GAS-ASSISTED GRAVITY DRAINAGE (GAGD) PROCESS FOR IMPROVED LIGHT OIL RECOVERY

Work Performed Under Cooperative Agreement
DE-FC26-02NT15323

By

Dandina N. Rao, Ph. D., P. Eng.
(Principal Investigator)

Subhash C. Ayirala, Ph.D.
Madhav M. Kulkarni, Ph.D.
Wagirin Ruiz Paidin, (Ph.D.)
Thaer N. N. Mahmoud, M.S.
Daryl S. Sequeira, M.S.
Amit P. Sharma, M.S.
(Graduate Research Assistants)

The Craft & Hawkins Department of Petroleum Engineering
Louisiana State University and Agricultural & Mechanical College
Baton Rouge, LA 70803

December 2006

Prepared for
United States Department of Energy
National Energy Technology Laboratory

DISCLAIMER

Abstract

This is the final report describing the evolution of the project "Development and Optimization of Gas-Assisted Gravity Drainage (GAGD) Process for Improved Light Oil Recovery" from its conceptual stage in 2002 to the field implementation of the developed technology in 2006. This comprehensive report includes all the experimental research, models developments, analyses of results, salient conclusions and the technology transfer efforts.

As planned in the original proposal, the project has been conducted in three separate and concurrent tasks: Task 1 involved a physical model study of the new GAGD process, Task 2 was aimed at further developing the vanishing interfacial tension (VIT) technique for gas-oil miscibility determination, and Task 3 was directed at determining multiphase gas-oil drainage and displacement characteristics in reservoir rocks at realistic pressures and temperatures.

The project started with the task of recruiting well-qualified graduate research assistants. After collecting and reviewing the literature on different aspects of the project such gas injection EOR, gravity drainage, miscibility characterization, and gas-oil displacement characteristics in porous media, research plans were developed for the experimental work to be conducted under each of the three tasks.

Based on the literature review and dimensional analysis, preliminary criteria were developed for the design of the partially-scaled physical model. Additionally, the need for a separate transparent model for visual observation and verification of the displacement and drainage behavior under gas-assisted gravity drainage was identified. Various materials and methods (ceramic porous material, Stucco, Portland cement, sintered glass beads) were attempted in order to fabricate a satisfactory visual model. In addition to proving the effectiveness of the GAGD process (through measured oil recoveries in the range of 65 to 87% IOIP), the visual models demonstrated three possible multiphase mechanisms at work, namely, Darcy-type displacement until gas breakthrough, gravity drainage after breakthrough and film-drainage in gas-invaded zones throughout the duration of the process. The partially-scaled physical model was used in a series of experiments to study the effects of wettability, gas-oil miscibility, secondary versus tertiary mode gas injection, and the presence of fractures on GAGD oil recovery. In addition to yielding recoveries of up to 80% IOIP, even in the immiscible gas injection mode, the partially-scaled physical model confirmed the positive influence of fractures and oil-wet characteristics in enhancing oil recoveries over those measured in the homogeneous (unfractured) water-wet models. An interesting observation was that a single logarithmic relationship between the oil recovery and the gravity number was obeyed by the physical model, the high-pressure corefloods and the field data.

Seeking to derive a sound and strong scientific basis for the new vanishing interfacial tension (VIT) technique through careful experimentation was the main objective of Task 2. This was accomplished by conducting gas-liquid and liquid-liquid interfacial tension (IFT) measurements at elevated pressures and temperatures using a high-pressure optical cell for two standard gas-oil systems (CO_2 + n-Decane and CO_2 + n-Decane + methane) as well as a standard ternary liquid system (water + ethanol + benzene). Both the pendent drop image capture technique and the capillary rise technique were used to measure low gas-oil interfacial tensions. The close agreement between the minimum miscibility pressure (MMP) obtained from the VIT technique for these standard fluid systems with those from slim-tube tests, rising bubble apparatus, phase diagram and analytical model predictions clearly validated the miscibility determination capabilities of the VIT technique.

The VIT technique was then applied to the study of miscibility between CO_2 and a live crude oil from a Louisiana oil field with the aim of examining the influence of the compositional path, if any, on the MMP measurements using the VIT technique. In various experiments involving a wide range of gas-oil ratios (GOR), detailed compositional measurements of both vapor and liquid phases were carried out using a gas chromatograph and densities of both phases were measured using a digital densitometer. In spite of the large GOR variations in the initial mixture compositions, all the extrapolated VIT miscibility pressures agreed well, with a standard deviation of 0.67%, thereby clearly establishing the robustness and compositional path independence of the VIT technique.

The Peng-Robinson equation of state (PR-EOS) and commercial phase behavior software were used to calculate MMPs for the various fluids systems used in the above VIT experiments. The MMP calculated using the untuned PR-EOS matched reasonably (within 3-5 MPa) with VIT results. Interestingly, this work also indicated that the calculated MMP can vary as much as 10 MPa (nearly 1500 psi) depending upon the choice of a tuning parameter for the EOS, raising questions about the utility of such non-unique results from EOS tuning , especially for MMP determination.

Another major accomplishment under Task 2 was the development of a new mechanistic Parachor model for the prediction of dynamic IFT in multicomponent hydrocarbon fluids. The 85-year old Parachor model was modified by incorporating a simple ratio of diffusivities (from oil-to-gas to gas-to-oil) raised to an exponent n, the value of which was to be determined by fitting the modified Parachor model to experimental IFT measurements. This bi-directional diffusivity ratio accounted well for the vaporizing- and condensing-type mass transfer interactions between the oil and gas phases, and the value and sign of the exponent, n, enabled the determination of the dominating mass transfer mechanism for miscibility development. A generalized regression model was also developed to determine the mechanistic model exponent (n) by

using only the compositional data of reservoir fluids. The modified Parachor model enabled the calculation of multicomponent gas-oil IFTs and MMPs, with excellent agreement with VIT-based MMPs.

Reservoir condition displacement tests involving 6-ft long Berea cores and 1-ft long reservoir cores were the focus of Task 3. CO_2 gas injection was carried out in several modes: continuous gas injection (CGI), water-alternating-gas (WAG) injection, Hybrid WAG (combination of CGI and WAG) and GAGD in order to develop a comparative evaluation of GAGD performance in the laboratory scale displacements at elevated pressures and temperatures. The GAGD process outperformed all the other modes of gas injection. Comparable oil recovery patterns in widely differing experimental systems, ranging from a uniform porous medium (Berea sandstone) to a heterogeneous fractured (Yates reservoir dolomite) cores, in both miscible and immiscible modes, clearly indicated the insensitivity of the GAGD process to reservoir heterogeneities, which remains a major concern in conventional horizontal gas floods. In fact, the presence of vertical fractures was found to be beneficial in increasing the rates and recoveries of oil – conforming to the findings from visual and physical model GAGD tests. The common logarithmic relationship found between recovery and the gravity number for all types of experiments conducted in this 4-year study clearly demonstrated the consistency of performance of the GAGD process.

The technology transfer efforts conducted during the course of this project have resulted in 15 technical reports, 20 conference presentations, 16 reviewed journal publications, 2 patent applications, one commercial license of the process, in addition to generating 5 M.S. theses, and 2 Ph.D. dissertations. The first field test of the GAGD process is anticipated in a Louisiana oil field during 2007.

Table of Contents

LIST OF TABLES

LIST OF FIGURES

1. Design and Development of a Scaled Physical Experimental GAGD Model

1.1 Dimensional Analysis and Scaling Criteria for Physical Model Design

1.1.1 Literature Review

In this section, a brief review of literature on the following topics is presented:

- Dimensional analysis
- Inspectional analysis

Buckingham (1914) developed the theory on physically similar systems resulting in the development of a general analytical method, called dimensional analysis. His theory states that any equation that completely describes a relation among a number of physical quantities is reducible to the form $\phi(\pi_1, \pi_2, ...\pi_n) = 0$, in which the π's are all the independent dimensionless products of some form of the original quantities. Thus, the effect of dimensionless groups, instead of the individual variables, can be investigated experimentally and theoretically resulting in global correlations between groups of variables representing different physical phenomena rather than numerous individual variables.

Ruark (1935) introduced the term "inspectional analysis." In an inspectional analysis, it is necessary to write down the differential equations describing the physical process and the associating boundary or initial conditions to determine the dimensionless groups governing the process. Ruark also compared dimensionless analysis and inspectional analysis and although dimensional analysis, based on Buckingham's PI theorem, generates complete and independent dimensionless groups for a specific problem, the groups are not unique. Instead, a large number of such dimensionless groups could exist. Dimensionless analysis works better if the system is small and the dimensionless groups are well understood beforehand. Inspectional analysis, on the other hand, takes the first step toward the actual solution of a problem. Dimensionless groups obtained from inspectional analysis are likely to bear clearer physical meaning than those from dimensional analysis.

Geertsma et al. (1956) derived dimensionless groups by inspectional analysis for three types of displacement processes: cold-water drive, hot-water drive and solvent injection. The form of the groups is given in such a way that they can be adapted to suit the various boundary conditions that are encountered in practice. The physical meaning associated with the various groups was also discussed.

By using dimensional and inspectional analysis, a new set of scaling groups for the immiscible displacement of heavy oil by CO_2 and water was derived by Rojas and Farouq Ali (1986). Studying the dynamics of sub-critical CO_2/brine floods for heavy oil

recovery, Rojas and Farouq Ali (1986) found that the immiscible displacement of viscous oils by carbon dioxide was dominated by viscous forces. Therefore, capillary and diffusive effects play a much less important role in the displacement process. Thus, in the scaled physical model, the following scaling groups were completely satisfied: geometric factors, morphologic factors, ratio of gravitational to viscous forces, ratio of viscous forces, and water-gas ratio of slug volumes. Other groups, such as ratio of capillary to viscous forces and ratio of convection time to transverse dispersion time, were only partially satisfied.

Islam (1995) reviewed emerging technologies in enhanced oil recovery (EOR) and pointed out the need for scaled model experiments for EOR applications. The author also stated that it is generally difficult to properly scale laboratory test results to field conditions, especially if the following conditions are involved: chemical reactions, horizontal wells, and unstable displacement fronts.

1.1.2 Inspectional Analysis of the Gravity Drainage Process

The gravity drainage process is difficult to model theoretically. Here, inspectional analysis is used to present the governing equations, derive their dimensionless forms, and combine variables into dimensionless groups. Similarity groups are then proposed based on these dimensionless groups and other considerations as well.

To begin this derivation, the following assumptions are made:

- One-dimensional downward flow.
- Isothermal condition.
- Immiscible gas/oil phases.
- Incompressible phases and porous media:

  The pressure in this process is not expected to vary in any significant way. Therefore, it is still reasonable to assume incompressible phases.
- Spreading system:

  $K = \sigma_{wg}-(\sigma_{og}+\sigma_{ow}) > 0$, where K is the spreading coefficient, and σ is the interfacial tension between the phases. When K is positive, oil spreads on water.
- Water-wet media:

  Water occupies the smallest pores and coats grain particles; water is immobile throughout the process.
- Three-phase co-existence, that can be simplified as an oil/gas two phase flow problem by assuming the connate water saturation for an oil/water system is the same for a gas/water system.

The problem is reduced to an oil/gas two-phase flow problem under the above assumptions. As shown in Figure 1.1, there is a constant production rate at u, which is

equal to the sum of u_1 (oil) and u_2 (gas). There are two regions in the column, one is the oil bank at connate water saturation, and the other is the gas-invaded zone.

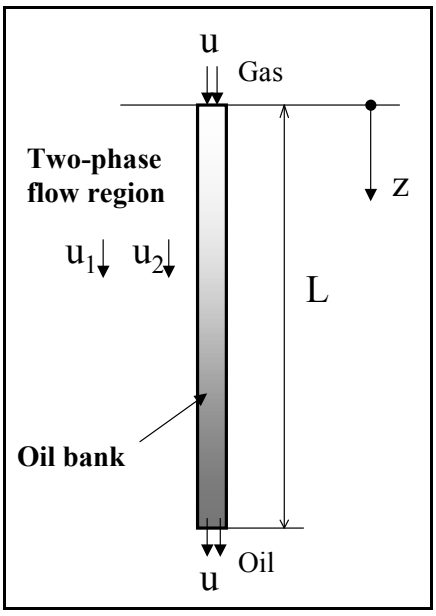

Figure 1.1: Schematic of 1-D Gravity Drainage in Porous Media

The mass conservation equation:

$$\phi \frac{\partial S_1}{\partial t} + \frac{\partial u_1}{\partial z} = 0 \quad \text{..... (1.1)}$$

, where subscript "1" refers to the oleic phase.
The flow equation is Darcy's law applied to the oil and gas phases:

$$u_1 = kk_{r1} / \mu_1 (\frac{dp_1}{dz} + \rho_1 g) \quad \text{..... (1.2)}$$

$$u_2 = kk_{r2} / \mu_2 (\frac{dp_2}{dz} + \rho_2 g) \quad \text{..... (1.3)}$$

, where k is the absolute permeability, k_r is the relative permeability, and μ and ρ are the viscosity and the density of the phases respectively.
From the incompressible assumption and capillary relation, we have

$$u_1 + u_2 = u \quad \text{..... (1.4)}$$

$$p_2 = p_1 + p_c \quad \text{..... (1.5)}$$

, where:

$$p_c = \sigma\sqrt{\frac{\phi}{k}}J(S_1) \quad \text{..... (1.6)}$$

$J(S_1)$ is the dimensionless capillary pressure Leverett J function, and σ is the interfacial tension.

The initial and boundary conditions are:

$$S_1 = S_{1i} \qquad at \quad t = 0, \qquad 0 \le z \le L$$

$$u_1 = 0 \qquad at \quad t > 0, \qquad z = 0$$

$$u_2 = 0 \qquad at \quad t < t_{BT}, \qquad z = L \quad \text{..... (1.7)}$$

, where t_{BT} is the gas breakthrough time.

Now the above equations are transformed to their dimensionless forms by applying the following transformations.

$$z_D = x / L$$
$$t_D = t / t^*$$
$$u_{1D} = u_1 / u$$
$$u_{2D} = u_2 / u \quad \text{..... (1.8)}$$
$$p_{1D} = p_1 /(\sigma\sqrt{\frac{\phi}{k}})$$
$$p_{2D} = p_2 /(\sigma\sqrt{\frac{\phi}{k}})$$
$$J(S_1) = p_c /(\sigma\sqrt{\frac{\phi}{k}})$$

, where t* is to be determined.

Substitute Eq. 1.8 into Eqs. 1.1-1.7 to get the following dimensionless form of the equations:

$$\frac{\partial S_1}{\partial t_D} + \frac{\partial u_{1D}}{\partial z_D} = 0 \quad \text{..... (1.1')}$$

$$u_{1D} = k_{r1}(D_1 \frac{dp_{1D}}{dz_D} + D_2) \quad \text{..... (1.2')}$$

$$u_{2D} = k_{r2}(D_3 \frac{dp_{2D}}{dz_D} + D_4) \quad \text{..... (1.3')}$$

In Eqs. 1.1'-1.8' we have:

$$t^* = \frac{\phi L}{u}$$

$$D_1 = \frac{k\sigma}{L\mu_1 u}\sqrt{\frac{\phi}{k}}$$

$$D_2 = \frac{\rho_1 g k}{\mu_1 u}$$

$$D_3 = \frac{k\sigma}{L\mu_2 u}\sqrt{\frac{\phi}{k}}$$

$$D_4 = \frac{\rho_2 g k}{\mu_2 u}$$

These dimensionless groups are not unique to the problem; other combinations may have a clearer physical meaning. Let us define $D_5 = D_2/D_4 = \rho_1/\rho_2$, then we can delete D_4 from the groups. Similarly, by defining $D_6 = D_1/D_3 = \mu_2/\mu_1$, we can delete D_1 from the groups, and D_7 such that $D_6/D_7 = D_2/D_3$, then $D_7 = \dfrac{\rho_1 g L}{\sigma\sqrt{\dfrac{\phi}{k}}}$.

Finally, our similarity groups after these transformations are:

$$\frac{\rho_1}{\rho_2}, \frac{\mu_2}{\mu_1}, \frac{\rho_1 g k}{\mu_1 u}, \frac{\rho_1 g L}{\sigma\sqrt{\dfrac{\phi}{k}}}$$

Groups 1 and 2 are density and viscosity ratios, group 3 is the ratio of gravity to the viscous forces, or a gravity number, and group 4 is the ratio of gravity force to capillary forces, also called the Bond number. The reason for these transformations is that the gravitational force is considered the most important among the viscous, capillary and gravitational forces in the drainage process being considered.

The dimensionless relative permeability terms of oil and gas appear in Eqs. 1.2' and 1.3'. The initial condition in Eq. 1.7 provides yet another dimensionless group, $S_{1i,}$ the initial oil saturation. To ensure the same relative permeability function in the model and in the field, it is ideal to use the same reservoir rock material in the physical model. However, this is not always possible. If different porous media are used, the pore size distribution in the prototype should be matched to that in the porous media of the physical model. In other words, the pore size distribution functions should be congruent functions as shown in Figure 1.2.

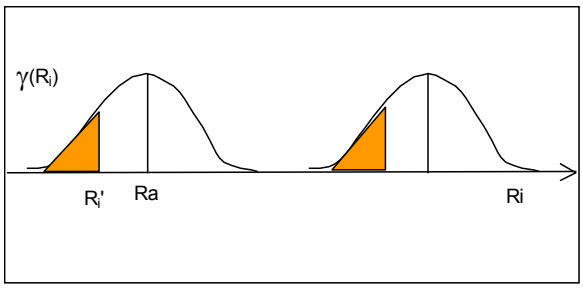

Figure 1.2: Congruent Pore Throat Size Distribution Functions

To ensure the same initial saturation condition, let us use Figure 1.2 to illustrate the point. The same saturation in the model as in the field means that the same proportion of space is occupied by the wetting phase within the same distribution function, represented by the dark-colored area. The entry pore throat size, R_i' that is determined by the capillary pressure, should correspond to each other in terms of their relative magnitude, that means R_i'/R_a should be the same for the model and field, where R_a can be the average pore throat size.

The initial drainage process in the oil reservoir is a capillary and gravity dominated process, i.e., oil migrates due to some force and enters the pores with a certain pore throat opening depending on the capillary pressure. The capillary pressure should be equal to the gravity force that drives water away, such that:

$P_c = 2\sigma\cos\theta/R_i'$ and

$R_i' = 2\sigma\cos\theta/ P_c$ …… (1.9)

, where the capillary pressure, P_c, is balanced by the gravity force. Thus the value of P_c can be determined by the oil-water contact and the density difference of oil and water in a specific reservoir. This quantity can be transformed by dividing it by the average pore throat radius, R_a, resulting in:

$2\sigma\cos\theta/ (P_c R_a)$

This dimensionless group serves as the dimensionless group for the same initial condition. Thus, the following list constitutes the final similarity groups for the gravity drainage process being discussed:

$$\frac{\rho_1}{\rho_2}, \frac{\mu_2}{\mu_1}, \frac{\rho_1 g k}{\mu_1 u}, \frac{\rho_1 g L}{\sigma\sqrt{\frac{\phi}{k}}}, \frac{2\sigma\cos\theta}{P_c R_a}, \gamma(R_i)$$

1.1.3 Development of a Scaled Physical Model

According to Stegemeier et al. (1980), a scaled physical model is developed through various steps. The governing equations for the process have to be identified in order to

adequately scale the process. The similarity groups have to be determined through dimensional or inspectional analysis. A prototype field has to be selected, in order to match the similarity parameters between the desired model and the selected field. Model properties are then determined through calculations, engineering judgment and resource availability. It has been attempted to follow this approach for developing a scaled physical model of the GAGD process.

1.1.3.1 Identification and Evaluation of the Scaling Parameters

It becomes necessary to identify the governing phenomena for a gravity drainage process in order to scale it. The similarity parameters usually involve the ratio of the various forces that govern the process. Viscous, capillary and gravity forces have been identified as the crucial forces that govern a gravity drainage process (Leverett, 1940, Craig, 1957, Hagoort, 1980, and Meszaros, 1990). Blunt et al. (1995) report that film flow plays an important role in gravity drainage of oil. A fluid property group, α, a function of interfacial tension and density difference of fluids was introduced by Kantzas et al. (1988). Blunt et al. (1995) used this relationship to show that for $\alpha>1$, oil only exists as a molecular film with negligible oil saturation above a critical height (Z_c). This implies that complete drainage of oil from the region above the critical height can be achieved, yielding very low oil saturations. The critical height Z_c is a function of the thickness of the oil bank (H) and α, where $Z_c = \alpha H/(\alpha-1)$. The similarity parameters for the calculation of the preliminary scaled physical model for the GAGD process have been adapted from literature while other similarity groups that could play a role in GAGD have been identified. Table 1.1, lists the similarity groups that were identified and used in calculating the physical model parameters for scaled experiments.

The relationship presented in equation 1.10 is the governing criterion for scaling the process, which is in agreement with the scaling laws presented by Rapoport (1955).

$$\gamma\left(\frac{L}{H}\sqrt{\frac{K_V}{K_H}}\right)=\gamma\left(\frac{v\mu}{\sigma}\right)=\gamma\left(\frac{\Delta\rho g\left(\frac{K}{\phi}\right)}{\sigma}\right)=\gamma\left(\frac{\Delta\rho_{og}gK}{\mu_o v_d}\right)=\gamma\left(\frac{\sigma_{ow}(\rho_0-\rho_g)}{\sigma_{go}(\rho_w-\rho_o)}\right)=1\ldots\ldots\ldots \quad (1.10)$$

Table 1.1: Similarity Groups for the GAGD Process

	Similarity Groups	Formula	References
1.	Geometric Aspect Ratio (R_L)	$R_L = \frac{L}{H}\sqrt{\frac{K_V}{K_H}}$	Shook et al., 1992
2.	Capillary Number (N_C) Ratio of viscous forces to capillary forces	$\frac{v\mu}{\sigma}$	Grattoni et al., 2000
3.	Bond Number (N_B) Ratio of Gravity forces to capillary forces	$\frac{\Delta\rho g\left(\frac{K}{\phi}\right)}{\sigma}$	Grattoni et al., 2000
4.	Fluid property group (α)	$\frac{\sigma_{ow}\left(\rho_0 - \rho_g\right)}{\sigma_{go}\left(\rho_w - \rho_o\right)}$	Kantzas et al., 1988
5.	Gravity Number (N_G) Ratio of gravity forces to viscous forces	$\frac{\Delta\rho_{og} gK}{\mu_o v_d}$	Shook et al., 1992

Where γ refers to the ratio of the similarity parameter of the prototype field to that of the scaled physical model. A model is said to be completely scaled if the above relationship is obeyed. Limitations of physical model arise because of the unavailability of materials and fluids having physical properties that will satisfy all scaling requirements (Stegemeier et al., 1980).

This study has investigated the effect of all these forces in addition to the spreading coefficient and wettability on GAGD performance. All the experiments conducted in this study have attempted to study the effect of the capillary number, the Bond number, the spreading coefficient, the mode of injection (secondary/tertiary), the rock wettability and the mode of gas injection (constant pressure/constant rate) on the performance of GAGD process.

1.1.3.2 The Bond and the Capillary Number

The Bond number, N_B, is defined as the ratio of gravitational forces and the capillary forces (Table 1.1). The Bond number is directly proportional to the absolute permeability of the sand pack, and the density difference between the fluids in the reservoir. The absolute permeability of an unconsolidated porous media is a strong function of the grain diameter and is given by the Carman-Kozeny equation (Equation 1.11).

$$D_P = \sqrt{\frac{72\tau(1-\phi)^2 K}{\phi^3}} \quad \text{..... (1.11)}$$

Where D_P is the grain diameter, τ is the tortuosity and ϕ is the porosity of the bead pack. However, it is out of the scope of this study to measure the tortuosity of the sand pack, therefore the typical value of 1.5 for sand packs is used as the tortuosity in the above equation. Moreover, the permeability decreases weakly with tortuosity and tortuosity does not vary vastly (White, 2004). In order to obtain favorable and realistic Bond numbers, fluid-fluid interaction parameters (interfacial tension) are also important. The Bond number ranges obtained from the field (Table 1.2) were the basis of the experimental design for studying their effect on GAGD recovery. Experiments were conducted by selecting appropriate grain sizes and fluids to simulate the Bond numbers obtained from field production data.

The capillary number, N_C, plays a very important role in deciding the stability of the gas displacement process. The importance of the capillary number and the viscosity ratio of the displacing and displaced fluid have been mentioned in the literature review section. Viscous forces have an effect on the drainage process. In this study the viscous forces were quantified with respect to the capillary forces by using the capillary number.

Table 1.2: Field Ranges of the Dimensionless Groups (Kulkarni, 2004)

Field Ranges	Capillary Number (N_C)	Bond Number (N_B)	Gravity Number (N_G)
Minimum	1.12E-09	1.21E-05	875
Maximum	4.18E-08	2.84E-07	0.39

1.2. The Physical Model Experiments

1.2.1 Introduction

The first sections contain the detailed literature review in which the design of the scaled model using the dimensional similarity approach will be discussed. Scaled experiments on a Hele-Shaw type physical model were carried to study the effect of the following parameters on GAGD performance during forced gravity drainage experiments:

- Bond number.
- Capillary number.
- Mode of gas injection.
- Type of gas injected.
- Wettability.
- Fractures.

1.2.1.1 Literature Review

A field review conducted on nine gravity drainage field projects by Kulkarni (2004), indicated that all those field projects in various parts of the world were successfully implemented. The oil recovery from these projects has been as high as 90% of the initial oil in place (IOIP) in tertiary mode after secondary waterfloods. Although two of the nine projects were deemed economically unsuccessful, the others were all lucrative. These projects were implemented on a large variety of geological settings, ranging from formations that were sandstone (mostly water-wet) to carbonates and dolomites (mostly oil-wet). This clearly indicates that gravity drainage can be implemented in a wide variety of geological setting.

However, these projects were implemented on pinnacle reefs type reservoirs. Gravity drainage using vertical wells might not yield similar recoveries if these were horizontal type reservoirs. Gravity override becomes a problem in conventional horizontal gas injection enhanced oil recovery (EOR) processes, where an unfavorable mobility ratio in such processes results in early gas breakthrough, lower gas utilization factor and poor oil recoveries. The inclusion of horizontal wells in horizontal type reservoirs to facilitate the gravity stable oil drainage appears to be a solution to this problem.

1.2.1.2 Horizontal Wells

Horizontal wells have long been used in several field applications. The key parameters that control the success of horizontal wells are: (i) fracture intensity, (ii) hydrocarbon pay zone thickness, (iii) well spacing, (iv) vertical communication, (v) formation damage and post drilling cleanup ability, (vi) geological control, (vii) multi-well prospect, and (viii) cooperation in geological, reservoir, drilling and completion departments (Lacy et al., 1992). Horizontal wells result in increased reservoir contact area, increased productivity

over vertical wells and reduce coning tendencies in reservoir with bottom water drive and top gas cap drive because of a low pressure drawdown around the well bore. The application of horizontal wells in GAGD will account for the stable displacement of oil from the top of the reservoir to the well, reduce early gas breakthrough and reduce the residual oil saturation (Joshi, 2003). However, the applicability of horizontal wells will depend on the parameters discussed above.

1.2.1.3 Scaled Model Studies

Displacement experiments in the laboratory have been extensively used to investigate the production behavior of petroleum reservoirs. Stahl et al. (1943) conducted the first scaled gravity drainage experiments. Air was used to displace various fluids from a column containing Wilcox sand. They reported results showing the dependence of liquid saturation on column height at both equilibrium and dynamic conditions. Scaled experiments investigating gravity segregation have been studied by Craig et al. (1957) and Templeton et al. (1961) in glass bead systems. Meszaros et al. (1990) used a series of partially scaled two-dimensional models to study the effect of inert gas injection on heavy oil recovery. As much as 70% of the oil in place was recovered in their study. Such experiments are representative of the reservoir if they are carried out in models that are properly scaled. The performance of oil reservoirs is governed by the value of a number of variables, which includes (i) fluid-fluid interfacial tension, (ii) fluid viscosities, (iii) wettability, (iv) spreading coefficient, (iv) fluid-fluid density difference, (v) rock porosity, (vii) absolute and relative permeability, and (vii) initial water saturation. These variables can be combined to form dimensionless groups. The derivation of these groups is done using two general methods:

- Dimensional Analysis (Geertsma et al., 1955).
- Inspectional Analysis (Ruark, 1935).

Dimensional analysis is the process of combining two or more variables into a group that would be dimensionless. The effect on a certain variable is then studied in terms of the group instead of individual variables in the group. Rapoport (1955) suggests that if the ratio of dimensionless groups at a larger geometric scale to dimensionless groups at a smaller geometric scale were kept equal to one, then the mechanisms occurring on both the scale would be similar. However, the above statement is true only if both of the scales are geometrically similar.

Inspectional analysis is a similar method for obtaining dimensionless groups to study the mechanistic behavior of a process. However, inspectional analysis is based on the underlying physical laws, usually expresses in the form of partial differential equations and boundary conditions. Inspectional analysis can be done even with an incomplete set of equations and through the analysis; at least some of the dimensionless groups can be obtained (Shook, 1992). Inspectional analysis is stronger than dimensional analysis in the

sense that it takes into account the underlying physical laws involved in the flow behavior. However, dimensional analysis has been found sufficiently useful for processes involving similar flow behavior (Hagoort, 1990).

1.2.1.4 Factors Affecting Gravity Drainage

Along with edge water drive and solution gas drive, gravity drainage has long been recognized as one of the three important natural drive mechanism for expelling oil from the reservoir rock. However, the quantification of oil recovery due to drainage has long been a concern. It has long been a concern to identify the contribution of oil recovery due to gravity drainage alone. Calhoun (1953) suggests that if drainage was occurring, those wells lowest in the structure should recover the highest amount of cumulative oil. During the early life of the reservoir, the reservoir tends to produce by solution gas drive, depending upon how much pressure drawdown is available. Although, the primary mechanism is solution gas drive, some drainage is still evident in the reservoir during production period at the lower part of the reservoir. However, when the reservoir pressure depletes, gravity drainage seems to be taking place at greater portions of the reservoir (Lewis, 1943).

Lewis (1943) suggests that the force of gravity provides sufficient mechanical energy to drain a large percentage of oil from the sand, but the important concern is not how much potential mechanical energy there is in the reservoir but how effective it will be in displacing oil. The distribution of oil within the pore space of a porous media plays an important role in the viability of the oil being recovered efficiently.

Oren et al., (1994), suggest that the static pore-scale distribution of three fluids in a porous media is determined by a complex interaction involving physical phenomena such as wettability (rock-fluid interactions), spreading phenomena, capillary pressure, mobility, viscosity and buoyancy.

Grattoni et al., (2002), reported that wettability in conjunction with the spreading characteristics of the oil plays an important role in displacing residual oil from the pores. They conducted experiments using large sintered packs, with different matrix wettability and with oils having different spreading coefficients for evaluating the performance of a depressurization process. Results from these experiment indicates that in a water-wet medium, for spreading oils, the physical form of the oil becomes transformed from immobile ganglia into mobile oil films, which can be transported by the gas. For non-spreading oils, oil has to be pushed out by the gas as discontinuous ganglia, so less oil is produced. In contrast, in an oil-wet system, the oil phase already exists as continuous film on the solid surface so that the generation of gas effectively expands the oil phase, enabling the oil to be produced in larger quantities even at lower gas saturations. It can be concluded from this work that rock wettability and oil spreading behavior have an influence on the performance of gas drives.

Moreover, most of the reservoirs have been reported as being mixed wet, in which continuous and distinct oil and water-wetting surfaces coexist in the porous media. Laboratory and network model studies conducted by Rao et al., (1992), Salatheil, (1973), Morrow (1991) and network model studies of Kovscek (1993), indicate that lower residual oil saturation can be obtained for a mixed wet porous media as compared to water-wet medium.

The preferential spreading of one fluid over the other in a porous media has been quantified using the spreading coefficient, S. Studies conducted by Blunt et al. (1995), Oren et al., (1995), Mani et al., (1996) and Grattoni et al., (2000) emphasized the importance of film flow behavior in a drainage dominated environment. Mani et al., (1996), report that for a spreading oil system where $S > 0$, the residual oil saturation is far less than in a non-spreading oil system. If $S > 0$, the interfacial energy of a three phase fluid system is decreased by having a film of oil between the gas phase and the water phase, and thus, oil spreads spontaneously between gas and water. The stability of the oil film becomes a crucial factor in facilitating the drainage of the film owing to gravity. Blunt et al., (1995) report that the thickness and stability of the oil film can be determined using a parameter α. This parameter governs the distribution of oil, water and gas in vertical equilibrium for a spreading system. Where:

$$\alpha = \sigma_{ow}(\rho_o - \rho_g)/\sigma_{go}(\rho_w - \rho_o) \quad \text{(1.12)}$$

, and ρ_o, ρ_g and ρ_w are the density of oil, gas and water respectively. Experiments conducted by the Blunt (1995) indicate that if $\alpha > 1$, there is a height above the oil/water contact, beyond which oil only exists as molecular film, with negligible saturation. When $\alpha < 1$, large quantities of oil remain in the pore space and gravity drainage is not efficient. The author also indicates that a negative spreading coefficient leaves behind large quantities of trapped oil in the reservoir, resulting in poor recoveries. Literature on spreading coefficient led to study its effect on the gravity drainage of oil assisted by invasion of gas into the model.

The distribution of oil, gas and water in the reservoir pores is controlled by their capillary interaction and the wetting characteristics of the reservoir rock. Whenever immiscible phases coexist in the porous media as in essentially all processes of interest, surface energy related to the fluid interfaces influences the distribution, saturations, and the displacement of the phases. Most of the EOR processes tend to reduce the interfacial forces existing across the interface of two phases. However, in immiscible processes capillary force exists and forces the denser fluid to retain in the pore spaces. Lewis et al., (1942) suggest that the self-propulsion of oil downward through sand under the impulse of its own weight occurs in two zones. At the top where the liquid is in contact with free gas, the sand is only partially oil saturated and capillarity controls the flow. Below the base of this capillary zone, which corresponds to a free surface, the sand is saturated or

nearly saturated with liquid and flow follows hydraulic laws. Therefore the complete knowledge of the capillary action in the porous media is necessary to predict the saturations and displacement of the displaced phase. Kantzas et al. (1988) presented equations to predict the saturations of each phase inside the capillaries of arbitrary pore sizes. Capillary pressure versus saturation plots for the three phase systems in capillaries of regular pore geometries were also developed. Li and Horne (2003) developed an analytical model based on capillary pressure curves to match and predict the oil production by free-fall gravity drainage. The model was able to match the experimental and numerical simulation data of oil recovery as well as the oil production data from Lakeview pool and Midway sunset field.

1.2.1.5 Summary of Literature Review

The effect of gravity tends to segregate fluids in the reservoir in order to maintain the density equilibrium (Muskat, 1949). Gravity segregation of fluids in horizontal reservoirs often leads to gas override and gas coning problems during a gas injection process. However, field reviews indicate that gravity stable gas injection is technically successful in dipping reservoirs and applicable to large variety of geological settings. Recent advances in horizontal well technology have demonstrated that the use of horizontal wells could minimize problems such as gas override and gas coning. Moreover, the use of horizontal wells in naturally fractured reservoirs often results in higher productivity. Horizontal wells could find favorable prospects in gravity stable gas injection processes in horizontal reservoirs.

Film flow characteristics of reservoir fluids are crucial for the implementation of gravity drainage processes. Rock wettability in conjunction with spreading coefficient determines the residual oil saturation for a drainage process. Capillarity plays an important role in the fluid distribution, fluid saturations and the displacement process. Viscosity ratio along with capillary number could determine the flow regime during a gas injection scheme. This study aims to determine the effect of all these parameters on GAGD performance.

1.2.1.6 The Effect of the Operating Mode

Lewis (1943) suggested the following modes of operating a gravity-stable gas injection process:

1. Gas injection at a constant pressure.
2. Restore and maintain or partially restore gas pressure after depletion of pressure
3. Reduce pressure gradually, so that gas and oil can segregate continuously by counter flow.
4. Produce field in two stages, first under solution gas-drive conditions until the gas has been practically eliminated from the oil, then by gravity drainage.

Methods 1 and 2, mentioned by Lewis (1943) are useful for commercial production from primary reservoirs. A thorough comparison between these two modes of gravity drainage process was deemed to be useful for the GAGD process. Experiments have been conducted to identifying the most favorable operating mode for GAGD.

Besides the two operating modes of gas injection, the effect of mobile and immobile or connate water saturation on GAGD was also investigated, achieved by conducting GAGD in primary recovery mode and secondary recovery mode (after waterflooding).

1.2.1.7 Wettability

Wettability is the term used to describe the relative adhesion of two fluids to a solid surface (Tiab et al., 1996). In a porous medium containing two or more immiscible fluids, wettability is a measure of the preferential tendency of one of the fluids to adhere to the surface. According to Morrow (1990), the reservoir wettability is determined by complex interface boundary conditions acting within the pore space of sedimentary rocks. These conditions have a dominant effect on interface movement and associated oil displacement.

The GAGD experiments in a 2-D Hele Shaw model also included experiments with oil-wet porous media. This experimentation was aimed as an extension of the water-wet 2-D Hele Shaw GAGD experiments and was designed to investigate the effects of reservoir wettability on secondary and tertiary mode GAGD process performance. Since the focus of this experimentation was to evaluate the performance of the GAGD process in oil-wet media, alteration of the wettability of the glass beads/silica sand from water-wet to oil-wet was essential for comparison on a similar basis. The wettability of the glass beads/silica sand was altered using an organosilane, dimethyldichlorosilane or $(CH_3)_2Cl_2Si$, and the steps involved (from the Fluorochem website) were:

1. Measure enough glass beads for use in one test run in a large glass vessel. Prepare the glass beads for the silylation process by rinsing the glass beads with the sample solvent (methylene chloride) to remove any manufacturing residues that might interfere with the silylation process.
2. Dry the glass beads by placing them in an oven and heat them at 180°C for at least 1 hour.
3. Cool the oven to approximately 50°C and immediately place the glass beads in a 5% solution of dimethyldichlorosilane ($(CH_3)Cl_2Si$), or DMDCS, in methylene chloride (CH_2Cl_2). Place a piece of laboratory stretch film over the reaction vessel. Soak the glass beads in the 5% DMDCS solution for 10 minutes. Use caution when removing the glass beads from the reaction vessel because anhydrous hydrochloric acid is formed during this reaction, as demonstrated in Figure 1.3.

4. Rinse the glass beads with the same solvent used in the DMDCS solution (methylene chloride) and then soak the glass beads in methanol for 10 minutes. Once again, cover the reaction vessel with laboratory stretch film.
5. Remove the glass beads from the methanol and allow them to air dry. Once dry, the beads are thoroughly deactivated and ready for use.
6. The described procedure must be performed entirely in the fume hood using gloves, an apron, a respirator, and suitable eye protection.

The interaction of certain silane compounds, in particular the chlorosilanes, with silica surfaces has important utility in their use as surface deactivating agents. When considering the reaction of dimethyldichlorosilane, or DMDCS ($(CH_2)_2Cl_2Si$), with the silica surface, two possible reactions can be presumed:

1. $S\text{-}_sOH + (CH_2)_2Cl_2Si \rightarrow Si_s\text{-}O\text{-}Si(CH_2)_2Cl + HCl$
2. $2\ S\text{-}_sOH + (CH_2)_2Cl_2Si \rightarrow (Si_s\text{-}O)_2\text{-}Si(CH_2)_2Cl + 2HCl$

A mixed, 1.6-order reaction has been observed suggesting that both reactions do occur. This implies that 40% of the freely vibrating surface hydroxyl groups reacts monofunctionally, but 60% must be present in a position sufficiently close to each other that they can react in a bifunctional manner (Hair, 1986). For this study it is assumed that only the first reaction occurs.

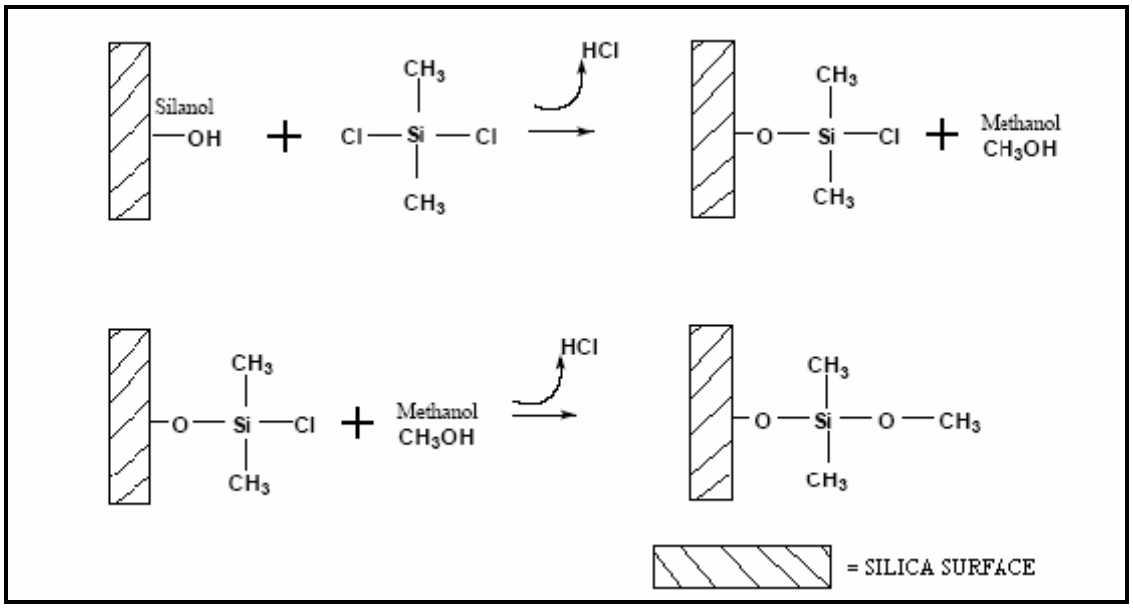

Figure 1.3: Reaction Mechanism of the Wettability Alteration Procedure

There are many different ways for measuring the wettability of a system. They include quantitative methods, such as contact angle measurement, imbibition/forced displacement (the Amott method), the United States Bureau of Mines (USBM) wettability method, and

qualitative methods, such as imbibition rates, microscope examination, flotation, glass slide method, relative permeability curves, and more. Although no single method is accepted by everyone, three quantitative methods are generally used:

1. Contact angle measurement.
2. The Amott method.
3. The USBM method.

The contact angle is a measure of the wettability of a specific surface, while the Amott and the USBM method measure the average wettability of a core.

The Contact Angle:

When two immiscible fluids are in contact the fluids are separated by a well-defined interface, which is only a few molecular diameters thick. When the interface is in intimate contact with a solid surface it intersects the surface at an angle, the contact angle, θ, which is a function of the relative adhesive tension of the liquids to the solid. The angle is described by Young's equation:

$$\cos\theta = \frac{\sigma_{s1} - \sigma_{s2}}{\sigma_{12}} \quad \text{..... (1.13)}$$

, where:

- σ_{s1} = interfacial tension between the solid and fluid 1;
- σ_{s2} = interfacial tension between the solid and fluid 2;
- σ_{12} = interfacial tension between the two fluids.

The contact angle is the best wettability measurement method when pure fluids and artificial cores are used because there is no chance of surfactants or other compounds altering the wettability (Anderson, 1986). Some of the methods used to measure the contact angle include: the tilting plate method, sessile drop or bubbles, vertical rod method, tensiometric method, cylinder method, capillary rise method, and the Dual Drop Dual Crystal method.

The Amott Method:

The Amott method combines imbibition and forced displacement to measure the average wettability of a core. In this method both reservoir core and fluids can be used. The Amott method is based on the principle that the wetting fluid will generally imbibe spontaneously into the core, displacing the non-wetting one. The ratio of spontaneous imbibition to forced displacement is used to reduce the influence of other factors, such as relative permeability, viscosity, and the initial saturation of the rock.

Usually the core is prepared by centrifuging under brine until the residual oil saturation is reached. The following four steps are then executed in the Amott method:

1. Immerse the core in oil and measure the volume of water displaced by the spontaneous imbibition of oil after 20 hours.

2. Centrifuge the core in oil until the irreducible water saturation is reached and measure the total amount of water displaced, including the volume displaced by spontaneous imbibition.
3. Immerse the core in brine and measure the volume of oil spontaneously displaced by the imbibition of water after 20 hours.
4. Centrifuge the core in brine until the residual oil saturation is reached and measure the total amount of oil displaced.

Note that the core may be driven to the irreducible water saturation and the residual oil saturation by flow rather than using a centrifuge. This is especially necessary for unconsolidated material that cannot be centrifuged.

The test results are generally expressed as follows:

1. The displacement-by-oil ratio:

   The ratio of the water displaced by spontaneous oil imbibition alone, V_{wsp}, to the total volume of water displaced by oil imbibition and forced displacement, V_{wt}.

   $$\delta_o = V_{wsp}/V_{wt} \quad \text{..... (1.14a)}$$

2. The displacement-by-water ratio:

   The ratio of the oil volume displaced by spontaneous imbibition of water, V_{osp}, to the total oil volume displaced by imbibition and forced displacement, V_{ot}.

   $$\delta_w = V_{osp}/V_{ot} \quad \text{..... (1.14b)}$$

Preferentially water-wet cores have a positive displacement-by-water ratio and a zero value for the displacement-by-oil ratio. The displacement-by-water ratio approaches one as the water-wetness increases. Similarly, oil-wet cores have a positive displacement-by-oil ratio and a zero displacement-by-water ratio. Both ratios are zero for neutrally wet cores. The time period for the spontaneous oil and water imbibition steps were chosen arbitrarily, but it is recommended that the cores be allowed to imbibe until either imbibition is complete or a pre-set maximum time limit has been reached. Imbibition can take from several hours to more than two months to complete.

1.2.1.8 Fracture Simulation within the GAGD Process

Darvish et al. (n.d.) conducted a numerical study in order to design oil-CO_2 gravity drainage laboratory experiments of a naturally fractured reservoir. They conducted the study using a fully compositional simulation model to investigate the drainage of CO_2 from a chalk core with artificial fractures. They also included the effects of molecular diffusion and interfacial tension. In their experiments, they used a cylindrical chalk core as the porous medium with a concentric hole through the middle of the core acting as an artificial fracture.

The numerical results examined the effects of core geometry, matrix permeability, pressure, and gas type in the fracture system on the oil recovery under CO_2/oil gravity drainage. Some of the most interesting results from their study can be summarized as follows:

1. The oil recovery scales up as the matrix permeability increases.
2. Increasing pressure postpones the oil recovery. The density difference reduces as the pressure increases and, consequently, this reduces the gravity force and results in less recovery at the early stage. The ultimate recovery for a high-pressure case is higher than for a low-pressure case, which is caused by the high extraction capability of CO_2 at high pressure.
3. The recovery performance for the injection of hydrocarbon gas versus CO_2 into the matrix is always higher at all stages due to the low hydrocarbon gas density compared with the CO_2 density.
4. In the case of CO_2 injection the recovery mechanism can be divided into two stages: (i) diffusion and gravity drainage and (ii) the extraction mechanism. In the initial stage, transport of the injection gas from the fracture into the matrix occurs primarily by lateral liquid-liquid diffusion between the undersaturated oil inside the matrix and the saturated oil with CO_2 at the inner surface of the matrix while at the same time the gas enters from the top of the block due to gravity drainage. This can be seen from the viscosity reduction of the oil along the core in the diffusion case. The CO_2 diffusion into the core causes the oil to swell followed by viscosity reduction and, consequently, less viscous forces and higher drainage rates. In the extraction mechanism, most heavy components of the residual oil are vaporized into the gas phase.

In addition to the secondary and tertiary water-wet and oil-wet runs, gas displacement runs were conducted in which the presence of a fracture was simulated. This was done by placing a mesh box inside the physical model prior to filling it up with glass beads. The mesh box consisted of strip metal wrapped in such a way as to form a framework with the length of the inside of the physical model and a height equal to the width of the model (dimensions: 13 7/8” by 1” by 1/2”). The framework was covered with 400-mesh sieve cloth to keep open an internal space that spanned the entire inner height of the model (the fracture) and, at the same time, to allow flow through it (see Figure 1.4).

In addition to the secondary and tertiary water-wet and oil-wet runs, gas displacement runs were conducted in which the presence of a fracture was simulated. This was done by placing a mesh box inside the physical model prior to filling it up with glass beads. The mesh box consisted of strip metal wrapped in such a way as to form a framework with the length of the inside of the physical model and a height equal to the width of the model

(dimensions: 13 7/8" by 1" by 1/2"). The framework was covered with 400-mesh sieve cloth to keep open an internal space that spanned the entire inner height of the model (the fracture) and, at the same time, to allow flow through it (see Figure 1.4).

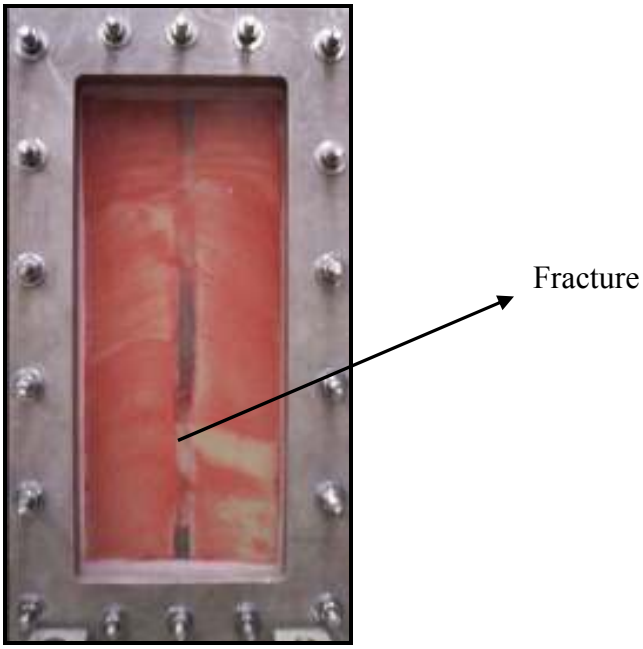

Figure 1.4: Physical Model with Vertical Fracture Simulation

1.2.2 Results and Discussion

1.2.2.1 Water-Wet Porous Media

This section summarizes the secondary and tertiary physical model GAGD experiments conducted to investigate the effect of the capillary number on the cumulative oil recovery, including three experiments studying the effect of the mobile water saturation, and consequently water shielding, on GAGD performance.

1.2.2.2 The Effect of the Capillary Number on GAGD Process Performance

Two immiscible secondary mode GAGD experiments with similar Bond numbers and varying capillary numbers were conducted to characterize the relationship between the capillary number and the total oil recovery, shown in Figure 1.5. It is interesting to note that this trend is confirmed by a miscible coreflood data point as well.

1.2.2.3 Tertiary Mode GAGD Experiments

The important distinction between secondary and tertiary oil recovery processes is the presence of mobile water saturation in the reservoir. Mobile water generally leads to

increased water shielding effects and water disposal problems in commercial gas injection projects.

Three 2-D physical model experiments to investigate the effects of mobile water on GAGD performance were completed. An additional experiment in the tertiary mode, Run TF4 with a gas injection rate of 400cc/min, was carried out during this quarter. The operational details of these floods, oil recoveries and capillary number variation(s) are reported in Table 1.3 and Figure 1.6.

The experimental results clearly demonstrate that the presence of mobile water in the physical model decreases the oil recoveries. Figure 1.7 shows the water production data during the GAGD run. The injected gas displaces the mobile water at the bottom of the model, mobilizing the residual oil and forming an oil bank at the bottom of the model. An average of 28.5% of the residual oil in place was recovered during these tertiary GAGD experiments as opposed to 63.5% IOIP during secondary GAGD floods for similar Bond and capillary number values. Water blocking effects are clearly noticeable in Figure 1.6 and Figure 1.7, where only 5% of the oil was recovered during early time. However, after the majority of the mobile water was produced, significant production of the residual oil was observed. Figure 1.8 shows the relationship between the oil recovery and the capillary number for the tertiary mode GAGD floods. It can be seen that relatively less oil is recovered (average of 24% IOIP) during tertiary mode GAGD compared to GAGD implemented in secondary mode (average of 63.5% IOIP). This implies that GAGD implementation in secondary mode is more beneficial compared to tertiary mode. The gravity-stable displacement of oil from the top of the reservoir to the bottom can be observed in Figure 1.9. This indicates that the immiscible GAGD process is not only capable of mobilizing large volumes of residual oil but is also an effective reservoir management tool.

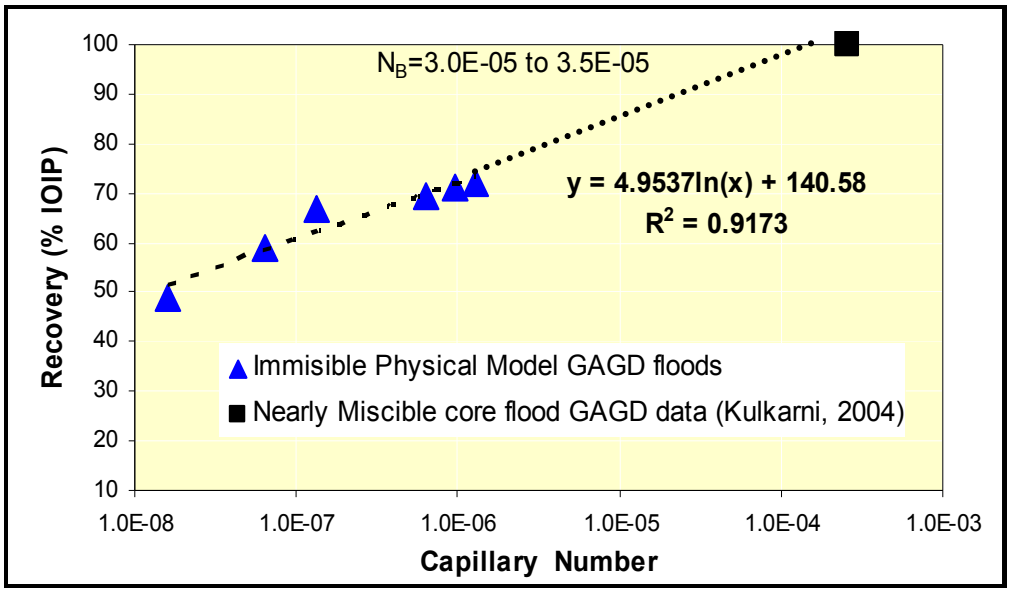

Figure 1.5: Variation in Total Oil Recovery with Capillary Numbers for Secondary GAGD

Table 1.3: Model Parameters for the Water-Wet Tertiary Mode GAGD Runs

Model Parameters	Run TF1 (20 cc/min)	Run TF2 (50 cc/min)	Run TF3 (5 cc/min)	Run TF4 (400 cc/min)
INITIAL CONDITIONS				
Connate Water Saturation (S_{wc}(%))	0.28	0.27	0.3	0.245
Porosity (%))	0.44	0.42	0.43	0.45
Initial Oil in Place, IOIP (cc)	401	405	384.5	430
WATER FLOOD				
Water Rate (cc/min)	3	3	3	3
Water Flood Oil Recovery (%IOIP)	45.8	51.7	52.4	49
Residual Oil Saturation, S_{or} (%)	39.4	35.2	33.6	36.1
Mobile Water Saturation, S_w (%)	60.6	64.8	66.4	63.9
GAS INJECTION				
Gas Rate (cc/min)	20	50	5	400
Oil Recovery (% ROIP)	21.4	29	27	36.6
Oil Recovery (% IOIP)	11.6	12.2	15.6	18.2
Bond Number (N_B)	3.9E-05	3.5E-05	3.6E-05	3.61E-05
Capillary Number (N_C)	5.35E-08	1.34E-07	1.6E-08	1.28E-06

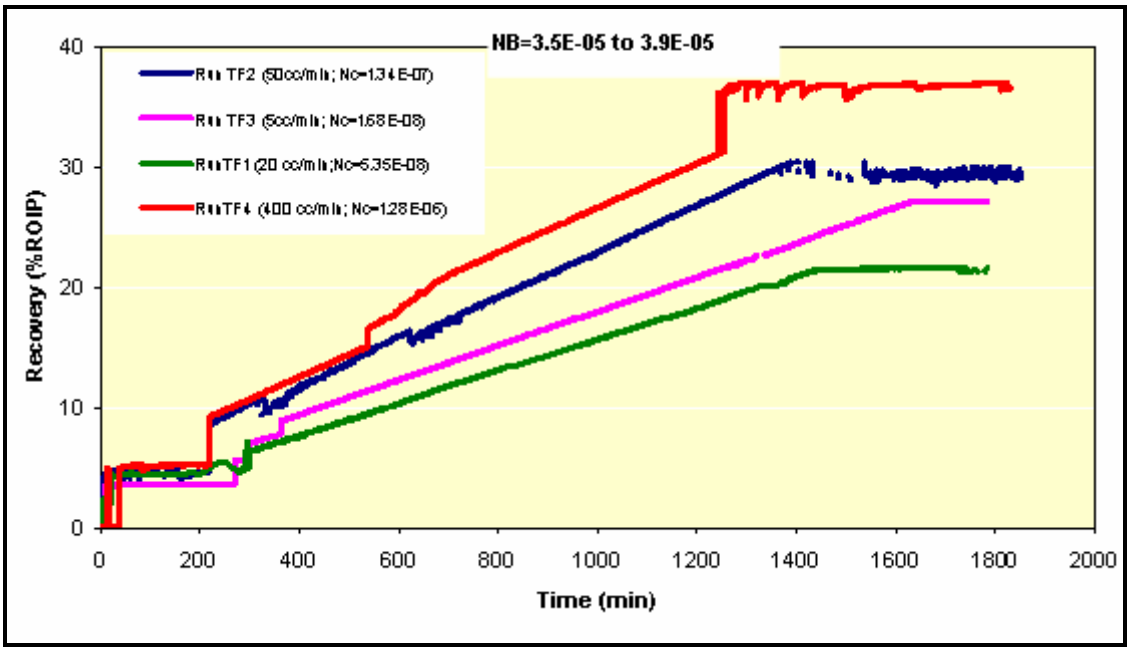

Figure 1.6: Oil Recoveries Obtained from Tertiary Mode GAGD Runs

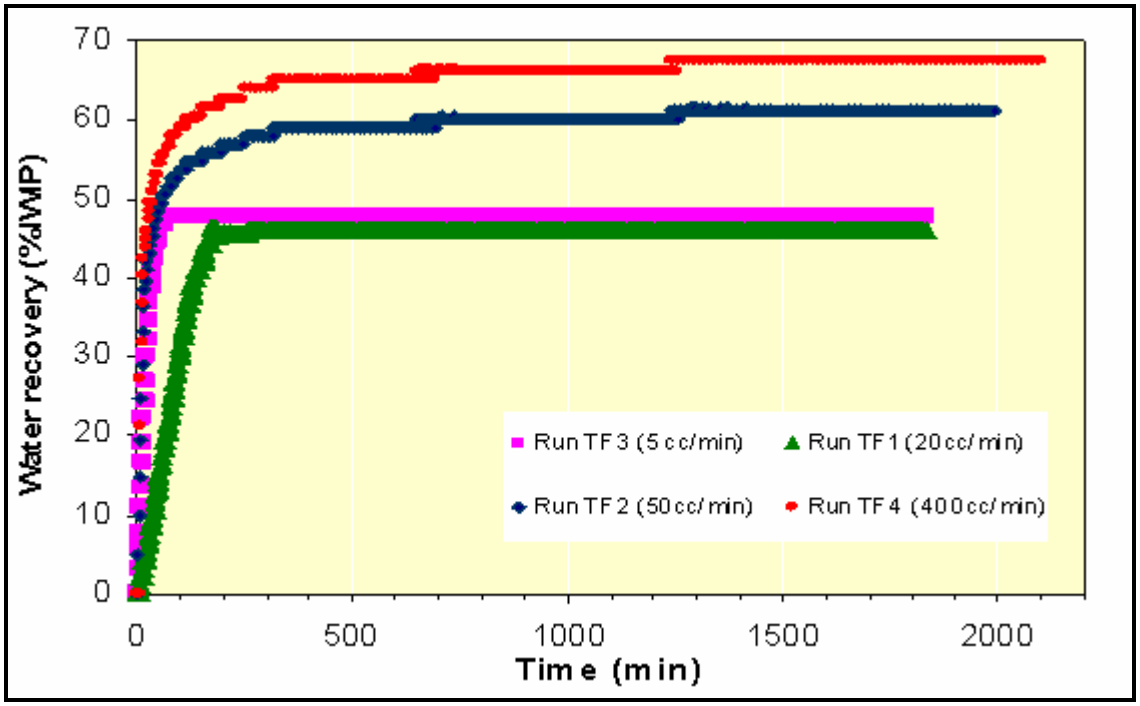

Figure 1.7: Water Recoveries Obtained from Tertiary Mode GAGD Runs

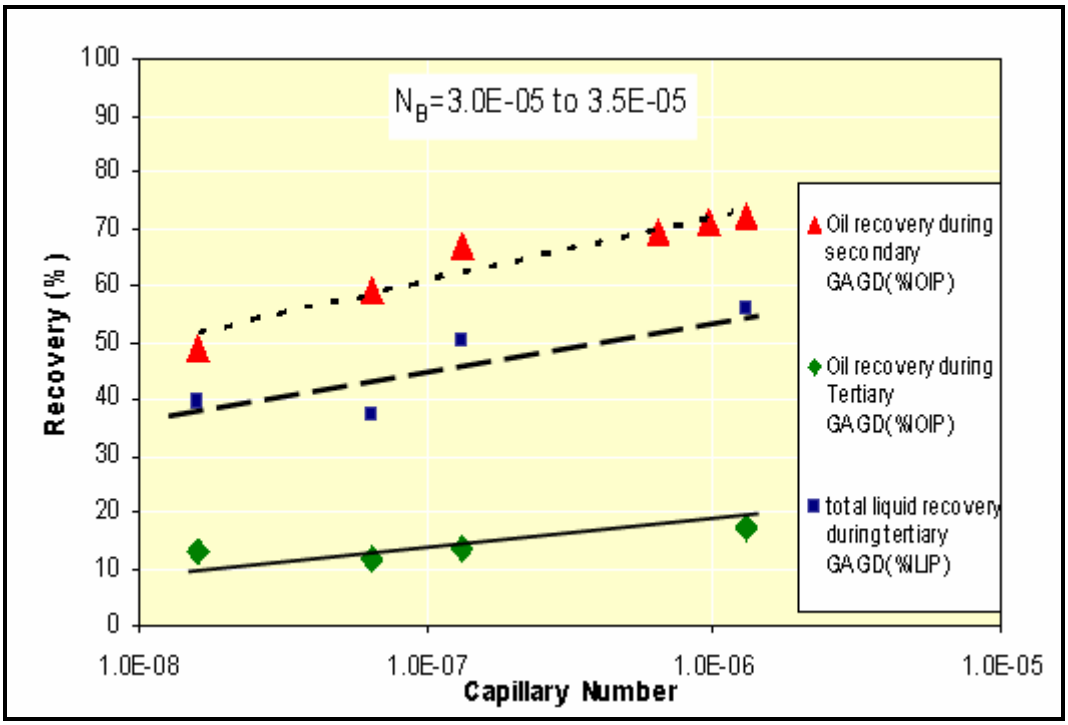

Figure 1.8: N_C versus Oil/Total Liquid Recoveries during Tertiary Mode GAGD

(A) Model placed horizontally for non-gravity stable water flood

(B) The presence of the oil bank at the top of the model at time = 1 min, after the start of GAGD in tertiary mode

(C) Movement of the oil bank to the bottom of the model at time = 200s

Figure 1.9: Flood Profile during Tertiary Mode GAGD

1.2.2.4 Oil-Wet GAGD Experiments

The Gas-Assisted Gravity Drainage (GAGD) experiments in a 2-D physical model packed were also conducted in oil-wet porous media and can be seen as an extension of the water-wet 2-D Hele Shaw physical model experiments of Sharma (2005). The experiments were designed to investigate the effect of reservoir wettability and the presence of a vertical fracture on secondary GAGD process performance. The procedure used to alter the wettability of glass beads from water-wet to oil-wet is described in the literature review section.

1.2.2.5 Overview of the Experiments

A total of six water-wet 2-D GAGD experiments were conducted to establish a baseline for comparison:

1. CP-S-WW-13-1: Constant pressure (4 psig), secondary mode, water-wet glass beads with an average diameter of 0.13 mm. Gas: N_2.
2. CF-S-WW-13-1: Constant mass flow rate (300 cc/min), secondary mode, water-wet glass beads with an average diameter of 0.13 mm. Gas: N_2.
3. CP-S-WW-15-1: Constant pressure (4 psig), secondary mode, water-wet glass beads with an average diameter of 0.15 mm. Gas: N_2.
4. CP-T-WW-13-3: Constant pressure (4 psig), tertiary mode, water-wet glass beads with an average diameter of 0.13 mm. Gas: N_2.
5. CP-T-WW-13-4: Constant pressure (4 psig), tertiary mode, water-wet glass beads with an average diameter of 0.13 mm. Gas: N_2.
6. CP-T-WW-15-1: Constant pressure (4 psig), tertiary mode, water-wet glass beads with an average diameter of 0.15 mm. Gas: N_2.

Eleven oil-wet 2-D GAGD experiments were also conducted during this reporting period, seven were run in the secondary mode, and four were conducted in the tertiary recovery mode:

1. CF-S-OW-13-1: Constant mass flow rate (75 cc/min), secondary mode, oil-wet glass beads with an average diameter of 0.13 mm. Gas: N_2.
2. CF-S-OW-13-2: Constant mass flow rate (75 cc/min), secondary mode, oil-wet glass beads with an average diameter of 0.13 mm. Gas: CO_2.
3. CP-S-OW-13-1: Constant pressure (4 psig), secondary mode, oil-wet glass beads with an average diameter of 0.13 mm. Gas: N_2.
4. CP-S-OW-13-2: Constant pressure (4 psig), secondary mode, oil-wet glass beads with an average diameter of 0.13 mm. Gas: CO_2.
5. CP-S-OW-13-3: Constant pressure (4 psig), secondary mode, oil-wet glass beads with an average diameter of 0.13 mm. Gas: N_2.
6. CP-S-OW-15-1: Constant pressure (4 psig), secondary mode, oil-wet glass beads with an average diameter of 0.15 mm. Gas: N_2.

7. CP-S-OW-15-2: Constant pressure (4 psig), secondary mode, oil-wet glass beads with an average diameter of 0.15 mm. Gas: N_2.
8. CF-T-OW-13-1: Constant mass flow rate (300 cc/min), tertiary mode, oil-wet glass beads with an average diameter of 0.13 mm. Gas: N_2.
9. CF-T-OW-13-2: Constant mass flow rate (300 cc/min), tertiary mode, oil-wet glass beads with an average diameter of 0.13 mm. Gas: N_2.
10. CP-T-OW-13-1: Constant pressure (4 psig), tertiary mode, oil-wet glass beads with an average diameter of 0.13 mm. Gas: N_2.
11. CP-T-OW-13-2: Constant pressure (4 psig), tertiary mode, oil-wet glass beads with an average diameter of 0.13 mm. Gas: N_2.

A total of five fractured secondary mode GAGD experiments were conducted, two of which were done using water-wet porous media and two were done with oil-wet porous media. The experiments are briefly described below:

1. CP-S-WW-13-2-F: Constant pressure (4 psi), secondary mode, water-wet silica sand with an average diameter of 0.13 mm. Gas: N_2. Fracture simulation.
2. CP-S-WW-15-1-F: Constant pressure (4 psi), secondary mode, water-wet glass beads with an average diameter of 0.15 mm. Gas: N_2. Fracture simulation.
3. CP-S-WW-15-2-F: Constant pressure (4 psi), secondary mode, water-wet glass beads with an average diameter of 0.15 mm. Gas: N_2. Fracture simulation.
4. CP-S-OW-13-2-F: Constant pressure (4 psi), secondary mode, oil-wet silica sand with an average diameter of 0.13 mm. Gas: N_2. Fracture simulation.
5. CP-S-OW-15-1-F: Constant pressure (4 psi), secondary mode, oil-wet glass beads with an average diameter of 0.15 mm. Gas: N_2. Fracture simulation.

The experimental results are summarized in Tables 2.2 to 2.6.

Table 1.4: Model Parameters for the Water-Wet Runs in Secondary Mode

Model Parameters	CP-S-WW-13-1	CF-S-WW-13-1	CP-S-WW-15-1
Gas	N_2	N_2	N_2
P (psig)	4	N/A	4
Rate (cc/min)	N/A	300	N/A
D_g(mm)	0.13	0.13	0.15
INITIAL CONDITIONS			
Pore Volume (cc)	524	528	558
Oil Flood Water (cc)	362.8	362.8	372.8
OOIP (cc)	362.8	362.8	372.8
Porosity ϕ (%)	36.5	36.5	38.6
S_{wc} (%)	30.8	31.3	33.2
S_{oi} (%)	69.2	68.7	66.8
GAS INJECTION			
k (Darcy)	4.7	4.9	3.8
Recovery (% OOIP)	66.7	60.1	72.7

Table 1.5: Model Parameters for the Tertiary Mode Water-Wet Runs

Model Parameters	CP-T-WW-13-3	CP-T-WW-13-4	CP-T-WW-15-1
Gas	N_2	N_2	N_2
P (psig)	4	4	4
Rate (cc/min)	N/A	N/A	N/a
D_g(mm)	0.13	0.13	0.13
INITIAL CONDITIONS			
Porosity ϕ (%)	37.4	36.8	38.7
OOIP (cc)	381.4	390.5	400.7
WATER FLOOD			
Water Flood Recovery (%IOIP)	55.5	56.5	63.7
S_{or} (%)	31.4	32.0	26.0
Post-WF S_w (%)	68.6	68.0	74.0
GAS INJECTION			
k (Darcy)	5.4	5.1	3.9
S_{wr} (%)	19.5	16.3	16.7
Recovery (% ROIP)	59.2	44.0	54.2
Recovery (% IOIP)	26.4	19.2	19.7
Total Recovery (%IOIP)	81.9	75.7	83.4

Table 1.6: Model Parameters for the Oil-Wet Runs in Secondary Mode

Model Parameters	CP-S-OW-13-1	CP-S-OW-13-2	CF-S-OW-13-1	CF-S-OW-13-2	CF-S-OW-13-3	CP-S-OW-15-1	CP-S-OW-15-2
Gas	N_2	CO_2	N_2	CO_2	N_2	N_2	N_2
P (psig)	4	4	N/A	N/A	N/A	4	4
Rate (cc/min)	N/A	N/A	75	75	300	N/A	N/A
D_g(mm)	0.13	0.13	0.13	0.13	0.13	0.15	0.15
INITIAL CONDITIONS							
Pore Volume (cc)	528	531	576	535	529	476	516.0
Oil Flood Water (cc)	357.8	450.5	475.5	415.5	430.5	347.7	433.7
OOIP (cc)	357.8	450.5	475.5	415.5	430.5	347.7	433.7
Porosity ϕ (%)	36.5	36.7	39.9	37.0	36.6	32.9	35.7
S_{wc} (%)	32.2	15.2	17.4	22.3	18.6	27.0	15.9
S_{oi} (%)	67.8	84.8	82.6	77.7	81.4	73.0	84.1
GAS INJECTION							
k (Darcy)	4.9	5.2	7.3	5.2	4.8	2.0	0.8
N_B	6.6E-06	7.4E-06	9.5E-06	7.2E-06	6.9E-06	3.0E-06	6.0E-06
N_C	1.2E-06	3.2E-07	4.7E-06	4.7E-06	1.9E-05	3.0E-07	6.3E-07
N_G	5.5	23.4	2.0	1.5	0.4	10.0	9.6
Recovery (% OOIP)	77.7	86.7	74.7	92.8	81.5	78.6	81.6

Table 1.7: Model Parameters for the Tertiary Mode Oil-Wet Runs

Model Parameters	CF-T-OW-13-1	CF-T-OW-13-2	CP-T-OW-13-1	CP-T-OW-13-2
Gas	N_2	N_2	N_2	N_2
P (psig)	N/A	N/A	4	4
Rate (cc/min)	300	300	N/A	N/A
D_g(mm)	0.13	0.13	0.13	0.13
INITIAL CONDITIONS				
Porosity ϕ (%)	37.8	39.8	36.2	39.1
OOIP (cc)	492.8	450.5	400.7	410.5
WATER FLOOD				
Water Flood Recovery (%IOIP)	37.4	47.6	50.4	46.4
S_{or} (%)	56.6	41.0	38.0	38.9
Post-WF S_w (%)	43.4	59.0	62.0	61.1
GAS INJECTION				
S_{wr} (%)	41.8	15.3	14.1	14.1
k (Darcy)	5.6	5.5	4.1	4.1
N_B	7.3E-06	6.8E-06	5.5E-06	8.1E-06
N_C	1.8E-05	1.8E-06	8.2E-07	6.2E-07
N_G	0.4	0.4	6.8	13.0
Recovery (% ROIP)	26.1	62.8	62.9	74.0
Recovery (% IOIP)	16.3	32.9	31.2	39.7
Total Recovery (%IOIP)	53.7	80.5	81.6	86.1

Table 1.8: Model Parameters for the Fractured Experiments

Model Parameters	CP-S-WW-13-2-F	CP-S-WW-15-1-F	CP-S-WW-15-2-F	CP-S-OW-13-1-F	CP-S-OW-15-1-F
Gas	N_2	N_2	N_2	N_2	N_2
Wettability State	Water-wet	Water-wet	Water-wet	Oil-wet	Oil-wet
P (psig)	4	4	4	4	4
D_g(mm)	0.13	0.15	0.15	0.13	0.15
INITIAL CONDITIONS					
Pore Volume (cc)	587.5	584.0	592.0	545.0	547.0
Oil Flood Water (cc)	363.7	303.7	338.7	463.7	468.7
OOIP (cc)	363.7	303.7	338.7	463.7	468.7
Porosity ϕ (%)	40.7	40.4	41.0	37.7	37.9
S_{wc} (%)	38.1	48.0	42.8	14.9	14.3
S_{oi} (%)	61.9	52.0	57.2	85.1	85.7
GAS INJECTION					
Recovery (% OOIP)	71.2	68.6	72.0	54.7	91.9

1.2.2.6 Confirmation of Wettability Alteration

During the oil flood the water-wet porous media always displayed a "mottled" appearance, i.e. the oil did not displace the water uniformly resulting in a swept red area speckled with unswept whiter portions. The oil-wet porous media, however, consistently showed a characteristic homogeneously red area indicating that the water was uniformly displaced by the injected n-decane (see Figure 1.10).

The results of the modified Amott test can be summarized as follows:

1. **Oil-wet 0.13 mm silica sand:**
   Pore volume = 456 cc
   Oil in cell = 368.7 cc
   V_{wsp} = 5 cc
   V_{wt} = 255 cc
   Oil after waterflood = 110.5 cc
   Oil in cell after oil flood = 365.5 cc
   V_{osp} = 7.3 cc
   V_{ot} = 224.9 cc
   $\delta_o = V_{wsp}/V_{wt} = 5/255 = 0.0196$
   $\delta_w = V_{osp}/V_{ot} = 7.3/224.9 = 0.0325$
2. **Oil-wet 0.15 mm glass beads:**
   Pore volume = 504 cc
   Oil in cell = 461.7 cc
   V_{wsp} = 4.4 cc
   V_{wt} = 225 cc
   Oil after waterflood = 293.9 cc
   Oil in cell after oil flood = 518.9 cc
   V_{osp} = 1.0 cc
   V_{ot} = 248.6 cc
   $\delta_o = V_{wsp}/V_{wt} = 4.4/225 = 0.0196$
   $\delta_w = V_{osp}/V_{ot} = 1.0/248.6 = 0.0040$

According to the criteria of the Amott test, an oil wet porous medium has a positive displacement-by-oil ratio, δ_o, and zero displacement-by-water ratio, δ_w. Because of the high porosity and permeability of the sand and bead packs used in these tests, the Amott tests were inconclusive due to the negligible capillary forces needed for imbibition. The confirmation of the wettability state of the porous media used was finally provided by the fractional flow curves (see Figures 1.10 and 1.11). They exhibit the characteristic shift to

the left of the fractional flow curve of the oil-wet silica sand or glass beads compared to the water-wet fractional flow curve.

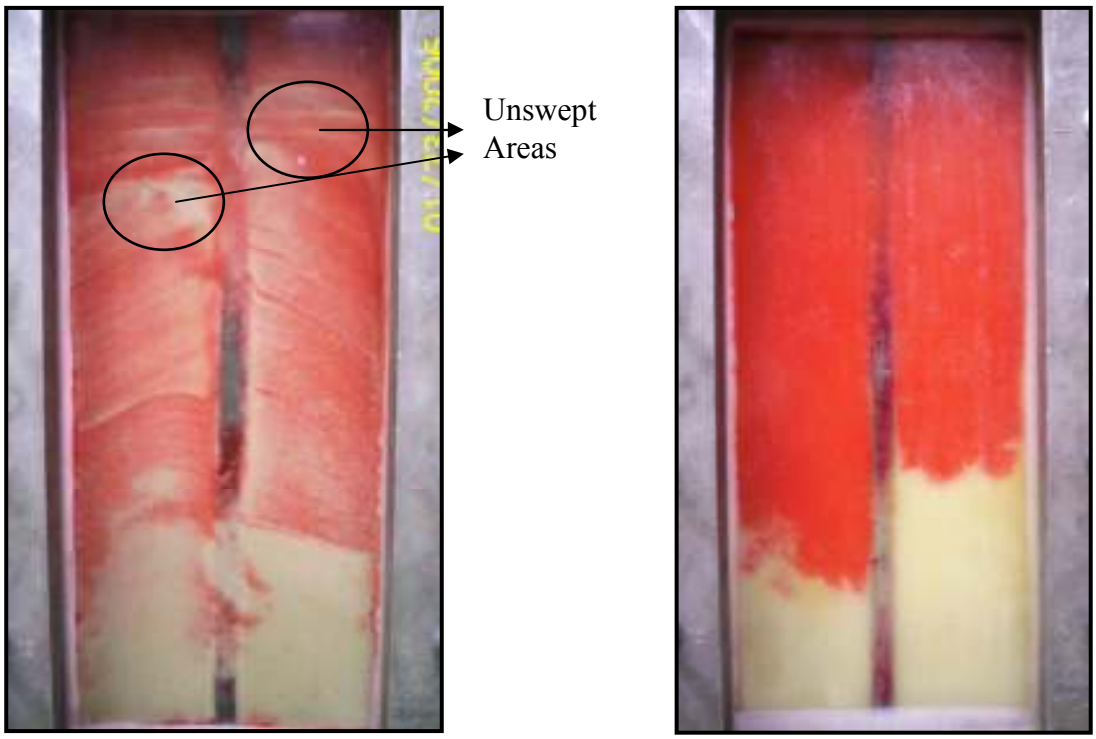

Figure 1.10: Visual Comparison of Water-Wet Porous Medium (Left) with Oil-Wet Porous Medium (Right) During Oil Flooding

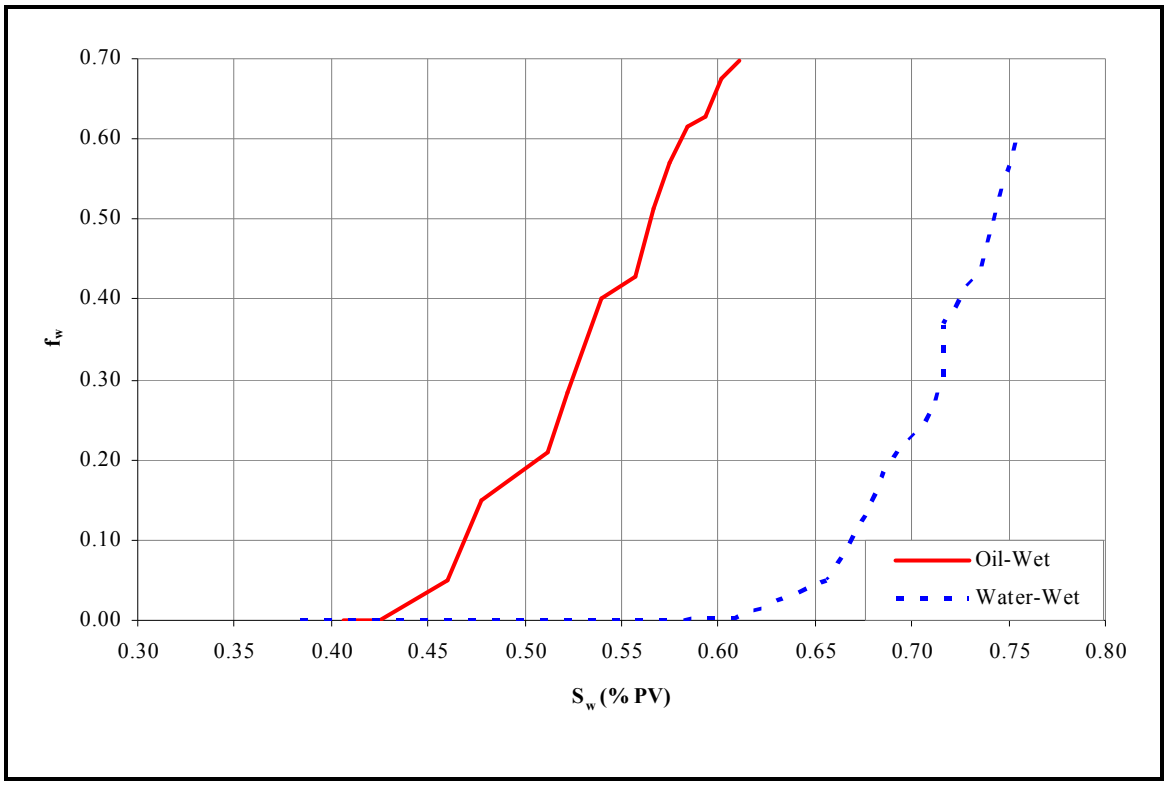

Figure 1.11: Fractional Flow Curves for the 0.13 mm Silica Sand

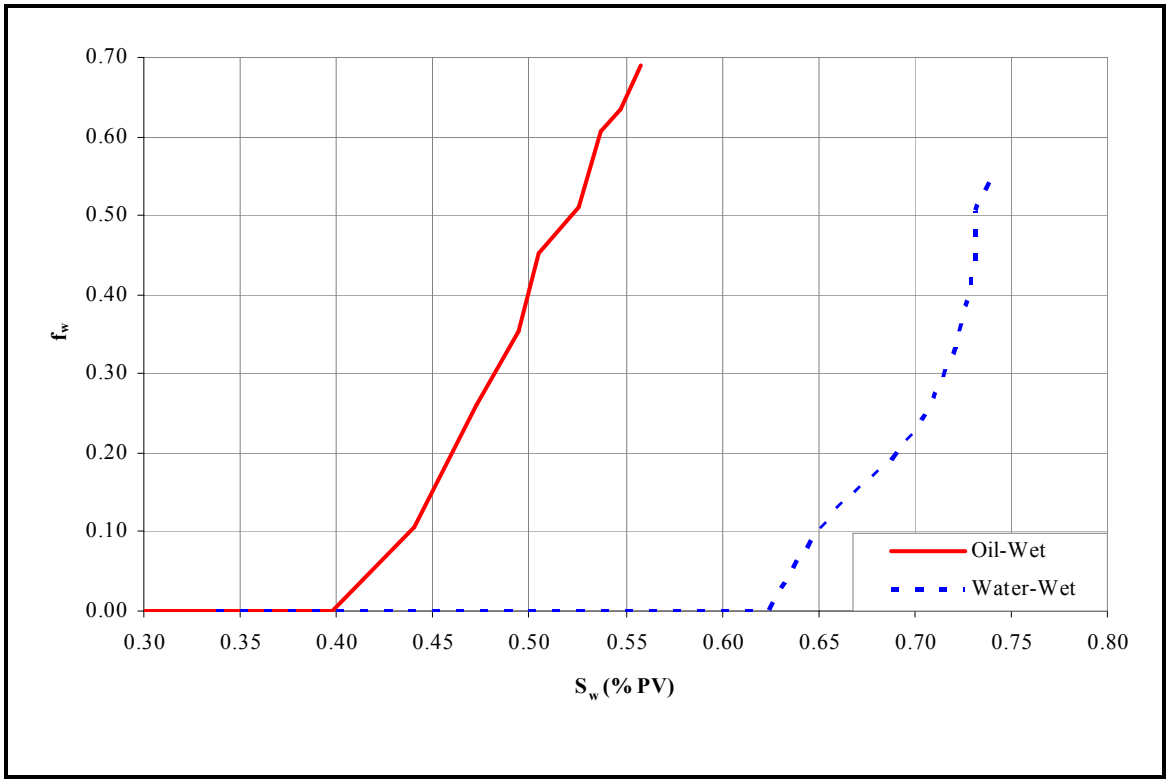

Figure 1.12: Fractional Flow Curves for the 0.15 mm Glass Beads

1.2.2.7 Effect of Wettability

The change in wettability from water-wet to oil-wet appears to significantly improve the oil recovery by N_2, as can be seen from Figures 1.13 to 1.17. The average incremental production of the oil-wet experiments compared to the water-wet experiments can be summarized as follows:

- Constant pressure secondary runs, 0.13 mm : +10 %OOIP.
- Constant pressure secondary runs, 0.15 mm : +5.9 %OOIP.
- Constant rate secondary runs, 0.13 mm : +18 %OOIP.
- Constant pressure tertiary runs, 0.13 mm : +14.8 %ROIP.
- Constant pressure tertiary runs, 0.15 mm : +3.9 %ROIP.

The high oil recoveries obtained in oil-wet systems when compared to water-wet systems in this study agree well with the field observations where oil recoveries due to gas injection are higher in oil-wet reservoirs. The displacement of fluids in these experiments is almost piston like because of appreciable gravity segregation effects. Therefore, the length of the two-phase (gas-oil) flow region is negligibly small to enable the application of diffuse flow theories and/or the use of relative permeabilities. The lower than expected incremental recovery in the constant pressure tertiary runs using the 0.15 mm grains can be attributed to deviation from normal experiment methodology (i.e. a hand packing method thereby decreasing the porosity and permeability, thus negatively affecting the oil recovery). This last experiment will be repeated using similar experimental procedures to those used in previous tests.

1.2.2.8 Effect of Gas Injection Mode

The constant flow rate experimental run CF-S-OW-13-1 demonstrated a lower oil recovery compared to the constant pressure run CP-S-OW-13-1 (an incremental production of 3%), because constant pressure gravity drainage has generally been suggested to be more efficient (Muskat, 1949). A similar phenomenon appears to be occurring when CP-T-OW-13-2 and CF-T-OW-13-2 are compared (an increase of 5.6% in oil recovery). This is illustrated in Figures 1.18 and 1.19.

1.2.2.9 Effect of Injection Gas

From the results (Figure 1.20) it appears that the type of injection gas does affect the oil recovery: whenever CO_2 was used as the displacement gas the oil recoveries were found to be higher than when N_2 was used; on average an increase in oil recovery of 13.6 % is achieved in the CO_2 experiments. This difference can probably be attributed to the effect of CO_2 on oil: the high solubility of CO_2 in oil causes the oil to swell thereby increasing its saturation and relative permeability, which results in significantly enhancing the oil recovery by improving the oil flowability (Darvish, et al., not dated).

1.2.2.10 Effect of a Vertical Fracture on GAGD Performance

The presence of the vertical fracture using water-wet 0.13 mm silica sand improved the GAGD recovery as evident from Figure 1.21. The average incremental increase in oil recovery is 7.9 %OOIP. The increase in oil recovery is mainly attributed to the presence of the fracture, which acts as a low resistance oil flow conduit, thus enhancing the oil recovery by gas injection. However, when we examine the water-wet fractured model runs using the 0.15 mm glass beads, it is evident that both of the fractured runs performed worse than the non-fractured run (Figure 1.22). This appears to be due to an incomplete oil flood, as there were parts of the porous medium that were consistently being bypassed by the n-decane. This is probably caused by the inherent higher permeability due to the use of a larger grain size creating easier flow paths to the fracture. From the results it can be seen that the oil-wet fractured cases outperform the non-fractured ones (Figures 1.23 and 1.24). On average, the incremental oil recovery was 6.7 %OOIP for the experiments using the 0.13 mm silica sand and 10.8 %OOIP for the 0.15 mm glass bead packs.

Effect of wettability on fractured GAGD performance:

All of the oil-wet experiments showed an increase in the oil recovery compared to the water-wet fractured runs (Figures 1.25 and 1.26):

1. Oil-wet, fractured 0.13 mm silica sand pack: an incremental oil recovery of 9.6 %OOIP on average.
2. Oil-wet, fractured 0.15 glass bead pack: an incremental oil production of 21 %OOIP.

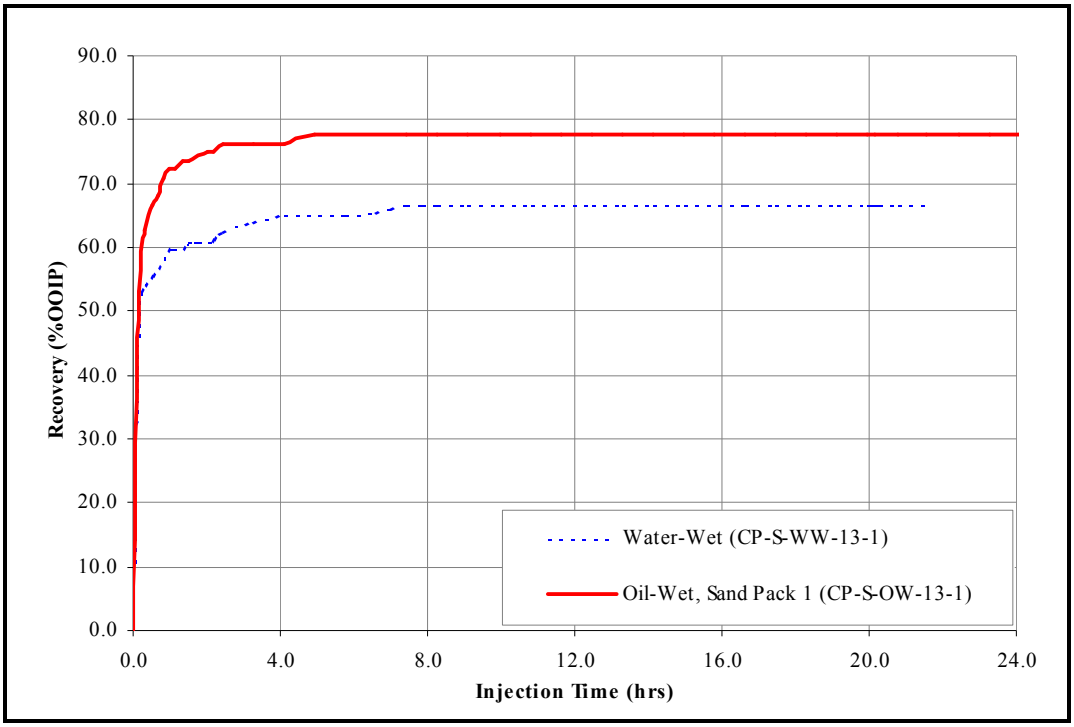

Figure 1.13: Effect of the Wettability on the Oil Recovery – Secondary Mode, Constant Pressure, 0.13 mm Sand Pack

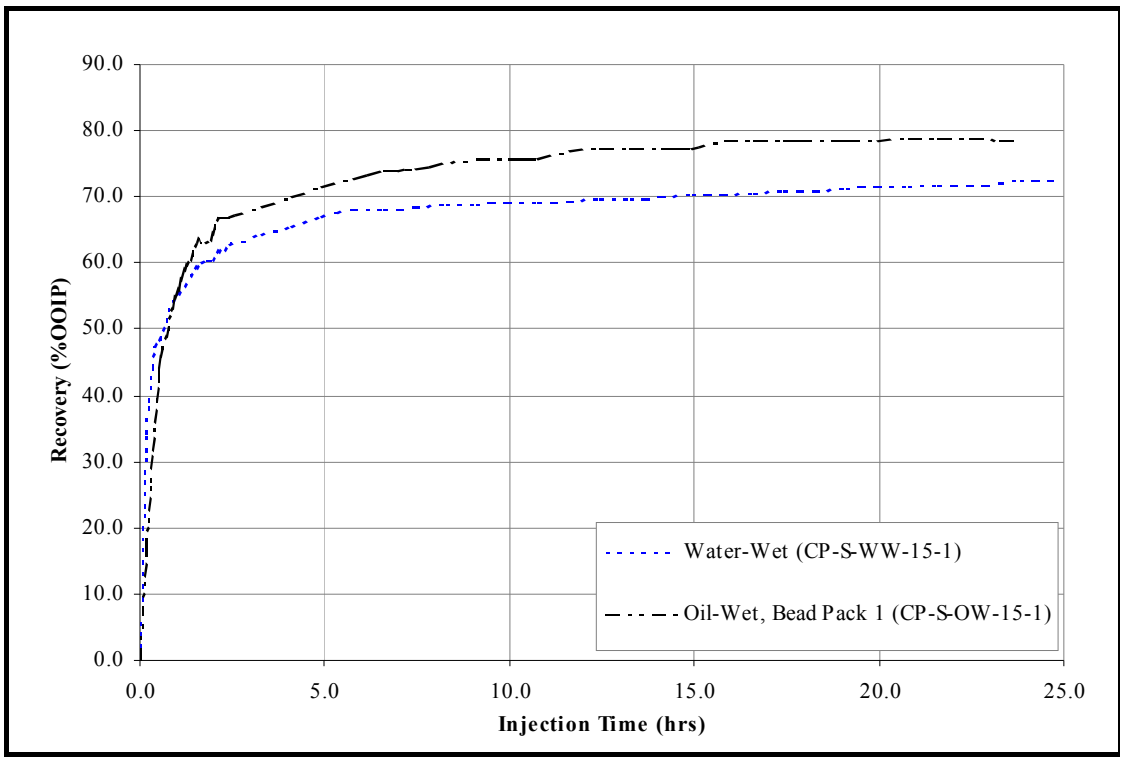

Figure 1.14: Effect of the Wettability on the Oil Recovery – Secondary Mode, Constant Pressure, 0.15 mm Glass Bead Pack

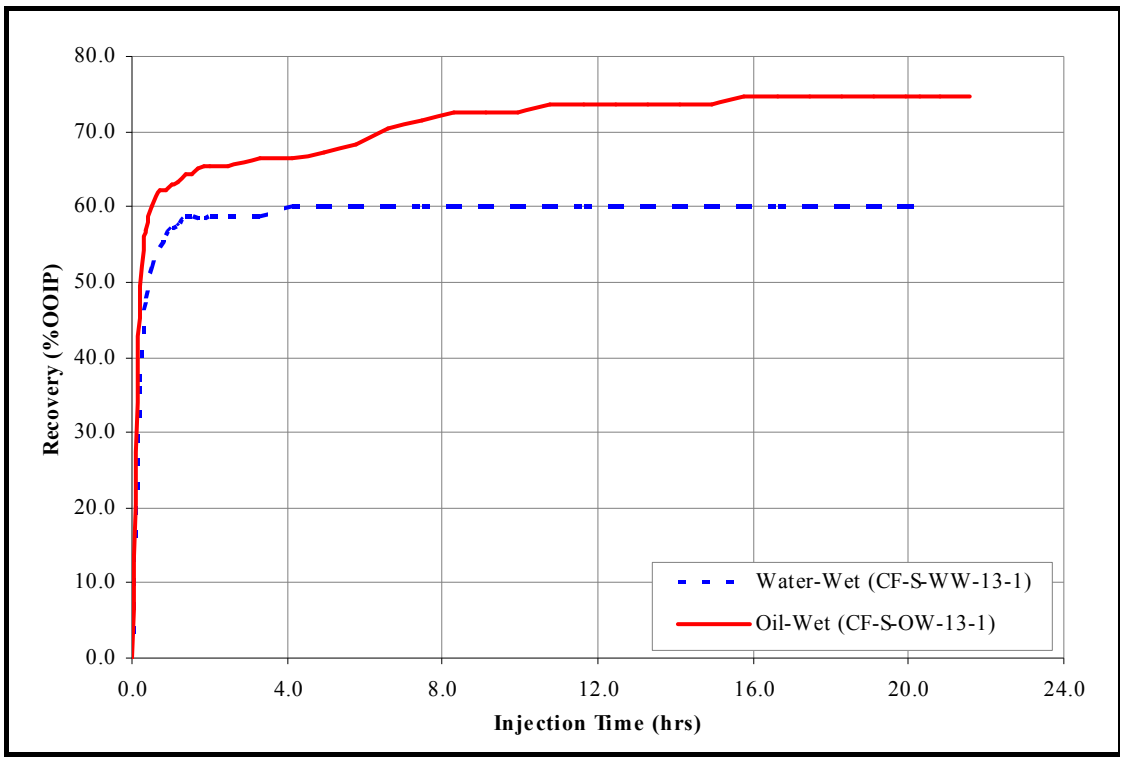

Figure 1.15: Effect of the Wettability on the Oil Recovery – Secondary Mode, Constant Rate, 0.13 mm Sand Pack

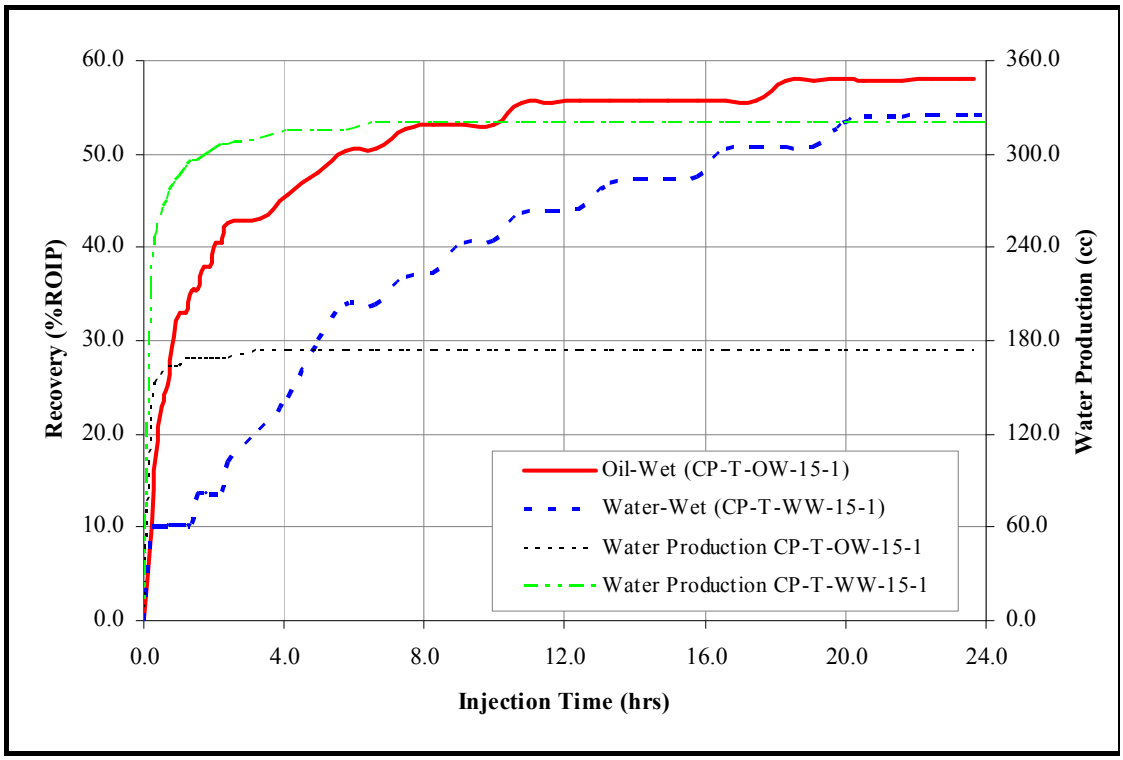

Figure 1.16: Effect of the Wettability on the Oil Recovery – Tertiary Mode, 0.15 mm Glass Bead Pack

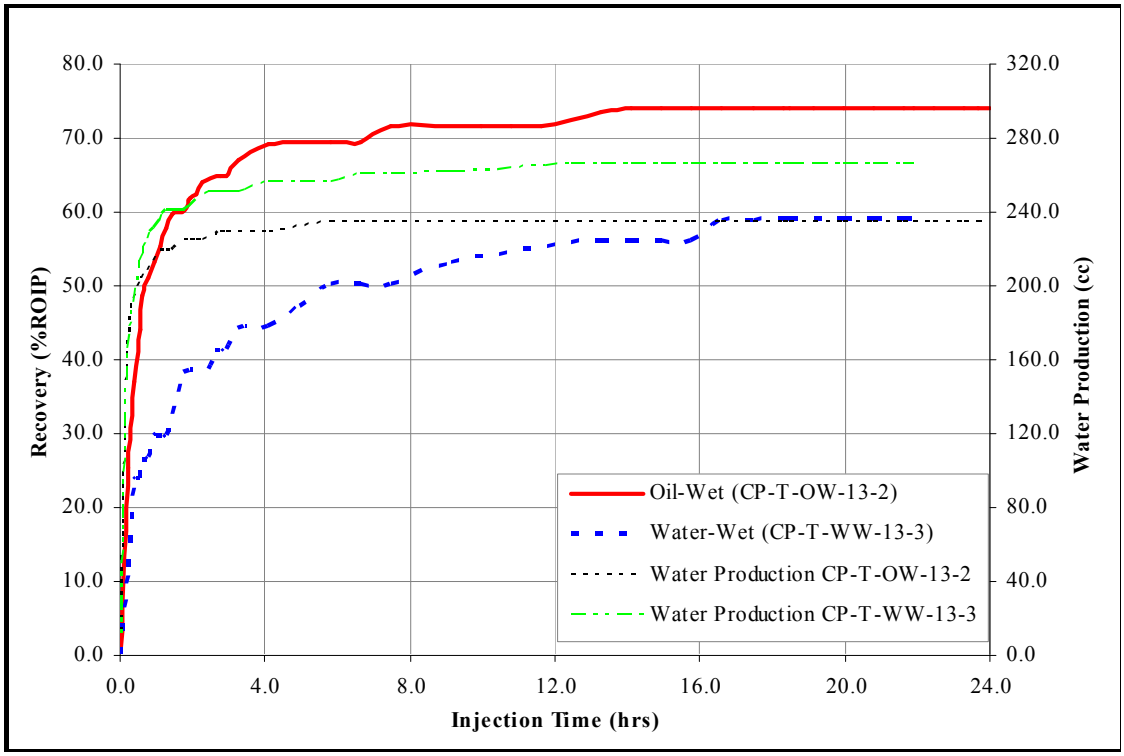

Figure 1.17: Effect of the Wettability on the Oil Recovery – Tertiary Mode, 0.13 mm Sand Pack

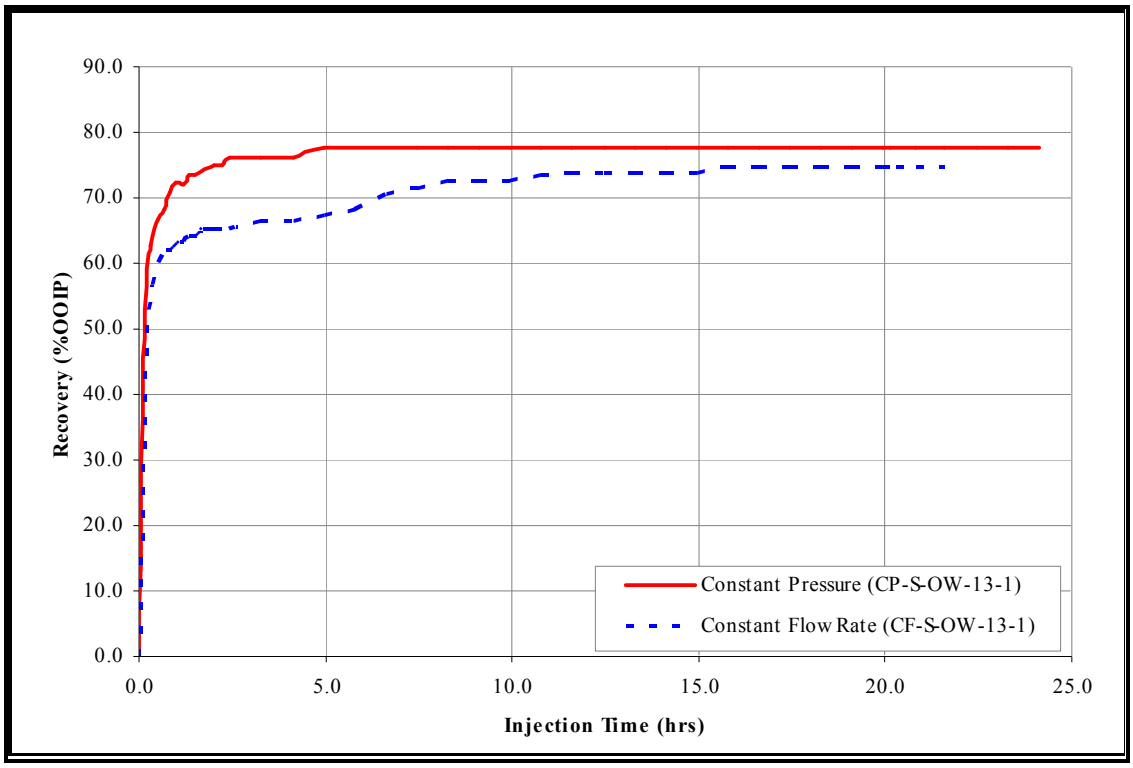

Figure 1.18: Effect of the Gas Injection Method on the Oil Recovery – Secondary Mode Runs, Oil-Wet Case, 0.13 mm Sand Pack

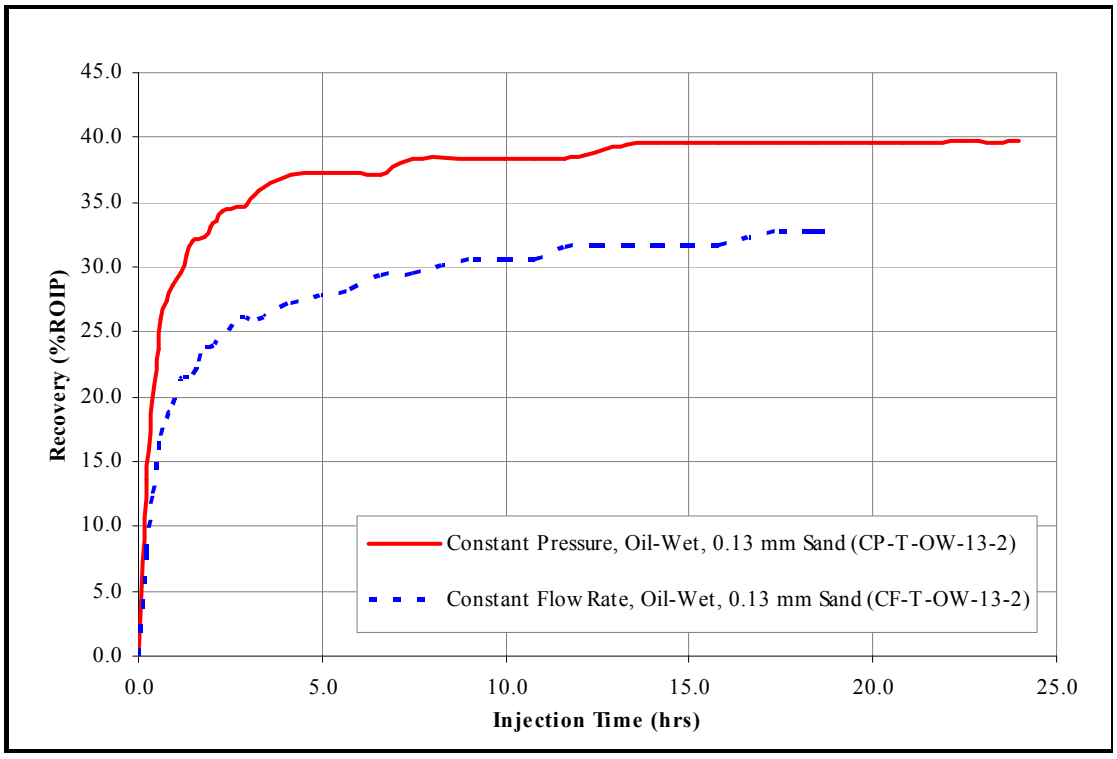

Figure 1.19: Effect of Gas Injection Method on the Oil Recovery – Tertiary Mode Runs

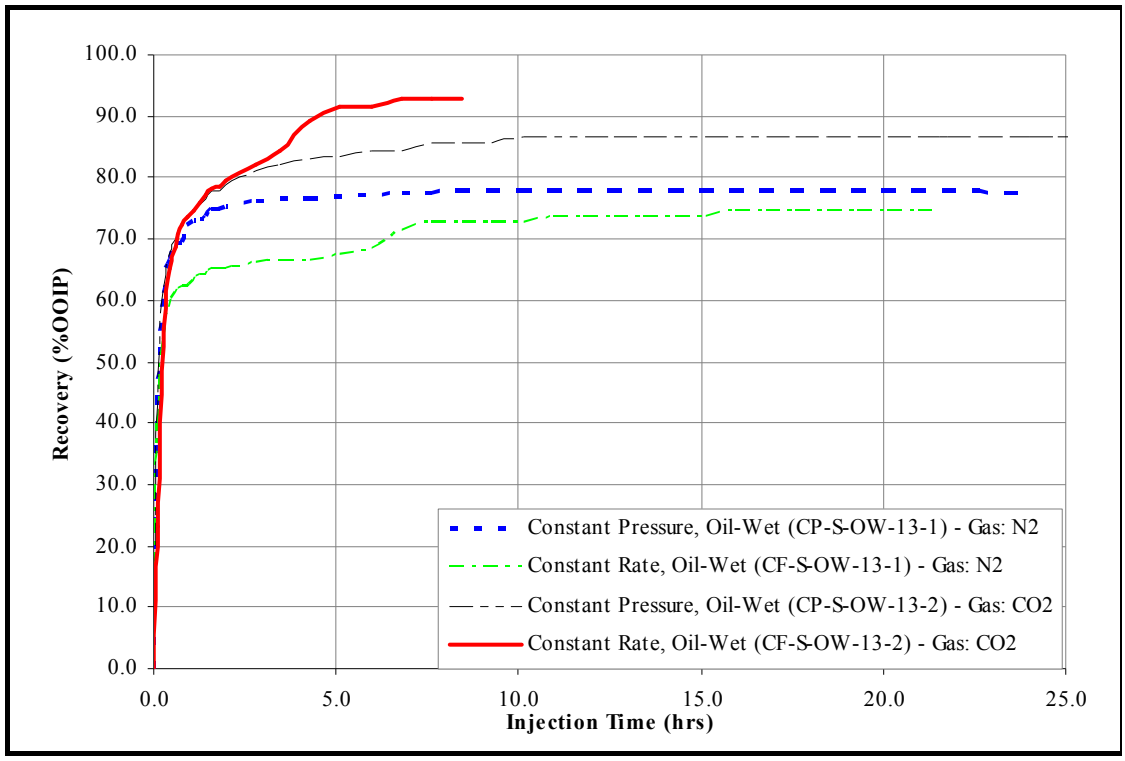

Figure 1.20: Effect of the Injected Gas on the Oil Recovery – Secondary Mode Runs

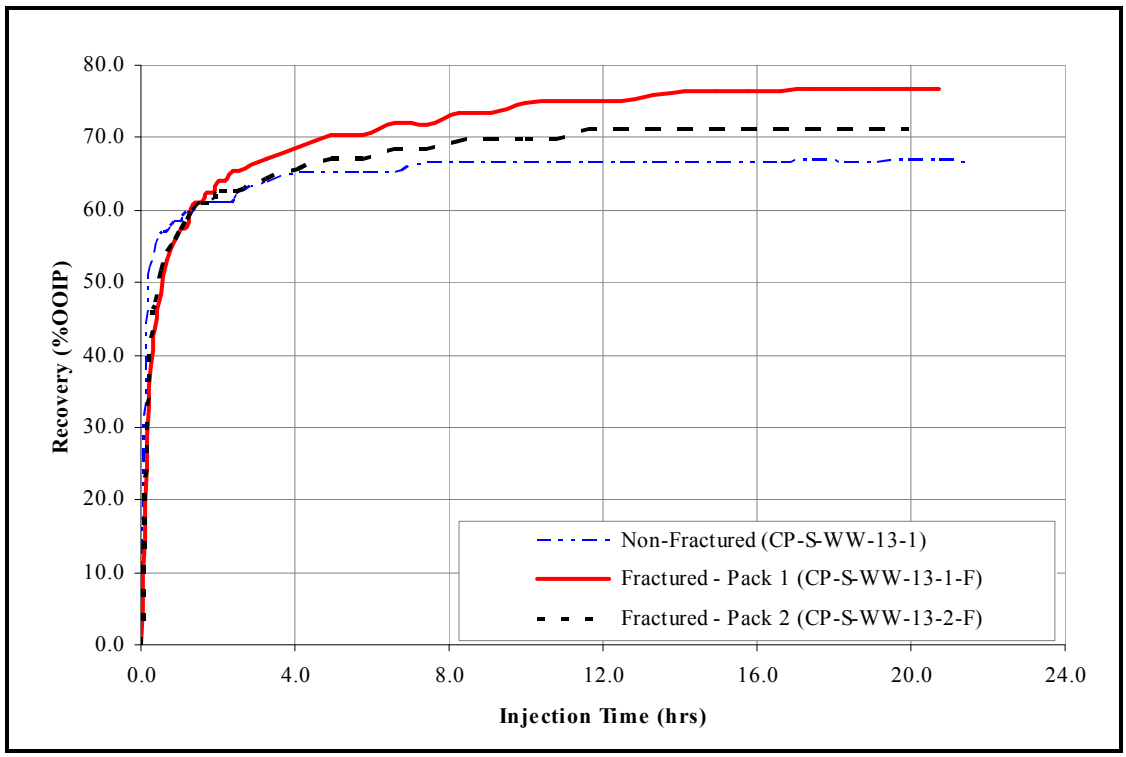

Figure 1.21: Effect of a Vertical Fracture on the Oil Recovery-Water-Wet Case, 0.13 mm

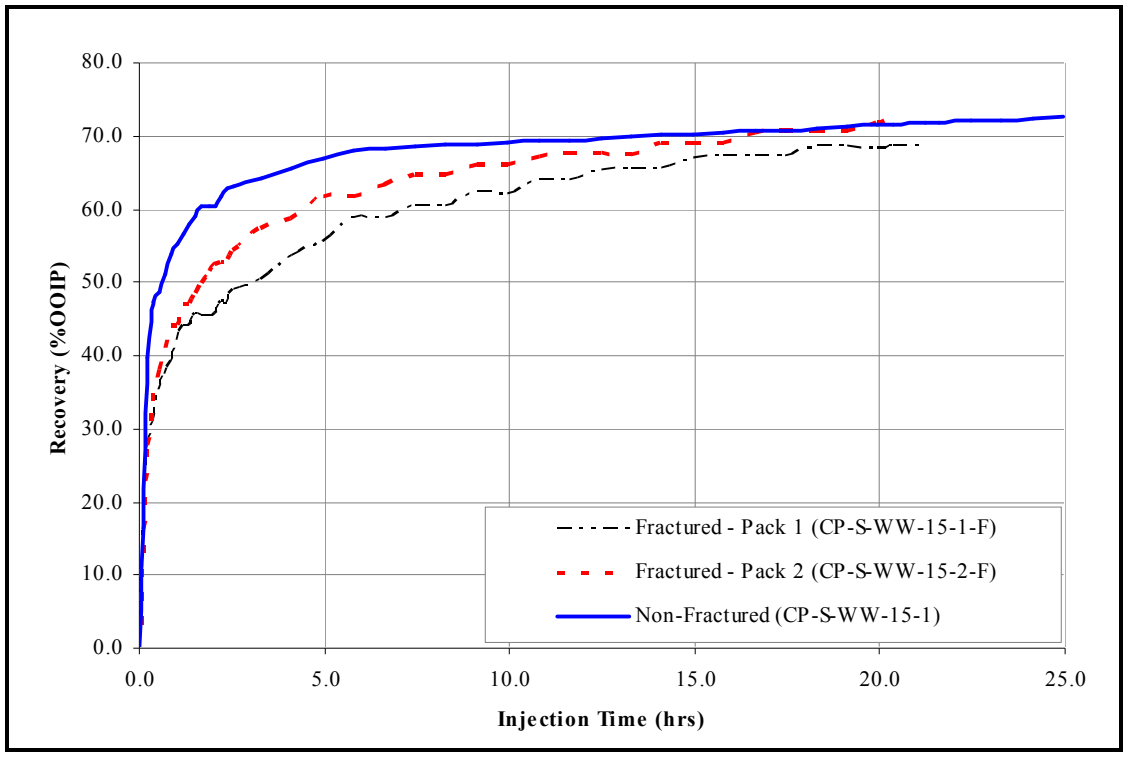

Figure 1.22: Effect of a Vertical Fracture on the Oil Recovery-Water-Wet Case, 0.15 mm

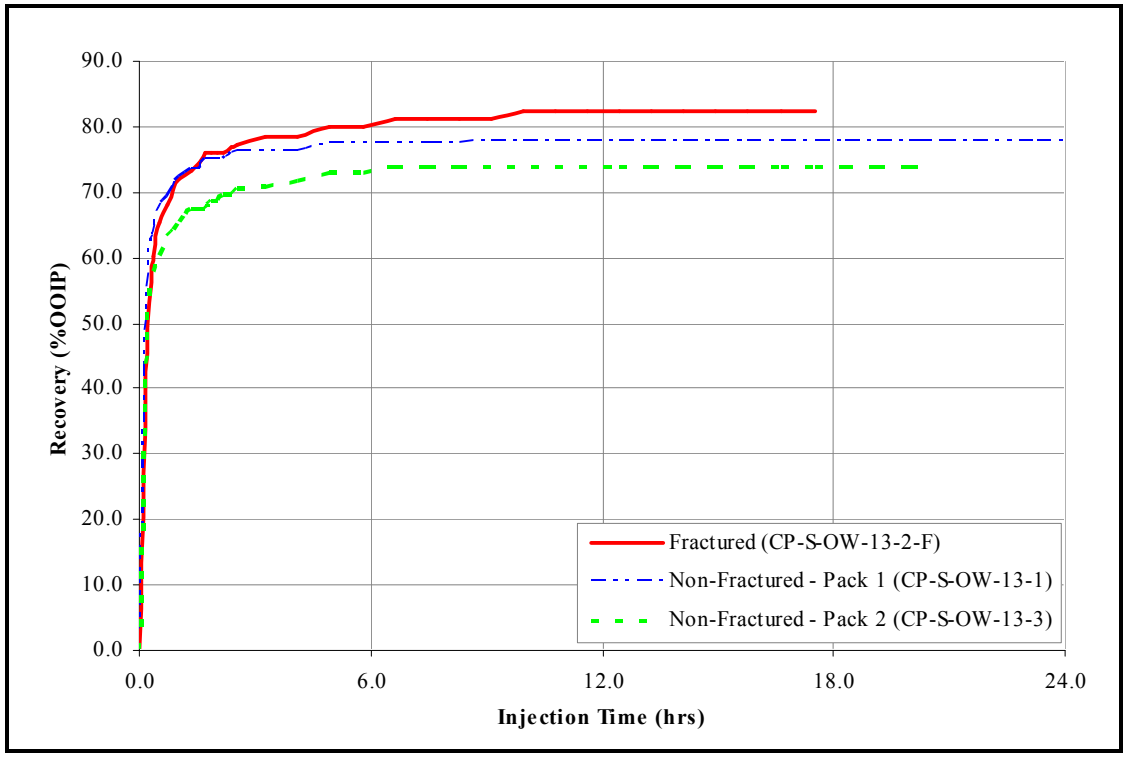

Figure 1.23: Effect of a Vertical Fracture on the Oil Recovery-Oil-Wet Case, 0.13 mm

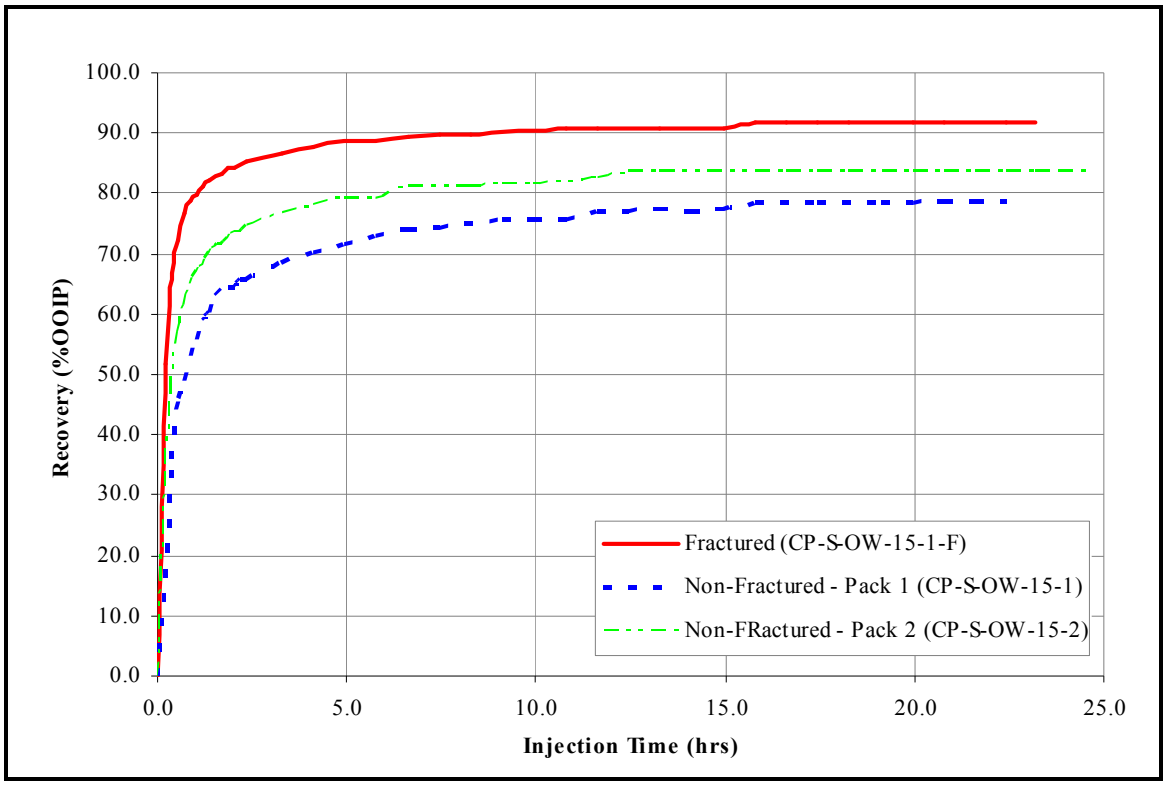

Figure 1.24: Effect of a Vertical Fracture on the Oil Recovery-Oil-Wet Case, 0.15 mm

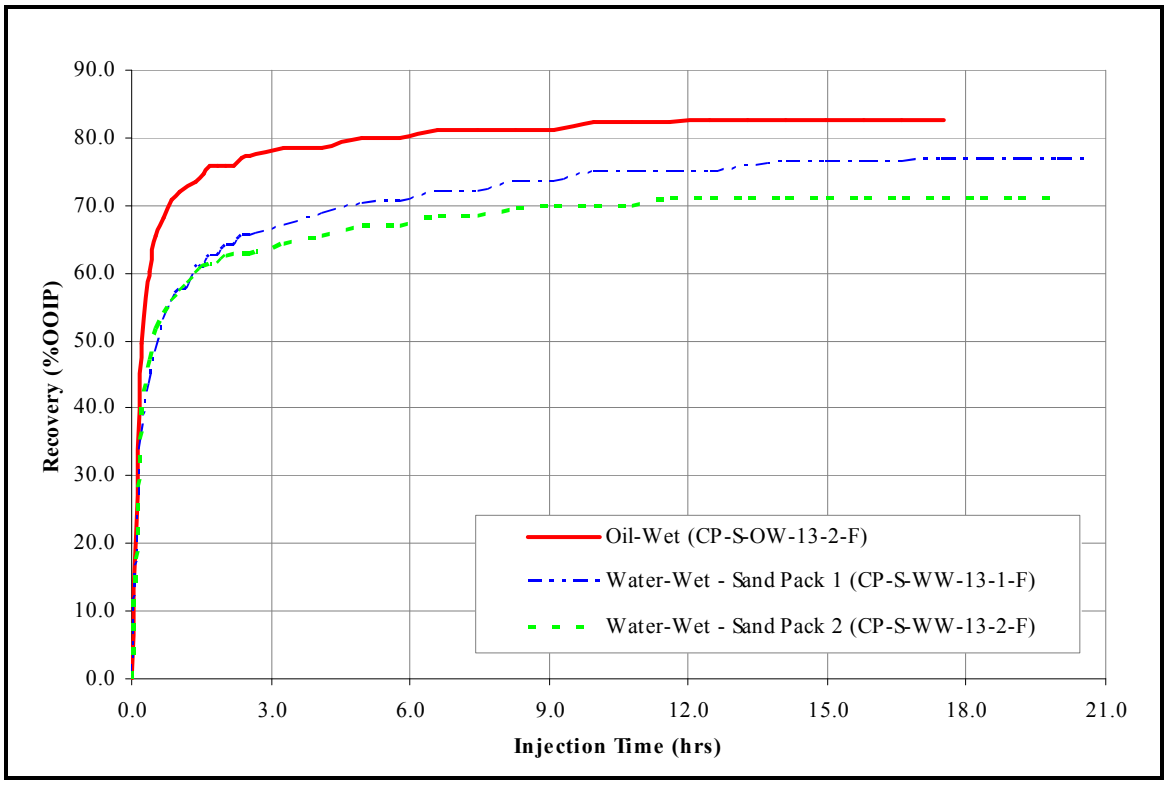

Figure 1.25: Effect of the Wettability on Fractured Runs – 0.13 mm Sand Pack

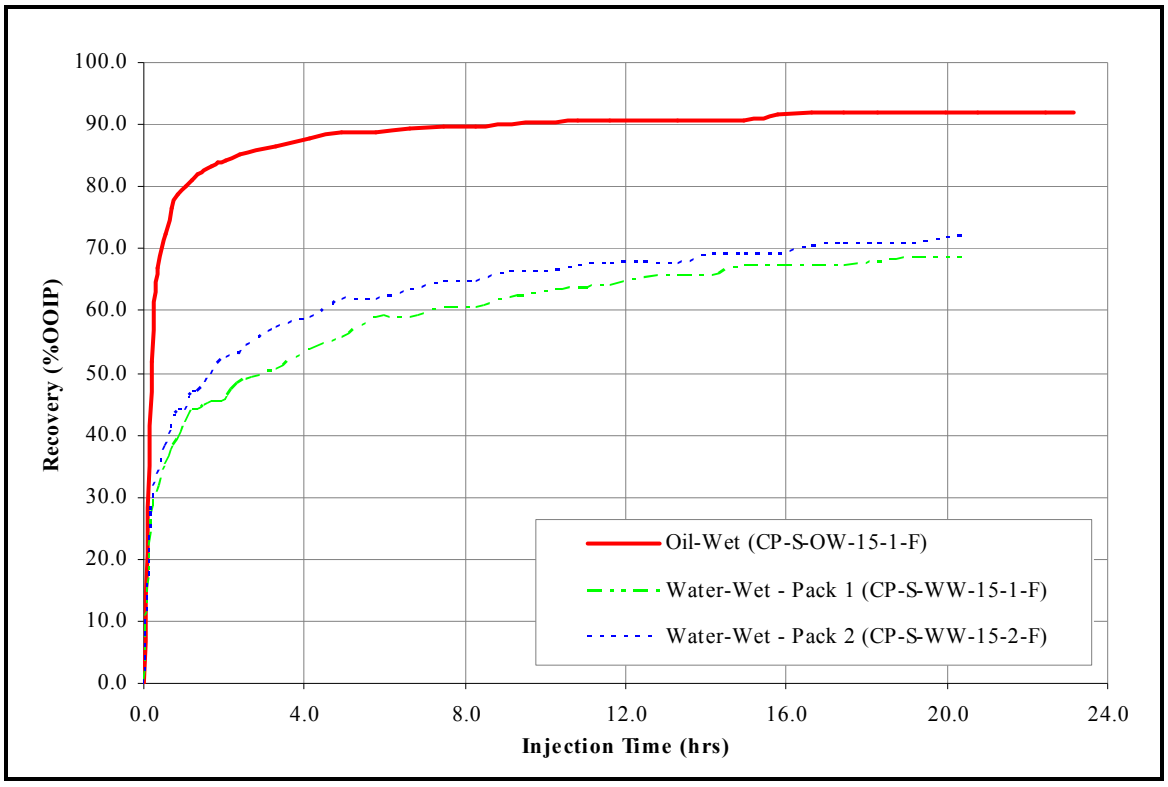

Figure 1.26: Effect of the Wettability on Fractured Runs – 0.15 mm Glass Bead Pack

1.2.3 Summary Findings and Conclusions

1.2.3.1 Water-Wet Experimentation

1. A simple 2-D Hele-Shaw type physical model has been used to study the Gas Assisted Gravity Drainage (GAGD) process. Experimental results have indicated the usefulness of physical models as a tool to investigate the performance of new processes such as GAGD.
2. The movement of gas-oil interface in the reservoir rock has been captured using this visual model. Experiments to study the effect of capillary, viscous and buoyancy forces have been conducted by simply using glass beads of different sizes, and injecting gas at various flow rates.
3. The performance of the GAGD process has been characterized using dimensionless numbers such as the Bond number, the capillary number and the gravity number. Furthermore, the experimental run time can be scaled to real time in the field by the use of a dimensionless time expression.
4. Slightly higher cumulative oil recovery (7-8% greater) as well as a higher rate of recovery is obtained during constant pressure gas injection as compared to constant rate gas injection.

5. A straight-line relationship between the total recovery and the natural log of Bond number is obtained from the experiments. This correlation fits well to both immiscible and miscible core flood experiments, which suggest that physical model experiments are a useful tool for predicting the GAGD performance at another scale.
6. A logarithmic relationship of total oil recovery and the capillary number is observed; this relationship also stands true for both immiscible and miscible core flood data. Therefore, immiscible physical model results could be extrapolated to predict oil recoveries during miscible conditions. Faster recoveries are obtained with higher values of capillary numbers.
7. Immiscible GAGD floods can yield recoveries up to 80% of the IOIP in secondary mode, as opposed to about 5-10% by the WAG process.
8. A logarithmic relationship between gravity number and recovery is observed when results from the physical model, core floods and field data are compared. It is very interesting to note that the recovery data from all the scales of operation corroborate well with this relationship.
9. A multi-variable regression model to fits the experimental and field data has been obtained. This analysis suggests that the Bond number has greater influence on ultimate GAGD oil recovery compared to the capillary number.
10. The type of gas injectant (gas composition) does not affect the oil recovery by GAGD in immiscible mode; in-fact the rate of recovery is quite identical for different gases. This can be attributed to the fact that the capillary number and Bond number for both the experiments were similar.

1.2.3.2 Oil-Wet Experimentation

In this part of the study, physical model experiments were conducted to study the effects of the wettability of the porous medium and the presence of a fracture on the performance of the GAGD process. The physical model used was a simple Hele-Shaw type model incorporating either soda glass beads or silica sand as the porous media and n-decane and deionized water as the fluids in the porous medium. The glass beads or silica sand were rendered oil-wet by a treatment with the organosilane dimethyldichlorosilane. The gas displacement experiments were conducted using nitrogen or carbon dioxide under constant pressure or under constant mass flow rate. The gas displacement strategy was also varied resulting in a series of experiments in the secondary mode and one in the tertiary mode (i.e. the gas displacement followed a water flood). The presence of a vertical fracture was simulated by placing a mesh box in the model prior to packing the bead or sand pack and conducting gas displacement experiments under the conditions described above.

The important conclusions that can be drawn from the experiments conducted in the study are:

1. The wettability affects the performance of the GAGD process – on average, the use of an oil-wet porous medium improved the performance of the GAGD process by an increase of 12.7 % in the recovery of the original oil in place.
2. The presence of a vertical fracture in the porous medium improves the performance of the GAGD process. The average incremental production because of the presence of the vertical fracture in the physical model experiments was 7.8 % (%OOIP).
3. The type of gas injected affects the performance of the GAGD process when using an oil-wet porous medium in the physical model experiments: an increase of 10.9 %OOIP was seen when using CO_2. Sharma (2005) had already shown that the type of gas does not affect the GAGD performance when the experiments are conducted in a water-wet porous medium.
4. The constant pressure gas displacement of the oil in the experiments results in a slightly higher recovery (2.6-3.0 %OOIP) compared to the constant rate displacement experiments.

1.3. A Visualization of the GAGD Process using a Glass Physical Model

1.3.1 Introduction

The purpose of building the scaled physical model was to incorporate the ability to visually very the movement of the gas front under the influence of viscous instability, capillary fingering, and stable displacement by trying to duplicate the various multiphase mechanics and fluids dynamics operating in the field scale.

Preliminary experimentation suggested that construction of the 2-D model from sintered glass beads was a feasible alternative. To facilitate faster and more precise experimental control during the model preparation, a high temperature furnace was used. The furnace was employed in the sintering step of construction and testing of multiple glass models to achieve the appropriate ranges of permeability and porosity. During the experimentation, the packing of physical model was changed from sintered glass beads to the traditional sand pack. The sand pack model construction was found to be much easier than the sintered glass beads and the model size is not limited to the furnace size.

The preliminary experimentation was started with mini-models (6” x 6”) instead of a full-scale model, since mini-models permitted the construction and testing to be carried out at relatively lower costs. They also allowed model optimization and to obtain the required permeability to simulate the field conditions. With the new sand pack model, 14 different experiments have been conducted to evaluate the GAGD process performance under different scenarios normally encountered in the field.

1.3.2 Model Construction

1.3.2.1 Sintered Glass Bead Model

In order to prepare the model for sintering, glass plates were cut to specific sizes. The mini-models generally consisted of a quarter inch thick glass with plates of 6" by 6", 3/8" inch spacers were glued between the glass plates to create the glass bead chamber. However, the least amount of glue was used for this purpose: once the model is sintered, most of the glue (if not all) had evaporated. Any excess glue fumes could possibly create a coating around the glass beads, and thereby affecting the wettability state.

During the assembly of most of the mini-models the sharp edges of the glass plates resulted in some leaks in the model, especially where two glass plates were joined perpendicular to each other. Silicone sealant was added at the joints to prevent any leaks from the unsintered glass bead pack. The temporary sealant was found to evaporate out during the sintering process. The next step in constructing the mini-model was to fill the model with glass beads of uniform or varying grain dimensions. Steel end caps were inserted in the model to hold the glass beads in place in the mini-model while it was filled with the glass beads, and this helped to minimize glass bead leakages.

According to the devised experimental protocol the mini-model was sintered at the chosen temperature for the selected time period. After the sintering the furnace exhaust was opened, and nitrogen, N_2, was injected at a low flow rate into the furnace to circulate the hot air out, thereby cooling the furnace down, as well as to stop the sintering process. The objective of N_2 injection was to lower the temperature inside the furnace as fast as possible without having to open the furnace, and to prevent any thermal shock to the mini-model or the ceramic frame inside the furnace. After the furnace temperature had lowered enough to open, usually under 100^{o}C, the mini-model was removed and allowed to completely cool in the ambient environment. Later, the steel end caps were removed and replaced with a 2" piece of 1/4" plastic line to serve as end caps. The plastic end caps were used instead of steel end caps, because plastic end caps could absorb vibrations that were introduced during the testing phase better than steel end caps. The plastic end caps were attached to the mini-model using high strength epoxy glue.

The last step before testing the mini-model was to seal the mini-model. Different kinds of sealants such as caulking and automotive sealants were attempted. The most appropriate sealant was found to be a silicone based automotive one, Permatex 66B ®. This sealant was found to cure and gain strength fast, usually within two hours. It required multiple coats of the sealant to be applied to the mini-model to create an effective seal. If the mini-model did not pass the vacuum seal test, then gas was usually injected at low pressure, 2-3 psig, followed by using Snoop® sprayed around the sealant to locate the leaks, after which they were sealed. The process of sealing is continued until the mini-model passes the vacuum test.

1.3.2.2 Sand Pack Model

The physical model was kept as simple as possible by using materials that were available locally and also easy to procure, such as regular window glass from the local glass shop, epoxy glue and sealant from the department store, and C clamps from hardware stores (Figure 1.27).

The physical model was constructed from two large glass plates of ¼ ” thickness, 23” in length and 13” in width, joined together using 3/8” thick spacers. The spacers were obtained by joining two different glass plates that were 0.25” and 0.125” in thickness respectively, using epoxy glue. Then, the spacers were glued to one side of the 23” by 13” glass plate forming the model assembly. Later, a 0.0625” hole drilled and 0.25” plastic tubing was attached to the model assembly using the glue. It is important to use small spacers, 1” long, 0.5” wide and 0.375” thick, in the middle of the glass model to create lateral support to withstand the fluid pressure. It is crucial to always maintain the pressure inside the glass model less than 2 PSI, as even this low pressure will exert 440 pounds of force on the glass plates.

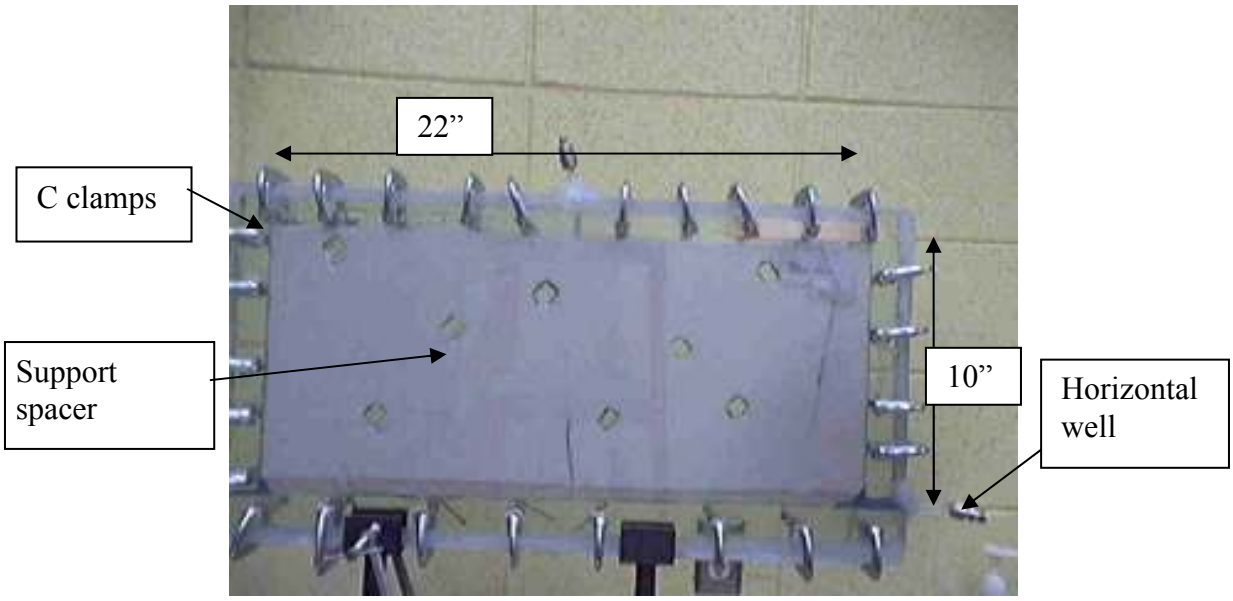

Figure 1.27: Photograph of the Fully Constructed Visual Model

Once all the spacers were glued to the glass plate assembly, the second large plate was attached to the assembly. Later, the glass model was filled with 50/70 mesh U.S. Silica sand to simulate the sand pack, and 0.25” tubing end caps were then attached. The last step was to apply automotive sealant to all of the sides and the edges to prevent any leaks. Once the sealant had cured, 1.5” or 2” C clamps were attached all around the outside of the glass model. The purpose of the clamps was to provide the mechanical

fastening that the model requires. However, care was taken while tightening the C clamps to avoid breakage.

1.3.3 Experimental Procedure

1.3.3.1 Sintered Glass Bead Model

After performing the final leak test, the mini-model porosity was measured by injecting distilled water in a gravity stable manner using burettes and 1/8" plastic lines. It is crucial to measure the exact amount of water injected in the mini-model through the lines. Another critical issue for the porosity measurement is calculating the lines' volume, the so-called dead volume. This dead volume needs to be deducted from the total volume of water injected. Finally, the porosity of the model is calculated by dividing the net water volume injected by bulk volume of the mini-model.

After the measurement of the mini-model's porosity, the following steps are employed to measure the mini-model's absolute permeability. This measurement is conducted by injecting distilled water into the model using the hydrostatic head from the burette to force the distilled water into and through the sintered glass bead pack. The distilled water is allowed to circulate inside the model to clean and stabilize the glass beads. After a water injection of at least two to three pore volumes, the mini-model is completely shut in. The mini-model is then opened to the water gravity feed line and injected water volume and time are measured to calculate the flow rate. It is important not to allow the water level in the burette to be lowered by more than one or 2", especially if the level of the gravity feed system is not very high. The top of the water in the burette that has been used in the testing the mini-models is set to equal 64" above the top of the glass beads. If the water level in the burette drops by a more than 2", the hydrostatic pressure will greatly vary between the beginning and the end of the test. In the permeability testing, 10 cc's of water is usually used, which is equal to a height of ½" in the burette for high accuracy. Finally, the permeability is calculated using Darcy's law.

1.3.3.2 Sand Pack Model

The following experimental protocol was used for the experiments with the sand pack model:

1. Start the experiment by flooding the glass model with distilled water in a gravity stable manner to measure the porosity and to check for leaks. Then, distilled water is allowed to circulate in the model for a while.
2. Measure the flow rate and the height of distilled water level to calculate the absolute permeability using Darcy's law. These steps are only performed when the glass model is first used. During later experiments it is recommended to check the absolute permeability for any changes.

3. Flood the model with red dyed N-decane from the top, while collecting the water that is produced from the horizontal well. At the end of the flood, the amount of N-decane in place is computed to be equal to the amount of the water produced minus the dead volume.
4. Attach the top end cap to the CO_2 line that is connected to a rotameter for flow rate measurement.
5. Set the rotameter at the desired flow rate and start the stopwatch.
6. Finally, open the horizontal well to the separator. The first fluid that flows out will be the N-decane, which is collected and measured in the separator, a burette, while the gases flow out through a second rotameter after breakthrough.

1.3.4 Results and Discussion

The research work was aimed at evaluating and characterizing the GAGD process using a glass model for visualization in addition to providing matching measurements for quantification of the performance. This visual model was found to be very useful in studying the GAGD process in the laboratory. Advantages provided by the model were the flexibility to test various configurations such as injection depth variation, injection location, and the ability to insert a horizontal well. The visual approach also provided the flexibility of seeing the results as they took place, rather than just imagining or speculating about the mechanisms. The main disadvantage was that the glass model could only be operated at ambient conditions of pressure and temperature. Visual experiments were conducted to compare the GAGD process with conventionally used processes. The visual experiments were divided into two sub groups: experiments conducted in the secondary recovery mode and in the tertiary recovery mode.

In the secondary recovery mode, it is assumed that the primary depletion drive has been completed, whether it is gas cap, gas in solution or water drive. Therefore, CO_2-driven GAGD was selected to be the secondary recovery process. In other cases, waterflooding was selected to be the secondary recovery, and then CO_2-driven GAGD was applied as the tertiary recovery method. The effect of following parameters on the GAGD performance was investigated during this reporting period: gas injection rate, miscibility, fluid viscosity, wettability of the porous medium, vertical fractures, the gas injection location, and the production configuration. The experiments are summarized in Table 1.9.

Effect of Injection Rate on GAGD:

Gas injection rate is an important factor that needs to be optimized for the GAGD process to be successful. The injection flow rate controls the flood front velocity and hence dictates whether the gravity force is dominating the process or not. If the injection rate is too high, two negative factors will be generated having an adverse effect on the performance of the GAGD process:

- The pressure will increase rapidly causing the viscous force to gain dominance.
- Another disadvantage of the high pressure is the increase of in-situ CO_2 density that could lead to the gravity forces becoming less dominant in the process.

However, a higher injection rate tends to decrease the time required to complete the GAGD process and makes it more economically attractive. Furthermore, increasing the CO_2 gas pressure in the reservoir is beneficial due to the increased CO_2 solubility in the oil. Higher CO_2 gas in solution lowers the interfacial tension, hence improving the microscopic displacement efficiency, E_D, and lowers the viscosity of the oil. Therefore, a balance between gravity domination, gas in solution and economic factors needs to be maintained for successful GAGD field implementation.

A set of GAGD experiments with three different injection rates were performed. The three injection rates used were 2 cc/min, 4 cc/min and 8 cc/min to simulate low, intermediate and high injection rates. Interestingly, it was observed that the higher the injection rate, the higher the ultimate GAGD oil recovery using the visual model (Figure 1.28).

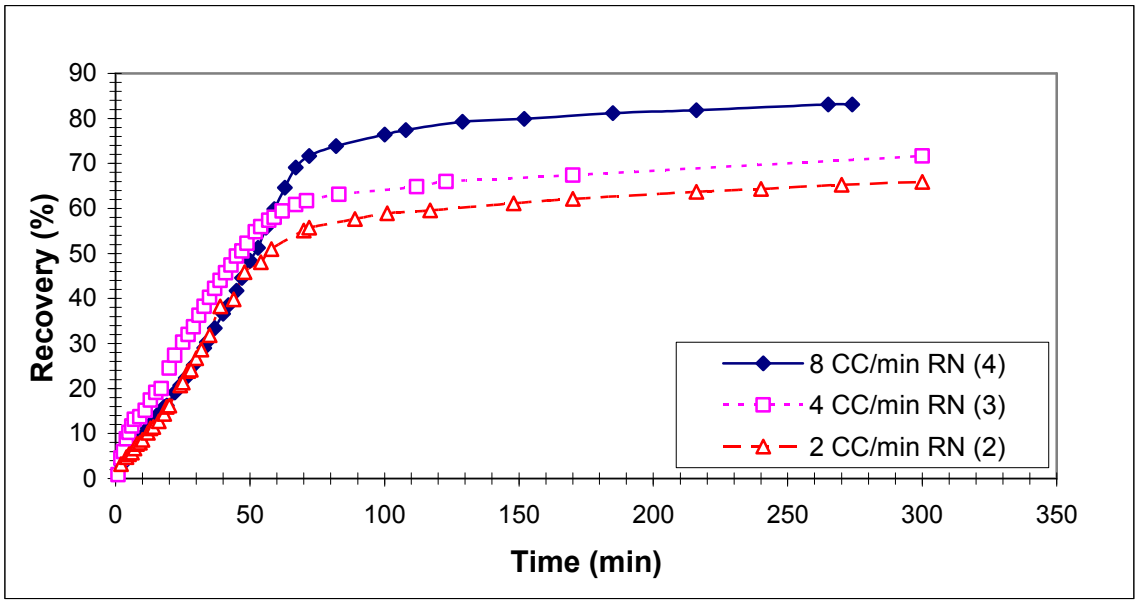

Figure 1.28: Effect of Injection Rate on GAGD Oil Recovery

The effect of the injection depth on GAGD:

It had been hypothesized that if the CO_2 gas was injected near the horizontal well, the production would begin sooner. It was believed that earlier production would be due to the formation of a gas chamber near the injection point, essentially draining the oil primarily from the gas zone. If the gas zone is close to the horizontal well, production would begin with very little time delay after injection. However, the author believes that the CO_2 gas chamber would rise to the top of the pay zone and form a (semi circular

shaped) gas cap that will eventually drain the oil from top to bottom in the entire pay zone.

Therefore, four injection depths were chosen for investigation of the effect of the gas injection location, namely the very top of the pay zone, 2.5", 5" and 7.5" from the top of the pay zone. These depths represent 0%, 25%, 50% and 75% of the physical model height, respectively. In order to eliminate or minimize any external effects on the recovery other than the injection depth, all four injection locations were fitted inside one visual model.

The formation of a CO_2 gas chamber was not observed in the experiments: the CO_2 gas always traveled to the top directly without forming a gas chamber around the injection point (Figure 1.29). The relatively loose packing of the sand around the outside periphery of the injection tube appeared to have been the reason for the gas to rise to the top immediately upon entering the model. However, it is believed that the vertical and horizontal permeability were nearly equal in the visual model, which is rarely true in real reservoirs. Therefore, the absence of this phenomenon could be attributed to permeability issues.

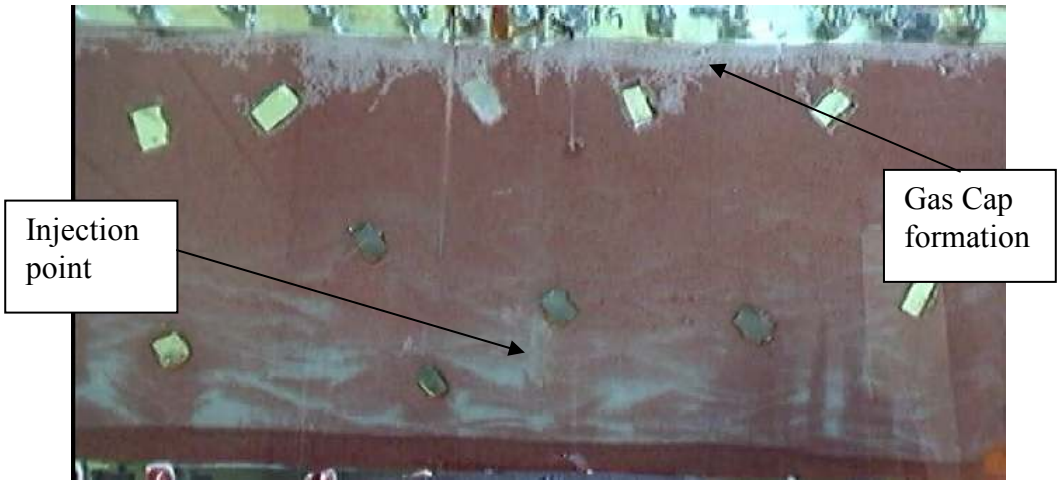

Figure 1.29: Varying Injection Depth Visual Model

However, it was observed that there were no significant variations in the oil recovery among the three the injection depths of 0", 2.5" and 7.5" from the top of the pay zone (Figure 1.30). However, the 5" injection depth recovered a little less oil than the other three injection depths and it is believed that the injection well was somehow filled with sand creating a flow restriction. The 5" depth injection pressure reached 0.9 psig, while the highest recorded injection pressure in the other three experiments was only 0.4 psig. This observation clearly indicates that the relatively low oil recovery obtained in the 5" injection depth case was due to well-related effects rather than the result of varying the gas injection location.

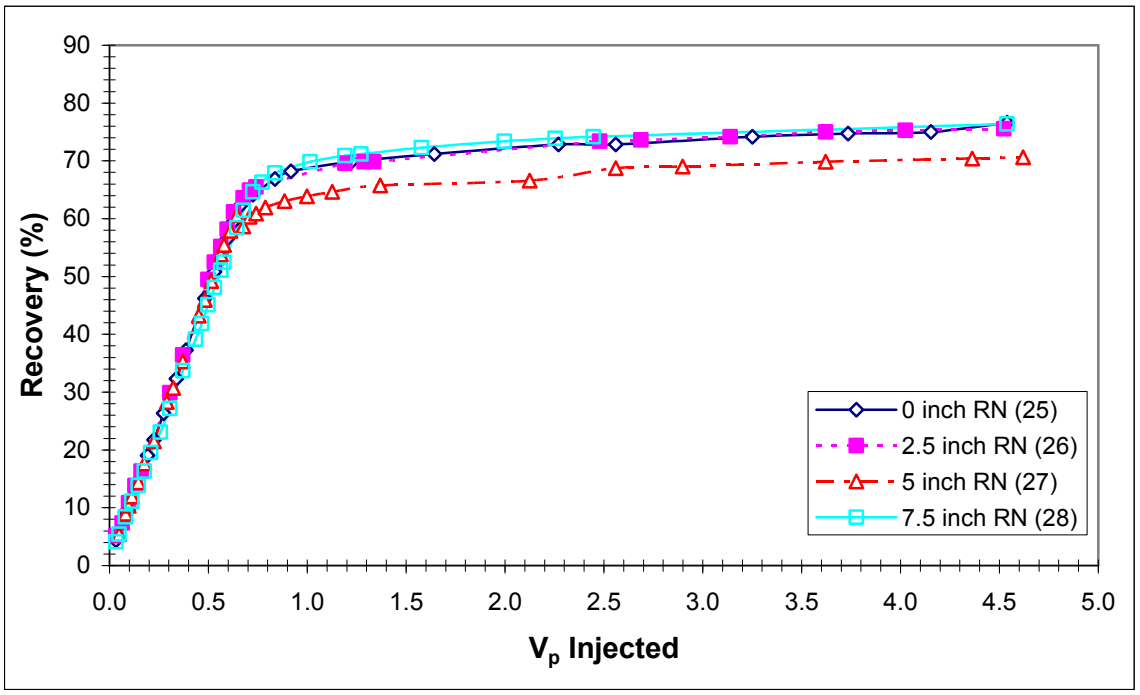

Figure 1.30: Effect of Injection Depth Variation on the Ultimate Recovery

Gas breakthrough times in these four experiments were between 39 and 45 minutes. The very comparable gas breakthrough times once again suggest that all four runs were gravity stable and the dominant force was gravity. The similar gas breakthrough times also suggest that the gas will always travel to the top of the zone immediately upon injection due to the density contrast. Furthermore, the breakthrough time is governed by the gas cap and not by the injection depth. Additionally, the initial overlap of the oil recovery plots for all four injection depths as shown in Figure 1.30 suggests that the initial process involving drainage and displacement is the same for all four gas injection depths.

The effect of miscible CO_2 gas injection on GAGD:

Miscible CO_2 gas injection has been practiced in the field extensively in different forms, such as Continuous Gas Injection and Water Alternating Gas injection. According to the literature, the microscopic displacement efficiency (E_D) of miscible gas injection is at or near 100% (Shedid et al., 2005, and Charkravarthy et al., 2006). Miscible experimentation was necessary to validate these hypotheses. However, due to the limitations of the glass visual model and the necessary high pressure required to achieve miscibility, it was not possible to simulate the miscibility conditions in the physical model using CO_2. Hence, two different miscible liquids were used instead to simulate the miscible GAGD tests. The fluids that were chosen for the miscibility simulation were red dyed naphtha for oil and clear decane for miscible CO_2 gas.

The experiment showed that E_D indeed approached 100% in miscible flooding (Figure 1.31A and B). It was visually verified by observing the complete disappearance of the red dye from the flooded area of the visual model. However, as is evident from Figure 1.31 the volumetric sweep efficiency (E_V) was less than 100%. In fact, initially E_V was considerably less than the immiscible E_V, but two different ways were identified to increase E_V. The first one is to allow enough time for the miscible injection, which would eventually sweep the whole model providing an E_V of 100%. However, this may require a large volume of the miscible CO_2 gas injection. The second way is to inject the miscible CO_2 gas at a very low rate.

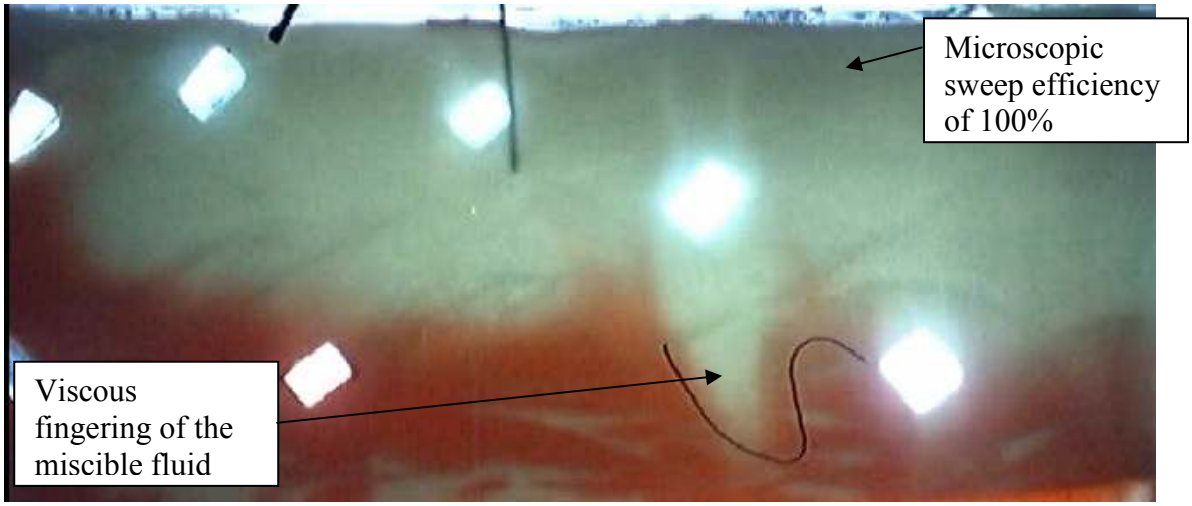

Figure 1.31A: Miscible Drainage Simulation (Injection Rate of 8cc/min)

Furthermore, it appears that the miscible injection in the visual model is quite sensitive to the injection rate. This can be attributed to the low density difference between the two liquids used (0.01655g/cc). This density difference is negligible compared to the immiscible case density difference of 0.7176g/cc. Therefore, any increase in rate will allow more viscous force domination which might lead to viscous fingering and premature gas breakthrough (Figure 1.31), which would lead to gas cycling, thereby raising the operational costs.

It is crucial to mention that the gravity effect on the process of the field miscible GAGD is expected to be better than the laboratory gravity domination. In the laboratory, the fluid density difference was negligible as was mentioned before. But in the field, the density difference would be much larger. The CO_2 gas density at 4000 psig and 239°F is 0.2111g/cc. This density value would result in a density difference of 0.67g/cc for typical 30 API Gravity oil. Therefore, the gravity force would be much higher than the laboratory gravity force which would lead to better GAGD oil recovery.

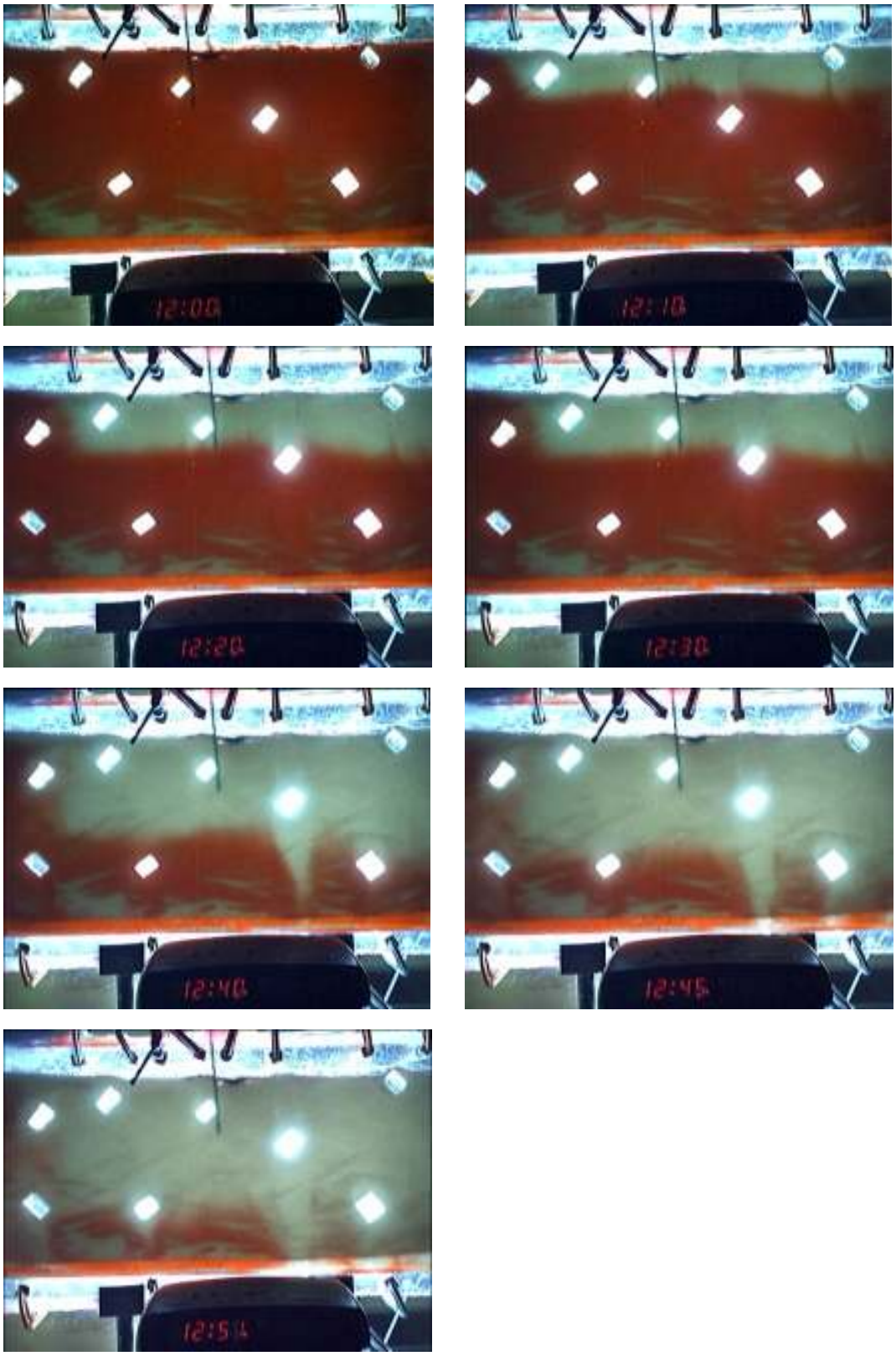

Figure 1.31B: Fluid Front Development Miscible Displacement

In the laboratory experiment, reliable recovery data could not be obtained from miscible injection because the two liquids were miscible with each other even in the separator. Unlike the two miscible liquids used, miscible CO_2 gas would evolve in the separator as soon as the pressure dropped. Therefore, the measurement of the naphtha volume in the separator was not recorded after decane breakthrough. Furthermore, the breakthrough time could not be observed accurately for the same reason. However, measurements of recoveries due to miscible fluid injection were made with some reliability up to the breakthrough time. Although limited quantitative results were obtained from this experiment, the data could be useful in providing a conceptual understanding of miscible injection.

It seems that the higher the injection rate, the lower the recovery is at breakthrough, which is obvious because the higher the injection rate results in a stronger viscous force and a lower the gravity number. However, with higher injection rates the oil recovery was also much faster (Figure 1.32) and this might be economically attractive as well.

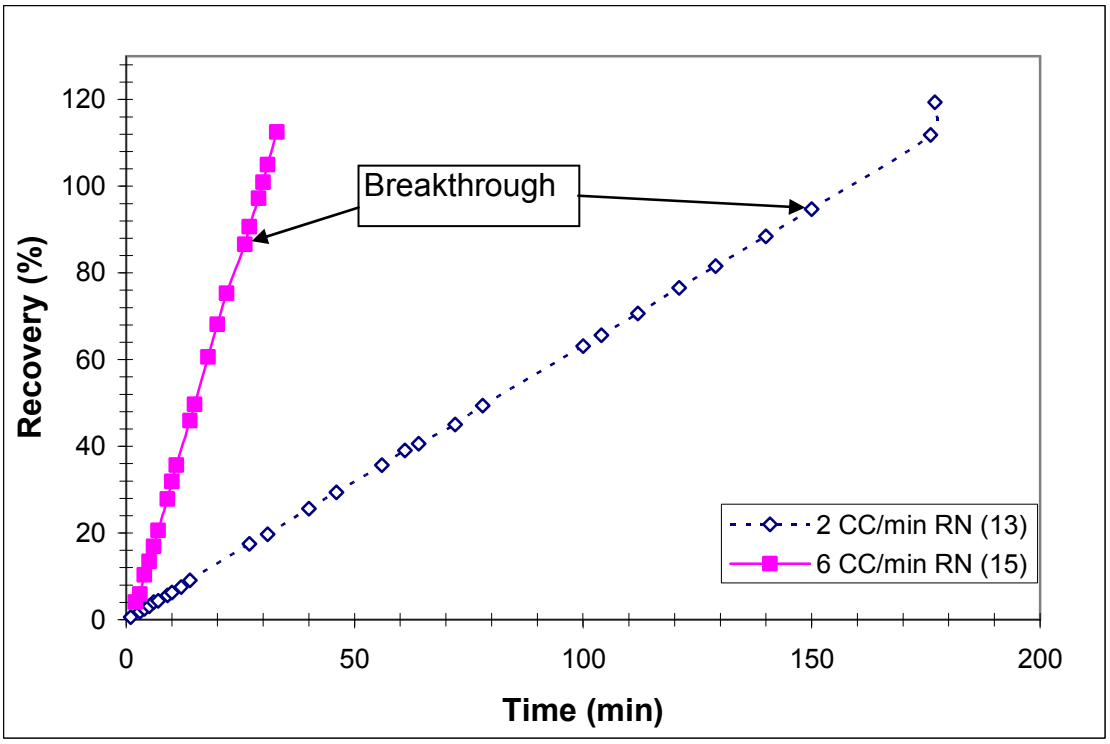

Figure 1.32: Miscible GAGD Recoveries

The effect of vertical fractures on GAGD:

Generally, naturally fractured reservoirs are considered as good candidates for gas EOR processes. This is mainly because these processes usually consist of horizontal flooding between two vertical wells, and the density contrast between the two fluids (CO_2 gas and oil), particularly in the immiscible mode, will cause the gas to find an easy path of low

Figure 1.33A: Fluid Front Development Fractured Immiscible Displacement

Figure 1.33B: Fluid Front Development Fractured Immiscible Displacement

resistance through the fracture to the production well thereby causing premature gas breakthrough and low oil recoveries. However, gravity drainage has been hypothesized to be an effective method of EOR in naturally fractured reservoirs.

Therefore, a set of experiments was conducted to investigate the impact of vertical fractures on GAGD. One of the visual models was built to simulate a vertically fractured reservoir by inserting two cylindrically shaped fine wire meshes inside the model. The results were as expected: immiscible GAGD proved to be a successful method of EOR even in the presence of fractures. The fractures did not show any detrimental effects on the GAGD oil recovery (Figures 1.33A and B). The observations are in good agreement with the findings of Wood et al. (2006). In fact, this laboratory study, as shown in Figure 1.34, clearly indicated that natural fractures would improve GAGD oil recoveries when compared to un-fractured ones as explained below.

When CO_2 gas is applied in a gravity stable manner, the gas will naturally try to stay on top of the pay zone and then slowly expand. If the gravity force is maintained to be the dominant force in place, then the natural fractures will work as an effective additional exchange path between the CO_2 and the oil contained in the matrix (Figure 1.35). However, if the viscous force dominates over the gravity force, then adverse effects are expected. These adverse effects include premature gas breakthrough, viscous fingering and lower volumetric sweep efficiency as shown in the miscible GAGD run in the fractured model (Figure 1.36).

The effect of oil viscosity on GAGD:

Thermal methods, especially steam injection, have been used as the primary methods to reduce the oil viscosity for heavy oil EOR, but CO_2 gas injection has been gaining ground in the heavy oil EOR (Luo et al., 2005). Hence, this particular set of experiments was conducted to simulate the application of GAGD for higher viscosity oil. Soltrol was selected to simulate oil due to its relatively high viscosity (2.93 cp) compared to decane with a viscosity of 0.966 cp. The higher viscosity experiments were conducted in both the miscible and the immiscible mode.

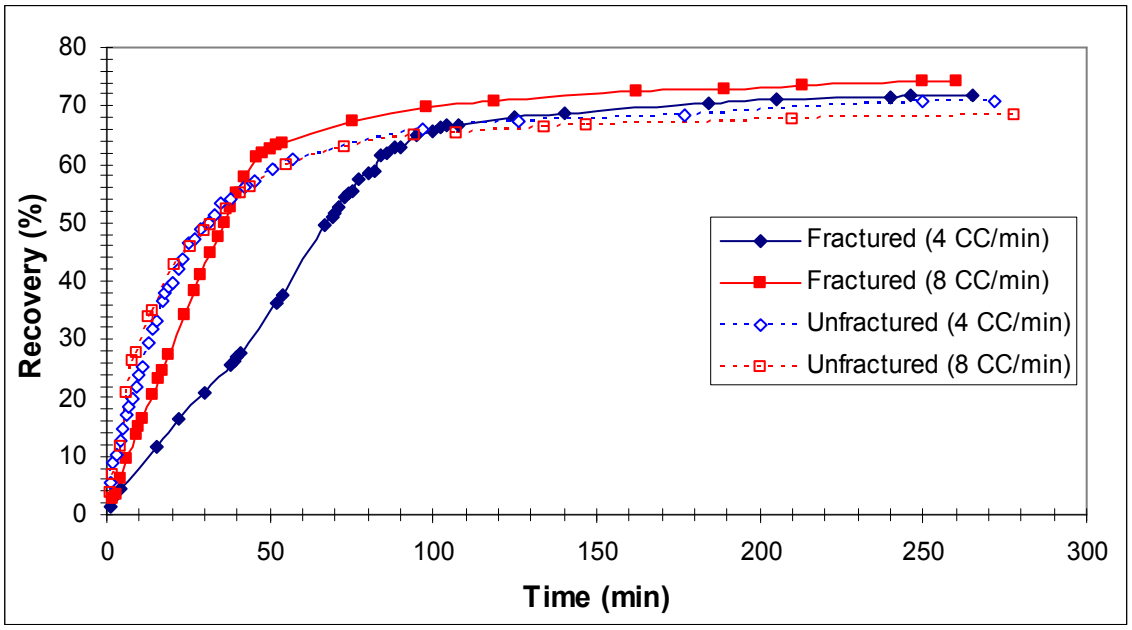

Figure 1.34: Effect of Vertical Fractures on GAGD Oil Recovery for the Immiscible Case

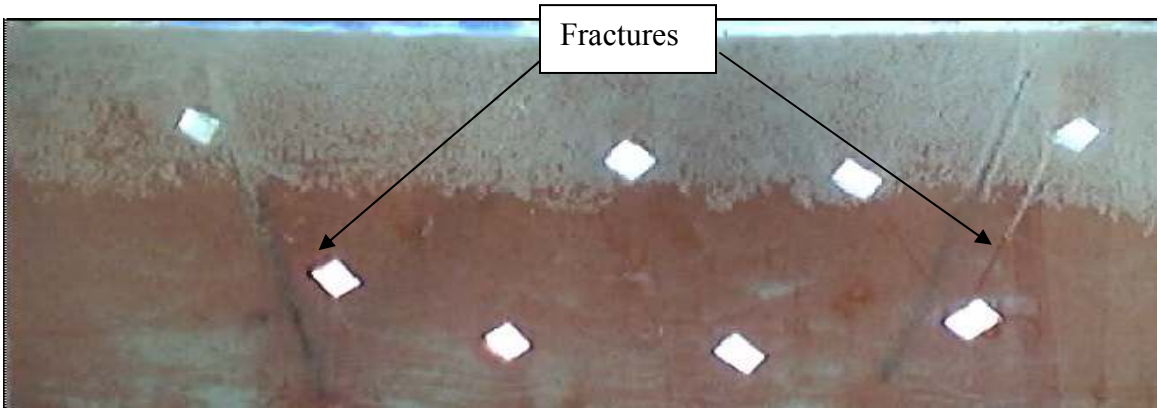

Figure 1.35: Vertically Fractured Porous Media in Immiscible CO_2 Flooding

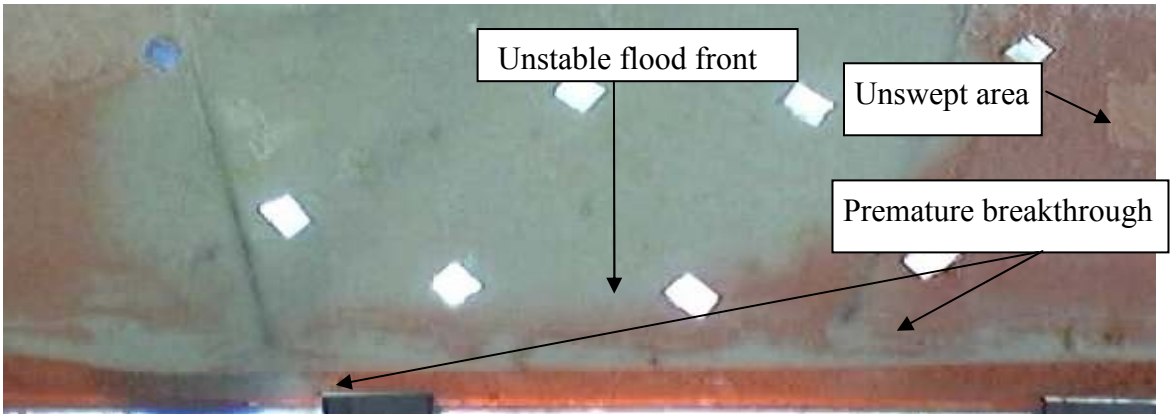

Figure 1.36: Miscible Injection in Vertically Fractured Porous Media

The immiscible recovery of Soltrol was lower compared to the experiments where decane was used for the oil phase under similar experimental conditions. The recovery of Soltrol was around 65% for the best case (Figure 1.37). Higher injection rates seem to have a positive influence on the process as was seen in the low viscosity experiments.
In contrast to the lower viscosity runs, the immiscible CO_2 volumetric sweep efficiency was significantly lower than 100% because of the adverse mobility ratio effect. The difference between the gas phase and liquid phase viscosity increased many folds in this case. Viscous fingering was observed very clearly, which lead to premature gas breakthrough and the loss of gas pressure, thus ending the displacement prematurely (Figure 1.38).

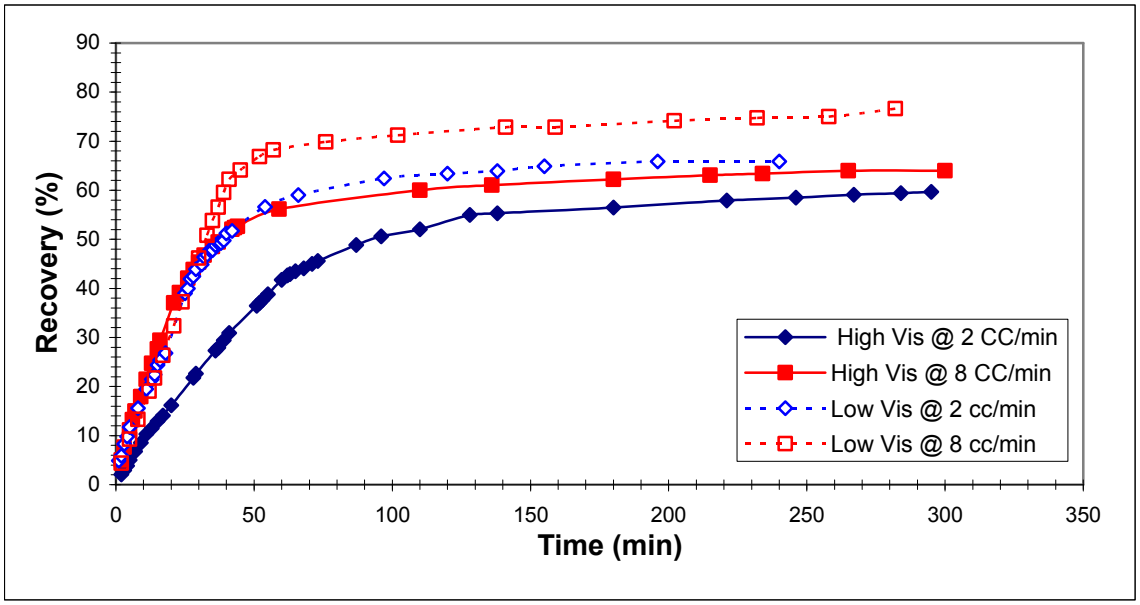

Figure 1.37: Immiscible GAGD Oil Recoveries – High versus Low Viscosity

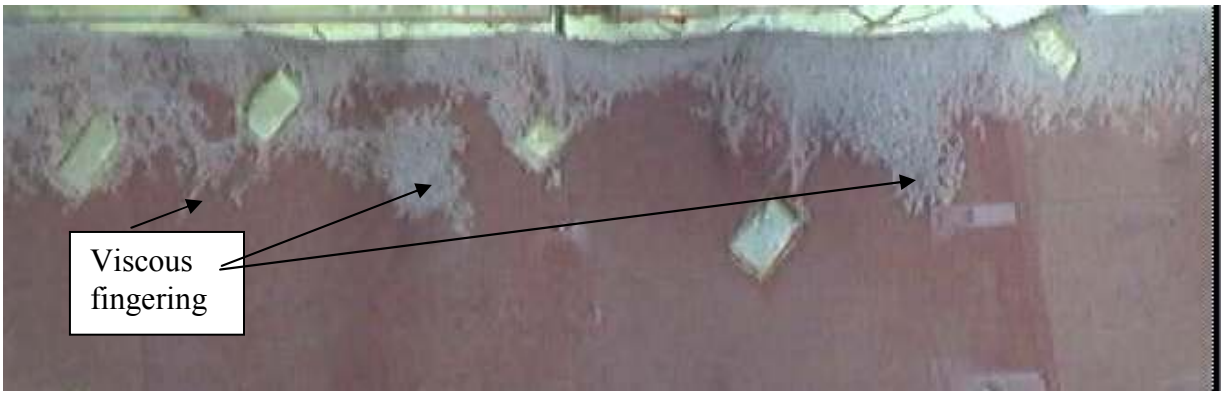

Figure 1.38: Immiscible GAGD Process with High Viscosity Oil

The miscible Soltrol experiment was conducted using red dyed Soltrol as oil and clear decane to represent miscible CO_2. The miscible recovery of Soltrol did not seem to be the ideal solution for the situation. Severe viscous fingering was observed even more clearly than the immiscible case (Figure 1.39) because of losing the gravity advantage of the gas. The density difference between fluid phases was 0.0509g/cc, which is relatively low. Consequently, the viscous force dominated. Furthermore, the adverse mobility ratio effects were present as well. However, it is expected that the gravity force will have more domination in field application due to the higher density difference between the fluids.

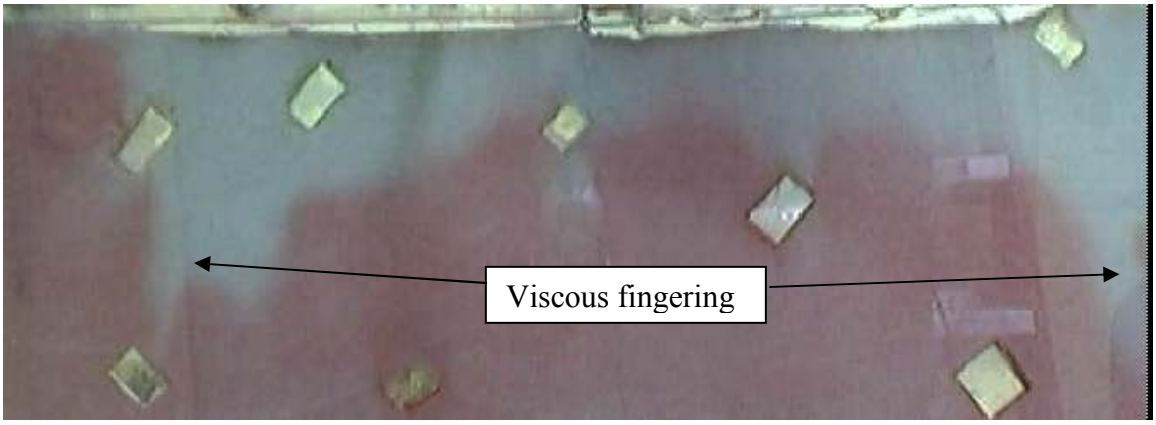

Figure 1.39: Miscible GAGD Process with High Viscosity Oil

The effect of wettability on GAGD:

Paidin (2006) studied the wettability effects on GAGD oil recovery in oil-wet porous media using a physical model. Hence, it was suggested to build a visual model for observation of the GAGD behavior in oil-wet porous media. As expected, the recovery was higher in oil-wet porous media compared to water-wet porous media (Figure 1.40). One advantage of oil-wet reservoirs is that they can utilize the beneficial effects of thin film oil flow. Oil flows more effectively in thin film through the reservoir matrix than in droplets that have to be pushed through the pore throats. Since the simulated case represents light oil with relatively low viscosity, E_V will be at or near 100% as proven before. Additionally, the thin film flow of oil facilitates a better E_D for the rock, which is evident from the very light color of the model after the GAGD flood (Figure 1.41 and Figure 1.42).

Single point horizontal well contact effects on GAGD:

Most of the experiments in this study utilized a horizontal well that was placed flat at the bottom throughout the visual model representing the line contact with the porous media for GAGD oil recovery. It was thought that this configuration might have had an advantageous effect on oil production due to the provision of a large contact area (line contact). However, in the field the horizontal well would not have relatively as much

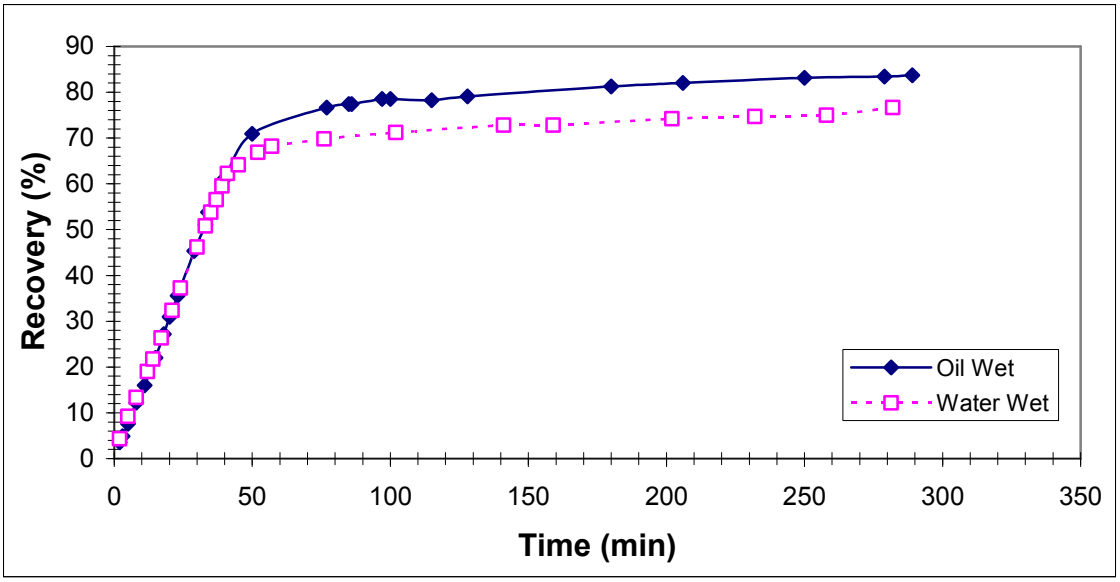

Figure 1.40: Recovery Graph Oil-Wet Model vs. Water-Wet Model

Figure 1.41: Oil-Wet Porous Media before GAGD

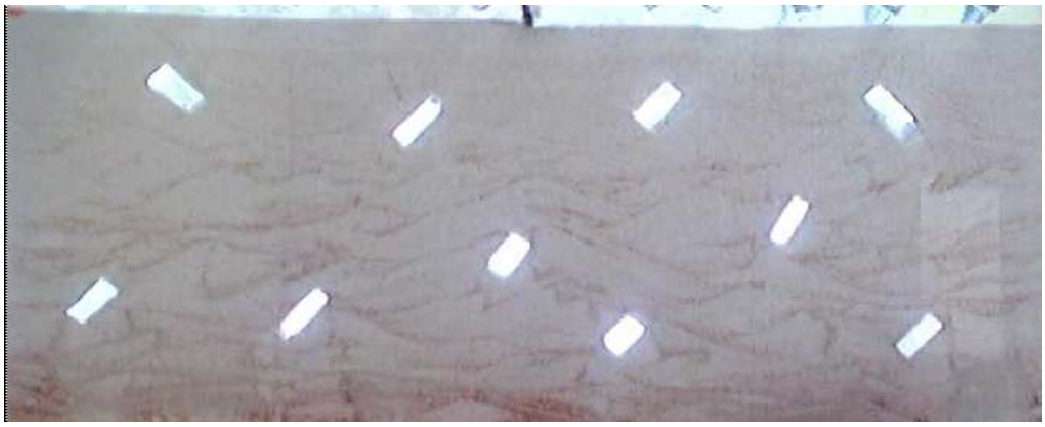

Figure 1.42: Oil-Wet Physical Model after Immiscible GAGD

contact with the porous media. Therefore, the horizontal well was placed as a point contact near the bottom of the visual model to test the influence of the horizontal well placement on the GAGD performance.

A visual model was constructed for this purpose, placing the horizontal well as a point contact within the porous media (Figure 1.43). It was decided to perform this experiment by injecting CO_2 at a rate of 8cc/min at the very top of the pay zone so as to compare the results with the other 8cc/min injection rate experiments.

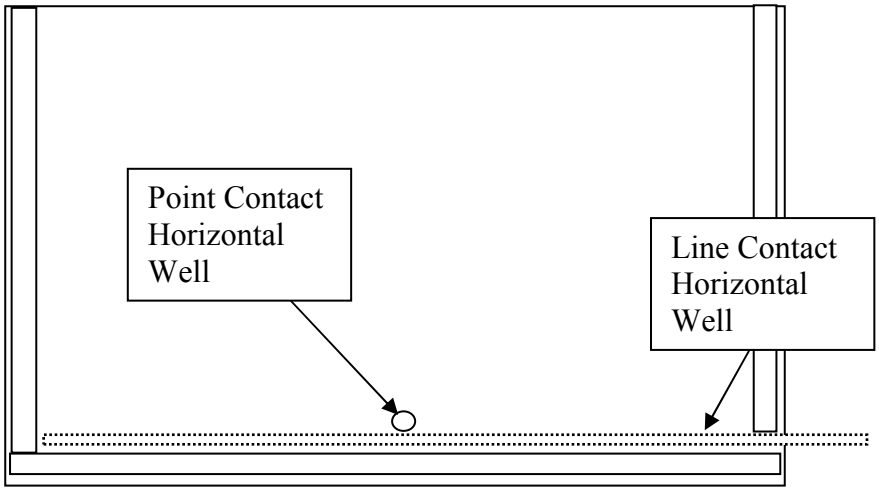

Figure 1.43: Diagram Demonstrating the Difference between Single Point and Conventional Horizontal Well

At the beginning of the experiment the CO_2 gas swept the model with a stable front. The gas flood front moved down through the model in a horizontal manner indicating a linear flow. However, when the CO_2 gas flood front approached the location of the production point, a semi circular shaped sweep pattern was observed indicating radial flow (Figure 1.44).

Figure 1.45 indicates that the configuration of the horizontal well placement in the visual model does not influence the GAGD oil recovery. Furthermore, it provides an additional proof that GAGD is a very effective process when gravity forces are predominant in the porous media and when the horizontal well is located at the bottom of the pay zone (Figure 1.43). Since two different visual models having unique characteristics were used, Figure 1.44 shows some difference between the two oil recoveries.

GAGD in the tertiary mode:

One of the most common practices in the industry is to perform waterflooding on the reservoir after the completion of primary depletion the reservoir. However, waterflooding may not always be the most efficient means of oil recovery for all reservoirs. After the secondary waterflooding in oil reservoirs, the residual oil could be as high as 70% of

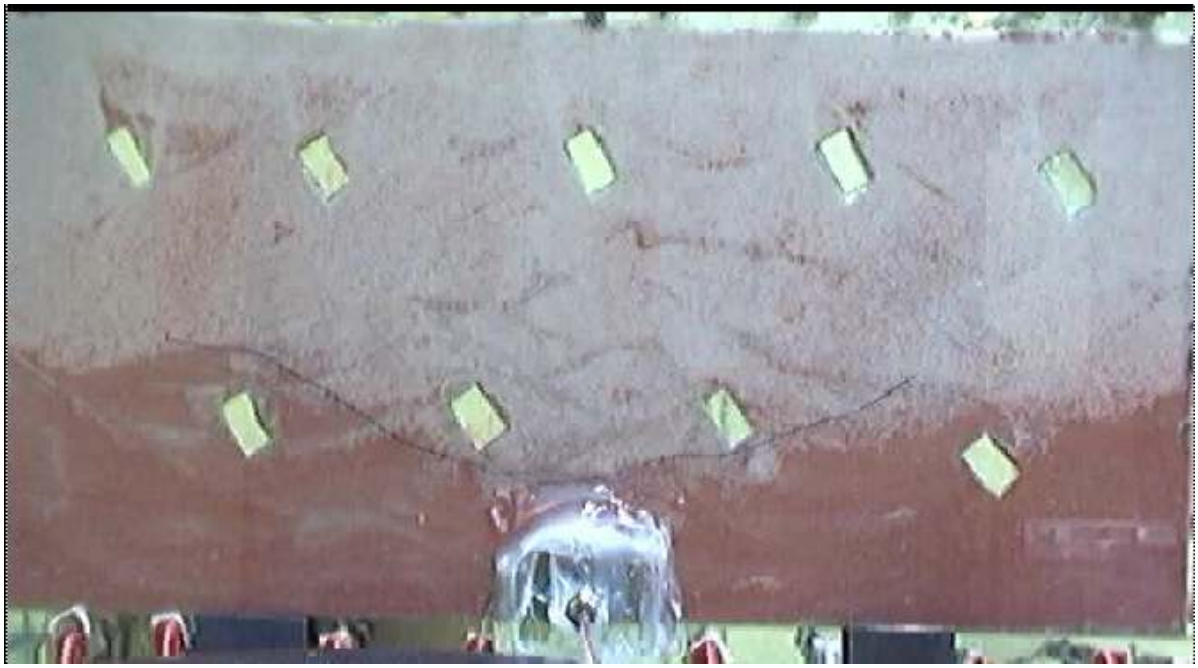

Figure 1.44: Point Contact Configuration of the Horizontal Producer

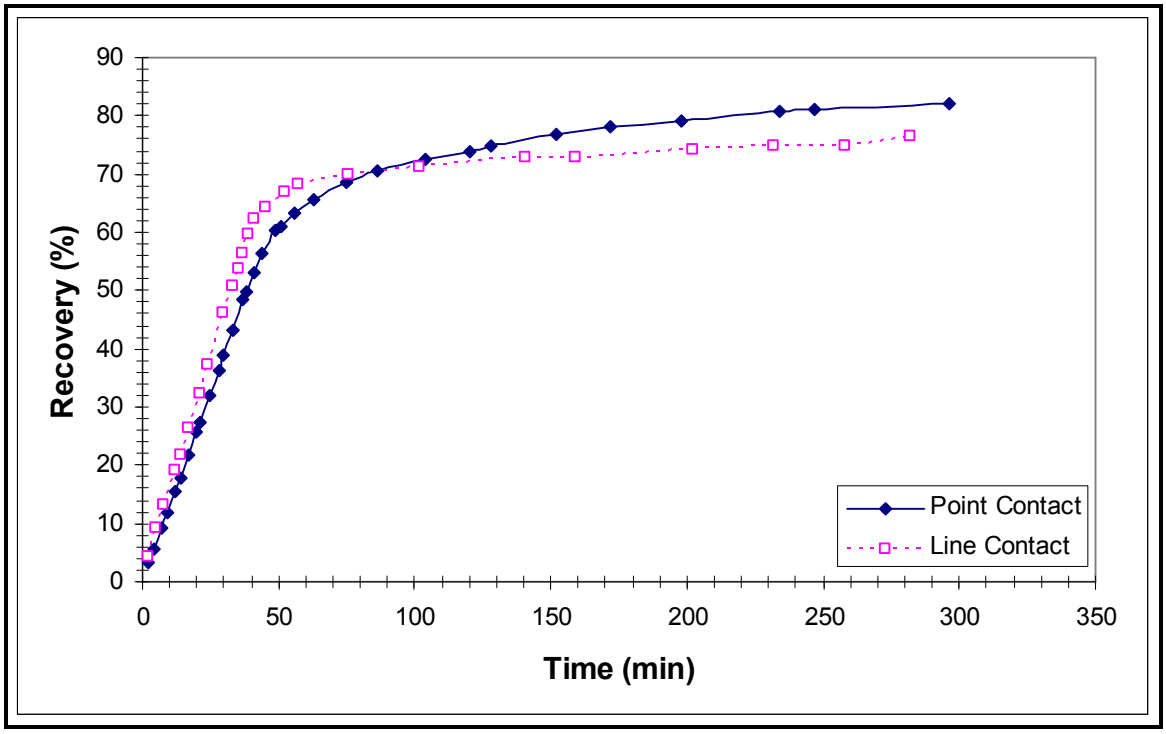

Figure 1.45: Oil Recovery – Point Contact vs. Line Contact

IOIP (DOE.gov). Therefore, some means of EOR will be required to recover the trapped oil from the reservoirs. It is to be expected that the lower density fluids (oil and gas) would travel to the top of the pay zone and the heavier density fluid (water) will sink to

the bottom of the pay zone. Therefore, a horizontal well can be placed at the bottom of oil zone and GAGD can be performed even if there is water in place that might shield the oil from coming in contact with CO_2 gas. Water shielding is not believed to be a big issue in this case because CO_2 is very soluble in water (Martin, 1992). Therefore, the CO_2 would contact the oil even after waterflooding.

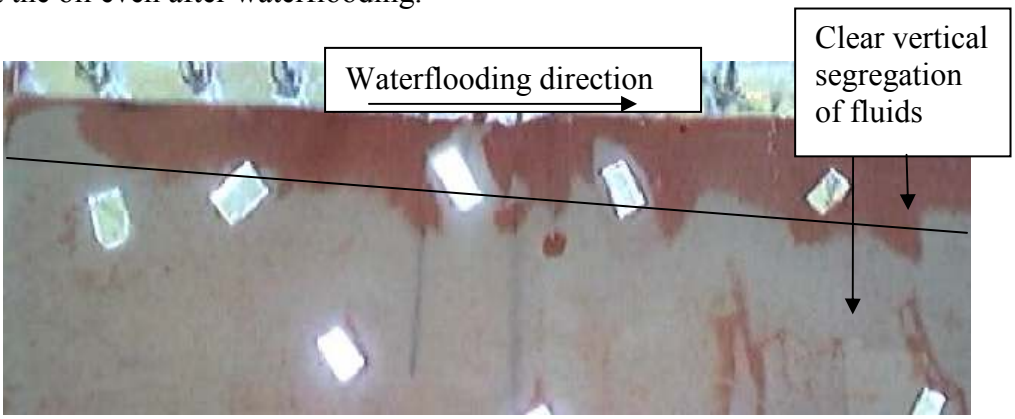

Figure 1.46: Waterflooding Effect on Porous Media

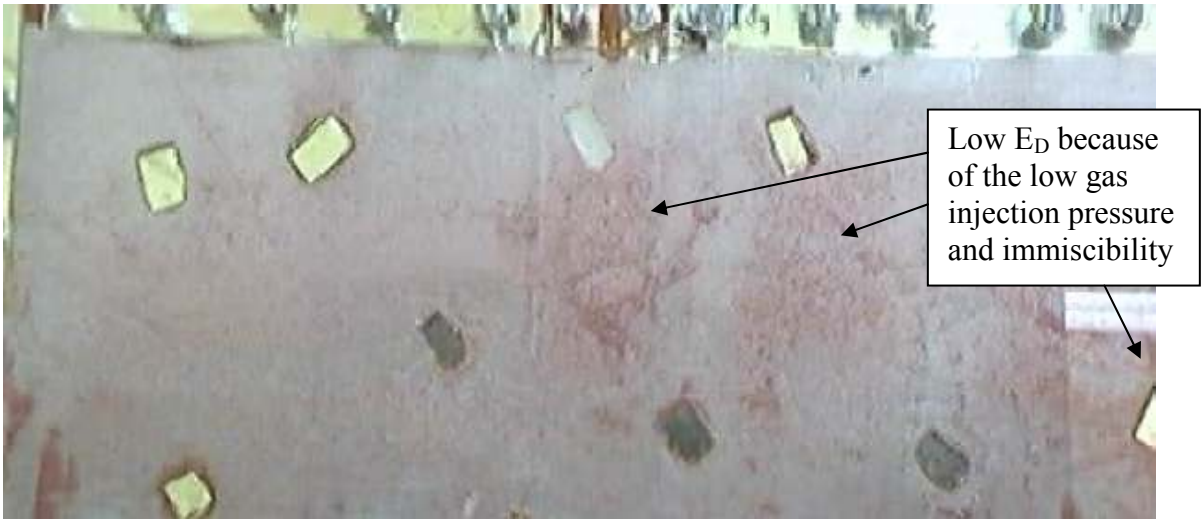

Figure 1.47: Conventional Waterflooding followed by Immiscible GAGD in Water-Wet Porous Media

A visual model was built to provide appropriate vertical wells to perform horizontal waterflooding first and then to conduct a CO_2 GAGD flood. It is important to keep in mind that the viscosity of decane is 0.96cp and the viscosity of water is equal to 1cp. Thus, the favorable mobility ratio provided a stable flood front during the waterflooding. Furthermore, the low density difference between the fluids (0.2809g/cc) and the relatively small model size yielded a good waterflood performance. The waterflooding experiment at a high injection rate (8cc/min) was dominated by viscous forces. The viscous forces allowed the water to be suspended in the matrix for a relatively long time

thereby combating the weak gravity force in place. This was further aided by the relatively small size of the visual model. The waterflooding was relatively very efficient with an oil recovery of 85.1%. Overall, the gravity force still forced the water to sink slightly to the bottom. Figure 1.46 shows that the oil height (red color) in the physical model is increasing as the distance increases from the injector. If the model was long enough the water height would eventually become very small.

Gas injection from top was performed on the waterflooded model afterwards. Because of the 85% oil recovery in the waterflood, only about 15%IOIP was available for CO_2 flooding in this case. The GAGD recovery provided an incremental 54.5%ROIP over the waterflooding, which is in good agreement with the literature (Martin et al, 1992). The volumetric sweep efficiency (E_V) was again nearly 100% (Figure 1.47), but E_D was relatively low because the injection pressure was very low in the immiscible GAGD test. Thus, the CO_2 solubility in water was very low leading to less contact between the CO_2 and the oil in place resulting in a low E_D (Figure 1.47).

Effect of wettability on waterflooding:

As mentioned before, waterflooding is a very common practice for secondary oil recovery in the field. However, waterflooding is known to be an ineffective oil recovery method, especially in oil-wet reservoirs. Therefore, there is a need to test the effectiveness of waterflooding in both water-wet and oil-wet porous media and to compare the results with secondary GAGD oil recovery.

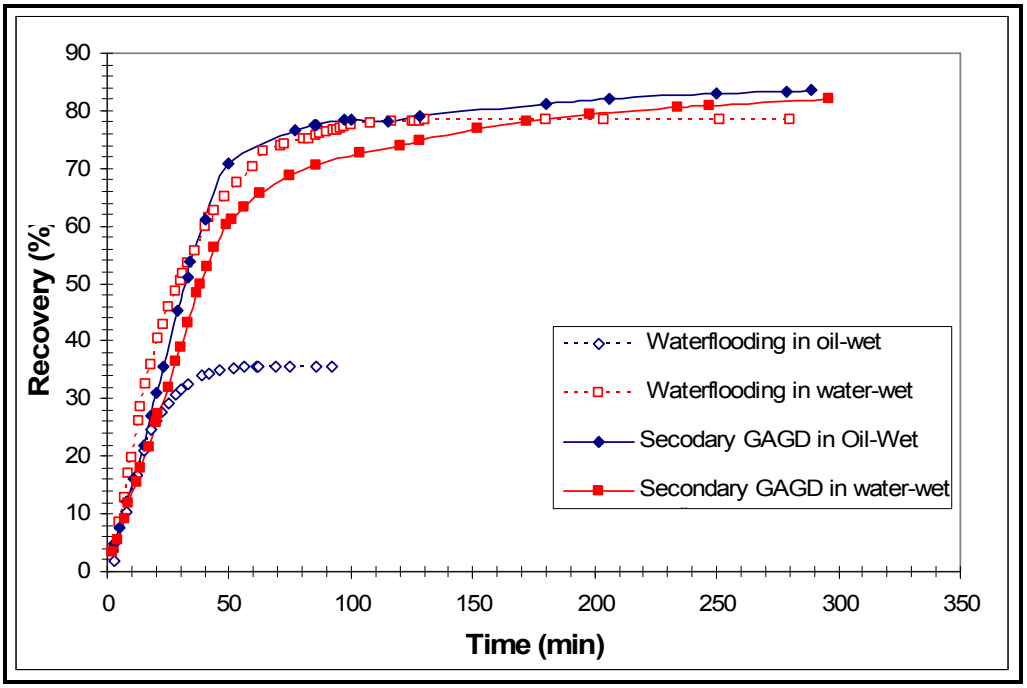

Figure 1.48: Comparison of Waterflood Oil Recovery in Oil-Wet and Water-Wet Porous Media

A visual model was constructed to perform secondary mode waterflooding in oil-wet porous media. The sand grains were treated with dimethyldichlorosilane and methylene chloride to render them oil-wet. The final waterflood oil recovery was 35.6%IOIP (Figure 1.48). Figure 1.48 compares the effectiveness of waterflooding in water-wet and oil-wet porous media. The waterflood oil recovery in oil-wet porous media is very poor. Furthermore, secondary GAGD is more efficient for oil recovery when compared with secondary waterflooding in oil-wet porous media.

The waterflooding was stopped in the oil-wet visual model after 90 minutes since the produced fluids consisted of 100% water. Furthermore, comparing Figure 1.49 to Figure 1.47 suggests that the oil-wet porous media had a strong resistance to water flow through the porous media. Hence, viscous forces lost their domination and as a result the gravity force dominated the process. Therefore, water sunk to the bottom of the porous media and only the oil at the bottom of the visual model was displaced.

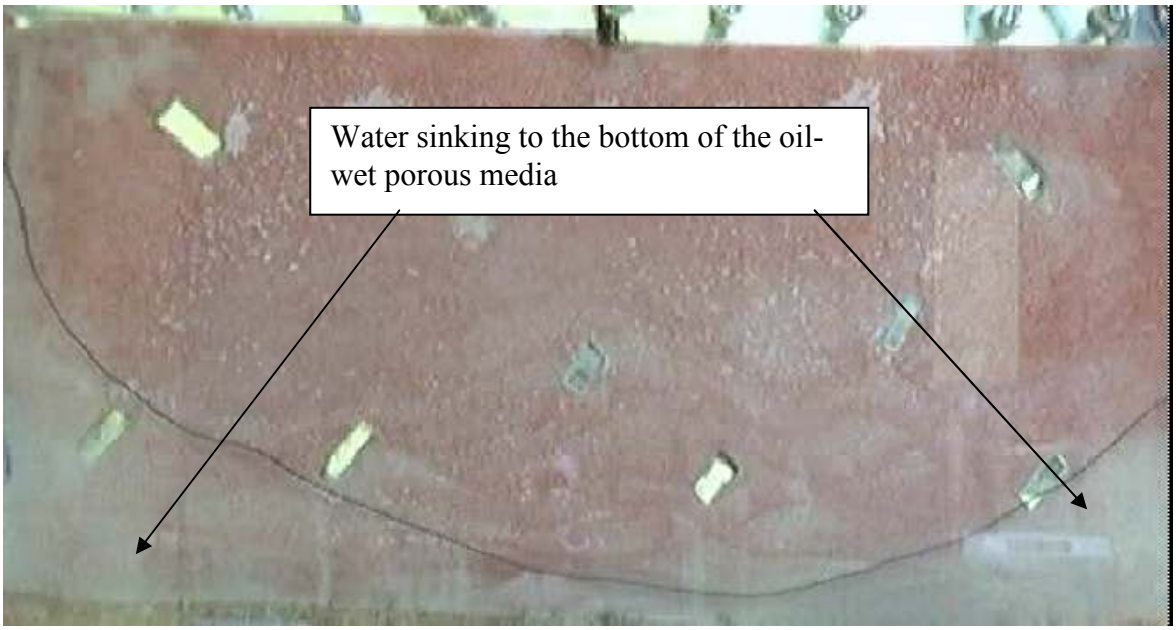

Figure 1.49: Oil-Wet Porous Medium after Waterflooding

In order to substantiate the wettability alteration, fractional water flow curves were generated for both oil-wet and water-wet porous media and are shown in Figure 1.50. There is a clear difference in the performance of both the porous media. As expected, the oil-wet fractional water flow lies to the left of water-wet fractional water flow curve. Furthermore, the water-wet porous media had much higher waterflood oil recovery than the oil-wet porous media, which is clearly evident from the end point water saturations.

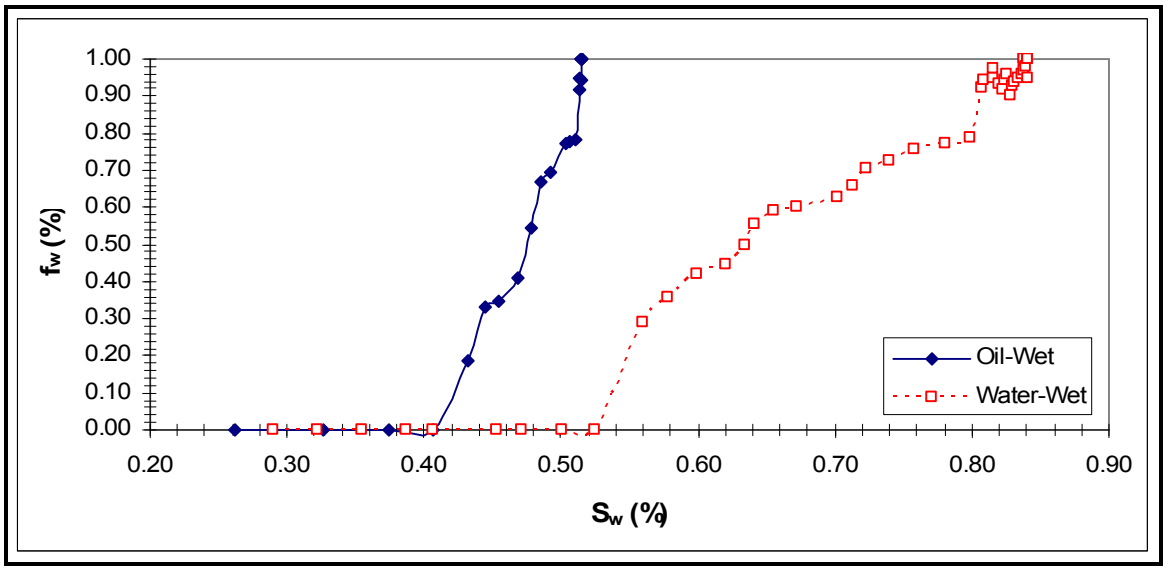

Figure 1.50: Comparison of Fractional Water Flow Curves of Oil-Wet and Water-Wet Porous Media

1.3.5 Summary and Conclusions

The visual model experimentation has provided conformational support for the GAGD theory and the important conclusions are summarized blow:

- The GAGD process is largely dependent on the domination of the gravity force. When the gravity force is dominating the process, no viscous fingering will be present thereby eliminating premature gas breakthrough. Furthermore, gravity force domination will overcome any permeability heterogeneity in the system and hence result in better ultimate oil recovery.
- Varying the gas injection depth in the pay zone did not have much effect on the ultimate GAGD oil recovery. The difference between the oil and CO_2 density resulted in the gas always traveling to the top of the visual model and forming a gas cap, thereby effectively draining the oil to the bottom.
- It was consistently observed that increasing the CO_2 injection rate tends to increase the ultimate GAGD oil recovery and with a faster recovery rate at late time. However, increasing the injection rate indefinitely is believed to have negative effects. Too high an injection rate may cause the gravity force to lose its domination and thereby allowing viscous forces to become stronger. Viscous force domination may lead to oil bypassing and premature gas breakthrough, creating the need for gas cycling and thereby increasing the operational costs.

  Immiscible CO_2 gas injection (as depicted in Figures 1.51A and B) in GAGD has resulted in oil recoveries between 65% and 87%IOIP with volumetric sweep efficiencies almost equal to 100%. Miscible injection in GAGD provided a nearly

perfect (100%) microscopic sweep efficiency. However, due to the low density difference and high CO_2 gas injection pressure, the viscous force has to be controlled. By maintaining the front velocity at low speeds, viscous fingering and oil bypassing can be avoided.

Figure 1.51A: Fluid Front Development Immiscible Displacement

- Wettability effects on GAGD were tested using the visual model. Oil-wet reservoirs are expected to have a continuous oil film flow on the matrix rather than droplets in between the pore space. The oil recovery in oil-wet porous media during the immiscible GAGD model was 83%, which was 10% higher than the corresponding water-wet porous media. Performing waterflooding on oil-wet porous media resulted

in very low oil recovery. It was observed that the gravity force dominated the process. Secondary GAGD oil recovery is much more efficient than the secondary waterflooding in oil-wet porous media.

Figure 1.51B: Fluid Front Development Immiscible Displacement

- Naturally fractured carbonate reservoirs appear to be good candidates for the GAGD process. The presence of the fracture can be exploited in the process as an effective gas-fluid exchange path between the fracture and the matrix. It is recommended to operate in the immiscible mode rather than the miscible mode to maintain gravity force domination. GAGD oil recoveries in fractured porous media were consistently higher than the non-fractured porous media recoveries by an average of 5%.
- The GAGD process can also be used to recover even higher viscosity oils. The visual model has provided evidence that miscible and immiscible CO_2 injections are applicable for heavy oil recovery. The most important consideration is to maintain the domination of the gravity force. Since the mobility ratio is highly adverse, viscous fingering could take place during the gas injection drainage of heavy oil if critical rates for gravity stable displacement are exceeded.
- The GAGD process is viable for both secondary and tertiary oil recovery. The GAGD was performed in the tertiary mode after conducting the waterflood. The oil recovery was 54.5%ROIP. It is believed that oil recovery would be better in field application

since the horizontal well can placed just above the oil-water contact thereby reducing the water production significantly.

Table 1.9: Summary of Experiments Performed with the Visual Model

Experiment #	Injection depth from top of model (inch)	Rate (cc/min)	Recovery (% IOIP)	Porosity (%)	K (D)	S_{wi} (%)	Comments
1	10	N/A	43	43.0	3.096	30.0	Free gravity flow was allowed to establish a base case.
2	7.5	2	67	43.0	3.096	30.0	
3	7.5	4	72	43.0	3.096	30.0	
4	7.5	8	83	43.0	3.096	30.0	
5	5	2	71	37.6	4.040	23.2	
6	5	4	88	37.6	1.730	30.0	The permeability of the visual model was relatively low in this experiment, and then it changed to a higher value after. Low permeability has shown to have a positive effect on recovery.
7	2.5	2	65	41.2	3.629	55.0	
8	2.5	4	71	41.2	3.629	55.0	
9	2.5	8	74	41.2	3.629	55.0	The model was shut-in near the end of experiment, and then restarted at later time with a jump of production due to phase segregation.
10	0	4	73	41.2	3.629	54.0	The model was shut-in near the end of experiment, and then restarted at later time with a jump of production due to phase segregation.
11	0	8	69	41.2	3.629	53.0	No shut-in was practiced to demonstrate the effect of shut-in time.
12	0	N/A	65	41.2	3.629	53.0	Water was used to simulate oil, and red dyed n-decane was used for gas to simulate a case with low density difference between the fluids.
13	0	2	94	41.2	2.787	30.0	Naphtha was used for oil and decane for CO_2 in the miscible mode. 100% microscopic sweep efficiency, but with less than 100% vertical sweep efficiency.

14	0	6	89	41.2	2.780	30.0	Naphtha was used for oil and decane for CO_2 in the miscible mode. Vertical sweep efficiency tends to improve with the lower injection rate.
15	0	8	85	41.2	2.780	30.0	Naphtha was used to simulate oil and decane for the gas phase in the miscible mode. 100% microscopic sweep efficiency; vertical sweep efficiency less than 100%. This experiment proved that recovery depends on injection rate in the miscible mode.
16	10	8	71	41.2	3.629	52.5	Intermittent injection of CO_2 in the horizontal well was tested.
17	0	2	71.9	45.7	2.957	22.4	2 fractures were introduced in the model.
18	0	4	71.8	45.7	2.957	22.4	2 fractures were introduced in the model.
19	0	8	74.2	45.7	2.957	20.0	2 fractures were introduced in the model. It seemed that in order to have a positive effect of the fractures on the overall recovery, injection rate had to be high.
20	0	8	85	45.7	2.957	20.0	2 fractures were used in the model; miscible flooding of the model (naphtha for oil, and decane for miscible CO_2)
21	0	2	64.1	42.0	2.787	25.7	Soltrol was used for oil. Soltrol has a higher viscosity (2.93 cp) compared to decane (0.92 cp).
22	0	8	64	42.0	2.787	25.7	Soltrol was used for oil.
23	0	2	53.5	42.0	2.787	25.7	Soltrol used for oil and decane for miscible CO_2. It was observed that just like in any other miscible case, microscopic sweep was 100%, but volumetric sweep was less 100%. Furthermore, the mobility ratio had an adverse effect, however, if the miscible fluid was circulated enough, volumetric sweep would reach 100%.
24	0	8	53.5	42.0	2.787	25.7	Soltrol used for oil and decane for miscible CO_2. The injection rate is irrelevant in this case: it is believed that it is only the effect of the mobility ratio.
25	0	8	76.6	45.7	2.500	26.0	This experiment was a repeated run: the previous the run had a permeability of 3600 mD and a recovery of 69%. It seemed that the permeability had an adverse effect up to a point. The purpose of this model was to run all four configurations (0", 2.5", 5", and 7.5" from top) in the same model for better comparison.

26	2.5	8	75.5	45.7	2.500	26.0	This experiment was a repeated run: the previous the run had a permeability of 3600 mD and a recovery of 74.1%. It seemed that the permeability had an adverse effect up to a point. The purpose of this model was to run all four configurations (0", 2.5", 5", and 7.5" from top) in the same model for a better comparison.
27	5	8	70.7	45.7	2.500	26.0	This experiment was a repeated run. The purpose of this model was to run all four configurations (0", 2.5", 5", and 7.5" from top) in the same model to have a better comparison.
28	7.5	8	76.4	45.7	2.500	26.0	This experiment was a repeated run. The purpose of this model was to run all four configurations (0", 2.5", 5", and 7.5" from top) in the same model to have a better comparison.
30	Vertical Well	8	85.1	45.7	2.500	26.0	The injection rate was believed to be too high to allow the gravity effect to take place; the viscous effect was the dominant effect in the process.
31	0	8	8.2	45.7	2.500	11.0	GAGD was performed after the horizontal water flooding. The water flooding was very efficient and it recovered 85.1% of IOIP.
32	0	8	83.7	45.7	4.000	26.0	This model was oil-wet resulting in film flow of the oil.
33	Vertical Well	2	71	45.7	4.000	26.0	WAG. The waterflooding part has out-performed the gas flooding part. CO_2 gas flooding was not effective because the gas traveled to the top immediately and bypassed the oil. Water injection performed just like waterflooding pattern
34	10	8 and 2	7.2	42.6	3.846	23.8	Toe to Heel. In this experiment the CO_2 gas injection was at the same height of production to simulate the Toe to Heel process. The outcome is not encouraging: it seems that due to the close proximity of the injection to the production the gravity force was not allowed to dominate the process. It is believed that the dominant force in place is the viscous. The horizontal production well acted like a vacuum attracting the CO_2. No gas cap formed.
35	0	8	82.2	44.7	1.365	20	Single point production. In this experiment the horizontal production well is simulated by a point contact outward instead of a horizontal well line contact with porous media.
36	Vertical	8	35.3	35.5	4.000	25	Oil-wet model. The need for oil- wet fractional flow curves arose, and therefore, this test was performed. The water sank to the bottom of the visual model (gravity force domination in this case).

2. Further Development of the Vanishing Interfacial Tension (VIT) Technique

Nearly two-thirds of original oil in place remains unrecovered in the crude oil reservoirs after the application of primary (pressure depletion) and secondary (waterflooding) oil recovery technologies. This remaining oil amounts to an enormous 377 billion barrels in the known oil fields of the United States alone. Hence, more attention is currently being paid to Enhanced Oil Recovery (EOR) processes to recover this huge amount of trapped oil.

Presently miscible CO_2 gas injection has become the most popular EOR process in the United States for light oil reservoirs. In addition to recovering the trapped oil, this EOR process has the added advantage of CO_2 sequestration for the reduction of greenhouse gas emissions into the atmosphere. The trapping of crude oil in oil reservoirs after primary and secondary oil recovery processes is mainly due to rock-fluids interactions including capillary forces, which prevent the oil from flowing within the pores of reservoir rock, thereby leaving huge amounts of residual oil in reservoirs. These capillary forces can be reduced to a minimum if the interfacial tension between the injected fluid and the trapped crude oil is decreased to zero. Zero interfacial tension is nothing but miscibility between the injected gas and crude oil. Thus there is a need for miscibility development between injected gas and the crude oil in a gas injection EOR process to remobilize the huge amounts of trapped oil and improve the oil recovery. Oil recovery in a miscible gas injection process can be maximized by choosing the operating conditions such that the injected gas becomes miscible with the crude oil. Hence an accurate prior laboratory evaluation of gas-oil miscibility conditions is essential for process design and economic success of miscible gas injection field projects. The primarily available experimental methods to evaluate gas-oil miscibility under reservoir conditions are the Slim-Tube Test (STT), the Rising Bubble Apparatus (RBA) and the method of constructing Pressure-Composition Diagrams (PXD). Apart from these experimental techniques, several computational models are also available to determine gas-oil miscibility. The most important and popular among these models are the equation of state (EOS) model and the analytical model.

In its very definition, fluid-fluid miscibility means the absence of an interface between the fluid phases, that is, the value of interfacial tension between the two phases is zero. However, none of the presently used conventional experimental techniques mentioned above for gas-oil miscibility evaluation satisfy this fundamental definition of miscibility. They do not provide direct and quantitative information on interfacial tension. Instead, they rely on indirect interpretation of miscibility from the amount of oil-recovered in a slim-tube test or qualitatively from the appearance of gas bubbles rising in a column of oil in the rising-bubble apparatus. Furthermore, some of these techniques are

time consuming (e.g. 4-5 weeks for a slim-tube test measurement) and also there exists neither a standard design nor a standard set of criteria to determine miscibility in slim-tube and rising bubble experimental techniques resulting in uncertainty and lack of confidence in the results obtained.

To overcome the disadvantages of the above-mentioned conventional approaches to determine gas-oil miscibility, recently a new technique of Vanishing Interfacial Tension (VIT) has been developed based on the fundamental definition of zero interfacial tension at miscibility (Rao, 1997; Rao et al., 1999; Rao and Lee, 2002; Rao and Lee, 2003). In this method, the gas-oil interfacial tension is measured at reservoir temperature and at varying pressures or enrichment levels of gas phase. The gas-oil miscibility condition is then determined by extrapolating the plot between interfacial tension and pressure or enrichment to zero interfacial tension. In addition to being quantitative in nature, this method is quite rapid (1-2 days) as well as cost effective. This new technique so far has been successfully implemented for optimization of two miscible gas injection field projects, namely Rainbow Keg River (RKR) in Alberta and the Canadian Terra Nova offshore field. However, this technique remains to be further verified for model fluid systems with known phase behavior characteristics and also needs to be compared with computational models of miscibility prediction. These concerns need to be addressed in further developing this promising new technique for gas-oil miscibility evaluation that has already demonstrated its usefulness and cost-effectiveness in two different field applications. Further development of the VIT technique is also required to enable its wide acceptance by industry and to answer the questions regarding the compositional dependence of this technique on mass transfer interactions between the fluids due to varying gas-oil ratios in the gas-oil mixture. This section of the report outlines the results of laboratory experiments as well as theoretical calculations carried out for further development of VIT technique, in the following three sub sections.

- VIT Experiments with Model Fluid Systems with Known Phase Behavior Characteristics
- Experimental Determination of Miscibility Conditions for CO_2 with Selected Crude Oil(s)
- Development of Computational Models for Miscibility Prediction

2.1 VIT Experiments with Model Fluid Systems with Known Phase Behavior Characteristics

2.1.1 VIT Experiments in Standard Gas-Oil Systems

2.1.1.1 Introduction

Minimum miscibility pressures (MMP) and minimum miscibility enrichments (MME) are the two important parameters used for assessing miscibility conditions for displacements of oil by gas. The minimum miscibility pressure as the name implies is the lowest possible pressure at which the injected gas (CO_2 or hydrocarbon) can achieve miscibility with reservoir oil at reservoir temperature. The minimum miscibility enrichment is the minimum possible enrichment of the injection gas with C_2-C_4 components at which miscibility can be attained with reservoir oil at reservoir temperature. Operating pressures below MMP or injection gas enrichments below MME result in immiscible displacements of oil by gas and, consequently, lower oil recoveries. Hence, prior laboratory evaluation of gas-oil miscibility conditions is essential for economic success of field miscible gas injection projects.

The widely used experimental methods to evaluate gas-oil miscibility conditions under reservoir conditions are the slim-tube displacement, the rising bubble apparatus, method of constructing pressure-composition (P-X) diagrams and the newly developed vanishing interfacial tension (VIT) technique.

Slim-Tube. Slim-tube test is the most common and has been widely accepted as the "petroleum industry standard" to determine gas-oil miscibility. The miscibility conditions are determined indirectly from oil recovery in this technique. Although the slim-tube is widely accepted, there is neither a standard design, nor a standard operating procedure, nor a standard set of criteria for determining miscibility conditions using this technique (Elsharkawy et al., 1996). Elsharkawy et al. (1996) comprehensively reviewed the literature and discussed several non-uniformities observed in the design and operation of this experimental technique. Slim tube length, diameter, type of packing, and the permeability and porosity of the packing have varied greatly in the designs used in industry. There is a considerable difference of opinion reported in literature on the effect of packing material and flooding rate on miscibility conditions determined using slim-tube (Elsharkawy et al., 1996). There exist no fixed criteria for determining miscibility within slim-tube and hence individual researchers have defined their own criteria to identify slim-tube miscibility. Klins (1987) described in detail these different available slim-tube miscibility definitions in the literature. Different oil recovery levels, such as 80% at gas breakthrough (Holm and Josendal, 1982), or 90-95% ultimate recovery at 1.2 pore volumes of gas injected (Jacobson, 1972; Graue and Zana, 1981), have been reported as miscibility defining criteria in a slim-tube. The miscibility determined from

slim-tube displacement might not necessarily represent the true thermodynamic miscibility, that is, the attainment of critical state condition. The presence of physical dispersion effects in slim-tube can prevent or delay the achievement of thermodynamic miscibility (Walsh and Orr, 1990; Johns et al., 1993). Slim-tube experiments can even give misleading results depending on the level of physical dispersion present (Johns et al., 2000). The actual displacement of fluids in a reservoir is strongly influenced by several factors such as viscous fingering, gravity over ride, dispersion and reservoir heterogeneity and it is impossible to simulate all these mechanisms in a slim-tube test. This technique is also time consuming and it may take several weeks (normally 4 to 5) to complete one miscibility measurement and hence is expensive. Thus, the lack of fixed design, operating procedure and miscibility defining criteria, inability to account for important reservoir scale mechanisms, indirect interpretation of miscibility from oil recovery, long times and high costs appear to be the main disadvantages associated with this technique. In spite of all these design, operational and conceptual uncertainties existing in slim-tube measurements, it is interesting to see that still this technique is most widely preferred by industry for miscibility evaluation. This primarily appears to be due to the fact that the industry still believes there exists no other effective alternative experimental technique that can measure gas-oil miscibility as accurately as slim-tube.

One of the often mentioned advantages of using the slimtube for miscibility determination is its ability to include the interaction of flow with phase behavior thereby accommodating the condensing and vaporizing modes of mass transfer that enable the development of the so-called multi-contact miscibility. However, the actual gas-oil contact occurring in the slimtube is a continuous interaction rather than one involving multiple discrete stages of contact. One can easily visualize the flow of injected gas (solvent) through a packed bed of sand in the slimtube that is saturated with crude oil. At the injection end, the gas contacts the oil for the first time when their mutual interactions begin. Depending on the extent of departure of their initial compositions from the equilibrium compositions, mass transfer begins to take place from each phase into the other. As the gas continues to flow through the slimtube, the previously oil-exposed gas contacts fresh oil residing in the unswept areas of the tube and the mutual mass transfer rates begin to slow down due to the continual decrease in the driving force as both phases approach their mutual equilibrium compositions. Thus the flow of the injected gas through the slimtube filled with oil essentially hastens the attainment of mass transfer equilibrium. However, this imposed flow does not have any effect on the final equilibrium compositions, which are governed by thermodynamics of phase behavior. Therefore it appears obvious that any other experimental method that allows for such mass transfer between phases to approach equilibrium could also be well suited for determining multi-contact miscibility. However, the low velocities used in typical slimtube displacements using 40-80 feet long sand-packed tubes render this technique to

be tedious and time consuming. Moreover, the definition of miscibility as the breakover point in the ultimate recovery curve makes it essential to run several slow rate displacement tests adding to the time and cost of miscibility determination using the slimtube. Another often mentioned advantage of slim-tubes is that it yields recovery factors. However, as Stalkup (1983) cautions, "it does not simulate many aspects of reservoir flooding, and the levels of ultimate recovery, both for immiscible and for miscible tests, should not be considered as indicative of the unit displacement efficiency to expect in reservoir rocks".

Rising Bubble. Rising bubble apparatus is another experimental technique, which is commonly used for quick and reasonable estimates of gas-oil miscibility. In this method, the miscibility is determined from the visual observations of changes in shape and appearance of bubbles of injected gas as they rise through in a visual high-pressure cell filled with the reservoir crude oil. A series of tests are conducted at different pressures or enrichment levels of the injected gas and the bubble shape is continuously monitored to determine miscibility. This test is qualitative in nature as miscibility is inferred from visual observations. Hence, some subjectivity is associated with the miscibility interpretation of this technique. Therefore, the results obtained from this test are somewhat arbitrary, but however this test is quite rapid and requires less than 2 hours to determine miscibility (Elsharkawy et al., 1996). This method is also cheaper and requires smaller quantities of fluids, compared to slim-tube. The subjective interpretations of miscibility from visual observations, lack of quantitative information to support the results and some arbitrariness associated with miscibility interpretation are the some disadvantages of this technique. There also appears to be no strong theoretical background associated with this technique and this technique provides only reasonable estimates of gas-oil miscibility conditions.

Pressure Composition Diagrams. The pressure composition (P-X) diagrams for gas-oil miscibility evaluation are constructed by conducting phase behavior measurements in high-pressure visual cells at reservoir temperature. On the diagram, the composition is expressed as a mole fraction of injection gas. Different amounts of injection gas are added to reservoir crude oil and the loci of bubble point and dew point pressures are determined to generate the phase boundaries. A single phase exists outside the phase boundaries, while the two phases coexist within the phase boundaries. In other words, miscibility develops outside the two-phase envelope, while immiscibility exists inside the two-phase envelope. The conditions needed for miscibility development between any composition of injection gas and reservoir crude oil at reservoir temperature can be determined from the diagram. However, this method is time consuming, quite expensive, cumbersome, requires large amounts of fluids and subject to some experimental errors.

Vanishing Interfacial Tension Technique. In its very definition, fluid-fluid miscibility means the absence of an interface between the fluid phases, that is, the value of

interfacial tension between the two phases is zero (Benham et al., 1965; Stalkup, 1983; Holm, 1987; Lake, 1989). The experimental technique of vanishing interfacial tension has been developed based on this fundamental definition of miscibility (Rao, 1997; Rao and Lee, 2002; Rao and Lee, 2003). In this method, the gas-oil interfacial tension is measured at reservoir temperature and at varying pressures or enrichment levels of gas phase. The gas-oil miscibility conditions are then determined by extrapolating the plot of interfacial tension against pressure or enrichment to zero interfacial tension. In addition to being quantitative in nature, this method is quite rapid (1-2 days) as well as cost effective. This technique has been successfully utilized to optimize the injection gas compositions for two gas injection projects, one in Rainbow Keg River (RKR) reservoir, Alberta and the other in Canadian Terra Nova offshore field. However, in spite of this technique being a direct and an easy route to determine miscibility based on the very fundamental definition, it has been criticized for certain perceived reasons such as the absence of compositional path specification during the laboratory gas-oil interfacial tension measurements and lack of calibration of this technique against well-known simple standard gas-oil systems. These concerns on the VIT technique are addressed in this section so as to enable the adoption of this promising new technique by the industry for accurate gas-oil miscibility evaluation in an easy, quick and cost-effective manner.

2.1.1.2 Objectives

The objectives are: (1) to carry out interfacial tension measurements in standard gas-oil systems of known miscibility conditions at elevated pressures and temperatures to calibrate the new VIT technique, and (2) to study the effect of compositional path on gas-oil miscibilities determined from VIT technique by varying gas-oil ratios during the interfacial tension measurements. For this purpose, two standard gas-oil systems of known miscibility conditions; (i) CO_2 against n-decane at 100^oF, and (ii) CO_2 against live decane consisting of 25 mole% methane, 30 mole% n-butane and 45 mole% n-decane at 160^oF have been chosen. The gas-oil interfacial tension measurements have been carried out using the pendent drop shape analysis (Kruss, 2000) and capillary rise techniques in the two standard gas-oil systems at elevated pressures and temperatures.

Table 2.1: Comparison between Target and Measured Compositions of Live Decane

Component	Target Composition (Mole%)	Measured Composition (Mole%)	% Dev. from Target
methane	25.00	24.57	1.72
n-butane	30.00	29.77	0.77
n-decane	45.00	45.66	1.47

2.1.1.3 Experimental Reagents, Apparatus, and Procedures Used

Reagents. Analytical grade reagents were used in the experiments. The cleaning solvents (toluene and acetone) and the oil (n-decane) used in the experiments were from Fisher Scientific, all having a purity of 99.9%. The pure gases methane and n-butane used in live decane preparation, the CO_2 gas used in the experiments and the N_2 gas used for drying and purging the flow lines were from Accurate Gas Products and have a purity of 99.7%, 99.5%, 99.9% and 99.9%, respectively. The live decane was prepared by adding appropriate amounts of light ends, methane and n-butane into n-decane to match the live decane composition. The target and the actual compositions of live decane (measured using Varian CP-3800 Gas Chromatograph) are shown in Table 2.1. As can be seen, an excellent match was obtained between these two compositions with a maximum deviation of about 1.7%.

Apparatus and Experimental Procedure. Figure 2.1 shows the photograph of the experimental apparatus used in this study for gas-oil interfacial tension measurements in the standard gas-oil systems at elevated pressures and temperatures. Part A in the picture is the high-pressure high-temperature optical cell (has a design rating of 400^{o}F and 20,000 psi), in which the glass capillary tube is stationed. Part B is the transfer vessel wound with heating tapes, used to hold the oil at test conditions of temperature and pressures. Part C is the centrifugal positive displacement pump used to pump oil into the optical cell. Part D is the Ruska pump, which can store and inject the CO_2 gas into the optical cell. Part E is the heating oven used to maintain the temperature of the optical cell and the fluids at the desired value. Part F is the PAAR DMA-512 density meter wrapped with heating tapes, used to measure the densities of equilibrated oil and gas phases during the experiments. Part G is the light source and part H is the digital video camera used to record the capillary rise observed in the capillary tube, inside the optical cell as well as to capture the pendent drops of oil for drop shape analysis (Kruss, 2000). We believe that this study may be the first one to adapt the capillary rise technique for interfacial tension measurements with complex hydrocarbon fluids at elevated pressures and temperatures. A capillary tube of known inside diameter (1.8 mm for n-decane-CO_2 system and 1.0 mm for live decane-CO_2 system) was carefully fitted into one of the crystal holders of the optical cell and is placed inside the cell. The cell was first filled with pure CO_2 gas using the Ruska pump and was heated to desired temperature using the temperature control system of the heating oven. Then, the oil (n-decane or live decane) maintained at the desired temperature (100^o or 160^{o}F) in the transfer vessel was injected into the cell using the pump so that the cell was filled with fluids at a fixed initial gas-oil ratio. Nearly about an hour was then allowed for the fluid phases to equilibrate in the cell. The capillary rise observed in the glass tube was then recorded using the light source, digital camera, which was measured precisely, using the magnification system of the camera and a computer. A calibration reference object with a magnification factor of about 50 times was used

during the capillary rise measurements. The equilibrated liquid and gas phases were allowed to flow through the density meter maintained at desired temperature for density measurements. These measurements were then repeated for different pressures. The pressure in the system was altered either by injecting or withdrawing small amounts of liquid or gas phases, while maintaining the initial gas-oil ratio in the cell as close to the initial gas-oil ratio.

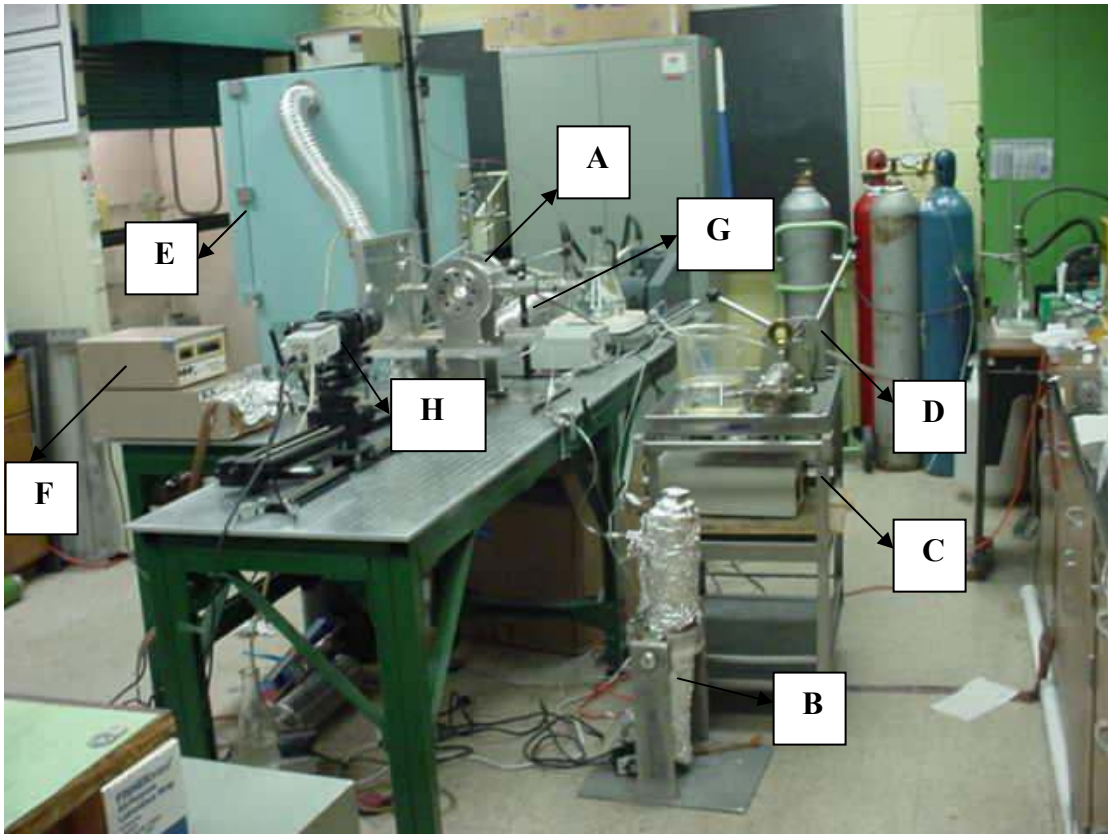

Figure 2.1: Photograph of the Equipment Used for IFT Measurements at Elevated Pressures and Temperatures

The measured capillary rise and the densities of equilibrated fluid phases were then used to calculate the interfacial tension using the capillary rise technique. A contact angle of $\theta = 0^o$ was used during the capillary rise interfacial tension calculations as it is reasonable to assume that the liquids wet the glass completely in preference to a gas phase. This procedure was then repeated by varying the initial gas-oil ratio of the fluids in the cell to study the effect of gas-oil ratio on interfacial tension. At certain pressures of specific gas-oil ratios in decane-CO_2 system at 100^oF, the pendent drop images of CO_2 gas in n-decane were captured and analyzed for interfacial tension using the drop shape analysis technique (Kruss, 2000). This was done to calibrate the newly adapted capillary rise technique for interfacial tension measurements at elevated pressures and

temperatures by comparing the results of capillary rise technique with those obtained using the pendent drop technique. The dynamic variations in capillary rise with time were also measured in live decane-CO_2 system at 160°F and 1100 psig at different gas-oil ratios to study the effect of gas-oil ratio on the dynamic interfacial tension in gas-oil systems.

2.1.1.4 Principles and Equations Used

Pendent Drop Shape Analysis. Mathematically, the force balance between the interfacial tension and gravity is well reflected in Laplace equation of capillarity. Hence, this equation has been used to fit the experimental drop profiles in pendent drop shape analysis technique. This equation represents the mechanical equilibrium between the two immiscible fluids. It relates the pressure difference across the interface to the interfacial tension and the curvature of the interface and is given by:

$$\sigma\left(\frac{1}{R_1}+\frac{1}{R_2}\right)=\Delta P \quad \text{..... (2.1)}$$

Where σ is the interfacial tension, R_1 and R_2 are the two principal radii of curvature and ΔP is the pressure difference across the interface.

This technique considers several points numbering about 50-100 on the actual measured drop profile of the pendent drop and fits a Laplacian curve to the measured profile. Then, an objective function is defined as the sum of the squares of the normal distances between the experimental points and the calculated curve to describe the deviation of the experimental profile from the theoretical profile. The objective function is finally minimized using a non-linear regression procedure to yield the interfacial tension. However, the major disadvantage of this technique is that it requires a drop shape to compute interfacial tension. In situations of low interfacial tension between the fluids, it is difficult to form pendent drops. Hence, this technique fails in such situations and therefore may not be applicable at conditions close to critical point, where the interfacial tension is close to zero. Hence, the capillary rise technique has been used to measure the low interfacial tensions occurring in this study, since the VIT technique requires very low interfacial tensions, as low a value as can be reliably measured, to accurately predict gas-oil miscibility.

Capillary Rise Technique. The equations governing the capillary rise in a circular glass tube are well known. The force acting along a vertical capillary due to the upward pull of interfacial tension is balanced by the oppositely directed force of gravity acting on the mass of liquid in the capillary above the outside level of the liquid. Thus, the force balance in a capillary is given by:

$$2\pi r\sigma\cos\theta=\pi r^2 h(\rho_l-\rho_g)\frac{g}{g_c} \quad \text{..... (2.2)}$$

Solving for interfacial tension (σ) gives,

$$\sigma = \frac{rh(\rho_l - \rho_g)g}{2\cos\theta g_c} \quad \text{..... (2.3)}$$

Where σ is the interfacial tension in mN/m, r is the capillary radius in cm, h is capillary rise in cm, ρ_l and ρ_g are the densities of liquid and gas phases, respectively in g/cc, θ is the equilibrium contact angle in degrees, g is the acceleration due to gravity in cm/s^2 and g_c is the conversion factor (1 g.cm/sec^2.dyne).

2.1.1.5 Results and Discussion

n-Decane-CO_2 System at 100^{o}F. This standard gas-oil system of n-C_{10}/CO_2 has a reported slim-tube miscibility of 1250 psig (Elsharkawy et al., 1996) and a rising-bubble miscibility of 1280 psig (Elsharkawy et al., 1996) at 100^{o}F. The interfacial tension measurements in this gas-oil system at 100^{o}F and at various pressures were carried out using the capillary rise and pendent drop techniques. Three different molar feed compositions of 100 mole% oil, 40/60 mole% gas and oil, and 80/20 mole% gas and oil were used during the experiments to study the effect of gas-oil ratio on miscibility. The interfacial tension measurements at the feed composition of 100 mole% oil were conducted using the pendent drop technique. Both the pendent drop and capillary rise techniques were used for IFT measurements at the feed composition of 40/60 mole% gas and oil, while only capillary rise technique was used for IFT measurements at the molar feed composition of 80/20 mole% gas and oil. The densities of pure as well as equilibrated fluid phases and the capillary rise heights measured at molar feed compositions of 40/60 mole% gas and oil and 80/20 mole% gas and oil are summarized in Table 2.2. The gradual decrease of capillary rise heights with pressure can be seen at both the gas-oil ratios used. The summary of all interfacial tensions measured at different gas-oil ratios and at various pressures using both the pendent drop and capillary rise techniques is given in Table 2.3 and shown in Figure 2.2. The standard deviations in interfacial tension values reported for pendent drop technique in Table 2.3 at the gas-oil ratios of 100 mole% oil and 40/60 mole% gas and oil were obtained from about 10-20 separate measurements.

From Table 2.3, a good match of interfacial tensions between capillary rise and pendent drop techniques can be seen at 40/60 gas-oil ratio in the feed. This validates the newly adapted capillary rise technique for IFT measurements at elevated pressures and temperatures. As can be seen in Table 2.3 and Figure 2.2, almost similar IFT values are obtained at each of the pressures for all the three gas-oil ratios used, which clearly indicates the absence of gas-oil ratio effects on interfacial tension and hence on miscibility. This indicates that interfacial tension becomes independent of gas-oil ratio, as

the fluid phases approach equilibrium and hence the miscibility conditions of pressure and enrichment determined from the VIT technique do not depend on gas-oil ratio in the feed mixture. All the interfacial tensions measured at different gas-oil ratios were fitted using linear regression to determine miscibility using the VIT technique as shown in Figure 2.2.

Table 2.2: Summary of Fluid Phase Densities and Capillary Rise Heights Measured in n-Decane-CO_2 System at 100^{o}F

Pressure (psig)	Fluid Phase Densities (gm/cc)				Capillary Height (mm)	
	Oil		Gas			
	Initial	Equilibrium	Initial	Equilibrium	40/60 Mole% Gas and Oil	80/20 Mole% Gas and Oil
0	0.7304	0.719	0.0002	0.0091	7.1	7.2
200	0.7320	0.722	0.0264	0.0185	6.4	6.5
400	0.7334	0.720	0.0556	0.0432	5.4	5.4
600	0.7349	0.678	0.0890	0.0698	3.8	3.8
800	0.7363	0.663	0.1294	0.1159	2.5	2.5
1000	0.7381	0.698	0.1820	0.2203	1.8	1.6
1100	0.7392	0.482	0.2010	0.2998	0.4	0.4

Table 2.3: Summary of Interfacial Tensions Measured in n-Decane-CO_2 System at Various Pressures and Gas-Oil Ratios in the Feed

Pressure (psig)	100 Mole% Oil	40/60 Mole% Gas and Oil		80/20 Mole% Gas and Oil
	Pendent Drop IFT (mN/m)	IFT (mN/m)		Capillary Rise IFT (mN/m)
		Pendent Drop	Capillary Rise	
0	22.29 ± 0.24	21.95 ± 0.054	22.29	22.45
200	19.70 ± 0.17	19.27 ± 0.121	19.86	20.13
400	15.76 ± 0.12	15.36 ± 0.051	16.09	16.24
600	11.29 ± 0.17	10.38 ± 0.098	10.19	10.27
800	8.24 ± 0.14	7.28 ± 0.103	5.97	6.07
1000	3.57 ± 0.14	3.28 ± 0.257	3.75	3.34
1100			0.33	0.33

As can be seen in Figure 2.2, a good linear correlation was obtained between interfacial tension and pressure in the standard n-decane-CO_2 system at 100^{o}F. The linear

regression equation obtained is also shown in Figure 2.2. The coefficient of determination (R^2) of 98.8% indicates a good fit. The extrapolation of the regression equation to zero interfacial tension gives a VIT miscibility of 1150 psig. This VIT miscibility is in good agreement with the reported miscibilities from slim-tube (1250 psig) and rising-bubble (1280 psig) experimental techniques. Considering the variabilities normally encountered in slim-tube and rising-bubble measurements, this can be treated as a good match. Thus, this VIT experiment conducted using the standard gas-oil system of n-decane-CO_2 at 100°F calibrates the VIT technique to measure miscibility in gas-oil systems.

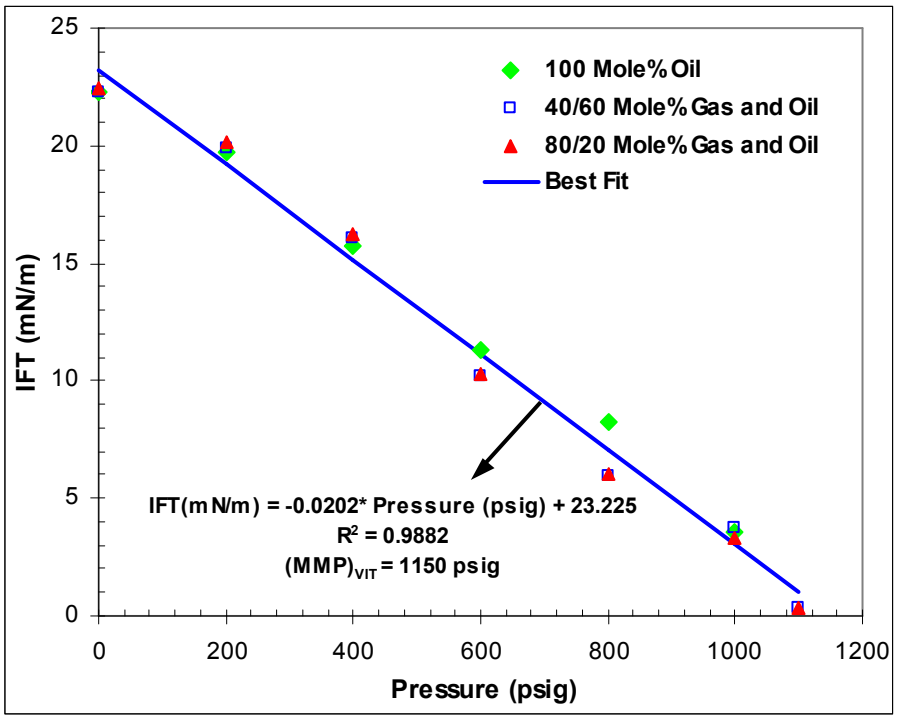

Figure 2.2: Effect of Gas-Oil Ratio on VIT Miscibility in n-Decane-CO_2 System at 100°F

Live Decane-CO_2 System at 160°F. The live decane refers to a composition of 25 mole% of methane, 30 mole% of n-butane and 45 mole% of n-decane. This standard gas-oil system has been reported to have a slim-tube minimum miscibility pressure (MMP) of 1700 psia at 160°F (Metcalfe and Yarborough, 1979). This miscibility pressure is further reproduced with phase diagram measurements (Metcalfe and Yarborough, 1979) and analytical model predictions (Monroe et al., 1990; Orr et al., 1993). The IFT measurements in this gas-oil system at 160°F and at various pressures were carried out using the capillary rise technique due to its suitability to measure low gas-oil interfacial tensions with good repeatability as judged from our earlier experiments in n-decane-CO_2 system. Two different molar feed compositions of 80/20 mole% gas and oil, and 20/80

mole% gas and oil were used during the experiments to examine the effect, if any, of gas-oil ratio on miscibility in this system as well. The summary of measured densities of pure as well as equilibrated fluid phases and capillary rise heights at the two different gas-oil ratios used are given in Table 2.4. The steady decline of capillary rise with pressure can be seen at both the gas-oil ratios used. The summary of interfacial tensions measured at both the gas-oil ratios and at various pressures in this standard gas-oil system at 160^{o}F is given in Table 2.5 and shown in Figure 2.3.

Table 2.4: Summary of Fluid Phase Densities and Capillary Rise Heights Measured in Live Decane-CO_2 System at 160^{o}F

Pressure (psig)	Fluid Phase Densities (gm/cc)				Capillary Height (mm)	
	Oil		Gas			
	Initial	Equilibrium	Initial	Equilibrium	20/80 Mole% Gas and Oil	80/20 Mole% Gas and Oil
1100	0.6509	0.6495	0.1636	0.2743	4.4	4.4
1150	0.6517	0.6509	0.1764	0.3028	4.1	4.1
1200	0.6524	0.6520	0.1892	0.3325	3.4	3.5
1250	0.6531	0.6538	0.2020	0.3543	3.2	3.3
1300	0.6538	0.6553	0.2148	0.3726	2.9	3.0
1350	0.6545	0.6571	0.2276	0.4060	2.9	2.9
1400	0.6552	0.6590	0.2404	0.4276	2.4	2.4
1500	0.6566	0.6630	0.2660	0.4586	2.3	2.2
1550	0.6573	0.6641	0.2788	0.4813	2.0	2.0
1600	0.6580	0.6677	0.2916	0.5186	1.7	1.6
1650	0.6587	0.6703	0.3044	0.5334	1.3	1.3
1700	0.6594	0.6717	0.3172	0.6252	1.1	1.1
1750	0.6601	0.6765	0.3300	0.6502	0.7	0.7

Table 2.5: Summary of Interfacial Tensions Measured in Live Decane-CO_2 System at Various Pressures and Gas-Oil Ratios in the Feed Using the Capillary Rise Technique

Pressure (psig)	20/80 Mole% Gas and Oil	80/20 Mole% Gas and Oil
	IFT (mN/m)	IFT (mN/m)
1100	4.05	4.06
1150	3.46	3.49
1200	2.67	2.71
1250	2.36	2.44
1300	2.02	2.04
1350	1.79	1.79
1400	1.37	1.37
1500	1.13	1.11
1550	0.88	0.89
1600	0.61	0.57
1650	0.43	0.44
1700	0.12	0.12
1750	0.04	0.04

From Table 2.5 and Figure 2.3, it can be seen that IFT is not changing with gas-oil ratio at all the pressures used. This clearly indicates the absence of gas-oil ratio effects on IFT and hence on miscibility. This further substantiates the compositional independence of miscibilities determined using the VIT technique, due to varying gas-oil ratios in the feed mixtures. Since interfacial tensions are found to be independent of gas-oil ratio, all the interfacial tensions measured at each pressure for the two gas-oil ratios are fitted using linear regression to determine miscibility using the VIT technique. The IFT measurements were fitted against pressure using a hyperbolic function in this particular gas-oil system as shown in Figure 2.3. This function was used especially to fit the curvature to the data due to almost one order of magnitude reduction in IFT observed near miscibility. A good linear relationship between IFT and the reciprocal pressure can be seen in Figure 2.3 with a determination coefficient (R^2) of 98.4%. The regression equation obtained is also shown in Figure 3. This regression equation is then extrapolated to zero IFT to determine MMP. A miscibility pressure of 1760 psig was obtained with the VIT technique, which agrees well with the miscibility pressure of 1700 psia reported from the slim-tube, phase diagram and analytical models. Thus, this VIT experiment conducted using the standard gas-oil system of live decane-CO_2 at 160^{o}F once again validates the VIT technique to measure fluid-fluid miscibility in gas-oil systems.

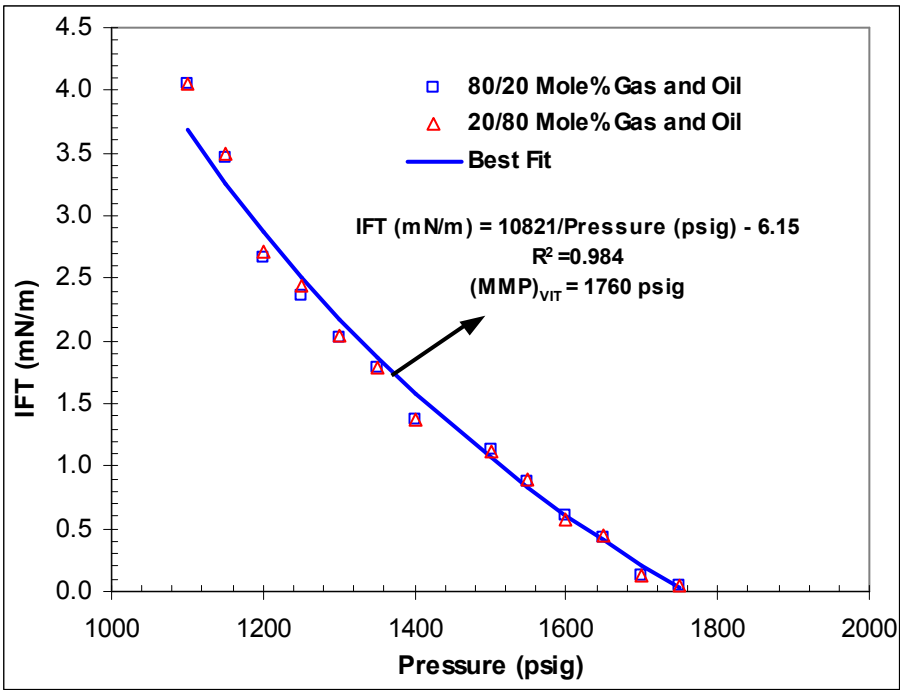

Figure 2.3: Effect of Gas-Oil Ratio on VIT Miscibility in Live Decane-CO_2 System at 160°F

Effect of Gas-Oil Ratio on Dynamic Interfacial Tension. The effect of gas-oil ratio on dynamic interfacial tension was studied by measuring the changes in capillary rise heights with time in the live decane-CO_2 system at 1100 psig and 160°F. The two gas-oil ratios of 20/80 mole% gas and oil and 80/20 mole% gas and oil were used. The densities of oil and gas phases required for dynamic interfacial tension calculations were obtained by fitting linear trend equations to the initial and equilibrated fluid phase densities as shown in Figure 2.4. The initial fluid phase densities are the densities of the pure fluid phases, while the equilibrated fluid phase densities are the densities of fluid phases that were measured during the previously reported interfacial tension measurements after allowing an aging period of about one-hour for saturation of fluid phases. The variations in capillary rise heights and fluid phase densities with time and the resulting dynamic interfacial tensions at both the gas-oil ratios used are summarized in Table 2.6. From Table 2.6, it can be seen that much of the changes in capillary rise heights were observed in the first one-hour for both the gas-oil ratios and hence it is reasonable to assume that the changes in fluid phase densities after one-hour is also negligible. Therefore, the fluid phase densities were assumed to be unchanged after one-hour during the dynamic interfacial tension calculations. The effect of gas-oil ratio on dynamic interfacial tension is shown in Figure 2.4.

Table 2.6: Variations in Fluid Phase Densities, Capillary Rise Heights, Interfacial Tensions with Time in Live Decane-CO_2 System at 1100 psig and 160^oF

Time (min)	Fluid Phase Densities (gm/cc)		80/20 Mole% Gas and Oil		20/80 Mole% Gas and Oil	
	Oil	Gas	Capillary Rise (mm)	IFT (mN/m)	Capillary Rise (mm)	IFT (mN/m)
1.0	0.6509	0.1717	4.92	5.78	4.74	5.57
2.0	0.6509	0.1734	-	-	4.65	5.45
3.0	0.6508	0.1751	4.83	5.63	4.64	5.40
4.0	0.6508	0.1768	4.78	5.55	4.60	5.34
5.0	0.6508	0.1785	4.74	5.49	4.58	5.30
5.5	0.6508	0.1794	4.71	5.44	-	-
6.0	0.6508	0.1802	4.67	5.39	-	-
6.5	0.6508	0.1811	4.65	5.36	-	-
7.0	0.6508	0.1819	4.64	5.33	-	-
8.0	0.6507	0.1836	4.60	5.27	4.55	5.21
9.0	0.6507	0.1853	4.58	5.23	-	-
10.0	0.6507	0.1870	4.57	5.19	4.50	5.11
12.0	0.4478	0.6507	-	-	4.48	5.05
13.0	0.6506	0.1921	4.55	5.11	-	-
15.0	0.6506	0.1955	4.53	5.05	4.46	4.97
20.0	0.6505	0.2040	4.51	4.94	4.42	4.84
30.0	0.6503	0.2210	4.48	4.71	4.41	4.64
60.0	0.6497	0.2720	4.46	4.13	4.39	4.06
120.0	0.6497	0.2720	4.44	4.11	4.39	4.06
360.0	0.4389	0.6497	-	-	4.39	4.06
720.0	0.6497	0.2720	4.42	4.09	4.37	4.05
1440.0	0.6497	0.2720	4.41	4.08	4.37	4.05
2880.0	0.6497	0.2720	4.39	4.06	4.37	4.05
4320.0	0.6497	0.2720	4.39	4.06	4.37	4.05
5760.0	0.6497	0.2720	4.39	4.06	4.37	4.05

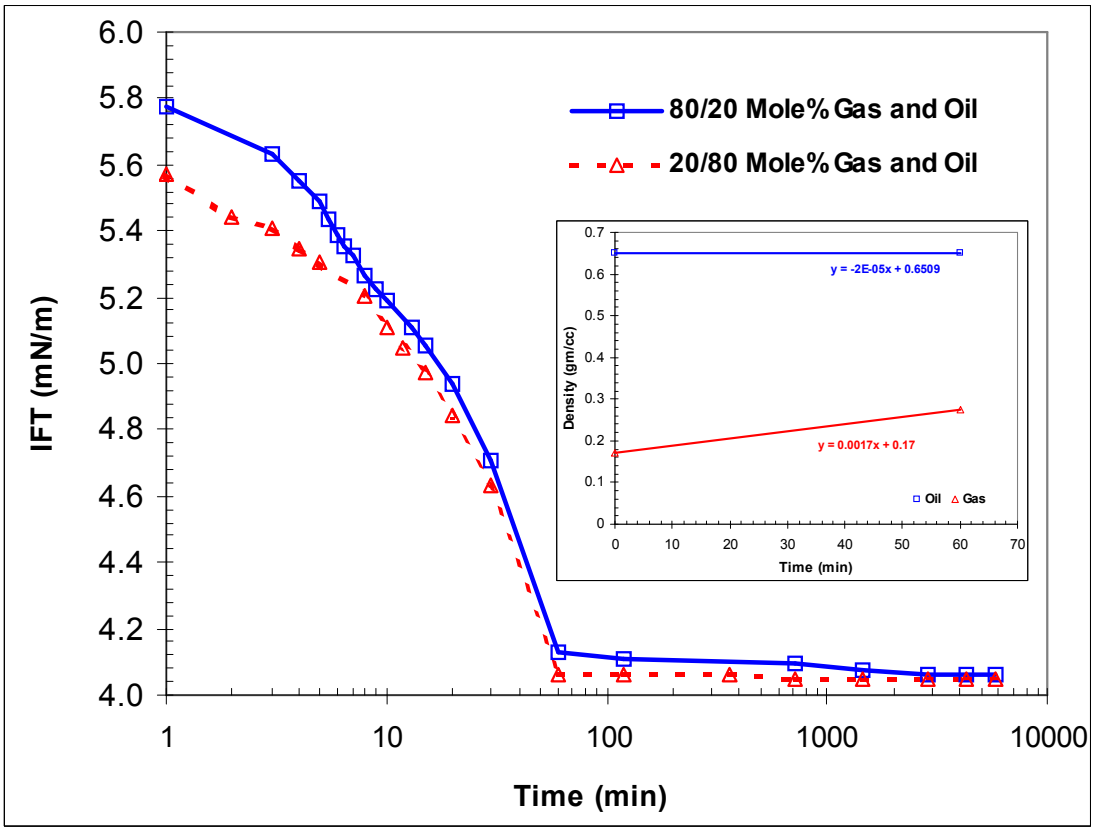

Figure 2.4: Effect of Gas-Oil Ratio on Dynamic Interfacial Tension in Live Decane-CO_2 System at 160°F and 1100 psig

From Figure 2.4, the dynamic nature of interfacial tension can be clearly seen at both the gas-oil ratios used. The interfacial tension is gradually decreasing with time for both the gas-oil ratios due to mass transfer interactions taking place between the fluid phases to reach the thermodynamic equilibrium. The dynamic nature of interfacial tension in multicomponent systems was first discovered experimentally by Plateau about five decades ago (Sternling and Scriven, 1959).

As can be seen in Figure 2.4, the changes in interfacial tension with time are much more rapid at 20/80 gas-oil ratio, when compared to 80/20 gas-oil ratio. The influence of changes in interfacial tension has more pronounced effects on mass transfer rates than the effect of variations in the static properties such as density, viscosity and diffusivity (Zuiderweg and Harmens, 1958). Therefore, the rapid changes in interfacial tension observed at 20/80 gas-oil ratio can be attributed to higher mass transfer rates between the two fluid phases. The possible reasons for the higher mass transfer rates at 20/80 gas-oil ratio in the feed mixture are as explained below.

The live decane contains significant amount of lighter components (55 mole% n-C_1 and n-C_4), which more easily tend to diffuse from oil to gas phase. Hence, the components n-C_1 and n-C_4 in oil can be considered as solutes for mass transfer between

oil and gas phases. At 20/80 gas-oil ratio, higher amounts of lighter components (solute) are available in oil to initiate the mass transfer and hence higher mass transfer rates to saturate the low amount of available gas, thereby resulting in quicker thermodynamic equilibrium. However, near thermodynamic equilibrium, the interfacial tensions become almost similar for both the gas-oil ratios used. This clearly indicates that when both the fluid phases approach equilibrium, interfacial tension becomes independent of gas-oil ratio. Thus the gas-oil ratio in the feed mixture has little or no effect on near equilibrium IFT values, but it determines the rate at which the thermodynamic equilibrium state is attained. In other words, gas-oil ratio has an impact on how fast the thermodynamic equilibrium can be reached when two immiscible fluid phases containing multiple components are brought into contact with each other. The following important observations can also be made from the dynamic interfacial tension measurements reported in Figure 2.4.

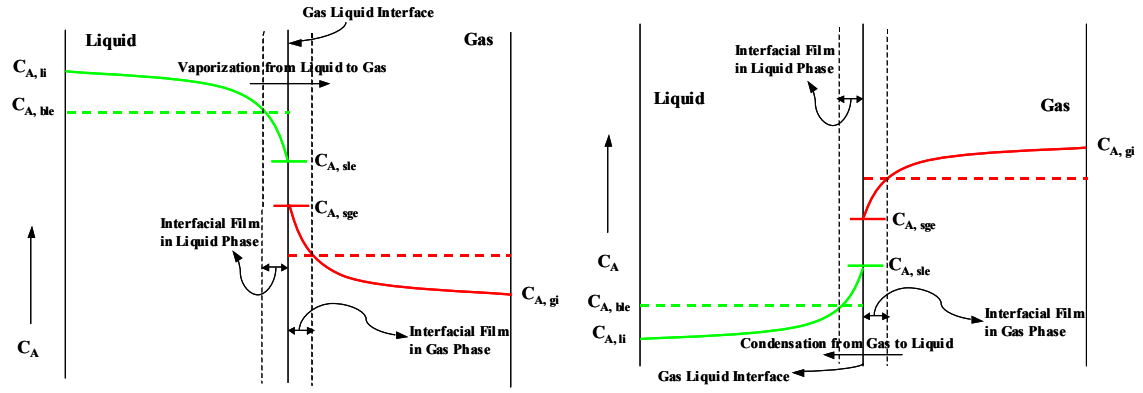

(a) Vaporizing Mode Mass Transfer **(b) Condensing Mode Mass Transfer**

Figure 2.5: Concentration Profiles of a Diffusing Component in Gas-Liquid Systems in Vaporizing and Condensing Modes

The interfacial tension first decreases rapidly with time up to 60 minutes for both the gas-oil ratios used. For 20/80 gas-oil ratio, much smaller changes in IFT were observed from 60-700 minutes and then IFT becomes almost constant after 700 minutes. However, for 80/20 gas-oil ratio, much smaller changes in IFT were observed until 3000 minutes and then it appeared to stay constant. This dynamic behavior of interfacial tension can be well understood using the schematic diagram of solute concentration profiles shown in Figure 2.5. Figure 2.5 depicts the changes in the concentration profile of a diffusing component in the bulk liquid, bulk vapor and at the interface due to mass transfer between the liquid and vapor phases in both vaporizing and condensing modes of mass transfer in a gas liquid system.

The initial concentrations of the diffusing component A in gas and liquid phases are $C_{A,gi}$ and $C_{A,li}$, respectively. In the vaporizing drive mechanism, mass transfer of component A takes place from liquid to gas by vaporization and in condensing mechanism, mass transfer of component A takes place from gas to liquid by condensation. In both these modes of mass transfer, the component A quickly reaches its equilibrium composition within the gas-liquid interfacial film due to the large concentration gradient of the diffusing component existing in the film on either side of the interface. Hence there will be less resistance to mass transfer within this film and $C_{A,sge}$ and $C_{A,sle}$ represent the equilibrium compositions of component A in the gas and liquid phases, respectively, at the interfacial film. However, the equilibrium compositions of the component A within the interfacial film are different from the equilibrium compositions of component A in the bulk liquid and vapor phases, $C_{A,ble}$ and $C_{A,bge}$, respectively. As a result, prolonged intra-phase mass transfer of component A takes place within the bulk fluid phases due to the small concentration gradient for much longer times to attain ultimate thermodynamic equilibrium in gas-liquid systems. The rapid mass transfer interactions of the diffusing components occurring within the interfacial film have significantly higher degree of influence on interfacial tension at the gas-liquid interface when compared to much slower mass transfer interactions taking place in the bulk fluid phases. These dynamic effects of interfacial tension will be especially significant in the complex hydrocarbon systems consisting of multicomponent crude oil and gas phases as crude oils contain thousands of chemical compounds (McCain, 1990). The one-hour aging period used during the interfacial tension measurements of standard gas-oil systems in this study accounted for nearly 99.5-99.7% of the equilibrium value, as shown in Figure 4 and thereby resulting in accurate measurements of gas-oil miscibility.

2.1.1.6 Summary and Conclusions

Interfacial tensions have been measured in two standard gas-oil systems of n-decane-CO_2 at 100^{o}F and live decane-CO_2 at 160^{o}F to calibrate VIT technique for gas-oil miscibility determination, using the pendent drop and capillary rise techniques. We believe that this is the first attempt to successfully adapt capillary rise technique for low interfacial tension measurements in complex gas-oil systems at elevated pressures and temperatures. The use of capillary rise technique in the present study has enabled us to measure low gas-oil interfacial tensions down to 0.04 mN/m, while the lowest gas-oil IFT measured with the conventional pendent drop shape analysis technique was about 0.6 mN/m. This has further enabled better accuracy in miscibility determination using the VIT technique.

For n-decane-CO_2 system at 100^{o}F, the minimum miscibility pressure of 1150 psig obtained from VIT experiments matched well with the reported miscibilities from slim-tube (1250 psig) and rising bubble (1280 psig) measurement techniques. A VIT minimum miscibility pressure of 1760 psig has been obtained in live decane-CO_2 system at 160^{o}F,

which also agreed well with the reported miscibilities of 1700 psia from phase diagram, slim-tube and analytical models. The close agreement of VIT miscibilities obtained in these two standard gas-oil systems clearly validates the new vanishing interfacial tension (VIT) technique to determine miscibility conditions in gas-oil systems.

As the fluid phases approached equilibrium, the interfacial tension is found to be unaffected by gas-oil ratio in both the standard gas-oil systems studied. Though gas-oil ratio has no effect on near equilibrium interfacial tension, it is found to have an impact on mass transfer rates that determine the duration needed for attaining the mass transfer equilibrium between the two phases. This experimental study has also pointed out the compositional path independence of the miscibilities determined using the VIT technique by varying the ratio of phases in the feed. Thus this experimental study conducted using standard gas-oil systems at elevated pressures and temperatures answers all the concerns expressed about the VIT technique and thereby strongly encourages the wide use of this technique for confident characterization of gas-oil miscibility conditions in an accurate, easy, quick and cost-effective manner for improved oil recovery field applications.

2.1.2 VIT Experiment in a Standard Ternary Liquid System

2.1.2.1 Introduction

The literature reviewed on solubility, miscibility, and their relation to IFT in ternary fluid systems are discussed in this section. The terms, miscibility, solubility and interfacial tension, are commonly used in phase behavior studies of ternary fluid systems. Review of literature shows that zero interfacial tension is a necessary and sufficient condition to attain miscibility (Benham et al., 1965; Stalkup, 1983; Holm, 1987; Lake, 1989).

Blanco et al. (1996) measured vapor-liquid equilibrium data at 141.3 kPa for the mixtures of methanol with n-pentane and n-hexane and then determined upper critical solubility for methanol, n-hexane mixtures from the measured miscibility data. This intuitively suggests the relationship of miscibility with upper critical solubility of a solute in solvent for ternary fluid systems. Lee (1999) modified the adsorption model proposed by van Oss et al. (1987) by the inclusion of equilibrium spreading pressure to calculate the liquid-liquid interfacial tension. This study related equilibrium interfacial film pressure and the interfacial tension for prediction of miscibility of liquids and also pointed out that the theory of miscibility of liquids can be applicable to the solubility of a solute in a solvent.

Fleming and Vinatieri (1981) explored the role of critical phenomena in oil recovery systems using surfactants. They found that for a surfactant system consisting of three phases, an aqueous phase, a microemulsion phase, and an oil phase, the interfacial tensions occurring in the neighborhood of the optimal salinity are associated with the critical end-points of aqueous phase-microemulsion and oil phase-microemulsion. They

were able to quantitatively describe the behavior of the other physical properties such as electrical conductivities, densities, viscosities, and compositions of the phases in terms of these critical-end points. They also concluded that these critical-end points influence the low interfacial tensions approaching the point of criticality where the interfacial tensions between the two phases vanish.

Huang and Kim (1985) investigated various thermodynamic paths through which a critical point can be reached in a microemulsion consisting of three components. The microemulsion studied consisted of 3% sodium di-2-ethyl-hexylsulfosuccinate (AOT), 5% distilled water and 92% n-decane. The different thermodynamic variables considered were temperature, oil composition, alkyl carbon chain length of oil and the salinity. The results showed the power law dependence of the thermodynamic singularity (correlation length) occurring near the critical point on all the reduced thermodynamic variables with a similar power law exponent (≈ 0.75). They called this power law exponent as the critical index, which describes the divergence of correlation length near the critical point. Based on these results, the authors concluded that the critical point of a microemulsion could be approached through different thermodynamic paths, but all of them would result in an apparently identical critical index.

Donahue and Bartell (1952) utilized the data on interfacial tensions and reciprocal solubilities for 31 water-organic systems at the same temperature (25^{o}C) to develop an empirical correlation between the solubility and the interfacial tension. They defined a quantity called "degree of miscibility (DM)", which is the sum of the mole fraction of water in the organic phase and the mole fraction of the organic liquid in the aqueous phase. They found an empirical relationship between the interfacial tension and logarithm of degree of miscibility. Glinski et al. (1994) later revisited the data of Donhue and Bartell (1952) to obtain the following relationship between interfacial tension and degree of miscibility (DM).

$$\sigma = -16.47 \log DM - 3.83 \quad \text{(2.4)}$$

Where, σ is the interfacial tension in mN/m. Chavepeyer et al. (1993) evaluated the correlation of Donahue and Bartell (1952) for several organic-organic and water-organic systems at different temperatures and found poor correlation of interfacial tension with degree of miscibility. Hence Glinski et al. (1994) supplemented the data of Donahue and Bartell (1952) with more results from their laboratory as well as from the literature and found a correlation between calculated reduced density difference and the logarithm of interfacial tension. Even though this relationship had an explicit shape, it lacked the definite proportionality to develop an empirical correlation.

Interfacial tension (IFT) being a property of the interface between two fluids is strongly dependent on mass transfer interactions occurring between the two fluid phases. The effect of molar ratio of the two fluids (solvent-oil ratio) in the feed mixture on fluid-fluid interfacial tension is rarely studied. Simon et al. (1978) measured the IFT of a

reservoir crude oil in CO_2 gas at various solvent-oil ratios in the feed using a high-pressure interfacial tensiometer. The results from this experimental study indicated strong dependence of IFT on solvent-oil ratio in the feed, in which an increase of IFT was observed with an increase in concentration of CO_2 gas in the feed. Such a dependence of IFT on solvent-oil ratio in the feed indicates the role of mass transfer effects on IFT. This gives raise the need to further explore solvent-oil ratio effects on IFT between fluids so as to clarify the role of mass transfer effects in fluid-fluid phase equilibria.

Thus from the literature reviewed above on solubility, miscibility and their relation to IFT, it is evident that the distinction between the terms miscibility and solubility still appears to be unclear, the correlation of solubility with interfacial tension is not definitive and the role of mass transfer effects on IFT at varying solvent-oil ratios needs to be explored. Moreover, further development of VIT technique is required in standard ternary liquid systems to enable the wide acceptance of this promising technique by the oil industry.

2.1.2.2 Objectives

The objectives are to correlate miscibility and solubility with interfacial tension, to study the solvent-oil ratio effects on IFT, and to investigate the applicability of the new VIT technique to determine the miscibility in ternary liquid systems. For this purpose, the standard ternary liquid system of ethanol, water and benzene is chosen since their phase behavior and solubility data are readily available (Chang and Moulton, 1953; Sidgwick and Spurrel, 1920). The IFT measurements were carried out using the drop shape analysis (Kruss, 2000) and capillary rise techniques. All the interfacial tension measurements reported in this study were conducted at atmospheric pressure and room temperature (23^oC).

2.1.2.3 Experimental Details

Reagents. Analytic grade reagents were used in the experiments. Benzene used in the experiments was from Fisher Scientific, having a purity of greater than 99%. Ethyl alcohol was from Aaper Alcohol and Chemical Company with a purity > 95%. Deionized water, from Water Quality Laboratory at Louisiana State University, was used. Acetone of purity 99.7%, from Fisher Scientific was used for cleaning the experimental apparatus.

Experimental Setup and Procedure. The schematic of the experimental setup used for IFT measurements using the drop shape analysis (DSA) technique is shown in Figure 2.6.

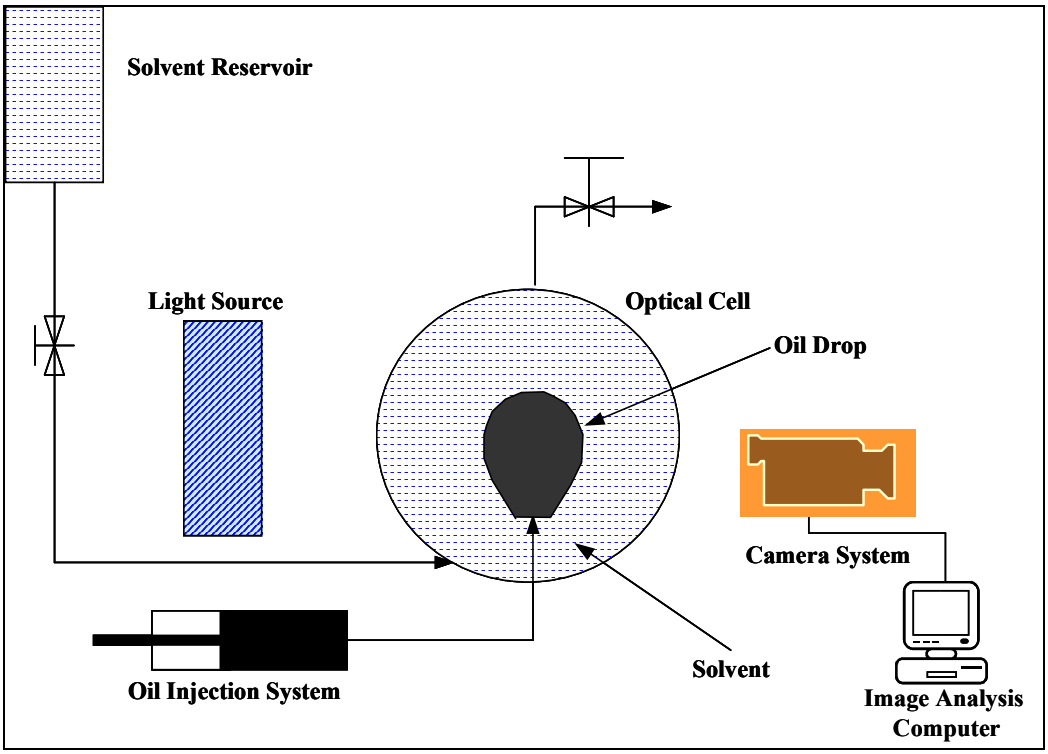

Figure 2.6: Schematic of the Experimental Setup Used for Pendent Drop IFT Measurements Using DSA Technique

It consisted of an optical cell, solvent reservoir, injection system to inject oil, light source and a camera system connected to a computer for image capture and analysis. Different molar solutions of ethanol and water were prepared using the desired volumetric percentages. These solutions were used as the non-equilibrated solvents in the experiments. For preparation of solvent solutions pre-equilibrated with benzene to study the benzene dissolution effects in aqueous ethanol and for equilibrium contact angle measurements, 1000 ml of the non-equilibrated solvent was taken in a glass flask and measured volume of benzene, slightly above the solubility limit corresponding to that solvent composition, was poured into the flask. The flask was tightly closed and rigorously mixed for 12 hours. After mixing, the solution was filtered to remove the formed oil-solvent emulsion drop-lets, using hardened ashless Whatman filter paper. Then, the filtered solution was allowed to settle for another 12 hours. Afterwards, the pre-equilibrated benzene and solvent phases of the solution were carefully collected and stored. The optical cell is first cleaned with deionized water and then with acetone. The non-equilibrated solvent is taken in a container (solvent reservoir), which was kept at a sufficient height to allow flow by gravity. The cell was gradually filled up and some solvent was allowed to drain from the top to ensure that there were no trapped air bubbles in the cell. The benzene is now injected into the cell, using the injection system, drop by drop. A few benzene drops, normally 10-20, were allowed to rise through the solvent and

rest at the top of the cell to allow for equilibration of the fluid phases. Now, a benzene drop was allowed to hang from the capillary tip in the pendent drop mode and the drop image is captured on the computer using the camera system. The captured drop image was then analyzed for IFT using the drop shape analysis technique. The volumes of benzene and the solvent in the cell were varied during the experiments to study the solvent-oil ratio effects on interfacial tension measurements. The detailed description of calculation procedure and equations used in pendent drop shape analysis technique to determine IFT is given in Section 2.1.1.4.

At molar concentrations above 40% ethanol enrichment in the aqueous phase, benzene pendent drops could not be formed as the benzene quickly escaped in streaks through the solvent. Therefore, the capillary rise technique was adapted and used to measure the low interfacial tensions occurring at these concentrations. The schematic diagram of the capillary rise technique used is shown in Figure 2.7. In the Figure 2.7 schematic, r is the inner radius of the capillary tube, ρ_o and ρ_l are the densities of oil and solvent phases, respectively, θ is the equilibrium contact angle and h is the capillary rise. More details on capillary rise technique can be seen in Section 2.1.1.4.

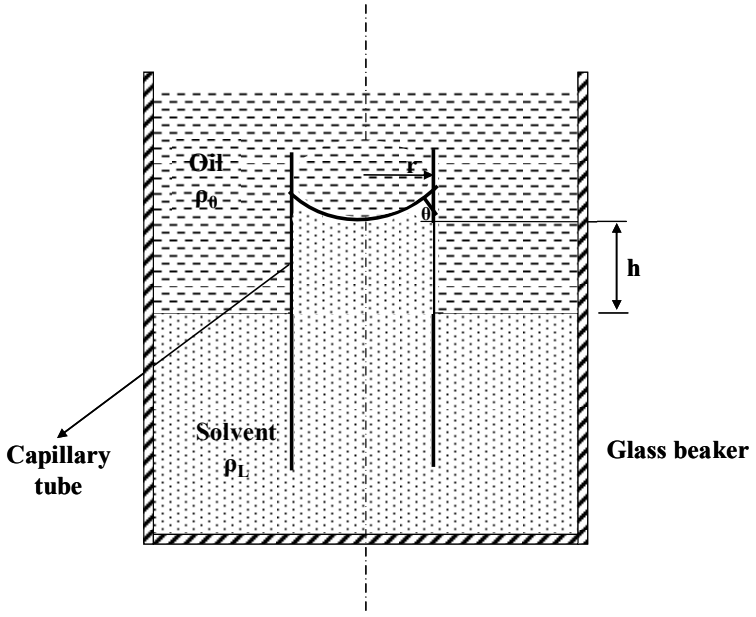

Figure 2.7: Schematic of Capillary Rise Technique Used

At first, certain volume of aqueous ethanol at particular ethanol enrichment above 40 mole% was taken in a glass beaker. Measured volume of benzene about one and one-half times above the solubility limit, was added to the aqueous ethanol. The two fluid phases were thoroughly mixed by shaking and allowed to settle for about one hour. Then, the solution clearly separated into two phases with less denser fluid phase at the top, while the denser fluid phase resting at the bottom. A glass capillary tube (radius r = 0.09 cm)

was then carefully inserted into the beaker using an adjustable stand so that it was completely immersed in the two fluid phases. Sufficient care was taken to avoid the contact of bottom end of the capillary tube with glass beaker. The interface between the fluid phases slowly raised through the capillary and stabilized at a definite height within a time of about 20 minutes. The capillary rise was then measured using a vernier-equipped cathetometer that reads in units of one-tenth of a millimeter. After the capillary rise measurements, the equilibrated aqueous ethanol solvent and benzene were allowed to flow through a PAAR DMA-512 density meter for density measurements.

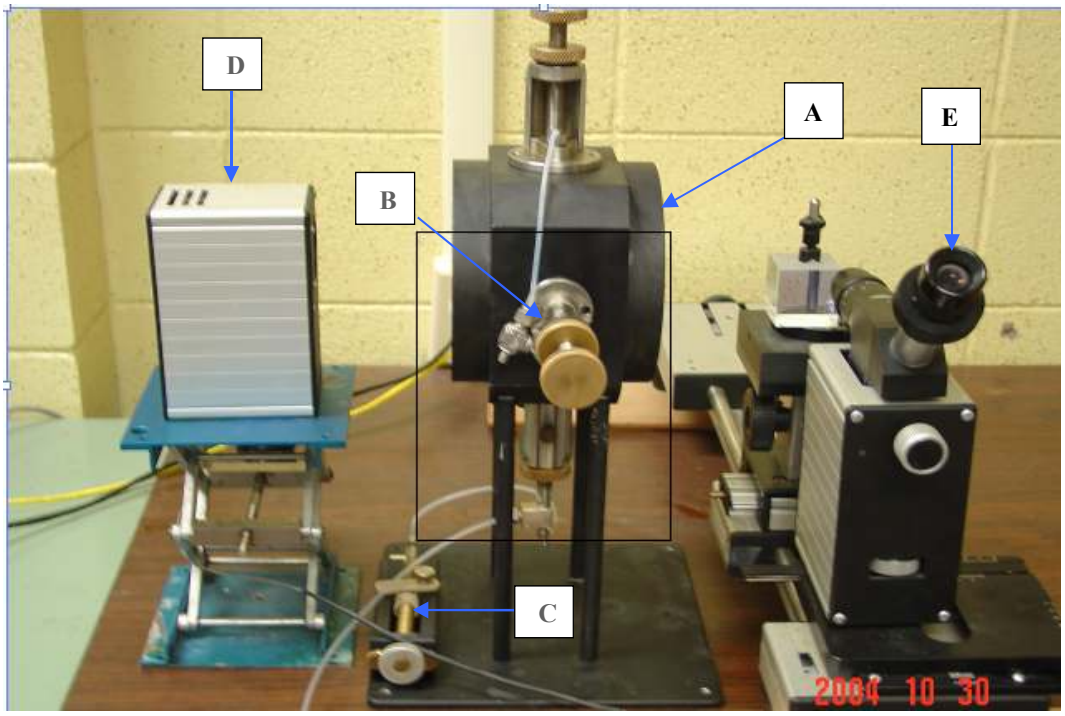

Figure 2.8: Photograph of the Equipment Used for Contact Angle Measurements
(A: Optical cell; B: Crystal holder; C: Injection system, D: Light source; E: Goniometer)

The equilibrium contact angles were measured using an ambient optical cell, pre-equilibrated fluid phases and glass substrates with which the capillary tubes were made. The photograph of the equipment used for equilibrium contact angle measurements is shown in Figure 2.8 and is described elsewhere (Vijapurapu and Rao, 2003). The procedure used for benzene equilibrium contact angle measurements was as followed. The glass substrate was first aged in pre-equilibrated aqueous ethanol solvent for about 24 hours. The aged glass substrate was then placed in a crystal holder and assembled carefully into the thoroughly cleaned optical cell. The pre-equilibrated aqueous ethanol solvent was taken in a large container kept at a sufficient height and allowed to flow into the cell by gravity. After the cell was filled, some solvent was allowed to drain from the top to ensure the removal of trapped air bubbles in the cell. Then, the pre-equilibrated

benzene drop was placed on the glass crystal using an injection syringe from the bottom of the cell. The cell was then set-aside with all the valves closed to age for 24 hours for the solvent-oil-crystal interactions to reach equilibrium. After 24 hours of aging, the equilibrium contact angle was measured using an eye-piece goniometer and light source. The interfacial tension is then calculated using the Eq. (3).

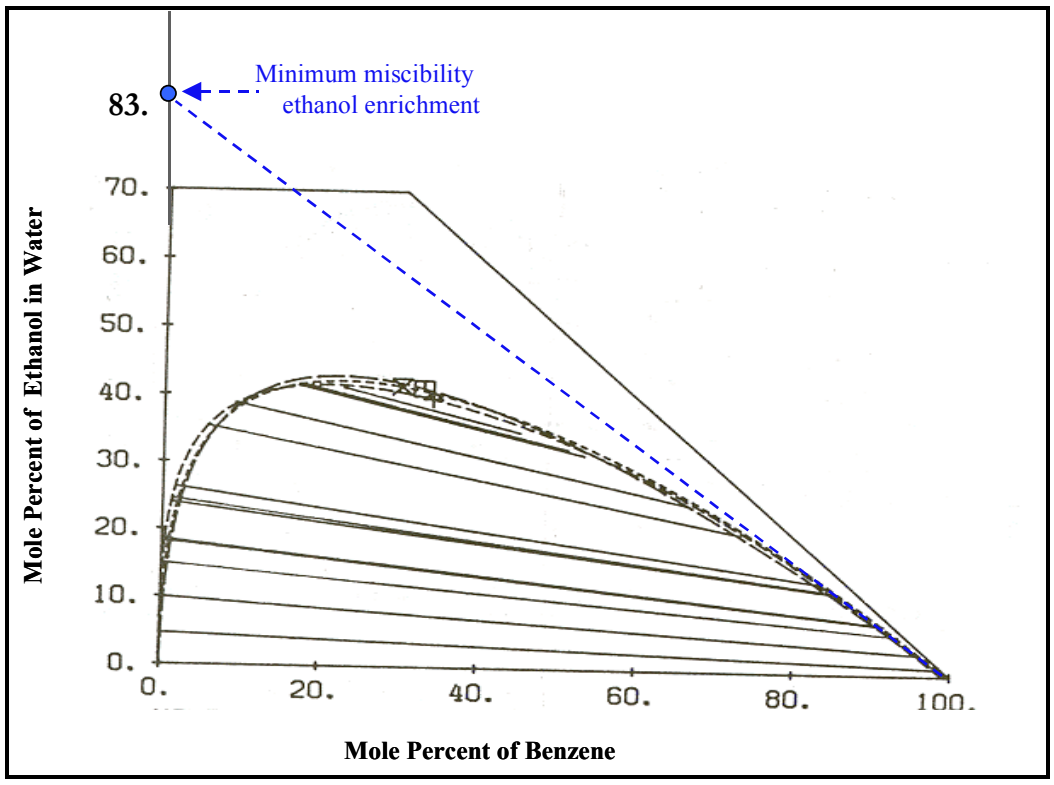

Figure 2.9: Phase Diagram of Benzene, Ethanol and Water Ternary System (After Chang and Moulton, 1953)

2.1.2.4 Results and Discussion

Miscibility and Solubility. The ternary phase diagram of the standard system of ethanol, water and benzene (Chang and Moulton, 1953) is shown in Figure 2.9. From the ternary phase diagram of Figure 2.9, it can be seen that the limiting tie-line passing through the oil (benzene) intersects the solvent (aqueous ethanol) at an ethanol enrichment of 83 mole% in aqueous phase. Hence, this becomes the minimum miscibility ethanol enrichment for the system to attain miscibility, since at any ethanol enrichment lower than this, the tie-line would pass through the two-phase envelope indicating the presence of two phases in equilibrium. The solubility of benzene in aqueous ethanol at various ethanol enrichments (Sidgwick and Spurrel, 1920) is given in Table 2.7 and shown in Figure 2.10. From the Table 2.7 and Figure 2.10, the following important observations can be made.

Table 2.7: Solubility of Benzene in Water at Various Ethanol Enrichments (Data from Sidgwick and Spurrel, 1920)

Solvent (Mole%)		Benzene Solubility
Ethanol	Water	(gms/liter)
34.8	65.2	134.3
46.6	53.4	343.2
53.3	46.7	629.1
61.2	38.8	1284.6
70.6	29.4	2351.6
78.0	22.0	5760.1

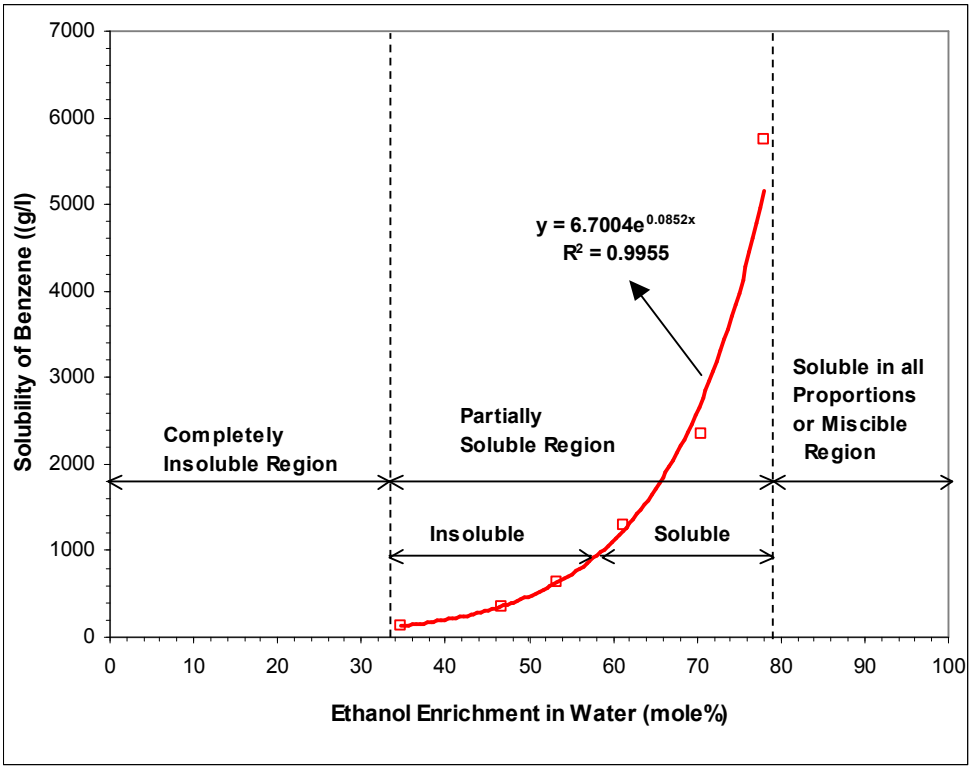

Figure 2.10: Solubility of Benzene in Water at Various Ethanol Enrichments (Using the Data from Sidgwick and Spurrel, 1920)

The solubility of benzene in aqueous ethanol begins at an ethanol enrichment of 35 mole% and then gradually increases to become completely soluble at about 78 mole% ethanol enrichment, exhibiting an exponential relationship between solubility and enrichment. As shown in Figure 2.10, the solubility characteristics can be divided into three regions: (1) Region 1 exists at ethanol enrichments below 35 mole%, where benzene is completely insoluble; (2) Region 2 exists at ethanol enrichments between 35 mole% and 78 mole%, where benzene is partially soluble. In this region, below the

solubility curve, benzene is completely soluble, whereas above the solubility curve, benzene is insoluble and (3) Region 3 exists at ethanol enrichments above 78 mole%, where benzene is soluble in all proportions and hence this can be called as the miscible region. Thus the minimum miscibility ethanol enrichments for this standard ternary fluid system by both the phase diagram (83 mole%) and the solubility data (>78 mole%) appear to be in good agreement.

IFT Measurements Using DSA Technique and Solvent-Oil Ratio Effects on IFT. At first, a calibration IFT experiment was conducted using the DSA technique for a known standard fluid pair of n-decane and water. An IFT value of 49.0 ± 0.15 mN/m was obtained, which is in good agreement with the published value of 50.5 mN/m reported by Jennings (1967). Then, different molar feed compositions corresponding to 0, 10 and 40 volume% oil in the solvent were used to study the solvent-oil ratio effects on IFT. The interfacial tensions between the fluids could not be measured above 40 mole% ethanol enrichment in aqueous phase, using the DSA technique. At these higher ethanol enrichments, pendent drops could not be formed as the oil quickly escaped in streaks through the solvent. All the measured IFT experimental data between the fluids at different ethanol enrichments in aqueous phase and at different solvent-oil ratios in aqueous ethanol-benzene feed mixtures are summarized in Table 2.8 and shown in Figure 2.11. The small standard deviations in the range of 0.03 to 0.11 obtained in measured IFT values indicate extremely low variation in the measurements. The summary of important observations from Table 2.8 and Figure 2.11 are as followed.

The IFT gradually decreases as the ethanol enrichment increases in aqueous phase. At ethanol enrichments up to 20 mole% in aqueous phase, IFT is found to be independent of solvent-oil ratio in the feed. However, at ethanol enrichments above 30 mole% in aqueous phase, a small increase in IFT is observed as the solvent-oil ratio in feed is decreased. The increase of IFT with decrease in solvent-oil ratio is low at 30 mole% ethanol enrichment and then becomes noticeable at 40 mole% ethanol enrichment in aqueous phase. The primary reasons responsible for the observed solvent-oil ratio effects on IFT are as discussed below.

As can be seen in Table 2.7 and Figure 2.10, benzene solubility in aqueous ethanol starts at 35 mole% ethanol enrichment and then gradually increases to become completely soluble at 78 mole% ethanol enrichment in aqueous phase. Hence solubility of benzene in aqueous ethanol does not come into picture during the IFT measurements in insoluble regions at ethanol enrichments below 35 mole%. Hence, absence of solvent-oil ratio effects on IFT is observed at ethanol enrichments below 30 mole% in aqueous phase. At ethanol enrichments above 30 mole% in aqueous phase, leaving of 10-20 drops of benzene in aqueous ethanol as well as different molar percentages of benzene used in

Table 2.8: Measured Benzene Interfacial Tensions in Aqueous Ethanol at Various Ethanol Enrichments and Feed Compositions using DSA Technique

Solvent (Mole%)		Feed Composition (Mole%)		Benzene IFT
Ethanol	Water	Solvent	Benzene	(mN/m)
0	100	100.0	0.0	32.58 ± 0.110
		97.8	2.2	32.59 ± 0.030
		88.0	12.0	32.62 ± 0.030
10	90	100.0	0.0	12.11 ± 0.110
		97.4	2.6	12.11 ± 0.060
		86.2	13.8	12.16 ± 0.045
20	80	100.0	0.0	4.85 ± 0.064
		97.0	3.0	4.84 ± 0.080
		84.4	15.6	5.00 ± 0.050
30	70	100.0	0.0	2.30 ± 0.035
		96.6	3.4	2.31 ± 0.040
		82.5	17.5	2.62 ± 0.030
40	60	100.0	0.0	1.23 ± 0.052
		96.2	3.8	1.41 ± 0.050
		80.7	19.3	1.99 ± 0.048

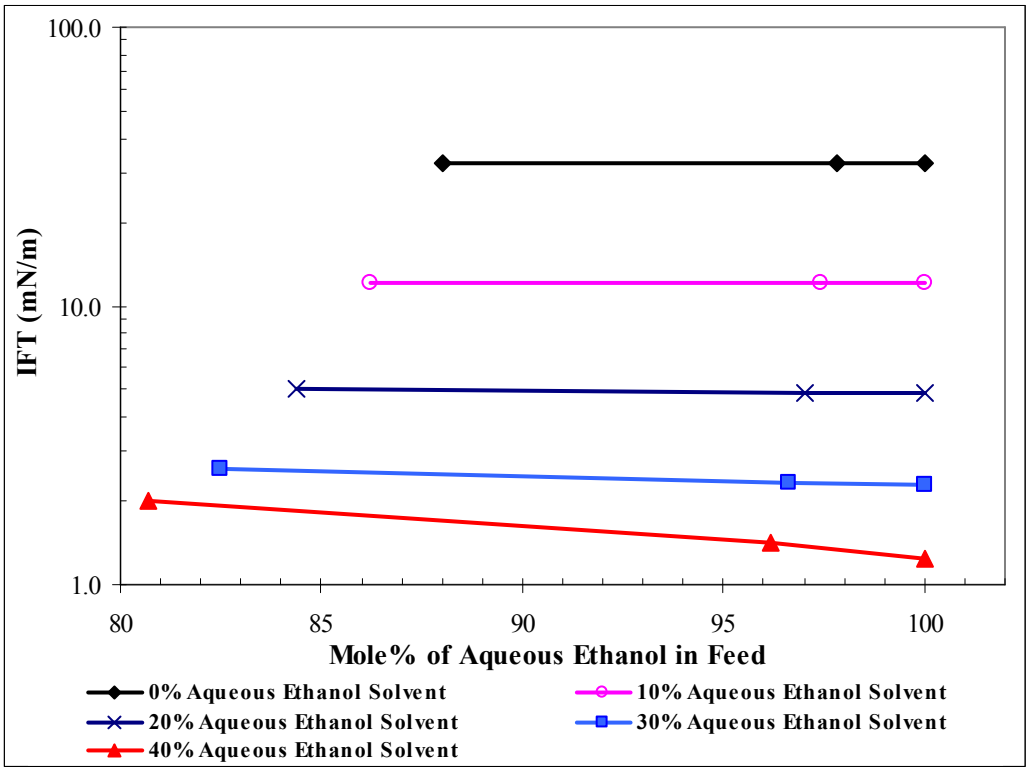

Figure 2.11: Effect of Solvent-Oil Ratio on IFT in Feed Mixtures of Benzene (Oil) and Aqueous Ethanol (Solvent)

the feed mixture are not sufficient to provide the complete equilibration of fluid phases so as to reach the solubility limit. As a result, the dissolution of benzene in aqueous ethanol interferes with IFT measurements due to varying amounts of benzene at different solvent-oil ratios in the feed mixture. This is probably the reason for small dependence of IFT on feed solvent-oil ratio observed in partially soluble regions at ethanol enrichments above 30 mole% in aqueous phase.

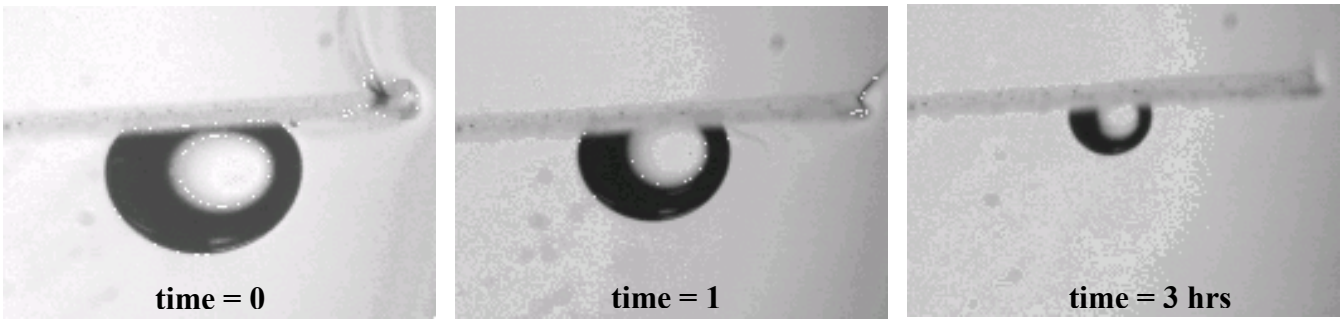

Figure 2.12: Photographs Showing the Effect of Benzene Dissolution in Non-Equilibrated Aqueous Ethanol Solvent at 30 Mole% Ethanol Enrichment

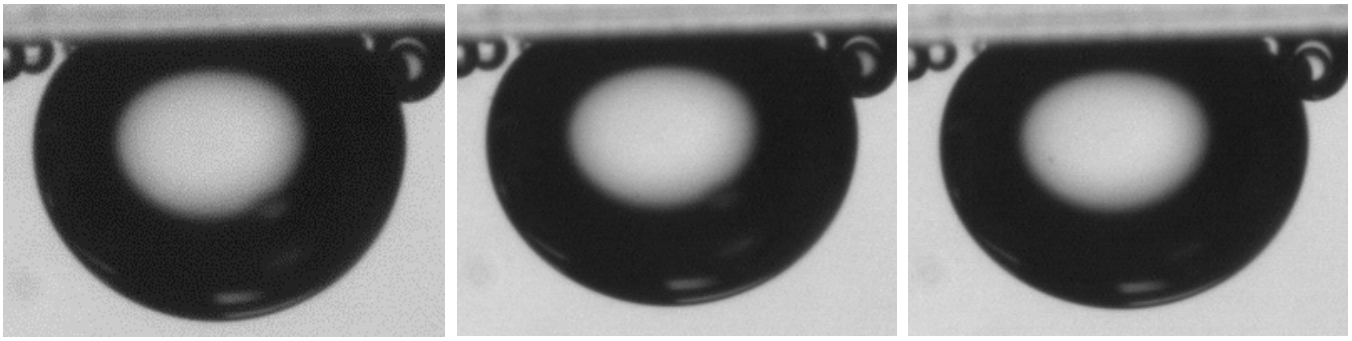

Figure 2.13: Photographs Showing the Absence of Benzene Dissolution in Pre-Equilibrated Aqueous Ethanol Solvent at 30 Mole% Ethanol Enrichment

The benzene solubility effects observed in aqueous ethanol in partially soluble regions at ethanol enrichments above 30 mole% can be removed by providing complete equilibration between benzene and aqueous ethanol solvent during IFT measurements. Figures 2.12 and 2.13 demonstrate the effects of benzene solubility on benzene drop size in non-equilibrated and pre-equilibrated 30 mole% aqueous ethanol solvent, respectively. As can be seen in Figure 2.12, benzene drop gradually reduces in size with time and completely vanishes within 4 hours in non-equilibrated aqueous ethanol solvent. This can be attributed to benzene dissolution in non-equilibrated aqueous ethanol. However, contrarily, absence of benzene solubility effects in aqueous ethanol pre-equilibrated with

benzene can be seen in Figure 2.13. The benzene drop is able to retain its original size and shape in the solvent even after 4.5 hours. These observations of Figures 2.12 and 2.13 clearly suggest that compositional effects on IFT in partially soluble regions are due to the absence of complete saturation between the fluid phases during the experiments. Thus the smaller IFT dependence on feed solvent-oil ratio observed with non-equilibrated fluids in partially soluble regions (Table 2.8 and Figure 2.11) appears to be due to benzene dissolution in aqueous ethanol. Hence pre-equilibrated solutions must be used in the partially soluble regions for IFT measurements to incorporate all the mass transfer effects. Equilibrium interfacial tension (which includes all the mass transfer effects) being a thermodynamic state property can be reached through several paths due to varying solvent-oil ratios in the feed, but all of them would result in a unique value. This is somewhat similar to approaching the critical point of a micro-emulsion through different thermodynamic paths with an apparently identical critical index (Huang and Kim, 1985).

IFT Measurements Using Capillary Rise Technique. This technique was adapted to measure low interfacial tensions that could not be measured using drop shape analysis technique at ethanol enrichments above 40 mole% in aqueous phase. At first, this technique was calibrated for a known low IFT standard fluid pair of n-butanol and water, using two different capillary sizes. IFT values of 1.72 and 1.79 mN/m were obtained for inner capillary glass tube radii of 0.09 and 0.025 cm, respectively. These values were in good agreement with the value of 1.8 mN/m reported by Mannhardt (1987) for this standard fluid system.

Table 2.9: Benzene Interfacial tensions in Aqueous Ethanol Solvent at Ethanol Enrichments above 40 Mole% in Aqueous Phase

Ethanol Enrichment (Mole%)	Phase Densities (gm/cc)		Contact Angle (degrees)	Capillary Rise (cm)	IFT (mN/m)
	Solvent	Oil			
50	0.8725	0.8597	25	0.53	0.3301
60	0.8641	0.8579	25	0.59	0.1780
70	0.8612	0.8594	25	0.68	0.0596
75	0.8579	0.8576	25	0.98	0.0143

All the measured capillary heights and the densities of the equilibrated fluid phases using the capillary rise technique at ethanol enrichments above 40 mole% in benzene, ethanol, water standard ternary liquid system are summarized in Table 2.9. From Table 2.9, it can be seen that as the ethanol enrichment in aqueous phase increases from 50 mole% to 75 mole%, the density difference between the fluid phases decreases from 0.0128 gm/cc to 0.0003 gm/cc. Contrarily, an increase in capillary rise from 0.53 cm to

0.98 cm can be seen as the ethanol enrichment in aqueous phase is increased. This indicates an inverse correlation between the density difference and the capillary rise and hence a good precision of IFT measurements can be made even in low IFT regions using this technique due to easily measurable heights in the capillary tube.

Table 2.10: Measured Equilibrium Benzene Contact Angles at Various Ethanol Enrichments in Aqueous Phase

Ethanol Enrichment (Mole%)	Equilibrium Time (hrs)	Benzene Contact Angle (^{o})
0	24	48
10	24	33
20	24	26
30	24	25
40	24	25

The equilibrium benzene contact angles measured for IFT calculations in capillary rise technique at different ethanol enrichments in aqueous phase are given in Table 2.10 and shown in Figure 2.14. From Table 2.10 and Figure 2.14, it can be seen that, the benzene equilibrium contact angles gradually decrease from 48^{o} at 0 mole% ethanol enrichment to 26^{o} at 20 mole% ethanol enrichment in aqueous phase and then remains unchanged (25^{o}) for ethanol enrichments 30 mole% and 40 mole% in aqueous phase. Therefore, it is reasonable to assume that there will be no change in benzene equilibrium contact angles from 25^{o} with ethanol enrichment at ethanol enrichments above 30 mole% in aqueous phase. Hence, an equilibrium contact angle of 25^{o} was used in capillary rise IFT calculations at all ethanol enrichments above 40 mole%, as indicated by the extrapolated line in Figure 2.14. The summary of all the measured parameters used in the IFT calculations of the capillary rise technique at ethanol enrichments above 40 mole% in aqueous phase is shown in Table 2.9. As can be seen in Table 2.9, an IFT value as low as 0.014 mN/m was measured at 75 mole% ethanol enrichment in aqueous phase using the capillary rise technique.

Correlation of Miscibility and Solubility with IFT. The correlation among all the three thermodynamic properties of solubility, miscibility and IFT in the standard ternary liquid system of benzene, ethanol and water is shown in Figure 2.15. The measured benzene interfacial tensions in aqueous ethanol using both the DSA and capillary rise techniques and the reported benzene solubility values are plotted against ethanol enrichment in aqueous phase to correlate solubility, miscibility and IFT.

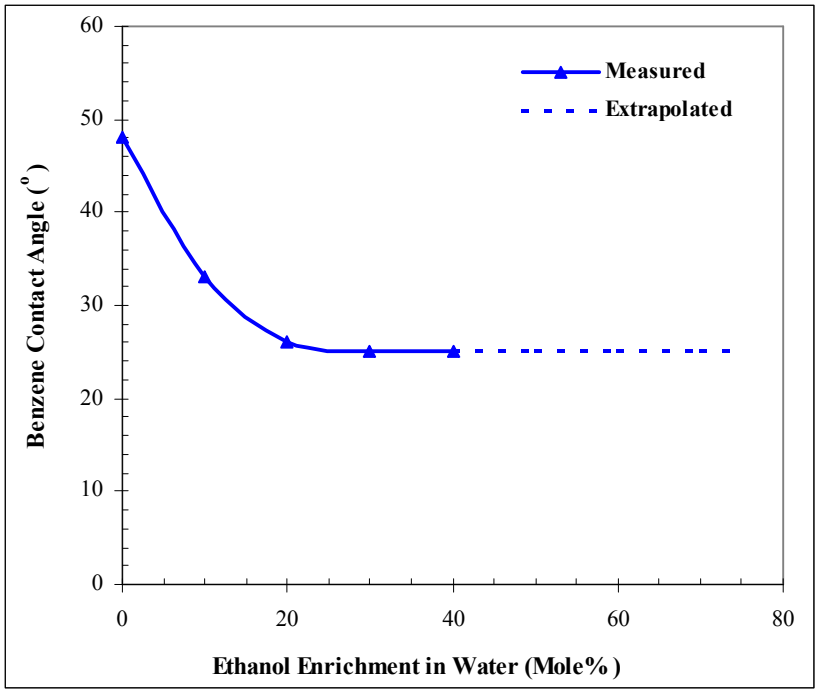

Figure 2.14: Benzene Equilibrium Contact Angles Measured Against Ethanol Enrichment in Aqueous Phase

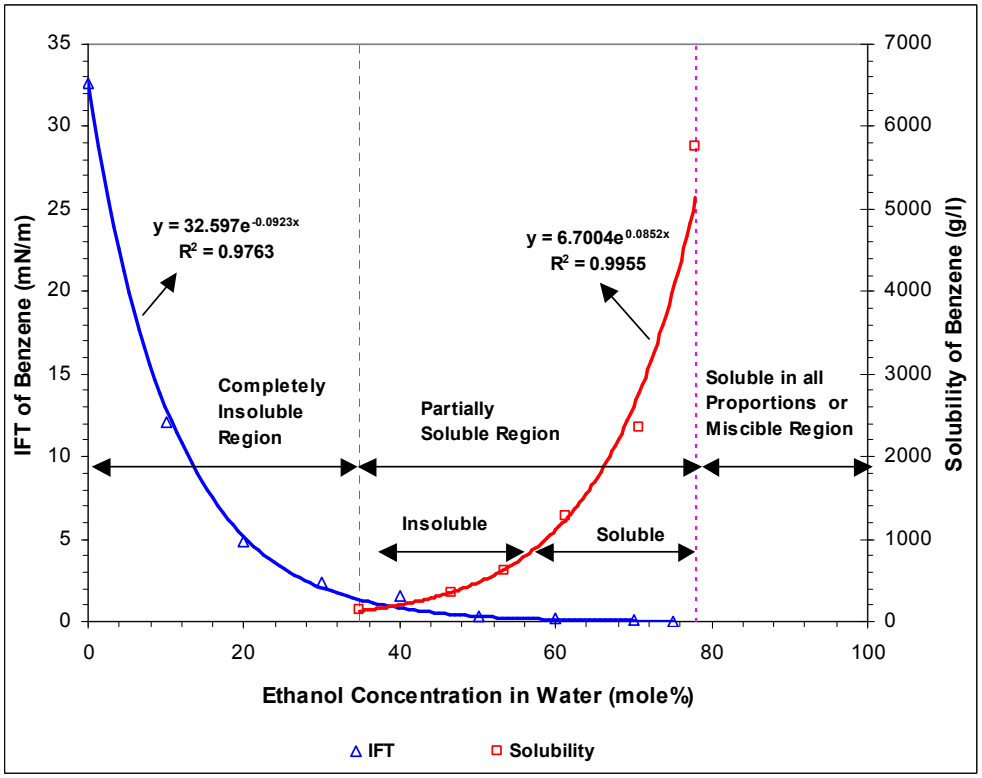

Figure 2.15: Correlation of Solubility and Miscibility with IFT

Since IFT is found to be independent of solvent-oil ratio, the average values of interfacial tensions obtained using DSA technique at each molar concentration for the three solvent-oil ratios are used in the plot. From Figure 2.15, it can be seen that IFT decreases exponentially as the ethanol enrichment in aqueous phase is increased and reduces to a low value of 0.014 mN/m at 75 mole% enrichment, as miscibility is approached. The regression equation obtained is IFT = 32.597 e $^{(-0.0923 * \text{Mole\% of Ethanol})}$ with a coefficient of determination (R^2) = 0.976.

Solubility of benzene is also exponentially correlated to ethanol enrichment by the regression equation, solubility = 6.7004 e $^{(0.0852*\text{Mole\% of Ethanol})}$ with a coefficient of determination (R^2) = 0.995. The positive slope in the exponential relationship between the solubility and ethanol enrichment shows an exponential growth. This is contrary to the negative slope of exponential decay obtained in the exponential correlation between IFT and ethanol enrichment. Furthermore, almost similar absolute values of the slope can be seen in both these exponential regression equations. These observations indicate a possible perfect inverse correlation between solubility and interfacial tension in ternary liquid systems.

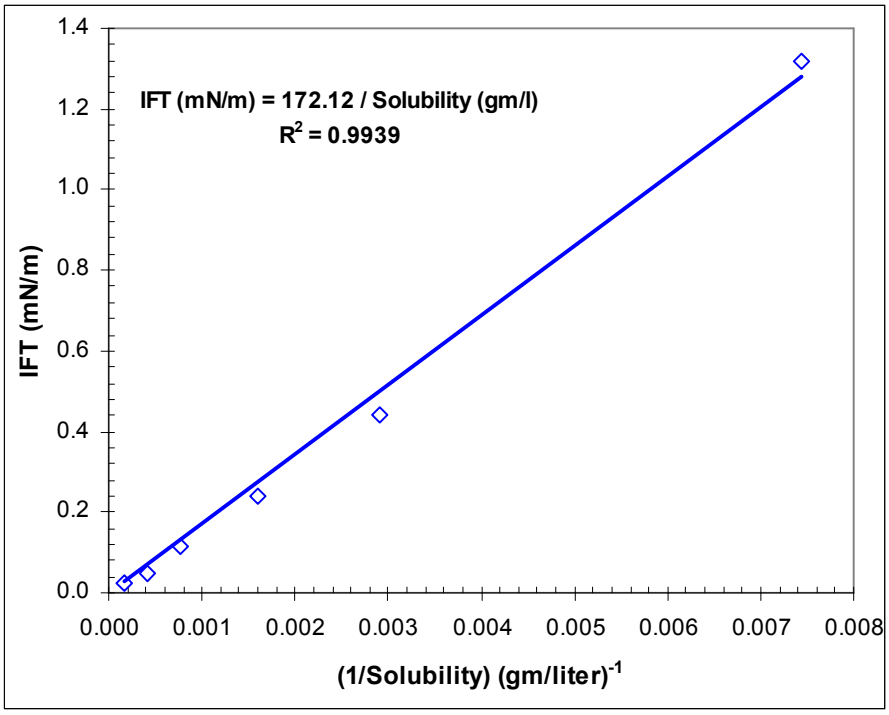

Figure 2.16: Correlation between IFT and Solubility

In order to determine such an inverse correlation between solubility and IFT, IFT is plotted against 1/solubility in Figure 2.16. The IFT values from the exponential regression equation of IFT vs. ethanol enrichment are used at ethanol enrichments

corresponding to the solubility values in the plot. As can be seen in Figure 2.16, IFT is linearly correlated to (1/solubility), indicating a strong mutual relationship between these two thermodynamic properties. The relationship obtained is IFT = 172.12 / solubility with a determination coefficient (R^2) = 0.994. Therefore, the correlation between solubility and IFT in ternary liquid systems can be generalized as solubility = C / IFT where C is a system dependent constant. Thus solubility is strongly correlated to IFT and hence can be used for IFT predictions.

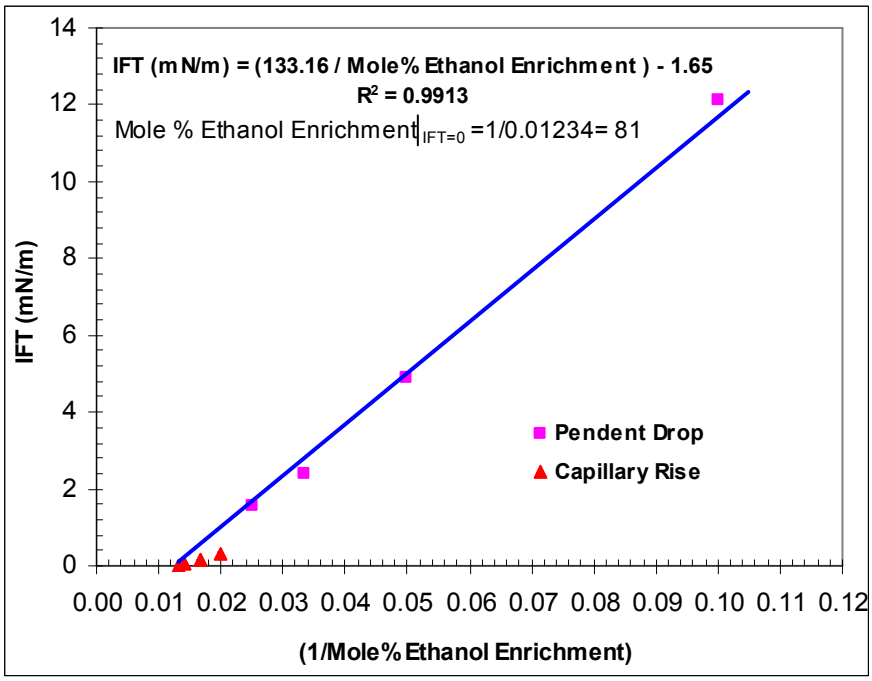

Figure 2.17: Plot of IFT vs. Ethanol Enrichment to Determine Miscibility

Determination of VIT Miscibility. All the IFT measurements obtained in the standard ternary liquid system of benzene, ethanol and water at various ethanol enrichments were fitted using a hyperbolic function to determine the miscibility using the VIT technique. The hyperbolic function was used especially to fit the curvature to the data due to almost one order of magnitude reduction in IFT observed near miscibility. The results are summarized in Figure 2.17. A good linear relationship between IFT and the reciprocal of ethanol enrichment can be seen with a determination coefficient (R^2) of 0.991. The regression equation obtained is also shown in Figure 2.17. The regression equation is then extrapolated to zero IFT, as required in the VIT technique, to determine miscibility in this standard ternary liquid system. A miscibility condition of 81 mole% ethanol enrichment was obtained with the VIT technique, which matches well with the miscibility conditions obtained from the phase diagram (83 mole%) and solubility data (>78 mole%). This clearly demonstrates the relationship of interfacial tension with

miscibility as the point of zero interfacial tension in phase equilibria. Since miscibility is a thermodynamic function associated with critical phase behavior, the observations from the study of Fleming and Vinatieri (1981) that relate interfacial tension with critical phenomena in surfactant containing systems also support such relationship of interfacial tension with miscibility. Thus, the VIT experiment conducted in this standard ternary liquid system further validates the VIT technique to determine the fluid-fluid miscibility conditions in multicomponent hydrocarbon systems.

2.1.2.5 Summary and Conclusions

An attempt has been made in this study to clarify the distinction between the terms solubility and miscibility and to relate them to interfacial tension. The selection of standard ternary liquid system of benzene, ethanol and water for experimentation was found to be useful. The distinction between the terms solubility and miscibility lies in partially soluble regions and solubility in all proportions implies miscibility. In addition, this study has demonstrated different regions of solubility characteristics and their relation to interfacial tension.

In insoluble regions, absence of solvent-oil ratio effects on interfacial tension is observed. Contrarily, small IFT dependence on solvent-oil ratio in the feed due to the absence of complete saturation between the fluids is observed in partially soluble regions. This study has thus identified the need to use pre-equilibrated solutions in the partially soluble regions to incorporate all mass transfer effects so as to eliminate the solvent-oil ratio effects on interfacial tension.

The two thermodynamic properties, solubility and miscibility, are strongly correlated to interfacial tension in that solubility is linearly related to reciprocal of interfacial tension and a condition of zero interfacial tension between the fluid phases implies miscibility. The new vanishing interfacial tension (VIT) technique applied so far to determine miscibility in gas-oil systems has been found to be applicable to determine miscibility even in ternary liquid systems. This once again exposes the sound conceptual basis of this new technique to determine fluid-fluid miscibility in multicomponent hydrocarbon systems.

2.2 Experimental Determination of Miscibility Conditions for CO_2 with Selected Crude Oil

2.2.1 Introduction

2.2.1.1 Current Status of EOR in United States

The cumulative production of oil reserves accounts for approximately one-third of the original oil in place. The U.S. Department of Energy (DOE) estimates 400 billion barrels of oil in place as a stranded resource (2006) and could be the target for EOR processes. The U.S. Department of Energy has further reported that the state-of-the-art enhanced oil recovery with carbon dioxide gas has now been recognized as a potential way of reducing greenhouse gas emissions and this would also help add another 89 billion barrels to the recoverable oil resources of the United States. Carbon dioxide flooding which is on the verge of an explosive growth due to technology advances, higher oil prices, reduced costs and environmental needs have made it a well-established method and the fastest-growing enhanced oil recovery technique in the United States. The types of gases injected into the reservoir for improved oil recovery are hydrocarbon, nitrogen, carbon dioxide, and flue gases.

Seventy-five active CO_2 floods operate in five countries producing 191 million bopd of incremental enhanced reserves. Projects in the U.S. comprise about 95% of the current worldwide CO_2 EOR production. Floods in Canada, Turkey and Trinidad produce the remaining CO_2 EOR reserves. As stated in SPE's CO_2 Monograph (1992), miscible CO_2 floods in the U.S. are the only EOR projects that have consistently and significantly increased annual EOR production. Martin and Taber (1992) reported that gas injection is one of the oldest methods used to improve oil recovery and its use has increased continuously and is proving to be effective in both carbonate and sandstone reservoirs. Ultimate incremental oil recovery from CO_2 floods in the U.S. was estimated to be 8 to 15 billion barrels depending on future oil prices and economic demand which continues to grow. On the field scale, incremental recoveries are projected at 7% to 23% of the original oil in place. All large CO_2 floods are miscible displacements of medium to high API gravity oils and are used either as secondary or tertiary injection operations. Most large CO_2 floods are used as tertiary injection operations in mature oil reservoirs that have been water flooded for years.

Oil and Gas Journal's exclusive EOR survey (2006) shows that the industry continues to increase the number of carbon dioxide injection projects. Table 2.11 shows that EOR has contributed 649,000 bpd to the US oil production, which is a 141,000 bopd decrease from the previous survey (OGJ, 2004) due the declining production from heavy oil projects in California (reached a maximum of 480,000 bopd in 1986 and has reduced to the 286,000 bopd in 2006). It can also be inferred from Table 2.11 that CO_2 miscible

injection increased oil recovery from 4.7% in 1986 to 54% in 2006. Table 2.12 indicated that the number of active US CO_2 miscible projects increased from 7.4% in 1986 to 52% in 2006.

Table 2.11: Summary of US EOR production (Ref.: Oil and Gas Journal, 2006)

Year	Thermal	Chemical	Gas	Other	Total	Carbon Dioxide Flood	
						Immiscible	Miscible
	b/d, 1000	b/d, 1000	b/d, 1000	b/d, 1000		b/d, 1000	b/d, 1000
1986	479.67	16.90	108.22	0.00	604.79	1.35	28.44
1988	464.91	22.50	131.00	0.00	618.40	0.42	64.19
1990	454.21	11.86	190.63	0.00	656.70	0.10	95.59
1992	460.69	2.19	298.02	0.00	760.91	0.10	144.97
1994	418.57	1.89	288.63	0.00	709.09	-	161.49
1996	424.08	0.14	299.35	0.00	723.57	-	170.72
1998	445.97	0.14	313.54	0.00	759.65	-	179.02
2000	417.68	1.66	328.76	0.00	748.09	0.07	189.49
2002	371.46	0.06	297.48	0.00	669.00	0.07	187.41
2004	345.51	0.06	317.88	0.00	663.45	0.10	205.78
2006	301.70	0.00	347.62	0.00	649.32	2.70	234.42

Table 2.12: Summary of active US projects (Ref.: Oil and Gas Journal, 2006)

Year	Thermal	Chemical	Gas	Other	Total	Carbon Dioxide Flood	
						Immiscible	Miscible
1986	201	206	104	1	512	28	38
1988	152	124	90	0	366	8	49
1990	154	50	91	0	295	4	52
1992	153	49	89	2	293	2	52
1994	116	30	79	1	226	1	54
1996	115	12	84	1	212	1	60
1998	100	11	87	1	199	-	66
2000	92	10	74	0	176	1	63
2002	65	4	78	0	147	1	66
2004	56	4	83	0	143	1	70
2006	55	0	97	0	152	2	80

Occidental Permian Limited initiated a CO_2 injection project in the North Hobbs Unit at the end of the Permian Basin, NM, in 2003 after a peak water flood resulted in a decline in oil production and reported an increase in oil production from 5000 bopd to more than 11,000 bopd. Thus it can be inferred from the above discussion that the CO_2 miscible displacement process, which results from multiple-contacts between the injected gas and reservoir oil to develop an in-situ composition alteration and generate miscibility,

is recognized as an important and the fastest growing enhanced oil recovery process in the oil industry.

2.2.1.2 Theory of CO2 EOR

Carbon Dioxide flooding processes are classified as immiscible or miscible even though CO_2 and crude oils are not actually miscible upon first contact in the reservoir (Martin and Taber, 1992).

Immiscible CO_2 Process. Immiscible CO_2 recovery is a technique, which is achieved primarily by reducing the oil viscosity, swelling of oil, and dissolved gas drive and is capable of sweeping the reservoir oil more effectively than water/polymer flooding. This combination of mechanisms enables a portion of the reservoir's remaining oil to be mobilized and produced. The areal sweep efficiency is increased by lowering the effective mobility ratio through a large reduction in oil viscosity.

Reservoirs with low pressures, stock tank oil gravities of 10° to 25°API and viscosities less than 100 centipoises are typical candidates for immiscible CO_2 displacements.

Miscible CO_2 Process. A miscible CO_2 displacement process is supposed to remobilize and reduce the post waterflooding residual oil saturation in the reservoir pore space. Miscible CO_2 recovery is a technique whereby CO_2 dissolves in the crude oil resulting in swelling the net oil volume, reducing oil viscosity, eliminating interfacial forces between reservoir oil and the displacing gas and achieving miscibility with the reservoir oil due to compositional changes and the mass transfer of hydrocarbon components between the reservoir oil and injection gas. These combined mechanisms improve the ability of the oil to flow out of the reservoir. Since the residual oil left in the reservoir after flooding is inversely proportional to the swelling factor, less oil will be left in the reservoir with greater swelling and the swollen oil droplets will force water out of the pore spaces thus creating drainage rather than imbibition (Klins, 1953).

A miscible CO_2 displacement process is subdivided into two processes: First-Contact Miscible and Multiple-Contact Miscible process.

In the First-Contact Miscible process (FCM) the injected solvent is directly miscible in all proportions and forms a single phase with the reservoir oil on first contact. LPG, propane, butane are the solvents used for achieving first contact miscible flooding. For first-contact miscibility to occur with the reservoir oil, the displacement pressure must be above the cricondenbar, since all solvent-oil mixtures above this pressure are single phase. The cricondenbar of CO_2 is high for first-contact miscibility to occur and hence at pressures lower than the cricondenbar, dynamic miscibility can be achieved with CO_2 (Stalkup, 1984). Thus first-contact miscibility between CO_2 and reservoir oil can be described as a process in which CO_2 first meets fresh reservoir oil and becomes miscible

with it on first contact to form a single phase fluid, without mass interaction between CO_2 and the reservoir fluid.

The advantage of FCM using LPG, propane and butane is that miscibility is developed at low pressures with crude oils. The high cost of solvents is a major disadvantage for using FCM. Sometimes small volumes of solvent slugs (diluted with oil and drive gas) are injected, but this has a disadvantage that the miscibility can to be lost and viscous fingering occurs whereby drive gas penetrates as small slugs and come into direct contact with oil, resulting in poor sweep efficiencies (Stalkup, 1984).

In the Multiple-Contact Miscible process, the injected fluid is not miscible with the reservoir oil on first contact. The process depends on the modification of the composition of the injected phase and oil phase through multiple contacts between phases in the reservoir and counter directional mass transfer of components between the fluid-fluid phases to such a degree that the fluids become miscible as the injection phase moves through the reservoir and the oil enriched CO_2 becomes undistinguishable from the CO_2 enriched oil. Under the optimum conditions of pressure, temperature and composition this compositional modification will generate miscibility between the displacing and displaced phases in the reservoir. Thus multiple-contact miscibility can be described as the thermodynamic state of equilibrium between the CO_2 and reservoir fluid in which there has been a complete mass transfer of components from the reservoir fluid to the CO_2 gas (vaporizing drive) and from the CO_2 gas into the reservoir fluid (condensing drive).

In miscible gas injection where by the oil/gas mixtures remain in single phase, the relative permeability between injected gas and oil and the relative wettability of the rock to oil and injected gas does not affect the recovery efficiency, as the process is one of purely fluid-fluid interaction. A miscible CO_2 injection process is effective in oil-wet and water-wet rocks and is not affected by mobile water remaining after a waterflood. The mechanisms involved in the displacement of oil by CO_2 in a dynamic multiple-contact miscible gas injection process are vaporizing, condensing or a vaporizing/condensing gas drive.

2.2.1.3 Discussion on CO2 Drive Mechanisms

Klins (1953) suggested that a number of mechanisms take place that may initiate oil displacement when CO_2 is injected into an oil reservoir. CO_2 may create a miscible front and hence miscibility is initiated by extraction of significant amounts of heavier hydrocarbons from C_5 through C_{30}, or at different reservoir conditions, CO_2 saturates the reservoir fluids to an extent where the swollen crude is miscible with the trailing CO_2 and may resemble enriched gas drive. This combination of mechanisms enables a portion of the remaining trapped oil to be mobilized and produced.

Rathmel (1971) proposed that the miscible-like recoveries achieved by CO_2 were a multiple-contact vaporization drive mechanism in which CO_2 strips intermediates from the liquid until the composition is rich enough to be miscible with the original oil.

Metcalfe and Yarborough (1979) have studied the phase behavior by performing various experiments on reservoir fluids using CO_2 as the displacing phase and have concluded that more than one mechanism (vaporizing and condensing) is possible for a CO_2-reservoir fluid system and that reservoir temperature and displacement pressure determine the type of mechanism (vaporization, condensing or vaporizing/condensing) that will control the displacement process.

Holm and Josendal (1982) conducted various displacement experiments by injecting CO_2 into crude oil to show that the drive mechanism was one of vaporization due to the extraction of hydrocarbons (C_5 through C_{30}) from the oil.

Stalkup (1984) and Zick (1986) performed various multiple-contact experiments backed by equation of state simulations to show that a combined condensing/vaporizing gas drive mechanism was responsible for several laboratory displacements of reservoir fluids by enriched gas.

It can be inferred from the above discussion that generally miscible CO_2 EOR involving the interaction between the injected CO_2 and reservoir fluid is a multiple-contact process in which CO_2 will vaporize the light to intermediate components of oil into the injected CO_2 phase and the rich CO_2 gas will transfer the light intermediates by condensing into the oil phase as it moves through the reservoir, thus leading to the CO_2 becoming miscible (mixing in all proportions) with the reservoir fluid. The miscibility between CO_2 and reservoir fluid is a function of displacement pressure, reservoir temperature, and composition of the oil and takes place due to compositional changes of the fluid-fluid phases resulting from the simultaneous counter-directional mass transfer of hydrocarbon components between fluid phases by the combined vaporization/condensing drive mechanism.

The injection of CO_2 into an oil reservoir would reduce the capillary forces to a minimum if the interfacial tension between the injected fluid and the trapped oil is reduced to zero. Hence, it is important to determine the gas-oil minimum miscibility pressure, because this is the lowest pressure at which miscibility is developed between the injected gas and reservoir fluid. Miscibility development results in the mobilization and the release of the trapped oil from the porous medium, thus improving the overall displacement efficiency and oil recovery. Interfacial tension through capillary forces plays an important role in the determination the flow behavior of hydrocarbon fluids in porous rocks (Asar and Handy, 1987).

In a miscible displacement process CO_2 directly mixes and forms a single phase with the reservoir oil when mixed at all proportions with it at the conditions existing at the interface between the injected gas and the reservoir oil being displaced. This result in the

elimination of interfacial tension forces between the oil and displacing fluid, the capillary number (ratio of capillary to viscous forces) becoming infinite (higher the capillary number lower the residual oil saturation) and a low residual oil saturation (Stalkup, 1984).

Determination of CO_2-reservoir fluid MMP is important in screening and selecting reservoirs for CO_2 injection in order to have economical attainable displacement efficiency over a significant volume of reservoir. A low CO_2 injection pressure would result in low displacement efficiency and a high CO_2 injection pressure would result in uneconomical high cost of injection pressures. Hence, an optimum miscible CO_2 displacement process can be applied to reservoirs by injecting CO_2 at pressures higher than the MMP but lower than the average reservoir pressure.

Minimum miscibility pressure is one of the most important parameters in the determination of optimum operating conditions involving miscible CO_2 displacement processes for evaluation of gas-oil miscibility and this value must be accurately determined by performing laboratory experiments.

2.2.1.4 Gas-Oil Minimum Miscibility Pressure (MMP)

The degree of miscibility is often expressed in terms of the MMP between the reservoir fluid and the injection gas. Definitions of multiple-contact miscibility relate to recovery performance curves from laboratory displacement tests. Miscible gas displacement is characterized by high oil recovery of greater than 90% in slim-tube displacement experiments. The following are some definitions of minimum miscibility pressure as reported in literature;

- Minimum Miscibility Pressure for a CO_2-reservoir fluid system is defined as the pressure at which 80% of the oil in place is recovered at CO_2 breakthrough and 94% of the oil in place at a production gas/oil ratio (GOR) of 40,000 SCF/BBL is ultimately recovered (Holm and Josendal, 1974). At MMP a sufficient volume of the extracted hydrocarbons is present at the displacement front to maintain the residual oil saturation at a minimum value throughout the flooding path.
- Minimum Miscibility Pressure is defined as the lowest pressure at which all oil available for recovery can be displaced by 1.2 pore volumes of injected solvent (Metcalfe, 1982).

Thus, the criteria used by various researchers for interpreting the displacements have included gas breakthrough, ultimate recoveries at a given volume of solvent injection, visual observations of core effluents, compositions of produced gases and liquids, shape of breakthrough, and ultimate recovery curves versus pressure. MMP is related to interfacial tension, thus when two fluids approach miscibility their interfacial tension approaches zero (Rao, 1997). Hence at MMP gas and oil must become a single phase.

The following conclusions are summarized by Holm and Josendal (1982) related to the development of miscibility in CO_2 displacements.

- Dynamic miscibility occurs when the density of CO_2 is sufficiently greater than dense gaseous CO_2, or when liquid CO_2 solubilizes the C_5 thorough C_{30} hydrocarbon components in the reservoir oil.
- Reservoir temperature has an effect on the pressure required to achieve the CO_2 density necessary for miscible displacement. As reservoir temperature increases MMP increases.
- MMP is inversely related to the total amount of C_5 through C_{30} hydrocarbon components present in the reservoir oil. The more these hydrocarbon components are present in the oil, the lower the MMP.
- MMP is affected by the molecular weight distribution of C_5 through C_{30} hydrocarbon components in the reservoir oil. Low molecular weight hydrocarbons in the gasoline range promote miscibility and result in a lower MMP.
- MMP is also affected to a lesser degree by the types of hydrocarbon components present in the reservoir oil, e.g. the presence of aromatics results in a lower MMP compared to paraffins of the same boiling range.
- Development of dynamic miscibility does not require the presence of C_2 through C_4 hydrocarbons.
- The presence of methane does not change the MMP appreciably.

2.2.1.5 Previous Work Relating Miscibility with Gas-Oil IFT

The disadvantages of the conventional miscibility measurement techniques and their inability to directly measure gas/oil interfacial tension can overcome by the new vanishing interfacial tension technique (VIT) which uses the concept that interfacial tension reduces as gas-oil miscibility approach. Rao (1997) first experimentally demonstrated the applicability of the VIT technique to determine miscibility in a live reservoir crude oil-gas system (Rainbow Keg F Pool reservoir, Canada) at reservoir temperature and varying pressures and gas enrichment levels (composition) using the drop shape analysis technique. The injection gas composition was successfully optimized for miscibility by performing VIT experiments at varying gas compositions at the experimental pressure of 30 MPa at the reservoir temperature of 60°C. Rao and Lee (2002) later extended VIT technique to an offshore Terra Nova reservoir to optimize the injection gas composition for developing miscibility with the crude oil of this reservoir.

Ayirala (2005) investigated the applicability of the vanishing interfacial technique to determine miscibility and measured dynamic gas-oil interfacial tension by using the capillary rise technique at elevated temperatures and pressures for two standard gas-oil systems of known phase behavior characteristics. The two standard gas-oil systems used

in this study are: CO_2-n-decane system at 100°F and CO_2-live decane (25 mole% methane+30 mole% n-butane+45 mole% n-decane) system at 160°F. The CO_2-n-decane system at 100°F showed a VIT miscibility of 1150 psi which agreed well with the reported minimum miscibility pressures from conventional slim tube (1250 psi) and rising bubble apparatus (1280 psi). The CO_2-live decane system at 160°F indicated a VIT minimum miscibility pressure of 1760 psi, which also agreed well with the reported minimum miscibility pressures from the conventional slim tube (1700 psi). This study in standard gas-oil systems thus further validated the VIT technique to measure gas-oil miscibility and also demonstrated the reliability and accuracy of VIT technique for gas-oil miscibility determination.

An attempt has been made in this section to extend these validation studies on VIT technique to an actual live crude oil-CO_2 system at reservoir conditions. It was also aimed to include a detailed compositional analysis to infer information on mass-transfer interactions and to determine the controlling mass transfer mechanism (vaporizing, condensing or both) that govern the attainment of gas-oil miscibility. Also, compositional dependence of VIT technique with varying gas-oil ratios (both molar and volumetric) in the feed mixture was planned for investigation in a live crude oil-CO_2 system.

2.2.2 Objectives

The objectives of this study are:

- To determine the minimum miscibility pressure of a CO_2- live reservoir fluid system at reservoir temperature by measuring the gas-oil interfacial tension, using the vanishing interfacial tension technique (VIT) by the pendant drop and capillary rise techniques.
- To characterize the mass transfer interactions between CO_2 and live reservoir fluid by carrying out compositional measurements and densities of the fluid-fluid phases at varying pressure at reservoir temperature.
- To investigate the gas-oil ratio effects on fluid phase compositions and interfacial tension, and hence on VIT miscibility conditions.

2.2.3 Experimental Apparatus and Procedure

For the purpose of simulating the fluid-fluid interactions and the variations in physical properties of the fluid phases occurring in the subsurface reservoir, all the experiments were conducted at reservoir conditions using live reservoir fluid that was prepared in the laboratory. The preliminary experimental tasks performed were: determination of composition of the stocktank oil, preparation of live reservoir fluid, determination of bubble point pressure, compositional analysis, and viscosity measurements of recombined reservoir fluid.

To investigate the compositional effects of interfacial tension and miscibility on a carbon dioxide-live reservoir fluid system at varying pressures from 1500 psig to 6000 psig at reservoir temperature of 238°F, it was necessary to set up instruments that could measure related vapor and liquid properties such as composition, density, molecular weight, and interfacial tension. These included the gas chromatograph for compositional analysis, densitometer for density measurements at high pressures and high temperatures, molecular weight apparatus for measuring the molecular weight of stocktank oils, and an optical cell for measuring the interfacial tension of the carbon dioxide-live reservoir fluid system provided with sampling ports for capturing fluids under actual test conditions to measure compositions and densities of the fluid phases with minimal disturbance.

This section provides the detailed description for each apparatus used, experimental design, and procedure involved in the preparation of the recombined live reservoir fluid, interfacial tension (IFT) measurements to determine the minimum miscibility pressure using the capillary rise and pendant drop techniques. The gas-oil system used was carbon dioxide-recombined reservoir fluid at the reservoir temperature of 238°F and at different pressures varying from 1500 psig to 6500 psig. The compositional analysis and density measurements of the equilibrated oil and gas phases were also carried out as a part of the experimental procedure.

2.2.3.1 Gas Chromatograph

Figure 2.18 shows the newly acquired Varian gas chromatograph (model CP-3800) along with an auto-sampler (model CP-8410) for measuring gas and oil compositions.

The basis of the gas chromatographic separation is the boiling point distribution of a sample between two phases. One of these phases is the stationary phase (high boiling liquid) and the other is the mobile (carrier) gas phase which percolates through the stationary phase. A non-polar packed or open tubular (capillary glass or ultimetal) gas chromatographic column is used to elute the hydrocarbon components of the sample in order of increasing boiling point. As the mixture of carrier gas and sample travels through this column, its components go back and forth at different rates between the gas phase and dissolve in the high-boiling liquid (stationary phase), and thus separating into pure components. After each component elutes from the column it passes through the detector. The detector sends an electronic message to the recorder, which responds by printing a peak. The column temperature is raised at a reproducible linear rate and the area under the chromatogram peak is recorded throughout the analysis. This Varian gas chromatograph system (CP 3800) has the capability of performing liquid and gas compositional analysis in a single setup.

Figure 2.18: Varian gas chromatograph with auto-sampler (model CP-3800 and model CP-8410)

2.2.3.2 Densitometer

Accurate density data are essential for the measurement of fluid-fluid interfacial tension as a function of pressure and temperature. For this purpose, a new Anton Paar DMA HP connected to the evaluation unit DMA 4500 has been acquired and the photograph of the equipment is shown in Fig 2.19. The density measurements of fluid phases in the CO_2-live reservoir fluid system at elevated pressures and temperatures were performed using this instrument.

2.2.3.2.1 Calibration Procedure

A density adjustment determines the apparatus constants 'A' and 'B'. To determine the apparatus constants, two samples of known density at the required temperature and pressure are required. The fluids used to calibrate the instrument were UHP grade nitrogen (99.997%) and de-ionized water. Apparatus constants 'A' and 'B' are determined by measuring the periods of oscillation directly from the DMA 4500 and are valid only for the temperature and pressure at which they have been determined. The equations 2.1 and 2.2 are used to calculate the apparatus constants A and B from the period of oscillations.

Figure 2.19: Pressure densitometer and flash separation unit

A. Heise Digital Pressure Indicator
B. DMA 4500 Evaluation Unit
C. DMA HP Density External Cell
D. Separator
E. Gas Sampling Cylinder
F. Ruska Gasometer
G. Gas Sampling Port
H. Liquid Sampling Port
I. Printer

$$A = \frac{\rho_1 - \rho_2}{P_1^2 - P_2^2} \quad \text{..... (2.5)}$$

$$B = \frac{P_2^2 * \rho_1 - P_1^2 * \rho_2}{P_1^2 - P_2^2} \quad \text{..... (2.6)}$$

Where:

A = Apparatus Constant

B = Apparatus Constant

ρ_1 = Density of Standard 1 (Nitrogen)

ρ_1 = Density of Standard 2 (De-Ionized Water)

P_1 = Period of Oscillation of Standard 1 (Nitrogen)
P_2 = Period of Oscillation of Standard 2 (De-Ionized Water)

The density of the unknown sample was then calculated using equation 2.7.

$$\rho = A * P^2 - B \quad \text{……...……...…} \quad (2.7)$$

Where:
ρ = Density of Unknown Sample (gms/cc)
P = Period of Oscillation of Unknown Sample
A = Apparatus Constant
B = Apparatus Constant

The apparatus constants A and B and the density of the unknown sample are automatically calculated by the evaluation unit DMA 4500. Initially, the external density cell is filled with a density standard 1 (Nitrogen) at the temperature and pressure. The value of the density of standard 1 obtained from the National Institute of Standards and Technology website (NIST) is then inputted into the density adjustment key on the evaluation unit. After the density adjustment is completed, the external density cell is thoroughly cleaned with toluene and acetone and blow dried with nitrogen. The external density cell is then filled with density standard 2 (de-ionized water) at the same temperature and pressure that was used for density standard 1. The value of the density of standard 2 obtained from the NIST website is then inputted into the density adjustment key on the evaluation unit. Once both the density adjustments are saved, the adjustment data are stored in the evaluation unit DMA 4500. The unknown sample is then filled in the density external cell at the same temperature and pressure that was used for calibration. The density of this unknown sample is directly read form the evaluation unit DMA 4500. If the density of the unknown sample is to be determined at a different pressure and temperature, the calibration procedure has to be repeated with the new pressure and temperature.

2.2.3.3 Molecular Weight Apparatus

The Cryette (Figure 2.20) measures the temperature at which samples freeze. The apparatus is a completely automatic system for holding the sample, cooling the sample to a definite temperature at a controlled rate, freezing the environment, measuring the temperature of the sample during the entire process and finally indicating the temperature of the sample automatically.

The Cryette WR apparatus determines the molecular weight of hydrocarbon samples by directly measuring the freezing point depression of the sample since freezing point

depression is linearly related to the solute concentration and the freezing point depression (K_f) of the solvent (Benzene).

Figure 2.20: Molecular weight determination apparatus

Where:

A. Molecular Weight Apparatus, Cryette WR (Model 5009)

B. Dispenser filled with Water Saturated Benzene

C. High Precision Sartorius Weighing Balance

2.2.3.3.1 Calibration Procedure

The measurement of the molecular weight of a sample is made by dissolving a known weight of the solute in a known weight of solvent. The range control on the apparatus is set to 6. The apparatus is calibrated using water saturated benzene (99.99%) and a mixture of about 0.2000 grams of n-nonane (99.95%) in 11.0000 grams of water saturated benzene. Initially 2.5 ml of water saturated benzene is placed in the glass tube that is lowered directly above the cold antifreeze bath by using the operating head. After seeding, indicated by the noise of the stirrer hitting against the glass tube, the display meter should read zero before the read light comes on. If not, adjust to zero using the zero control. Then a 2.5 ml of a mixture of about 0.2000 grams of n-Nonane (99.95%) in about 11.0000 grams of water saturated benzene is placed in the glass tube that is lowered directly above the cold antifreeze bath by using the operating head. After seeding, which is indicated by the noise of the stirrer hitting against the glass tube, set the display meter

to read a ΔF_P calculated by the equation 2.8 before the read light comes on, using the slope control.

$$\Delta F_p = \frac{K_f * 1000 * 1000 * W_{solute}}{MW * W_{solvent}} \quad \text{..... (2.8)}$$

ΔF_p = Meter Reading (Freezing Point Depression)
K_f = molal freezing point depression of solvent i.e. 5.12°C/m
W_{solute} = weight of solute (oil) in grams
$W_{solvent}$ = weight of solvent (benzene) in grams
MW = Molecular weight of n-Nonane (128 gm/mole)

After calibration, verification of the instrument is performed by running pure n-tetradecane (99.95%). The meter display should read a ΔF_P which when calculated according to equation 2.9 gives a molecular weight of 198 gm/mole (n-tetradecane).

$$MW = \frac{K_f * 1000 * 1000 * W_{solute}}{\Delta F_p * W_{solvent}} \quad \text{..... (2.9)}$$

After calibration and verification of the instrument, the molecular weight of the unknown sample is then determined by placing 2.5 ml from a mixture of about 0.2000 grams of unknown sample in about 11.0000 grams of water saturated benzene in a glass tube, lowering the tube directly above the cold antifreeze bath by using the operating head and reading the display meter. The meter display should read a ΔF_P which when calculated according to equation 2.8 gives the molecular weight of the unknown sample.

2.2.3.4 Determination of Current Depleted Reservoir Fluid Composition Using CMG-WinProp

Initially, the composition of the stocktank crude oil was determined using the Varian gas chromatograph shown in Section 2.2.3.1. Then, the compositions of separator gas (historical data) and separator oil (measured stocktank crude oil) were used as inputs into the CMG-WinProp software. These separator products were then recombined at the initial gas oil ratio of 1052 SCF/STB and at a separator pressure and temperature of 268 psi and 54°F to obtain the original reservoir fluid composition at the initial conditions.

The equation of state was then tuned to match the known saturation pressure of the original reservoir fluid at 238°F (4050 psi). Tuning the equation of state (EOS) is nothing more than a calibration of the EOS against the known experimental data by adjusting the input values of some uncertain parameters in the EOS to minimize the difference between the predicted and the measured values. The Peng-Robinson equation of state was chosen

for the bubble point pressure calculations. Tuning of this equation of state was performed by adjusting the volume shift parameter of the hexanes plus (C_{6+}) fraction to match the bubble point pressure at the initial reservoir conditions. A relatively high weight factor of 50 was used for the measured saturation pressure value during the tuning calculations, since this data was believed to be more accurate.

Once the equation of state was tuned to match the saturation pressure, the two-phase flash calculations were performed on the original reservoir fluid to deplete it down to the current reservoir pressure of 1100 psi. The liquid phase composition obtained from the two-phase flash calculations can be considered as the representative reservoir fluid composition at the current depleted reservoir conditions.

2.2.3.5 Procedure for Preparation of Live Reservoir Fluid by Recombination

At first, the composition, density, and molecular weight of stocktank crude oil were determined using the procedures described in Sections 2.2.3.1, 2.2.3.2, and 2.2.3.3 respectively. Before beginning the recombination, transfer vessels, stainless steel tubings and the PVT cell were thoroughly cleaned with toluene and acetone, and blown dried with nitrogen. Stocktank crude oil containing a C_{6+} mole fraction of about 0.76146 and the pure methane gas (99.99%) were physically recombined in a PVT cell to create a representative reservoir fluid sample at the current reservoir conditions for interfacial tension measurements with CO_2.

In this procedure a known volume of stocktank oil was transferred into a high pressure PVT cell at 500 psi and 75°F. Knowing the molecular weight and density of the stocktank oil at 500 psi and 75°F, the moles of stocktank oil in place were calculated. Pure component methane gas (99.99%) was then added to the known volume of stock tank oil at a pressure dictated by the vapor pressure of the pure gas component. The volume of pure hydrocarbon gas (methane) to be added was determined from the mole fraction of the gas (i.e.C_1) present in the live oil, the compressibility factor, density and charge pressure of the gas, and the calculated moles of stocktank oil in place at the start. After the addition of all components, the recombined reservoir fluid was then pressurized to 4000 psig (the reservoir pressure is about 4000 psi). The PVT cell was then inverted at that pressure several times to bring the reservoir fluid to single-phase conditions. The PVT cell was also rocked for 24 hours to ensure equilibrium single-phase conditions of the reservoir fluid.

2.2.3.6 Procedure for Determination of Bubble Point of the Recombined Reservoir Fluid

The PVT cell, consisting of a floating piston, separates water from live reservoir fluid. Initially the live reservoir fluid was pressurized with water to 4000 psig and ambient temperature to keep the fluid in single phase. About 1 to 2 cm^3 of water was drained through the valve from the waterside of the PVT cell to bring the pressure down to a fixed value. The PVT cell was then agitated several times until a constant pressure reading was obtained indicating equilibrium. The exact volumes of the water collected as well as the stabilized pressure reading obtained were recorded. This procedure was repeated until the live reservoir fluid went into a two-phase region. All these measurements represent the region above bubble point pressure. Similarly pressure-volume readings were taken in the two-phase region, below the bubble point pressure. A plot of cumulative volume of water collected versus pressure was then prepared and the bubble point pressure is indicated by the intersection of two distinct linear portions of the plot i.e. one above the bubble point region and one below the bubble point region.

2.2.3.7 Composition Measurement of Recombined Reservoir Fluid

The composition of the recombined reservoir fluid was determined by flashing the fluid from 4000 psig and ambient temperature to atmospheric conditions. This enabled the fluid to separate (glass flask) into stable gas and liquid phases. Figure 2.19 shows the separator (glass flask denoted by 'D') that was used to perform the flash separation for the recombined reservoir fluid. The flashed oil was collected in the separator (glass flask 'D') and the flashed gas was allowed to flow through the gas collection cylinder (denoted 'E') and then eventually into the gasometer. The volume of flashed gas was measured using the Ruska gasometer and the weight of oil was measured using the Sartorius weighing balance. The resultant properties measured for the flashed oil and flashed gas were:

- The molecular weight of the flashed oil
- The composition of the gas sample collected in the cylinder
- The composition of the flashed oil collected in the separator

The resultant composition of the recombined fluid was then determined using the measured gas-oil ratio at ambient conditions (i.e. volume of flashed gas and weight of oil) for the flash separation performed, composition of the flashed oil, composition of the flashed gas, molecular weight of the flashed oil and the calculated average molecular weight from the flashed gas composition.

2.2.3.8 Experimental Procedure for the IFT Measurements

Figure 2.21 shows the setup of the equipment used to conduct the interfacial tension measurements using the capillary rise technique and the pendant drop technique at elevated pressures and reservoir temperature of 238°F. The different components are described below:

A. Optical Cell

The optical cell is placed in an insulated oven. The optical cell houses a traveling injector tube N of 1.5875 mm I.D. (Figure 2.22). The injector tube is made of Hastelloy. The optical cell also houses the glass capillary tube O of 1.000 mm I.D and 2.000 mm O.D (Figure 2.22). The design rating of the optical cell is 20,000 psig at 392°F.

Figure 2.21: Various equipments used for measuring interfacial tension at different experimental pressures at 238°F

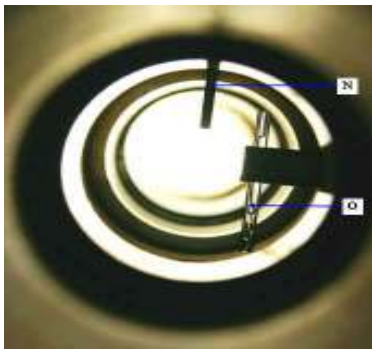

Figure 2.22: Inside of the optical cell

B. Anton Paar Densitometer (DMA HP and DMA 4500)

The apparatus is capable of measuring densities at high pressures and high temperatures. The design rating of the densitometer is 10,000 psig at 392°F.

C. Ruska Positive Displacement Pump (Model 2014)

This pump is a high pressure precision metering and volumetric pump capable of delivering accurate fluid rates at elevated pressures. The pump consists of a piston and a cylinder. The piston is injected into the cylinder thereby displacing an accurate and equivalent volume of fluid. The design rating of the pump is 10,000 psig at 80°F. The pump was filled with 99.997% carbon dioxide and was used to charge accurate amounts into the optical cell.

D. Ruska Positive Displacement Pump (Model 2014)

The pump specifications are the same as described in C. The pump was filled with the recombined reservoir fluid and was used to charge accurate amounts into the optical cell.

E. Sensotec Digital Pressure Indicator (Model No. SC 3004)

The Sensotec digital pressure indicator has a design rating of 10,000 psig at 105°F. The two positive displacement pumps are connected to the Sensotec digital pressure indicator via pressure transducers.

F. Heise Digital Pressure Indicator (Model No. 901A)

The pressure in the optical cell was continuously monitored using the Heise digital pressure gauge. The digital pressure gauge has a design rating of 25,000 psig at 72°F.

G. Floating Piston Transfer Vessel (CFT-50-400)

The recombined reservoir fluid was prepared in the floating piston 316 stainless steel transfer vessel. The design rating of the transfer vessel was 5000 psig at 250°F.

H. Temperature Indicator

Temperature on the optical cell is displayed by the temperature indicator, which is connected to the optical cell by a thermocouple.

I. Heating Oven

The heating oven provides and maintains a stable temperature of 238°F to the fluid phases in the optical cell.

J. Digital Camera

The drop shapes and the heights of the fluid phases was recorded using a Sony digital video camera provide with a zoom lens (Model DXC-190) which was connected to a video cassette recorder.

K. Gas Sampling Outlet

The top of the optical cell was provided with a sampling port for collection of gas samples to be used in pressure density measurements and compositional analysis.

L. Liquid Sampling Outlet

The bottom of the optical cell was provided with a sampling port for collection of liquid samples to be used in pressure density measurements and compositional analysis.

M. Gas Chromatograph

Gas and liquid compositional analysis was performed using the new Varian gas chromatograph with auto-sampler (Models CP 3800 and CP 8410).

N. Hastelloy tube (I.D. = 1/16 inches)

O. Glass capillary tube (I.D. = 1.0 mm)

The experimental design setup described above and the following detailed experimental procedure was devised to conduct the IFT measurements at reservoir conditions with compositional analysis and high pressure density measurements in an efficient, accurate and safe manner, and to keep the integrity of the equilibrated fluid-fluid phases thus allowing representative samples to be collected for performing the various fluid property measurements throughout the experimental study.

1. Fill the Ruska pump C with CO_2 gas at the experimental pressure of 1500 psig.
2. Fill the Ruska pump D with live recombined reservoir fluid and stabilize it at the experimental pressure of 1500 psig.
3. Carefully insert a capillary tube of 1.0 mm I.D into the optical cell.
4. Heat the high-pressure high-temperature optical cell to 238°F.
5. Connect the heated stainless steel tubing from the laboratory cylinder containing live oil to the top of the optical cell.
6. Evacuate the optical cell using the vacuum pump to remove any traces of contaminants.
7. Using the Ruska pump C, charge an accurate amount of CO_2 into the optical cell, required for the experimental pressure. Using Ruska pump D, charge an accurate amount of the recombined reservoir fluid into the optical cell required for the experimental pressure. The amounts of CO_2 gas and live reservoir fluid to be charged

at the various pressures (1500 to 6000 psig) for the two sets of gas/oil molar ratios and two sets of gas/oil volume ratios are described in Section 2.2.3.9.

8. Capture the image of the first pendant drop of live crude oil at the tip of capillary tube in the optical cell as soon as it contacts the gas phase through the digital video camera 'J' that is connected to a computer equipped with the drop shape analysis software. Use the densities of the pure fluid phases initially during the first-contact gas-oil interfacial tension calculations.
9. Allow approximately 6 hours for the fluids to reach equilibrium in the cell at the experimental pressure and 238°F.
10. Form a pendant drop of the recombined reservoir fluid at the tip of capillary tube in the optical cell in the gas phase that has already interacted with the oil residing at the bottom of the cell. Capture this pendant oil drop image using the drop shape analysis software program (Kruss, 2000). Repeat the same procedure for about 8-10 pendant oil drops.
11. Allow approximately 24 hours for the fluids to reach equilibrium in the cell at the experimental pressure and 238°F.
12. Record the capillary rise observed in the capillary tube using the digital video camera 'J'.
13. Measure the density of the equilibrated gas phase using the Anton Paar densitometer.
14. Remove the equilibrated gas sample from the densitometer by flashing the gas to ambient conditions and analyze for composition using Varian CP-3800 gas chromatograph.
15. Measure the density of the equilibrated oil phase using the Anton Paar densitometer.
16. Remove the equilibrated oil sample from the densitometer by flashing the oil to ambient conditions and analyze for compositions using the Varian CP-3800 gas chromatograph. Measure the molecular weight of the stocktank oil sample using the Cryette WR apparatus.
17. Use the equilibrated gas and oil phase densities, and captured pendant drop images in the drop shape analysis software program to calculate the average equilibrium gas-oil interfacial tension. Also, use the equilibrated gas and oil phase densities, the capillary rise, and the capillary radius in the conventional capillary rise technique equation to compute the gas-oil interfacial tension.
18. Drain the fluids from the optical cell, clean with toluene and acetone and blow dry with nitrogen gas.
19. Evacuate the cell using the vacuum pump to remove any traces of remaining residual fluid phases.
20. Repeat the steps 7-19 to obtain the first-contact by drop shape analysis technique as well as the equilibrium interfacial tensions at different experimental pressure steps till the pressure reaches 6000 psig using drop shape as well as capillary rise techniques.

21. Steps 1 to 20 were performed for two sets of constant gas-oil molar ratios and two sets of constant gas-oil volume ratios.

The following constant gas-oil molar ratios and constant gas-oil volume ratios and variations of the above procedure with respect to pendant drop and capillary rise were conducted depending on the practicality of the experiment at each selected pressure:

- Multiple-contact (equilibrium) miscibility was performed using the pendant drop and capillary rise techniques for the 0.893 mole fraction of CO_2 and 0.107 mole fraction of recombined reservoir fluid (Rm=0.893/0.107=8.346) at each experimental pressure of 1500, 2000, 2500, 3000, 3500, 4000, 5000, 5500 and 6000 psig.
- Multiple-contact (equilibrium) miscibility was performed using the capillary rise technique for the 0.700 mole fraction of CO_2 and 0.300 mole fraction of recombined reservoir fluid in the feed mixture (Rm=0.700/0.300=2.333) at each experimental pressure of 2000, 3000, 3500, 4000, 5000 and 6000 psig.
- First-contact miscibility using the pendant drop and multiple-contact (equilibrium) miscibility using the pendant drop and capillary rise techniques were performed for the 0.850 volume fraction of CO_2 and 0.150 volume fraction of recombined reservoir fluid in the feed mixture (Rv=0.850/0.150=5.667) at each experimental pressure of 2000, 3000, 4000, 5000 and 6000 psig.
- Multiple-contact (equilibrium) miscibility using the capillary rise technique was performed for the 0.450 volume fraction of CO_2 and 0.550 volume fraction of recombined reservoir fluid in the feed mixture (Rv=0.450/0.550=0.818) at each experimental pressure of 2000, 3000, 4000, 5000 and 6000 psig.

2.2.3.9 Calculation Procedure for the Constant Gas-Oil Molar Ratios and the Constant Gas-Oil Volume Ratios Used as Feed in the Mixture

The equations 2.6 and 2.7 given below were used for calculating the charge ratios.

$$moles = \frac{mass(gms)}{molecularweight(g/mole)} \quad \text{(2.10)}$$

$$density(g/cc) = \frac{mass(gms)}{volume(cc)} \quad \text{(2.11)}$$

$$V_1 = \frac{V_2 \times \rho_2}{\rho_1} \quad \text{(2.12)}$$

Where:

V_1 = volume of reservoir oil at pressure at 75°F

V_2 = volume of reservoir fluid at pressure at 238°F

ρ_2 = density of reservoir fluid at pressure at 238°F

ρ_1 = density of reservoir fluid at pressure at 75°F

$$V = \frac{znRT}{P} \quad \text{.....} \quad (2.13)$$

Where:

V = volume of carbon dioxide gas at pressure at 75°F

z = compressibility of carbon dioxide at pressure at 75°F

n = mole fraction of carbon dioxide in the feed mixture

R = gas constant =1205.91 $\left(\frac{psia \times cm^3}{gmole \times °K} \right)$

T = temperature in Kelvin

P = charge pressure in psig

Initially the mass in grams was obtained by multiplying the gram moles of each fluid (CO_2 and reservoir fluid) with the corresponding molecular weight of that fluid. Volume in cm^3 was obtained by dividing the mass in grams of each fluid by the density of that fluid at the experimental pressure at 238°F, from which a volume percent was then calculated. Since the measured volume of the optical cell was 80 cm^3 at 238°F, the volume percent for each fluid was multiplied by the cell volume (80 cm^3) to obtain the amounts in cm^3 of the each fluid phase that would be present at the experimental pressure at 238°F. The volume of each reservoir fluid to be charged at the experimental pressure at 75°F (ambient temperature) was then obtained by using the equation 2.12. The volume of CO_2 gas to be charged at the experimental pressure at 75°F was similarly obtained by using the equation 2.13.

2.2.4 Results and Discussion

2.2.4.1 Calibrations Experiments Performed

2.2.4.1.1 Hydrocarbon Liquid Compositional Analysis

Before performing liquid composition analysis, the performance of the flame ionization detector was checked. This was achieved by injecting 0.3 microliter of certified hydrocarbon mixture (n-paraffin mixture) from C_6 through C_{44} of known composition diluted with carbon disulphide into the Varian gas chromatograph instrument. The procedures and methods used in the calibration were based on methods ASTM D2887 and ASTM D4626.

The relative response factors were calculated for each n-paraffin (relative to n-decane) in accordance with the method ASTM D4626. The method assumes that the detector response is proportional to the mass of individual components. Table 2.13 and Figure 2.23 indicated that the percent deviation of relative response factor F_n for the n-paraffin mixture was less than about 1.5% and was much less than $\pm$10% deviation

recommended by ASTM D4626 method. This validates the precision and accuracy with which the gas chromatograph can perform hydrocarbon liquid compositional analysis.

Table 2.13: Relative response factors of n-paraffin mixture (relative to n-decane)

Component	Carbon Number	Peak Area	Weight% Gas Chromatograph	Weight% (Standard n-Paraffin Mix) ASTM D2887	Relative Response F_n	% Deviation
n-Hexane	nC_6	822085	7.784	7.781	1.0	1.2
n-Heptane	nC_7	622101	5.891	5.957	1.0	1.1
n-Octane	nC_8	819153	7.756	7.861	1.0	1.3
n-Nonane	nC_9	838635	7.941	7.822	1.0	-1.5
n-Decane	nC_{10}	1264562	11.974	11.831	1.0	-1.2
n-Undecane	nC_{11}	1241582	11.756	11.758	1.0	0.0
n-Dodecane	nC_{12}	1239986	11.741	11.758	1.0	0.1
n-Tetradecane	nC_{14}	1215275	11.507	11.571	1.0	0.6
n-Hexadecane	nC_{16}	1042146	9.868	9.824	1.0	-0.4
n-Octadecane	nC_{18}	524148	4.963	4.961	1.0	0.0
n-Eicosane	nC_{20}	208010	1.970	1.973	1.0	0.2
n-Tetracosane	nC_{24}	206168	1.952	1.968	1.0	0.8
n-Octacosane	nC_{28}	103525	0.980	0.981	1.0	0.1
n-Dotriacontane	nC_{32}	101731	0.963	0.981	1.0	1.8
n-Hexatriacontane	nC_{36}	103108	0.976	0.986	1.0	1.0
n-Tetracontane	nC_{40}	104630	0.991	1.006	1.0	1.5
n-Tetratetracontane	nC_{44}	104124	0.986	0.981	1.0	-0.5
Total		10560969	100.000	100.000		

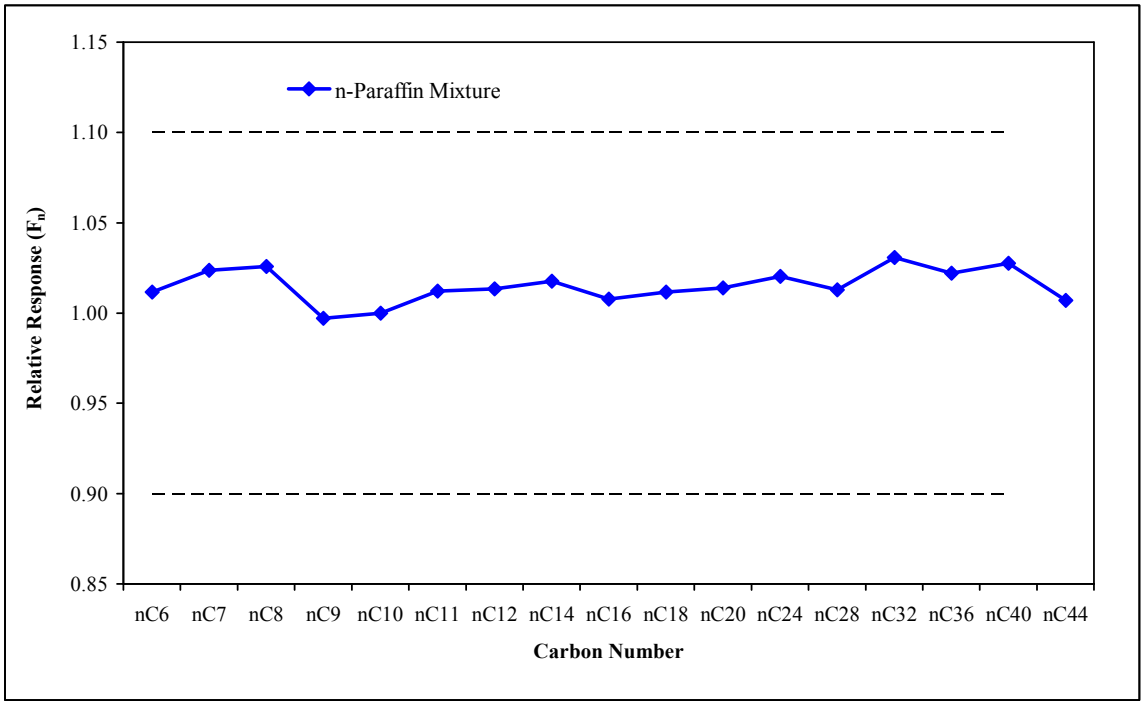

Figure 2.23: Linearity plot of relative response factor of n-paraffin mixture

2.2.4.1.2 Gas Composition Analysis

Components to be determined in the gaseous sample are physically separated by the gas chromatograph and compared to calibration data obtained under identical operating conditions. The method of calibration GPA2286 was used to calculate the response factor from a certified calibration gas reference standard of known composition. The response factor of each component determined from the reference gas standard using the thermal conductivity detector and the flame ionization detector are presented in Table 2.14. The appropriate mole or weight percentage of each component was used depending on whether the peak was taken from the thermal conductivity detector or the flame ionization detector.

Table 2.14: Response factor of components in the reference gas standard

Component	Carbon No.	Reference Gas Standard	Peak Area (From GC)	Response Factors
Column 1 (Porous Polymer Column) - Thermal Conductivity Detector				
Nitrogen	N_2	5.002	24686	0.0002026
Methane	C_1	67.994	276869	0.0002456
Column 3 (Partition Column) - Thermal Conductivity Detector				
Nitrogen	N_2	5.002	19508	0.0002564
Methane	C_1	67.994	223557	0.0003041
Carbon Dioxide	CO_2	4.995	22666	0.0002204
Ethane	C_2	7.985	39660	0.0002013
Propane	C_3	6.025	37539	0.0001605
i-Butane	iC_4	3.000	21775	0.0001378
n-Butane	nC_4	3.001	22121	0.0001357
i-Pentane	iC_5	0.999	8307	0.0001203
n-Pentane	nC_5	0.999	8201	0.0001218
Column 4 (Glass Capillary Column) - Flame Ionization Detector				
Methane	C_1	67.994	386195	0.0001761
Ethane	C_2	7.985	90380	0.0000883
Propane	C_3	6.025	101325	0.0000595
i-Butane	iC_4	3.000	66525	0.0000451
n-Butane	nC_4	3.001	66155	0.0000454
i-Pentane	iC_5	0.999	26864	0.0000372
n-Pentane	nC_5	0.999	26253	0.0000381

Validation checks for the gas compositions were performed for each analysis by comparing the percent of component eluted from one column with the percent of the same component eluted out from another column. For example the $\%C_1$ component eluted from column 1 can be compared with the $\%C_1$ component eluted out from column 3 and column 4.

2.2.4.1.3 Densitometer

The newly acquired Anton Paar densitometer DMA HP was calibrated using pure standard fluids UHP grade Nitrogen (99.997%) and de-ionized water covering a range of pressures from 1500 psig to 6000 psig at the reservoir temperature of 238°F. Densities of pure methane (99.999%) were then measured to validate the precision of the instrument covering a range of pressures from 1500 psig to 6500 psig at 238°F and the results are presented in Table 2.15.

Table 2.15: Measured densities of pure methane from DMA HP

Pressure (psig)	Temperature (°F)	Measured Density (g/cc)	NIST Density (g/cc)	%Deviation
1500	238	0.0538	0.0541	-0.5
2000	238	0.0720	0.0721	-0.2
2500	238	0.0893	0.0898	-0.5
3000	238	0.1065	0.1067	-0.2
3500	238	0.1225	0.1226	-0.1
4000	238	0.1374	0.1376	-0.1
4500	238	0.1511	0.1514	-0.2
5000	238	0.1638	0.1642	-0.2
5500	238	0.1755	0.1760	-0.3
6000	238	0.1865	0.1868	-0.2
6500	238	0.1960	0.1968	-0.4
NIST: National Institute of Standards and Testing				

These measured density data showed excellent agreement with the published values from NIST (average absolute deviation less than 0.13%). This proves the accuracy with which this new instrument can be used to measure densities of unknown samples at elevated pressure at 238°F.

2.2.4.2 Preliminary Experimental Tasks Performed

2.2.4.2.1 Stocktank Crude Oil Composition

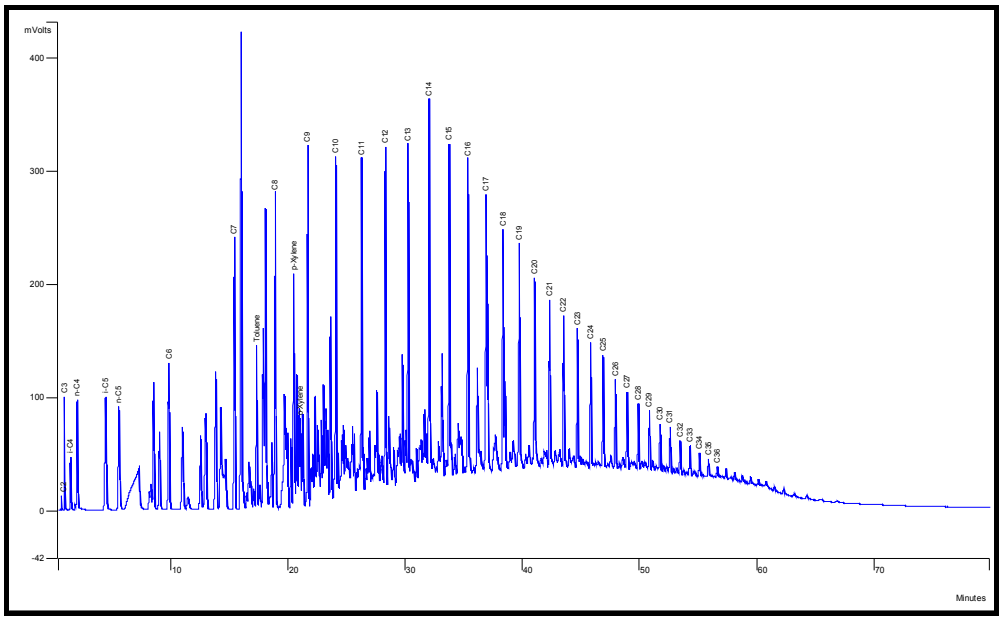

Figure 2.24: Chromatogram of the stocktank crude oil

The composition of the stocktank crude oil sample obtained from the depleted oil reservoir was analyzed using the newly acquired Varian gas chromatograph (Model CP-3800). The results of the compositional analysis performed are presented in Table 2.16. The chromatogram obtained from this compositional analysis is shown in Figure 2.24.

A portion of the stocktank crude oil sample was also sent to a commercial laboratory to verify the precision and accuracy of the results obtained from the newly acquired Varian gas chromatographic system. It can be seen from Table 2.16 that the results of the compositional analysis provided by the commercial laboratory was in good agreement with the results of the compositional analysis obtained by performing a compositional analysis of duplicate samples (STO 1 and STO 2) of the stocktank crude oil using the newly acquired Varian gas chromatograph

Figure 2.25 shows the excellent match between the results provided by the commercial laboratory to that obtained from the new gas chromatograph in which the hydrocarbon component mole% of the stocktank crude oil approximately falls on a 45^{o} straight line. This confirms the validity check of the instrument and the precision and accuracy with which compositional analysis can be performed on oil samples in our reservoir fluids laboratory at the Louisiana State University.

Table 2.16: Compositional analysis of stocktank crude oil

Components	Carbon No.	STO 1	STO 2	Comm. Lab
		Mole%	Mole%	Mole%
Methane	C_1	0.003	0.004	0.002
Ethane	C_2	0.030	0.025	0.042
Propane	C_3	0.514	0.486	0.566
i-Butane	iC_4	0.451	0.434	0.440
n-Butane	nC_4	1.132	1.115	1.160
i-Pentane	iC_5	1.610	1.574	1.502
n-Pentane	nC_5	1.359	1.331	1.447
Hexanes	C_6	3.753	3.735	3.830
Benzene	C_6	0.000	0.000	0.000
Heptanes	C_7	8.510	8.621	8.677
Toluene	C_7	1.100	1.118	0.095
Octanes	C_8	10.877	11.169	12.067
M/P-Xylene	C_8	1.580	1.620	1.066
O-Xylene	C_8	0.528	0.545	0.936
Nonanes	C_9	6.115	6.312	5.785
Decanes	C_{10}	7.003	7.153	7.567
Undecanes	C_{11}	5.777	5.846	5.765
Dodecanes	C_{12}	5.033	5.058	4.659
Tridecanes	C_{13}	4.997	4.976	4.938
Tetradecanes	C_{14}	4.674	4.637	4.309
Pentadecanes	C_{15}	3.717	3.670	3.918
Hexadecanes	C_{16}	3.436	3.409	3.266
Heptdecanes	C_{17}	3.006	2.965	2.950
Octadecanes	C_{18}	2.960	2.920	2.865
Nonadecanes	C_{19}	2.876	2.831	2.467
Eicosanes	C_{20}	2.051	2.092	2.012
Heneicosanes	C_{21}	1.776	1.470	1.751
Docosanes	C_{22}	1.468	1.611	1.520
Tricosanes	C_{23}	1.469	1.425	1.416
Tetracosanes	C_{24}	1.326	1.302	1.282
Pentacosanes	C_{25}	1.183	1.154	1.168
Hexacosanes	C_{26}	1.024	0.991	0.990
Heptacosanes	C_{27}	0.945	0.909	0.864
Octacosanes	C_{28}	0.822	0.798	0.823
Nonacosanes	C_{29}	0.769	0.743	0.738
Triacontanes	C_{30}	0.702	0.674	0.667
Hentriacontanes	C_{31}	0.615	0.597	0.610
Dotriacontanes	C_{32}	0.535	0.515	0.522
Tritriacontanes	C_{33}	0.479	0.458	0.463
Tetratriacontanes	C_{34}	0.419	0.415	0.394
Pentatriacontanes	C_{35}	0.396	0.367	0.378
Hexatriacontanes Plus	C_{36+}	2.980	2.925	4.083
Total		100.000	100.000	100.000
Properties of Stocktank Oil				
Average Molecular Weight		201.1	201.1	203.1
Specific Gravity @ 60/60°F		0.8261	0.8261	0.8321
Properties of Hexanes Plus (C_{6+}) Stocktank Oil				
Mole%	95.031			
Molecular Weight	208.3			
Specific Gravity @ 60/60°F	0.8311			
Properties of Heptanes Plus (C_{7+}) Stocktank Oil				
Mole%	91.296			
Molecular Weight	213.3			
Specific Gravity @ 60/60°F	0.8346			

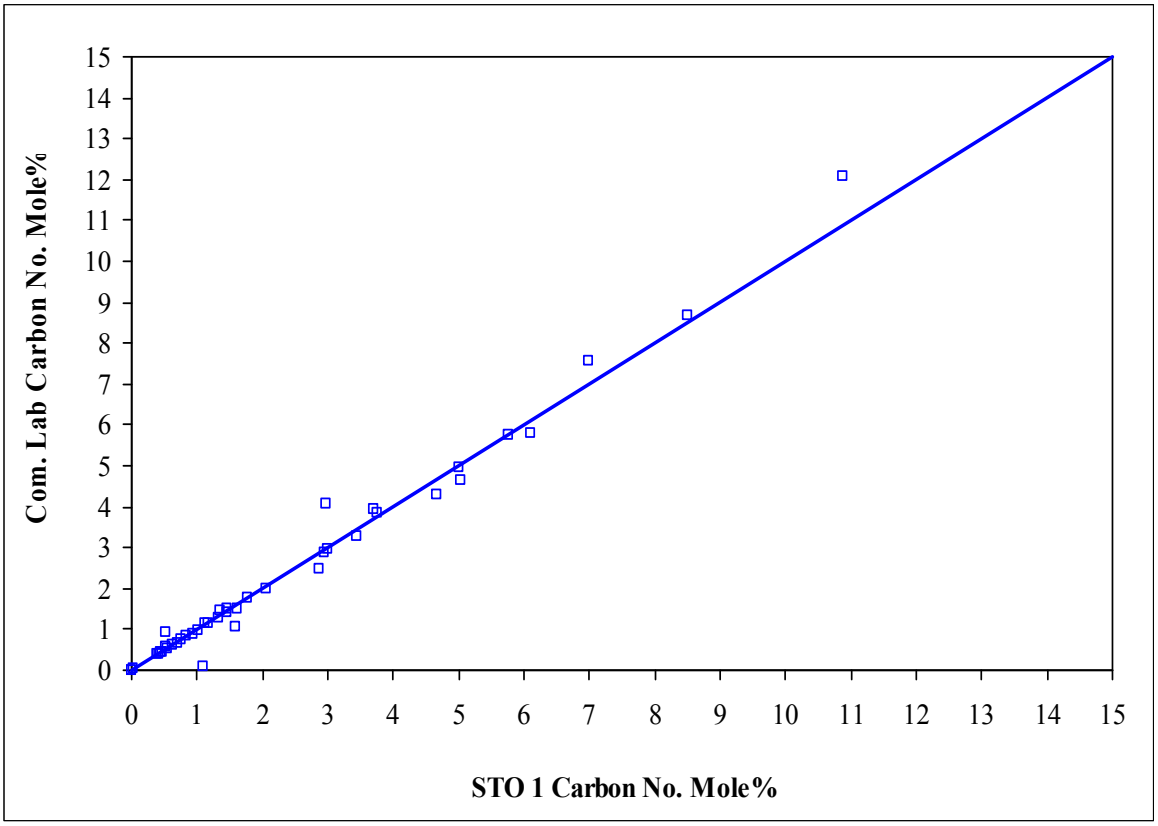

Figure 2.25: Comparison plot of carbon number mole% between commercial lab and newly acquired Varian gas chromatograph

2.2.4.2.2 Current Depleted Reservoir Fluid Composition Obtained by Using WinProp

Since the reservoir fluid sample at the current reservoir conditions was not available and only the stocktank crude oil of the depleted reservoir was provided, it was necessary to perform a compositional tuning using the CMG-WinProp software from previous available historical data in order to obtain the reservoir fluid composition at the current depleted reservoir pressure of 1100 psi and 238°F. The data used as input into the CMG WinProp software were separator gas composition, separator liquid composition (stocktank crude oil), gas-oil ratio (SCF/STB), separator pressure and temperature.

The separator gas composition, separator liquid composition (stocktank crude oil) and the recombined reservoir fluid composition are presented in Tables 2.17, 2.18, and 2.19 respectively. The Peng Robinson equation of state was used in order to match the bubble point pressure of this resultant recombined reservoir fluid composition to the initial bubble point pressure of 4050 psi at 238°F of the reservoir by using various tuning parameters.

Table 2.17: Separator gas composition

Components	Carbon No.	Separator Gas
		Mole %
Hydrogen Sulphide	H_2S	0.000
Carbon Dioxide	CO_2	2.355
Nitrogen	N_2	1.134
Methane	C_1	83.351
Ethane	C_2	6.878
Propane	C_3	2.797
i-Butane	iC_4	0.599
n-Butane	nC_4	1.009
i-Pentane	iC_5	0.543
n-Pentane	nC_5	0.397
Hexanes Plus	C_{6+}	0.939
Total		100.000
Average Molecular Weight		20.45
Properties of Hexanes Plus (C_{6+}) Separtor Gas		
Mole %		0.939
Molecular Weight		86.20
Specific Gravity @ 60/60°F		0.7084
Gas Compressibility Factor, Z (14.73 psia @ 60°F)		0.997

Table 2.18: Separator liquid composition

Components	Carbon No.	Separator Oil
		Mole %
Hydrogen Sulphide	H_2S	0.000
Carbon Dioxide	CO_2	0.000
Nitrogen	N_2	0.000
Methane	C_1	0.004
Ethane	C_2	0.025
Propane	C_3	0.486
i-Butane	iC_4	0.434
n-Butane	nC_4	1.115
i-Pentane	iC_5	1.574
n-Pentane	nC_5	1.331
Hexanes Plus	C_{6+}	95.031
Total		100.000
Average Molecular Weight		201.1
Properties of Hexanes Plus (C_{6+}) Separtor Oil		
Mole %		95.031
Molecular Weight		208.3
Specific Gravity @ 60/60°F		0.8311

Table 2.19: Recombined reservoir fluid composition at original reservoir conditions

Separator Pressure (psi)	268			
Separator Temperature (°F)	54			
Recombination Gas/Oil Ratio (SCF/STB)	1052			
Components	**Carbon No.**	**Separator Gas**	**Separator Oil**	**Recombined Fluid**
		Mole %	**Mole %**	**Mole %**
Hydrogen Sulphide	H_2S	0.000	0.000	0.000
Carbon Dioxide	CO_2	2.355	0.000	1.550
Nitrogen	N_2	1.134	0.000	0.747
Methane	C_1	83.351	0.004	54.883
Ethane	C_2	6.878	0.025	4.537
Propane	C_3	2.797	0.486	2.007
i-Butane	iC_4	0.599	0.434	0.543
n-Butane	nC_4	1.009	1.115	1.045
i-Pentane	iC_5	0.543	1.574	0.895
n-Pentane	nC_5	0.397	1.331	0.716
Hexanes Plus	C_{6+}	0.939	95.031	33.077
Total		100.000	100.000	100.000
Average Molecular Weight		20.5	201.1	82.93
Properties of Hexanes Plus (C_{6+})				
Mole %		0.939	95.031	33.077
Molecular Weight		86.2	208.3	-
Specific Gravity @ 60/60°F		0.7084	0.8311	-
Gas Compressibility Factor, Z (14.73 psia @ 60°F)		0.997	-	-

A two-phase flash was then preformed on this tuned reservoir fluid composition to obtain current reservoir composition of the depleted reservoir at reservoir conditions of 1100 psi (bubble point pressure) and 238°F (Table 2.20). The liquid phase composition from this two-phase flash was then used to prepare a recombined live reservoir fluid in the laboratory.

Table 2.20: Reservoir fluid composition at current depleted reservoir conditions

Flash Conditions at Bubble Point (psi)	1100			
Weight Shift	50			
Components	**Carbon No.**	**Recombined Fluid**	**Liquid Phase**	**Vapor Phase**
		Mole %		
Hydrogen Sulphide	H_2S	0.000	0.000	0.000
Carbon Dioxide	CO_2	1.550	0.762	2.247
Nitrogen	N_2	0.747	0.147	1.278
Methane	C_1	54.883	18.691	86.870
Ethane	C_2	4.537	3.093	5.813
Propane	C_3	2.007	2.069	1.952
i-Butane	iC_4	0.543	0.704	0.401
n-Butane	nC_4	1.045	1.448	0.689
i-Pentane	iC_5	0.895	1.444	0.410
n-Pentane	nC_5	0.716	1.191	0.296
Hexanes Plus	C_{6+}	33.077	70.451	0.045
Total		100.000	100.000	100.000
Average Molecular Weight		82.9	155.1	19.13

2.2.4.2.3 Preparation of Recombined Reservoir Fluid

While preparing the recombined live reservoir fluid using the liquid phase composition obtained from the two-phase flash calculations, the ethane and propane components were lumped into the methane portion. This can be considered reasonable, since there were no significant amounts of ethane and propane components present in the liquid phase composition obtained from the two-phase flash, as the reservoir was depleted from the original pressure of 4050 psi at 238°F to the current depleted pressure of 1100 psi at 238°F. The remaining components N_2, CO_2, i-C_4 and n-C_4 were lumped into the hexanes plus fraction to simplify the live recombined reservoir fluid preparation procedure. Also, these components were present in small quantities in the liquid phase composition obtained from the two-phase flash as the reservoir was depleted, thus would not significantly affect the minimum miscibility pressure determinations after the preparation of the recombined reservoir fluid. Furthermore, various miscibility correlations provided by Holm and Josendal (1974), Yellig and Metcalf (1980), and Cronquist (1978) predict that the light ends in oils such as methane and nitrogen, and the intermediate molecular weight hydrocarbons in oil, such as ethane, propane and butane, have a small effect on CO_2 miscibility pressure (Stalkup, 1984). The results of the calculation spreadsheet used for obtaining the volume of methane (cc) to be added per mole of live fluid are described in Table 2.21.

Table 2.21: The composition of live reservoir fluid used in all the experiments

Components	Carbon No.	Molecular Weight gm/mole	Live Fluid Mole%	Live Fluid (C_1 lumped) Mole%	Pressure psig	Density at P and 75°F gm/cc	Volume Added cc gas/mol Live Oil
Hydrogen Sulphide	H_2S	34.08	0.000	0.000	-	-	0.000
Carbon Dioxide	CO_2	44.01	0.762	0.000	-	-	0.000
Nitrogen	N_2	28.01	0.147	0.000	-	-	0.000
Methane	C_1	16.04	18.691	23.854	2000	0.1129	33.894
Ethane	C_2	30.07	3.093	0.000	-	-	0.000
Propane	C_3	44.10	2.069	0.000	-	-	0.000
i-Butane	iC_4	58.12	0.704	0.000	-	-	0.000
n-Butane	nC_4	58.12	1.448	0.000	-	-	0.000
i-Pentane	iC_5	72.15	1.444	0.000	-	-	0.000
n-Pentane	nC_5	72.15	1.191	0.000	-	-	0.000
Hexanes Plus	C_{6+}	208.30	70.451	76.146	500	0.8270	191.794*
Total			100.000	100.000			225.688
Properties of Hexanes Plus (C_{6+}) Stocktank Oil							
Molecular Weight			208.30				
Specific Gravity @ 60/60°F			0.8311				
*** Volume of Stocktank Oil per Mole of Live Fluid.**							

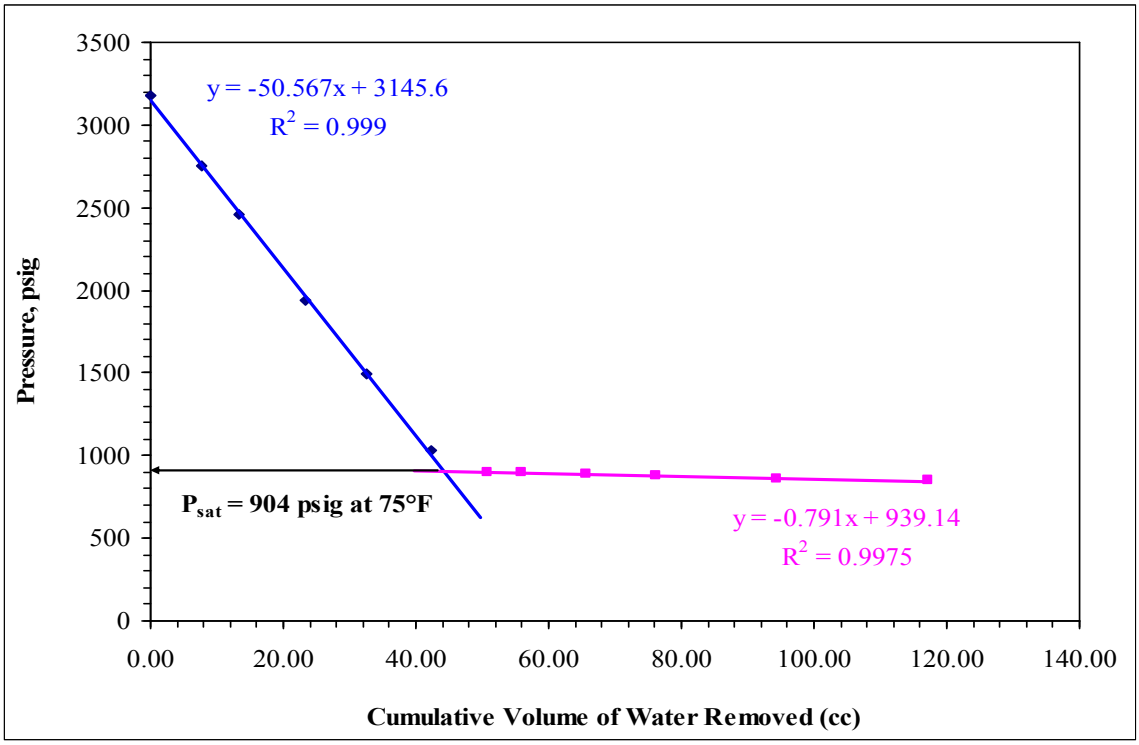

Figure 2.26: Bubble point pressure of live reservoir fluid at ambient temperature

2.2.4.2.4 Bubble Point Pressure Determination of the Recombined Reservoir Fluid

Figure 2.26 shows a plot of the cumulative volume of water collected versus the pressure obtained during the determination of the bubble point pressure of the live reservoir fluid at ambient conditions. Two different linear sections were identified, one above the bubble point and one below the bubble point. Values of above 99% of the coefficient of determination (R^2) were obtained when these two identified different linear sections were fitted separately using linear regression, thus indicating excellent fits. These two linear regression equations were then solved to obtain the point of their intersection, which was the bubble point pressure of the recombined reservoir fluid.

The experimentally measured bubble point pressure value of 904 psig at 75°F was in good agreement with the value of the bubble point pressure obtained using the CMG-WinProp software (927 psig at 75°F). The recombined live reservoir fluid was pressurized to 4000 psig and was kept at that pressure in order to maintain single-phase conditions of the fluid at all times.

2.2.4.2.5 Compositional Analysis of Recombined Reservoir Fluid

The composition of the recombined live reservoir fluid prepared in the laboratory was determined by flashing a portion of the sample to ambient conditions, and analyzing the compositions of the flashed separated products using gas chromatography. The results of the flashed gas, flashed oil and recombined oil are presented in Table 2.22. An excellent

match was obtained between the target and measured live reservoir fluid composition, thus confirming the use of a representative recombined reservoir fluid for conducting IFT experiments using the drop shape analysis and capillary rise techniques.

A compositional analysis was again performed later to check the stability of the prepared live oil sample. The compositional analysis results presented in Table 2.23 indicated that the composition measured on January 7, 2006 was approximately identical to that measured on June 3, 2006, thus confirming the integrity of the sample.

A new batch of recombined reservoir fluid was prepared and the compositional analysis was performed on this batch (August 5, 2006). The compositional analysis of this new batch presented in Table 2.23 was almost identical to the compositions performed on the previous batch. This confirms that true representative fluids were used throughout the experimental study.

Table 2.22: Composition of prepared recombined reservoir fluid

Components	Carbon No.	Flashed Gas	Flashed Oil	Recombined Fluid
		Mole %	Mole %	Mole %
Hydrogen Sulphide	H_2S	0.000	0.000	0.000
Carbon Dioxide	CO_2	0.026	0.000	0.006
Nitrogen	N_2	0.047	0.000	0.011
Methane	C_1	95.610	0.039	23.141
Ethane	C_2	0.000	0.001	0.000
Propane	C_3	0.275	0.026	0.085
i-Butane	iC_4	0.331	0.089	0.148
n-Butane	nC_4	0.782	0.336	0.444
i-Pentane	iC_5	0.850	0.973	0.943
n-Pentane	nC_5	0.625	1.000	0.908
Hexanes	C_6	0.790	3.488	2.835
Benzene	C_6	0.000	0.000	0.000
Heptanes	C_7	0.619	7.815	6.076
Toluene	C_7	0.000	1.151	0.873
Octanes	C_8	0.021	10.835	8.220
M/P-Xylene	C_8	0.000	1.727	1.309
O-Xylene	C_8	0.000	0.545	0.414
Nonanes	C_9	0.024	6.053	4.595
Decanes	C_{10}		7.118	5.397
Undecanes	C_{11}		6.007	4.555
Dodecanes	C_{12}		5.347	4.055
Tridecanes	C_{13}		5.340	4.049
Tetradecanes	C_{14}		5.041	3.823
Pentadecanes	C_{15}		4.013	3.043
Hexadecanes	C_{16}		3.725	2.825
Heptadecanes	C_{17}		3.260	2.472
Octadecanes	C_{18}		3.217	2.440
Nonadecanes	C_{19}		3.140	2.381
Eicosanes	C_{20}		2.325	1.763
Heneicosanes	C_{21}		1.852	1.404
Docosanes	C_{22}		1.598	1.212
Tricosanes	C_{23}		1.600	1.213
Tetracosanes	C_{24}		1.448	1.098
Pentacosanes	C_{25}		1.292	0.980
Hexacosanes	C_{26}		1.126	0.854
Heptacosanes	C_{27}		1.021	0.774
Octacosanes	C_{28}		0.901	0.683
Nonacosanes	C_{29}		0.821	0.622
Triacontanes	C_{30}		0.748	0.568
Hentriacontanes	C_{31}		0.659	0.500
Dotriacontanes	C_{32}		0.565	0.428
Tritriacontanes	C_{33}		0.507	0.385
Tetratriacontanes	C_{34}		0.432	0.328
Pentatriacontanes	C_{35}		0.408	0.309
Hexatriacontanes Plus	C_{36+}		2.411	1.831
Total		100.000	100.000	100.000
Average Molecular Weight		18.55	210.0	163.7
Flash Gas-Oil Ratio, SCF/STB				166.9
Properties of Hexanes Plus (C_{6+}) Recombined Reservoir Fluid				
Mole %		74.314		
Molecular Weight		213.0		
Specific Gravity @ 60/60°F		0.8325		
Properties of Heptanes Plus (C_{7+}) Recombined Reservoir Fluid				
Mole %		71.479		
Molecular Weight		218.0		
Specific Gravity @ 60/60°F		0.8359		

Table 2.23: Composition of recombined reservoir fluid

Components	Carbon No.	Recombined Reservoir Fluid		
		January 7, 2006	June 3, 2006	August 5, 2006
		Mole %	Mole %	Mole %
Hydrogen Sulphide	H_2S	0.000	0.000	0.000
Carbon Dioxide	CO_2	0.006	0.038	0.063
Nitrogen	N_2	0.011	0.051	0.005
Methane	C_1	23.141	22.984	24.216
Ethane	C_2	0.000	0.015	0.011
Propane	C_3	0.085	0.083	0.021
i-Butane	iC_4	0.148	0.131	0.068
n-Butane	nC_4	0.444	0.380	0.190
i-Pentane	iC_5	0.943	0.854	0.638
n-Pentane	nC_5	0.908	0.823	0.597
Hexanes	C_6	2.835	2.647	2.353
Benzene	C_6	0.000	0.000	0.000
Heptanes	C_7	6.076	5.868	5.378
Toluene	C_7	0.873	0.807	0.188
Octanes	C_8	8.220	7.404	7.658
M/P-Xylene	C_8	1.309	1.303	1.248
O-Xylene	C_8	0.414	0.404	0.382
Nonanes	C_9	4.595	4.765	4.693
Decanes	C_{10}	5.397	5.508	5.451
Undecanes	C_{11}	4.555	4.621	4.636
Dodecanes	C_{12}	4.055	4.197	4.179
Tridecanes	C_{13}	4.049	4.108	4.232
Tetradecanes	C_{14}	3.823	4.000	4.024
Pentadecanes	C_{15}	3.043	3.006	3.163
Hexadecanes	C_{16}	2.825	2.878	2.949
Heptadecanes	C_{17}	2.472	2.537	2.592
Octadecanes	C_{18}	2.440	2.492	2.557
Nonadecanes	C_{19}	2.381	2.515	2.498
Eicosanes	C_{20}	1.763	1.427	1.680
Heneicosanes	C_{21}	1.404	1.726	1.590
Docosanes	C_{22}	1.212	1.258	1.321
Tricosanes	C_{23}	1.213	1.253	1.285
Tetracosanes	C_{24}	1.098	1.145	1.170
Pentacosanes	C_{25}	0.980	1.004	1.020
Hexacosanes	C_{26}	0.854	0.891	0.913
Heptacosanes	C_{27}	0.774	0.786	0.817
Octacosanes	C_{28}	0.683	0.713	0.733
Nonacosanes	C_{29}	0.622	0.649	0.663
Triacontanes	C_{30}	0.568	0.595	0.610
Hentriacontanes	C_{31}	0.500	0.516	0.533
Dotriacontanes	C_{32}	0.428	0.437	0.463
Tritriacontanes	C_{33}	0.385	0.395	0.412
Tetratriacontanes	C_{34}	0.328	0.340	0.359
Pentatriacontanes	C_{35}	0.309	0.302	0.337
Hexatriacontanes Plus	C_{36+}	1.831	2.144	2.104
Total		100.000	100.000	100.000
Average Molecular Weight		163.7	164.2	165.6
Flash Gas-Oil Ratio, SCF/STB		166.9	167.1	165.6
Properties of Hexanes Plus (C_{6+}) Recombined Reservoir Fluid				
Mole %		74.314	74.641	74.191
Molecular Weight		213.0	212.9	216.5
Specific Gravity @ 60/60°F		0.8325	0.8320	0.8362
Properties of Heptanes Plus (C_{7+}) Recombined Reservoir Fluid				
Mole %		71.479	71.994	71.838
Molecular Weight		218.0	217.5	220.7
Specific Gravity @ 60/60°F		0.8359	0.8351	0.839

2.2.4.2.6 Density Measurements of the Recombined Reservoir Fluid

Densities of the recombined reservoir fluid sample were measured at a wide range of pressures at 75°F and 238°F using an old DMA 512P and the newly acquired DMA HP densitometers. These measurements of densities over a wide range of pressures at 75°F and 238°F are summarized in Tables 2.24 and 2.25, respectively. Two sets of experiments were performed using constant gas-oil molar ratios and two sets of more experiments were performed using constant gas-oil volume ratios over a wide range of pressures at 238°F. Densities of the fluid-fluid phases were measured for one set of constant gas-oil molar ratio (Rm=0.893/0.107=8.346) experiments using the old DMA 512P. Densities of the fluid-fluid phases for gas-oil molar ratio Rm=0.700/0.300=2.333, gas-oil volume ratio Rv=0.850/0.150=5.667 and gas-oil volume ratio Rv=0.450/0.550=0.818 were performed using the new DMA HP.

Table 2.24: Measured densities of recombined reservoir fluid at 75°F

Pressure psig	Temperature °F	Measured Density DMA 512P gm/cc	Measured Density DMA HP gm/cc	Comm. Lab Density gms/cc	%Deviation DMA 512P	%Deviation DMA HP
1500	75.0	0.8687	0.8060	0.810	7.8	-0.5
2000	75.0	0.8721	0.8087			
2500	75.0	0.8752	0.8114			
3000	75.0	0.8786	0.8140	0.818	7.9	-0.5
3500	75.0	0.8817	0.8166			
4000	75.0	0.8850	0.8187			
4500	75.0	0.8881	0.8216	0.825	8.1	-0.4
5000	75.0		0.8237			
5500	75.0		0.8265			
6000	75.0		0.8287			
6500	75.0		0.8313			

Table 2.25: Measured densities of recombined reservoir fluid at 238°F

Pressure psig	Temperature °F	Measured Density DMA 512P gm/cc	Measured Density DMA HP gm/cc	Comm. Lab Density gms/cc	%Deviation DMA 512P	%Deviation DMA HP
1500	238.0	0.8404	0.7416	0.744	13.3	-0.3
2000	238.0	0.8450	0.7455			
2500	238.0	0.8497	0.7487			
3000	238.0	0.8543	0.7525	0.755	13.5	-0.3
3500	238.0	0.8586	0.7562			
4000	238.0	0.8630	0.7595			
4500	238.0	0.8673	0.7632	0.765	13.6	-0.2
5000	238.0		0.7665			
5500	238.0		0.7696			
6000	238.0		0.7735			
6500	238.0		0.7758			

A portion of the recombined reservoir fluid was also sent to a commercial laboratory for density measurements at 75°F and 238°F, to verify the accuracy and precision of the instruments. The linear curve fit equations were obtained by plotting the densities of the recombined reservoir fluid versus pressure for all the measurements of DMA 512P, DMA HP and the values obtained from the commercial laboratory. They are shown in Figures 2.27 and 2.28, respectively. The coefficients of determination (R^2) values of above 99% obtained for all the equations indicate good correlations.

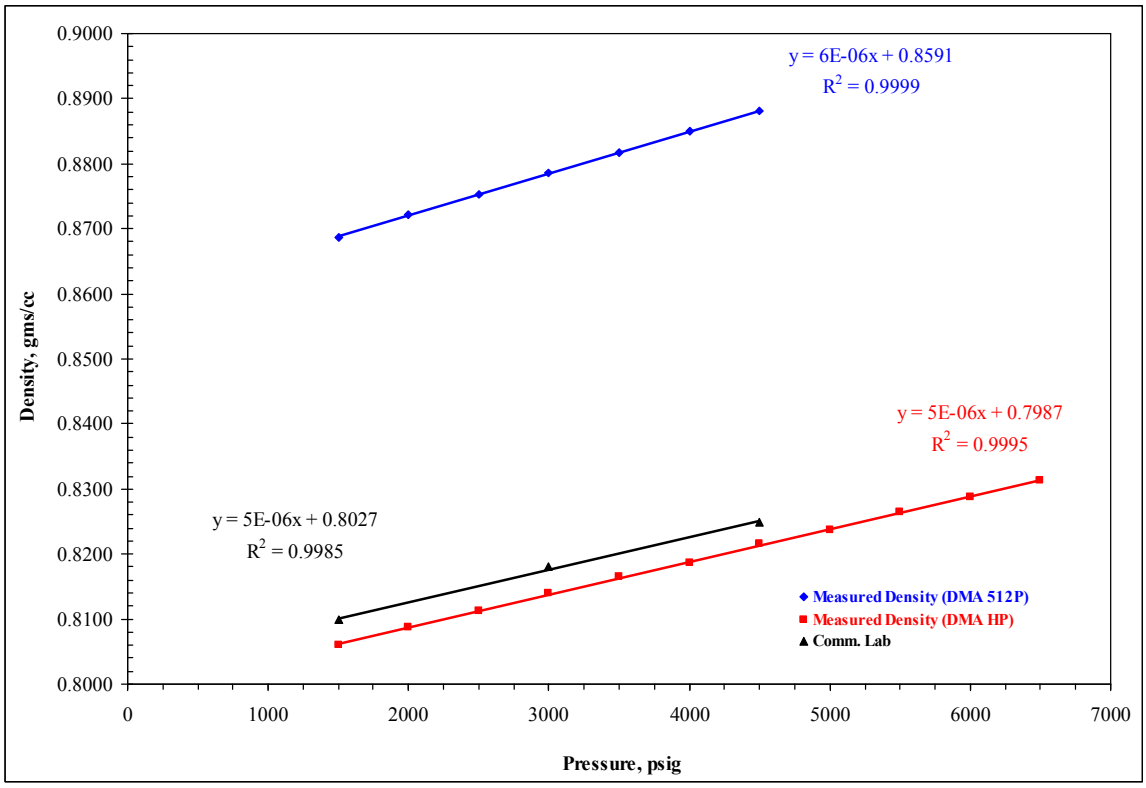

Figure 2.27: Measured pressure densities of recombined reservoir fluid at 75°F

It can be seen from Figures 2.27 and 2.28 that there was a noticeable deviation of about 13.5% between the oil densities measured using the old DMA 515P and that obtained from the commercial laboratory. Since the experimental study for the first set of constant gas-oil molar ratio (Rm=0.893/0.107=8.346) had already started, a correction factor of 0.0955 was applied to all the equilibrated oil phase densities obtained while performing the gas-oil IFT measurements using the old DMA 512P. However, an excellent agreement was obtained for the recombined oil densities measured using the new DMA HP to that obtained from the commercial laboratory, needing no correction.

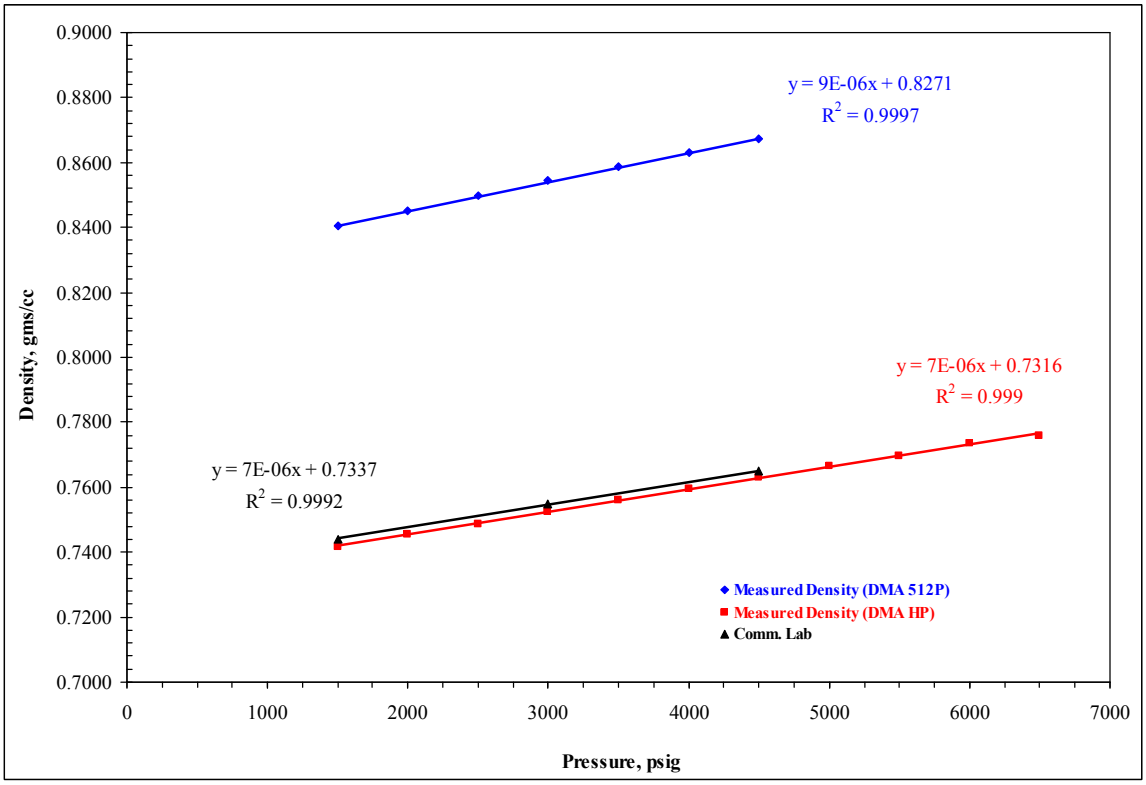

Figure 2.28: Measured pressure densities of recombined reservoir fluid at 238°F

Table 2.26: Fluid properties at 75°F

Pressure (psig)	Injection Gas Carbon Dioxide (CO_2)		Recombined Reservoir Fluid
	Compressibility, z (CMG-WinProp)	Density, (g/cc) (NIST)	Measured Density (g/cc)
1500	0.232	0.8337	0.8060
2000	0.288	0.8727	0.8087
2500	0.342	0.9013	0.8114
3000	0.396	0.9243	0.8140
3500	0.448	0.9436	0.8166
4000	0.499	0.9604	0.8187
4500	0.550	0.9753	0.8216
5000	0.600	0.9888	0.8237
5500	0.649	1.0011	0.8265
6000	0.697	1.0125	0.8287
6500	0.745	1.0230	0.8313
Molecular Weight of Carbon Dioxide = 44.01 g/mole Molecular Weight of Recombined Reservoir Fluid = 163.72 g/mole NIST - National Institute of Standards and Technology			

The properties of carbon dioxide and recombined reservoir fluid at 75°F and 238°F are summarized in the Tables 2.16 and 2.17, respectively.

Table 2.27: Fluid properties at 238°F

Pressure (psig)	Injection Gas Carbon Dioxide (CO_2)		Recombined Reservoir Fluid Measured Density (g/cc)
	Compressibility, z (CMG-WinProp)	Density, (g/cc) (NIST)	
1500	0.774	0.1822	0.7416
2000	0.720	0.2641	0.7455
2500	0.685	0.3531	0.7487
3000	0.670	0.4388	0.7525
3500	0.671	0.5123	0.7562
4000	0.684	0.5720	0.7595
4500	0.705	0.6202	0.7632
5000	0.729	0.6599	0.7665
5500	0.757	0.6933	0.7696
6000	0.786	0.7219	0.7735
6500	0.817	0.7469	0.7758
Molecular Weight of Carbon Dioxide = 44.01 g/mole Molecular Weight of Recombined Reservoir Fluid = 163.72 g/mole NIST - National Institute of Standards and Technology			

2.2.4.3 IFT Measurements of CO_2-Reservoir Fluid System at 238°F

Gas-oil interfacial tension (IFT) measurements, densities of the equilibrated fluid phases and compositional analysis of the equilibrated fluid-fluid phases were performed with the recombined reservoir fluid as the liquid phase and carbon dioxide as the gas phase after equilibrating them in the high pressure optical cell. First two sets of experiments were carried out using constant gas-oil molar ratios and the later two sets of experiments using constant gas-oil volume ratios at the reservoir temperature of 238°F and varying experimental pressures from 1500 psig to 6000 psig. This was done to investigate the compositional effects on interfacial tension and gas-oil miscibility.

The densities of the equilibrated fluid phases at the different pressures for the constant gas/oil molar ratio Rm=8.346 at 238°F were performed using the old DMA 512P densitometer and a correction factor of 0.0955 was subtracted from each liquid phase density to correct for the consistent deviations observed. The densities of the equilibrated fluid phases at different pressures for the constant gas/oil molar ratio Rm=2.333, constant gas-oil volume ratio Rv=5.667 and constant gas/oil volume ratio Rv=0.818 were performed using the new DMA HP densitometer. The compositions of the equilibrated gas and liquid phases at each experimental pressure were measured using the gas chromatograph.

The optical cell was thoroughly cleaned at the end of each pressure test, evacuated and reloaded with fresh recombined reservoir fluid and CO_2 to the start the test at the next pressure. This was to avoid compositional interference from the previous experiment. This procedure is distinctly different from previously conducted tests (Ayirala, 2005) wherein all IFT measurements were made at varying pressures but with the same initial load of live oil and gas phases.

One batch of prepared recombined reservoir fluid was used in performing the IFT measurements at the constant gas/oil molar ratio Rm=8.346 and a second batch of prepared recombined reservoir fluid was used in performing the IFT measurements at the constant gas/oil molar ratio Rm=2.333, constant gas/oil volume ratio Rv=5.667 and constant gas/oil volume ratio Rv=0.818. However as described previously in Subsection 2.2.4.2.5 (Table 2.23), this recombined reservoir fluid composition in all cases were quite similar.

2.2.4.3.1 Constant Gas/Oil Molar Ratio Experiments

Gas-oil IFT measurements were carried out at various pressures using a constant gas-oil molar ratio of 0.893 mole fraction of carbon dioxide gas and 0.107 mole fraction of recombined reservoir fluid as feed in the mixture (Rm=0.893/0.107=8.346). Gas-Oil IFT measurements were also carried out using a constant gas-oil molar ratio of 0.700 mole fraction of carbon dioxide gas and 0.300 mole fraction of recombined reservoir fluid as feed in the mixture (Rm=0.700/0.300=2.333). The measured densities of the equilibrated gas and liquid phases at 238°F and equilibrium interfacial tension values obtained from the drop shape and the capillary rise techniques for the constant gas-oil molar ratio of Rm=8.346 are summarized in the Table 2.28. The compositional analysis of the equilibrated gas and liquid phases at 238°F for the constant gas/oil molar ratio Rm=8.346 are summarized in the Tables 2.29 and 2.30 respectively.

Table 2.28: Summary of the equilibrated fluid densities and gas-oil IFT measurements at constant gas/oil molar ratio of 0.893 mole fraction of CO_2 and 0.107 mole fraction of recombined reservoir fluid (Rm=0.893/0.107=8.346) at 238°F

Gas Mole Fraction	0.893							
Oil Mole Fraction	0.107							
Pressure	Equilibrated Phase Densities		Density Diff.	Capillary	Equilibrium IFT		Corresponding Volume Fraction	
	Oil	Gas	Δρ	Height	Capillary Rise	Pendant Drop		
(psig)	(g/cc)	(g/cc)		(cm)	(dyne/cm)	(dyne/cm)	Gas	Oil
1500	0.7660	0.1670	0.5990	0.475	6.97	7.30	0.901	0.099
2000	0.7665	0.2482	0.5183	0.358	4.54	6.00	0.864	0.136
2500	0.7725	0.3590	0.4135	0.317	3.21	4.85	0.826	0.174
3000	0.7775	0.4170	0.3605	0.237	2.09	3.00	0.794	0.206
3500	0.7975	0.5070	0.2905	0.211	1.50	1.70	0.768	0.232
4000	0.8005	0.5830	0.2175	0.192	1.02	1.35	0.749	0.251
5000	0.8055	0.7020	0.1035	0.133	0.34	0.13	0.723	0.277
5500	0.8115	0.7790	0.0325	0.121	0.10	*	0.714	0.286
6000	0.8145	0.7980	0.0165	0.026	0.01	*	0.706	0.294
* Could not form drop due to approaching miscibility between fluid phases								

Table 2.29: Compositional analysis of the equilibrated gas phase at constant gas/oil molar ratio of 0.893 mole fraction of CO_2 and 0.107 mole fraction of recombined reservoir fluid (Rm=0.893/0.107=8.346) at 238°F

Gas Mole Fraction	0.893									
Oil Mole Fraction	0.107									
Component	**Carbon No.**	**Pressure (psig)**								
		1500	**2000**	**2500**	**3000**	**3500**	**4000**	**5000**	**5500**	**6000**
		Gas Phase Mole%								
Hydrogen Sulphide	H_2S	0.000	0.000	0.000	0.000	0.000	0.000	0.000	0.000	0.000
Carbon Dioxide	CO_2	97.249	97.286	97.125	96.769	96.893	97.300	97.589	96.885	96.900
Nitrogen	N_2	0.051	0.013	0.014	0.034	0.108	0.048	0.029	0.004	0.128
Methane	C_1	1.958	2.024	2.066	2.263	2.253	2.269	2.007	2.196	2.236
Ethane	C_2	0.000	0.000	0.000	0.000	0.000	0.000	0.000	0.000	0.000
Propane	C_3	0.008	0.014	0.007	0.009	0.008	0.000	0.000	0.007	0.029
i-Butane	iC_4	0.013	0.019	0.012	0.013	0.012	0.011	0.010	0.013	0.028
n-Butane	nC_4	0.038	0.044	0.033	0.037	0.033	0.029	0.026	0.035	0.053
i-Pentane	iC_5	0.069	0.071	0.063	0.069	0.061	0.048	0.044	0.068	0.070
n-Pentane	iC_5	0.065	0.068	0.059	0.064	0.057	0.042	0.038	0.063	0.074
Hexanes	C_6	0.157	0.141	0.156	0.170	0.146	0.086	0.082	0.171	0.116
Heptanes Plus	C_{7+}	0.392	0.320	0.465	0.572	0.429	0.167	0.175	0.558	0.366
Total		100.000	100.000	100.000	100.000	100.000	100.000	100.000	100.000	100.000
Density, at Pressure (g/cc)		0.1670	0.2482	0.3590	0.4170	0.5070	0.5830	0.7000	0.7790	0.7980
Molecular Weight		43.81	43.75	43.83	43.86	43.74	43.54	43.62	43.87	43.70
Charged GOR, SCF/STB		16698	12654	9524	7980	7063	6490	5828	5617	5451

Table 2.30: Compositional analysis of the equilibrated liquid phase at constant gas/oil molar ratio of 0.893 mole fraction of CO_2 and 0.107 mole fraction of recombined reservoir fluid (Rm=0.893/0.107=8.346) at 238°F

Gas Mole Fraction	0.893										
Oil Mole Fraction	0.107										
Component	**Carbon No.**	**Pressure (psig)**									
		1250 Recombined Reservoir Fluid*	**1500**	**2000**	**2500**	**3000**	**3500**	**4000**	**5000**	**5500**	**6000**
		Liquid Phase Mole%									
Hydrogen Sulphide	H2S	0.000	0.000	0.000	0.000	0.000	0.000	0.000	0.000	0.000	0.000
Carbon Dioxide	CO2	0.006	45.015	52.302	58.088	62.244	66.425	69.088	72.756	73.896	75.852
Nitrogen	N2	0.011	0.013	0.000	0.002	0.000	0.018	0.017	0.013	0.005	0.016
Methane	C1	23.141	0.651	0.829	0.907	1.120	1.236	1.374	1.371	1.601	1.462
Ethane	C2	0.000	0.004	0.007	0.006	0.006	0.003	0.002	0.007	0.014	0.006
Propane	C3	0.085	0.012	0.013	0.011	0.012	0.011	0.012	0.008	0.013	0.009
i-Butane	iC4	0.148	0.026	0.027	0.021	0.021	0.020	0.021	0.016	0.021	0.016
n-Butane	nC4	0.444	0.088	0.088	0.067	0.067	0.065	0.061	0.049	0.061	0.049
i-Pentane	iC5	0.943	0.247	0.262	0.177	0.169	0.148	0.141	0.102	0.134	0.104
n-Pentane	iC5	0.908	0.264	0.230	0.185	0.173	0.151	0.141	0.099	0.129	0.105
Hexanes	C6	2.835	1.048	1.152	0.716	0.642	0.561	0.492	0.314	0.386	0.306
Heptanes Plus	C7+	71.479	52.632	45.090	39.820	35.546	31.362	28.651	25.265	23.740	22.075
Total		100.000	100.000	100.000	100.000	100.000	100.000	100.000	100.000	100.000	100.000
Density, at Pressure (g/cc)		0.7403	0.7660	0.7665	0.7725	0.7775	0.7975	0.8005	0.8055	0.8115	0.8145
Molecular Weight (Recombined Oil)		163.7	145.2	129.5	122.1	113.8	108.3	105.1	104.4	101.3	98.2
Molecular Weight C_{7+} (Recombined Oil)		218.0	235.5	232.7	239.6	240.0	248.9	257.5	283.7	286.2	290.6
Flash GOR, SCF/STB		0	410	560	686	825	961	1061	1148	1236	1340
*** Bubble Point Pressure**											

Table 2.31: Summary of the equilibrated fluid densities and gas-oil IFT measurements at constant gas/oil molar ratio of 0.700 mole fraction of CO_2 and 0.300 mole fraction of recombined reservoir fluid (Rm=0.700/0.300=2.333) at 238°F

Gas Mole Fraction	0.700							
Oil Mole Fraction	0.300							
Pressure	Equilibrated Phase Densities		Density Diff.	Capillary	Equilibrium IFT		Corresponding Volume Fraction	
	Oil	Gas	Δρ	Height	Capillary Rise	Pendant Drop		
(psig)	(g/cc)	(g/cc)		(cm)	(dyne/cm)	(dyne/cm)	Gas	Oil
2000	0.7689	0.2362	0.5327	0.112	3.27	*	0.639	0.361
3000	0.7703	0.3749	0.3954	0.160	1.55	*	0.518	0.482
3500	0.7709	0.4326	0.3383	0.105	0.87	*	0.481	0.519
4000	0.7720	0.4965	0.2755	0.080	0.54	*	0.454	0.546
5000	0.7726	0.5807	0.1919	0.040	0.19	*	0.421	0.579
6000	0.7795	0.6781	0.1014	0.004	0.01	*	0.402	0.598
* Equilibrium IFT of the pendant drop could not be calculated as the optical cell was filled with significant amount of reservoir fluid								

Table 2.32: Compositional analysis of the equilibrated gas phase at constant gas/oil molar ratio of 0.700 mole fraction of CO_2 and 0.300 mole fraction of recombined reservoir fluid (Rm=0.700/0.300=2.333) at 238°F

Gas Mole Fraction	0.700						
Oil Mole Fraction	0.300						
Component	Carbon No.	Pressure (psig)					
		2000	3000	3500	4000	5000	6000
		Gas Phase Mole%					
Hydrogen Sulphide	H2S	0.000	0.000	0.000	0.000	0.000	0.000
Carbon Dioxide	CO2	81.305	81.419	83.423	84.131	84.269	84.027
Nitrogen	N2	0.086	0.050	0.066	0.073	0.073	0.286
Methane	C1	18.131	17.609	15.445	14.529	14.324	14.568
Ethane	C2	0.000	0.000	0.000	0.000	0.000	0.000
Propane	C3	0.014	0.017	0.013	0.017	0.011	0.016
i-Butane	iC4	0.025	0.027	0.023	0.027	0.026	0.027
n-Butane	nC4	0.055	0.059	0.057	0.062	0.066	0.061
i-Pentane	iC5	0.091	0.107	0.116	0.123	0.156	0.123
n-Pentane	iC5	0.070	0.098	0.094	0.109	0.134	0.110
Hexanes	C6	0.110	0.193	0.241	0.260	0.279	0.258
Heptanes Plus	C7+	0.113	0.421	0.522	0.669	0.662	0.524
Total		100.000	100.000	100.000	100.000	100.000	100.000
Density, at Pressure (g/cc)		0.2362	0.3749	0.4326	0.4965	0.5807	0.6781
Molecular Weight		39.10	39.49	40.18	40.54	40.61	40.39
Charged GOR, SCF/STB		3607	2677	2472	2342	2189	2098

The measured densities of the equilibrated gas and liquid phases and equilibrium interfacial tension values obtained from the capillary rise technique for the constant gas-oil molar ratio Rm=2.333 are summarized in Table 2.31. The compositional analysis of the equilibrated gas and liquid phases at 238°F for the constant gas/oil molar ratio Rm=5.667 are summarized in the Tables 2.32 and 2.33 respectively.

Table 2.33: Compositional analysis of the equilibrated liquid phase at constant gas/oil molar ratio of 0.700 mole fraction of CO_2 and 0.300 mole fraction of recombined reservoir fluid (Rm=0.700/0.300=2.333) at 238°F

Gas Mole Fraction	0.700							
Oil Mole Fraction	0.300							
Component	**Carbon No.**	**Pressure (psig)**						
		1250 Recombined Reservoir Fluid*	**2000**	**3000**	**3500**	**4000**	**5000**	**6000**
		Liquid Phase Mole%						
Hydrogen Sulphide	H2S	0.000	0.000	0.000	0.000	0.000	0.000	0.000
Carbon Dioxide	CO2	0.063	40.034	59.786	64.775	65.971	69.951	72.702
Nitrogen	N2	0.005	0.004	0.000	0.006	0.014	0.010	0.037
Methane	C1	24.216	3.073	3.719	3.815	3.948	4.240	5.052
Ethane	C2	0.011	0.017	0.008	0.005	0.009	0.004	0.008
Propane	C3	0.021	0.015	0.011	0.009	0.010	0.009	0.008
i-Butane	iC4	0.068	0.035	0.029	0.025	0.023	0.022	0.022
n-Butane	nC4	0.190	0.101	0.083	0.066	0.067	0.062	0.061
i-Pentane	iC5	0.638	0.334	0.240	0.202	0.186	0.185	0.168
n-Pentane	iC5	0.597	0.324	0.234	0.189	0.178	0.176	0.156
Hexanes	C6	2.353	1.382	0.873	0.719	0.665	0.177	0.536
Heptanes Plus	C7+	71.838	54.681	35.017	30.189	28.929	24.657	21.250
Total		100.000	100.000	100.000	100.000	100.000	99.493	100.000
Density, at Pressure (g/cc)		0.7403	0.7689	0.7703	0.7709	0.7720	0.7726	0.7795
Molecular Weight (Recombined Oil)		165.7	144.3	110.2	102.1	98.9	89.7	84.0
Molecular Weight C_{7+} (Recombined Oil)		220.7	227.6	234.6	240.0	236.2	232.4	237.3
Flash GOR, SCF/STB		0	389	866	1062	1149	1452	1736
*** Bubble Point Pressure - New Batch**								

Effect of Constant Gas/Oil Molar Ratio on Fluid Phase Compositions, Densities and Molecular Weights

The following observations can be made regarding the effects of the two selected constant gas/oil molar ratios on the compositions, densities and molecular weights of the equilibrated gas and liquid phases using the Figures 2.29-2.35 and the Tables 2.28 and 2.31, respectively.

1. Figure 2.29 shows the plot of gas/oil volume ratio versus pressure for the two selected constant gas-oil molar ratios and indicates the decreasing trend of gas/oil volume ratios with increasing pressures in the feed mixtures used for conducting the IFT experiments at various pressures. It can be seen from Figure 2.29 that the gas/oil volume ratio decreases rapidly until a pressure of 4000 psig and then remains approximately constant for the constant gas/oil molar ratio Rm=8.346, and is an indication of approximately constant volumes of gas and constant volumes of oil in the feed mixture at each pressure. The gas/oil volume ratio displays a limited variation (3500 psig to 6000 psig) for the constant gas/oil molar ratio Rm=2.333. This

is also an indication of approximately of constant volumes of gas and constant volumes of oil in the feed mixture at each pressure.

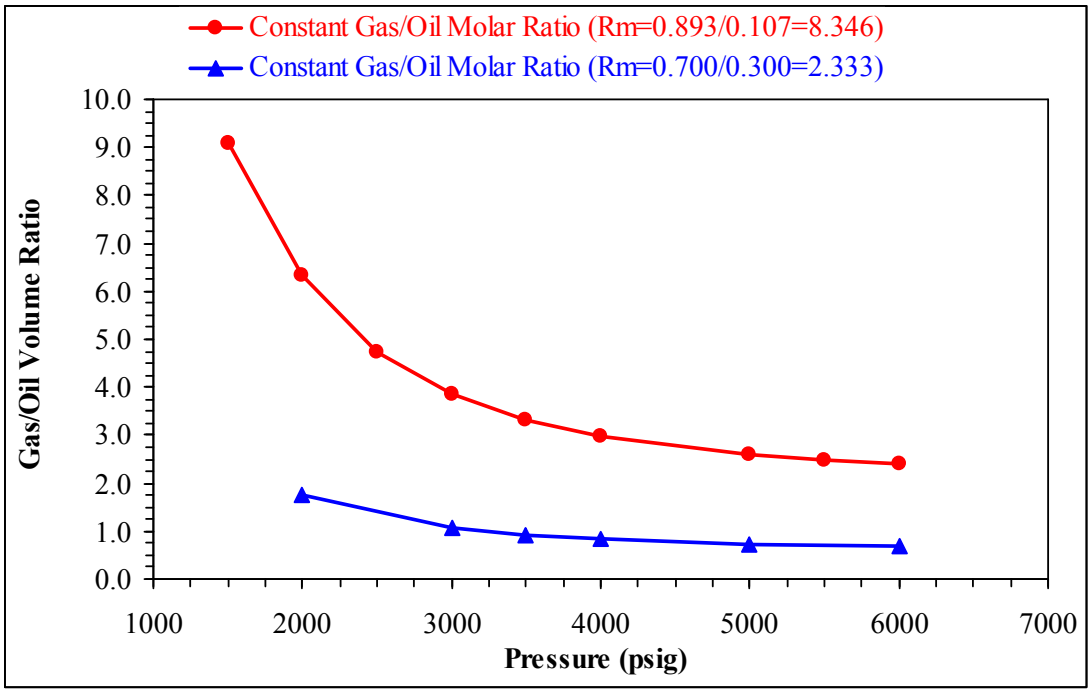

Figure 2.29: The dependence of gas/oil volume ratio on pressure at constant gas/oil molar ratios

2. Figure 2.30 is a plot of the equilibrated fluid phase densities versus pressure for the two selected constant gas/oil molar ratios. As can be seen from Figure 2.30, the equilibrated gas phase density increases very rapidly with pressures and the equilibrated liquid phase density increases very slowly with pressures. The difference in the densities between the equilibrated gas and liquid phase gradually decreases with pressure, which provides evidence for CO_2 gas approaching the miscibility pressure with this particular reservoir fluid. At Rm=2.333 the difference in densities of the equilibrated gas and liquid phase large when compared to that at Rm=8.346. This was due to the more reservoir fluid in the feed mixture that resulted in more extraction of hydrocarbons from the liquid phase by CO_2 for Rm=2.333 when compared to Rm=8.346 which had less reservoir fluid in the feed mixture that resulted in less extraction of hydrocarbons from the liquid phase by CO_2.

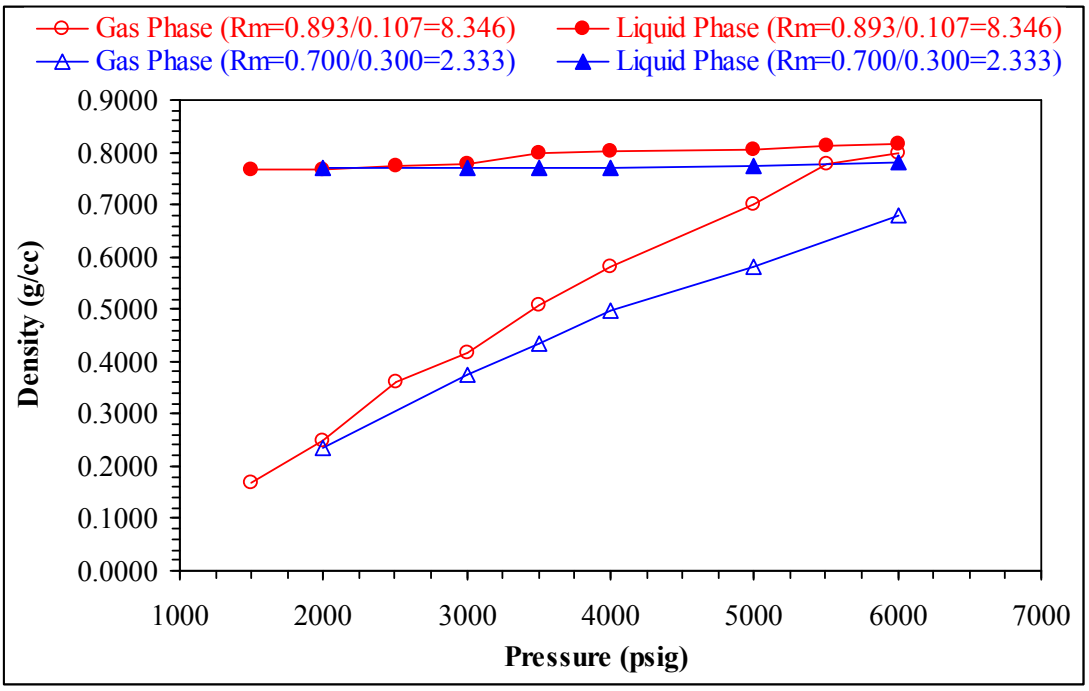

Figure 2.30: The effect of equilibrated gas and liquid phase densities at constant gas/oil molar ratios at 238°F

3. Figure 2.31 is a plot of CO_2 mole% content in the equilibrated fluid phases versus pressure for the two selected gas/oil molar ratios. The equilibrated gas phase compositions for the constant gas/oil molar ratio of Rm=8.356 indicated a CO_2 composition of about 97 mole% as shown in Figure 2.31 at various experimental pressures at 238°F. This confirms that the extraction of light components from the liquid phase into gas phase is quite low. The densities of pure CO_2 gas and the measured densities of the equilibrated gas phase (shown in Table 2.28) are almost similar at all the pressures, which proves that the gas phase is predominantly CO_2. It can also be seen from Figure 2.31 that the CO_2 component from the equilibrated gas phase compositions for the second gas/oil molar ratio of Rm=2.333 is approximately constant at about 83 mole% for the various experimental pressures at 238°F. This once again confirms the interpretations of negligible extraction of light components from the liquid phase into the gas phase for this particular reservoir crude oil.

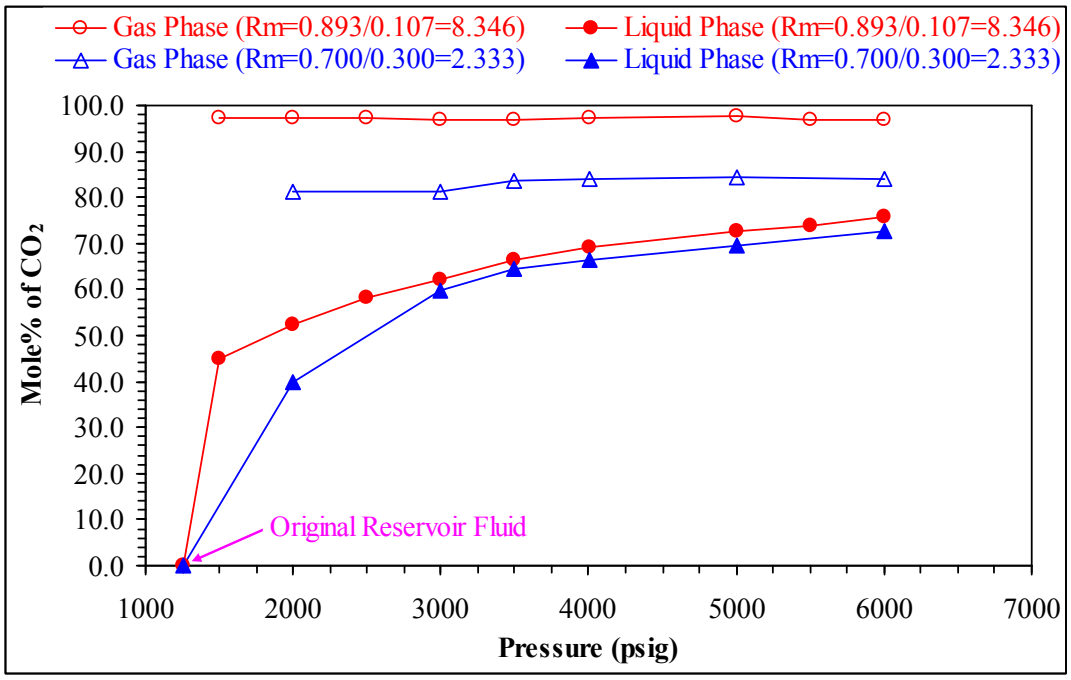

Figure 2.31: CO_2 content in the equilibrated gas and liquid phases at 238°F

Thus it can be concluded that mole% of CO_2 component in the equilibrated gas phase does not change appreciably with increase in pressure for the two selected gas-oil molar ratios. The absence of light hydrocarbon components (C_2-C_5) in this particular depleted reservoir fluid seems to be the cause of less vaporization of components from the liquid phase into the gas phase.

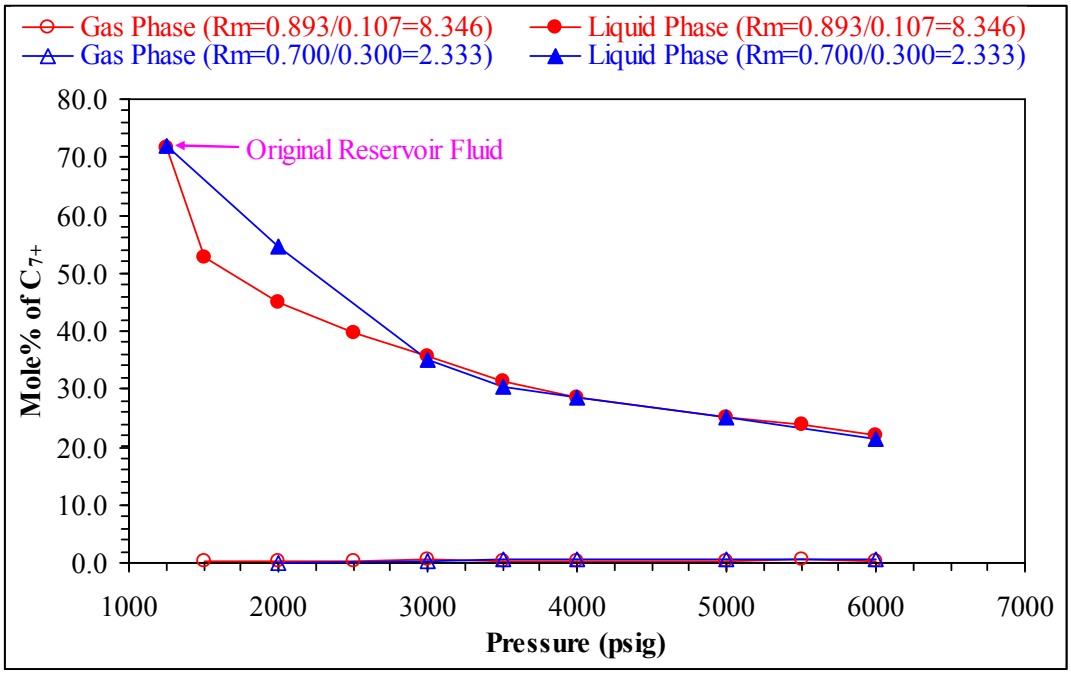

Figure 2.32: C7+ content in the equilibrated gas and liquid phases at 238°F

4. Figure 2.32 is a plot of C_{7+} mole % content in the equilibrated fluid phases versus pressure. Figure 2.33 is a plot of molecular weights of the equilibrated fluid phases versus pressure. The amount of CO_2 dissolving in the reservoir fluid has increased rapidly with pressure as indicated by the decline in heptanes plus content and molecular weight of the reservoir fluid with increasing experimental pressures at 238°F as indicated in Figures 2.32 and 2.33, respectively. It can also be seen from Figure 2.31 that the CO_2 concentration in the liquid phase increases significantly with increase in pressure until 4000 psig and then slowly up to 6000 psig. This indicates that the recombined reservoir fluid was gradually saturated with CO_2 leading to the development of miscibility between CO_2 and recombined reservoir fluid.

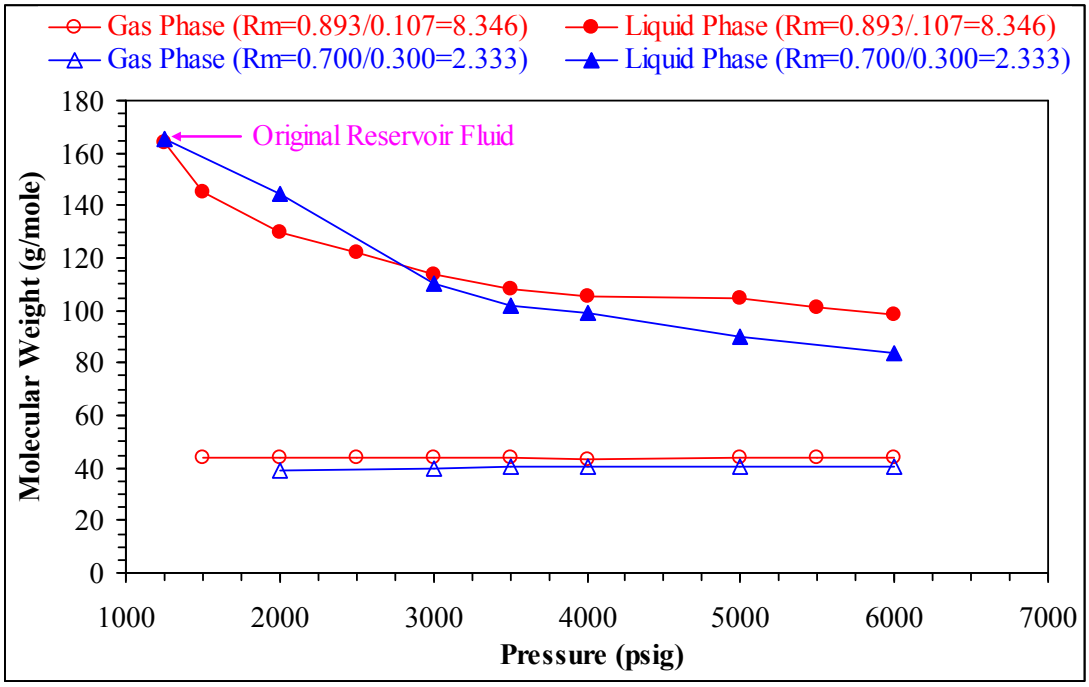

Figure 2.33: Equilibrated gas and liquid phase molecular weights as a function of pressure at constant initial gas/oil molar ratio at 238°F

Figure 2.34 is a plot of flash GOR of the liquid phase versus pressure. The solubility of CO_2 in the recombined reservoir fluid was also indicated by the increasing gas-oil ratios obtained by performing a flash separation analysis on the equilibrated liquid phases with increasing pressures (Figure 2.34). Due to this phenomenon the molecular weights of the equilibrated liquid phase decreased quite rapidly up to a pressure of about 3000 psig and then remained approximately constant for the various pressures from 3500 psig to 6000 psig as shown in Figure 2.33. As a result of this, the difference in the molecular weights of the equilibrated gas phase and equilibrated liquid phase decreased continuously with increasing pressure, due to continuous dissolving of CO_2 gas in the

liquid phase with increasing pressure. This is an indication of the approaching miscibility between the two fluid phases.

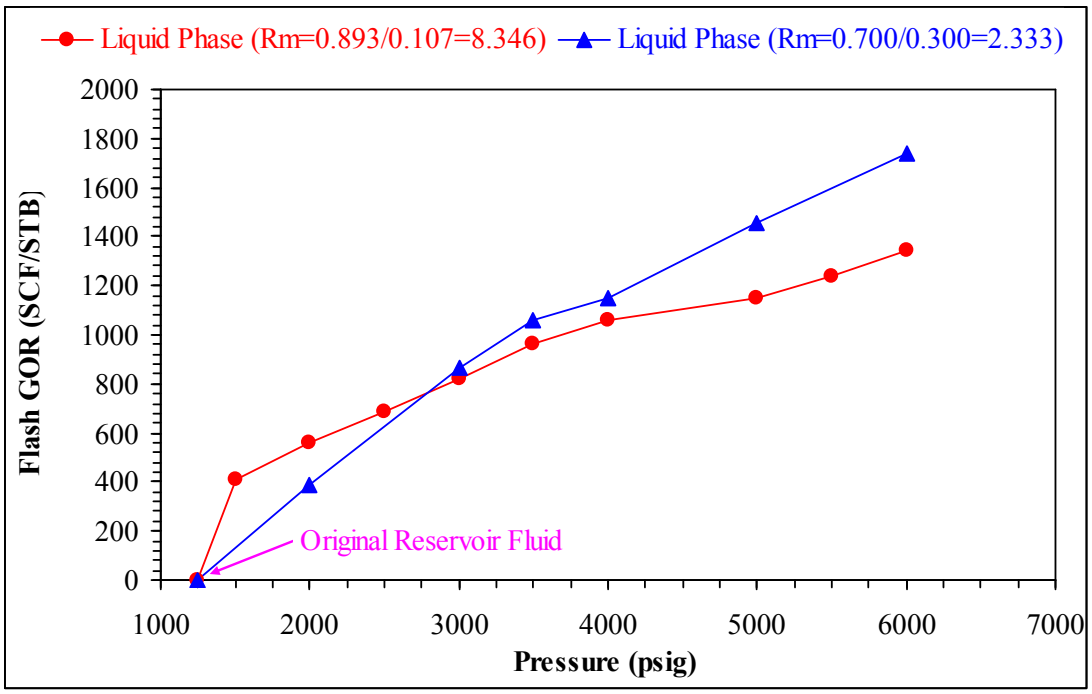

Figure 2.34: Effect of CO_2 dissolution in the liquid phase on GOR at 238°F

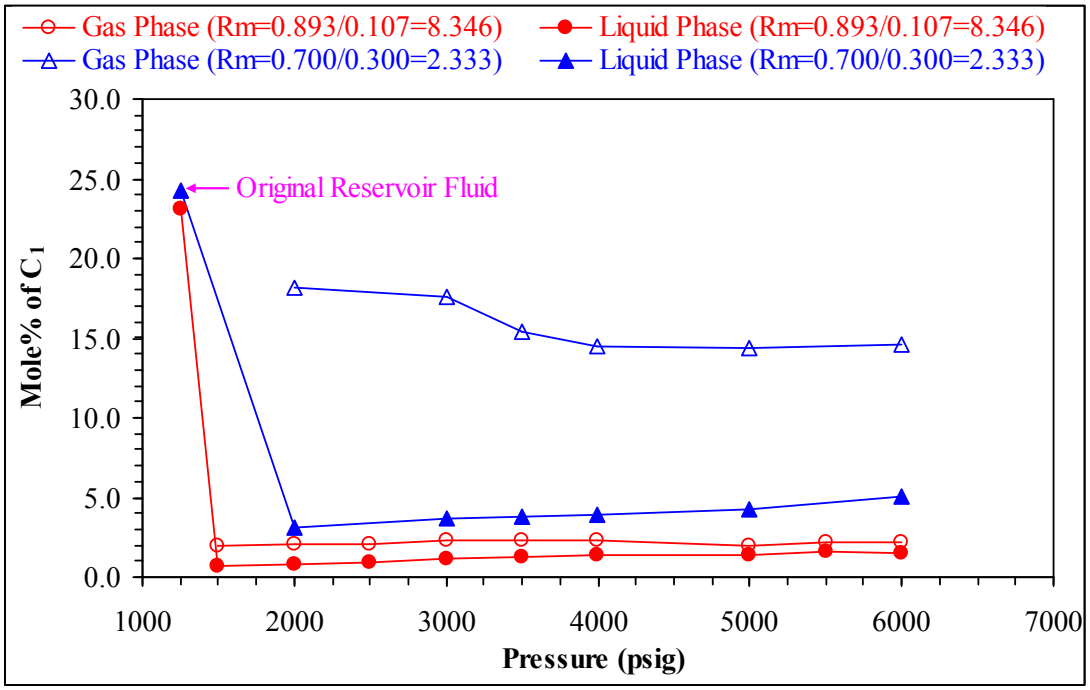

Figure 2.35: C1 content in the equilibrated gas and liquid phases at 238°F

5. Figure 2.35 is a plot of C_1 content in the equilibrated fluid phases versus pressure. The amount of C_1 extracted by CO_2 from the liquid phase into the gas phase as shown in Figure 2.35 is less at the constant gas-oil molar ratio Rm=8.346 when compared to the case of lower gas-oil molar ratio Rm=2.333. This is due to the less amount of reservoir oil present in the feed mixture and hence less C_1 available in the feed mixture for extraction at the gas-oil molar ratio of Rm=8.346 than the lower gas/oil molar ratio of Rm=2.333.
6. There appears to be less interaction of the CO_2 with the liquid phase as can be seen from the compositional analysis data shown in Figures 2.31, 2.32 and 2.35 and hence there is less transfer of components from the liquid phase into the gas phase. The role of CO_2 in these experiments was interpreted to be continuous dissolving in the liquid phase with increase in pressure. This is due to the absence of C_2-C_5 components in the depleted reservoir fluid. This indicates that a condensing gas drive mechanism is mainly responsible for the miscibility development in this type of reservoir system.

Effect of Gas/Oil Molar Ratios on Interfacial Tension

The following important observations can be made from the gas/oil IFT measurements conducted for the two selected constant gas/oil molar ratios at 238°F.

1. Figure 2.36 are video images of the drop shapes captured by a digital video camera at various pressures for the gas/oil molar ratio Rm=8.346. Figure 2.37 are video images of the capillary heights of the liquid phase captured using the digital video camera at various pressures for the same gas/oil molar ratio Rm=8.346.

   The equilibrium IFT measured from the pendant drop technique is slightly high compared to that measured using the capillary rise technique at the constant gas/oil ratio Rm=8.346 (Table 2.28 and Figures 2.36 and 2.37). This is due to the less contact time of 6 hours between the fluid phases for the pendant drop technique as compared to the more equilibration time of 24 hours for the capillary rise technique, at the same gas/oil molar ratio Rm=8.346.

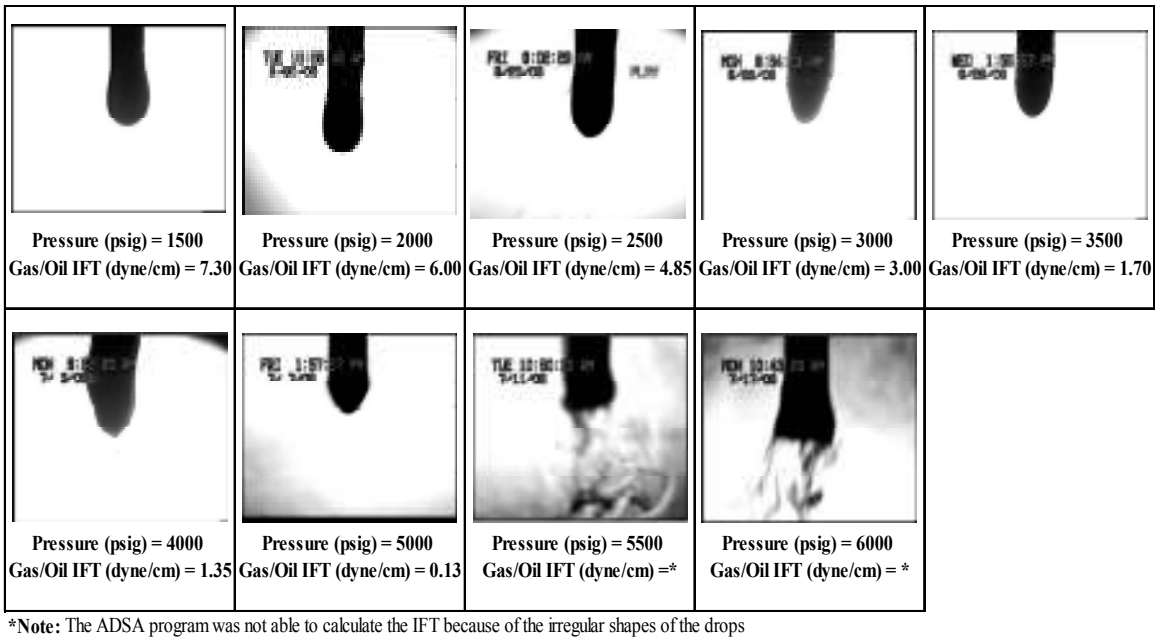

***Note:** The ADSA program was not able to calculate the IFT because of the irregular shapes of the drops

Figure 2.36: Gas/Oil IFT using the pendant drop shape images at constant initial gas/oil molar ratio at 238°F (Rm=0.893/0.107=8.346)

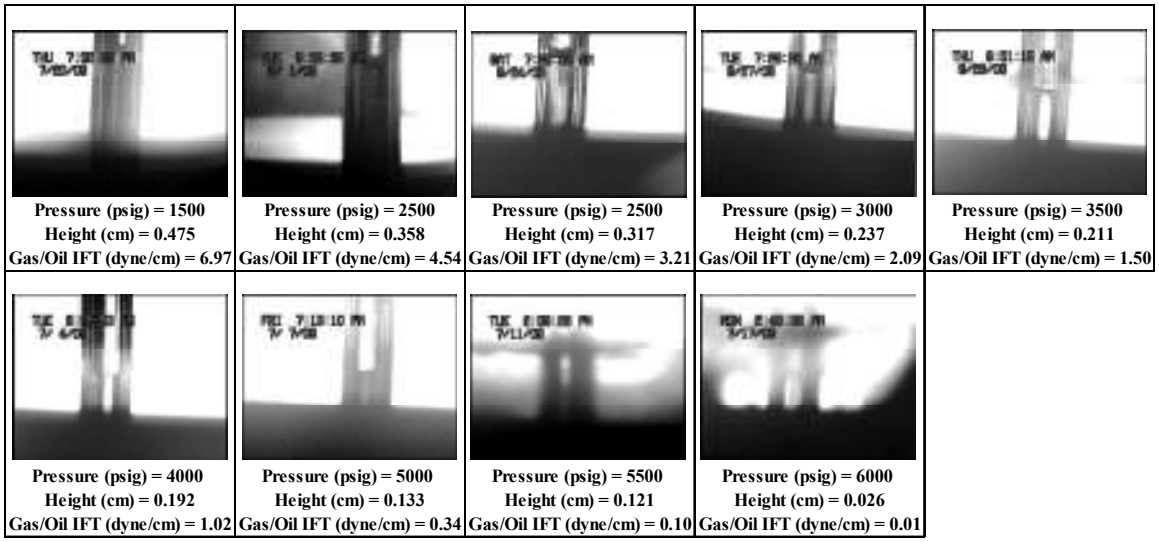

Figure 2.37: Gas/Oil IFT using the capillary rise at constant initial gas/oil molar ratio at 238°F (Rm=0.893/0.107=8.346)

2. It can also be seen from Figure 2.36 that the IFT measurements at pressures of 5000, 5500 and 6000 psig could not be determined using the pendant drop technique due to the irregular shapes of the oil drops and the oil drops disappearing into the gas phase as the miscibility pressure is approached. This is an indication of the CO_2-reservoir fluid system approaching miscibility and consequently becoming a single- phase fluid system.

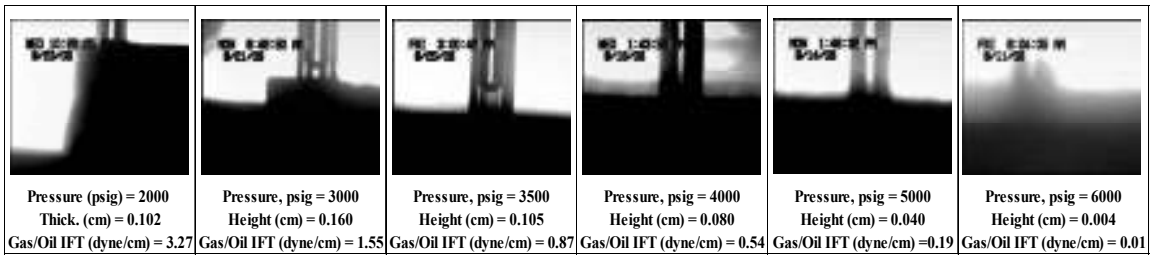

Figure 2.38: Gas/Oil IFT using the capillary rise at constant initial gas/oil molar ratio at 238°F (Rm=0.700/0.300=2.333)

3. Figure 2.38 shows capillary height images of the liquid captured using the digital video camera at various pressure for the constant gas/oil molar ratio Rm=2.333. The measured capillary heights decreased (Figures 2.37 and 2.38) as the experimental pressures increased. This is due to the lowering of the IFT between CO_2 and the live reservoir fluid as pressure increases. The interfacial forces between carbon dioxide and recombined reservoir fluid approach zero as fluids approach miscibility.
4. Figure 2.39 is a plot of gas/oil IFT values versus pressure obtained using the pendant drop and capillary rise techniques for the constant gas/oil molar ratio of Rm=8.346. From Figure 2.39 it can be seen that the equilibrium IFT values measured using the pendant drop and capillary rise techniques agree reasonably well and that an exponential curve appears to fit IFT measurements at different pressures. However, the exponential curve cannot be extrapolated to zero interfacial tension to determine the minimum miscibility pressure. It was also noticed from Figure 2.39 that the last seven pressure points could provide a linear fit between the IFT measurements.

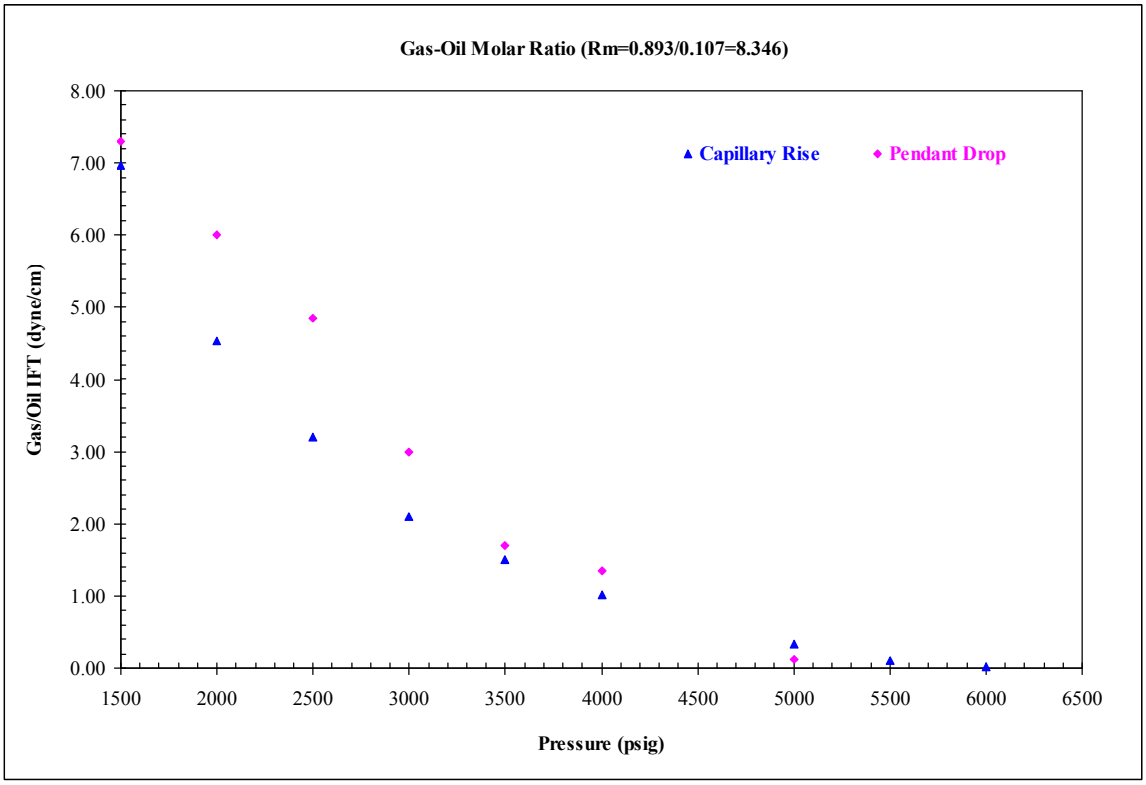

Figure 2.39: Comparison of IFT measurements using pendant drop and capillary rise techniques at constant initial gas/oil molar ratio at 238°F (Rm=0.893/0.107=8.346)

5. Figure 2.40 shows that a good linear fit exists at the constant gas/oil ratio Rm=8.346 using the capillary rise technique when the equilibrium IFT measurements are plotted against the reciprocal of pressure using a hyperbolic function with a coefficient of determination (R^2) of 0.9952. The linear regression equation when extrapolated to zero interfacial tension axis provides a minimum miscibility pressure of 6180 psig for the constant gas-oil molar ratio Rm=8.346 and indicates a condition where there is no interface between the fluid-fluid phases and CO_2 and live reservoir form a single phase.

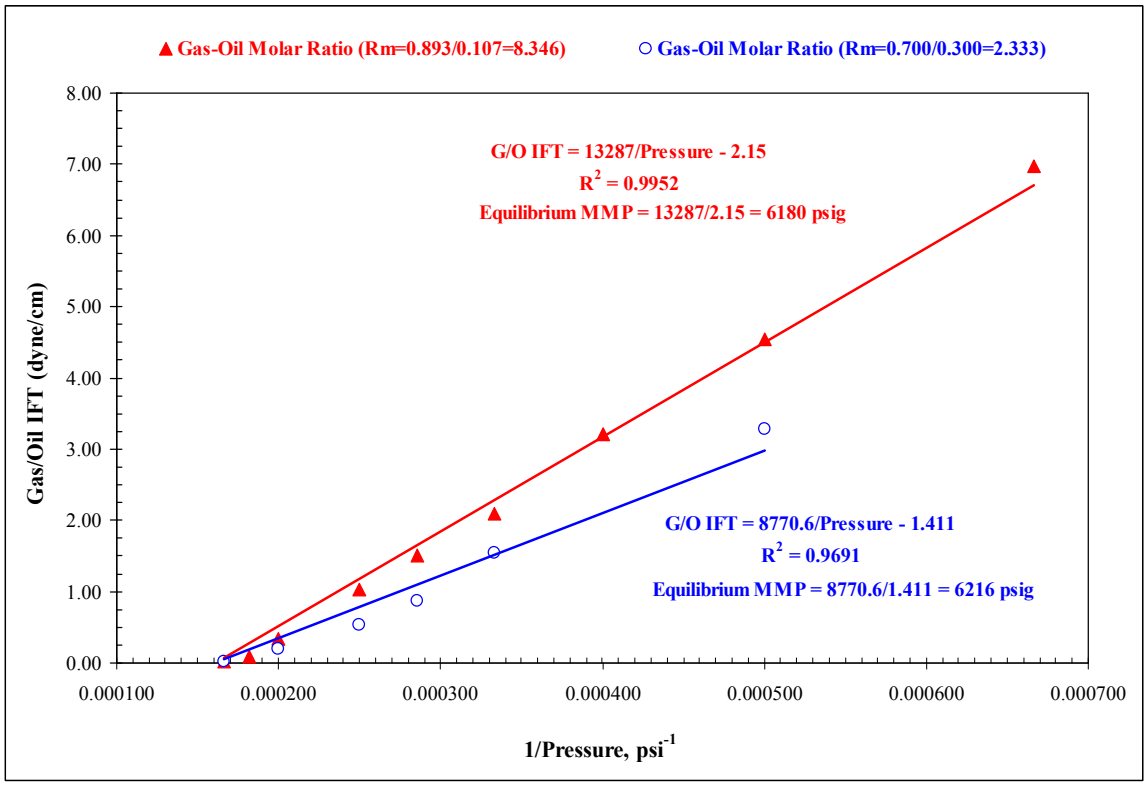

Figure 2.40: Effect of initial gas/oil molar ratio on gas-oil IFT and equilibrium MMP using VIT at 238°F

Figure 2.40 also shows that a good linear fit also exists when the equilibrium IFT measurements are plotted against the reciprocal of pressure at the constant gas-oil molar ratio Rm 2.333 using a hyperbolic function with a coefficient of determination (R^2) of 0.9691. The linear regression equation when extrapolated to zero interfacial tension provides a minimum miscibility pressure of 6216 psig for the constant gas-oil molar ratio of Rm=2.333.

6. From Figure 2.40 it can be seen that equilibrium IFT values measured for the Rm=8.346 were high compared to the case when Rm=2.333. This appears to be due to less amount of reservoir oil available in the feed at Rm=8.246 and hence less interaction of CO_2 with the reservoir fluid. This has resulted in the lower extraction of components from the liquid phase. However, relatively more amount of reservoir oil is available in the feed when Rm=2.333 and hence the interaction of CO_2 with the reservoir fluid appears to be more due to the greater amount of components available in the liquid phase for extraction.
7. It can be seen from Figure 2.40 that the equilibrium IFT values measured at the two widely different gas/oil molar ratios of Rm=8.346 and Rm=2.333 converge almost to the same point of zero interfacial tension. This indicates that the equilibrium IFT measurements for the two selected gas-oil molar ratios move along different paths,

but they both appear to converge at about the same end point of zero interfacial tension to yield similar minimum miscibility pressures, within about 0.6% of each other.

2.2.4.3.2 Constant Gas/Oil Volume Ratio Experiments

In the previous section, IFT measurements were performed using the constant gas-oil molar ratios as feed in the mixture. The following section discusses the results of the gas-oil IFT measurements performed with constant gas-oil volume ratio using the recombined reservoir crude oil as the liquid phase and carbon dioxide as the gas phase. These experiments were conducted at the reservoir temperature of 238°F and varying experimental pressures from 1500 psig to 6000 psig. This was done mainly to investigate the effect of compositional paths on the gas-oil IFT measurements using the constant gas/oil volume ratio approach.

Measurements were carried out using a constant gas-oil volume ratio of 0.850 volume fraction of carbon dioxide gas and 0.150 volume fraction of recombined reservoir fluid as feed in the mixture (Rv=0.850/0.150=5.667) and a constant gas-oil volume ratio of 0.450 volume fraction of carbon dioxide gas and 0.550 volume fraction of recombined reservoir fluid as feed in the mixture (Rv=0.450/0.550=0.818).

The measured densities of the equilibrated gas liquid phases at 238°F and interfacial tension values obtained from the pendant drop and the capillary height techniques at the constant gas/oil volume ratio Rv=5.667 are summarized in the Table 2.34.

Table 2.34: Summary of the equilibrated fluid densities and gas-oil IFT measured at constant gas/oil volume ratio of 0.850 volume fraction of CO_2 and 0.150 volume fraction of recombined reservoir fluid (Rv=0.850/0.150=5.667) at 238°F

Gas Volume Fraction	0.850								
Liquid Volume Fraction	0.150								
Pressure	Equilibrated Phase Densities		Density Diff.	Capillary	Equilibrium IFT		First-Contact IFT	Corresponding Mole Fraction	
	Oil	Gas	Δρ	Height	Capillary Rise	Pendant Drop	Pendant Drop		
(psig)	(g/cc)	(g/cc)		(cm)	(dyne/cm)	(dyne/cm)	(dyne/cm)	Gas	Oil
2000	0.7760	0.2167	0.5594	0.480	6.58	6.85	7.30	0.882	0.118
3000	0.7922	0.4250	0.3672	0.375	3.37	3.75	4.21	0.925	0.075
4000	0.8104	0.5349	0.2756	0.195	1.32	1.44	2.15	0.941	0.059
5000	0.8280	0.6158	0.2122	0.125	0.65	0.75	1.00	0.948	0.052
6000	0.8583	0.6861	0.1722	-	*(1)	*(2)	*(3)	0.952	0.048

*(1) IFT could not be determined due to less oil in the feed mixture and the approaching miscibility between the fluid phases

*(2) and *(3) drop shapes could not be formed due to the approaching misciblity between the fluid phases

Table 2.35: Compositional analysis of the equilibrated gas phase at constant gas/oil volume ratio of 0.850 mole fraction of CO_2 and 0.150 mole fraction of recombined reservoir fluid (Rv=0.850/0.150=2.333) at 238°F

Gas VolumeFraction	0.850					
Liquid Volume Fraction	0.150					
Component	Carbon No.	Pressure (psig)				
		2000	3000	4000	5000	6000
		Gas Phase Mole%				
Hydrogen Sulphide	H2S	0.000	0.000	0.000	0.000	0.000
Carbon Dioxide	CO2	96.616	97.962	98.316	98.640	98.622
Nitrogen	N2	0.084	0.050	0.045	0.032	0.048
Methane	C1	2.820	1.667	1.218	0.987	0.940
Ethane	C2	0.000	0.000	0.000	0.000	0.000
Propane	C3	0.008	0.006	0.007	0.000	0.000
i-Butane	iC4	0.010	0.007	0.004	0.003	0.003
n-Butane	nC4	0.023	0.009	0.010	0.007	0.008
i-Pentane	iC5	0.049	0.036	0.026	0.021	0.022
n-Pentane	iC5	0.044	0.033	0.024	0.019	0.020
Hexanes	C6	0.103	0.083	0.076	0.063	0.070
Heptanes Plus	C7+	0.243	0.147	0.275	0.228	0.267
Total		100.000	100.000	100.001	100.000	100.000
Density, at Pressure (g/cc)		0.2167	0.4250	0.5349	0.6158	0.6861
Molecular Weight		43.44	43.68	43.89	43.91	43.96
Charged GOR, SCF/STB		10935	11359	11448	11429	11372

Table 2.36: Compositional analysis of the equilibrated liquid phase at constant gas/oil volume ratio of 0.850 mole fraction of CO_2 and 0.150 mole fraction of recombined reservoir fluid (Rv=0.850/0.150=2.333) at 238°F

Gas VolumeFraction	0.850						
Liquid Volume Fraction	0.150						
Component	Carbon No.	Pressure (psig)					
		1250 Recombined Reservoir Fluid*	2000	3000	4000	5000	6000
		Liquid Phase Mole%					
Hydrogen Sulphide	H2S	0.000	0.000	0.000	0.000	0.000	0.000
Carbon Dioxide	CO2	0.063	51.063	65.903	69.532	73.337	76.195
Nitrogen	N2	0.005	0.009	0.019	0.017	0.009	0.024
Methane	C1	24.216	1.126	0.870	0.739	0.734	0.819
Ethane	C2	0.011	0.007	0.003	0.006	0.006	0.005
Propane	C3	0.021	0.007	0.006	0.004	0.001	0.000
i-Butane	iC4	0.068	0.017	0.009	0.005	0.004	0.004
n-Butane	nC4	0.190	0.046	0.024	0.017	0.014	0.013
i-Pentane	iC5	0.638	0.173	0.114	0.057	0.042	0.036
n-Pentane	iC5	0.597	0.175	0.119	0.058	0.041	0.035
Hexanes	C6	2.353	0.821	0.375	0.262	0.159	0.132
Heptanes Plus	C7+	71.838	46.556	32.558	29.303	25.653	22.737
Total		100.000	100.000	100.000	100.000	100.000	100.000
Density, at Pressure (g/cc)		0.7403	0.7760	0.7922	0.8104	0.8280	0.8583
Molecular Weight (Recombined Oil)		165.7	134.3	116.1	116.1	115.8	115.5
Molecular Weight C_{7+} (Recombined Oil)		220.7	237.6	265.6	290.1	324.4	359.2
Flash GOR, SCF/STB		0	526	859	917	987	1045
*** Bubble Point Pressure - New Batch**							

The effect of constant gas/oil volume ratio Rv=5.667 in the feed mixture on the first-contact and equilibrium miscibility for the CO_2-recombined reservoir fluid system was investigated at different pressures at 238°F using the pendant drop technique and these results are also presented in Table 2.34. The compositional analysis of the equilibrated gas and liquid phases at 238°F for the constant gas/oil volume ratio Rv=5.667 are summarized in the Tables 2.35 and 2.36 respectively.

Another set of gas-oil IFT experiments were performed with the constant gas-oil volume ratio of 0.450 volume fraction of CO_2 and 0.550 volume fraction of recombined reservoir oil in the feed mixture (Rv=0.450/0.550=0.818) using the capillary rise technique. The measured densities of the equilibrated gas and liquid phases and equilibrium interfacial tension values at Rv=0.450/0.550=0.818 are summarized in Table 2.37.

Table 2.37: Summary of the equilibrated fluid densities and gas-oil IFT measured at constant gas/oil volume ratio of 0.450 volume fraction of CO_2 and 0.550 volume fraction of recombined reservoir fluid (Rv=0.450/0.550=0.818) at 238°F

Gas Volume Fraction	0.450							
Liquid Volume Fraction	0.550							
Pressure	**Equilibrated Phase Densities**		**Density Diff.**	**Capillary**	**Equilibrium IFT**		**Corresponding Mole Fraction**	
	Oil	**Gas**	**Δρ**	**Height**	**Capillary Rise**	**Pendant Drop**		
(psig)	**(g/cc)**	**(g/cc)**		**(cm)**	**(dyne/cm)**	**(dyne/cm)**	**Gas**	**Oil**
2000	0.7645	0.2125	0.5520	0.175	2.37	*	0.519	0.481
3000	0.7728	0.3471	0.4256	0.114	1.19	*	0.640	0.360
4000	0.7664	0.4932	0.2732	0.066	0.44	*	0.696	0.304
5000	0.7856	0.6160	0.1696	0.033	0.14	*	0.724	0.276
6000	0.7971	0.7183	0.0788	0.010	0.02	*	0.740	0.260
* **Equilibrium IFT could not be calculated from the drop shapes due to significant amounts of reservoir oil in the optical cell**								

Table 2.38: Compositional analysis of the equilibrated gas phase at constant gas/oil volume ratio of 0.450 mole fraction of CO_2 and 0.550 mole fraction of recombined reservoir fluid (Rv=0.450/0.550=00.818) at 238°F

Gas Volume Fraction	0.450					
Liquid Volume Fraction	0.550					
Component	**Carbon No.**	**Pressure (psig)**				
		2000	**3000**	**4000**	**5000**	**6000**
		Gas Phase Mole%				
Hydrogen Sulphide	H2S	0.000	0.000	0.000	0.000	0.000
Carbon Dioxide	CO2	86.674	90.070	92.446	95.010	88.638
Nitrogen	N2	0.107	0.099	0.048	0.050	0.041
Methane	C1	12.476	8.882	6.669	4.419	4.709
Ethane	C2	0.000	0.000	0.000	0.000	0.001
Propane	C3	0.008	0.006	0.008	0.003	0.005
i-Butane	iC4	0.017	0.015	0.016	0.008	0.011
n-Butane	nC4	0.041	0.038	0.037	0.022	0.030
i-Pentane	iC5	0.084	0.086	0.077	0.050	0.083
n-Pentane	iC5	0.071	0.075	0.069	0.044	0.073
Hexanes	C6	0.164	0.198	0.175	0.117	0.275
Heptanes Plus	C7+	0.358	0.531	0.455	0.277	6.134
Total		100.000	100.000	100.000	100.000	100.000
Density, at Pressure (g/cc)		0.2125	0.3471	0.4932	0.6160	0.7183
Molecular Weight		40.85	41.99	42.55	43.02	51.92
Charged GOR, SCF/STB		1754	2153	2311	2380	2411

Table 2.39: Compositional analysis of the equilibrated liquid phase at constant gas/oil volume ratio of 0.450 mole fraction of CO_2 and 0.550 mole fraction of recombined reservoir fluid (Rv=0.450/0.550=0.818) at 238°F

Gas Volume Fraction	0.450						
Liquid Volume Fraction	0.550						
Component	**Carbon No.**	**Pressure (psig)**					
		1250 Recombined Reservoir Fluid*	**2000**	**3000**	**4000**	**5000**	**6000**
		Liquid Phase Mole%					
Hydrogen Sulphide	H2S	0.000	0.000	0.000	0.000	0.000	0.000
Carbon Dioxide	CO2	0.063	47.194	60.436	67.281	72.017	78.022
Nitrogen	N2	0.005	0.021	0.035	0.024	0.029	0.018
Methane	C1	24.216	4.333	4.047	4.122	4.170	3.289
Ethane	C2	0.011	0.007	0.005	0.004	0.007	0.003
Propane	C3	0.021	0.008	0.007	0.006	0.007	0.005
i-Butane	iC4	0.068	0.030	0.023	0.023	0.020	0.015
n-Butane	nC4	0.190	0.092	0.065	0.056	0.054	0.039
i-Pentane	iC5	0.638	0.299	0.194	0.171	0.155	0.117
n-Pentane	iC5	0.597	0.289	0.181	0.159	0.145	0.109
Hexanes	C6	2.353	1.235	0.707	0.616	0.554	0.418
Heptanes Plus	C7+	71.838	46.492	34.300	27.538	22.842	17.965
Total		100.000	100.000	100.000	100.000	100.000	100.000
Density, at Pressure (g/cc)		0.7403	0.7645	0.7728	0.7664	0.7856	0.7971
Molecular Weight (Recombined Oil)		165.7	126.8	107.7	95.4	88.3	80.2
Molecular Weight C_{7+} (Recombined Oil)		220.7	223.2	231.9	233.6	241.3	249.3
Flash GOR, SCF/STB		0	556	911	1248	1553	2037
*** Bubble Point Pressure - New Batch**							

The compositional analysis of the equilibrated gas and liquid phases at 238°F for the constant gas/oil volume ratio Rv=0.818 are summarized in the Tables 2.38 and 2.39 respectively.

Effect of Constant Gas/Oil Volume Ratio on Fluid Phase Compositions, Densities and Molecular Weights

The following observations are made on the effects of the two selected constant gas-oil volume ratios on the compositions, densities and molecular weights of the equilibrated gas and liquid phases from Figures 2.41-2.47 and Tables 2.34 and 2.37 respectively.

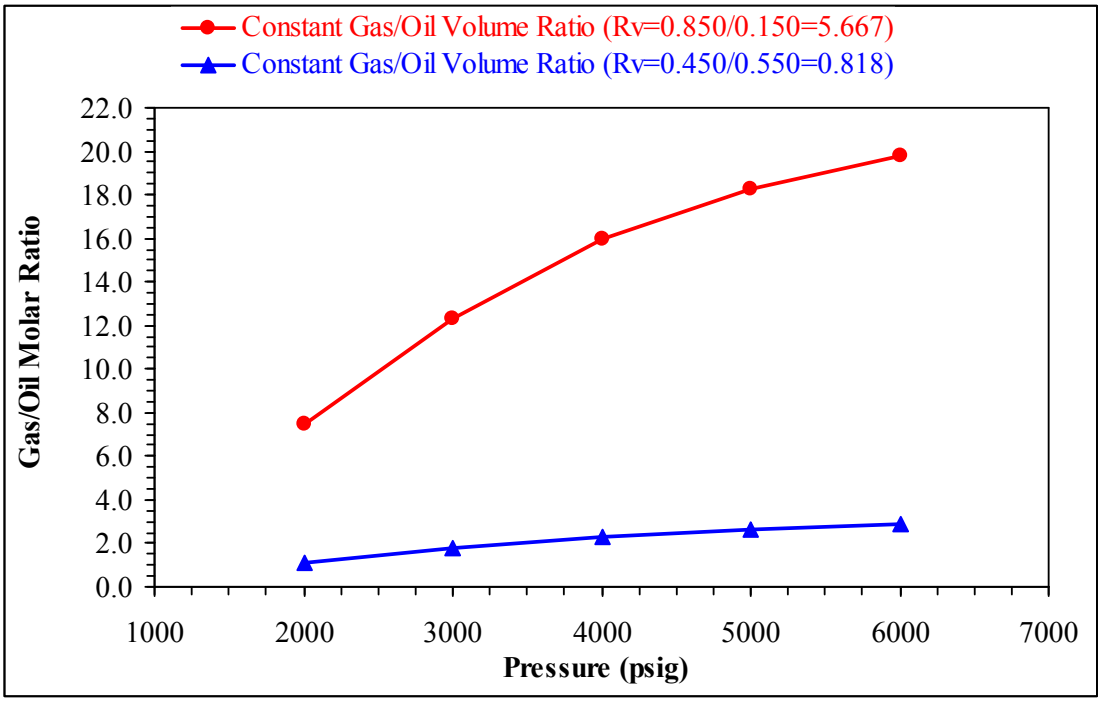

Figure 2.41: The dependence of gas/oil molar ratio on pressure at constant gas/oil volume ratios

1. Figure 2.41 shows the plot of gas/oil molar ratio versus pressure for the two selected constant gas-oil molar ratios. It can be seen from Figure 2.41 that the gas/oil molar ratio increases rapidly with pressure at the constant gas/oil volume ratio Rv = 5.667 and is an indication of approximately constant low amounts of reservoir oil in the feed mixture with increasing pressures. However it remains approximately constant for the constant gas/oil volume ratio Rv = 0.818 in the feed mixtures used in conducting the gas-oil IFT experiments at various pressures indicating approximately constant amounts of gas and constant amounts of oil in the feed mixture.

2. Figure 2.42 is a plot of densities of equilibrated fluid phases versus pressure for the two selected constant gas/oil volume ratios. As can be seen from Figure 2.42 the equilibrated gas phase density increases rapidly with pressure and the equilibrated liquid phase density changes slightly with pressure. The decrease in the difference in the densities between the equilibrated gas and liquid phase with increase in pressure provides evidence of CO_2 gas approaching the miscibility pressure with this particular reservoir fluid.

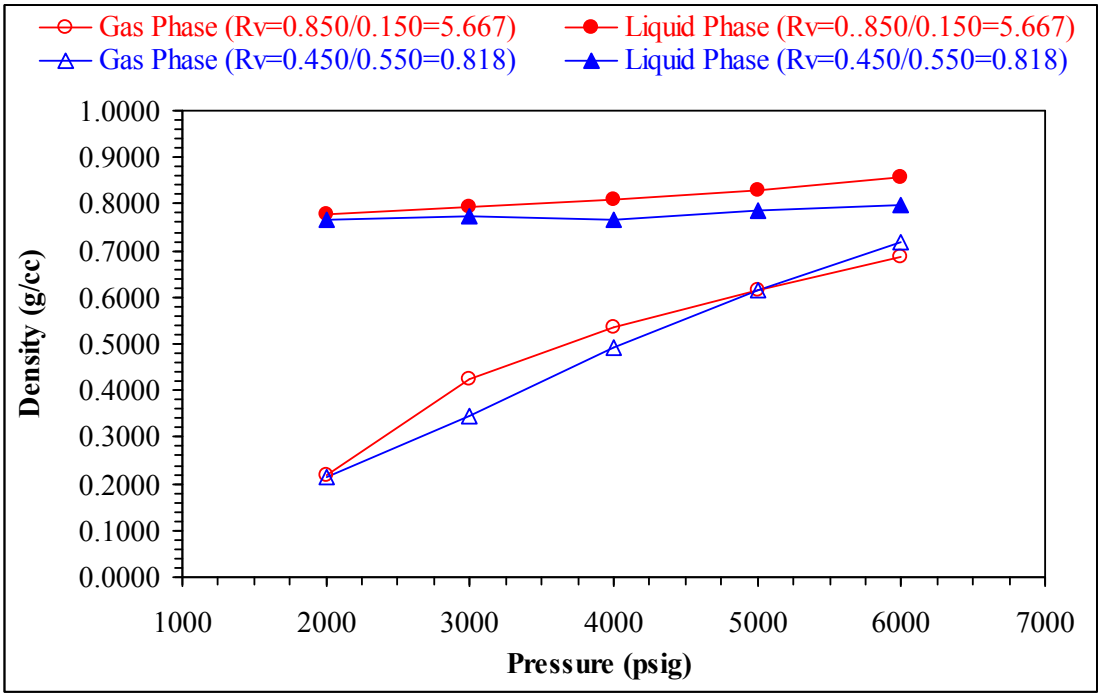

Figure 2.42: The effect of equilibrated gas and liquid phase densities at constant initial gas/oil volume ratio at 238°F

3. Figure 2.43 is a plot of CO_2 mole% in the equilibrated fluid phases versus pressure for the two selected constant gas/oil volume ratios. It can be seen from Figure 2.43 that CO_2 in the equilibrated gas phase for the constant gas/oil volume ratio of Rv = 5.667 was approximately 98 mole% at the various experimental pressures at 238°F. It was also observed that the densities of pure CO_2 (Table 2.27) are approximately similar to the measured densities of the equilibrated gas phase shown in Table 2.34. This observation confirms that the gas phase contains predominantly CO_2 and there has been very little extraction of light components from the liquid phase into the gas phase.

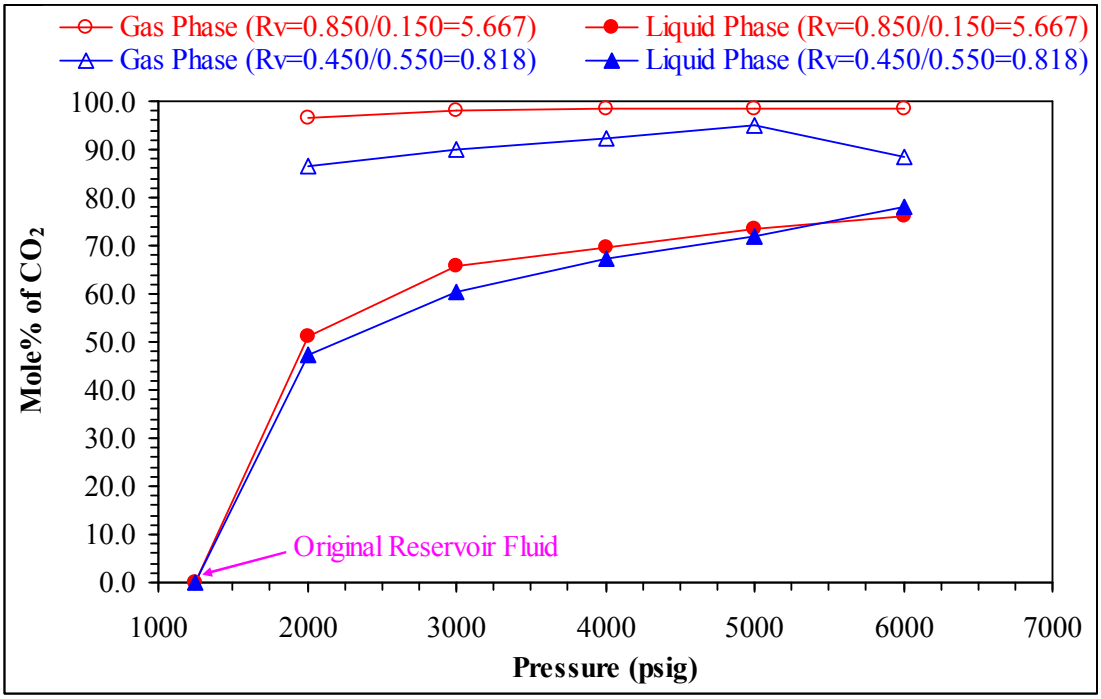

Figure 2.43: CO_2 content in the equilibrated gas and liquid phases at 238°F

4. Figure 2.43 also shows that the CO_2 in the equilibrated gas phase for the constant gas/oil volume ratio of Rv = 0.818 increases with pressure until 5000 psig and then decreases slightly at 6000 psig. This was attributed to the presence of about 6 mole% of C_{7+} in the gas phase at 6000 psig. It was also observed while performing flash separation on the equilibrated gas phase at 6000 psig at the constant gas/oil volume ratio of Rv = 0.818, there was light brown condensate condensing into the separator. This is due to the gas being rich in C_{7+} components which have resulted in liquids dropping out of gas phase.
5. Figure 2.44 is a plot of C_{7+} mole% in the equilibrated fluid phases versus pressure for the two selected constant gas/oil volume ratios. Figure 2.45 is a plot of flash GOR of the equilibrated liquid phase versus pressure.

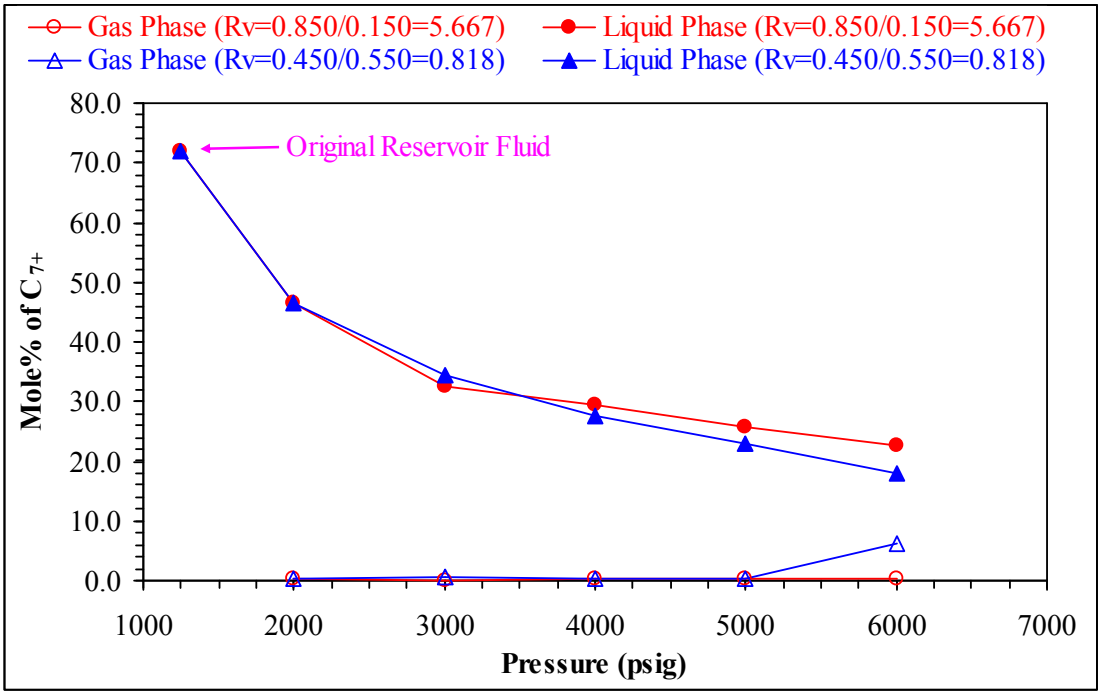

Figure 2.44: C7+ content in the equilibrated gas and liquid phases at 238°F

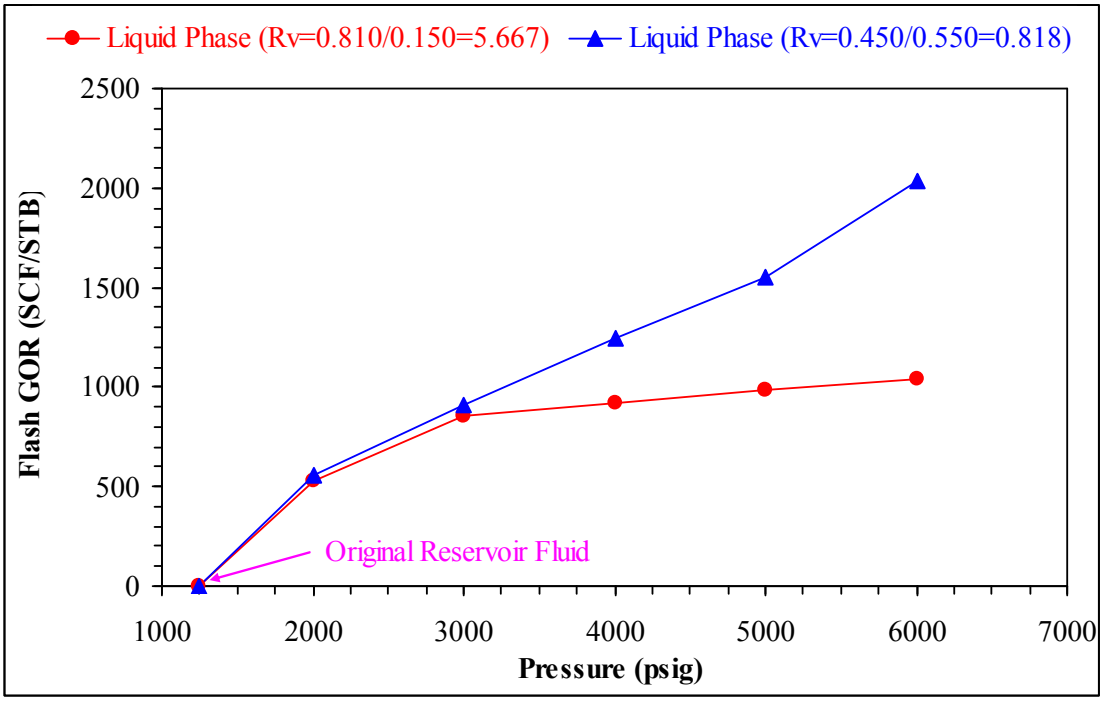

Figure 2.45: Effect of CO_2 dissolution in the liquid phase on GOR at 238°F

Figure 2.43 indicated that the concentration of CO_2 dissolving in the liquid phase increases appreciably with increase in pressure until 4000 psig and then increases slowly up to 6000 psig. Due to these phenomena the amount of C_{7+} mole% in the liquid phase

has decreased with increasing pressures (Figure 2.44). This indicates that the recombined reservoir fluid was fully saturated with CO_2 and that miscibility between CO_2 and recombined reservoir fluid was approached. Increasing gas-oil ratios with increasing pressures obtained by performing a flash separation analysis on the equilibrated liquid phases at each pressure as shown in Figure 2.45, was also an indication that CO_2 is continuously dissolving into the liquid phase.

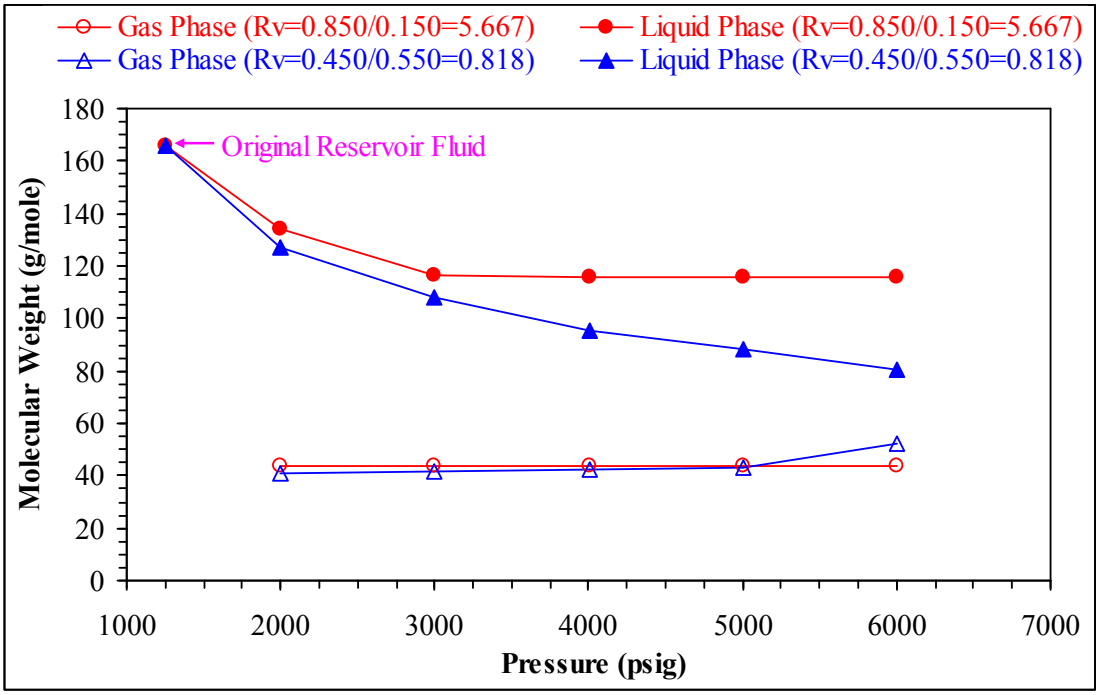

Figure 2.46: Equilibrated gas and liquid phase molecular weights as a function of pressure at constant initial gas/oil volume ratio at 238°F

6. Figure 2.46 is plot of molecular weights of the equilibrated fluid phases versus pressure for the two selected constant gas/oil volume ratios The molecular weights for the equilibrated gas phase increases slightly with increase in pressure and molecular weights for the equilibrated liquid phase decreases rapidly until 3000 psig and then remains approximately constant up to 6000 psig for the constant gas/oil volume ratio Rv = 5.667 as shown in Figure 2.46. Due to this, the difference in molecular weights for the constant gas/oil volume ratio Rv = 5.667 between the equilibrated fluid phases decreases very slowly with increase in pressure. This could be due to the less interaction of CO_2 with liquid phase, due to the less amount of reservoir fluid available in the feed mixture at the high gas/oil volume ratio Rv = 5.667.
7. Figure 2.46 also shows that at the constant gas/oil volume ratio Rv = 0.818, the molecular weights of the equilibrated gas phase is almost constant until 5000 psig and then shows a slight increase at 6000 psig. At 6000 psig the gas phase is rich in C_{7+} components since it is able to extract these components from the liquid phase, due to

more reservoir fluid being available in the feed mixture. Due to these phenomena the difference in molecular weights of the equilibrated fluid phase is gradually decreasing with increase in pressure. The molecular weights at 6000 psig for the equilibrated gas and liquid phase at the constant gas/oil volume ratio Rv = 0.818 approach each other and is an indication that the compositions of the fluid-fluid phases will eventually become similar when miscible condition between CO_2 and the reservoir fluid is approached.

8. Figure 2.47 is a plot of C_1 content in the equilibrated fluid phases versus pressure for the two constant gas/oil volume ratios. A very small amount of C_1 component has been extracted by CO_2 from the liquid phase into the gas phase as shown in Figure 2.47, and the amount of extraction decreases very slowly with increase in pressure for the constant gas/oil volume ratio Rv = 5.667. But a large amount of C_1 component is extracted by CO_2 from the liquid phase at the constant gas/oil volume ratio Rv = 0.818 and the extent of extraction decreases with increase in pressure. This is due to the less amount of reservoir oil present in the feed mixture (less C_1 available in the feed mixture for extraction) for the constant gas/oil volume ratio of Rv 5.667 and more amounts of reservoir oil present in the feed mixture (more C_1 available in the feed mixture for extraction) for the constant gas/oil volume ratio of Rv = 0.818.

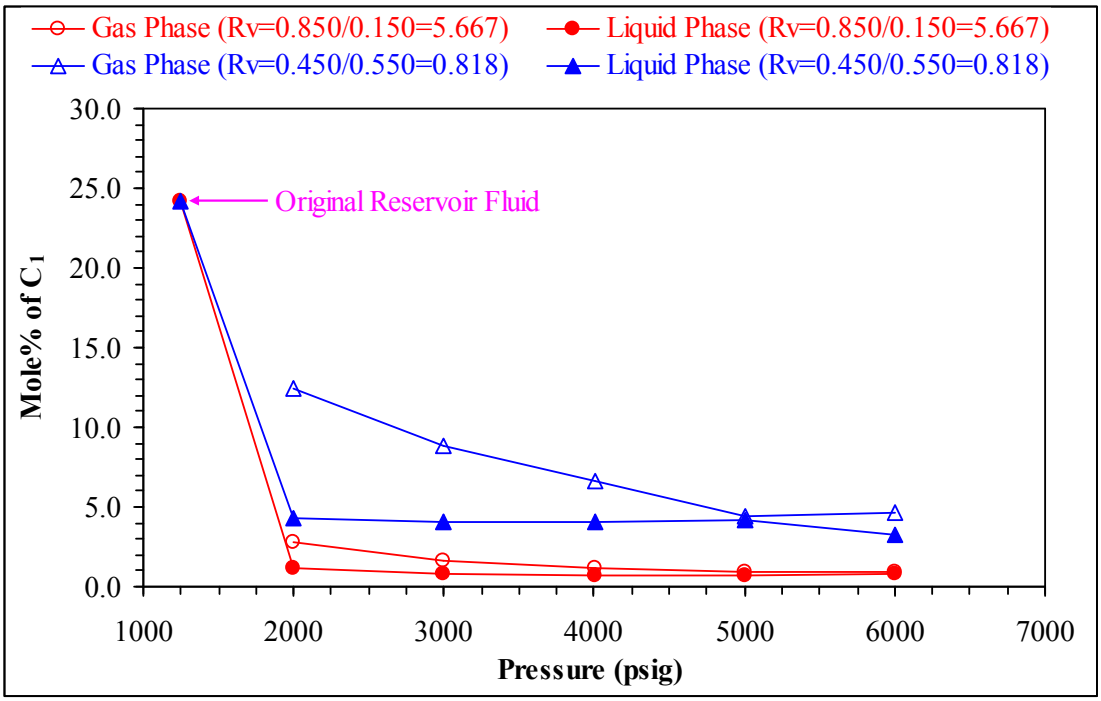

Figure 2.47: C1 content in the equilibrated gas and liquid phases at 238°F

9. There appears to be less interaction of the CO_2 with the liquid phase as can be seen from the compositional analysis data shown in Figures 2.43, 2.44 and 2.47 and hence there is less transfer of components from the liquid phase into the gas phase. It also

appears that the amounts of extraction of components by CO_2 from the liquid phase are dependant on the volume of reservoir fluid available in the feed mixture. The compositional analysis results of the liquid phase at each pressure also indicate that CO_2 was continuously dissolving in the liquid phase with increase in pressure. This is due to the absence of C_2-C_5 components in the depleted reservoir fluid, leading to less extraction of hydrocarbon components from the liquid phase into the gas phase. All these observations indicate that a condensing gas drive mechanism was responsible for developing miscibility in this CO_2-reservoir oil system.

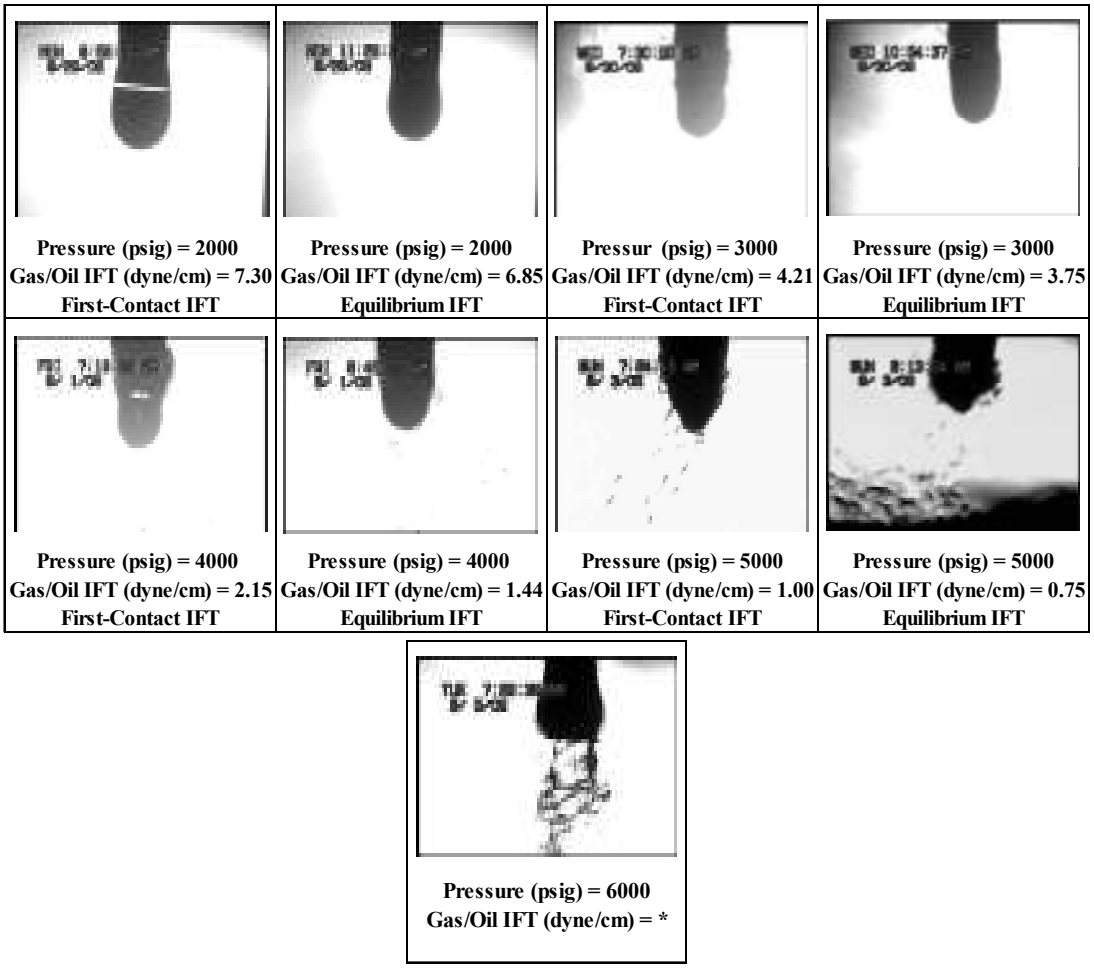

***Note:** The DSA program was not able to calculate the IFT because of the irregular shapes of the drops

Figure 2.48: FCM and equilibrium gas/oil IFT using the pendant drop shape images at constant initial gas/oil volume ratio at 238°F (Rv=0.850/0.107=5.667)

Effect of Gas/Oil Volume Ratios on Interfacial Tension

Figure 2.48 shows the drop shape images captured by the digital video camera for the first-contact miscibility and equilibrium IFT performed at the constant gas/oil ratio of

Rv=5.667. The first-contact process corresponds to the IFT of the first drop of fresh reservoir fluid when it first meets CO_2 gas without any liquid at the bottom of the optical cell i.e. the CO_2 gas has not been exposed to the crude oil. The equilibrium IFT corresponds to the drops of reservoir fluid with the CO_2 gas that attained complete mass transfer equilibrium by placing certain amount of reservoir oil at the bottom of the optical cell. Hence these equilibrium measurements represent the thermodynamic condition at which the fluid phases are in equilibrated and stabilized state.

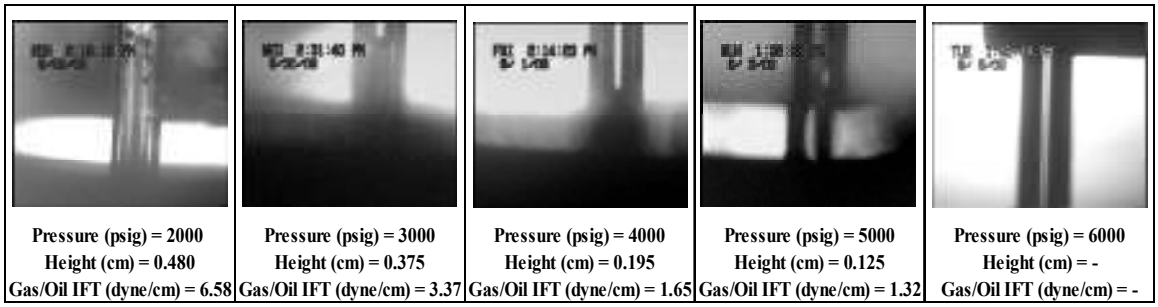

Figure 2.49: Gas/Oil IFT using the capillary rise technique at constant initial gas/oil volume ratio at 238°F (Rv=0.850/0.107=5.667)

Figures 2.49 and 2.50 show the capillary height images captured using the digital video camera for the constant gas/oil volume ratio corresponding to Rv=5.667 and Rv=0.818, respectively.

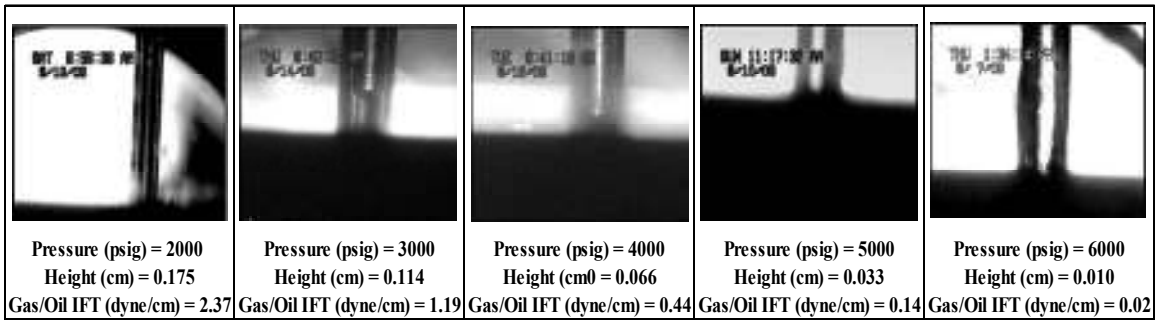

Figure 2.50: Gas/Oil IFT using the capillary rise technique at constant initial gas/oil volume ratio at 238°F (Rv=0.450/0.550=0.818)

The IFT data measurements using pendant drop and capillary rise techniques are for the two gas/oil volume ratios are summarized in Tables 2.34 and 2.37 respectively.

The following observations can be inferred from the first-contact and equilibrium gas/oil IFT measurements for two selected the constant gas/oil volume ratios Rv = 5.667 and Rv = 0.818, respectively.

1. The drop shape images shown in Figure 2.48 indicate that the IFT values calculated using the drop shape analysis software (DSA) is high for the first-contact miscibility

when compared to the equilibrium IFT values. These high first-contact IFT values clearly describe a situation where the fresh reservoir fluid contacts CO_2 and hence no mass transfer and interaction of the CO_2 with the reservoir fluid has occurred. The low equilibrium IFT values calculated from the drop shape images using the DSA program very much resemble multiple-contact miscibility where a complete counter directional mass transfer of components between the CO_2 and reservoir fluid takes place and hence the two fluid phases are in complete equilibrium.

There is a small difference observed between the equilibrium IFT values of the pendant drop and capillary rise techniques at the constant gas/oil volume ratio Rv = 5.667 as shown in Figures 2.48 and 2.49 respectively (Table 2.34). This can be attributed to the less contact time between the fluid phases (6 hours) for the pendant drop technique as compared to the high stabilization time of 24 hours for the capillary rise technique at the constant gas/oil volume ratio Rv = 5.667.

2. Figure 2.51 shows the plot of IFT measurements against the reciprocal pressure using a hyperbolic function. This plot indicates that a good linear fit exists for first-contact and equilibrium experimental IFT data using the pendant drop and capillary rise methods at the constant gas/oil volume ratio Rv = 5.667 with a coefficient of determination (R^2) values of 0.9953, 0.9919 and 0.9927 respectively. These linear regression equations when extrapolated to zero interfacial tension provide a minimum miscibility pressure value for the first-contact and equilibrium conditions to be 6845 psig and 6103 psig, respectively, based on pendant drop technique and a minimum miscibility pressure of 6142 psig for the equilibrium IFT data obtained using the capillary rise technique at the constant gas/oil volume ratio Rv = 5.667.

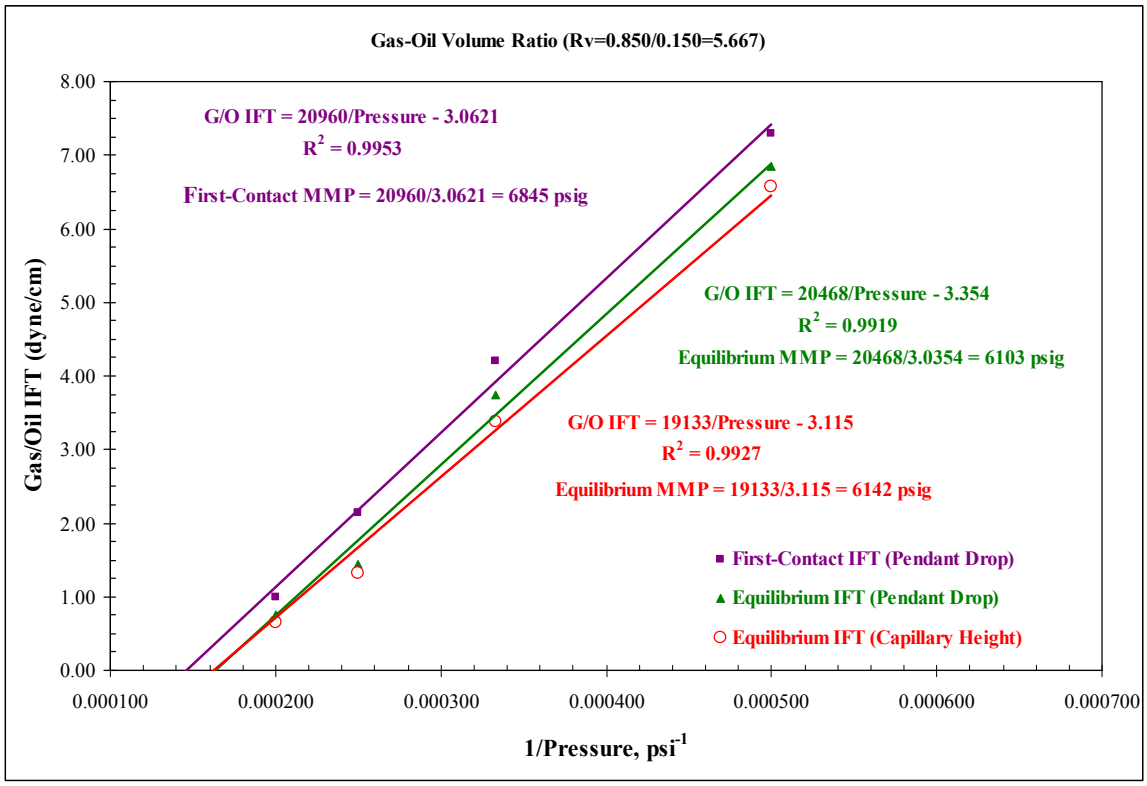

Figure 2.51: First-contact and equilibrium MMP using VIT technique at the constant gas/oil volume ratio Rv=5.667 at 238°F

The extrapolated linear regression equations to zero interfacial tension indicate the condition where the interface between the fluid-fluid phases vanishes and as a result the entire fluid-fluid system becomes a single-phase fluid. As expected the MMP for the first-contact was higher than that of equilibrium MMP, since no mass transfer and interaction of components between CO_2 and the reservoir fluid had occurred during the first-contact due to the fresh reservoir fluid contacting the CO_2 for the first time. While the low MMP for the equilibrium IFT is a stabilized state of fluid-fluid phases due to the complete counter directional mass transfer of hydrocarbon between the fluid-fluid phases.

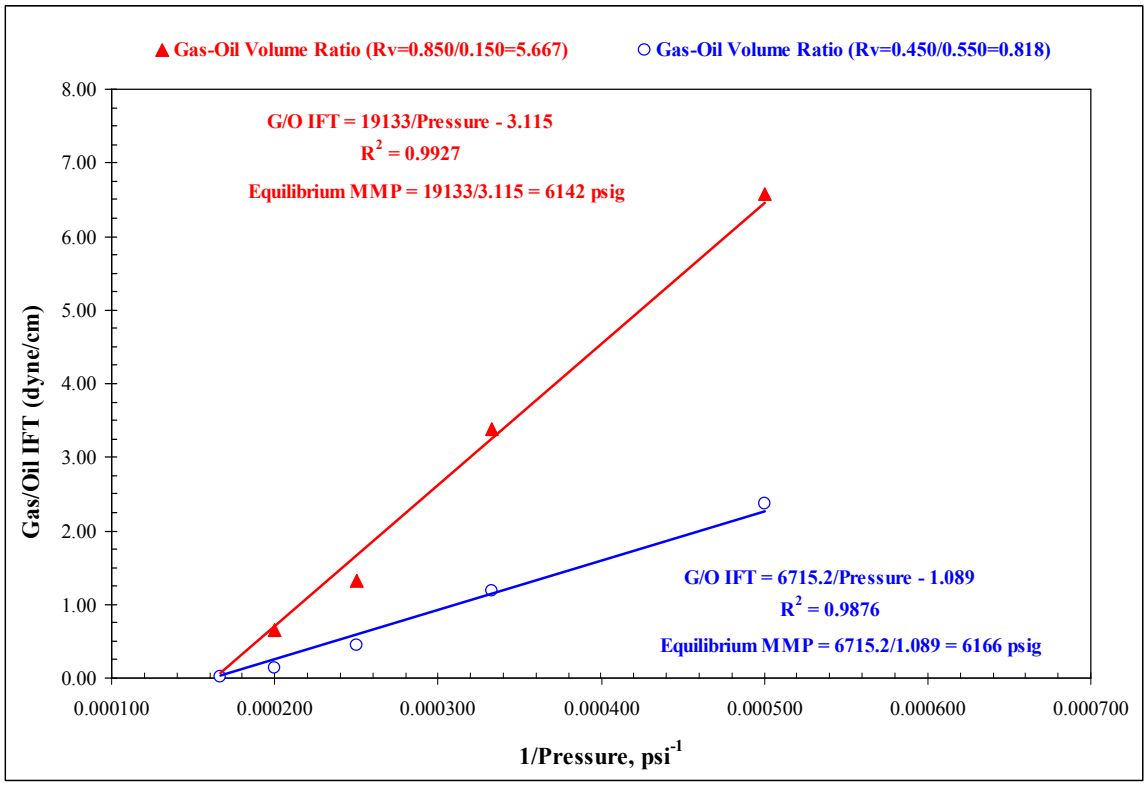

Figure 2.52: Effect of initial gas/oil volume ratio on gas-oil IFT and equilibrium MMP using VIT at 238°F

3. Figure 2.52 shows that IFT data for the two constant gas/oil volume ratios of Rv = 5.667 and Rv = 0.818 when plotted against reciprocal pressure using the hyperbolic function converge to similar end point on zero IFT axis. The linear curve fit gives an equilibrium MMP of 6142 psig for the constant gas-oil volume ratio of Rv = 5.667 at zero interfacial tension with a coefficient of determination (R^2) of 0.9927and an equilibrium MMP of 6166 psig for the constant gas-oil volume ratio Rv = 0.818 at zero interfacial tension with a coefficient of determination (R^2) of 0.9876. The equilibrium IFT measurements at the widely different two gas/oil volume ratios clearly indicate that although the initial mixture composition of the phases affects the gas/oil IFT yielding different relationships for its dependence on pressure, they all converge at same end point of zero interfacial tension yielding an almost identical miscibility pressure.

2.2.4.3.3 Compositional Effects on IFT at Varying Gas/Oil Ratios (Molar and Volumetric) in the Feed Mixture

Since gas-oil IFT is dependant on gas/oil ratio, it may appear that the minimum miscibility pressure, determined from VIT technique, may also depend on gas/oil ratio. However, Figures 2.40 and 2.52 indicated that although IFT varies with gas-oil ratio and

pressure at constant reservoir temperature for this type of CO_2-reservoir fluid system, all of them would eventually converge to similar miscibility pressures at zero interfacial tension.

Table 2.40: Summary of MMP data at varying gas/oil ratios

Case	Gas/Oil Ratio	Equilibrium MMP (psig)
1	Gas/Oil Molar Ratio (Rm=8.346)	6180
2	Gas/Oil Molar Ratio (Rm=2.333)	6216
3	Gas/Oil Volume Ratio (Rv=5.667)	6142
4	Gas/Oil Volume Ratio (Rv=0.818)	6166
Average MMP (psig)		6176
Standard Deviation		0.31
% Maximum Deviation		1.20
% Variation in Gas/Oil Molar Ratio		72
% Variation in Gas/Oil Volume Ratio		86

Table 2.40 shows the MMP data obtained from performing the gas/oil IFT measurements using the VIT technique at the varying gas/oil molar ratios (72%) and the varying gas/oil volume ratios (86%). Table 2.40 indicated that a 4-fold increase in gas/oil molar ratio and a 7-fold increase in gas/oil volume ratio resulted in a standard deviation of only 0.31% and maximum deviation of only 1.20% in equilibrium MMP. These results clearly indicate that the compositional paths followed by the fluids to attain mass transfer equilibrium do not affect MMP derived from IFT measurements. This experimental study has also demonstrated that the VIT technique for miscibility determination is independent of the compositional path followed by gas and oil in their approach to equilibrium.

The VIT technique involved contacting of fresh reservoir oil with already pre-equilibrated CO_2 gas by placing a small amount of oil at the bottom of the optical cell. This simulates a dynamic (multiple-contact) displacement process occurring in the reservoir where the injected gas interacts with reservoir oil as it moves ahead in the reservoir and gradually becomes altered in composition due to mass transfer between fluid phases so as to become miscible with the original oil. The definition of multiple-contact is an approximation which serves well to explain the “continuous interaction” that actually occurs in the reservoir (or in the slim-tube) by means of several discrete steps or contacts (Ayirala and Rao, 2006). It is an approximation because infinite number of such contacts between phases will be required in order to truly approach the result of their continuous interaction.

Since the IFT measurements were made using the pendant drop and capillary rise technique after complete equilibrium and stabilization of the mass transfer between the fluid phases, it was concluded that the terms "Equilibrium IFT" and Equilibrium Miscibility" are appropriate to use for this type of an experimental study. Equilibrium IFT typically simulates a real reservoir where the injected CO_2 gas interacts continuously with crude oil as it flows to the producing well. This continuous interaction enables counter-directional mass transfer (vaporizing and condensing) between the fluid phases thereby allowing the system to attain equilibrium miscibility.

2.2.5 Summary of Conclusions

The following important conclusions were drawn from the results of various VIT experiments conducted in this section using a live crude oil-CO_2 system at reservoir conditions.

1. The experimental procedure used in this study for IFT measurements closely resembles the continuous interaction between the injected gas and the crude oil occurring in the reservoir. At the leading edge of the CO_2 slug, the gas which has attained compositional equilibrium with live reservoir oil through its continuous interaction as it flows through the reservoir, contacts fresh live reservoir oil ahead of the gas slug. This is exactly what is simulated in the VIT technique by allowing the gas and live reservoir oil to continuously interact and attain equilibrium before exposing the gas phase to fresh oil drops that are injected into the higher pressure optical cell for measuring the IFT through the pendant drop technique. Additional care was taken to restart each experiment at each new pressure to avoid compositional interference from the previous experiment.
2. The validation of the vanishing interfacial tension technique to determine the fluid-fluid miscibility in a real CO_2-live reservoir fluid system using the pendant drop and capillary rise techniques once again proved that VIT is a fast and cost effective method, requiring small amounts of fluid samples.
3. For the first time an in-depth insight into the phase behavior interactions between the fluid-fluid phases was gained from the compositional analysis of the fluid phases at two different gas/molar ratios and at two different gas/oil volume ratios in the feed mixture and at actual reservoir temperature.
4. The compositional analysis data of the equilibrated fluid phases at constant gas/oil molar ratios and constant gas/oil volume ratios indicated that the gas phase contained predominantly CO_2 and the CO_2 continuously dissolved into the liquid phase with increase in pressure. The CO_2 content in the liquid phase rapidly increased up to a certain pressure and then slowed down, until the liquid phase becomes fully saturated with CO_2 near miscibility conditions. This type of behavior of CO_2 gas observed with

the depleted reservoir fluid clearly indicated that condensing gas drive mechanism was the dominant mass transfer mechanism for miscibility development.

5. The dominance of condensing gas drive mechanism for obtaining the miscibility with the depleted reservoir crude oil can be attributed to the least interaction of CO_2 with the reservoir fluid to extract C_2-C_5 components from the reservoir fluid. This was confirmed by the compositions of the original reservoir fluid which showed negligible amounts of C_2-C_5 (about 2.528 mole%) components. This reservoir oil was depleted starting from an initial reservoir pressure of 4050 psi to the current reservoir pressure of 1100 psi at 238°F. Hence most of the lighter components of C_2-C_5 present in the original live oil were produced since the reservoir pressure was well below the bubble point pressure. This type of gas-oil interfacial tension measurements and their direct dependence on hydrocarbon fluid phase compositions at constant initial gas/oil (molar and volumetric) ratios provided an effective means to determine the mass transfer drive mechanisms responsible for miscibility development.
6. An interesting finding of using the constant gas-oil ratio in the feed mixture for this type of a condensing mode gas-oil fluid system was that the amount of hydrocarbon components extracted by the CO_2 gas from the reservoir fluid was dependent on the volume of oil present in the feed. More amount of reservoir fluid in the feed mixture had resulted in more extraction of n-C_1 by CO_2 from the liquid phase. Similarly less amount of reservoir fluid in the feed mixture had resulted in less extraction of n-C_1 by CO_2 from the liquid phase. Therefore, it can be concluded that the amount of extraction of hydrocarbon components from the reservoir fluid by CO_2 is dependent on the gas-oil ratio in the depleted reservoir fluid-CO_2 system.
7. Minimum miscibility pressures of 6180 psig and 6216 psig were obtained for the two constant gas/oil molar ratios of Rm=8.346 and Rm=2.333, respectively. Hence, it can be concluded that although the equilibrium gas-oil interfacial tensions for the two gas/oil ratios exhibit different dependences on pressure, they converge to the same end point of zero interfacial tension with similar minimum miscibility pressures.
8. The first-contact miscibility of 6845 psig obtained was distinctly higher than the equilibrium MMP of 6103 psig using the pendant drop technique at the constant gas-oil volume ratio Rv=5.667 at 238°F when the gas-oil interfacial tension values were extrapolated to zero interfacial tension. These observations were in good agreement with the published literature (Rao, 1997). During a first-contact miscible displacement process, CO_2 gas becomes miscible with the reservoir fluid to form a single-phase fluid on the first-contact itself. Hence no mass transfer of hydrocarbon components between the fluid phases will take place in a first-contact miscible displacement process. The lower value of MMP for equilibrium miscibility compared to first-contact miscibility is due to the fact that in equilibrium miscibility the CO_2 gas attains equilibrium with the reservoir fluid due to complete mass transfer of

components during their continuous interaction, and hence a thermodynamic equilibrium state is reached between the injected gas and reservoir oil. The equilibrated minimum miscibility pressure at the constant gas/oil volume ratio Rv=5.667 at 238°F was 6142 psig using the capillary rise technique and this was in good agreement (within 0.64%) with the MMP value obtained from the equilibrium IFT values using the pendant drop technique at the same gas/oil volume ratio.

9. The minimum miscibility pressure at the constant gas/oil volume ratio Rv=5.667 was 6142 psig and at Rv=0.818 was 6166 psig using the capillary rise technique. These observations show that although the nature of dependence of equilibrium interfacial tension on pressure varies with gas-oil ratio, but all of them would eventually converge at the same point of zero interfacial tension to yield similar miscibility pressures. This once again proves the compositional independence of minimum miscibility pressures determined using the VIT technique.
10. The experimentally determined VIT miscibility value (from 6103 psig to 6215 psig) at 238°F was in good agreement (within 7%) with the predicted MMP of 6675 psi at 238°F calculated from modified Peng-Robinson (1987) equation of state model using the CMG-WinProp. The equation of state models for MMP calculations have been known to over predict the minimum miscibility pressure. Interestingly, the governing mass transfer mechanism of condensing drive mechanism inferred from the measured compositional data also agreed well with the predictions of PR-EOS calculations.
11. The gas-oil interfacial tensions measured for the CO_2-live reservoir fluid system using the capillary rise technique at reservoir conditions in this study proved that the capillary rise technique is accurate, and reliable, and can be successfully used to measure very low values of gas-oil interfacial tension for obtaining the minimum miscibility pressure through the VIT technique.

2.3 Development of Computational Models for Miscibility Prediction

2.3.1 EOS Computational Model for Gas-Oil Miscibility

2.3.1.1 Introduction

Apart from the experimental techniques discussed previously in Section 2.1.1.1, a computational approach based on equations of state calculations is also available to determine minimum miscibility pressures. With the advances in computer implemented equations of state models, the predictions of phase behavior by this approach have become more reliable (Kuo, 1985). However, this approach requires the availability of compositional data for the reservoir fluids, which can be obtained from the laboratory PVT measurements that are considered to be somewhat tedious.

An analytical model (Wang and Orr, 1998; Jessen et al., 1998; Wang and Peck, 2000) has been widely used in recent years to calculate the MMP and MME for real systems. The main principle involved in this analytical approach is that all key tie-lines intersect each other in a multicomponent system and hence these tie-line intersections can be used to determine the MMP or MME. The key tie-lines are first determined for various increasing pressures. MMP is then defined as the pressure at which one of the key tie-lines becomes a critical tie-line, that is, a tangential tie-line of zero length to the critical locus. Besides speed and accuracy, the main advantage of this method is that the computed MME and MMP are dispersion-free. Oil and gas mixing due to dispersion affects the displacement efficiency and hence the oil recovery. Dispersional effects are much likely to be greater in the field than observed in the laboratory. The main disadvantage of this analytical technique is that a good equation of state fluid characterization is required.

Lee and Reitzel (1982) determined the miscibility conditions of Pool A crude oil from the Brazeau River Nisku field with injection gas containing 90 mole% of methane by conducting laboratory slim-tube tests. They compared the experimental result with that obtained from PR-EOS calculations and found that the EOS predictions were higher by about 4.0 MPa than the experimental slim-tube measurement. They attributed this deviation to inaccuracies in estimating the critical points as well as to lack of suitable experimental PVT data to fine tune the PR-EOS. Firoozabadi and Aziz (1986) compared the slim-tube miscibility conditions with PR-EOS calculations for four different reservoir fluids. They found that PR-EOS predictions were consistently higher by about 0.7-9.0 MPa for the four systems studied. Hagen and Kossack (1986) measured the MMP of methane-propane-n-decane systems using a high-pressure sapphire cell and compared their experimental results against slim-tube displacements and modified three-parameter PR-EOS calculations. They were able to accurately match the sapphire cell measurement of MMP with the three-parameter PR-EOS, using binary interaction coefficients as

regression variables. Ahmed (1997) used a new "miscibility function" in PR-EOS and matched the slim-tube experimental results of several already existing systems with an absolute average deviation of around 3.4%. Wang and Orr (1998), Wang and Peck (2000) used an analytical model to calculate the MMP and evaluated their model results with numerical simulation and slim-tube displacements. Jessen et al. (1998) developed a model based on Wang and Orr (1998) to predict the MMP and matched their model with slim-tube experimental results and compositional simulators.

2.3.1.2 Objectives

The objective is to compare the VIT experimental results of MMP with those obtained from phase behavior calculations based on a PR-equation of state computational model. For this purpose, two reservoir fluids of Rainbow Keg River and Terra Nova were used, since all the PVT data needed for EOS calculations and the VIT experimental values of MMP were readily available (Rao, 1997; Rao et al., 1999; Rao and Lee, 2002). VIT experimental results of two standard gas-oil systems of n-decane-CO_2 at 37.7^oC and live decane (consisting of 25 mole% methane, 30 mole% n-butane and 45 mole% n-decane)-CO_2 at 71.1^oC, reported in Section 2.1.1.5, were also used for comparison with EOS calculations. All the phase behavior calculations were carried out using the commercial simulator, Winprop (Computer Modelling Group Ltd., 2002). This is a multiphase equilibrium program equipped with Peng-Robinson (PR) (Peng and Robinson, 1976) and Soave-Redlich-Kwong (SRK) (Redlich and Kwong, 1949; Soave, 1972) equations of state and accommodates most of the phase behavior calculations efficiently.

2.3.1.3 EOS Tuning

The phase behavior calculations of reservoir fluids are routinely made using equations of state in petroleum industry today. It is common practice to tune equations of state prior to use for accurate phase behavior prediction of reservoir fluids. EOS tuning is nothing but the calibration of EOS against the experimental data by adjusting the input values of some uncertain parameters in the EOS so as to minimize the difference between the predicted and measured values. The effectiveness of each experimental property is introduced into the EOS model through its weight factor. The weakness of EOS towards calculation of some specific properties, the reliability of data and the target for the fluid properties study affect the values of these weight factors. Coats and Smart (1986), Coats (1988) and Bahbahaninia (2001) recommended a universal set of weight factors for experimental data to ensure proper tuning of EOS, which are shown in Table 2.41.

However, if the input parameters of EOS were adjusted widely by assigning weight factors other than those suggested by Coats and Smart (1986), Coats (1988), Bahbahaninia (2001) to match the experimental data, it would lead to unrealistic results. This is known as over tuning of EOS. Pederson et al. (1988) discussed the dangers of

over tuning of EOS and provided many examples of reliable predictions without any tuning, but only by a proper analysis and characterization of real reservoir fluids. Danesh (1998) suggested that, in general, any leading EOS, which predicts the phase behavior data reasonably well without tuning, would be the most appropriate choice for phase behavior calculations.

Table 2.41: Optimum Weight Factors Proposed for Proper EOS Tuning (Coats and Smart, 1986; Smart, 1988; Behbahaninia, 2001)

Property	Weight Factor
Saturation Pressure	50
Oil Specific Gravity	5 – 10
Gas Compressibility Factor	2 – 3
All Other Properties	1

Table 2.42: Composition of Rainbow Keg River Fluids Used

Reservoir Temperature: 87°C Saturation Pressure: 17.15 MPa
Reservoir Pressure: 17.50 MPa (bubble point)

Component	Mol % in live oil	Mol % in lean gas (Primary)	Mol % in rich gas (Makeup)
Hydrogen Sulfide	1.37	0.00	0.00
Carbon Dioxide	0.82	1.24	0.80
Nitrogen	0.57	1.76	0.40
Methane	35.13	81.01	14.73
Ethane	10.15	11.14	21.34
Propane	6.95	3.95	41.83
iso-Butane	1.10	0.50	7.35
n-Butane	3.16	0.34	11.67
iso-Pentane	2.29	0.00	0.00
n-Pentane	1.74	0.07	1.89
Hexanes	3.68	0.00	0.00
Heptanes plus	33.04	0.00	0.00
Total	100	100	100
$C_{2+} + CO_2$	62.93	17.24	84.88

C_{7+} Properties:
Specific Gravity: 0.8397
Molecular Weight: 205

From the Table 2.41, it is observed that saturation pressure has the highest weight factor of 50. The higher the weight factor, the more accurate is the measurement of that data and hence more importance must be given to match that property. Hence, in this study, EOS has been tuned to match saturation pressures as done by Jessen et al. (1998) and Glaso (1990). Peng-Robinson EOS has been chosen as it is most widely used in the

industry. The reservoir fluid compositions, reservoir temperatures and saturation pressures described in Tables 2.42 and 2.43 form the basis for this study. Before tuning the EOS, the heptanes plus fraction was characterized using two-stage exponential distribution (Whitson and Brule, 2000). Then the PR-EOS was tuned to match the saturation pressures using different tuning approaches. The detailed description of the equations and the procedures used for obtaining the optimum values of regression parameters while tuning PR-EOS to match the saturation pressure can be seen elsewhere (Computer Modeling Group Ltd., 2002).

Table 2.43: Composition of Terra Nova Fluids Used

Reservoir Temperature: 96°C Saturation Pressure: 24.79 MPa
Reservoir Pressure: 38.04 MPa (bubble point)

Component	Mol % in live oil	Mol % in lean gas (Primary)	Mol % in rich gas (Makeup)
Nitrogen	0.15	0.33	0.21
Carbon dioxide	0.69	1.1	1.18
Methane	45.06	90.11	51.55
Ethane	5.37	6.01	12.8
Propane	5.44	2.09	16.31
iso-Butane	0.98	0.12	2.63
n-Butane	2.85	0.21	6.71
iso- Pentane	1.24	0.02	2.12
n- Pentane	1.8	0	2.35
n- Hexane	9.13	0	3.86
Heptanes plus	27.29	0	0.29
Total	100	100	100
CO_2+ C_{2+}	54.79	9.56	48.24

C_{7+} Properties:
Specific Gravity: 0.879
Molecular Weight: 241

The regression parameters tuned are:

1. The critical temperature, T_c, of the heaviest component in the characterized heptanes plus fraction
2. The critical pressure, P_c, of the heaviest component in the characterized heptanes plus fraction
3. The acentric factor, ω, of the heaviest component in the characterized heptanes plus fraction
4. The binary interaction coefficient (BIC), K_{ij}, between methane and the heaviest component in the characterized heptanes plus fraction

5. Volume shift parameter, S, of the heaviest component in the characterized heptanes plus fraction
6. EOS parameter, Ω_b, of the heaviest component in the characterized heptanes plus fraction
7. Molecular weight of the heaviest component in the characterized heptanes plus fraction

The initial and final values of tuned parameters and predicted saturation pressures for different tuning approaches of RKR and Terra Nova crude oil systems are given in Tables 2.44 and 2.45, respectively. The deviations of EOS predicted saturation pressures without tuning and without heptanes plus characterization from experimental values were reasonable (less than 5%). The tuning of volume shift parameter and molecular weight of the heaviest component in C_{7+} fraction were ineffective in improving the match of EOS predictions. The EOS predictions from the tuned parameters of critical temperature, critical pressure, binary interaction coefficient, acentric factor and Ω_b of the heaviest component in C_{7+} fractions matched well with the experimental saturation pressure. The best fit of saturation pressures was obtained with the tuned parameter of binary interaction coefficient for both the cases studied. Furthermore, in order to match the experimental saturation pressure, an absolute change of less than 5% was needed in all these parameters. Knowing the uncertainty in the experimental measurements, these variations in EOS parameters can be considered as reasonable.

2.3.1.4 MMP Determination Using EOS

The compositions of the lean and rich gases used for making up the solvent and the compositions of various solvents used in VIT experiments as well as in EOS calculations are shown in Tables 2.42, 2.46 and 2.43, 2.47 for RKR and Terra Nova reservoirs, respectively.

The following steps are used in the commercial simulator, Winprop (Computer Modelling Group Ltd., 2002) to calculate the MMP at a given temperature.

1. An initial pressure below MMP is chosen to start the computation.
2. The reservoir temperature, crude oil composition, primary and makeup gas compositions, makeup gas fraction, pressure increment, solvent to oil ratio increment, equilibrium gas/original oil mixing ratio and equilibrium liquid/original solvent mixing ratio are then provided as inputs to the program.
3. The composition of solvent obtained by mixing of primary and makeup gases is then calculated using the specified ratio.
4. Solvent is added to the crude oil at specified solvent to oil molar ratio increments and flash calculations are performed until two-phase region is detected. The absence of two-phase region implies first contact miscibility and the program stops.

5. For the presence of two- phase region, the program checks the relative positions of solvent and crude oil compositions with respect to limiting tie line. If the solvent composition is to the left, while that of crude oil to the right of limiting tie line, then the process is a vaporizing gas drive. Otherwise, the process is a condensing gas drive (Green and Willhite, 1998).
6. For vaporizing gas drive, using the first point in the two-phase region detected in step 4, the flashed vapor is mixed with the original oil at the specified ratio of equilibrium gas to original oil and the flash calculation is performed.
7. For condensing gas drive, using the first point in the two-phase region detected in step 4, the flashed liquid is mixed with the original solvent at the specified ratio of equilibrium liquid to original solvent and the flash calculation is performed.
8. The procedure is repeated until the liquid composition is same as the vapor composition and MMP is the pressure at which this occurs and the program stops.
9. Otherwise, the pressure is increased at specified pressure increment and the steps 4 to 8 are repeated.

Table 2.44: Comparison of MMP from VIT Measurements and EOS Calculations Using Various Tuning Approaches for Rainbow Keg River Fluids

Parameter	**Initial Value**	**Tuned Value**	**Psat (MPa)**	**Deviation* (%)**	**Solvent #1 (C_{2+}=51.0%) MMP (MPa)**	**Solvent #2 (C_{2+}=52.5%) MMP (MPa)**	**Solvent #3 (C_{2+}=59.7%) FCM (MPa)**
Experimental (VIT)	-	-	17.15	0.00	14.8	14.0	14.8
No tuning and without C_{7+} characterization	-	-	17.68	3.07	17.8	16.7	19.5
No tuning and with C_{7+} characterization	-	-	17.32	1.02	15.6	16.4	24.7
T_c (^oC)	667.817	642.33	17.15	0.00	21.8	23.7	22.3
P_c (MPa)	1.0367	0.9903	17.14	-0.05	21.8	23.6	23.5
ω	1.09313	1.04037	17.15	0.00	21.9	21.7	22.7
Volume Shift Parameter, S	0.085167	0.035171	17.33	1.05	15.6	16.4	24.7
K_{ij} ($C_1 - C_{27+}$)	0.111198	0.105836	17.15	0.00	15.9	23.6	23.6
Ω_b	0.077796	0.079139	17.15	0.00	24.1	23.7	23.1
M_w (g/mole)	480.611	480.611	17.33	1.05	15.6	16.4	24.7

Table 2.45: Comparison of MMP from VIT Measurements and EOS Calculations

Parameter	Initial Value	Tuned Value	P_{sat} (MPa)	Deviation* (%)	Solvent #1 (C_{2+}=9.56%) MMP (MPa)	Solvent #2 (C_{2+}=21.4%) MMP (MPa)	Solvent #3 (C_{2+}=29.4%) MMP (MPa)	Solvent #4 (C_{2+}=32.3%) MMP (MPa)	Solvent #5 (C_{2+}=41.2%) MMP (MPa)
Experimental (VIT)	-	-	24.793	0.00	62.85	57.80	31.80	-	-
Visible MMP	-	-	-	-	60.70	55.00	30.60	30.00	26.20
No tuning and without C_{7+} characterization	-	-	26.241	5.84	56.20	54.80	44.40	40.00	29.30
No tuning and with C_{7+} characterization	-	-	25.683	3.59	38.00	38.00	31.50	35.95	34.59
T_c (^oC)	741.47	723.098	25.510	2.89	38.70	38.70	32.87	37.32	34.93
P_c (MPa)	0.9453	0.8282	24.917	0.50	39.04	38.70	38.01	37.32	34.58
ω	1.20948	1.16924	25.497	2.84	38.70	38.40	31.85	36.64	34.93
Volume Shift Parameter, S	0.07201	0.122	25.683	3.59	38.00	38.00	31.50	35.95	34.59
K_{ij} ($C_1 - C_{31+}$)	0.119124	0.106069	24.828	0.14	38.70	38.70	30.48	37.32	34.24
Ω_b	0.077796	0.082574	24.834	0.17	39.40	39.40	38.40	36.64	34.60
M_w (g/mole)	577.624	606.549	25.683	3.59	38.00	38.00	37.67	35.95	34.58

Using Various Tuning Approaches for Terra Nova Fluids

*** Deviation (%) = ($P_{sat,calc} - P_{sat,exp}$) / ($P_{sat,exp}$)**

Table 2.46: Composition (in Mole %) of Solvents Used in VIT Tests as well as in EOS Calculations of Rainbow Keg River Fluids

Component	Solvent #1	Solvent #2	Solvent #3
Hydrogen Sulfide	0.00	0.00	0.00
Carbon Dioxide	1.01	1.00	0.96
Nitrogen	1.06	1.03	0.89
Methane	46.93	45.47	38.46
Ethane	16.38	16.61	17.69
Propane	23.42	24.26	28.27
iso-Butane	4.02	4.17	4.90
n-Butane	6.16	6.41	7.61
iso-Pentane	0.00	0.00	0.00
n-Pentane	1.01	1.05	1.24
Hexanes	0.00	0.00	0.00
Heptanes plus	0.00	0.00	0.00
Total	100.00	100.00	100.00
C_{2+}	51.00	52.50	59.70
Makeup (%)	51.417	53.621	64.198

Table 2.47: Composition (in Mole %) of Solvents Used in VIT Tests as well as in EOS Calculations of Terra Nova Fluids

Component	Solvent #1	Solvent #2	Solvent #3	Solvent #4	Solvent #5
Nitrogen	0.33	0.2933	0.2684	0.2594	0.2318
Carbon dioxide	1.1	1.1245	1.141	1.1471	1.1654
Methane	90.11	78.306	70.3285	67.4085	58.5642
Ethane	6.01	8.0894	9.4932	10.0071	11.5635
Propane	2.09	6.4444	9.3848	10.4611	13.7211
iso-Butane	0.12	0.8886	1.4076	1.5976	2.173
n-Butane	0.21	2.2004	3.5445	4.0365	5.5266
iso- Pentane	0.02	0.663	1.0973	1.2562	1.7377
n- Pentane	0	0.7196	1.2055	1.3834	1.9222
n- Hexane	0	1.182	1.9802	2.2723	3.1573
Heptanes plus	0	0.0888	0.1488	0.1707	0.2372
Total	100	100	100	100	100
$CO_2 + C_{2+}$	9.56	21.4	29.4	32.33	41.2
Makeup (%)	0	30.62	51.3	58.87	81.8

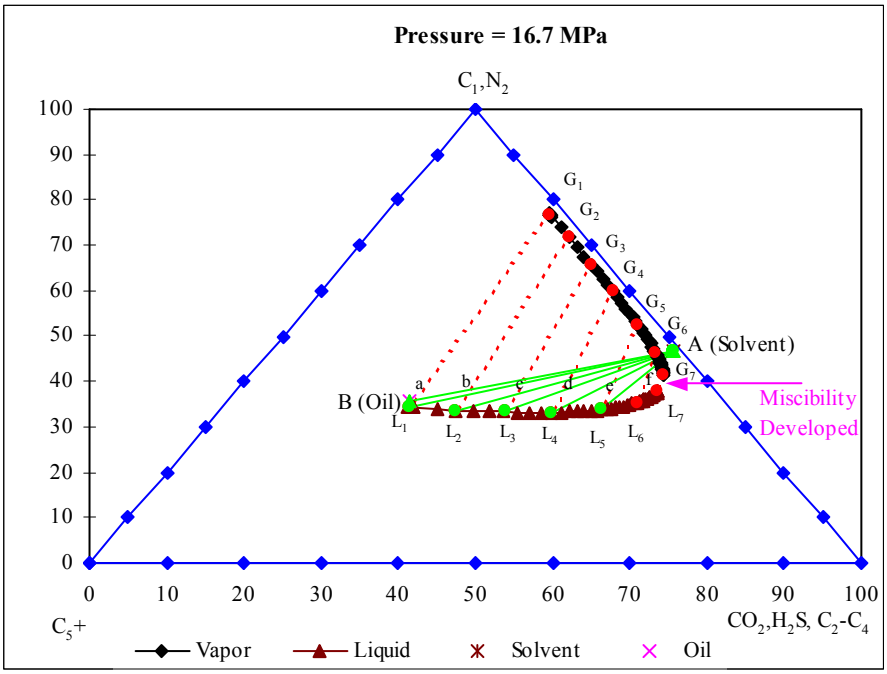

Figure 2.53: Representation of Condensing Drive Mechanism on a Pseudo-Ternary Diagram for Rainbow Keg River Fluids at a C2+ Concentration of 52.5% in Solvent

2.3.1.5 Results and Discussion

Rainbow Keg River Reservoir. Figure 2.53 (for a pressure of 16.7 MPa) shows the development of multiple-contact miscibility by condensing drive mechanism at a C_{2+} concentration of 52.5% in the solvent, as an example case. Since the 7 th contact-line between solvent (A) and the liquid phase (L_7) lies outside the two-phase envelope, the

MMP is 16.7 MPa. The summary of VIT experimental results and EOS calculations for different tuning approaches is shown in Table 2.44. The comparison is shown in Figure 2.54, which indicates that the MMP predictions from untuned PR-EOS and without C_{7+} characterization were consistently higher by about 3-5 MPa than VIT measurements at all C_{2+} enrichments. This is in good agreement with other studies (Lee and Reitzel, 1982; Firoozabadi and Aziz, 1986), which show that EOS calculations generally yield more conservative results than laboratory measurements.

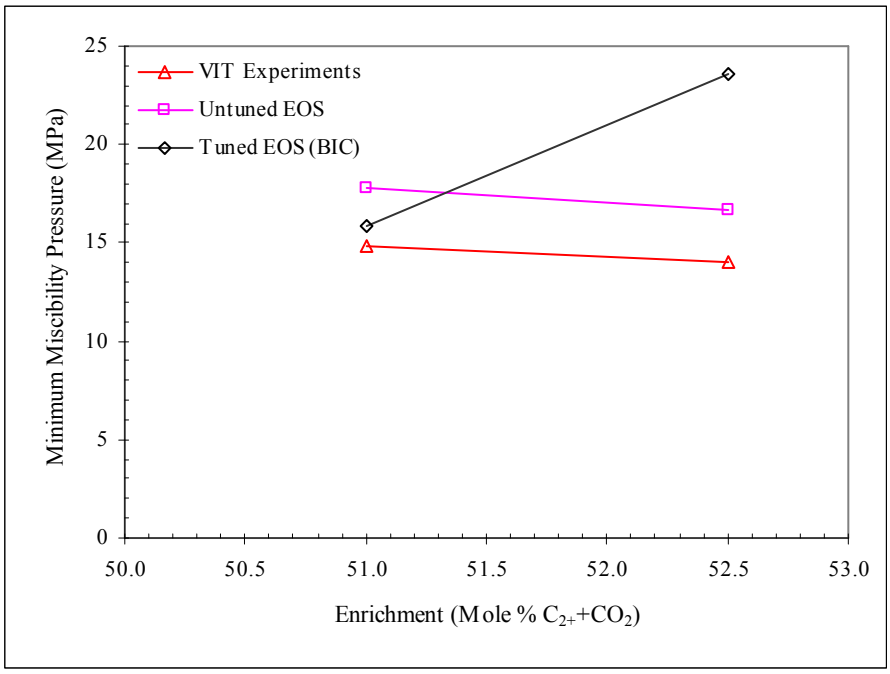

Figure 2.54: Comparison of Miscibility Conditions of RKR Fluids Obtained from VIT Experiments and EOS Calculations

As can be seen in Table 2.44, the MMP predictions from tuned EOS of critical temperature, critical pressure, acentric factor, binary interaction coefficient, and Ω_b parameter are nearly the same. Interestingly, all these tuned parameters also resulted in similar saturation pressure predictions. But these MMP predictions significantly differed from the VIT experimental values. Thus, in spite of matching the saturation pressure with acceptable change in EOS parameters, the significantly different MMP predictions obtained in this study for different tuning approaches clearly indicate that tuning of EOS may not be always suitable while calculating the MMP. However, it also raises question as to the effect of choosing another measured property to match other than saturation pressure, on MMP prediction.

Terra Nova Reservoir. Table 2.45 shows the summary of VIT experimental values and EOS calculations for this reservoir. The comparison between various experimental

techniques and EOS calculations is shown in Figure 2.55. The important observations are:

- Large differences exist between untuned and tuned EOS at low C_{2+} enrichments below 25%.
- Untuned EOS prediction is much closer to VIT and visible MMP experimental values than tuned EOS predictions.
- Sharp decline in MMP is indicated at C_{2+} enrichments above 21.4% by almost all the techniques including VIT, visible observation, untuned and tuned EOS.
- Both tuned and untuned EOS indicate that calculated MMP is insensitive to enrichment when the C_{2+} enrichment level is between 9.5-21.4%. This does not appear to be reasonable, since the doubling of enrichment should be expected to yield a significant drop in MMP.

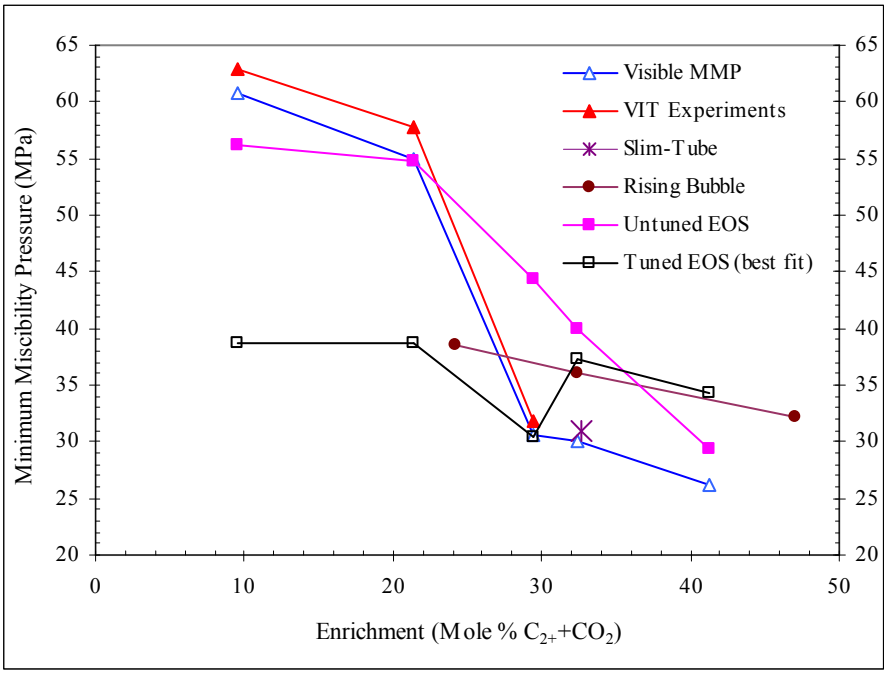

Figure 2.55: Comparison of Miscibility Conditions of Terra Nova Fluids Obtained from VIT Experiments and EOS Calculations

In three out of total of five cases studied, the predicted MMP from untuned PR-EOS and without C_{7+} characterization reasonably matched the visible MMP from VIT experiments. Interestingly, the C_{2+} concentration in the solvent is around 30% for the two particular cases where the strong disagreement is observed. In one out of three cases where reasonable match is obtained, the EOS prediction is about 3.0 MPa higher than the VIT experimental value. The C_{2+} concentration in the solvent for this case is around 40%. Similar situation was observed at 50% C_{2+} concentrations in the RKR case. Furthermore,

the slim-tube measurement exactly lies on the line joining the visible MMP experimental points (Figure 2.55).

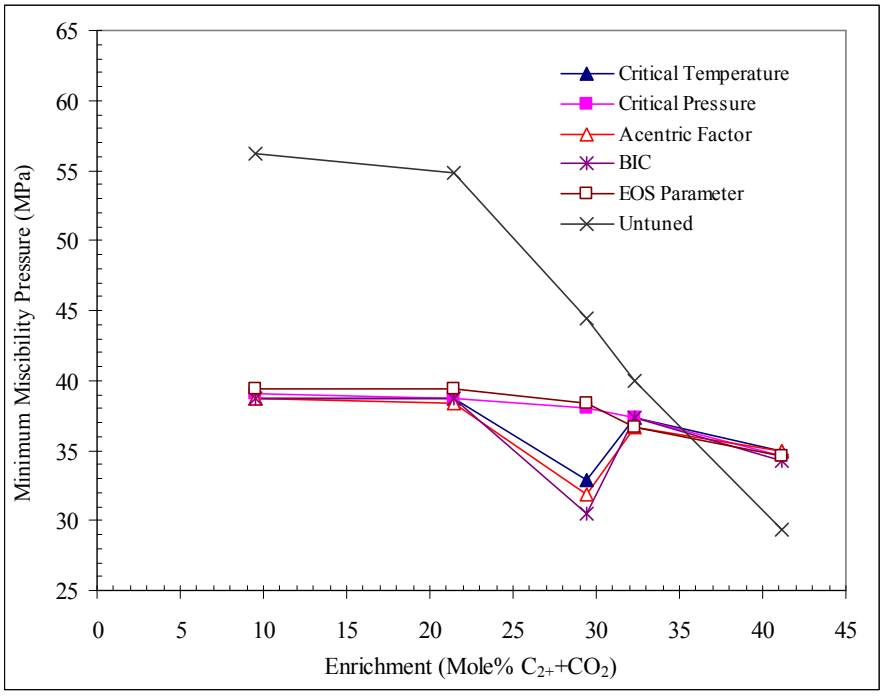

Figure 2.56: Effect of Tuning on EOS MMP Predictions for Terra Nova Fluids

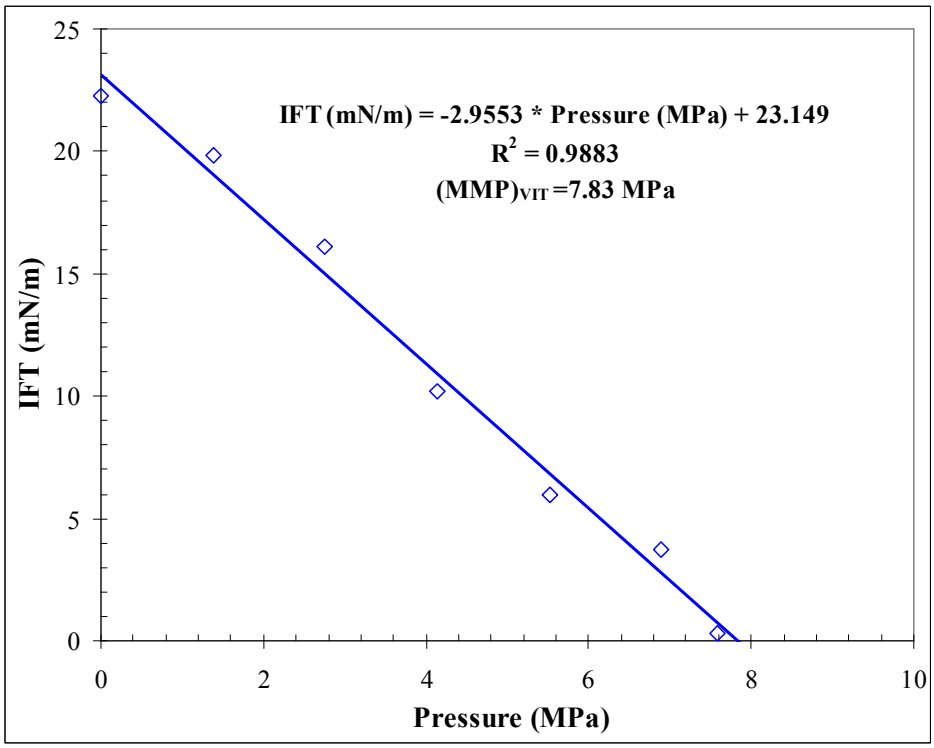

Figure 2.57: Determination of VIT Miscibility in Decane-CO_2 System at 37.7°C

The comparison of predicted MMP from different tuning approaches is shown in Figure 2.56. The overall range of predicted MMP from tuned EOS was from 30 to 40 MPa throughout the range of enrichments studied. However, the experimental (VIT) MMP ranged from 31.8-62.85 MPa. The untuned EOS prediction did cover the same range as experimental data. While critical temperature, acentric factor and binary interaction coefficient show a sharp decline in predicted MMP at a C_{2+} concentration above 21.4%, the remaining tuned parameters did not show such a decline. This clearly points out that any MMP value within the range of 10 MPa can be matched by suitably choosing a tuning parameter, which in turn raises questions about the utility of such non-unique results from EOS tuning.

Standard Gas Oil Systems. The interfacial tensions measured in n-decane-CO_2 system at a molar composition of 40 mole% gas and 60 mole% oil in the feed are plotted against pressure in Figure 2.57 to determine miscibility using the VIT technique. A good linear relationship between interfacial tension and pressure can be seen with a coefficient of determination (R^2) value of 98.8%. The regression equation obtained is also shown in Figure 2.57. The extrapolation of this relation to zero interfacial tension gives a VIT miscibility of 7.83 MPa. This VIT miscibility agrees well with the slim-tube miscibility of 8.27 MPa reported for this gas-oil system at 37.7°C (Elsharkawy et al., 1996).

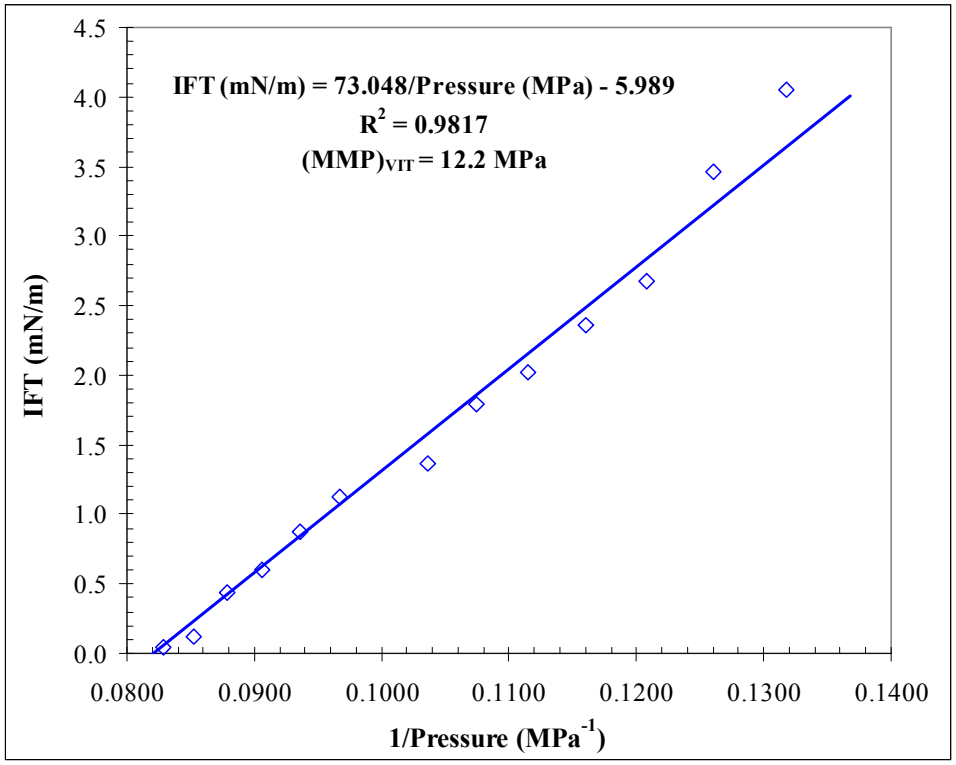

Figure 2.58: Determination of VIT Miscibility in Live Decane-CO_2 System at 71.1°C

The standard gas-oil system of live decane-CO_2 has been reported to have a slim-tube MMP of 11.7 MPa at 71.1^{o}C (Metcalfe and Yarborough, 1978). The same MMP has been obtained even with phase diagram measurements (Metcalfe and Yarborough, 1978) and analytical model calculations (Monroe et al., 1990; Orr et al., 1993). The interfacial tensions measured in this gas-oil system at 71.1^{o}C and at a molar composition of 20 mole% gas and 80 mole% oil in the feed are plotted against pressure in Figure 2.58 to determine the VIT miscibility. The IFT measurements were fitted using a hyperbolic function. This function was mainly used to fit the curvature to the data that resulted due to almost one order of magnitude reduction in IFT observed near miscibility. A good linear relationship between IFT and reciprocal pressure can be seen with a determination coefficient (R^2) of 98.1%. The regression equation obtained is also shown in Figure 2.58, which when extrapolated to zero IFT yielded an MMP of 12.2 MPa. This VIT miscibility agrees well with the miscibility pressures reported from the slim-tube, phase diagram and analytical models (11.7 MPa).

The comparison of VIT miscibilities measured in the two standard gas-oil systems with untuned PR-EOS calculations are given in Table 2.48. From Table 2.48, close match between the VIT miscibilities and EOS calculations can be seen for both the gas-oil systems with low absolute deviations in the range of 3.5-8.7%. Thus the good match of VIT miscibilities with slim-tube measurements (with small absolute deviations in the range of 4.1-5.6%) as well as untuned EOS calculations obtained once again validate VIT technique to determine fluid-fluid miscibility in multicomponent hydrocarbon systems.

Reality Check on EOS Tuning. The best set of tuning parameter (binary interaction coefficient) obtained in this study that matched the saturation pressures for both the reservoir crude oils perfectly, was used to predict the laboratory PVT data as a reality check. The weight factors proposed by Coats and Smart (1986), Coats (1988) and Bahbahaninia (2001) were used to improve the PR-EOS predictive capabilities. These predictions were then compared against the actual laboratory PVT measurements of reservoir crude oil samples. The comparisons of tuned PR-EOS predictions against the PVT experimental data for RKR and Terra Nova crude oils are shown in the Figure 2.59 and Figure 2.60, respectively. It is observed that, the best set of tuned EOS parameter was unable to predict the other PVT measurements such as oil specific gravity, gas compressibility factor and gas-oil ratio as accurately as the saturation pressure, for the two reservoir cases. This raises another question: Is tuning an EOS based on saturation pressure alone enough to provide capability to predict other PVT properties and miscibility conditions? This study therefore recommends further work, using different tuning strategies, to address this question. The recent efficient EOS tuning strategy proposed by Zurita and McCain (2002) has been identified as one such approach for future use to improve the tuned EOS predictions reported in this study.

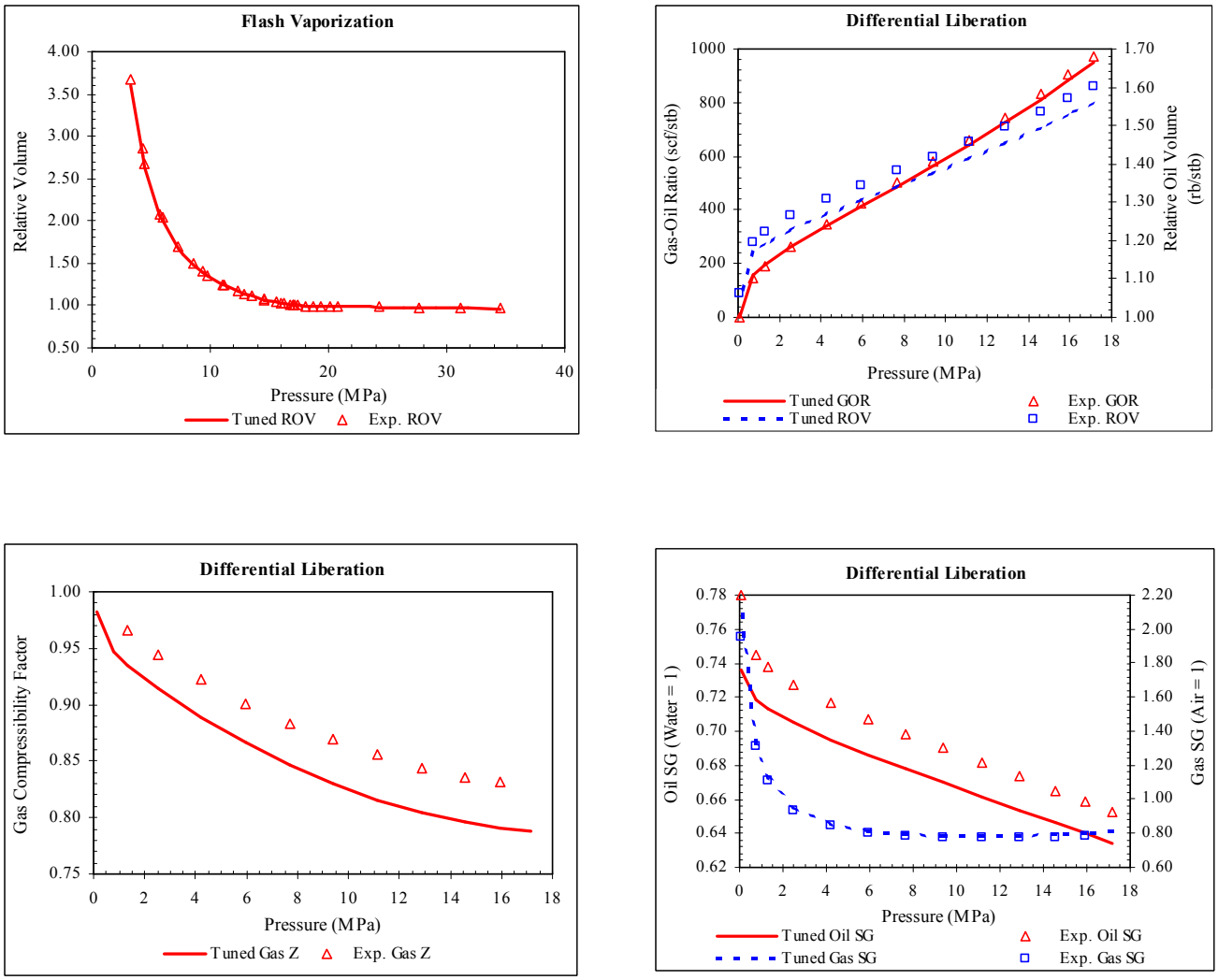

Figure 2.59: Comparison of Tuned PR-EOS Predicted and Experimental PVT Data of RKR Fluids

Table 2.48: Comparison of Measured VIT Miscibilities with Slim-Tube Miscibilities and EOS Calculations in Standard Gas-Oil Systems

Standard Gas-Oil System	VIT Miscibility (MPa)	Slim-Tube Miscibility		EOS Miscibility	
		MMP (MPa)	Abs. Dev. from VIT (%)	MMP (MPa)	Abs. Dev. from VIT (%)
Decane - CO_2 at 37.7°C	7.83	8.27	5.6	7.56	3.5
Live Decane -CO_2 at 71.1°C	12.2	11.7	4.1	13.27	8.7

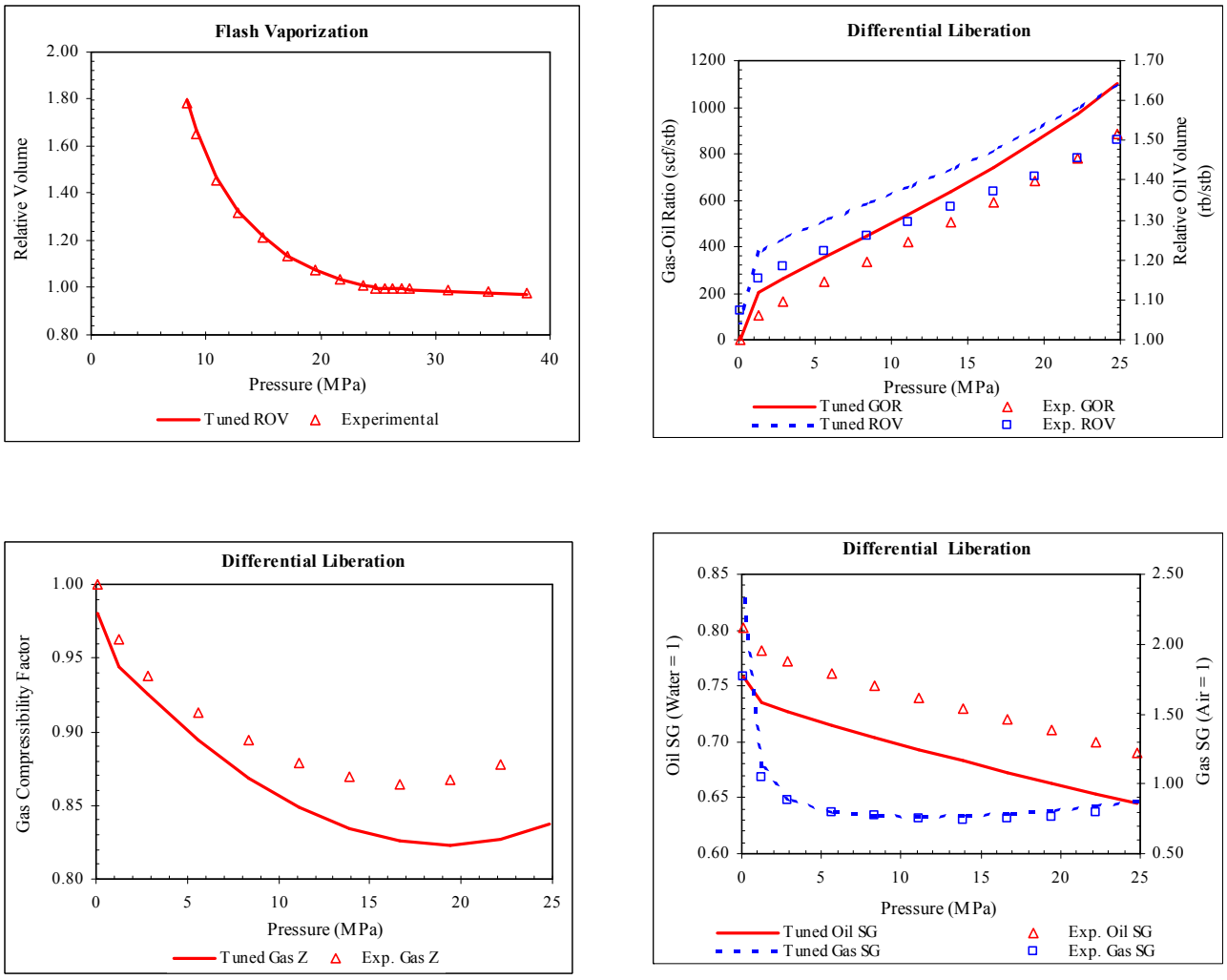

Figure 2.60: Comparison of Tuned PR-EOS Predicted and Experimental PVT Data of Terra Nova Fluids

2.3.1.6 Conclusions

1. Tuning of critical temperature, critical pressure, binary interaction coefficient, acentric factor, and Ω_b of the heaviest component in C_{7+} fraction were effective in matching the experimental saturation pressure of RKR and Terra Nova crude oils.
2. Tuning of volume shift parameter and molecular weight of the heaviest component in C_{7+} fraction were found to be ineffective in improving the EOS prediction of saturation pressure for RKR and Terra Nova crude oils.
3. The MMP calculated using untuned PR-EOS and without C_{7+} characterization reasonably matched the VIT experimental values (within 3-5 MPa) for RKR reservoir.
4. For Terra Nova reservoir, in three out of total five cases studied, the visible MMP from the VIT experiments reasonably matched the untuned PR-EOS calculations.

5. The MMP calculated using the tuned EOS with different tuning approaches showed strong disagreement with the experimental MMP from the VIT technique for both the RKR and Terra Nova reservoirs. This clearly indicates that tuning of EOS is not advisable for calculating the MMP of these reservoirs.
6. This work also indicates that MMP can be matched within a 10 MPa range by suitably choosing a tuning parameter, which raises questions about the utility of such non-unique results from EOS tuning.
7. The good match of VIT miscibilities obtained with slim-tube measurements as well as untuned EOS calculations in the two standard gas-oil systems studied once again validate VIT technique to determine fluid-fluid miscibility in multicomponent hydrocarbon systems.

2.3.2 Parachor Computational Model for Gas-Oil Miscibility

2.3.2.1 Introduction

Need for Gas-Oil Miscibility. More than half of the crude oil found in petroleum reservoirs is left behind at the end of primary recovery and secondary water floods. This is due to rock-fluids interactions including capillary forces, which prevent the oil from flowing within the pores of reservoir rock, trapping huge amounts of residual oil in reservoirs. These capillary forces can be reduced to a minimum if the interfacial tension between the injected fluid and the trapped crude oil is reduced to zero. Zero interfacial tension is nothing but miscibility between the injected fluid and reservoir crude oil (Benham et al., 1965; Stalkup, 1983; Holm, 1987; Lake, 1989). Thus there is a need for miscibility development between the gas injected (natural gas or CO_2) and the crude oil to remobilize these huge amounts of trapped oil and improve the oil recovery.

Mass Transfer Mechanisms in Miscibility Development. Miscible displacement of crude oil in a reservoir can be carried out by the injection of gases such as hydrocarbon solvents, CO_2, flue gas and nitrogen. The compositional changes resulting from the mass transfer between reservoir oil and injected gas promote miscibility attainment. During displacements of oil by gas, miscibility develops mainly due to three types of mass transfer mechanisms between the fluids in reservoir, namely vaporizing gas drive, condensing gas drive and combined condensing/vaporizing gas drive.

In the vaporizing gas injection process, the injected gas is relatively a lean gas consisting of mostly methane and other low molecular weight hydrocarbons. As the injected fluid moves through the reservoir, it contacts the reservoir oil several times and becomes enriched in composition by vaporizing the intermediate components (C_2 to C_4) in the crude oil. This process continues till the injected gas attains miscibility with reservoir oil.

In the condensing gas injection process, the injected gas contains significant amounts of intermediates (C_2 to C_4). During the multiple contacts of the injected gas with crude oil in the reservoir, the intermediates condense from gas phase into the oil phase. The continuation of this process modifies the reservoir oil composition to become miscible with additional injected gas, resulting in miscible displacement.

In the combined condensing/vaporizing process, the light intermediate compounds in the injected gas (C_2 to C_4) condense into the reservoir oil, while the middle intermediate compounds (C_5–C_{10} to C_{30}) in the crude oil vaporize into the injected gas. This prevents miscibility between fluids near the injection point as the oil becomes heavier. As the injection of gas continues, there will be no further condensation of light intermediates from the injected gas into this saturated oil. However, the vaporization of middle intermediates continues from the oil enriching the injected gas further. As this condensation/vaporization process continues farther into the reservoir, the gas becomes enriched to greater and greater extents as it contacts more and more oil and eventually becomes miscible with reservoir oil. This mechanism involving simultaneous counter-directional mass transfer of components between the phases is shown to be the one that most frequently occurs during the displacements of oil by gas (Zick, 1986).

Parachor Model for Gas-Oil Miscibility. A model based on Parachor IFT calculations has been investigated in this study for gas-oil miscibility determination. Just as the VIT experimental technique, this model is also based on the concept of zero interfacial tension at miscibility. In this model, the interfacial tension between the fluids is calculated using Weinaug and Katz's Parachor method (Weinaug and Katz, 1943) at reservoir temperature as a function of pressure or gas enrichment. Then the extrapolation of the plot between interfacial tension and pressure or enrichment to zero interfacial tension yields the conditions of miscibility.

2.3.2.2 Objectives

The objectives are to utilize the Parachor model to calculate interfacial tension in complex vapor-liquid systems involving multi-components in both phases and to evaluate the performance of the proposed Parachor model by comparing the miscibility conditions of pressure and enrichment determined from the model with VIT experiments and equations of state (EOS) calculations. For this purpose, Rainbow Keg River (RKR) reservoir fluids were used, since all the phase behavior data needed for miscibility calculations and the VIT experimental results were readily available (Rao, 1997; Rao et al., 1999). The calculations were carried out using the commercial simulator, Winprop (Computer Modelling Group Ltd., 2002).

2.3.2.3 EOS Calculations

Our previous study on effects of tuning an equation of state (EOS) on miscibility calculations (reported in Section 2.3.1) indicated that EOS tuning based on saturation pressures is not suitable for miscibility calculations of this reservoir. Hence, untuned Peng-Robinson EOS has been chosen to perform all the miscibility calculations. The reservoir fluid compositions, reservoir temperature, the compositions of lean and rich gases used for making up the solvent and the resultant solvent compositions are given in Tables 2.42 and 2.46. Detailed description of EOS miscibility calculation procedure is already provided in the previous Section 2.3.1.4.

The comparison between the MMP's from VIT experiments and EOS calculations for RKR fluids at C_{2+} enrichments of 51.0% and 52.5% in the injected gas phase (solvent) is given in Table 2.49 and shown in Figure 2.61. From these results, it can be seen that EOS MMP predictions are higher than the experimental MMP's (by about 3.5 MPa). This is in good agreement with other reports (Lee and Reitzel, 1982; Firoozabadi and Aziz, 1986) that EOS calculations yield more conservative results than laboratory measurements.

Table 2.49: Comparison of VIT MMP's with EOS Calculations and Parachor Model (5: Rao, 1997; 6: Rao et al., 1999)

MMP Determination Method	Solvent #1 (C_{2+} = 51.0 %) MMP (MPa)	Solvent # 2 (C_{2+} = 52.5%) MMP (MPa)
Experimental (VIT) [5,6]	14.8	14.0
PR - EOS calculation	18.3	17.4
Parachor model (Weinaug & Katz)	19.4	18.7

2.3.2.4 Parachor Model Calculations

Background. Macleod-Sudgen (Macleod, 1923; Sudgen, 1924) related surface tension of a pure compound to the density difference between the phases, as:

$$\sigma^{1/4} = P(\rho_M^L - \rho_M^V) \quad \text{.....} \quad (2.14)$$

Where σ is the surface tension in dynes/cm, ρ_M^L and ρ_M^V are the molar density of the liquid and vapor phases, respectively, in gmole/cm^3 and the proportionality constant, P is known as the Parachor. The Parachor values of various pure compounds have been determined from measured surface tension data using the Eq. (2.14). The Parachor values of different pure compounds are reported in the literature by several investigators (Quale, 1953; Fanchi, 1990; Ali, 1994; Schechter and Guo, 1998).

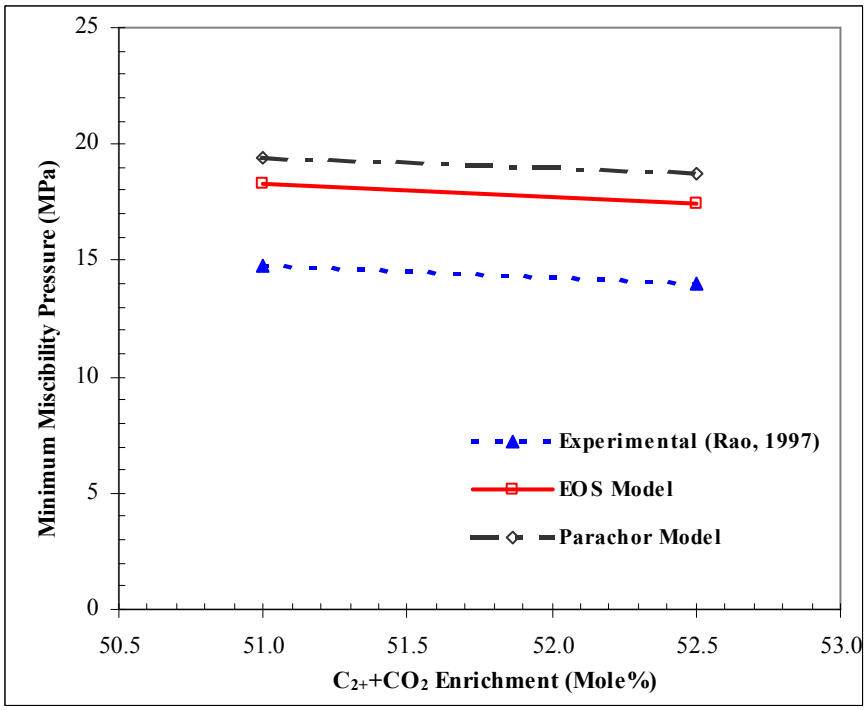

Figure 2.61: Comparison of VIT MMP's with EOS Calculations and Parachor Mode

The equation proposed by Macleod-Sudgen (Macleod, 1923; Sudgen, 1924) was later extended to hydrocarbon mixtures using the simple molar averaging technique of Weinaug and Katz's (Weinaug and Katz, 1943) for the mixture Parachor,

$$\sigma^{1/4} = \rho_M^L \sum x_i P_i - \rho_M^V \sum y_i P_i \quad \text{..... (2.15)}$$

Where x_i and y_i are the mole fractions of component i in the liquid and vapor phases, respectively, and P_i is the Parachor of the component i. Parachor values of pure compounds are used in Eq. (2.15) to calculate the interfacial tension of the mixtures, considering the Parachor value of a component in a mixture is the same as that when pure (Danesh, 1998). This method is most widely used in petroleum industry to estimate the interfacial tension between fluids.

Gas-Oil IFT Calculations. In order to apply the Parachor model to the current reservoir case study, a mixture consisting of 10 mole% of crude oil and 90 mole% of solvent is used as the feed composition in the computational model to match the composition used in VIT experiments. Flash calculations are performed with the mixed feed at the specified pressure and reservoir temperature at varying C_{2+} enrichments in solvent. The resultant molar liquid, vapor densities, equilibrium liquid and vapor compositions of different components along with their Parachors reported in the literature, are then used in IFT computations.

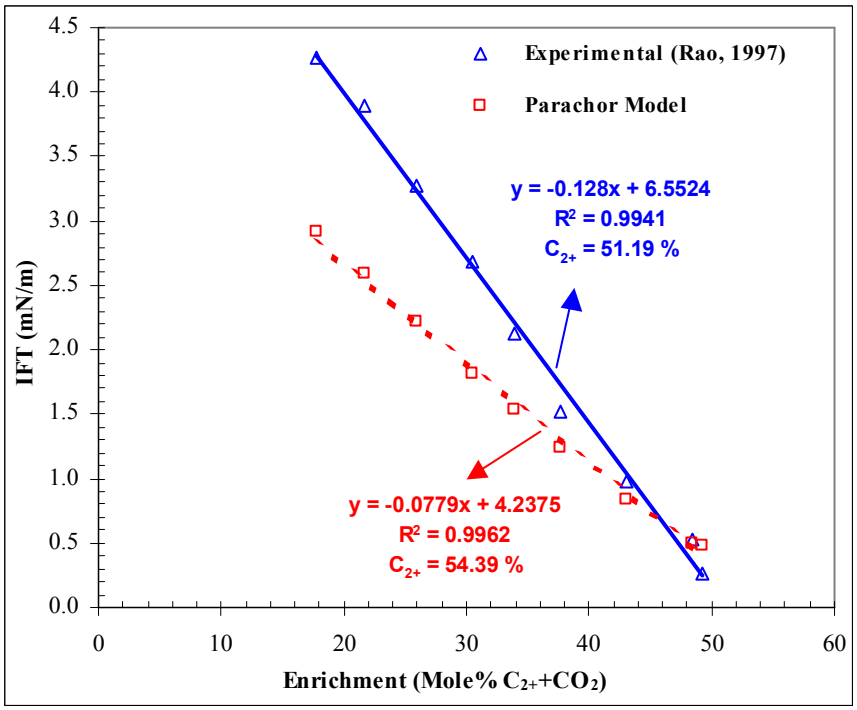

Figure 2.62: Comparison of Experimental IFT's with Parachor Model for RKR Fluids at 14.8 MPa

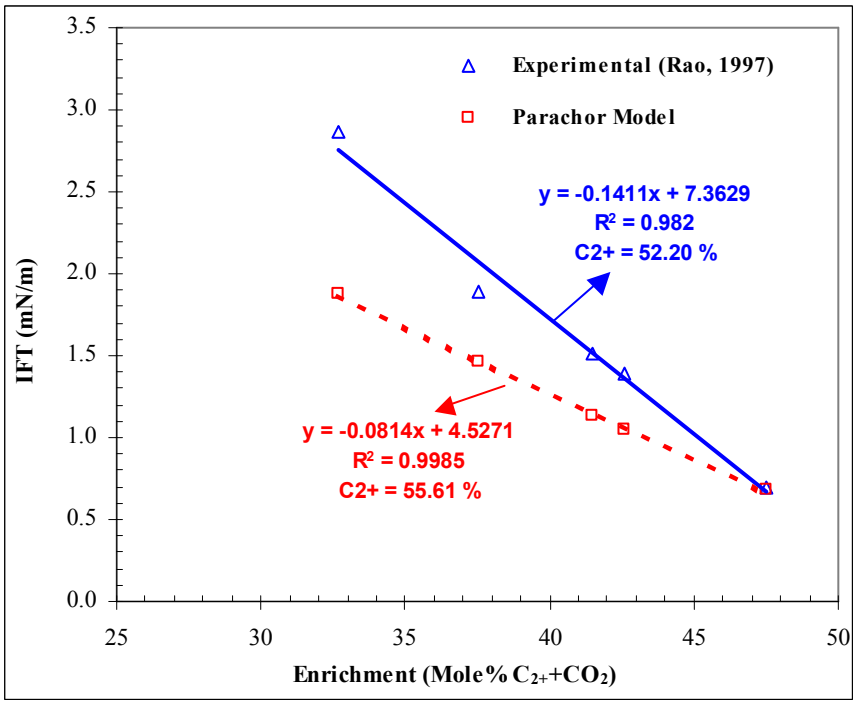

Figure 2.63: Comparison of Experimental IFT's with Parachor Model for RKR Fluids at 14.0 MPa

The summary of experimental IFT's and the calculated IFT's using the Parachor computational model for RKR fluids at different C_{2+} enrichments in solvent is given in Table 2.50 for pressures of 14.8 MPa and 14.0 MPa. Similar trends are observed at both the pressures. Parachor computational model under predicts the interfacial tension in high IFT regions. However, the difference between the experimental and the calculated IFT's gradually decreases and consequently the Parachor model predictions match with experimental measurements in the low IFT regions. This is in good agreement with Cornelisse et al. (1993) where similar observations are made. The calculated IFT's are then plotted against C_{2+} enrichment to determine MME's in Figures 2.62 and 2.63, for pressures of 14.8 MPa and 14.0 MPa, respectively. As can be seen in these figures, conservative estimates of MME's are obtained with Parachor model when compared to experimental MME's (by about 3.2-3.4%) at both the pressures.

Table 2.50: Comparison of Measured IFT's with Parachor Model Predictions (5: Rao, 1997; 6: Rao et al., 1999)

Pressure = 14.8 MPa			**Pressure = 14.0 MPa**		
Enrichment (C_{2+} %)	IFT (dynes/cm)		Enrichment (C_{2+} %)	IFT (dynes/cm)	
	Experimental [5,6]	Parachor		Experimental [5,6]	Parachor
17.79	4.26	2.91	32.68	2.86	1.88
21.64	3.89	2.59	37.55	1.89	1.46
25.85	3.27	2.21	41.45	1.51	1.14
30.57	2.69	1.81	42.61	1.39	1.04
33.86	2.13	1.54	47.48	0.70	0.68
37.70	1.52	1.24			
43.07	0.97	0.85			
48.39	0.53	0.50			
49.28	0.27	0.48			

MMP Calculations. The sequence of steps followed in MMP calculation procedure using Parachor computational model are:

- Oil composition, solvent composition, reservoir temperature, mole fraction of oil in the feed, pressure and the pressure increment are provided as inputs to the model.
- Flash calculations are performed with mixed feed at reservoir temperature and specified pressure.
- The resulting molar liquid, vapor densities, equilibrium liquid and vapor compositions of different components along with their Parachors are used to calculate the IFT's.
- The pressure is incremented at the specified pressure increment and the steps 2 to 3 are repeated.

In the low interfacial tension region, pressure is incremented in smaller steps to clearly identify the point of vanishing IFT pressure. Then this vanishing IFT pressure becomes the MMP for the system.

The comparison between VIT experimental MMP's and the calculated MMP's from Parachor computational model for RKR fluids at C_{2+} enrichments of 51.0% and 52.5% in solvent is given in Table 2.49 and shown in Figure 2.61. The calculated IFT's using the Parachor model at these C_{2+} enrichments are plotted against pressure to determine MMP's in Figure 2.64. From these results, it is quite evident that Parachor model has resulted in MMP over-predictions, when compared to VIT experiments (by about 4.5 MPa). Moreover, these over-predictions are greater than those obtained in EOS calculations.

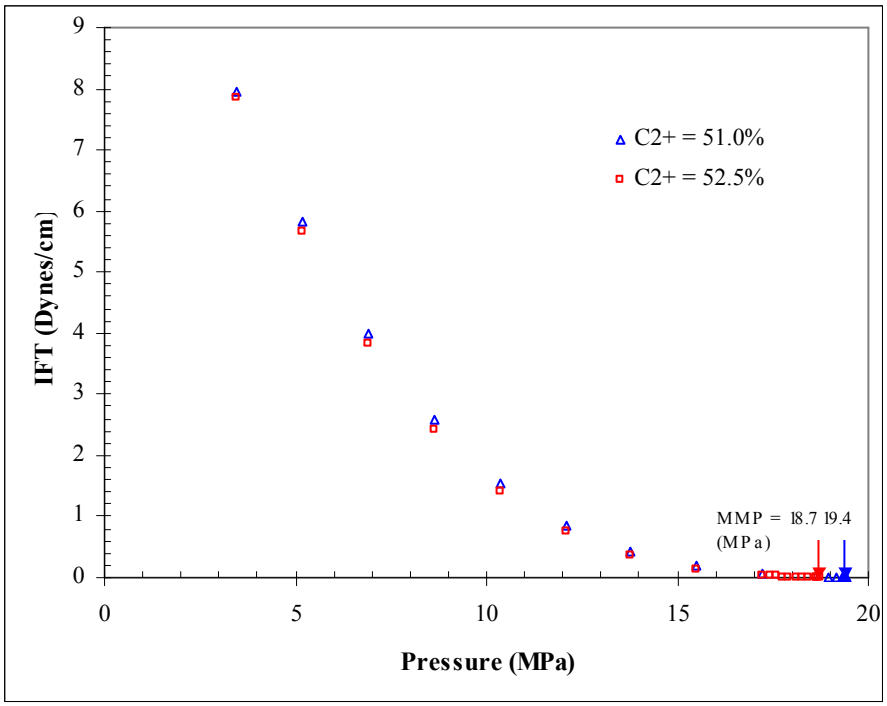

Figure 2.64: MMP Determination using Parachor Computational Model for RKR Fluids

2.3.2.5 Mass Transfer Effects on Miscibility Predictions

Since IFT, a good indicator of mass transfer effects, was used to interpret miscibility in this study, the reasons for the miscibility over-predictions by the computational models appear to be the following.

In VIT experiments, equilibrated fluids are used in IFT measurements. Hence various types of mass transfer mechanisms are allowed to take place between the fluids (condensing gas drive, vaporizing gas drive and combined condensing/vaporizing gas drive). Thus VIT measurements include all the mass transfer effects and hence predict true MMP's. In EOS calculations, mass transfer effects are taken into account only

through either condensing gas drive or vaporizing gas drive, which is quite evident in the MMP calculation procedure of EOS model. This limited mass transfer resulted in MMP over-predictions (about 3.5 MPa) by the EOS model. In Parachor computational model, the Parachor values are based on surface tension measurements of pure compounds. Hence these values are incorporated in the computational model considering each component of the mixture as if all the others were absent. Because of this assumption, any type of mass transfer effect is not considered at all in the calculation procedure. This appears to be responsible for even larger over-predictions of MMP (about 4.5 MPa) by the Parachor model.

Further, it can be seen that the difference in the over-predictions of miscibility is not significant (only about 1 MPa) between the EOS and Parachor models. This means incorporation of either condensing or vaporizing mass transfer mechanism in the EOS model has not resulted in any significant improvement in accuracy of miscibility prediction. This observation intuitively suggests that the combined vaporizing/condensing mechanism involving simultaneous counter-directional mass transfer of components between the fluid phases is the main mechanism that controls fluid-fluid miscibility. This is in good agreement with the experimental observations of Zick (1986). Thus the ability of any miscibility computational procedure to account for the counter-directional mass transfer effects between the fluids governs the extent of agreement with miscibility pressures and enrichments determined from VIT experiments. This clearly demonstrates the importance of mass transfer effects in fluid-fluid miscibility computations and hence identifies the need to develop methods to incorporate these mass transfer effects in the models used to compute miscibility.

2.3.2.6 Conclusions

1. The interfacial tensions computed using the Parachor model are found to differ from the experimental measurements by about 0.1 to 1.4 dynes/cm, except in low IFT regions where the agreement is good.
2. Parachor computational model over-predicts minimum miscibility pressures, when compared to VIT experiments (by about 4.5 MPa) and EOS calculations (by about 1.0 MPa).
3. The combined vaporizing/condensing mechanism involving simultaneous counter-directional mass transfer of components between the fluid phases appears to be the main mass transfer mechanism that governs the attainment of fluid-fluid miscibility.
4. The disagreement with IFT measurements and over-predictions of miscibility obtained using the proposed Parachor model appears to be due to the inability of the model to account for counter-directional mass transfer effects that can occur in reality between the fluids.

5. This study exemplifies the importance of counter-directional mass transfer effects in interfacial phenomena and hence gives raise to the need to develop methods to incorporate these mass transfer effects in the proposed Parachor model for interfacial tension and miscibility calculations.

2.3.3 Development of a New Mechanistic Parachor Model for Gas-Oil IFT and Miscibility

2.3.3.1 Introduction

Interfacial tension is an important property for many processes such as enhanced oil recovery by gas injection and flow through porous media, and in mass and heat transfer applications. However, the experimental data on interfacial tension for complex fluid systems involving multicomponent phases are scarce. Therefore, there has long been a need for a simple and accurate computational model for prediction of interfacial tension in multicomponent hydrocarbon systems. Several models have been proposed for the calculation of interfacial tensions of simple fluids and mixtures in the past few decades. The most important among these models are the Parachor model (Macleod, 1923; Sudgen, 1924), the corresponding states theory (Brock and Bird, 1955), thermodynamic correlations (Clever and Chase, 1963) and the gradient theory (Carey, 1979).

While most of the thermodynamic properties refer to individual fluid phases, interfacial tension (IFT) is unique in the sense that it is a property of the interface between the phases. The IFT, being a property of interface, is strongly dependent on the compositions of fluid phases in contact, which in turn depend on the mass transfer interactions between the phases. The commonly occurring mass transfer mechanisms between the fluid phases to attain equilibrium are vaporization, condensation or a combination of the two. In the vaporizing drive mechanism, the vaporization of lighter components (C_1 to C_3) from the liquid (crude oil) to hydrocarbon vapor phase promotes the attainment of miscibility of the two phases. In condensing drive mechanism, the condensation of intermediate and heavy components (C_4 to C_8) from hydrocarbon gas to the crude oil is responsible for attaining miscibility between fluid phases. In combined condensation and vaporization drive mechanism, the simultaneous counter-directional mass transfer mechanisms, that is, vaporization of lighter components from crude oil to gas and condensation of intermediate and heavy components from gas to crude oil, are responsible for attaining miscibility of the phases. These mass transfer interactions affect the compositions of both phases and hence their interfacial tension. Therefore, the dynamic changes in IFT can be used to infer information on mass transfer interactions taking place prior to the attainment of thermodynamic fluid phase equilibrium and miscibility.

Almost all currently available IFT models have been extensively tested for either pure compounds or binary mixtures. The use of these models to predict interfacial tension in complex hydrocarbon systems involving multicomponents in both the phases is limited and not well documented. Furthermore, none of these models provides information on mass transfer interactions occurring prior to attaining fluid phase equilibria. Hence, a mass transfer enhanced mechanistic model, based on the Parachor model, has been proposed in this study for prediction of interfacial tension as well as to identify the governing mass transfer mechanism for fluid phase equilibria in complex multicomponent hydrocarbon systems.

2.3.3.2 The Proposed New Mass Transfer Enhanced Mechanistic Parachor Model

The conventional Parachor model (described in Section 2.3.2) has been extensively used for prediction of surface tension of pure compounds and binary mixtures. However, the model gives poor IFT predictions for complex multicomponent hydrocarbon mixtures (Danesh et al., 1991). Several attempts have been already made in the past to improve the Parachor model IFT predictions in multicomponent systems. Fawcett (1994) has reviewed these reported studies in detail. All these attempts are mostly directed at improving the Weinaug and Katz's molar averaging technique (Weinaug and Katz, 1943) for the mixture Parachor determination. The Hough-Stegemeier correlation (Hough and Stegemeier, 1961) is almost the same as the Weinaug-Katz correlation, but with a slight change in the values of empirical parameters. Other investigators have modified the Weinaug-Katz correlation using more complex mixing rules for multicomponent mixtures (Hugill and Van Welsenes, 1986), or incorporating a parameter that depends on the density difference between the fluid phases (Danesh et al., 1991). The Lee-Chien's modification (Lee and Chien, 1984) is based on critical scaling theory and still retains the same functional form of Weinaug-Katz correlation. All these modifications are intended to match the experimental data based on empirical correlations and there appears to be no strong theoretical background associated with them.

In the application of the conventional Parachor model to multicomponent mixtures, Parachor values of pure components are used in IFT predictions, considering each component of the mixture as if all the others were absent. Significant interactions take place between the various components in a multicomponent mixture and hence the inability of pure component Parachor values to account for these interactions of each component with the others in a multicomponent mixture appears to be the main reason for poor IFT predictions from the Parachor model in multicomponent hydrocarbon systems.

In the present study, a mechanistic Parachor model has been proposed, in which the ratio of diffusivity coefficients raised to an exponent is introduced into the Parachor model to account for mass transfer effects. The mass transfer interactions for phase

equilibria between any two fluid phases take place by diffusion due to concentration gradient and by dispersion. Hence diffusivities are used in the proposed mechanistic model to account for mass transfer interactions. Furthermore, only diffusivities can reasonably represent mass transfer interactions in complex multicomponent systems like crude oil-hydrocarbon gas mixtures involving multicomponents in both the phases. The ratio of diffusivities in both directions (vaporizing and condensing) between the fluid phases raised to an exponent used in the mechanistic model, enables the retention of the same dimensions of the original Parachor model. The proposed mechanistic model is given by:

$$\sigma^{1/4} = \left(\frac{D_{os}}{D_{so}}\right)^{n} (\rho_M^L \Sigma x_i P_i - \rho_M^V \Sigma y_i P_i) \quad \text{..... (2.16)}$$

Where, D_{os} is the diffusivity of oil in gas (solvent), D_{so} is the diffusivity of gas (solvent) in oil and n is the exponent, whose sign and value characterize the type and extent of governing mass transfer mechanism for fluid phase equilibria. If n > 0, the governing mechanism is vaporization of lighter components from the oil to the gas phase. If n < 0, the governing mechanism is condensation of intermediate to heavy components from the gas to the crude oil. The value of n equal to zero (n ≈ 0) indicates equal proportions of vaporizing and condensing mass transfer mechanisms to be responsible for fluid phase equilibria. This condition of equal mass transfer in both the directions of vaporization and condensation appears to be most common in binary mixtures where the conventional Parachor model has shown to result in reasonably accurate interfacial tension predictions (n = 0 in the mechanistic Parachor model). The higher the numerical value of n (irrespective of its sign), the greater is the extent of that governing mass transfer mechanism.

Sigmund (1976) used Wilke equation (Wilke, 1950) for comparison with the experimental data of diffusivities between two nine-component gas mixtures and found that Wilke equation is capable of giving good estimates of diffusivities even for the cases where one mixture diffuses into another mixture. Fayers and Lee (1992) compared the diffusivity data of multicomponent systems at reservoir conditions obtained from various correlations with experiments and concluded that Wilke-Chang equation (Wilke and Chang, 1955) is the best available empirical correlation to compute the diffusivities in multicomponent hydrocarbon systems. Hence, in this study, the diffusivities between the fluid phases are computed, using the empirical correlation of Wilke and Chang (Wilke, 1949; Wilke and Chang, 1955), given by:

$$D_{AB} = \frac{(117.3\times10^{-18})(\varphi M_B)^{0.5} T}{\mu v_A^{0.6}} \quad \text{..... (2.17)}$$

Where D_{AB} = diffusivity of solute A in very dilute solution in solvent B, m^2/sec

M_B = molecular weight of the solvent, kg/kmol

T = temperature, K

μ = solution viscosity, kg/m.sec

v_A = solute molal volume at normal boiling point, m^3/kmol

φ = association factor for solvent, set equal to unity since the solvents used in this study are unassociated.

Eq. (2.17) is extended to multicomponent hydrocarbon mixtures, using:

$$M_B = \sum x_{Bi} M_{Bi} \quad \text{(2.18)}$$

$$v_A = \sum x_{Ai} v_{Ai} \quad \text{(2.19)}$$

Where, x_i is the mole fraction of the component i in the mixture, M_{Bi} is the molecular weight of the component i and v_{Ai} is the molal volume of the component i at normal boiling point.

An objective function (Δ) is defined as the sum of weighted squared deviations between the original Parachor model predictions and experimental IFT values and is given by:

$$\Delta = \sum_{j=1}^{N} \left[w_j \left(\frac{\sigma_j^{pred}(X) - \sigma_j^{\exp}}{\sigma_j^{\exp}} \right) \right]^2 \quad \text{(2.20)}$$

Where, each element of the objective function expresses the weighted difference between the predicted and experimental interfacial tension values, σ^{pred} and σ^{exp}, respectively; w is the weighting factor; N represents the number of measured data points to be fitted and X designates the correction factor to the original Parachor model prediction.

The mass transfer enhancement parameter (k), a correction to the original Parachor model to account for mass transfer effects, is then defined as the correction factor (X) at which the objective function (Δ) becomes the minimum. The mechanistic Parachor model is now given by:

$$\sigma^{1/4} = (k)(\rho_M^L \sum x_i P_i - \rho_M^V \sum y_i P_i) \quad \text{(2.21)}$$

From Eqs. (2.16) and (2.21), the exponent n, characterizing the governing mass transfer mechanism for fluid phase equilibria, can be computed using:

$$k = \left(\frac{D_{os}}{D_{so}} \right)^n \quad \text{(2.22)}$$

2.3.3.3 Objectives

The objectives are to utilize the newly proposed mechanistic Parachor model to (1) calculate interfacial tension in complex vapor-liquid systems involving multicomponents in both phases, (2) evaluate the model effectiveness by comparing the interfacial tensions determined from the model with experimental measurements, and (3) identify the

governing mass transfer mechanism responsible for fluid phase equilibria in multicomponent hydrocarbon systems. For this purpose, two reservoir crude oil-gas systems of Rainbow Keg River (RKR) and Terra Nova have been used, since the fluids compositions and the phase behavior data needed for IFT calculations and the experimental IFT measurements are readily available (Rao, 1997; Rao and Lee, 2002). These gas-oil interfacial tension measurements are made using the axisymmetric drop shape analysis (ADSA) technique by fitting the images of the captured pendent drops of crude oil in gas phase with the drop profile calculated using the Laplace capillary equation. An aging period of about 2 hours was allowed between the fluid phases to reach equilibrium during these experiments. Flash calculations needed for gas-oil interfacial tension calculations are carried out using QNSS/Newton algorithm (Nghiem and Heidemann, 1982) and Peng-Robinson equation of state (Peng and Robinson, 1976), within a commercial simulator (Computer Modelling Group Ltd., 2002).

2.3.3.4 Results and Discussion

Rainbow Keg River Reservoir. The crude oil and hydrocarbon gas compositions and the reservoir temperature from Rao (1997) are used in IFT computations for this reservoir. The IFT measurements at various C_{2+} enrichments in hydrocarbon gas phase and at various pressures reported by Rao (1997) are used for comparison with model predictions. A mixture consisting of 10 mole% of crude oil and 90 mole% of hydrocarbon gas is used as the feed composition in the computations to match the composition used in the reported experiments.

The comparison of IFT predictions by the original Parachor model with experiments at various C_{2+} enrichments in gas phase is given in Tables 2.51 and 2.52, for pressures 14.8 MPa and 14.0 MPa, respectively. These results are also shown in Figures 2.65 and 2.66, respectively, at these pressures. As can be seen, similar trends in IFT are observed for both the pressures. The match between the experiments and the model predictions is not good and IFT under-predictions are obtained with the Parachor model.

Table 2.51: Comparison of IFT Measurements with Parachor and Mechanistic Parachor Models for RKR Fluids at 87°C and 14.8 MPa

Enrichment (Mole% C_{2+}+CO_2)	IFT (mN/m)			Weighted Squared Deviation	
	Experimental (Rao, 1997)	Parachor Model	Mechanistic Parachor Model	Parachor Model	Mechanistic Parachor Model
17.79	4.26	2.91	3.79	0.1000	0.0123
21.64	3.89	2.59	3.36	0.1124	0.0184
25.85	3.27	2.21	2.88	0.1043	0.0144
30.57	2.69	1.81	2.36	0.1065	0.0155
33.86	2.13	1.54	2.00	0.0762	0.0035
37.70	1.52	1.24	1.61	0.0347	0.0034
43.07	0.97	0.85	1.10	0.0166	0.0175
48.39	0.53	0.50	0.65	0.0028	0.0535
49.28	0.27	0.48	0.63	0.0061	0.0173
			Objective Function (Π) =	0.5595	0.1558

Table 2.52: Comparison of IFT Measurements with Parachor and Mechanistic Parachor Models for RKR Fluids at 87°C and 14.0 MPa

Enrichment (Mole% C_{2+}+CO_2)	IFT (mN/m)			Weighted Squared Deviation	
	Experimental (Rao, 1997)	Parachor Model	Mechanistic Parachor Model	Parachor Model	Mechanistic Parachor Model
32.68	2.86	1.88	2.37	0.1167	0.0290
37.55	1.89	1.46	1.84	0.0518	0.0007
41.45	1.51	1.14	1.43	0.0610	0.0026
42.61	1.39	1.04	1.32	0.0620	0.0029
47.48	0.70	0.68	0.86	0.0007	0.0518
			Objective Function (Π) =	0.2921	0.0871

The disagreement between the experiments and the model predictions, as seen in Figures 2.65 and 2.66, are attributed mainly to the absence of mass transfer effects in the original Parachor model. Hence correction factors are used for original Parachor model predictions to minimize the objective function (Δ), which is the sum of weighted squared deviations between the model predictions and experimental values. The correction factors and the resulting objective functions for this crude oil-gas system are shown in Figure 2.67. The mass transfer enhancement parameters (k), the correction factors at which objective function becomes the minimum, are estimated to be 1.30 and 1.26, respectively for pressures of 14.8 MPa and 14.0 MPa.

The computed diffusivities between the fluid phases at various C_{2+} enrichments in hydrocarbon gas phase for RKR fluids at pressures of 14.8 MPa and 14.0 MPa are given in Table 2.53. The mass transfer interactions between the fluid phases declined slightly as the C_{2+} enrichment in hydrocarbon gas phase is increased for both the pressures. However, the ratio of diffusivities in both directions (oil to gas and gas to oil) remains almost the same at all C_{2+} enrichments in gas phase.

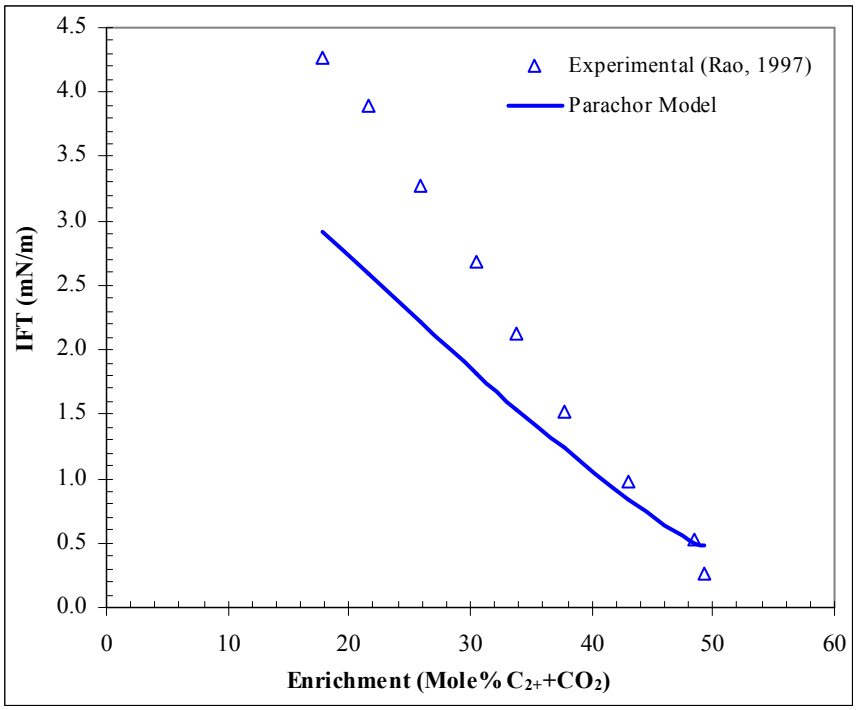

Figure 2.65: Comparison between IFT Measurements and Parachor Model for RKR Fluids at 87°C and 14.8 MPa

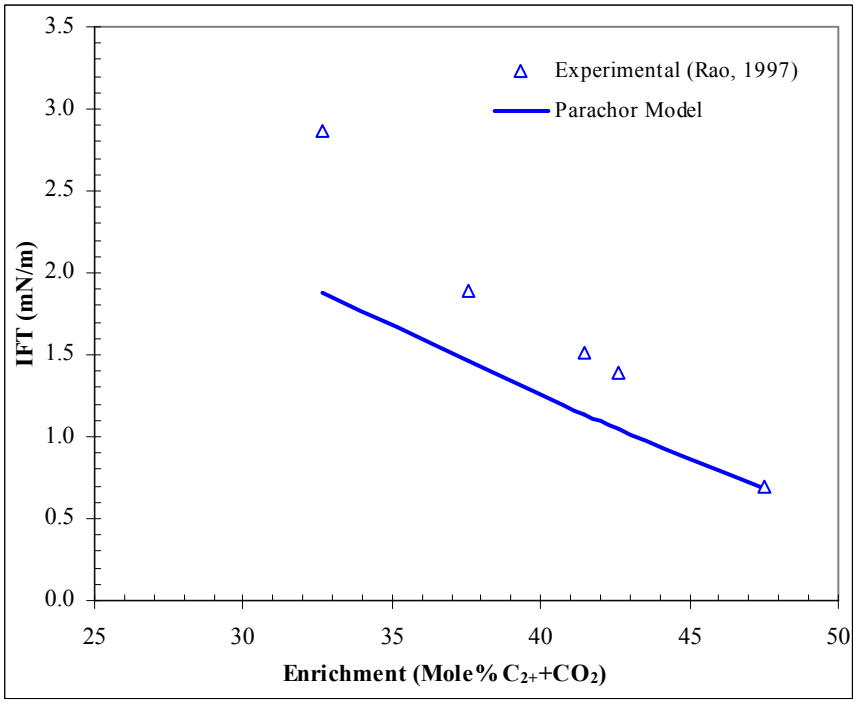

Figure 2.66: Comparison between IFT Measurements and Parachor Model for RKR Fluids at 87°C and 14.0 MPa

The average ratios of diffusivities between the fluids at all C_{2+} enrichments are 3.70 and 3.92, respectively for pressures 14.8 MPa and 14.0 MPa. From the mass transfer enhancement parameters and the average ratios of diffusivities between the fluid phases, the exponents (n) characterizing the governing mass transfer mechanism are found to be +0.20 and +0.17, respectively for pressures 14.8 MPa and 14.0 MPa. These values of n being greater than zero, indicate that the vaporization of light components from the crude oil into the gas phase is the mass transfer mechanism that governs the fluid phase equilibria of these reservoir fluids. This can be attributed to the presence of significant amounts of lighter components (52 mole% C_1 to C_3) in the crude oil of this reservoir (Rao, 1997).

The comparison between the IFT predictions of mass transfer enhanced mechanistic Parachor model with experiments at various C_{2+} enrichments in gas phase is given in Tables 2.51 and 2.52, respectively, for pressures of 14.8 MPa and 14.0 MPa. These results are also shown in Figures 2.68 and 2.69, respectively, at these pressures. Since the optimization of the mass transfer enhancement parameter (k) is based on minimizing the sum of squared deviations between the experimental and calculated values, the mechanistic model predictions matched well with the experiments for both the pressures.

Table 2.53: Diffusivities between Oil and Gas at Various C2+ Enrichments for RKR Fluids

14.8 MPa				14.0 MPa			
(Mole% C_{2+}+ CO_2)	D_{os} (m^2/s)	D_{so} (m^2/s)	D_{os}/D_{so}	(Mole% C_{2+}+CO_2)	D_{os} (m^2/s)	D_{so} (m^2/s)	D_{os}/D_{so}
17.79	3.45E-08	9.69E-09	3.56	32.68	3.44E-08	8.67E-09	3.97
21.64	3.45E-08	9.40E-09	3.68	37.55	3.34E-08	8.39E-09	3.98
25.85	3.42E-08	9.11E-09	3.75	41.45	3.21E-08	8.18E-09	3.93
30.57	3.36E-08	8.81E-09	3.81	42.61	3.17E-08	8.12E-09	3.91
33.86	3.29E-08	8.62E-09	3.82	47.48	2.99E-08	7.89E-09	3.79
37.70	3.19E-08	8.41E-09	3.80				
43.07	3.03E-08	8.14E-09	3.73				
48.39	2.85E-08	7.89E-09	3.61				
49.28	2.83E-08	7.88E-09	3.59				
		Average =	3.70			Average =	3.92

Terra Nova Reservoir. The crude oil and gas compositions, the reservoir temperature and the IFT measurements needed for gas-oil interfacial tension calculations of these reservoir fluids are obtained from the reference of Rao and Lee (2002). IFT calculations are performed using a feed composition of 8 mole% of crude oil and 92 mole% of gas in the mixture since the same composition is used during the reported interfacial tension measurements.

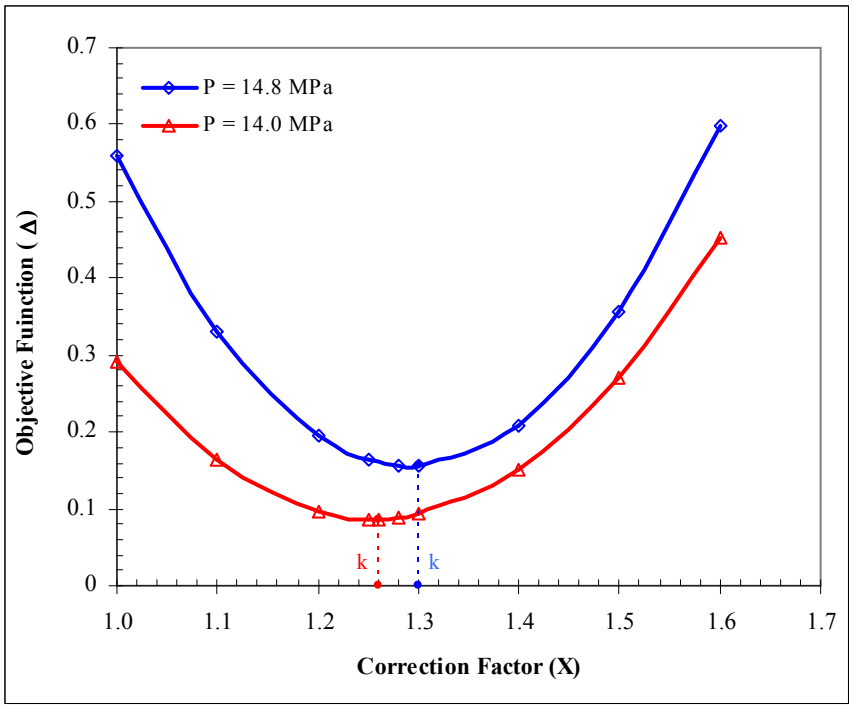

Figure 2.67: Determination of Mass Transfer Enhancement Parameters for RKR Fluids

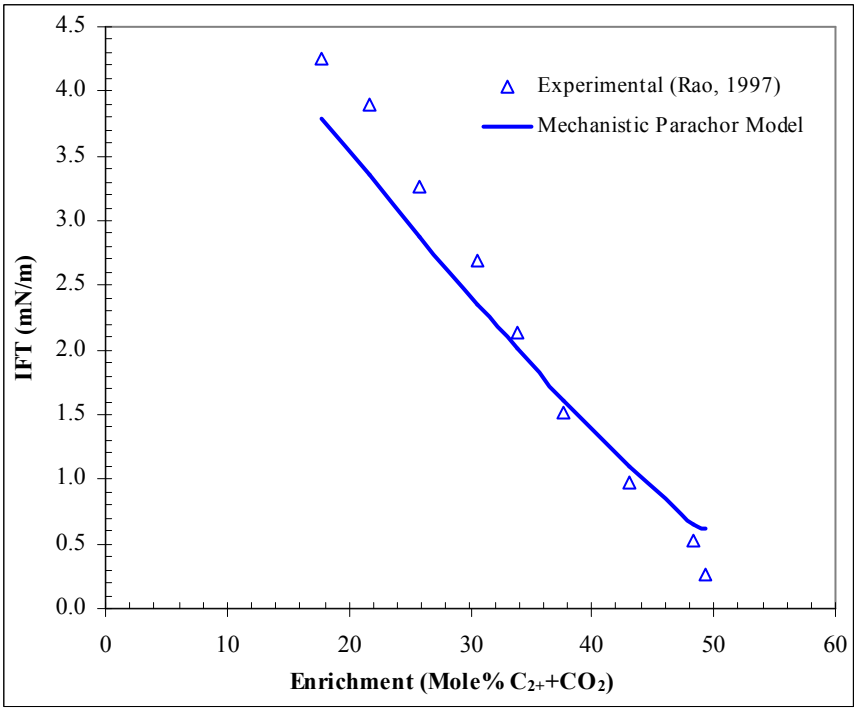

Figure 2.68: Comparison between IFT Measurements and Mechanistic Parachor Model for RKR Fluids at 87°C and 14.8 MPa

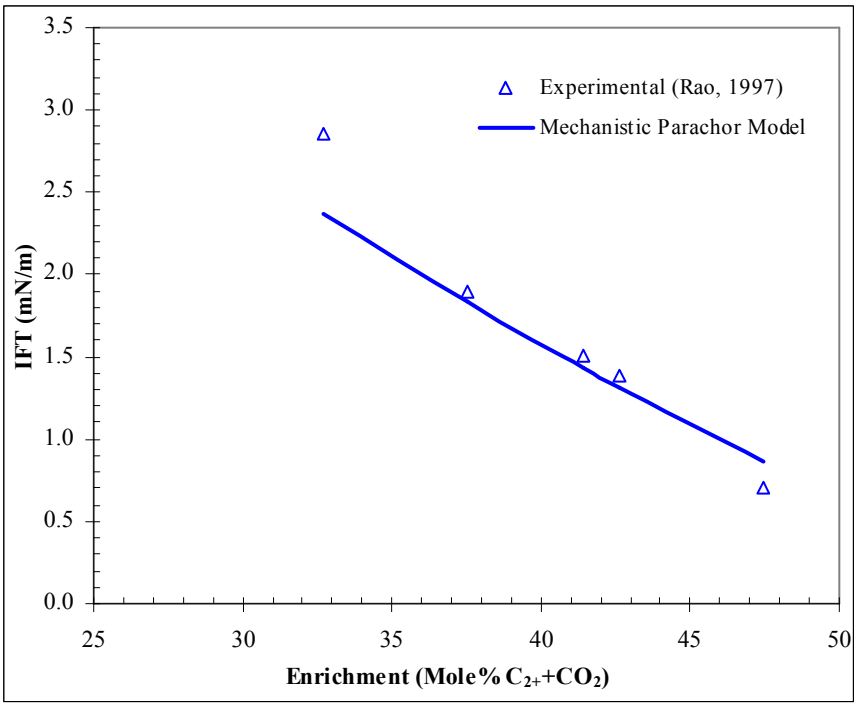

Figure 2.69: Comparison between IFT Measurements and Mechanistic Parachor Model for RKR Fluids at 87°C and 14.0 MPa

Table 2.54: Comparison of IFT Measurements with Parachor and Mechanistic Parachor Models for Terra Nova Fluids at 96°C and 30.0 MPa

Enrichment (Mole% C_{2+}+CO_2)	IFT (mN/m)			Weighted Squared Deviation	
	Experimental (Rao and Lee, 2002)	Parachor Model	Mechanistic Parachor Model	Parachor Model	Mechanistic Parachor Model
9.49	3.19	0.78	3.59	0.5694	0.0154
11.79	3.09	0.66	3.00	0.6204	0.0008
14.22	2.60	0.58	2.64	0.6052	0.0003
18.57	2.02	0.41	1.86	0.6376	0.0060
24.64	1.07	0.23	1.06	0.6147	0.0001
27.77	0.73	0.15	0.70	0.6265	0.0020
			Objective Function ( ) =	3.6738	0.0245

The results of comparison of experimental IFT measurements with original Parachor model predictions at different C_{2+} enrichments in gas phase and at a pressure of 30 MPa are summarized in Table 2.54 and shown in Figure 2.70. From Table 2.54 and Figure 2.70, it can be seen that significant IFT under-predictions are obtained with the Parachor model when compared to the experiments due to the absence of mass transfer effects in the Parachor model. Therefore, as before, an objective function (Δ), the sum of weighted squared deviations between the model predictions and experimental values, has been defined and then minimized using the correction factors for the original Parachor model predictions.

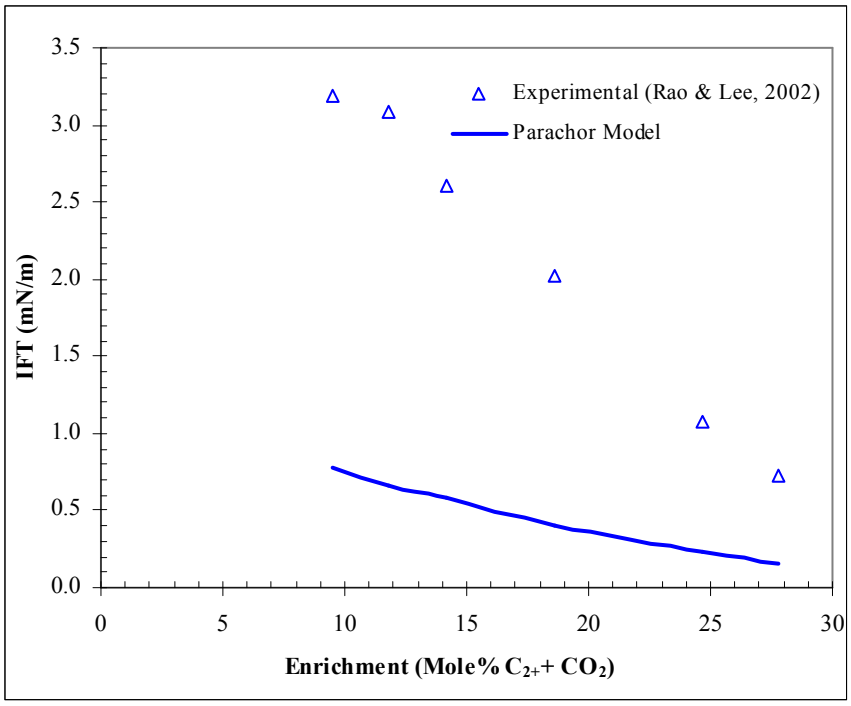

Figure 2.70: Comparison between IFT Measurements and Parachor Model for Terra Nova Fluids at 96°C and 30.0 MPa

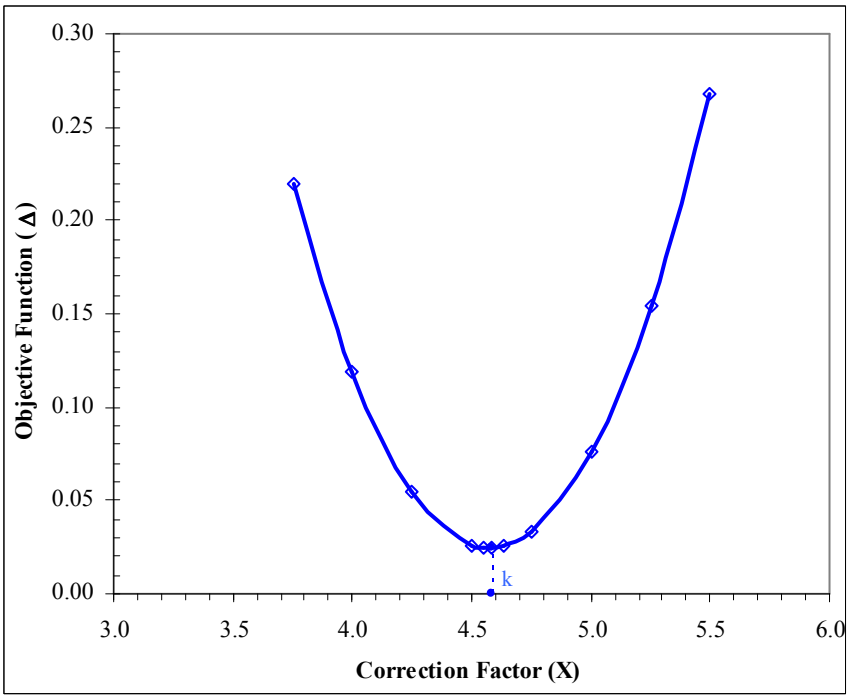

Figure 2.71: Determination of Mass Transfer Enhancement Parameter for Terra Nova Fluids

The minimization of the objective function and the determination of resulting mass transfer enhancement parameter (k) for this crude oil-gas system are depicted in Figure 2.71. The mass transfer enhancement parameter (k), the correction factor at which objective function becomes the minimum, is estimated to be 4.58.

Table 2.55: Diffusivities between Oil and Gas at Various C2+ Enrichments for Terra Nova Fluids at 96^{o}C and 30.0 MPa

(Mole% C_{2+}+ CO_2)	D_{os} (m^2/s)	D_{so} (m^2/s)	D_{os}/D_{so}
9.49	2.39E-08	7.39E-09	3.23
11.79	2.34E-08	7.14E-09	3.28
14.22	2.32E-08	7.05E-09	3.29
18.57	2.24E-08	6.77E-09	3.31
24.64	2.12E-08	6.44E-09	3.29
27.77	2.04E-08	6.25E-09	3.27
		Average =	3.28

Table 2.56: Model Exponents for different Single Experimental IFT Measurement Points in the Mechanistic Parachor Model for RKR Fluids at 14.8 MPa

Enrichment (Mole% C_{2+} + CO_2)	IFT (mN/m)			C.F (k)	D_{os}/D_{so}	n
	Experimental (Rao, 1997)	Parachor	Mechanistic Parachor			
17.79	4.26	2.910	4.26	1.46	3.56	0.30
21.64	3.89	2.590	3.89	1.50	3.68	0.31
25.85	3.27	2.210	3.27	1.47	3.75	0.29
30.57	2.69	1.810	2.69	1.48	3.81	0.29
33.86	2.13	1.540	2.13	1.39	3.82	0.25
37.70	1.52	1.240	1.52	1.23	3.80	0.16
43.07	0.97	0.850	0.97	1.15	3.73	0.11
48.39	0.53	0.500	0.53	1.10	3.61	0.07

The calculated diffusivities between the fluid phases at different C_{2+} enrichments in gas phase for Terra Nova fluids at a pressure of 30 MPa are summarized in Table 2.55. The slight decline of mass transfer interactions between the fluid phases with the increase of C_{2+} enrichment in gas phase can be seen. Furthermore, the ratio of diffusivities between the fluids remains nearly constant irrespective of C_{2+} enrichment in gas phase. Both these findings are similar to those observed with RKR fluids. From Table 2.55, it can be seen that the average ratio of diffusivities between the fluids at various C_{2+} enrichments is obtained as 3.28. From the mass transfer enhancement parameter and the average ratio of diffusivities between the fluid phases, the exponent (n) characterizing the governing mass transfer mechanism is computed to be +1.28. The positive sign of n indicates that even for these reservoir fluids, vaporization of components from the crude

Table 2.57: Model Exponents for different Single Experimental IFT Measurement Points in the Mechanistic Parachor Model for Terra Nova Reservoir

Enrichment (Mole% $C_{2+} + CO_2$)	IFT (mN/m)			C.F (k)	D_{os}/D_{so}	n
	Experimental (Rao and Lee, 2002)	Parachor	Mechanistic Parachor			
9.49	3.19	0.783	3.19	4.08	3.23	1.20
11.79	3.09	0.656	3.09	4.71	3.28	1.30
14.22	2.60	0.577	2.60	4.51	3.29	1.27
18.57	2.02	0.407	2.02	4.97	3.31	1.34
24.64	1.07	0.231	1.07	4.63	3.29	1.29
27.77	0.73	0.152	0.73	4.80	3.27	1.33

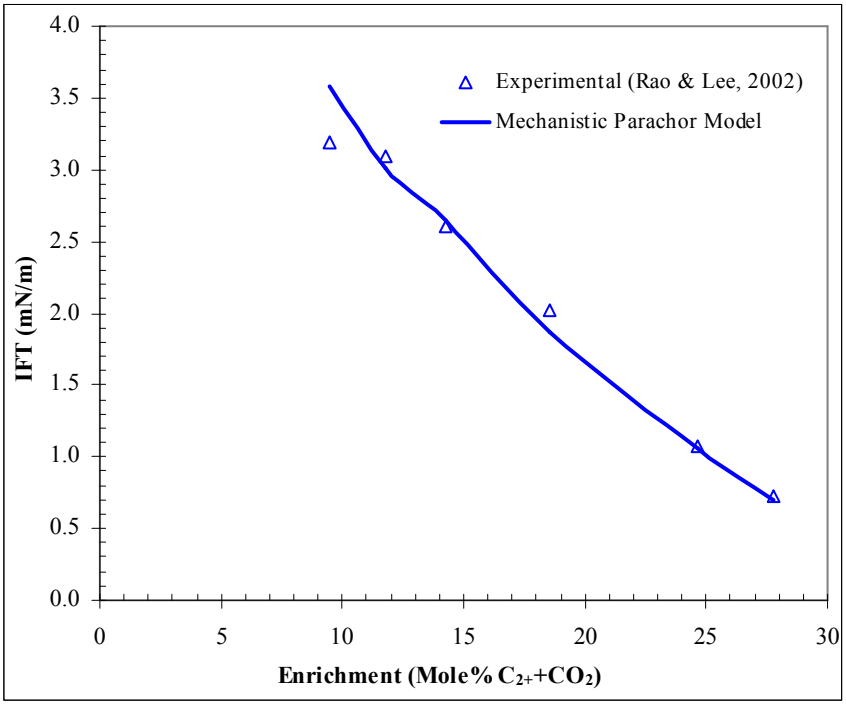

Figure 2.72: Comparison between IFT Measurements and Mechanistic Parachor Model for Terra Nova Fluids at 96°C and 30.0 MPa

oil into the gas phase is the dominating mass transfer mechanism for attaining the fluid phase equilibria. Furthermore, relatively higher value of n obtained for this crude oil-gas system compared to RKR fluids imply more pronounced vaporization mass transfer effects in the Terra Nova reservoir fluids. This can be attributed to the presence of relatively larger amounts of lighter components (56 mole% C_1 to C_3) in the Terra Nova crude oil compared to 52 mole% C_1 to C_3 in RKR crude oil (Rao, 1997; Rao and Lee, 2002).

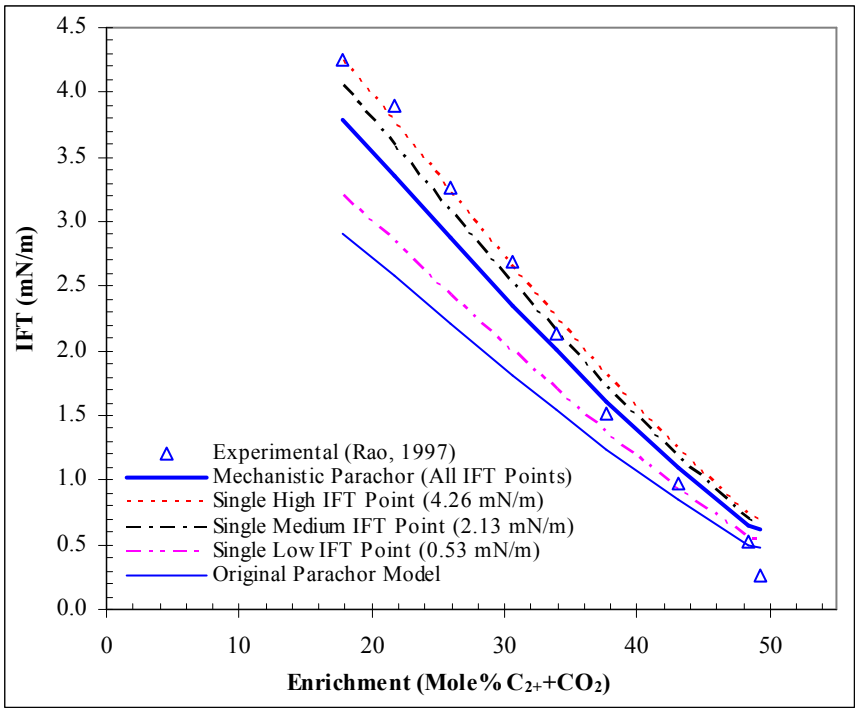

Figure 2.73: Sensitivity Studies on Mechanistic Model Results for RKR Fluids at 87°C and 14.8 MPa

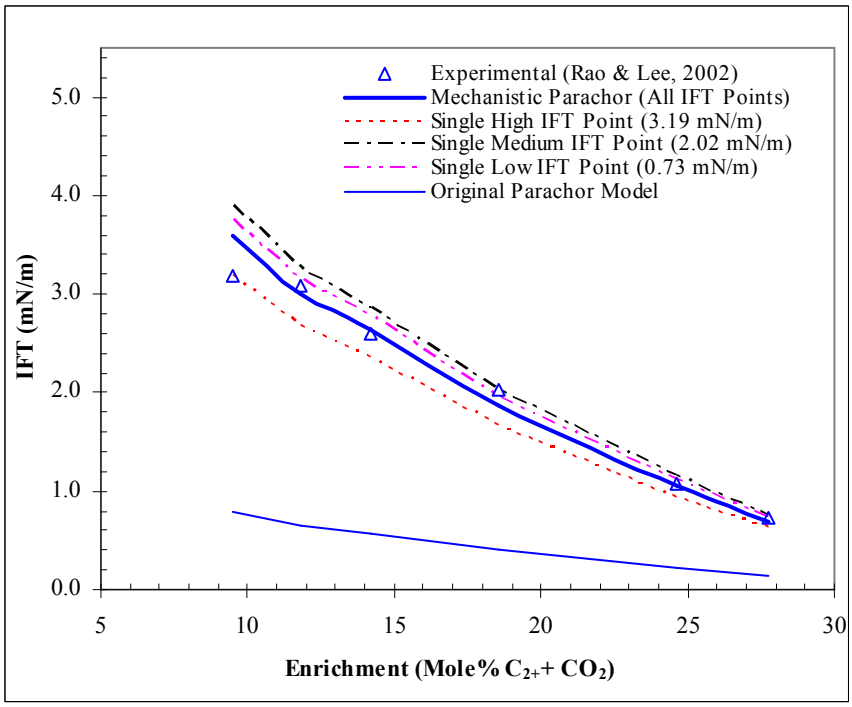

Figure 2.74: Sensitivity Studies on Mechanistic Model Results for Terra Nova Fluids at 96°C and 30.0 MPa

The comparison between the mechanistic Parachor model IFT predictions and the experiments at various C_{2+} enrichments in gas phase is given in Table 2.54 and shown in Figure 2.72 for a pressure of 30 MPa. As expected, an excellent match is obtained between the experiments and the mechanistic model predictions.

Sensitivity Studies on Proposed Mechanistic Model. Sensitivity studies were carried out for RKR and Terra Nova fluids to determine the effect of number of experimental IFT measurement data points on the mechanistic model results. The exponents obtained by using different single experimental IFT measurements in the mechanistic model are shown in Table 2.56 and Table 2.72 for RKR fluids at 14.8 MPa and Terra Nova fluids at 30.0 MPa, respectively. The comparison of IFT predictions from the mechanistic model obtained by using three different single IFT measurements namely high IFT, medium IFT and low IFT with the original Parachor model and the mechanistic model with all the available experimental data are shown in Figures 2.73 and 2.74 for RKR and Terra Nova fluids, respectively. From Figure 2.73 for RKR fluids, it can be seen that there is no significant differences among the mechanistic model IFT predictions using single high and medium IFT measurement points and all the experimental data in the mechanistic model. However, the use of low single IFT measurement point in the mechanistic model resulted in significantly deviating IFT values when compared to the mechanistic model with all the experimental points. It is important to note that even the provision of single low IFT measurement point as input to the mechanistic model yielded better IFT predictions compared to original Parachor model. Similar results are obtained even for Terra Nova fluids. From Figure 2.74 for Terra Nova fluids, it can be seen that the provisions of single high, medium and low IFT measurement points as well as all the experimental data in the mechanistic model resulted in almost similar IFT predictions. The IFT predictions from all these combinations matched extremely well with experiments when compared to original Parachor model. Based on these observations, it can be concluded that the provision of a single high or medium experimental IFT measurement in the proposed mechanistic model is sufficient for reasonable IFT predictions from the model.

Development of a Generalized Multiple Regression Model. In crude oil-solvent systems such as RKR and Terra Nova fluids, simultaneous counter-directional mass transfer interactions occur from both the oil and solvent (gas) phases. These include vaporization of lighter components (C_1-C_3) from crude oil phase to solvent (gas) phase and condensation of intermediate to heavier components (C_4-C_{7+}) from the solvent (gas) phase to crude oil phase. CO_2 has also been included in the model, as it is the active component involved in both the mechanisms of vaporization from crude oil and condensation from the injection gas Therefore, the compositions of (C_1-C_3 + CO_2) in crude oil and (C_4-C_{7+} + CO_2) in gas constitute the solute composition. These compositions are normalized as a molar ratio: (C_1-C_3 + CO_2) / (C_4-C_{7+}) in crude oil to

represent vaporizing drive mechanism from the oil and (C_4-C_{7+} + CO_2) /(C_1-C_3) in gas phase to represent condensing drive mechanism from the gas. The mechanistic model exponents resulted by the provision of different single experimental IFT measurements in the mechanistic model for the two crude oil-solvent systems of RKR and Terra Nova reservoirs (as given in Table 2.56 for RKR fluids and Table 2.57 Terra Nova fluids) are now related to the normalized solute compositions using multiple regression analysis. The results are summarized in Figure 2.75. From Figure 2.75, it can be seen that a good linear relationship between the exponent and the normalized solute compositions is obtained for both the crude oil-solvent systems with a multiple determination coefficient of 0.984. The regression equation obtained for predicting the exponent (n) values is also shown in Figure 2.75 and is given by,

$$n = -9.4473 + 8.26206\left(\frac{Mole\%CO_2 + C_1 - C_3}{Mole\%C_4 - C_{7+}}\right)_{Oil} - 1.00635\left(\frac{Mole\%CO_2 + C_4 - C_{7+}}{Mole\%C_1 - C_3}\right)_{Gas} \quad \ldots$$

……...…….. (2.23)

Higher absolute value of the slope for vaporizing mechanism (8.262) when compared to condensing mechanism (1.006) in the regression equation further substantiates that the vaporization of lighter components from crude oil to gas phase is the governing mass transfer mechanism for the attainment of fluid phase equilibria between the vapor and liquid phases of these two crude oil-solvent systems. This regression model can be used for *a priori* estimation of exponent (n) in the mechanistic model for crude oil-solvent systems. Thus, the exponent (n) in the mechanistic model can be simply determined by using the compositions of crude oil and solvent and thereby completely eliminating the need for even a single experimental IFT data in the proposed mechanistic model. Although this regression model incorporates both the mechanisms of vaporization and condensation, the regression correlation obtained is based on the systems where vaporization mechanism is dominant and hence the application of the model is suggested mainly for vaporizing drive crude oil-gas systems.

Validation of the Proposed Generalized Multiple Regression Model. The proposed generalized multiple regression model was utilized to predict the exponent in the mechanistic model and consequently interfacial tensions in Prudhoe Bay gas-oil system for validation. The experimental IFT data on Prudhoe Bay reservoir fluids at 200^{o}F reported by Dorshow (1995) were used for comparison with the results from the proposed regression model. The crude oil and solvent compositions for Prudhoe Bay reservoir fluids needed in the calculations were obtained from the references of Spence and Ostrander (1983) and McGuire and Moritz (1992), respectively.

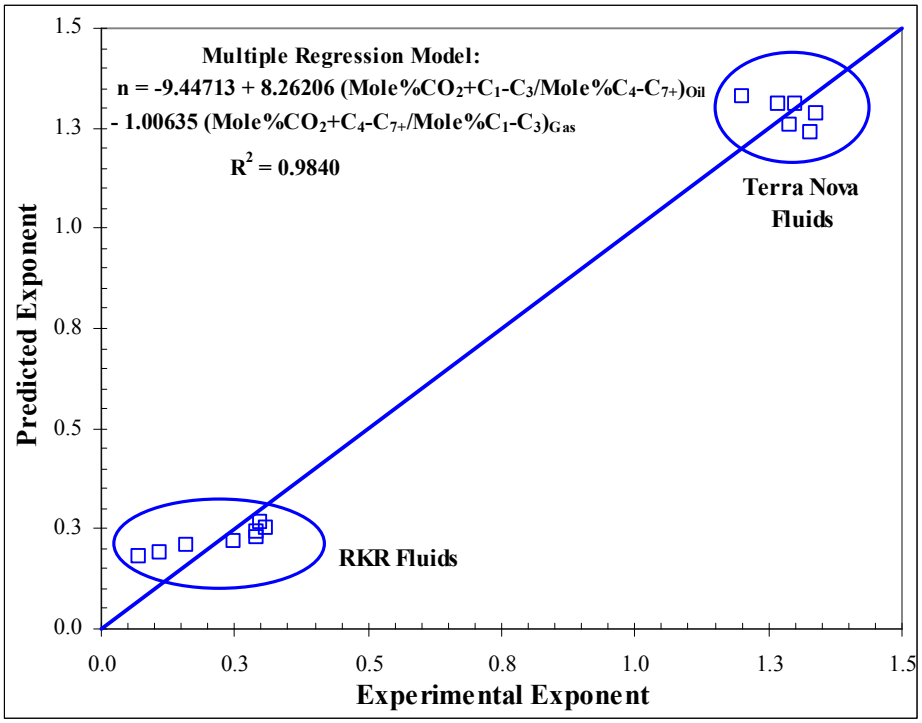

Figure 2.75: Multiple Linear Regression Model for the Mechanistic Model Exponent Prediction in Vaporizing Drive Gas-Oil Systems

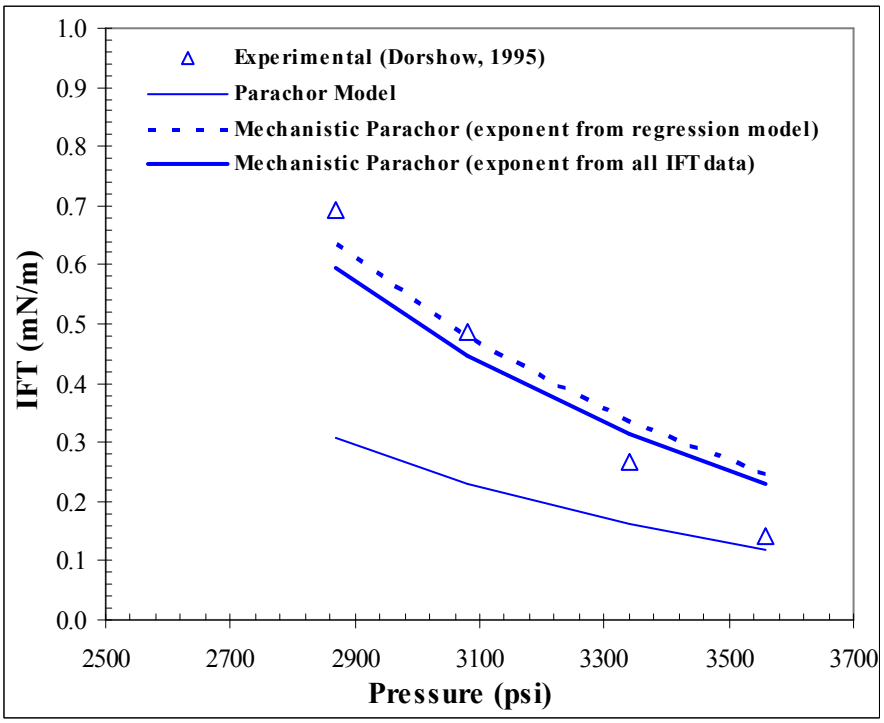

Figure 2.76: Validation of Multiple Linear Regression Model for Mechanistic Model Exponent Prediction Using Prudhoe Bay Crude Oil-Solvent System

Table 2.58: Summary of IFT Measurements, Parachor Model Predictions and Diffusivities between Fluid Phases for Prudhoe Bay Reservoir Fluids at 200°F

Pressure (psi)	IFT (mN/m)		D_{os}	D_{so}	D_{os}/D_{so}
	Experimental (Dorshow, 1997)	Parachor Model			
2869	0.694	0.307	1.704E-08	5.831E-09	2.923
3082	0.486	0.230	1.614E-08	5.294E-09	3.048
3340	0.268	0.162	1.525E-08	5.627E-09	2.710
3560	0.143	0.119	1.459E-08	5.485E-09	2.659
				Average =	2.835

A feed composition of 65 mole% of crude oil and 35 mole% of solvent was used in IFT computations to match the composition used in the experiments. The comparison between the experimental IFT measurements and the original Parachor model predictions is given in Table 2.58 and is also shown in Figure 2.76. As can be seen from Table 2.58 and Figure 2.41, IFT under-predictions are obtained with Parachor model, when compared to experiments due to lack of mass transfer effects in Parachor model. Hence correction factors are applied for Parachor model predictions to minimize the objective function and consequently a mass transfer enhancement parameter (k) of 1.94 has been obtained. The calculated diffusivities between fluid phases for Prudhoe Bay reservoir fluid are also given in Table 2.58, which indicates an average ratio of diffusivities between the fluid phases to be 2.835. From the average ratio of diffusivities and the mass transfer enhancement parameter, the exponent in the mechanistic model is computed as 0.636. A mechanistic model exponent of 0.699 has been obtained for Prudhoe Bay crude oil-solvent system by using only the compositional data of reservoir fluids in the proposed generalized regression model. This exponent calculated using the regression model thus deviates by only about 9.9% from the mechanistic model exponent of 0.636 obtained by using all the available IFT experimental data. The positive exponent obtained indicates that vaporization of lighter components from crude oil into the gas is the governing mass transfer mechanism for fluid phase equilibria of these reservoir fluids.

The comparison of the IFT measurements with the predictions of mechanistic Parachor model with the exponent calculated using the compositional data of reservoir fluids is shown in Figure 2.76. The mechanistic Parachor model IFT predictions with the exponent obtained by fitting all the available experimental IFT data are also shown in Figure 2.76 for better comparison. From Figure 2.76, better match of IFT predictions with experiments can be seen with the mechanistic Parachor model of both the exponents. Moreover, the IFT predictions from the mechanistic model for both the exponents used are almost similar. Therefore, this validates the proposed regression model to predict the exponent in the mechanistic model without the need for even a single IFT measurement in the mechanistic Parachor model.

Extension of the Proposed Mechanistic Parachor Model for Gas-Oil Miscibility. The use of diffusivities in the proposed mechanistic model and the ability of model to provide information on mass transfer mechanisms indicate that the IFT measurements modeled in this study are dynamic in nature. This is further supported with the already published works of the other investigators as cited below.

Rosen and Gao (1995) and Campanelli and Wang (1999) used their models to compute the diffusion coefficients from the measured short-time and long-time dynamic interfacial tension data in aqueous surfactant solutions. Diamant et al. (2001) discussed the kinetics of surfactant adsorption and provided a general method to calculate dynamic interfacial tension at fluid-fluid interfaces using diffusion-controlled models. Taylor and Nasr-EI-Din (1996) modeled the measured dynamic interfacial tensions in crude oil-brine-surfactant systems with diffusion coefficient as one of the parameters in their model. Ayirala (2005) experimentally proved the dynamic nature of interfacial tension in gas-oil systems by measuring the variations in interfacial tension with time in live decane consisting of 25 mole% methane, 30 mole% n-butane and 45 mole% n-decane and CO_2 system at 160^{o}F and 7.7 MPa. The dynamic changes in interfacial tension were observed in this live decane-CO_2 system for about 48 hours, after which the IFT remained reasonably constant. Ayirala (2005) reported that even after such long aging periods between the two fluid phases, minute changes in interfacial tension may occur, but are not measurable with the available experimental system and instrumentation. It is also worth mentioning that the provision of one hour aging period between the fluid phases in this experimental study has been found to be sufficient for attaining nearly 98% of the equilibrium interfacial tension value. We also believe that these dynamic effects of interfacial tension will be especially significant in the complex hydrocarbon systems consisting of multicomponent crude oil and gas phases. Crude oils contain thousands of chemical compounds (McCain, 1990) and hence it is difficult to attain thermodynamic equilibrium compositions of these various components within short aging periods. Therefore, in crude oil-gas systems such as the ones used for IFT modeling in this study, even after aging for much longer times, there may be still some infinitesimal amounts of mass transfer interactions occurring between the fluid phases to reach the ultimate thermodynamic equilibrium. However, after certain finite aging periods, the changes in interfacial tension with time become so minute that it is reasonable to approximate these interfacial tensions to near equilibrium interfacial tension. Therefore, considering the aging period of about 2 hours allowed between the fluid phases during the reported experiments, the IFT measurements modeled in this study appear to be at near equilibrium condition. Thus, these near equilibrium interfacial tensions appear to be amenable to calculations using the diffusivity included mechanistic Parachor model proposed in this study. Fluid-fluid miscibility means the absence of interface between the fluids, that is, zero interfacial tension between the fluid phases (Benham et al., 1965;

Stalkup, 1983; Holm, 1987; Lake, 1989). Therefore, the interfacial tension predictions from the proposed mechanistic model can be plotted against pressure or solvent enrichment and the extrapolation of the plot to zero interfacial tension gives the dynamic miscibility conditions in multicomponent hydrocarbon systems.

Miscibility Prediction in Standard Gas-Oil Systems Using Mechanistic Parachor Model. The fluid phase compositions for dynamic gas-oil IFT and miscibility in the two standard gas-oil systems of n-decane-CO_2 at 37.7^oC and live decane (consisting of 25 mole% methane, 30 mole% n-butane and 45 mole% n-decane)-CO_2 at 71.1^oC were obtained by performing flash calculations using QNSS/Newton algorithm (Nghiem and Heidemann, 1982) and PR-EOS (Peng and Robinson, 1976) incorporated in the commercial simulator, Winprop (Computer Modeling Group Ltd., 2002). The IFT's and miscibilities measured at an initial gas-oil ratio of 80 mole% gas and 20 mole% oil in the two standard gas-oil systems were used for comparison with model predictions. The viscosities of the fluid phases were computed using the Pederson's corresponding state model (Pederson and Fredenslund, 1987) within the commercial simulator, Winprop (Computer Modeling Group Ltd., 2002). The measured densities of the equilibrated fluid phases and the pure component Parachor values reported by Danesh (1998) were used during gas-oil IFT calculations.

Table 2.59: Comparison of IFT Measurements with Parachor Model in n-Decane-CO_2 System at 37.8^oC

Pressure (MPa)	IFT (mN/m)	
	Experimental	Parachor Model
0.103	22.45	22.21
1.483	20.13	19.90
2.862	16.24	16.10
4.241	10.27	10.10
5.621	6.07	5.96
7.000	3.34	3.21
7.690	0.33	0.13

The comparison between IFT predictions from the Parachor model and the experiments at various pressures for n-decane-CO_2 system at 37.7^oC is given in Table 2.59. The results are also shown in Figure 2.77. As can be seen in Table 2.59 and Figure 2.77, a good match between the experiments and the model predictions is obtained with the Parachor model. This agrees well with the already published reports that the Parachor model predicts IFT reasonably well in binary mixtures (Weinaug and Katz, 1943; Fawcett, 1994). The good match of experimental IFT measurements with Parachor model indicates an exponent of zero in the mechanistic Parachor model. The zero value for the exponent in the mechanistic model implies equal proportions of vaporizing and

condensing drive mechanisms to be responsible for dynamic gas-oil miscibility development in this standard gas-oil system. This means that the amount of CO_2 dissolving in n-decane is about the same as the amount of n-decane vaporizing into CO_2 gas. Now, the model IFT predictions were fitted using the simple linear regression. The relation obtained is indicated in Figure 2.77. A predicted VIT miscibility of 7.84 MPa was obtained by extrapolation of this relation to zero IFT. This predicted miscibility deviates by only about 0.13% from the experimental VIT miscibility of 7.83 MPa (Figure 2.57) obtained from the IFT measurements.

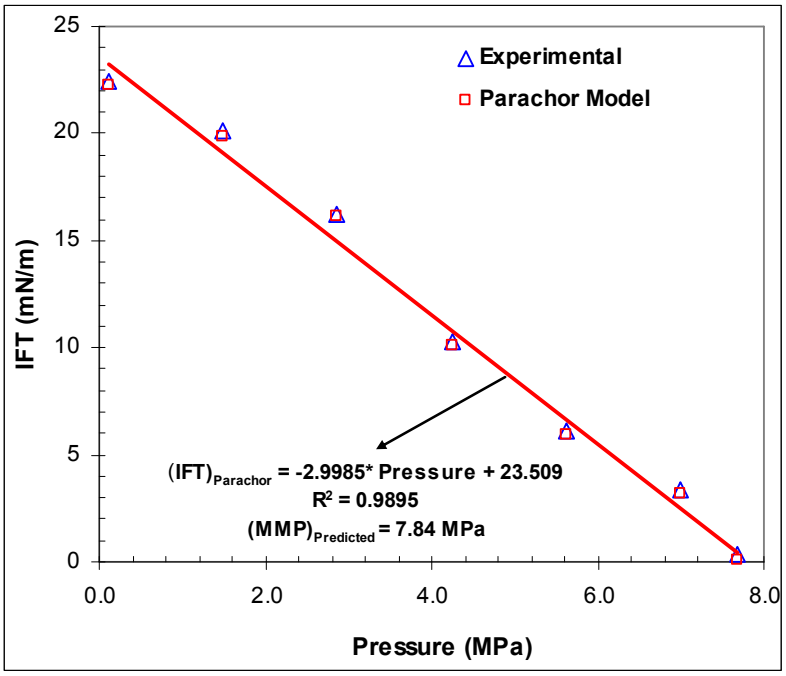

Figure 2.77: Comparison of IFT Measurements with Parachor Model in n-Decane-CO_2 System at 37.8°C

The comparison between IFT predictions from the Parachor model and the experiments at various pressures for live decane-CO_2 system at 71.1°C is given in Table 2.60 and shown in Figure 2.78. As can be seen, the match between the experiments and the model predictions is not good and IFT under-predictions are obtained with the Parachor model. This was not the case in the binary system of n-decane-CO_2 discussed earlier. The disagreement between the experiments and the model predictions in this gas-oil system indicates significant effect of interaction of one component with the others in terms of Parachor values in multicomponent hydrocarbon systems. This furthermore substantiates the poor performance of Parachor model for IFT predictions in multicomponent hydrocarbon systems, as reported by the other researchers also (Danesh et al., 1991; Fawcett, 1994).

Table 2.60: Comparison of IFT Measurements with Parachor and Mechanistic Parachor Models for Live Decane - CO_2 System at 71.1°C

Pressure (MPa)	IFT (mN/m)		
	Experimental	Parachor Model	Mechanistic Parachor Model
7.69	4.061	2.394	4.908
8.03	3.490	1.936	3.969
8.38	2.712	1.526	3.128
8.72	2.437	1.263	2.589
9.07	2.041	1.056	2.165
9.41	1.791	0.776	1.591
9.76	1.373	0.614	1.259
10.45	1.115	0.411	0.843
10.79	0.887	0.300	0.615
11.14	0.571	0.185	0.379
11.48	0.441	0.138	0.283
11.83	0.125	0.028	0.057
12.17	0.044	0.014	0.029

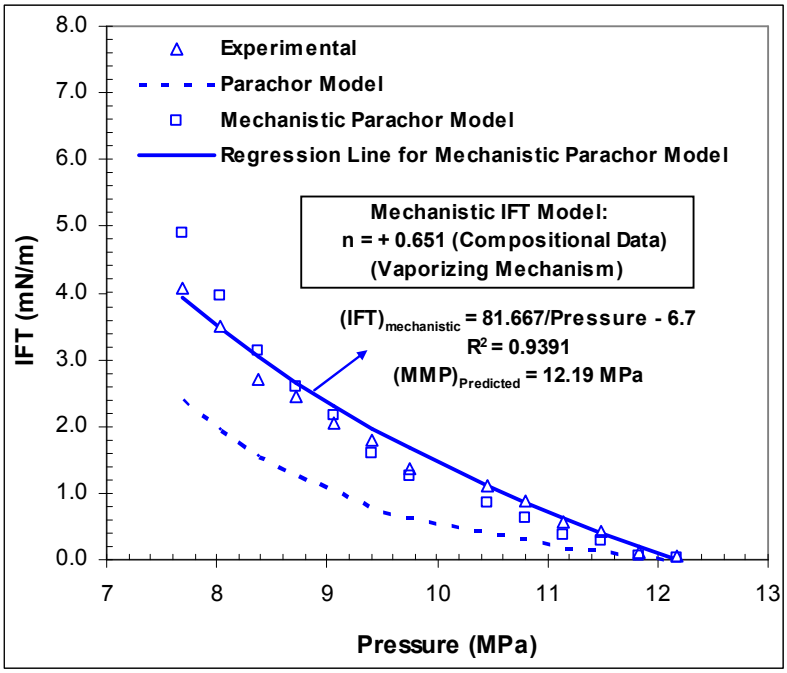

Figure 2.78: Comparison of IFT Measurements with Parachor and Mechanistic Parachor Models for Live Decane-CO_2 System at 71.1°C

The mechanistic Parachor model has been applied to improve the IFT predictions in this live decane-CO_2 system by accounting for counter-directional mass transfer effects. Correction factors are used for the original Parachor model predictions to minimize the objective function, that is, the sum of weighted squared deviations between the original

Parachor model predictions and the experimental IFT values. The mass transfer enhancement parameter (k), the correction factor at which the objective function becomes the minimum was found to be 2.20. The diffusivities between the fluid phases at various pressures in this gas-oil system are given in Table 2.61. From Table 2.61, it can be seen that the average ratio of diffusivities between the fluids at all pressures is 3.0. From the mass transfer enhancement parameter and the average ratios of diffusivities between the fluid phases, the exponent (n) characterizing the governing mass transfer mechanism is found to be + 0.716 (Eq. 13). The positive sign of n indicates that vaporization of components from the oil into the gas phase is the controlling mass transfer mechanism for attaining dynamic gas-oil miscibility in this standard gas-oil system. This can be attributed to the presence of significant amounts of lighter components (55 mole% n-C_1 and n-C_4) in the live decane.

Table 2.61: Diffusivities between Oil and Gas at Various Pressures in Live Decane-CO_2 System at 71.1^oC

Pressure (MPa)	$D_{oil-gas}$ (m^2/s)	$D_{gas-oil}$ (m^2/s)	$D_{oil-gas}/D_{gas-oil}$
7.69	4.178E-08	1.251E-08	3.339
8.03	4.100E-08	1.244E-08	3.295
8.38	4.024E-08	1.238E-08	3.251
8.72	3.952E-08	1.231E-08	3.210
9.07	3.881E-08	1.224E-08	3.171
9.41	3.797E-08	1.217E-08	3.119
9.76	3.716E-08	1.211E-08	3.068
10.45	3.521E-08	1.198E-08	2.940
10.79	3.438E-08	1.192E-08	2.885
11.14	3.333E-08	1.185E-08	2.812
11.48	3.234E-08	1.180E-08	2.742
11.83	3.141E-08	1.173E-08	2.677
12.17	3.043E-08	1.167E-08	2.607
		Average =	3.009

The generalized regression model (Eq. 14) proposed for mechanistic model exponent prediction in vaporizing crude oil-solvent systems was then utilized to determine the exponent. In this standard gas-oil system, the solvent is the pure CO_2 gas. Therefore, the term representing condensing drive mechanism of intermediate to heavy components from solvent to oil in the regression model is not applicable and hence can be ignored. But, the portion of the regression model representing the vaporizing drive mechanism holds good even for this case, as the lighter components (solute) vaporizing from oil into gas are almost the same. Furthermore, it is reasonable to add the component n-C_4 to the numerator in the term representing vaporizing drive mechanism, as its tendency will be primarily towards vaporization in this standard gas-oil system. With these assumptions, a

mechanistic model exponent of + 0.651 is obtained using the compositional data of live decane in the generalized regression model. This exponent calculated using the compositional data in the regression model deviates by about 8.6% from the mechanistic model exponent of 0.716 obtained by using all the measured IFT experimental data.

The comparison between experiments and the predictions obtained using the exponent from the compositional data of live decane in the mechanistic Parachor model is given in Table 2.60 and shown in Figure 2.78. From Table 2.30 and Figure 2.78, a good match of IFT predictions from the mechanistic model with IFT measurements can be seen. The mechanistic model IFT predictions were then fitted against pressure using the hyperbolic function and the relationship obtained is shown in Figure 2.78. Extrapolation of this relationship to zero interfacial tension gives a predicted VIT miscibility pressure of 12.19 MPa. This predicted VIT miscibility is almost identical to the experimentally measured VIT miscibility of 12.2 MPa (Figure 2.58) and deviates by only about 0.08%.

2.3.3.5 Conclusions

1. A new mass transfer enhanced mechanistic Parachor model has been proposed for prediction of dynamic gas-oil interfacial tension as well as to characterize the governing mass transfer mechanism responsible for fluid phase equilibria and miscibility in multicomponent hydrocarbon systems.
2. The ratio of diffusivities between the fluid phases raised to an exponent is introduced into the Parachor model for mass transfer effects. The sign and value of the exponent in the proposed mechanistic model characterize the type and the extent of governing mass transfer mechanism for fluid phase equilibria and miscibility.
3. The performance of the proposed mechanistic model has been tested for two reservoir crude oil-gas systems of Rainbow Keg River and Terra Nova to evaluate its effectiveness in multicomponent hydrocarbon systems.
4. For Rainbow Keg River reservoir fluids, the positive exponents (+0.20, +0.17) obtained in the mechanistic model indicate that the governing mass transfer mechanism is the vaporization of lighter components from crude oil into the gas phase for attaining the fluid phase equilibria and miscibility.
5. For Terra Nova reservoir fluids, the positive exponent (+1.28) in the mechanistic model indicates the vaporization of light hydrocarbon components from crude oil into the gas phase to be the governing mass transfer mechanism for fluid phase equilibria and miscibility.
6. The relatively higher value of positive exponent in the mechanistic model for Terra Nova fluids compared to RKR fluids indicates more pronounced vaporization mass transfer effects in Terra Nova fluids. This is substantiated by the presence of relatively higher amount of light hydrocarbon components (C_1 to C_3) in Terra Nova crude oil.

7. The sensitivity studies on proposed mechanistic model results for RKR and Terra Nova reservoir fluids indicate that the provision of a single high or medium range IFT measurement in the proposed model is sufficient for reasonable IFT predictions.
8. A generalized multiple regression model has been developed correlating the exponent (n) in the mechanistic model with normalized solute compositions present in both the fluid phases for RKR and Terra Nova reservoir fluids. The proposed regression model has been validated for mechanistic model exponent prediction using Prudhoe Bay reservoir fluids and hence can be used for *a-priori* estimation of exponent (n) in the mechanistic model in predominantly vaporizing drive gas-oil systems.
9. The dynamic nature of interfacial tensions observed in the experiments justifies the use of diffusivity coefficients in the mechanistic model. Hence, IFT predictions from the mechanistic model can be used to determine dynamic gas-oil miscibility conditions in multicomponent hydrocarbon systems.
10. The proposed mechanistic model can be utilized to identify the predominating mass transfer mechanism in the combined vaporizing/condensing mode and to determine dynamic interfacial tension and miscibility in multicomponent hydrocarbon systems by using only the compositional data of fluid phases.
11. The miscibilities determined using the mechanistic Parachor model deviated by only about 0.08-0.13% from the measured VIT miscibilities for both the standard gas-oil systems studied. Hence accurate miscibility predictions can be obtained using the mechanistic Parachor model in multicomponent hydrocarbon systems by knowing only the fluids compositional data.

3. Determination of Multiphase Displacement Characteristics in Reservoir Rocks

This comprehensive section of the final progress report includes the entire experimental work aimed at evaluating the multiphase displacement characteristics of gravity stable gas injection processes in Berea and reservoir rocks for the project period starting Oct 1, 2002 to Sept 30, 2006. This final report also summarizes the previous progress reports to the DOE (15323R01, Jan 2003 to date).

This work attempts to address six key questions: (i) do we continue to 'fix the problems' of gravity segregation in the horizontal gas floods or find an effective alternative?, (ii) is there a 'happy-medium' between single-slug and water-alternating-gas (WAG) processes that would outperform both?, (iii) what are the controlling multiphase mechanisms and fluid dynamics in gravity drainage processes?, (iv) what are the mechanistic issues relating to gravity drainage?, and (v) how can we model the novel gas assisted gravity drainage (GAGD) process using traditional analytical and empirical theories and (vi) what are the roles of the classical displacement, versus drainage in the GAGD process?

To facilitate fair and effective performance comparisons between the WAG and GAGD processes, as well as to decipher the controlling operational multiphase mechanisms and fluid dynamics in the GAGD processes, the dimensional analysis approach was employed and ten gravity stable and eight WAG field applications in the U.S., Canada and rest of the world were analyzed. A newly defined 'index of productivity' and five dimensionless groups, namely Capillary (N_C), Bond (N_B), Dombrowski-Brownell (N_{DB}), Gravity (N_G), and Grattoni et al.'s N group were calculated for these gravity stable field projects. This dimensional analysis not only provides an effective starting point to elucidate the mechanisms and dynamics associated with the gravity stable gas injection processes, but also serves as an effective means for 'field-scaled' experimental design. This dimensionless experimental design appeared to capture and characterize most of the spectrum of the operational forces in field gas injection projects.

Extensive literature review and laboratory experimentation (GAGD corefloods) were conducted to investigate and characterize the effects of various parameters on the GAGD process. The parameters investigated were: (i) gravity segregation, (ii) miscibility development, (iii) spreading coefficient, (iv) reservoir heterogeneity, (v) reservoir wettability, (vi) injection fluid type, (vii) injection mode, and (viii) gas cap control.

This work has resulted in several original contributions to our current understanding of the multiphase mechanisms and fluid dynamics of gas injection processes. The original contributions of this work to the existing literature are summarized as: (i) first

demonstration of the GAGD concept through high pressure experimentation, (ii) experimental demonstration of the superior oil recovery performance of the GAGD process in secondary (immiscible recovery range: 62.3% to 88.6% ROIP) and tertiary (immiscible recovery range: 47.3% to 78.9% ROIP) processes, in both miscible (avg. secondary miscible recoveries: near 100% ROIP; avg. tertiary miscible recoveries: near 100% ROIP) and immiscible modes, and in varying wettability and rock types of porous media, (iii) experimental verification of the hypothesis that the GAGD process is largely immune to the deteriorating effects of reservoir heterogeneity and that the presence of vertical fractures possibly aid the GAGD oil recoveries, (iv) experimental demonstration of the possibility of gas breakthrough control, (v) definition of a new 'combination' process between single-slug and WAG processes, (vi) preliminary mechanistic and dynamic differences between the drainage and displacement phenomenon have been identified and a new mechanism to characterize the GAGD process fluid mechanics has been proposed, (vii) a new parameter was introduced in the Li and Horne (2003) model to accurately predict the dynamic behavior of the GAGD process which resulted in more accurate predictions of GAGD oil recoveries, and (viii) a new dimensionless number to predict GAGD oil recoveries in both the miscible as well as the immiscible modes has been identified. Excellent correlation between the newly proposed number and GAGD immiscible recoveries was observed, and although the correlation's regression fit was not as good in GAGD miscible floods, the holistic nature of this correlation, makes it a useful tool for predicting GAGD oil recoveries.

To ensure continuity this report has been subdivided into four major sections: (i) literature review on gas injection enhanced oil recovery (EOR) processes, (ii) literature review on gravity stable gas injection and introduction of the GAGD process, (iii) experimental design for gravity stable and horizontal mode gas injection laboratory corefloods, (iv) gravity stable and horizontal mode gas injection coreflood experimental results, (v) analytical and conceptual modeling of GAGD process. It is important to note that the items (iii) and (iv) correspond to Tasks 3.1 and 3.2; whereas item (v) illustrates the Task 3.3 of the original statement of work submitted to the DOE for this research.

3.1 Introduction to EOR by Gas Injection

3.1.1 Need for Enhanced Oil Recovery (EOR)

In 1978, the United States Congress commissioned the Office of Technology (OTA, 1978) to evaluate the state of the art in U.S. oil production. The OTA concluded that the 300 billion barrels of known U.S. oil were economically unproducible by conventional methods in practice at that time. The OTA report (OTA, 1978) also evaluated a range of Enhanced Oil Recovery (EOR) techniques and their potential for improving the prospects of extracting a sizeable fraction of this known resource base. These major political and

administrative amendments triggered increased interest in EOR in late 70's and early 80's, most notably in California and the Permian Basin of West Texas.

Now, 25 years later, there is again a strong interest in improving domestic oil production (Nummedal et al., 2003), and the total 'unproducible oil' referred to in the OTA report (OTA, 1978), has increased to a whopping 377 billion barrels (Maddox, 2004). The need for oil in the U.S., as well as globally, has been constantly on the rise, except for the temporary drop during 1979 - 1983 (Figure 3.1) (USGS, 2000).

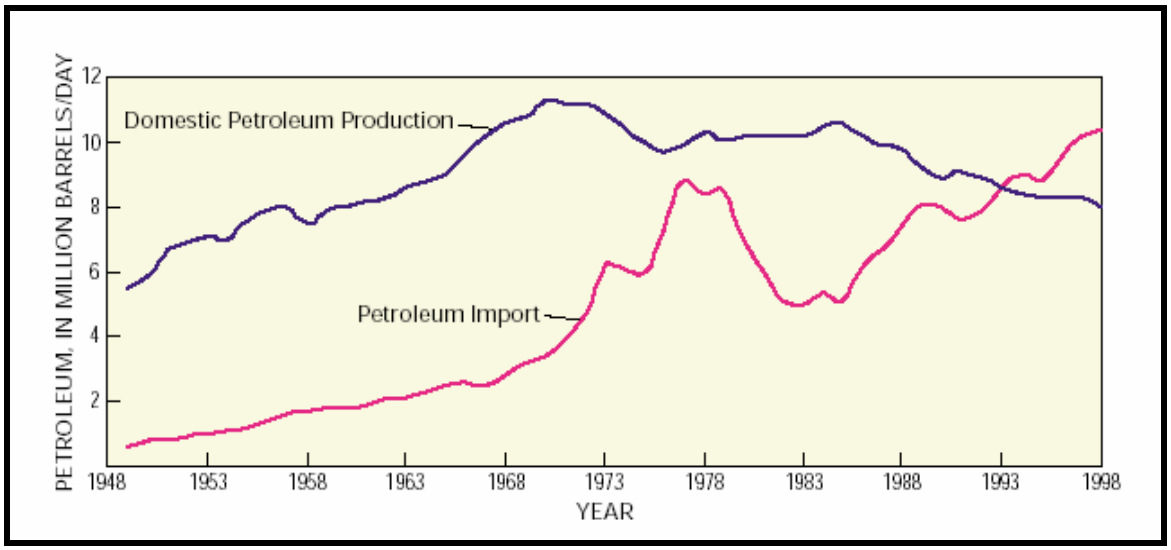

Figure 3.1: Oil Production and Imports of the U.S. (USGS, 2000)

The U.S. Geological Survey (USGS, 2000) notes that the proven U.S. reserves (Maddox, 2004), about 21.9 billion barrels, as of January 01, 2005 (USEIA, 2005), would be depleted quickly at the current production rates (USEIA, 2005) of 5.4 million barrels per day, and the probability of finding newer reserves is diminishing (Maddox, 2004, USEIA, 2005). The most important conclusion of this report, from oil self-reliance point of view, is that the EOR techniques have not been tried for most of these reservoirs. Therefore, the potential for EOR applications in the U.S. are very large with a target of 377 billion barrels (Moritis, 2004).

3.1.2 U.S. EOR Scene

The National Petroleum Council (NPC) defines Improved or Enhanced Oil Recovery (IOR or EOR) as "…incremental oil that can be economically produced…over that which can be economically recoverable by conventional primary and secondary methods". The main goals of any EOR method are increasing the capillary number and providing 'favorable' ($M < 1.0$) mobility ratios. The EOR processes today contribute a significant portion (~ 12% (EOR Survey, 2004)) to the U.S. domestic production, and its importance continues to rise in light of the recent high crude oil prices of about $70 per barrel.

The U.S. EOR scene is dominated by thermal methods used in heavy oil production, followed by CO_2 gas injection (mostly miscible) and finally hydrocarbon gas injection. These three processes account for almost 98% of the U.S. EOR production.

The changes in the U.S. EOR application and distribution scenario from 1984 to 2004 are shown in Figure 3.2 (Kulkarni, 2004). Figure 3.2 shows that except for the CO_2 and hydrocarbon processes, all the other EOR processes, namely thermal, and Nitrogen, have significantly decreased and the and chemical methods are nearly extinct. The share of CO_2 and hydrocarbon gas processes has increased from 18% (1984) to 48% (2004) in just two decades.

3.1.2.1 EOR Status

The U.S. EOR share patterns (Figure 3.3) demonstrate a clear shift in the oil industry towards more efficient EOR processes, and the steep rise and equally quick downfall of the chemical based EOR in the past 3 decades. The thermal methods are indispensable due to the presence of extensive heavy oil reserves. The gas injection process applications have steadily grown in use to become the main EOR process for light oil applications (using CO_2 or hydrocarbon (HC) gas). EOR survey (Moritis, 2004) shows that the gas injection processes are applicable to almost all medium-to-light oil reservoirs, with various fluid and reservoir characteristics. Thus, the gas injection processes hold the promise of significantly enhancing the recovery of the oil left behind by primary and secondary operations.

3.1.2.2 Gas Injection EOR Status

As demonstrated earlier, the gas injection EOR processes would be instrumental in tapping the 377 billion barrels of oil left behind in the U.S. reservoirs after primary and secondary processes. Moreover, as most of the U.S. oil reserves can be classified as medium to light, with average API gravities of over 28^o, except for the 'Thums' and 'Kern River' oils (Platt, 2005); gas injection process has become indispensable in the U.S. EOR scenario.

Further scrutiny of the gas injection EOR performance shows that within the last twenty years the miscible CO_2 projects have increased (Moritis, 2004) from 28 in 1984 to 70 in 2004 and their production during the same time period has grown by 6 folds (Moritis, 2004) from 31,300 BPD to 205,775 BPD. The production from miscible hydrocarbon gas injection projects in the U.S. has also steadily increased from 14,439 BPD in 1984 to 124,500 BPD in 2000 in spite of their decreasing numbers. However, this trend was reversed in 2002 and 2004 when the production from hydrocarbon gas floods fell to 97,300 BPD, perhaps due to the increasing price of natural gas (Rao et al., 2004).

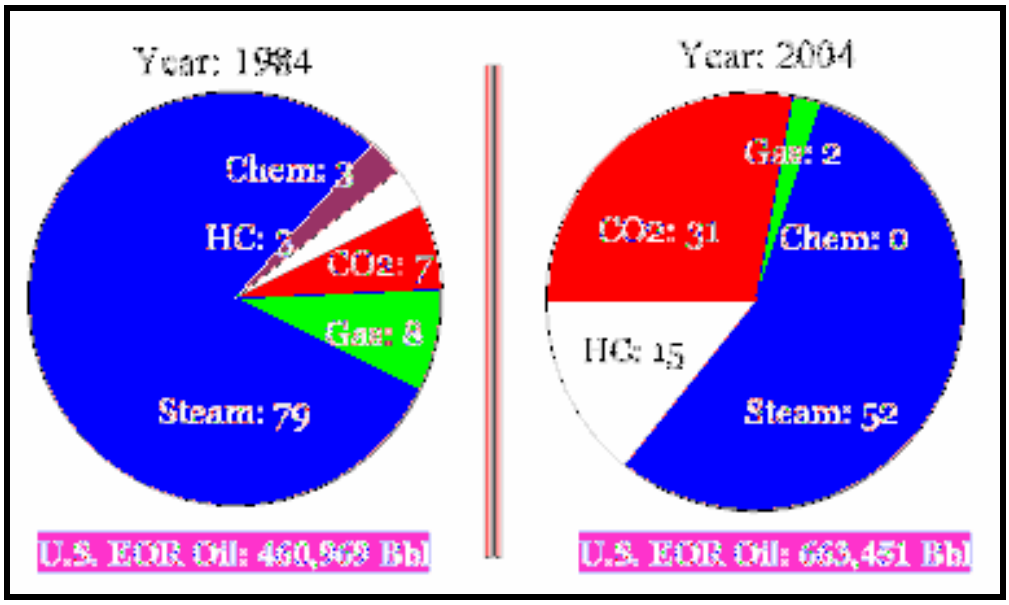

Figure 3.2: EOR Application and Distribution Scenario 1984 – 2004 (Kulkarni, 2004)

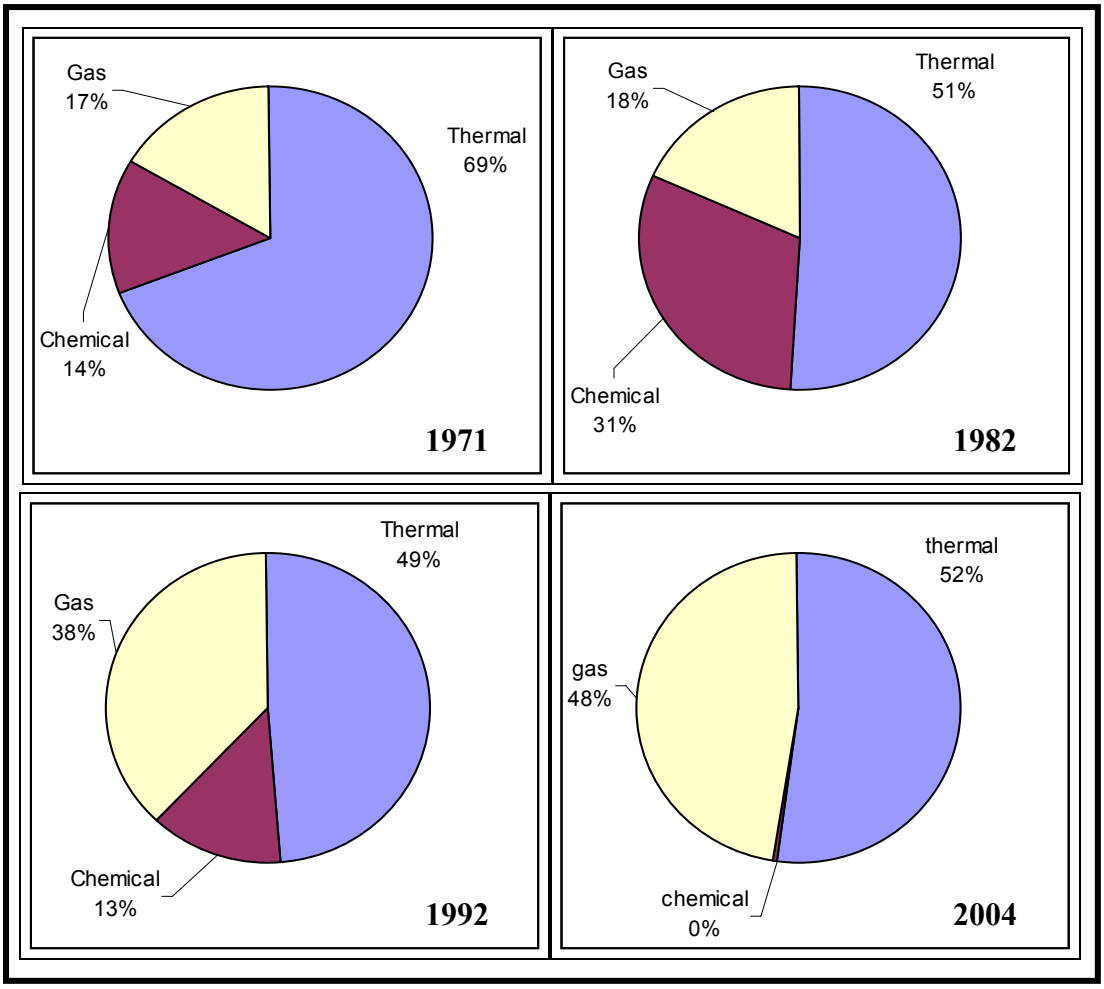

Figure 3.3: EOR Project Distribution Changes from 1971 – 2004

Studies of the gas injection EOR status (Figure 3.4) show that only two injectants, CO_2 (miscible) and hydrocarbon (miscible and immiscible) gas, have continued to grow, while all the other injectants namely, CO_2 (immiscible), N_2 and flue gas have declined or become extinct. The overall effect is that the share of production from gas injection EOR in the U.S. has more than doubled from 18% in 1984 to 47.9% in 2004. This clearly demonstrates the growing commercial interest that the U.S. oil industry has in gas injection EOR projects – especially CO_2.

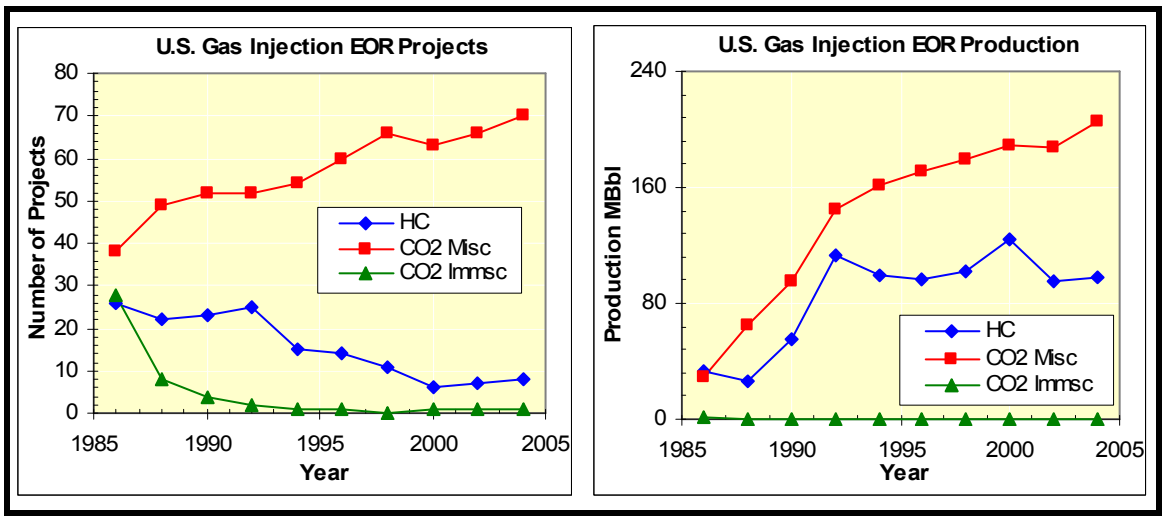

Figure 3.4: EOR Project and Production Distribution Dynamics (1986 – 2004)

3.1.2.3 EOR by Gas Injection

The target oil for the gas injection processes is the 'left-behind' oil in reservoirs that have been already discovered and deemed unproducible by current technology, which amounts to 377 billion barrels of left behind U.S. oil identified in OGJ surveys (Moritis, 2004). The growing importance of the recovery of this oil is evident from increased efforts in EOR, especially gas injection EOR.

Injection of gases such as hydrocarbon (HC), carbon dioxide (CO_2), air, Nitrogen (N_2), flue gas etc. for improved light oil recovery has been practiced since the early 1920's. Gas injection refers to those enhanced oil recovery (EOR) techniques whose main oil recovery function is extraction, vaporization, solubilization, and condensation. However, some of the injectants such as CO_2 possess other, important oil recovery mechanisms such as oil viscosity reduction, oil swelling and solution gas drive.

In the earliest applications of gas injection, both liquefied petroleum gas (LPG) and lean hydrocarbon gases constituted the major share of injectants for gas injection EOR. However, this process became economically unattractive with increasing natural gas prices. In the 1970's, renewed interests in gas injection methods, especially CO_2, were

observed, mainly due to the increasing oil prices and improved capabilities in oil recovery estimates by gas injection (Stalkup Jr., 1985). The last two decades have shown a significant increase in CO_2 injection EOR and the hydrocarbon gas injection is losing its applicability due to sustained high natural gas prices (Moritis, 2004). Hydrocarbon injection is still widely practiced in large offshore fields such as Prudhoe Bay, where limited gas processing and transportation facilities are available.

3.1.2.4 Importance of CO_2 as Injectant: U.S. Perspective

CO_2 injection remains an important EOR method in the U.S. in-spite of oil price swings and ownership realignments. The CO_2 process leads the gas injection processes spectrum, complimented with nitrogen and hydrocarbon (HC) processes. This is especially true in the Permian Basin of West Texas and New Mexico. Over 95% of the CO_2 flooding activity is in the United States and mainly in the mature Permian Basin of the southwestern U.S. and dominated by injection under miscible conditions (Christensen et al., 1998; Moritis, 1995).

CO_2 floods demonstrate lower injectivity problems due to its higher viscosity, compared to other common gas injectants. Furthermore, the lower formation volume factor (FVF) of CO_2 and lower mobility ratio make the volumetric efficiency higher for CO_2 than other solvents and solvent mixtures. Another beneficial effect of CO_2 usage is the likelihood of higher gravity segregation within the high water saturation zones of the reservoir than in the higher oil saturation zones. This effect is useful when targeting pockets and bypassed areas of oil and drain them effectively (Hadlow, 1992). The increasing price of natural gas, higher incremental oil recoveries by CO_2, compared to hydrocarbon gases (Rogers and Grigg, 2000) as well as the additional benefit of carbon sequestration tips the scales in favor of CO_2 for future gas injection projects.

The lower costs for implementing CO_2 floods (Figure 3.5) are due to large gas processing facilities as well as huge reserves of almost pure CO_2 (Mississippi, West Texas, New Mexico, Oklahoma, North Dakota, Colorado and Wyoming), supported with extensive CO_2 pipeline infrastructure (Kulkarni, 2003). Projected oil recoveries from these projects are in the order of 7-15% OOIP (Christensen et al., 1998; Rogers and Grigg, 2000). Improved simulation capabilities and reduced development costs have made the CO_2-based processes even more attractive for commercial applications in recent years.

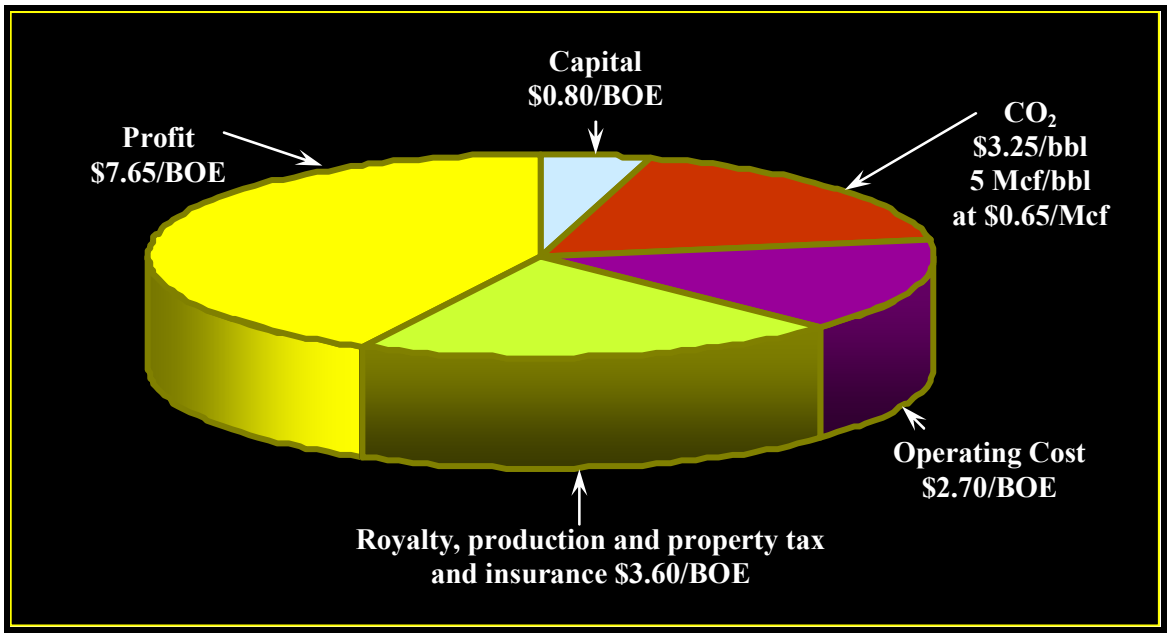

Figure 3.5: Estimated Cost of New CO_2 Flood based on $18/BOE Price (Shows a Profit Potential of more than $7/BOE (Petroleum Engineering International, 1995).

3.1.3 U.S. EOR Scene

Field-scale gas injection applications have almost always been associated with design and operational difficulties. Although, the gas processes demonstrate high microscopic displacement efficiencies, especially under miscible conditions, the volumetric sweep of the flood has always been a cause of concern (Hinderaker et al., 1996). The mobility ratio, which controls the volumetric sweep, between the injected gas and displaced oil bank in gas processes, is typically unfavorable due to the relatively low viscosity of the injected phase. This difference results in severe gravity segregation of fluids in the reservoir, consequently leading to poor flood conformance controls.

Commercial gas injection has traditionally been classified into primarily four types of applications: water-alternating-gas (WAG) injection, down-dip injection, crestal (gas cap) injection, and gas recycle mode injection. WAG injection is generally practiced in normal horizontal reservoirs, where down-dip injection is difficult; and the beneficial gravity effects are difficult to obtain. During WAG applications, water and gas are alternatively injected in predetermined slugs to offset the gravity segregation phenomenon and achieve a uniform and stable flood front (Christensen et al., 1998).

The down-dip injection, with or without WAG, is mostly favored in sloping reservoirs for targeting waterflood residual as well as the 'attic oil' (Jayasekera & Goodyear, 2002). Down-dip injection has been proven to be beneficial even under immiscible injection modes and in cases where reservoir characteristics do not permit a miscible flood, mainly due to interfacial and three phase relative permeability effects.

Crestal injection has been generally found useful to increase reservoir sweeps, in saturated reservoirs with gas cap, and gravity stable displacements using miscible or immiscible gas. Crestal type gas injection has also been employed on some continental shelves (such as U.K. Offshore), but this has usually been driven by the need for gas storage or to manage the position of oil rims under gas caps rather than enhanced recovery (Jayasekera & Goodyear, 2002). Furthermore, improving the liquid recoveries from rich gas condensate reservoirs has also successfully utilized the crestal gas recycle mode process (Jayasekera & Goodyear, 2002).

3.1.3.1 The WAG Process

To increase the extent of reservoir contacted by the injected gas, the water-alternating-gas (WAG) process is the most commonly employed commercial field gas injection process. Conceptually, the WAG process, proposed by Caudle and Dyes (1958), is meant to 'break-up' the continuous slug of gas into smaller slugs by alternating them with water. In the WAG process, the counter tendencies of gas to rise upward and water to descend within the reservoir are supposed to 'compensate' each other to provide a more uniform reservoir sweep of the entire reservoir (Figure 3.6). The WAG process attempts to combine the good microscopic displacement arising from gas injection with improved macroscopic efficiency by injection water to improve the flood mobility ratio.

Today the WAG process is applied to nearly 83% (49 out of 59 field reviews reported (Christensen, 1998)) of the miscible gas injection field projects, and is the default process for commercial gas injection projects. The large-scale WAG applications have been driven by proven improved EOR performances over continuous gas injection (CGI) and their successes on both the laboratory as well as the field-scale(s) (Kulkarni, 2003).

3.1.3.2 Problems Associated with the WAG Process

Since the WAG principle is to improve the flood conformance and 'combat' the natural forces of gravity segregation, the best 'WAG-effects' have been observed in reservoirs with negligible gravity force components i.e. in thin or low permeability reservoirs (Jayasekera & Goodyear, 2002). However, these types of reservoirs represent an insignificant fraction of the gas flood candidate reservoirs, which results in lower than expected WAG recoveries. Even though in most of the reservoirs, the WAG process helps dampen the water-oil-gas segregation due to gravity in the near-wellbore region, the gravity segregation effects' prominence increases as the injected fluids progress away from the wellbore, resulting in a large bypassed zone attributable to the gas over-ride and water under-ride as shown in Figure 3.7. Figure 3.7 clearly shows that although good conformance is achieved by employing the WAG process in the near-well bore region, the natural gravity segregation tendencies of gas and water eventually dominate the

process, thereby resulting in a large un-swept region in the central portion of the reservoir.

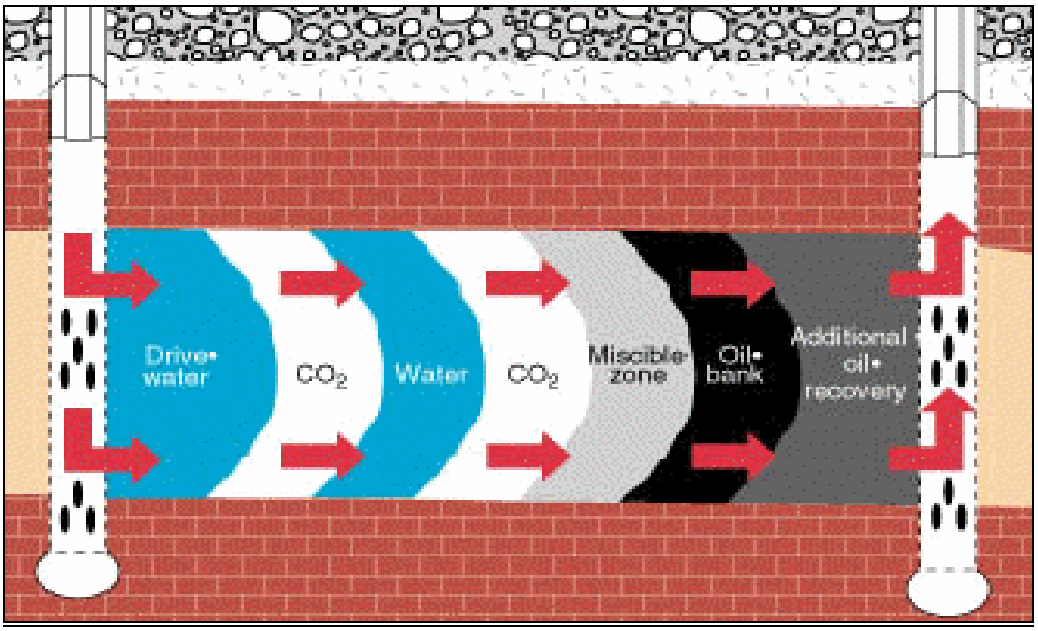

Figure 3.6: Schematic of the WAG Process (Kinder Morgan CO_2 Company Website)

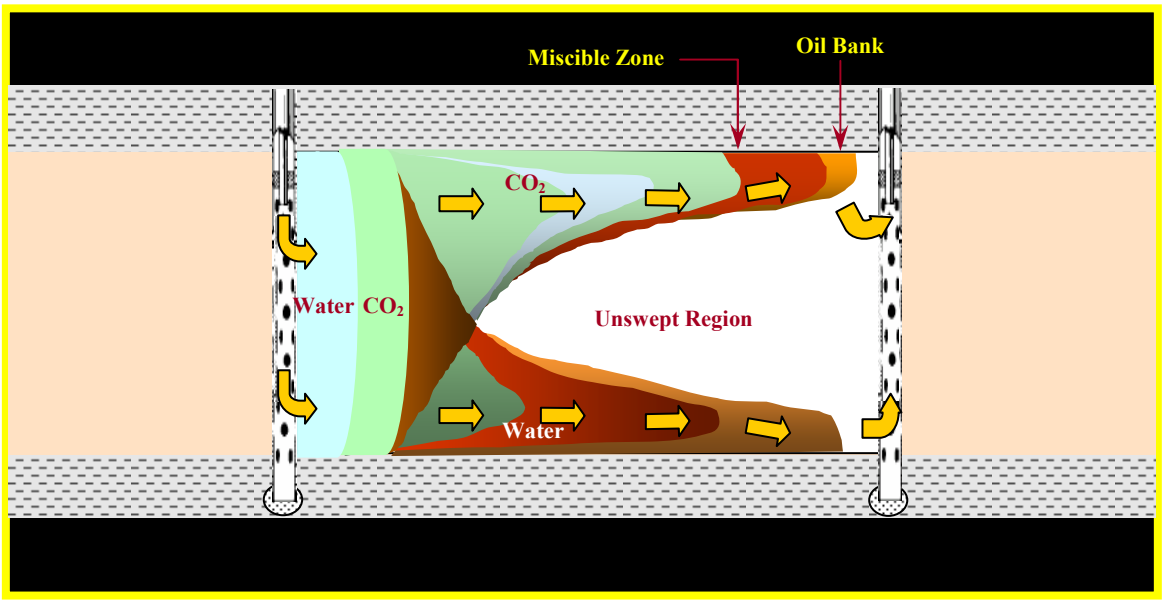

Figure 3.7: More Probable WAG Displacement (Conceptually in Horizontal Reservoirs) (Rao et al., 2004)

Furthermore, water injection for conformance control leads to other mechanistic problems such as increased three-phase relative permeability and water-shielding effects and decreased gas injectivity. These effects could collectively result in injectivity and

operational problems, as well as difficulties in effectively establishing gas-oil contact and miscibility in the reservoir.

Apart from these reservoir problems such as high initial water production, water shielding effect of mobile water, decreased oil relative permeabilities and decreased gas injectivity; operational problems for WAG implementation like corrosion, asphaltene and hydrate formation, and premature gas breakthrough are also perennial (Jackson et al., 1985; Christensen et al., 1998; Rogers and Grigg, 2000).

A review of 59 WAG field experiences by Christensen et al. (1998) clearly concluded that although the WAG process is conceptually sound, its field recovery performance has been low. Of the 59 WAG field experiences they examined (Christensen et al., 1998), a majority of the projects reviewed reported an incremental oil recovery in the range of only 5 to 10% OOIP, with an average incremental recovery of 9.7% for miscible WAG projects and 6.4% for immiscible WAG projects.

3.1.3.3 Proposed Solutions for Mitigating Field WAG Implementation Problems

Although, significant research has been put forth to increase tertiary recoveries from WAG floods have provided with better understanding of the injectivity limitations and WAG ratio optimizations (Christensen et al., 1998), they have had limited success in terms of incremental tertiary recoveries. Proposed modifications for WAG implementation such as the Hybrid-WAG, Denver Unit WAG (DUWAG), Simultaneous WAG (SWAG), foam injection etc. have also met with limited success (Moritis, 1995).

Other research efforts such as gas thickeners (Enick et al., 2000) with gas-soluble chemicals (McKean et al., 1999), and injectant slug modifications (Moritis, 1995) targeted at specific formation types have also been proposed. Although these methods appear promising on a laboratory / simulator scale; important issues such as feasibility, cost, applicability, safety and environmental impact still need to be addressed (Moritis, 1995 and 2004). Furthermore, most of these process modifications are still at inception or experimental stage and are yet to be tested in the field and hence are not accepted as part of the current commercial technology.

It is important to note that all the above newly proposed gas injection methods are still aimed at overcoming the gravity force (consequently the natural phenomenon of gravity segregation) and an ‘attempt’ to improve the flood profile (Moritis, 1995 and 2004). Hence the full utilization of EOR potential (377 billion barrels of target oil) in the United States requires the development of new and more efficient gas injection processes that would overcome the conceptual limitations of the WAG process and its successors.

3.1.4 WAG Process Literature Review

The objective of this section was to summarize the literature's perspective on WAG process. It is important to note that the continuous gas injection (CGI) process has been also classified as a type of WAG process with a WAG ratio of 0:1.

3.1.4.1 Mobility Control Processes

The overall efficiency of the EOR process depends on both, the microscopic as well as the macroscopic sweep efficiencies. Specifically, the mobility ratio controls the aerial sweep in the reservoir, and the vertical sweep is controlled by the difference in the densities of the injected and displaced fluids. The low residual oil saturations in swept zones, and overall poor volumetric reservoir sweep are the main concerns in a gas flood. The 'unfavorable' mobility ratio in gas floods being the main cause, flood profile control in gas floods is instrumental for a successful project.

Continuous research efforts are being made to improve the flood profile control in gas floods[(2)(3)]. These include preparation of direct thickeners with gas-soluble chemicals like Telechelic Disulfate, Polyfluoroacrylate and Fluoroacrylate-Styrene copolymers, which can increase the viscosity of gases several folds (e.g. For CO_2 viscosity increase from 2 – 100 fold). Other methods such as, modifications in the injected slug such as the use of Natural Gas Liquids (NGL) instead of water for highly viscous oils in low pressure, poorly producing and unconsolidated formations are also proposed (Moritis, 1995). Although they seem promising on the laboratory/simulator scale, important issues like feasibility, cost, applicability, safety and environmental impact still need to be addressed (Moritis, 1995).

Most of these process modifications are still at inception or experimental stage and are not accepted as part of the current commercial flooding technology. Moritis (1995), comments on the National Petroleum Council's (NPC) survey conducted for about 27 production, 16 deepwater development and 34 developmental technologies. He predicts that gas thickeners and combustion, thermal and microbial EOR processes will have lower impact in future Research, Development and Demonstration (RD&D). New directional drilling techniques, stimulation and re-completion techniques along with reservoir characterization will be the keys for cost-effective production in the oil and gas industry.

Almost all the commercial miscible gas floods today employ the WAG method (Hinderaker, et al., 1996). The WAG process is shown schematically as Figure 1 below. Gas injection projects contribute about 40% of the total US-EOR production: most of which are WAG floods. Almost 80% of the WAG flood projects in the US are reported an economic success (Hadlow, 1992).

The WAG survey conducted by Hadlow (1992) reported an ultimate recovery of about 8–14% OOIP, based on simulation and pilot tests. However, the more recent survey

of 2001 by Christensen et al. (1998) shows that the average increases in oil recovery were only 5 – 10%. The survey encompassed 59 projects. The popularity of the WAG process is evident from the increasing number of projects and many successful field wide applications (Enick, 2000).

The survey (Christensen et al., 1998) also sheds light on the application scenario and distribution of the WAG process. U.S. had the largest share of WAG applications of 62.7%, followed by Canada at 15.3%. The process was seen mostly applied to onshore reservoirs (88%), but applicable to a wide range of reservoir types, from chalk to fine sandstone. The popularity of the miscible flood was evident from the fact that 79% of the WAG projects employed are miscible. The CO_2 floods lead the WAG applications with a share of 47% of total projects, closely followed by hydrocarbon gas at 42%.

3.1.4.2 WAG Process Classification

The large-scale reservoir applications need a good classification system for better understanding and design of WAG process. Although Claudle and Dyes (1958) suggested simultaneous injection of oil and gas to improve mobility control, the field reviews show that they are injected separately (Christensen et al., 1998). The main reason for this injection pattern is the better injectivity when only one fluid is injected.

Christensen et al. (1998) have attempted to systematically classify the WAG process. They grouped the process into four types: Miscible, Immiscible, Hybrid and Others based on injection pressures and method of injection. Many reservoir specific processes developed have been patented and are generally grouped under the 'other' WAG classification. Some of the examples are the 'Hybrid-WAG' process patented by UNOCAL (Huang and Holm, 1986), and the 'DUWAG' process of Shell (Tanner et al., 1992). These patented processes namely; Hybrid-WAG and DUWAG were developed to optimize recoveries from gas injection processes wherein a large slug of CO_2 is injected followed by 1:1 WAG.

3.1.4.3 Design Parameters for the WAG Process

The WAG review showed that this process has been applied to rocks from very low permeability chalk up to high permeability sandstone. Most of the applied processes were miscible. The miscibility issue is generally based on gas availability, but is mainly reported as an economic consideration and the extent of reservoir repressurization required for process application. The major design issues for WAG are reservoir characteristics and heterogeneity, rock and fluid characteristics, composition of injection gas, injection pattern, WAG ratio, three-phase relative permeability effects and flow dispersion. It is important to note that plain gas injection is considered as a part of WAG process with a WAG ratio of 0:1, hence the design issues pertinent to WAG are applicable to plain gas injection as well.

Reservoir Heterogeneity and Stratification

Stratification and heterogeneities strongly influence the oil recovery process. Reservoirs with higher vertical permeability are influenced by cross flow perpendicular to the bulk flow direction. Viscous, capillary, gravity and dispersive forces generally influence this phenomenon (Rogers and Grigg, 2000). Cross-flow may influence to increase the vertical sweep, but generally the effects are detrimental to oil recovery – mainly due to the gravity segregation and decreased flow velocity in the reservoir. This leads to reduced frontal advancement in lower permeability layer. WAG recoveries and continuous gas injections are more strongly affected by these phenomena. Reservoir heterogeneity controls the injection and sweep patterns in the flood. The reservoir simulation studies (Jackson et al., 1985) for various k_v/k_h (vertical to horizontal permeability) ratios suggest that higher ratios adversely affect oil recovery in WAG process.

Gorell (1990) reported that the vertical conformance of WAG displacements is strongly influenced by conformance between zones. In a non-communicating-layered system, vertical distribution of CO_2 is dominated by permeability contrasts. Flow into each layer is essentially proportional to the fractional permeability of the overall system (average permeability * layer thickness (k*h)) and is independent of WAG ratio, although the tendency for CO_2 to enter the high permeability zone with increasing WAG ratio cannot be avoided. Due to the cyclic nature of the WAG, the most permeable layer has the highest fluid contribution, but as water is injected it quickly displaces the highly mobile CO_2 and all the layers attain an effective mobility nearly equal to the initial value. These cause severe injection and profile control problems. The higher permeability layer(s) always respond first. WAG will reduce mobility not only in the high permeability layer but also in the low permeability layer, resulting in a larger amount of the CO_2 invading in the highest permeability layer.

The ratio of viscous to gravity forces is the prime variable for determining the efficiency of WAG injection process and controls vertical conformance of the flood. Cross-flow or convective mixing can substantially increase reservoir sweep even in the presence of low vertical to horizontal permeability ratios. Heterogeneous stratification causes physical dispersion, reduces channeling of CO_2 through the high permeability layer, and delays breakthrough. This is attributed to permeability and mobility ratio contrasts (Rogers and Grigg, 2000). This is unfavorable and greatly influences the performance of the flood. However, the effects are reservoir specific and the overall effect is dependent on various parameters like permeability, porosity, reservoir pressure, capillary pressure and mobility ratio (Gorell, 1990; Rogers and Grigg, 2000; McCoy et al., 2000; Alvarez et al., 2001).

Rock and Fluid Characteristics

Fluid characteristics are generally black-oil or compositional PVT properties obtained in the laboratory by standardized procedures (Rogers and Grigg, 2000). Very accurate determination of fluid properties can be obtained with current techniques.

However, rock-fluid interactions such as adhesion, spreading and wettability affect the displacement in the reservoir. In reservoir simulators all these rock-fluid interactions are generally lumped into one parameter – relative permeability. The relative permeability is the connecting link between the phase behavioral and transport properties of the system. Relative permeability is an important petrophysical parameter, as well as a critical input parameter in predictive simulation of miscible floods. Relative permeability data are generally measured in the laboratory by standardized procedures with actual reservoir fluids and cores and at reservoir conditions (Rogers and Grigg, 2000).

Injection Gas Characteristics

This issue is more related to the location than the applicability of the reservoir. The question of availability is most important as far as the design criteria are concerned. The CO_2 design criteria suggest a minimum depth limitation as well as dictate the specific gravity and viscosity criteria of the oil to be produced from the concerned reservoir. In offshore fields, the availability of hydrocarbon gas directly from production makes hydrocarbon gas injection feasible. Good example of this issue is the Ekofisk field where miscible hydrocarbon WAG was suggested to be more suitable for Ekofisk, even though CO_2 WAG yielded higher incremental production under laboratory conditions (Jensen et al., 2000). Christensen et al. (1998) suggest that all the offshore fields use hydrocarbon WAG, however the option to use CO_2 is being tested for environmental concerns.

Injection Pattern

The WAG process review (Christensen et al., 1998) clearly shows the popularity of the 5-spot injection pattern with close well spacing on shore. In spite of higher costs, the 5-spot injection pattern with closed well spacing is still popular since it gives better control over the process. Inverted 9-spot patterns are also reported in DUWAG and the Hybrid WAG projects of Shell and Unocal respectively.

Tapering

Tapering is the decrease in gas-to-water ratio as the flood progresses. This is generally done to control the gas mobility and channeling as well as to prevent early breakthrough of the gas. This step is important especially when the injected gas is expensive and needs recycling. Tapering is generally done in most of the CO_2 and hydrocarbon floods and prevailed even in the earliest WAG flood trials (Hadlow, 1992; Christensen et al., 1998).

WAG Ratio

The optimum WAG ratio is influenced by the wetting state of the rock (Jackson et al., 1985). WAG ratio of 1:1 is the most popular for field applications (Christensen et al., 1998). However, gravity forces dominate water-wet tertiary floods while viscous fingering controls oil-wet tertiary floods. High WAG ratios have a large effect on oil recovery in water-wet rocks resulting in lower oil recoveries. Tertiary CO_2 floods controlled by viscous fingering had a maximum recovery at WAG ratio of about 1:1. Floods dominated by gravity tonguing showed maximum recovery with the continuous CO_2 slug process. The optimum WAG ratio in secondary floods was a function of the total CO_2 slug size.

For water-wet rocks, 0:1 WAG ratio (continuous gas injection) is suggested for secondary as well as tertiary floods (Jackson et al., 1985). For a partially oil-wet rock, tertiary gas injection with 1:1 WAG ratio is suggested. The recovery depends on the slug size with larger slug size yielding better results. A 0.6 PV slug size gives maximum recovery, but 0.2 – 0.4 PV slug size is dictated by economics. Tertiary and secondary CO_2 floods (in both oil-wet and water-wet reservoirs) are viscous (or finger) dominated (Jackson et al., 1985). In these cases, miscible CO_2 floods would greatly enhance oil recovery since miscibility reduces fingering considerably.

Flow Dispersion Effects

The WAG injection results in a complex saturation pattern as both gas and water saturations increase and decrease alternatively. This results in special demands for the relative permeability description for the three phases (oil, gas and water). There are several correlations for calculating three-phase relative permeability in the literature[15], but these are in many cases not accurate for the WAG injection since the cycle (water / gas) dependant relative permeability modification and application in most models are not considered. Stone II model is the most common three-phase relative permeability model used in commercial reservoir simulators today; however, it is necessary to obtain experimental data for the process planned.

Gravity Considerations in WAG

Green and Willhite (1998) suggest that the same density difference, between injected gas and displaced oil, that causes problems of poor sweep efficiencies and gravity override in these types of processes can be used as an advantage in dipping reservoirs. Gravity determines the ‘gravity segregation’ of the reservoir fluids and hence controls the vertical sweep efficiency of the displacement process. Gravity-stable displacements of oil by plain gas injection or WAG in dipping reservoirs as secondary or tertiary process results in very high oil recovery. This has been confirmed by laboratory tests, pilot tests as well as field applications (Tiffin and Kremesec, 1986; Chatzis et al., 1988; Thomas et al.,

1990; Bangla et al., 1991; Mungan, 1991; Karim et al., 1992; Kalaydjian et al., 1993; Hinderaker et al., 1996; Audolfo and Jourdan, 1996). Although the purpose of WAG injection is to mitigate the gravity segregation effects and provide a stable injection profile, WAG in downdip reservoirs have shown better profile control and higher recoveries. Hence the gravity considerations in WAG design are indispensable.

Laboratory Studies and Simulation

Detailed laboratory studies coupled with reservoir simulation are of paramount importance for successful WAG design (Sanchez, 1999). The quality of data input to the simulator is the key to provide quality predictions (Prieditis et al., 1991). For compositional simulations phase behavior and slim-tube experiments should be performed and used to tune the EOS model. This tuned model helps in accurate characterization of reservoir fluid. Also relative permeability and capillary pressure hysteresis modeling for three-phase flow is a requirement when simulating miscible WAG floods. Although these compositional effects do not affect immiscible floods to the same extent as in miscible floods, a tuned EOS coupled with an accurate three-phase relative permeability model is required for reliable predictions from the simulation. Significant improvements are being made in three-phase relative permeability models (Blunt, 1999; Moulu et al., 1999; Hustad, 2000; Christensen et al., 2000; Larsen et al., 2000; Dijke et al., 2002). As a result, accuracy of the simulation studies is improving.

3.1.4.4 Need for Miscibility Development

Most of the gas injection processes could be segregated as miscible or immiscible. Gas injection processes are most effective when the injected gas is nearly or completely miscible with the oil in the reservoir (Jakupstovu et al., 2001). The immiscible gas flood increases oil recovery by raising the capillary number due to the relatively low interfacial tension values between the oil and injected gas. In miscible flooding, the incremental oil recovery is obtained by one of the three mechanisms: oil displacement by solvent through the generation of miscibility (i.e. zero interfacial tension between oil and solvent – hence infinite capillary number), oil swelling and reduction in oil viscosity (Schramm et al., 2000).

Miscible flooding has been used with or without WAG for the control of viscous fingering and reduction in gas-oil interfacial tension of the system. Miscibility is achieved by repressurization in order to bring the reservoir pressure above the minimum miscibility pressure (MMP) of the fluids. Christensen et al. (1998) observed that it is difficult to distinguish between miscible and immiscible processes since in many cases multi-contact gas-oil miscibility may have been obtained. This leads to uncertainty about the actual displacement process. Loss of injectivity and/or failure of pressure maintenance in the actual reservoir, attributable to many factors, cause the process to

fluctuate between miscible and immiscible during the life of the process. The author (Hadlow, 1992) also point out that the earlier miscible processes used expensive solvents like propane, which are uneconomical in the present price context. The injectivity problems and pressure loss dictate closer well spacing – hence increased costs – although no severe impairments in the project economics have been reported attributable only to these problems (Hadlow, 1992).

There seems to be no consensus in the literature for the need for development of miscibility in gas floods (Thomas et al., 1995; Schramm et al., 2000; Jakupstovu et al., 2001). Rogers and Grigg (2000) suggest that interfacial tension is the most sensitive and the most easily modified parameter in the capillary number, and suggest that considerable decrease in interfacial tension at relatively low cost is the benefit of miscible flooding. However, overlapping values of interfacial tension for immiscible, near-miscible and miscible floods have been reported (Taber et al., 1996; Christensen et al., 1998; Rao, 2001). Although Rogers and Grigg (2000) suggest a way to improve the capillary number, the issue of viscous forces still needs to be addressed. Viscous forces strongly depend on the reservoir heterogeneities, petrophysical properties and cross-flow in the reservoir, hence are strongly reservoir dependant. Rao (2001) suggests the use of chemicals to alter wettability in non-water wet reservoirs where miscibility achievement (for reduction in interfacial tension) may not be as important as the water-wet reservoirs where miscibility is useful to maximize pore-level displacement efficiency.

3.1.4.5 Effect of Brine Composition

The migration of small solid materials (‘fines’) within porous media has long been recognized as a source of potentially severe permeability impairment in reservoirs (Eng et al., 1993). This impairment has a strong effect on the flow capability (relative permeability) of the reservoir rock. Fines migration occurs when loosely attached particles are mobilized by fluid drag forces caused by the motion of fluid within the pore space. One of the primary factors that determine the migration of clay particles is the brine composition. Laboratory studies (Eng et al., 1993) have shown that brine salinity, composition and pH can have a large effect on the microscopic displacement efficiency of oil recovery by waterflooding and imbibition.

Gray and Rex (Scheuerman and Bergersen, 1990) in their study of the migration of mica needles and kaolinite, found that fines migration, consequently permeability reduction, could be induced by salinity changes or abrupt reductions in the ratio of divalent to monovalent ions present in the brines. Mungan (1965) studied the effects of permeability reduction (‘Core Damage’) due to changes in pH and salinity of the injected brine. He concluded that the permeability reduction occurs, regardless of the type of clay, due to changes in brine salinity.

Capabilities of divalent cations like [Ca^{2+}] and [Mg^{2+}] to control permeability impairment of reservoir due to swelling of clays have been long recognized[39][41][42]. This phenomenon is attributable to the cation exchange properties of clays, which inherently favor the adsorption of [Ca^{2+}] and [Mg^{2+}] ions over [Na^{+}]. The clays in their calcium-form are less easily dispersed compared to the clays with sodium, and they are easily interchangeable by flowing a solution containing other cations (Jones, 1964).

Even though the literature is unison about the effects of brine composition on permeability reduction and fines migration, there seems to be little consensus about the effects of brine composition on oil recovery (either by waterflooding or imbibition). Kwan et al. (1989), in their study of permeability damage via fines migration in extracted core material, concluded that permeability and oil recovery were nearly independent of brine composition. Contrarily, other experimental studies (Jones, 1964; Khilar et al., 1990; Filoco and Sharma, 1998; Tang and Morrow, 1999), suggested that changes in brine composition could have a large effect on oil recovery. This is especially apparent based on wettability.

Waterflooding and core imbibition experiments conducted by Tang and Morrow (1999) with 1% solutions of NaCl, $CaCl_2$ and $AlCl_3$ showed increased waterflood recoveries (forced displacement) and decreased (natural) imbibition rates with increase in cation valency. Generally, oil recovery was found to increase with decrease in brine salinity.

In contrast to the observations of Tang and Morrow (1999), Sharma and Filoco (1998) conducted centrifuge experiments on Berea cores and found that oil recovery via imbibition increases significantly with increasing salinity of connate brine.

3.1.4.6 WAG Literature Review Summary

The gas injection EOR processes today contributes a substantial portion of the oil from light oil reservoirs, next only to thermal processes used in heavy oil reservoirs and their importance is continuing to rise.

Nearly all the commercial gas injection projects today employ the WAG method. The WAG process has long been considered as a tertiary gas injection mobility control process after a secondary waterflood. Previous research and field applications have repeatedly proven the inadequacy of the WAG process, yet it has remained the default process due to absence of a viable alternative. The low recoveries from the WAG process lead to substantial research of the process and consequently some of its limitations are eliminated. In spite of these improvements, the field performance of WAG process is disappointing. Hence the full utilization of EOR potential in the U.S. requires the development of new and more efficient gas injection processes that overcome the limitations of the WAG process.

In the United States, most of the WAG applications are onshore, employing a wide variety of injection gases for a wide range of reservoir characteristics in the miscible mode. Although many types of injectant gases have been used in the commercial WAG floods, CO_2 and Hydrocarbon gases form the major share of injectant types (~ 90%).

The main design parameters that need to be evaluated on a laboratory scale so as to evaluate the feasibility of the process are: Reservoir heterogeneity, rock type, fluid characteristics, injection gas, WAG ratio and gravity considerations. Other important parameters that are important for gas injection and tertiary recovery in general are those of miscibility development and oil / brine composition (characteristics).

CO_2 is ideally suited for the use as an EOR gas in the U.S. scenario. Abundance of reserves of almost pure CO_2 and availability of technical know-how can be instrumental in the growth of CO_2 injection process. Carbon sequestration is an added advantage of the CO_2 injection projects.

3.1.5 Scope for Improvement – Gravity Stable Gas Injection (Gravity Drainage)

In summary, the literature review (Kulkarni 2003) clearly shows that WAG process, plagued with operational problems and poor recovery performance, has prevailed in the oil field, primarily due to the absence of a viable alternative. Although less popular as n EOR method, the gravity stable gas injection, is an attractive method of oil recovery. The drainage of oil under gravity forces, either through gas cap expansion or by gas injection at the crest of the reservoir, has proven to be an efficient gas injection method since it can reduce the residual oil saturation to very low values, when applied in both secondary as well as tertiary modes. These claims are well substantiated via both corefloods and field investigations. These studies experimentally prove that a large amount of incremental tertiary oil can be recovered using gravity assisted tertiary gas injection. Recoveries as high as 85 – 95% OOIP have been reported in field tests and nearly 100% recovery efficiencies have been observed in laboratory floods (Ren et al., 2003).

Conceptually, the gravity stable gas injection takes advantage of the density difference between injected gas and reservoir oil that controls the extent of gravity segregation within the reservoir. The density difference, between injected gas and displaced oil, often cause problems of poor sweep efficiencies and gravity override in horizontal gas floods (such as WAG), but can be effectively used as an advantage in dipping reservoirs (Green and Willhite, 1998). Ironically, although the primary purpose for employment of WAG injection is to mitigate the gravity segregation effects and provide a stable injection profile, WAG or continuous gas injection (CGI) in downdip reservoirs, in secondary as well as tertiary mode, have demonstrated better profile control and higher oil recoveries (Hinderaker et al., 1996). These reviews underscore the benefits of working in tandem with nature by exploiting the natural buoyancy tendency of injected

gas to displace oil downwards (Rao et al., 2004), and indicate that the gravity stable gas injection process appears to be a promising alternative to WAG.

3.1.6 Newly Proposed Gas Assisted Gravity Drainage (GAGD) Process

EOR field applications have repeatedly proven the inadequacies of the WAG process and underscored the viability of the gas gravity drainage process. Furthermore, the consistently successful field applications of the gravity stable gas injections in dipping reservoirs and pinnacle reefs with widely varying reservoir and fluid characteristics, in both secondary and tertiary mode, are also encouraging.

This leads us to the question: why not always inject gas in a gravity-stable mode at the top of the pay zone in order to drain the oil downwards into a horizontal producer? The newly proposed Gas Assisted Gravity Drainage (GAGD) process (Rao, 2001) aims to address this question and to provide with a process which extrapolates the highly successful gravity stable gas injection processes, that have been applied only to dipping reservoirs and pinnacle reefs, to horizontal type reservoirs. The concept of GAGD is depicted in Figure 3.8.

The GAGD process consists of placing a horizontal producer at the bottom of the pay zone and injecting gas through existing vertical wells at the top (into the gas cap) to provide gravity stable displacement and uniform reservoir sweep. CO_2 injected through the vertical wells accumulates at the top of the pay-zone due to gravity segregation and displaces oil, which drains to the horizontal producer straddling several injection wells. With increased cumulative gas injection, the CO_2 chamber grows downward and sideways which results in larger and larger portions of the reservoir being swept, without any increases in the reservoir water saturation, thus maximizing the volumetric sweep efficiency. The natural gravity segregation of CO_2 not only helps in delaying (or even eliminating) the premature CO_2 breakthrough to the producer, but also eliminates the co-current gas-liquid flow mechanics, resulting in lower pressure drops and increased gas injectivity. The oil displacement efficiency within the CO_2 filled chamber can be further maximized by maintaining the injection pressure near the minimum miscibility pressure (MMP), which helps in lowering of the reservoir capillary forces: consequently the residual oil saturations.

For GAGD applications in water-wet formations, it is hypothesized that water is likely to be held back in the rock pores by capillary and surface forces while the oil will preferentially drain to the producer. Opposingly, GAGD applications in oil-wet formations will be aided by the continuity of the oil phase, which would help create continuous oil drainage flow paths to the horizontal producer.

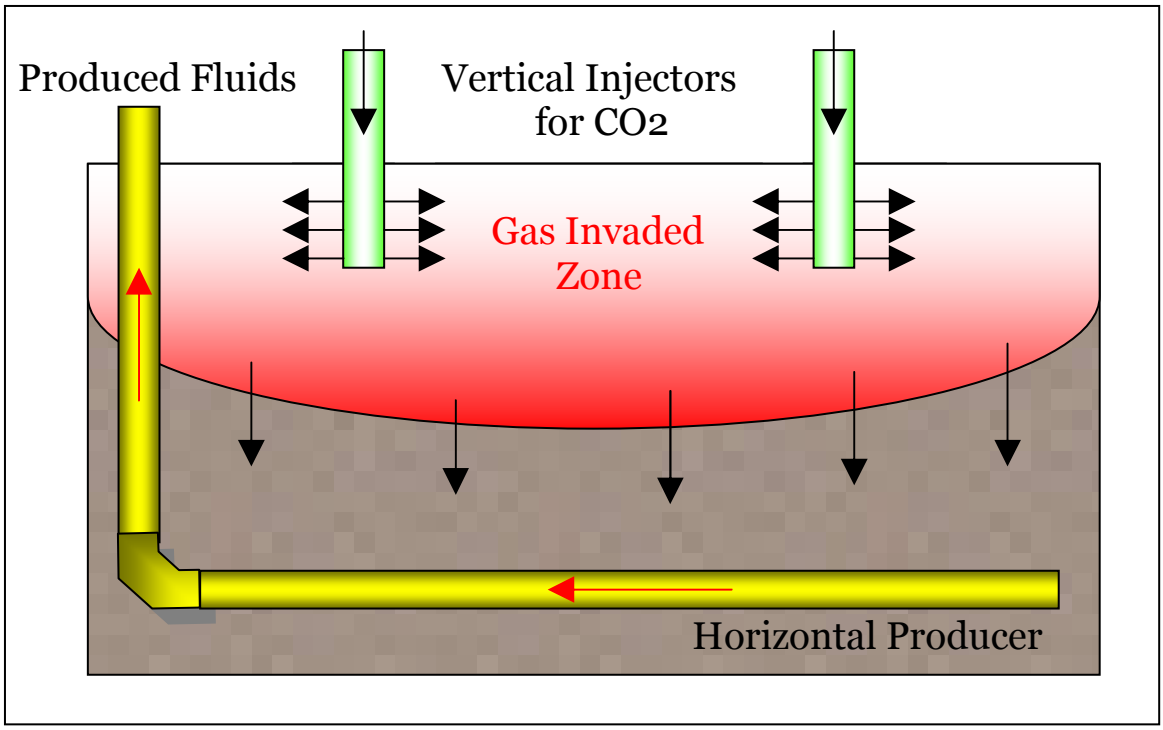

Figure 3.8: Concept of the Gas Assisted Gravity Drainage (GAGD) Process (Rao, 2001)

The proposed GAGD process appears to be capable of not only eliminating the two major limitations (poor sweep and water-shielding) of the conventional WAG processes, but also of significantly increasing oil relative permeabilities in the near producing well-bore regions due to the absence of high water saturation and consequently increasing recoveries.

Because the GAGD process utilizes the candidate field's existing vertical wells for CO_2 injection and requires the drilling of only a few horizontal wells, GAGD capital costs could be kept low. Additionally, the drilling costs of horizontal wells have been continuously dropping due to advancements in drilling technology.

In summary, the proposed GAGD process not only possesses the potential of significantly enhancing ultimate oil recovery, but also holds the promise of delivering this incremental recoveries at production rates comparable to (or even higher than) those achieved by the widely-applied conventional WAG process.

3.2 Problem Definition and Research Objectives

3.2.1 Problem Definition

Although the gas injection EOR has seen steady commercial growth in the last two decades, the overall recoveries have been disappointly low (in the range of 5 – 10% OOIP). This implies that inspite of their economic success, the WAG projects do leave

behind significant quantities of residual oil in the reservoirs. Furthermore, the high saturations of injected water existing at the end of a WAG project, makes the recovery of the remaining oil even more difficult.

This raises several questions: Is there any harm done if the previous secondary recovery was by water flooding? Just for the benefit of 5 – 10% additional oil recovery, have we done more harm than good by injecting large quantities of water into the reservoir during the WAG projects? Has the increased waster saturation rendered the remaining oil even more remote to access? How are the mechanisms of oil recovery and multiphase flow behavior by gas injection affected by increased water saturation? Is there a happy medium between CGI and WAG that could outperform both? Should the gas injection be in secondary or tertiary mode? Is gravity drainage an effective alternative to WAG considering the fact that gravity stable gas injection projects have performed well in dipping reservoirs and pinnacle reefs? How would the relative roles of gravity, capillary and viscous forces change in gravity drainage process versus WAG or CGI? How would the reservoir characteristics (heterogeneity and wettability) affect the gas-oil-water multiphase dynamics in gravity drainage? How would the fluid characteristics (miscibility and gas composition) affect oil recovery performance in gravity drainage? These are some of questions that this research project seeks to address in addition to gaining a better understanding of the underlying mechanisms responsible for the success or failure of any gas injection EOR project.

3.2.2 Research Objectives

The major objectives of this study are to:

1. Study the operative mechanisms of multiphase coexistence in reservoirs:
   (i) Identification of operative mechanisms via dimensional analyses.
   (ii) Investigating the effect(s) of positive and negative spreading coefficients, obtained by using various fluid triplets, on gravity stable gas injection performance.
   (iii) Investigation of the effects of miscibility development on various commercial modes of gas injection, namely CGI, WAG, Hybrid-WAG and the newly proposed Gas Assisted Gravity Drainage (GAGD) process.
   (iv) Identifying the effects of reservoir mobile water saturation, by comparison of the performance characteristics of gas injection floods in secondary and tertiary modes.
   (v) Characterization of the effects of reservoir wettability and possible wettability alteration effects (if any) operational during gas injection EOR processes.
   (vi) Identification and characterization of the relative importance of gravity / capillary / viscous force effects in gas injection processes.
   (vii) Investigation of the effects of reservoir heterogeneity on gas injection EOR performance.
2. Study the multiphase fluid dynamic characteristics in gas injection EOR:

(i) Characterization of the effect(s) of multiphase mechanisms (such as gravity segregation, wettability, spreading coefficient, miscibility, etc.) on fluid dynamics namely relative permeability and oil recovery.
(ii) Comparing and correlating various laboratory and field scale studies.

3.3 Gravity Drainage Literature Review

Schechter and Guo (1996) provided a comprehensive review of the gravity drainage literature and suggested that three different gravity drainage processes can occur in porous media, namely: (i) forced gravity drainage by gas injection at controlled flow rates into steeply dipping reservoirs, (ii) simulated gravity drainage by centrifuging (existing only in laboratories), and (iii) free-fall (or pure) gravity drainage which takes place in naturally fractured reservoirs after depletion of oil from fractured or gas injection into a depleted fractured reservoirs.

Since only the first and third gravity drainage processes discussed above are relevant to the GAGD process being developed in this study, this literature review focuses on these two gravity drainage processes. The literature review details: (i) displacement stabilities for gravity stable gas flow through porous media, (ii) gravity drainage fundamentals and traditional models, (iii) various laboratory studies on gravity drainage and (iv) various field applications of gravity drainage.

3.3.1 Displacement Instabilities for Gravity Stable Gas Flow through Porous Media

Although less popular as an EOR method, the gravity stable crestal or downward displacement type injection, either through gas cap expansion or by gas injection at the crest of the reservoir is an attractive method of oil recovery. The drainage of oil primarily under the influence of gravity forces (gravity drainage) has been found to be an efficient improved recovery method (Rao et al., 2004), since it can reduce the remaining oil saturation to below that obtained after secondary recovery techniques. It is important to note that the literature review on the mechanistic characterizations of gas injection processes is applicable to all processes; however the emphasis of this review is on gravity stable gas injection.

The presence of viscous forces in a gas injection process may result in unstable flood fronts. Gas injection for EOR results in a finite viscous force acting on the gas-liquid interface. Because in any gas injection process (horizontal or gravity stable), the mobility ratio is typically unfavorable, the development of unstable fingers during gas displacements is imperative. The macroscopic and microscopic heterogeneities result in unequal displacement rates between the gas and in-situ fluids, thus magnifying this 'fingering' phenomenon. In horizontal mode floods, various modifications in gas injection protocol are followed to mitigate this phenomenon, but have met with limited success – mainly due to the unfavorable gravity forces (as discussed in Chapter 1).

On the other hand, in vertical (gravity stable) gas floods, this unfavorable mobility ratio is generally attempted to overcome by reducing the viscous force magnitude (by decreasing the injection rates), and allowing the favorably acting gravity forces to stabilize the gas front. The maximum (vertical) gas injection rate allowable in a given reservoir to achieve a stable flood front is called as the 'critical rate'. Mechanistically, the critical rate represents the injection rate wherein the favorable gravity force effects are overcome by the increased magnitude of viscous forces.

For miscible gravity stable flood, Hill (1952) derived a critical velocity expression to predict the rates above which viscous instabilities can occur due to gravity forces being overshadowed by viscous forces. This equation (Equation 3.1) assumed a single interface contact between the injected and displaced phase with no mixing of solvent and oil behind the front.

$$V_C = \frac{2.741 \Delta\rho k Sin\theta}{\phi \Delta\mu} \quad \text{..... (3.1)}$$

Where:

V_C = Critical vertical injection rate (ft/d)

$\Delta\rho$ = Density difference (gm/cc)

k = Permeability (D)

θ = Dip angle (degrees – measured from horizontal)

ϕ = Porosity (fraction)

$\Delta\mu$ = Viscosity difference (cP)

Dietz (1953) also proposed a method of analysis of stability of a vertical flood front with the following assumptions: homogeneous porous medium, vertical equilibrium of oil and water, piston displacement of oil by water, no oil-water capillary pressures, and negligible compressibility effects of rock and fluid. The Dietz equation is given by Equation 3.2 below.

$$\tan\beta = \frac{1 - M_e}{M_e N_{ge} Cos\theta} + \tan\theta \quad \text{.....with } \beta > 0 \text{ being the stability criterion.....} \quad \text{(3.2)}$$

Where,

M = Mobility Ratio

N_{ge} = Gravitational force

Dumore (1964) eliminated the limitation of the Hill (1952) equation which assumed that for vertical gas-liquid displacements, the solvent and oil do not mix, and derived a new frontal stability criterion (summarized in Equation 3.3). Interestingly, the Dumore stability criterion is more stringent than the Hill criterion, and for all rates lower than V_{st}; each infinitesimal layer of the mixing zone is stable with respect to each successive layer.

$$V_{st} = \frac{2.741 k Sin\theta}{\phi} \left(\frac{\partial\rho}{\partial\mu}\right)_{\min} \quad \text{..... (3.3)}$$

Where

V_{st} = Critical velocity for stable vertical flow of gas (ft/D)

Rutherford (1962; Mahaffey et al., 1966) developed a stability criterion for miscible vertically oriented corefloods in laboratory. The equation is given as Equation 3.4 below.

$$(q/A)_{CRITICAL} = 0.0439\frac{k*(\rho_O - \rho_S)}{\mu_O - \mu_S}Sin(\theta) \quad \text{..... (3.4)}$$

Where,

(q/A) = Critical velocity for stable flow (ft/D)

μ_O = Viscosity of Oil (cP)

μ_S = Viscosity of Solvent (cP)

Brigham (1974) observed that the estimate of stability of a coreflood front could be obtained by measuring mixing zone length. The mixing zone length could then be used to calculate the effective mixing coefficient (α_e) an important reservoir simulation parameter. Perkins (1963) and Brigham (1974) solved the diffusion-convection equation and concluded that by measuring the mixing zone between 10% and 90% injected fluid concentrations at the core exit; the effective mixing coefficient (α_e) can be easily determined. Brigham (1974) suggested that in the absence of viscous mixing, the effective mixing coefficient (α_e) is a function of the porous medium only and typical values for Berea are 0.005 ft in laboratory scale systems.

Slobod and Howlett (1964) derived a critical injection velocity equation for gravity stable displacements' frontal stability in homogeneous sand packs and is given in Equation 3.5.

$$V_C = \frac{k_o}{\Delta\mu}(\Delta\rho g) \quad \text{..... (3.5)}$$

Among all the available analytical models in the literature to determine the critical gas injection rates (and promote stable displacement fronts) in gravity stable (vertical) gas injection floods, the Dumore (1964) criterion appears to be the most popular in the industry. The Dumore criterion has been widely applied, inspite of newer models being available (Piper and Morse, 1982; Skauge and Poulsen, 2000; Pedrera et al., 2002; Muggeridge et al., 2005).

3.3.2 Gravity Drainage Fundaments and Traditional Models

Gravity drainage is defined as a recovery process in which gravity acts as the main driving force and where gas replaces the voidage volume (Hagoort, 1980). Gravity drainage has been found to occur in primary phases of oil production through gas cap expansion, as well as in the latter stages wherein gas is injected from an external source. Muskat (1949) provides a detailed review on the effects of gravity forces in controlling oil and gas segregation during the primary-production phase of gas drive reservoirs. It

was suggested that the most efficient type of gravity-drainage production would be an idealized case wherein no free gas is allowed to evolve in the oil zone by maintaining the reservoir pressure above its bubble point, or by pressure maintenance at current GOR levels (Muskat, 1949).

The literature employs the words 'gravity stable gas injection' and 'gas gravity drainage' interchangeably. Identification of the conceptual mechanistic differences between gravity stable gas injection, and 'pure' gas gravity drainage has been attempted in this study, and are detailed in following sections.

The importance of gravity drainage as an important oil recovery mechanism has been well recognized. Gravity drainage has been observed to occur during gas injection (Muskat, 1949) as well as in the stripper stages of volumetric reservoirs (Matthews and Lefkovits, 1956). Field and laboratory experience has shown that that gravity drainage, under certain conditions, can result in very high oil recoveries and also, that gravity drainage is one of the most effective mechanisms of developing an oil field (see Section 3.4).

In spite of the fact that one of the earliest gravity drainage models appeared in 1949, the "…characterization and modeling of the (gravity drainage) process are still a great challenge (Li and Horne, 2003)". This review attempts to provide a mechanistic understanding of the forced gravity drainage process, the fundamental mechanism involved in the GAGD process.

3.3.2.1 Drainage or Displacement?

Literature seems to use the words 'gravity stable gas displacement' and 'drainage' interchangeably. Many authors suggest the drainage process to be a type of displacement mechanism with the classical theories of Buckley-Leverett (1942), Darcy's law, relative permeability, continuity equation, and decline curve analysis (material balance equation) to be applicable (Terwilliger et al., 1951; Hagoort, 1980; Li et al.; 2000).

However, Muskat (1949) suggested that although the classical theories of Darcy and Buckley-Leverett are relevant, the decline curve equation, applicable to most displacements, does not in itself provide any information regarding the gravity drainage phenomenon. The decline curve method represents only the thermodynamic equilibrium between the net liquid / gas phases in the reservoir and hence cannot characterize the mechanistic and fluid-dynamic aspects of the gravity drainage process. This statement of Muskat (1949) seems to be supported by many researchers (Cardwell and Parsons, 1948; Richardson and Blackwell, 1971; Pedrera et al., 2002; Li and Horne, 2003) which suggest that "Gravity drainage can be modeled by conservation equation, Darcy's law and capillary pressure relationship (Pedrera et al., 2002)".

Most of this confusion about gravity drainage characterization appears to stem from ignoring the injection gas pressure distribution as well as due to the application of 'pure'

or ‘free’ gravity drainage theory (Cardwell and Parsons, 1948) to forced gravity drainage applications or vice-versa.

3.3.2.2 Gravity-Drainage / Buckley-Leverett Displacement Mechanisms and Models

To facilitate the differentiation between displacement and drainage, the original Buckley-Leverett (1942) displacement theory and the gravity drainage theory (Cardwell and Parsons, 1948) were critically examined and the resulting inferences are summarized below.

Classical Displacement Theory

Buckley and Leverett (1942) first described the mechanism of displacement and also proposed an analytical model to determine the oil recovery by gas or water injection into a linear (horizontal mode) oil reservoir. The Buckley-Leverett (B-L) model (Equation 3.6) considers a small element within a porous medium and expresses the displacement rates in terms of accumulation of the displacing fluid (material balance theory is applicable).

The B-L displacement theory also suggests that after displacing phase breakthrough, the oil production rate changes (generally decreases) in proportional to its saturation. Since the oil saturation decreases continually after breakthrough, the oil production rate also drops with time. Additionally, for pure piston-like displacement (B-L displacement) in water-wet systems (ignoring the capillary pressure effects), water floods demonstrate a ‘clear’ breakthrough, i.e. no additional oil is produced after the water breaks through at the producing well. If the capillary pressure effects are included, the size of the oil bank increases with proportional decrease of the oil saturation from the leading to the trailing edge (Buckley and Leverett, 1942; Welge, 1952)

$$\left(\frac{\partial S_D}{\partial \theta}\right)_u = -\frac{q_T}{\phi A}\left(\frac{\partial f_D}{\partial u}\right)_\theta \qquad \text{(3.6)}$$

Where, S_D is the saturation of the displacing fluid, A is the cross-sectional area of flow, θ is the time, q_T is the total rate of flow through the section, u is the distance along the path of flow, ϕ is the porosity, and f_D is the fraction of flowing stream comprising of the displacing fluid.

However, inspite the fact that the original B-L model was hypothesized to be applicable to gas floods as well, the two assumptions used by B-L model, no mass transfer between phases and incompressible phases, result in severely limiting its application to GAGD type (gravity drainage) floods.

Buckley-Leverett's Perspective about Gravity Drainage

The original paper by Buckley and Leverett (1942) suggests that the gravity drainage phenomenon is "exceedingly slow" and is defined as the 'mechanism in which no other forces in the reservoir, except gravity, are available to expel the residual oil'. Although Buckley and Leverett (1942) suggest that the 'mechanism by which the area of high gas saturation invades the area of high oil saturation is very similar to that by which water encroaches into and displaces oil from a sand'; they also acknowledge that 'in gas displacing oil systems, simultaneous three phase flow in the reservoir results in non-piston like displacements and complete displacement never occurs!'.

Classical Drainage Theory

The earliest known analytical theory on gravity drainage was that of Cardwell and Parsons (1948), which derived a gravity drainage model based on hydrodynamic equilibrium equations in vertically oriented sand packs. The original theory assumed a free gas phase draining a single liquid phase, and suggested that the liquid recovery is equal to the percentage of the total area above the height versus saturation curve. One of the most important requisites to gravity drainage is the absolute pressure equilibrium between the gaseous and liquid phases. In other words, the gas zone does not exert a vertical pressure gradient on the gas-liquid interface.

Interestingly, Cardwell and Parsons (1948) acknowledge that only a slight pressure gradient in the gas zone is sufficient for the B-L theory to be applicable. This statement seems to be the reason for non-distinction between displacement and drainage, since in real oil-gas-water systems, reservoir pressure maintenance and gas injection result in a finite pressure gradient on the gas-liquid flood front.

A gravity drainage model similar to that of Cardwell and Parsons (1948) was proposed by Terwilliger et al. (1951). Terwilliger et al. (1951) applied the B-L immiscible displacement theory and the 'shock-front' technique (using fractional gas flow equations (Welge, 1952)) to match the steady state gravity drainage laboratory experiments (assuming steady-state relative permeability and static capillary pressure distribution). Terwilliger et al. (1951) also showed that recovery by gravity drainage is inversely proportional to production (conversely, injection) rates and recommended a "maximum rate of gravity drainage" or "gravity drainage reference rate" (Equation 3.7). Equation 6 appears to be the theoretical basis for the "critical injection rate" and "frontal stability" equations developed by various researchers (Hill, 1952; Dietz, 1953; Perkins and Johnston, 1963; Dumore, 1964; Brigham, 1974; Moissis et al., 1987; Ekrann, 1992; Virnovsky et al., 1996) for commercial gravity drainage applications.

$$GRR = \frac{K_L A}{\mu_L} g \Delta p Sin\alpha \quad \text{..... (3.7)}$$

Where, K_L is the effective permeability to liquid at 100% liquid saturation, A is the cross-sectional area of flow, μ_L is the liquid viscosity, g is the gravitational constant, $\Delta\rho$ is the density difference between liquid and gas, and α is the angle of dip.

3.3.2.3 Traditional Gravity Drainage Models

Although Cardwell and Parsons (1948) and Terwilliger et al. (1951) models first presented the governing equations for the gravity drainage process, the non-linearity of the equations forced them to ignore two important parameters: (i) the capillary pressure variation with saturation and (ii) capillary pressure dependence on permeability.

Although, Nenniger and Storrow (1958) provided an approximate series solution (obtained from film flow theory) to predict the gravity drainage rates on a glass bead pack, the next important development in gravity drainage modeling was the generalization of the Cardwell and Parsons (1948) theory (Dykstra, 1978) by improving the capillary pressure representation in the governing equations. Using similar analysis and procedures, Hagoort (1980) also developed a theoretical analysis to predict forced gravity drainage recoveries, by simultaneously employing the B-L and Cardwell and Parsons (1948) theory. Although the model was significantly improved over the classical gravity drainage theory by modeling the capillary function as a Leverett J function, analytical solution of the model is not feasible due to the resulting non-linear governing equation.

Richardson and Blackwell (1971) presented a radically different 'hybrid' approach to predict gravity drainage recoveries for a variety of scenarios such as: vertical flow conditions, water under running viscous oils, gravity segregation of water banks in gas caps, and for control of coning by oil injection. They combine the Buckley and Leverett (1942), Cardwell and Parsons (1948) and Welge (1952) theories with the Dietz (1953) frontal stability criterion to predict the ultimate oil recoveries, when the injection rate is less than one-half of the Dietz's (1953) critical rate.

Pavone et al. (1989) and Luan (1994) revisited the 'demarcator' concept introduced by Cardwell and Parsons (1948) to generate analytical models for gravity drainage in low IFT conditions and fractured reservoir systems, respectively. The 'demarcator' is defined (Cardwell and Parsons, 1948) as the region of minimum gas saturation in the systems. They also showed that assuming the demarcator at the bottom (or outlet) of the reservoir, improves the model prediction.

Blunt et al. (1994) developed a theoretical model for three-phase gravity drainage flow through water-wet porous media based on a wide range of experiments, from molecular level to glass bead packs. These studies suggest that best tertiary gravity drainage efficiency in water-wet systems occurs when the oil spontaneously spreads as a layer between water and gas (under positive spreading coefficient conditions).

Li and Horne (2003) claim that "…the analytical models do not work well…" for gravity drainage recovery predictions, an empirical approach is more suitable. They proposed an empirical oil recovery model to match and predict oil production, which was tested against experimental, numerical and field data.

3.3.3 Gravity Drainage Fundaments and Traditional Models

Mechanistic reviews (provided earlier in Section 3.3.2) on pure gravity drainage and gravity stable gas injection processes suggest that they are the two ends of the gravity stabilized (vertical) gas injection processes. This section therefore summarizes the laboratory experiments conducted for the characterization and optimization of the vertical gas injection process, since the forced as well as free gravity drainage processes are relevant to the GAGD process.

Although, Leverett's (1941) studies on capillary behavior in porous media appear to be foremost of the documents suggesting the importance of gravitational and capillary forces in immiscible gas injection processes; Katz's (1942) studies on vertical sand packs supplied the experimental evidence to confirm Leverett's (1941) hypothesis. The experimental as well as analytical studies (Stahl et al., 1943; Lewis, 1944; Terwilliger et al., 1951; Higgins, 1953) that followed this pioneering work, stressed on the importance of 'gravity-stabilization' of the flood front by controlling flow rates, fluid properties and injection temperatures, for improved oil recovery factors from gravity stable gas injection (gravity drainage) floods.

Since most of the latter (mid 1950's to early 1970's) experimental work involving gravity drainage experimental studies, conducted for improved understanding of the gravity drainage process, was focused on solving the non-linear gravity drainage models resulting from application of Darcy's law, Buckley-Leverett theory and continuity equations to gravity drainage process (see Section 3.2), minimal mechanistic and fluid dynamic studies are resulted during this period.

Dumore and Schols (1974) conducted gravity stable gas displacement experiments in high permeability oil saturated cores. They observed that the presence of connate water is critical for achieving very low oil residual saturations during gravity drainage floods, under high gas-oil capillary pressures, irrespective of whether or not the oil spreads on water in the presence of gas. Interestingly, Dumore and Schols (1974) attribute the achievement of low residual oil saturations to possible 'film flow'. This appears to contradict their previous inference that the oil spreading need not occur in presence of gas, and that the contribution of oil from film flow in secondary gas caps is negligible.

Centrifuge gravity drainage experiments by Hagoort (1980) conducted using various consolidated outcrop and field cores suggested that the gravity drainage was a "very effective" process in water-wet, connate water bearing reservoirs. The results were analyzed using the Buckley-Leverett displacement theory (forced gravity drainage) and

the author suggested that the oil relative permeability was a key parameter during the gravity drainage process. It was also suggested that the centrifugal relative permeabilities are representative of the gravitational relative permeabilities if the microscopic flow regimes in the centrifuge were similar to those in reservoir floods, as characterized by the Dombrowski-Brownell (N_{DB}) number. Hagoort (1980) suggested that a value of less than 10^{-5} for the Dombrowski-Brownell number, results in the microscopic flow being capillary dominated, and that a N_{DB} value of greater than 10^{-3} would make the centrifugal gravity drainage experiments unrealistic. These observations appear to be supported by the experimental results presented by Danesh et al. (1989).

Tiffin and Kremesec (1986) conducted a series of gravity-assisted vertical core displacements of both first contact miscible and multiple contact miscible type, with CO_2 – recombined crude oil systems at various pressures and temperatures. The authors suggested that downward gravity assisted displacement recoveries, even at injection rates significantly higher than the critical rates, are more efficient than horizontal floods at similar rates. This inference appears to contradict the original gravity drainage theory (hypothesized by Terwilliger et al. (1951)) which predicts similar recoveries for both scenarios. Tiffin and Kremesec (1986) also attempted to experimentally determine the mixing lengths required for miscibility development, and reported that while miscibility development in vertical core displacements was at similar pressures as their horizontal counterparts; miscibility was achieved in the downward gravity assisted displacements at a considerably shorter core length. This study also demonstrates that component mass transfer, similar to those in multiple contact miscible processes, strongly (negatively) affect flood front stability and that displacement efficiency increases at lower fluid cross flow and mixing conditions.

Kantzas et al. (1988) identified two possible mechanisms for gravity drainage processes by conducting gravity assisted inert gas injection experiments in 2-D micromodels and unconsolidated columns of glass beads. Along with excellent oil recoveries observed (99% in unconsolidated columns and about 80% in the others), they identified two distinct displacement mechanisms for gas injection into discontinuous oil films, termed gravity drainage mechanism and leakage mechanism. For gravity drainage mechanism, the injected gas (air) was observed to advance at slow flow rates, and an oil bank was formed behind the free water zone and the bulk gas zone. On the other hand, during the leakage mechanism, the injected gas advanced rapidly to the production end and bypassed the isolated oil globules, resulting in poor sweeps. Interestingly, these experiments demonstrated that the discontinuous oil globules can be reconnected and displaced by decreasing (or stopping) the injection rate.

Chatzis et al. (1988) carried out downward displacements of oil by injection of inert gas at initial and waterflood residual oil saturations. Very high recovery efficiencies under strongly water-wet systems in consolidated or unconsolidated porous media were

observed. Further experimentation with CT scans and regular capillary tubes for immiscible gravity stable inert gas displacements concluded that very high recoveries under these conditions were only possible when oil spread over water, the reservoir was strongly water-wet and a continuous film of oil existed over the water in the corners of the pores invaded by gas. The spontaneous spreading of oil at the water-gas interface occurred in the case of water-wet rock samples and positive spreading coefficients. It should be noted that this inference appears to contradict all the previously summarized gravity drainage studies, which suggested that spreading of the oil is not required for achieving very low residual oil saturations.

Meszaros et al. (1990) examined the potential use of inert gas (N_2 and / or CO_2) injection using horizontal injection and production wells in scaled physical model studies at experimental pressures ranging from atmospheric to about 609 psi (4200 kPa). This investigation appears to be aimed at the verification of the Dumore (1964) stability criterion and experimental verification of the two extreme scenarios obtainable during gravity stable gas injection, namely pure gravity drainage and vertical gas injection performance approaching horizontal floods (as proposed by Terwilliger et al. (1951)). Numerical simulation coupled with physical model studies clearly demonstrated the need for gravity-stabilization of the flood front for higher recovery factors and that a slanting or horizontal front propagation (probably due to increased injection rates) results in severe reduction in recoveries.

The experimental and numerical observations of Meszaros et al. (1990) appear to fortify the original assumptions (hypothesis) of gravity drainage proposed by Terwilliger et al. (1951) and Muskat (1949) (but contradict the inferences of Tiffin and Kremesec (1986)). The two extreme possible scenarios hypothesized are clearly observed in the experimental results, however the oil production patterns appear to contradict the Muskat's (1949) theory. Muskat (1949) suggested that the ideal scenario for gravity drainage would be wherein the reservoir pressure is held constant and oil is allowed to drain only under the influence of gravity. Two important observations from the experimental results of Meszaros et al. (1990) are interesting: (i) the pure gravity drainage experiment produces at the lowest rate (i.e. higher pressured gravity stable experiments demonstrate higher production rates), and (ii) the pure gravity drainage flood continues to produce for a significantly longer time as compared to its higher pressure counterparts.

CO_2 cyclic (or huff-and-puff) injection in Berea cores using live oil samples for gravity stable (vertical) displacements and dead oil samples with horizontal cores were studied by Thomas et al. (1990). It was found that an existence of a gas cap, gravity segregation as well as higher residual oil saturations increased overall oil recovery in gravity-stable floods. Moreover, it was observed that gravity segregation (beneficial in

gravity-stable floods) helped deeper penetration of CO_2 (hence better recovery), and accidental injection of CO_2 in gas cap did not have detrimental effects on recovery.

Mungan (1991) conducted miscible and immiscible coreflood experiments using heavy and light oils with CO_2. It was concluded that CO_2 could increase heavy oil recovery even without miscibility development. Furthermore an increase in breakthrough recovery from 30% to 54% was observed when CO_2 was used instead of CH_4 as a displacing fluid.

Karim et al. (1992), similar to Thomas et al. (1990), conducted CO_2 cyclic (huff-and-puff) coreflooding experiments using 6-ft long Berea cores and Timbalier Bay light crude. The core inclination was found to substantially influence the oil recovery efficiencies and gas utilization factors of the coreflood and the 'best' performance was observed when CO_2 was injected into the lower end of a core tilted at a 45 or 90^o angle.

Barkve and Firoozabadi (1992) derived the initial (also the maximum) gravity drainage rate (q_o) for an immiscible process in a homogeneous rock matrix, and is given by Equation 3.8.

$$q_o = \frac{k_o}{\mu_o}(\Delta\rho g - (P_c^{(TH)} / L)) \quad \text{(3.8)}$$

Where:

k_o = Single phase oil permeability

μ_o = Oil viscosity

$\Delta\rho$ = Density difference between injected / displaced fluids

g = gravitational acceleration

$P_c^{(TH)}$ = Threshold capillary pressure

L = Height

Infinite gas mobility during displacement is one in the assumptions used in the Barkve and Firoozabadi's (1992) derivation. The authors reported that in the initial phase, the gravity drainage rate in fractured media does not exceed the un-fractured media, provided the fractures have negligible storage. In developed flow conditions, the capillary pressure contrast between the matrix and fracture, results in lower gravity drainage rates in case of fractured media.

For miscible displacements (capillary pressure = 0), the ($P_C^{(TH)}$/L) term in Equation 3.8 becomes negligible and therefore, the initial (also the maximum) gravity drainage rate (q_{om}) in a homogeneous rock matrix is simplified as (Equation 3.9):

$$q_{om} = \frac{k_o}{\mu_o}(\Delta\rho g) \quad \text{(3.9)}$$

Interestingly, comparison of Equations 3.5 and 3.7 shows that the capillary force term becomes negligible during miscible gravity dominated flows. The decrease in the density difference ($\Delta\rho$) term due to miscibility development also decreases the maximum

miscible oil drainage rate (q_{om}) achievable, as compared to immiscible critical rates (q_{oc}) wherein the density difference ($\Delta\rho$) term is high due to negligible injected gas viscosity.

Kalaydjian et al. (1993) conducted sand-pack experiments in both horizontal and gravity stable modes. These results were similar to the previous experimental findings that the gravity stable floods had higher (approx. 30% OOIP) incremental recoveries over horizontal floods.

Longeron et al. (1994) studied the influence of capillary pressure on oil recovery by compositional simulation. The gas-oil capillary pressures were always found to be higher in the presence of connate water, as compared to the capillary pressures displayed in the absence of connate water saturation. However, the authors suggested that recovery was very sensitive to capillary pressure input data, and "using scaled capillary pressures from mercury-air data, the recovery is underestimated by about 6% PV". These inferences reinforce the general notion that effective modeling of the capillary pressures in gravity drainage floods is still a challenge (see Section 3.2).

Catalan et al. (1994) reported the results on low pressure inert gas injection assisted by (forced) gravity drainage experiments on short core plugs with varying wettability and heterogeneity characteristics. They concluded that tertiary gravity drainage in water-wet systems is most efficient when the oil can spread on water in the presence of gas. Furthermore, the experimental results also suggested that the oil-wet nature of the porous medium was not detrimental to the oil recovery factors. These observations appear to be supported by both theoretical as well as experimental gravity drainage floods in both secondary as well as tertiary modes (Blunt et al., 1994; Oyno et al., 1995).The additional contribution of Oyno et al. (1995) was that they experimentally demonstrated the dependence of the time required to reach gravity/capillary equilibrium on oil-gas density difference, oil-gas interfacial tension, and molecular diffusion between the two bulk phases. However, the identification of the conditions at which individual factors dominate is still an open question.

Chalier et al. (1995) employed the gamma ray absorption technique to visualize fluid saturation distribution in the core as a function of injected gas volume at reservoir conditions. The authors experimentally demonstrated that gravity drainage proves to be a "very efficient" process in a water-wet (sandstone) reservoir under positive spreading coefficient conditions.

Vizika and Lombard (1996) discussed the effect of spreading and wettability on gravity drainage oil recovery in water-wet, oil-wet and fractionally-wet porous media. The authors experimentally demonstrated that in water-wet porous media, oil recovery depends on the spreading coefficient value, while the spreading coefficient "does not affect the process efficiency" in oil-wet media. The highest oil recoveries were obtained with water-wet and fractional wet media under positive spreading coefficient conditions; while the oil recoveries were found to deteriorate when the spreading coefficient value

was less than zero (or negative). Numerical simulation to match the experimental results showed that the lowest oil recoveries were obtained in oil-wet porous media. However, continuous oil (wetting) films were still observed, but were found to be subjected to strong capillary retention. This observation is extremely important for commercial GAGD applications in oil-wet reservoirs, and suggests that miscibility development (to alleviate the capillary retention of oil) would be beneficial in such cases.

Saputelli et al. (1998) examined the physics of gravity effects that compete with capillary forces, under different scenarios of wettabilities, density differences, and low IFT differences for multi-phase coexistence in porous media. The authors reported that for the same positive spreading coefficient values, the gravity drainage is significantly less efficient in oil-wet system as compared to the water-wet system. Furthermore, the oil recovery by gravity drainage was found to be independent of spreading conditions. The authors also stressed the need for incorporation of the wettability effects and spreading coefficient in Bond number correlation, since "…it does not describe wettability, spreading coefficient or saturation effects, which are important at the microscopic scale".

Sargent et al. (1999) performed a series of gas/oil and water/oil gravity drainage experiments on sandpacks, with permeabilities representative of United Kingdom's Continental Shelf (UKCS) viscous oil fields. Experimental results showed that an effective residual oil saturation of about 10% was obtained for gravity drainage of viscous oils (about 100 cP). For gravity drainage experiments with oils with 1 – 1000 cP viscosities, very low residual oil saturations (at gas breakthrough) were obtained with gravity drainage at a range of reservoir permeabilities (1 – 5 Darcy) and gravity stable displacement rates (about 10 ft/month and below).

Wylie and Mohanty (1999) conducted secondary near-miscible mass transfer and gas flood experiments in both oil-wet and water-wet sandstones to study the effects on wettability on oil recovery. The reported experimental results of higher oil recoveries in oil-wet media, as compared to water-wet media; agree with the similar miscible gas flood experiments reported previously (Rao and Sayegh, 1992). Gas flood experiments by Rao and Sayegh (1992) also observed a significant enhancement in the incremental oil recovery in intermediate-wet systems, while the lowest incremental increase was observed in water-wet media. Rao and Sayegh (1992) attributed this incremental oil recovery in oil-wet media to wettability alteration, while Wylie and Mohanty (1999) suggested it to be due to the higher water-shielding effects in water-wet porous media.

Although, the wettability alteration phenomenon, reported by Rao and Sayegh (1992), was experimentally verified by contact angle measurements, the water-shielding phenomenon, reported by Wylie and Mohanty (1999), does not appear to be the dominant factor for the observed oil recovery increases, since Wylie and Mohanty's (1999) experiments were conducted in secondary mode and no water production was observed in either of the gravity drainage miscible floods. Previous studies (Blunt et al., 1994; Oyno

et al., 1995; Vizika and Lombard, 1996; Saputelli et al., 1998) on spreading and wettability effects on immiscible gravity drainage have attributed the relatively lower oil recovery performance of oil-wet porous media either to the absence of continuous oil films (the inability of oil to spread under negative spreading coefficient conditions) or strong capillary retention of the continuous wetting phase (oil) films on rock surface. The probable reason for improved oil recoveries in oil-wet systems, with minimal improvements in water-wet recoveries, is probably due to alleviation of the strong capillary retention forces due to miscibility development.

Li et al. (2000) discuss the results of the experimental work on CO_2 gravity drainage on artificially fractured Berea sandstone cores at reservoir conditions (Spraberry Trend Area, West Texas). The authors suggested that fractures could improve the efficiency of CO_2 flooding, but suggest further experimental investigation for further clarification.

Pedrera et al. (2002) examined the effects of wettability on (air) immiscible gravity drainage by conducting secondary mode experiments with varying core wettabilities. Their results appear to agree with the previous observations (Meszaros et al., 1990) that higher production times are required for oil-wet systems as compared to water-wet systems. However, the authors observed higher oil recoveries for oil-wet systems (64%) as compared to the water-wet systems (52%), which appear to contradict the previous experimental results (Blunt et al., 1994; Oyno et al., 1995; Vizika and Lombard, 1996; Saputelli et al., 1998). The important contribution of Pedrera et al. (2002) towards improved mechanistic understanding of the gravity drainage process was the identification and characterization of two flow regimes operating sequentially during gas gravity drainage: bulk flow followed by film flow. The authors' numerical modeling studies suggested that wettability has a weak influence on the bulk flow regime (consisting of bulk displaced fluid, and capillary fringe region of high and medium oil saturation (or oil bank)) of gravity drainage, whereas it has "great influence" during the late film flow regime.

Li and Horne (2003) developed an empirical model for the prediction of oil recovery patterns in free-fall gravity drainage. This model was used to predict the recovery patterns of Lakeview Pool, Midway Sunset Field, resulting in a good match.

Ren et al. (2003) suggests that the incremental oil recovery obtainable by tertiary gas gravity drainage consists of two-parts: firstly the bypassed oil, existing as a continuous oil phase in previously unswept areas (by secondary waterflood), and secondly the residual oil existing, at the microscopic scale, as isolated ganglia. It is suggested that the injected gas improves the reservoir sweep by reestablishing the hydraulic continuity of the residual oil, under positive spreading conditions, resulting in assured flow of this isolated oil into the dynamic oil bank. This connectivity of the oil bank, with both the bypassed oil as well as the isolated oil ganglia, is implicit to facilitate their drainage via the oil bank to the production well.

Muggeridge et al. (2005) studied the effect of the presence of discontinuous shale barriers in the reservoir on miscible gas gravity drainage, both experimentally and through numerical simulation. The experimental (as well as simulation) results indicate that all the oil in the vicinity of the shales will ultimately be recovered; and that "regardless of the miscible displacement conditions" it is "surprisingly difficult" to bypass oil in the vicinity of shales over significant times.

Dastyari et al. (2005) investigated gravity dominated immiscible gas injection in a single-matrix block using 2D glass micromodels, in both free and forced gravity drainage modes. The authors reported that the free gravity drainage is initially a very fast process, but slows down at longer times. This observation appears to be supported by the original gravity drainage theories (Cardwell and Parsons, 1948; Terwilliger et al., 1951) as well as other macroscopic experimentation (Meszaros et al., 1990). However, three other conclusions of Dastyari et al. (2005) appear to contradict the previous observations. Firstly, the authors suggested that the oil recovery in an un-fractured system appears to be higher than that of a fractured system. This observation contradicts the observations of Catalan et al. (1994) and Li et al. (2000) which indicate that the presence of fractures in the direction of flow enhanced the oil production rates. Secondly, the authors stated that the residual oil saturation increases to more than twice of the natural gravity drainage, which contradicts the observations of Thomas et al. (1990) and Karim et al. (1992). Thirdly, the authors reported that gas injection in both un-fractured and fractured models results in higher residual oil saturations, which appears to contradict almost all the experimental studies summarized in this section, which suggest that gravity stabilized gas injection can result in very low residual oil saturations.

3.3.3.1 Laboratory Studies Summary

1. Gravity stable gas injection and pure gravity drainage appear to be on the two extreme ends of the vertical gas injection EOR processes spectrum.
2. Literature does not attempt to mechanistically differentiate between these two processes, and the precise distinction between these two processes is not available.
3. Two different schools of thought are evident from the literature review on gravity stabilized gas injection: (i) the drainage process is a type of displacement mechanism with the classical theories of Buckley-Leverett, Darcy's law, relative permeability, continuity equation, and decline curve analysis (decline curve equation) are applicable; and (ii) although the classical theories of Darcy and Buckley-Leverett are relevant, the decline curve equation, applicable to most displacements, does not in itself provide any information regarding the gravity drainage phenomenon.
4. Most of this confusion about gravity drainage characterization appears to stem from ignoring the injection gas pressure distribution as well as due to the application of

'pure' or 'free' gravity drainage theory to forced gravity drainage applications or vice-versa.

5. Characterization and modeling of the gravity drainage process is still a challenge.
6. Non-linear nature of the fundamental gravity drainage equation (Cardwell and Parsons (1948)) has prompted application of numerical and empirical techniques to gravity drainage process characterization. No single model to adequately define the gravity drainage process is available.
7. The forced gravity drainage process has been suggested to be consisting of two flow regimes: bulk flow and film flow, and a 'lumped' approach between the Buckley-Leverett (1942) and Cardwell and parsons (1948) theory to accurately model forced gravity drainage has been advocated.
8. Characterization and quantification of conditions of displacement instabilities and critical injection rates are important for flood profile control and need to be evaluated using 3D physical models and / or reservoir simulation. Various models for the mitigation of these displacement instabilities in gravity drainage have been proposed.
9. Wettability influences on gravity drainage oil recoveries are not very clear. Although the literature appears to be in unison about the beneficial effects of oil spreading and film flow in water-wet and mixed wet systems, conflicting reports about the effects of wettability on gravity drainage recoveries in oil-wet systems have been found.
10. The effects of spreading coefficient (coupled with wettability) on gravity drainage performance in oil-wet systems are also not clear. However, most of the literature appears to agree that positive spreading coefficient in water-wet or intermediate-wet systems is beneficial to gravity drainage by promoting film flow.
11. Although, miscibility development has demonstrated improved oil recoveries in both water-wet as well as oil-wet systems; the screening criteria for miscible flood applications have not been defined.
12. The literature review on miscible gravity stable gas injection into depleted reservoirs (gas cap injection) yielded only a few studies. This is probably due to the notion that immiscible gravity drainage can eventually recover nearly 100% of the reservoir oil given enough drainage time. Further characterization and optimization of the miscible gravity drainage process presents an excellent future research opportunity.
13. Vertical coreflood displacement studies suggest the use of CO_2 over hydrocarbon gases due to the higher recovery efficiency and injectivity characteristics of CO_2; although economical and assured supply of CO_2 for EOR applications could be an issue in some cases.
14. Reservoir heterogeneity and fractures may not negatively influence the recovery characteristics of gravity drainage processes. Some studies suggest that the fractures may actually aid the gravity drainage process.

15. Gravity stabilized gas injection remains an active research area and has continued to demonstrate superlative oil recovery performance in laboratory applications inspite of the meager mechanistic understanding of the process.

3.3.4 Review of Field Applications of Gravity Stable Gas Injection (Gravity Drainage)

In the previous section, the laboratory and numerical studies on gravity stable gas injection (gravity drainage) were summarized. Although, the gravity stabilized gas injection process demonstrated superlative oil recovery performance on the laboratory scale; the performance evaluation of this process on a field scale is required. This section details the various field scale applications of the gravity stable gas injection (gravity drainage) process.

Since gravity stable gas injection and WAG are the two main commercial gas injection application processes, in the vertical and horizontal modes respectively; examination of each of the process' 'report-card' is important. Preliminarily, two field reviews by Howes (1988) and Christensen et al. (1998) are compared for this evaluation. Howes (1988) summarized 51 gravity stable 'vertical' floods (Table 3.1) conducted for recovery of light – to – medium crude oils in Canada upto 1986.

Table 3.1: Summary of Canadian 'Vertical' Hydrocarbon (HC) Miscible Field Applications (Howes, 1988) (Table continued on next page)

Year	Project	Operator	Area (ha)	OOIP MMm^3	Ult. Recovery %OOIP	Prodn %OOIP (till 1986)
1964	Golden Spike D3A Pool	Esso	590	49.60	58.0	56.1
1968	Rainbow Keg River A Pool	Canterra	253	14.30	88.1	61.5
1969	Wizard Lake D3A Unit	Texaco	1075	62.00	95.2	79.9
1969	Rainbow Keg River T Pool	Esso	87	3.18	81.8	55.7
1970	Rainbow Keg River O Pool	Canterra	281	6.21	79.9	61.0
1970	Rainbow Keg River EEE Pool	Canterra	24	1.91	70.2	36.6
1972	Rainbow Keg River E Pool	Canterra	69	3.97	85.4	44.3
1972	Rainbow Keg River G Pool	Canterra	65	2.38	77.3	56.3
1972	Rainbow Keg River AA Pool	Mobil	259	15.90	78.0	40.9
1972	Rainbow Keg River B Pool	Amoco	223	6.52	79.9	50.9
1973	Rainbow Keg River H Pool	Canterra	19	2.35	74.9	59.1
1973	Rainbow Keg River Z Pool	Esso	181	1.49	65.8	44.3

1973	Rainbow Keg River FF Pool	Esso	92	2.50	66.0	41.2
1976	Rainbow Keg River D Pool	Canterra	34	1.13	82.3	53.1
1980	Bigoray Nisku B Pool	Amoco	67	1.50	60.0	28.7
1980	Brazeau River Nisku A Pool	Petro-Canada	108	5.30	75.1	45.5
1980	Brazeau River Nisku E Pool	Petro-Canada	142	2.30	65.1	38.7
1981	Brazeau River Nisku D Pool	Petro-Canada	157	2.70	65.2	28.9
1981	Pembina Nisku G Pool	Texaco	133	3.00	70.0	32.0
1981	Pembina Nisku K Pool	Texaco	58	2.43	70.0	31.7
1981	Westpem Nisku A Pool	Chevron	62	2.65	75.1	34.0
1981	Westpem Nisku D Pool	Chevron	74	2.20	70.0	34.1
1982	Rainbow Keg River B Pool	Canterra	1090	43.00	71.6	43.5
1983	Pembina Nisku M Pool	Canadian Reserve	78	2.85	75.1	27.0
1983	Pembina Nisku O Pool	Texaco	85	1.70	70.0	20.6
1983	Pembina Nisku P Pool	Texaco	170	4.25	75.1	22.4
1983	Rainbow Keg River II Pool	Mobil	73	3.49	75.1	48.7
1984	Rainbow Keg River I Pool	Esso	146	1.88	70.2	N/A
1984	Westpem Nisku C Pool	Chevron	60	4.00	80.0	31.5
1984	Brazeau River Nisku B Pool	Chevron	90	2.30	80.0	29.1
1985	Pembina Nisku A Pool	Chevron	124	2.80	70.0	30.0
1985	Pembina Nisku D Pool	Chevron	143	4.80	72.1	31.7
1985	Pembina Nisku F Pool	Chevron	170	2.10	61.9	3.8
1985	Pembina Nisku L Pool	Texaco	253	5.00	82.0	25.4
1985	Pembina Nisku Q Pool	Texaco	122	2.80	83.9	12.5
1986	Bigoray Nisku F Pool	Chevron	52	2.80	76.1	32.5
1987	Acheson D3 A	Chevron	N/A	3.70	83.8	N/A

The performance evaluation of the projects show that gravity stable oil recoveries are much higher, in the range of 15 – 40 % OOIP, for gravity stable gas floods in the pinnacle reefs of Alberta, as compared to WAG recoveries of 5 – 10 % OOIP in horizontal floods as reported by Christensen et al. (1998). Additionally, comparison of secondary gas flood recoveries from Howes' (1988) review with secondary (horizontal) waterflood recoveries from Christensen et al.'s (1998) review clearly showed the benefit of gas injection applications over plain waterfloods (secondary mode gravity stabilized gas injection recovery factors: 59% versus waterflood recovery factors of 32% OOIP).

3.3.4.1 Screening Criteria for Gravity Stable Gas Injection

As suggested earlier, up-dip (gravity stable) gas injection into dipping or a reef type reservoir is one of the most efficient oil recovery methods in both secondary and tertiary modes. Furthermore, the gravity drainage concept has been applied and has been successfully implemented in many field applications and pilots (individually discussed in the following sections). Potential candidates for gas injection EOR are generally selected using various empirically based screening criteria (Taber et al., 1996; Lepski and Bassiouni, 1998). The empirical screening criteria for identification of potential reservoirs (Table 3.2) for gravity stable gas injection projects were presented by Lepski and Bassiouni (1998). These screening criteria provide with a critical tool for preliminary selection, screening and evaluating the application of the gravity stable gas injection EOR processes to potential reservoirs.

Table 3.2: Screening Criteria for Gravity Assisted Gas Injection

Parameter	Value
Waterflood Residual Oil Saturation	Substantial (range not specified)
Reservoir Permeability (Vertical)	> 300 mD
Bed Dip Angle	$> 10^{o}$
Oil Viscosity	Free flow
Spreading Coefficient	Positive

3.3.4.2 Review of Ten Commercial Gravity Drainage Field Projects

Ten gravity stable field projects (summarized in Table 3.3) in various parts of the world were critically examined to decipher the controlling multiphase mechanisms and fluid dynamics operational in gravity stable gas injection processes. This section summarizes the unique characteristics of each of the gravity drainage project. This review has enabled the duplication of the multiphase mechanisms and fluid dynamics operational in the field into the laboratory through proper strategy for experimental design.

1. West Hackberry Field, Louisiana (Gillham et al., 1996)

The Hawkins (Woodbine) field is a salt dome reservoir in southwest Louisiana, with average porosity of 28% and a connate water saturation of 19%. This reservoir production history was subjected to sidetracking as well as waterflooding.

Amoco Production Company, U.S. Department of Energy and Louisiana State University jointly initiated the air injection project into the West Hackberry Field (Cameron Parish) Louisiana. This air injection project was initiated to improve recovery from this watered-out reservoir, by creating an artificial gas cap thereby allowing the gravity drainage of liquids (termed as the Double Displacement Process (DDP)). DDP is

the gas displacement of a water invaded oil column to recover additional oil (and by default free water) through the gravity drainage process.

Laboratory and field studies on the steeply dipping, high permeability West Hackberry field clearly demonstrated the superiority of the gravity drainage process which exhibited recoveries of nearly 90% OOIP as against the 50 – 60% water drive recoveries. The gravity drainage based DDP process has proved to be a success on both engineering and economic fronts in the West Hackberry field.

2. Hawkins (Woodbine) Field, East Texas (King and Lee, 1976; Carlson, 1988)

The Hawkins (Woodbine) field is highly faulted with a 6^{o} dip and a strong aquifer support. The oil gravity was 12-30 ^{o}API with viscosity varying from 2-80 cP. The reservoir characteristics include 10,000 acres of area, with greater than 1000 ft of hydrocarbon column. A reservoir characterization study of the Hawkins (Woodbine) field was completed using 35,900 ft of conventional cores obtained from 193 wells in the field.

Detailed phase behavior and modeling studies (Carlson, 1988) suggested gas injection to prevent oil encroachment in the gas cap and prevent further shrinking. These studies concluded that the gas gravity drainage process had a recovery efficiency of > 80% compared to the water drive efficiency of only 60%. Coreflood investigations (Carlson, 1988) confirmed that even under immiscible conditions, the gas could recover additional oil from the water invaded portions of the reservoir and thereby reducing the residual oil saturation in water invaded oil column from 35% to about 12%. The above conclusion helped the development of the 'Double Displacement Process' (DDP) (both in the West Hackberry and Hawkins Fields) and initiation of a field DDP pilot in the east fault block of the reservoir.

Predictive simulation studies indicated that about 189 million bbl of additional oil recovery was feasible, of which nearly 116 million bbl would be produced by converting the water-drive areas into gas-drive/gravity drainage, and 67 million bbl from prevention of the oil loss caused by gas cap shrinkage. The central inference of this reservoir study was that the gas-drive / gravity drainage combination process would help produce nearly 33% more oil than what was possible in a water drive.

3. Weeks Island: S-RB Field Pilot, Louisiana (Johnston, 1988)

Shell initiated an immiscible gravity stable CO_2 (diluted with methane gas) flood at Weeks Island S-RB reservoir in Louisiana, in 1978. The pilot was conducted in a dipping 13,000 ft and 225 ^{o}F fault block similar to West Hackberry reservoir. The S-RB reservoir was chosen due to the small, well confined nature and exceptional sand quality and continuity. Reservoir characteristics include vertical permeability of 1200 mD and a bed dip of 26^{o}. The reservoir oil properties are not specified, however residual oil saturation before the pilot was 22% based on Special Core Analysis (SCAL). Low oil rates, water

cuts and increasing GOR made tertiary recovery (CO_2 injection) necessary in the field. Interestingly, the residual oil saturation was lower than the minimum saturation recommended by the screening criteria for gravity assisted gas injection (Lepski and Bassiouni, 1998)

A 25.5% PV gravity stable miscible CO2 + HC slug (24% PV & 1.5% PV) was injected resulting in additional 205 MBbl or 60% waterflood residual oil. The core-analysis of gas swept zones showed that gas injection has decreased the residual oil saturation from 22% to 1.9%.

The displacement efficiencies were found greater than 90% (based on sidewall core data) and a CO_2 usage rate of 7.90 MCF/Bbl considering the recycled gas. Although the pilot's expected oil recovery was 66% of the ROIP and a technical success, it was deemed as a non-profitable venture, probably due to the low oil prices prevalent at the time.

4. Bay St. Elaine Field, Louisiana (Cardenas et al., 1981; Ray, 1994; Nute, 1983)

A miscible gravity stable CO_2 flood, in the dipping Louisiana Gulf Coast field, Bay St. Elaine, was initiated by Texaco in 1981. Laboratory studies conducted to study the injection slug characteristics demonstrated that after miscibility was achieved, the injected CO_2 solvent mixture was effectively able to recover all of the waterflood residual oil.

Pressure pulse testing during field implementation of the EOR process indicated the process to be "successful" (Nute 1983), but EOR surveys (Moritis, 1995) deem the flood to be "discouraging and non-profitable" probably due to the low oil prices prevalent at the time. No oil recovery data was found in the literature for this flood.

5. Wizard Lake D3A Pool, Alberta, Canada (Backmeyer et al., 1984)

The Wizard Lake D3A reservoir is a dolomitized bioherm reef of Devonian age with oil zone of 648 ft with a bottom water drive (Cooking Lake Aquifer). The reservoir characteristics include vuggular and matrix porosities with average horizontal permeability of 1375 mD and average vertical permeability of 107 mD with original reservoir pressure of 2270 psi. Reservoir oil is paraffin based 38 ^{o}API crude with a saturation pressure of 2131 psi at 160 ^{o}F.

Texaco Canada initiated a secondary miscible HC flood in this reservoir in 1969. The HC miscible slug size was 7.5% HCPV, which projected the incremental recovery increase to 28.5 MMSTB. This flood was highly successful with an overall reservoir recovery factor of about 95% OOIP.

6. West Pembina Nisku 'D' Pool, Alberta, Canada (Da-Sle and Guo, 1990)

Westpem Nisku D pool, a pinnacle reef type carbonate reservoir, is located 100 miles southwest of Edmonton, Canada. The reservoir oil is light (45 ^{o}API) with a viscosity of 0.19 cP. Chevron Canada Resources implemented a miscible flood in May 1981, employing a miscible slug composed of 80% Methane and 20% C_{2+} fraction(s). The slug design was later changed to 85% C_1, and 15% C_{2+} fraction at 4800 psi working pressure to assure miscibility development.

Flood analysis demonstrated that the solvent/oil interface was consistently flat across the reef, affirming the applicability of the Dumore stability criterion. Furthermore, the core-analysis results indicated very low residual oil saturation in the order of 5% making the flood an economic as well as a technical success. Chevron expected an overall recovery factor of about 84% OOIP from this flood.

7. Wolfcamp (Wellman Unit) Reef, W. Midland, Texas (Bangla et al., 1991)

Union Texas Petroleum Corp. conducted a gravity stable vertical tertiary CO_2 flood in Wellman unit of the Wolfcamp reef (limestone) reservoir, located in the western Midland basin of Terry county, Texas. Reservoir oil was light (43.5 API) with 0.43 cP viscosity, making it a good gas flood candidate. A tertiary CO_2 miscible flood was planned after a successful waterflood with residual oil saturation (ROS) of 35%. CO_2 was injected into the crest of the reservoir with water injection continued in the water zone to maintain the reservoir pressure above the MMP of 1900 psi.

Numerical model studies predicted the CO_2 ultimate recovery efficiency to be 78%, which was exceeded in the actual field flood (84%). The gas flood reduced the residual oil saturation to only 10.5% with a net gas utilization ratio of the 6.5 MSCF/STB. This flood ultimately produced 68.8% of the OOIP, of which CO_2 incremental recovery was 27%. This flood was an economic and a technical success, and Union Texas Petroleum expects the final recovery of about 74.8% of the OOIP.

8. Intisar D Reef, Libya (DesBrisay et al., 1960; 1975; 1981)

Occidental Libya initiated a vertical gravity stable miscible flood in the Intisar 'D' reservoir in the Libyan Sirte basin. Geologic studies show the reservoir as an upper Paleocene pinnacle reef, roughly circular (diameter ~ 3 miles) in plan with original hydrocarbon column of 950 ft. The reservoir oil was highly undersaturated, very light (40^{o} API) with 0.46 cP viscosity. Laboratory studies show that the minimum miscibility pressure (MMP) of 4000 psi for this oil with hydrocarbon gas from nearby fields, was lower than the original reservoir pressure of 4257 psi. The highly undersaturated nature of the reservoir prompted simultaneous peripheral water and crestal gas injection to maintain the reservoir pressure above the MMP. Occidental predicts that almost 1.6 billion bbl of OOIP (of which 496 million bbl) recovered till date (1981) would be

ultimately recovered yielding a recovery factor of about 67%, and most of which is attributable to miscible gas gravity drainage, making this flood a success.

9. Handil Main Zone, Indonesia (Gunawan and Caie, 1999)

Handil is a giant oil field located in the Mahakam Delta of the island of Borneo in Indonesia. The reservoir is simple anticline, 2.49 mile (4 km) long and 1.86 mile (3 km) wide, with a main East-West fault dividing the reservoir into North and South area. The reservoir geology is complex, and the field comprises of more than 500 hydrocarbon accumulations, stacked between 984.25 ft (300 m) to 1312.34 ft (4000 m) (ss), and trapped in channel-sand and sand-bar reservoirs deposited in a fluvio-deltaic environment of the Miocene age. The reservoir permeability ranges from 10 to 2000 mD, with 25% porosity and connate water saturation around 22%. The oil accumulations consist of a large oil column (in excess of 328.08 ft (100 m)) underlying a variable sized gas-cap. The reservoir structural dip ranges from 5^o to 12^o, which connects an underlying aquifer (weak in the main and deep zones).

Total's gravity stable lean gas injection into the waterflooded Handil reservoir in Indonesia, has increased the oil recovery factor by 1.2% during 1979 to 1982, and is deemed successful. Total expects that the reservoir would yield additional 30 MMSTB EOR oil, and ultimately extend the productive life of the near abandonment Handil reservoir in the Mahakam delta of Borneo, Indonesia.

10. Albian Paluxy Formation, East Texas (Hyatt and Hutchison, 2005)

The clastic Paluxy formation is a large, fault dependent closure with a moderately strong water drive producing from the lower Cretaceous Albian Paluxy formation of the East Texas basin. This formation is composed of fluvial channel sands intercalated with shaly, silty interfluves and estuarine mudstones. The reservoir interval is over 300 ft thick and was deposited during the transgression of the early Cretaceous seaway over the central North American continent. The channel sands have a porosity of 25% and an average permeability of 2200 mD. The channel sands predominantly fine upward resulting a lower permeability (10 to 500 mD) at the top and margins with considerably higher permeability (2000 to 6000 mD) at the channel bases.

Table 3.3: Summary of Gravity Drainage Field Applications

Property	West Hackberry	Hawkins Dexter	Weeks Island	Bay St. Elaine	Wizard Lake	Westpem Nisku	Wolfcamp Reef	Intisar D Reef	Handil Main	Paluxy Formation
Location	Louisiana USA	Texas USA	Louisiana USA	Louisiana USA	Alberta Canada	Alberta Canada	Texas USA	Libya	Borneo Indonesia	East Texas, USA
RESERVOIR CHARACTERISTICS										
Rock Type	Sand Stone	Sand Stone	Sand Stone	Shaly Sand	Dolomite	Carbonate	Limestone	Biomicrite/ Dolomite	Sand Stone	Fluvial-Deltaic
Reservoir Type	$23 – 35^o$	8^o Dip	26^o Dip	36^o Dip	Pinnacle	Pinnacle	Pinnacle	Pinnacle	$5 – 12^o$ Dip	Channel

	Dip				Reef	Reef	Reef	Reef		Sand - Thk
Porosity (%)	23.9 - 27.6	27	26	32.9	10.94	12	8.5	22	25	25
Permeability (mD)	300-1000	3400	1200	1480	1375	1050	110	200	10 - 2000	10 - 6000
Kv/Kh Ratio	1.0	~ 1.0	1.0	1.0	0.08	0.033 - 0.2	Not Avbl	0.75	1.0	1.0
Pay (ft)	30 - 31	230	186	35	648	292	824	950	50 - 82	300
Swc	19 - 23	13	10	15	5.64	11	20	Not Avbl	22	Not Avbl
Res. Temp (^oF)	195 - 205	168	225	164	167	218	151	226	197.6	Not Avbl
PROCESS DATA										
Project Scope	Fieldwide	Fieldwide	Pilot Fld	Lab Study	Fieldwide	Fieldwide	Fieldwide	Fieldwide	Fieldwide	Pilot
Start Date	11/1994	08/1987	01/1979	01/1981	01/1969	05/1981	07/1983	01/1969	01/1994	01/2001
Project Area (Ac)	381	2,800	8	9	2,725	320	1,400	3,325	1,500	~ 640
Injection Gas	Air	N_2	CO_2/HC	CO_2	HC	HC	CO_2	HC	HC	HC (?)
Injection Mode	Secondary	Tertiary	Tertiary	Secondary	Secondary	Secondary	Tertiary	Secondary	Tertiary	Tertiary
Injection Strategy	Immsc	Immsc	Immsc	Immsc	Misc	Misc	Misc	Misc	Immsc	Immsc
Displ. Velo. (ft/D)	.095 – .198	Not Avbl	.04 – 1.2	Not Avbl	.021- .084	.020 - .203	.116	.06	Not Avbl	Not Avbl
Status (Date)	C (‘02)	NC (‘02)	NC (‘86)	NC (‘86)	NC (‘02)	HF (‘92)	HF (‘98)	NC (‘02)	Not Avbl	NC (’05)
PHASE BEHAVIOR DATA										
Oil API Gravity	33	25	32.7	36	38	45	43.5	40	31 – 34	23
Oil Viscosity (cP)	0.9	3.7	0.45	0.667	0.535 (Pb)	0.19	0.43	0.46	0.6 – 1.0	23
Oil FVF at Pb	1.285	1.225	1.62	1.283	1.313	2.45	1.284	1.315	1.1 – 1.4	Not Avbl
GOR (SCF/STB)	500	900	1386	584	567	1800	450	509	2000	10
MMP (psi)	Not Avbl	Not Avbl	Not Avbl	3334	2131	4640	1900	4257	Not Avbl	Not Avbl
KEY RESULTS										
Wtr flood Sor (%)	26	35	22	20	35	Not Avbl	35	Not Avbl	27	Not Avbl
WF Recvry (OOIP)	60	60	60 - 70	Not Avbl	Not Avbl	Not Avbl	Not Avbl	Not Avbl	58	35
Gas flood Sor (%)	8	12	1.9	Not Avbl	24.5	5	10	Not Avbl	3	Not Avbl
So at Start (%)	Not Avbl	Not Avbl	22	20	93	90	35	80	28	Not Avbl
So at End (%)	Not Avbl	Not Avbl	2	5	12	5	10	18	Not Avbl	Not Avbl
Enh. Prd (GF: b/d)	150 - 400	1,000	160	7	1,300	2,300	1,400	40,000	2,383	175
Ult. Recvry (OOIP)	90.0	> 80.0	64.1	Not Avbl	95.5	84.0	74.8	67.5	Not Avbl	Not Avbl
Conclusion	Successful	Successful	Successful	Discorgng	Successful	Successful	Successful	Successful	Successful	Successful
Profit?	Profit	Profit	No Profit	No Profit	Profit	Profit	Profit	Profit	Profit	Not Avbl

The oil is about 23^o API with a viscosity of 23 cP at reservoir conditions. The reservoir is highly undersaturated with original pressure of 1900 psig with a solution GOR of 10 SCF/Bbl. The reservoir pressure is maintained by a moderately strong aquifer. Since the start of the production of this field in 1930’s, it has been marred with high production water-cut, due to the unfavorable mobility ratio in the production water-drive.

After about 70 years of water-drive production, ExxonMobil initiated an immiscible gas injection pilot in this field in the early 2000’s. A full-field reservoir simulation study suggested that this field would reach its economic production limit at about 35% OOIP production. Simulation studies also suggested excellent EOR potential (5% incremental OOIP in 3 years and 10+% incremental OOIP recoveries after 10 years) by immiscible

gas injection, and gravity drainage of the oil to the lowest point of the channel sands with the help of horizontal wells. The results of the pilot are being awaited, but production logs and reservoir monitoring has demonstrated the feasibility of the gravity drainage process in significantly improving the oil recoveries primarily driven by film flow behind the advancing gas flood front.

3.3.4.3 WAG and Gravity Drainage Field Production Rates

The general perception about gravity drainage processes appears to be that the production rates are lower than conventional flooding / displacement processes.

To compare the enhanced production flow rates between gravity stable and WAG projects, four miscible and four immiscible WAG projects and ten gravity stable projects were evaluated. Furthermore, to provide with a common comparison basis for performance evaluation of the WAG and gravity stable gas injection processes, a parameter 'Index of Productivity' was defined as:

I.P. = [Enhanced Production (Bbl/D)] / [Flood Volume (Ac-ft)]…….....…(10)

The immiscible WAG projects considered were: (i) Painter Field, Wyoming (Sandstone reservoir, using N_2 injectant), (ii) ARCO Block 31, Texas (Limestone reservoir using HC/N_2 mixture as injectant), (iii) Timbalier Bay, Louisiana (Sandstone reservoir using CO_2 as injectant), and (iv) Yates Field, Texas (Dolomite reservoir using CO_2 as injectant). The miscible WAG projects considered were: (i) Slaughter Estate, Texas (Dolomite reservoir, using CO_2 injectant), (ii) Levelland, Texas (Limestone reservoir using Enriched HC/CO_2 mixture as injectant), (iii) Quarantine Bay, Louisiana (Sandstone reservoir using CO_2 as injectant), and (iv) Prudhoe Bay, Alaska (Sandstone reservoir using Enriched HC injectant).

The comparison of the gravity stable gas injection projects and WAG projects was based on the index of productivity. The range of productivity indices calculated for the miscible and immiscible projects is depicted in Table 3.4, which clearly shows that the gravity drainage processes have comparable enhanced production rates and that gravity drainage rates can sometimes be several folds higher than in WAG projects. This comparison clearly demonstrates that gravity drainage processes could outperform the WAG processes, not only on a production rate basis, but also on overall recovery factors.

Table 3.4: Index of Productivity Comparisons between Nine Gravity Drainage and Eight WAG Field Projects

Index of Productivity (Bbl/D-Ac)			
Immiscible WAG Projects		Immiscible Gravity Drainage Projects	
Field Name	**I.P.**	**Field Name**	**I.P.**
Painter Field, Wyoming	1.07	West Hackberry, Louisiana	0.72

ARCE Block 31, Texas	0.56	Hawkins Dexter Sands, Texas	0.04
Timbalier Bay, Louisiana	0.23	Weeks Island, Louisiana	20.00
Yates, Texas	3.64	Bay St. Elaine, Louisiana	0.78
Average P.I.	**1.37**	Handil Main Zone, Borneo	1.59
Miscible WAG Projects		**Average P.I.**	**4.62**
		Miscible Gravity Drainage Projects	
Field Name	**I.P.**	**Field Name**	**I.P.**
Slaughter Estate, Texas	0.88	Wizard Lake D3A, Alberta	0.48
Levelland, Texas	1.41	West Pembina Nisku D, Alberta	7.19
Quarantine Bay, Louisiana	2.19	Wolfcamp Reef, Texas	1.00
Prudhoe Bay, Alaska	1.09	Intisar D, Libya	12.03
Average I.P.	**1.39**	**Average I.P.**	**5.17**

3.3.4.4 Field Reviews Summary

The important characteristics of the field scale gravity drainage projects are:

1. Up dip / crestal gas injection into oil reservoirs is one of the most efficient methods to recover residual oil.
2. Gas gravity drainage process has been applied as secondary as well as tertiary recovery processes with encouraging results.
3. Gas gravity drainage process has been applied to all reservoir types, from extremely geo-complex reservoirs like Biomicrite / Dolomite to high quality turbidite (fluvial-deltaic sands) reservoirs.
4. Various field injectant gases such as Air, Nitrogen (N_2), Hydrocarbon (HC) and Carbon Dioxide (CO_2) have been successfully employed for the gas gravity drainage process.
5. Gas gravity drainage process is applicable to low permeability (110 mD) – low porosity (8.5%) reservoirs as well as high permeability (3400 mD) – high porosity (32.9%) formations, and is not greatly affected by the variation of common reservoir and fluid parameters such as reservoir heterogeneity, bubble point pressure, gas oil ratio (GOR), reservoir temperature and oil formation volume factor (FVF).
6. Gas gravity drainage process is best applicable to light oil reservoirs, low connate water saturations, positive spreading coefficient (to promote film flow), thicker formations, moderate-high vertical permeability, highly dipping or reef structured reservoirs, and minimal reservoir re-pressurization requirements (for miscible GAGD applications).
7. Corefloods and field investigations confirm that a large amount of incremental tertiary oil can be recovered using gravity assisted gas injection.

8. Recoveries as high as 85 – 95% OOIP have been reported in field tests, with the calculated average ultimate recoveries for all the field projects reviewed in this study being 77 %OOIP, and laboratory gas gravity drainage floods yielding nearly 100% recovery efficiencies.

3.3.5 Multiphase Mechanisms Operational in Gas Injection EOR Projects

Multiphase mechanisms strongly influence the fluid distribution and microscopic displacement behavior in gas injection process. The multiphase mechanisms are displayed through the rock-fluid and fluid-fluid interactions occurring in gas injection processes.

This section identifies and details on the various multiphase mechanisms operational in gas injection EOR processes. This study places special emphasis on gravity stable gas injection (consequently the GAGD process), and evaluates the various interplays of these reservoir specific interactions that eventually determine the recovery efficiency of the project. The relevant multiphase mechanisms identified through the review of literature are: (i) gravity segregation, (ii) wettability, (iii) spreading coefficient, (iv) miscibility development, and (v) mobile water saturation.

3.3.5.1 Gravity Segregation

The gravity segregation phenomenon is one of the dominant mechanisms that dictate the recovery performance during horizontal type gas injection projects. Although the WAG process is deployed to minimize this effect, significant differences in viscosities and densities between the injected water, gas and reservoir fluids, results in severe in-situ gravity segregation effects ultimately causing the water to 'under-ride' while the gas to 'over-ride'. As discussed previously, this negatively influences the flood performance.

Slight mitigation of this negative influence is possible in reservoirs with high vertical-to-horizontal permeability (K_V/K_H) ratios, where higher cross-flow and / or convective mixing tendencies may slightly increase the local vertical sweep. However, this phenomenon of convective mixing has been found to be generally detrimental to the overall flood oil recovery; mainly due to the increased gravity segregation tendencies and loss of miscibility due to decreased frontal velocities.

On the other hand, contrary to the horizontal floods, gravity stable (vertical) gas injections demonstrate marked benefits due to this phenomenon of gravity segregation. In vertical floods the gravity segregation phenomenon assuredly increases the oil recoveries by improved volumetric sweep, increased gas injectivity and decreased flow competition between injected gas and liquids to the producing well.

3.3.5.2 Effect of Wettability

The strong effect of the reservoir rock's wetting properties on the gas flood performance has been experimentally proven in the laboratory (for some examples see: Rao et al., 1992; Wylie and Mohanty, 1999; Rao, 2001). The wetting nature of the reservoir rock not only governs the oil-gas-water distribution in the reservoir pore space, but also influences the fluid flow behavior during oil production.

In water-wet porous media the sand grains are covered with a thin film of water and the oil and gas occupy the central portions of the pore space. On the other hand, in oil-wet media, the rock grains are covered with a thin oil layer, whereas the gas and water now occupy the central portion of pore. Two more wettability states have been observed in oil reservoirs: neutral or intermediate wet and mixed wet. For neutral or intermediate wet media, the rock has no preference for either oil or water, and the fluid saturations dictate the film type on the rock grains. For mixed-wet systems, the smaller pores are water-wet whereas the larger pores are oil-wet. This reservoir fluid distribution, dictated primarily by the native wettability state of the rock, seriously influences the primary, secondary as well as the tertiary recoveries from the reservoir.

The gravity stable gas injection studies can be categorized in two groups: immiscible floods and miscible floods. Only two experimental studies (Rao and Sayegh, 1992; Wylie and Mohanty, 1999) evaluating the gravity stable miscible gas flood performance dependence on various reservoir wettability states were found. These two studies proved that the water-wet system resulted in the poorest oil recoveries during miscible gas injection.

The experimental studies on the effects of reservoir wettability on immiscible gravity stable gas injection result in conclusions contradictory to the miscible floods. The detailed literature review is included in Section 3.2 of this dissertation. Immiscible gravity drainage experimental studies demonstrated that the highest oil recoveries were obtained in water-wet porous media followed by mixed-wet media; whereas the lowest oil recoveries were obtained in oil-wet porous media. The poor recoveries were attributed to the strong capillary retention (or surface) forces acting on the wetting phase films and the inability of the oil to spread (even under positive spreading conditions (discussed later)).

3.3.5.3 Effect of Spreading Coefficient

The spreading coefficient, along with wettability, affects the gas-oil-water distributions, consequently the recoveries during a gas injection program. The spreading coefficient is a 'balance' between the three interfacial tensions (IFT) in Oil/Water/Gas systems. Equation 3.11 below defines the spreading coefficient.

$$S_O = \sigma_{G/W} - \sigma_{G/O} - \sigma_{W/O} \quad \text{(3.11)}$$

The spreading coefficient value (as well as the reservoir wettability) is also critical in determining the equilibrium spreading characteristics between the three co-existing reservoir phases. The fluid spreading characteristics are critical in determining the oil recoveries in gas floods, especially in gas assisted gravity drainage. Furthermore, the equilibrium value of the spreading coefficient also determines the orientation and continuity of the fluid phase in the reservoir pores. Rao (2002) conceptually summarized the phase orientation dependence on spreading coefficient and wettability. He reported that the positive spreading coefficient conditions appear to be favorable from an oil recovery point of view.

The presence of continuous oil films (in the center of the pores) over the water films covering the rock grains not only increases the oil drainage phenomenon (during gas injection) at lower pressure drops, but also provides with continuous 'conduits' that guide isolated oil globules toward the production well. The continuity of these oil films is an interfacial phenomenon and depends on the ability of the oil phase to spread on the water phase in presence of gas. The spreading coefficient can be positive or negative depending on the in-situ fluids' composition and reservoir temperature and pressures.

Micromodel experiments (Oren and Pinczewski, 1994) to visualize and characterize the effects of wettability and fluid-fluid spreading on gas flood oil recovery prove that the positive value of the spreading coefficient helps ensure development and maintenance of continuous oil films between injected gas and reservoir water, thereby resulting in minimal losses of the injected gas to the reservoir water. On the other hand a negative value signifies a lens-type discontinuous distribution of oil between water and gas, thereby enabling gas-water contact and consequently lowers the oil recoveries.

Although horizontal mode gas injection literature agrees with the inferences of Oren and Pinczewski (1994), the gravity drainage literature does not appear to be in unison about the effects of spreading coefficient on oil recoveries. Most of the gravity drainage literature (Blunt et al., 1994; Oyno et al., 1995; Vizika and Lombard, 1996; Saputelli et al., 1998) suggests that the presence of oil films is instrumental in increasing the oil recoveries in water-wet and mixed-wet porous media. Conversely, the absence of these oil films is responsible for the observed lower recoveries in oil-wet media. However, no agreement on the effects of spreading coefficient value (positive, zero or negative) on oil recovery appears in the gravity drainage literature. Interestingly, the gravity drainage literature from 1998 to 2005 (see Section 3.2 and 3.3) focuses on the numerical experimentation of the gravity drainage process, and no experimental studies on the effects of spreading coefficient were found.

3.3.5.4 Effect of Miscibility Development

Currently, almost all of the commercial CO_2 / hydrocarbon gas injection projects operating in the United States and Canada are miscible. Oil and Gas Journal's biannual

EOR survey (2002) clearly demonstrates the industry inclination towards miscible gas floods and that the commercial immiscible projects have significantly decreased over the past few decades with no immiscible floods planned for the immediate future.

The capillary number (N_{ca}) controls the microscopic displacement efficiency in gas floods. The capillary number is defined by Equation 3.12.

$$N_{ca} = \frac{V\mu}{\sigma Cos\theta} \quad \text{..... (3.12)}$$

The fundamental definition of miscibility (Stalkup Jr., 1985) implies that the necessary and sufficient condition for miscibility development is the absence of an interface between the injected and the reservoir fluids (in other words, a condition of zero interfacial tension). Interestingly this results in a capillary number of infinity, and theoretically all the oil in the reservoir can be produced. Furthermore, as the capillary number controls the microscopic displacement efficiency of the flood, miscible floods have the potential to demonstrate nearly 100% microscopic displacement efficiencies in the gas swept zones.

The need for miscibility development for improved oil recovery processes can be best explained using the Klins (1984) plot. The Klins plot (Figure 3.9) correlates the reservoir residual oil saturation to the capillary number, and suggests that significantly higher recoveries are obtained by increasing the capillary number. It is important to note that when miscibility is achieved, the σ term in Equation 12 becomes zero; thereby resulting in an infinite capillary number (consequently very low oil saturations) at miscibility.

The CO_2 flood design criteria (for both miscible and immiscible floods) (Green and Willhite, 1998) suggest a minimum depth limitation as well as dictate the density and viscosity of the oil to be produced from the concerned reservoir. Hence in shallow and medium gravity (22^o to 31^o API) oil reservoirs, the flood is by default immiscible. However, the immiscible nature of gas injection may not be always due to reservoir limitations. The operational, economic and design factors may sometimes result in immiscible floods. Although the recoveries for immiscible floods are lower than those of miscible floods, the costs of reservoir re-pressurization may be prohibitive in certain cases for miscible flooding. It is important to note that although the performance of horizontal immiscible floods is significantly lower than horizontal miscible floods (WAG as well as CGI) (Christensen et al., 1998), the miscible and immiscible horizontal flood oil recoveries have been comparable to gravity stable (vertical) gas injection projects.

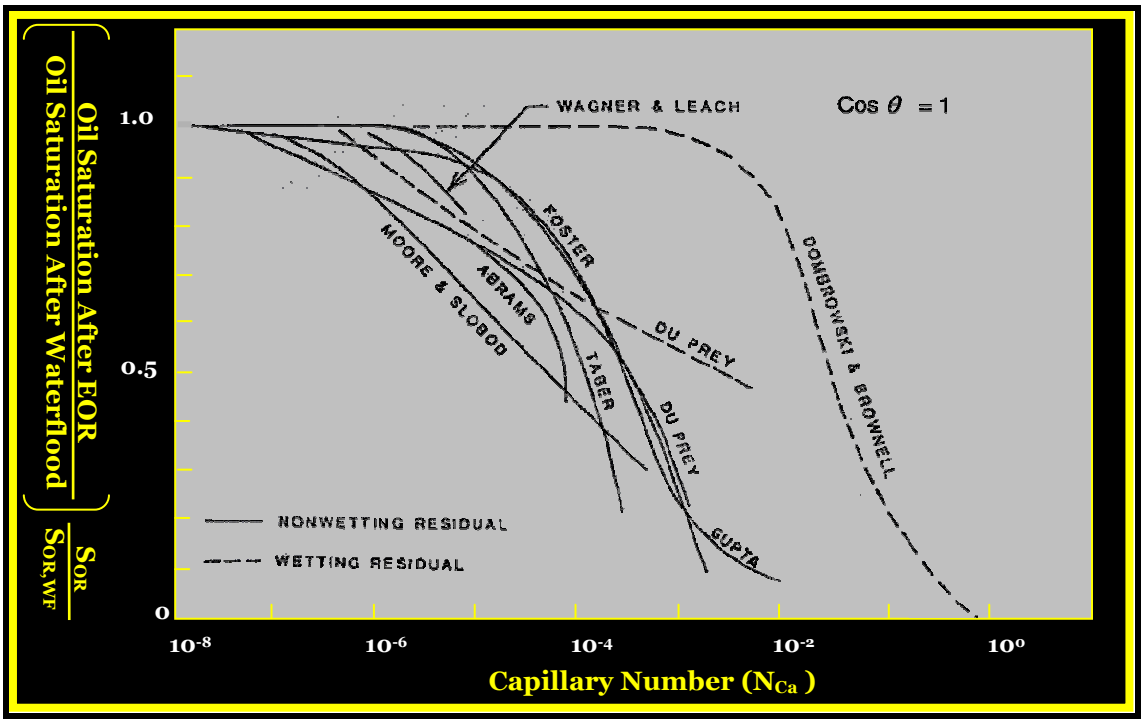

Figure 3.9: Dependence of Capillary Number Value on Reservoir Residual Oil Saturation (After Any EOR Process) for Water-wet Reservoirs (Klins, 1984)

In miscible flooding, the incremental oil recovery is obtained by one of the three mechanisms, namely oil displacement by solvent through the generation of miscibility (i.e. zero interfacial tension between oil and solvent – hence infinite capillary number), oil swelling and reduction in oil viscosity (Schramm et al., 2000).

Although both immiscible and miscible floods appear to have their own merits and demerits, there seems to be no consensus in the literature for the need for development of miscibility in gas floods (Thomas et al., 1995, Schramm et al., 2000, Rao 2001, Jakupsstovu et al., 2001). This debate could be partially due to the 'industry-definition' of the capillary number, which leaves out the contact angle (Cos θ) term (Rao, 2001), which eliminates the reservoir wettability from consideration. The general belief is that the IFT is the most easily modifiable term in the capillary number definition (Rogers and Grigg, 2000), which resulted in increased research efforts for the development of new and better surfactants for IFT reduction. However, overlapping values of interfacial tension for immiscible, near-miscible and miscible floods for similar fluid system have been reported (Taber et al., 1996, Christensen et al., 1998, Rao, 2001). If the ultimate goal is to make the value of capillary number large, gas injection in a neutral-wet reservoir (or made neutral wet using surfactants: where the condition of $\theta = 90^{o}$ or $\text{Cos}\ \theta = 0$ makes capillary number infinity), could theoretically yield the results similar to zero IFT conditions (Rao, 2001). Inspite of these different schools of thought on miscible gas injection, the inclination of the industry towards miscible flooding is very evident (EOR survey, 2002).

However, the gravity drainage literature review appears to advocate immiscible gas injection. Literature review on gravity drainage studies yielded only two miscible gravity stabilized gas injection floods. The inclination towards immiscible flooding in gravity drainage applications appears to stem from the two notions: (i) the Bond number is the controlling parameter in gravity drainage floods, and (ii) immiscible floods result in good oil recoveries in water-wet and mixed-wet porous media. The Bond number value is directly proportional to the density difference ($\Delta\rho$) between injected gas and reservoir oil. Therefore, it appears that to maximize the Bond number value, immiscible injection has been preferred, since the $\Delta\rho$ value significantly decreases in the near miscible region. The second notion appears to be attributable to the erroneous assumption that all reservoirs are water-wet.

The gravity drainage literature (Section 3.2) suggests that the lower oil recovery in oil-wet media is attributable to the strong surface retention forces on the wetting phase films. It is hypothesized that for such scenarios, miscibility would be beneficial to alleviate these surface retention forces and improve oil recoveries. This hypothesis appears to be supported by the experimental results of miscible gravity stable floods (Rao and Sayegh, 1992; Wylie and Mohanty, 1999).

3.3.5.5 Effect of Mobile and Connate Water Saturation

Reservoir water saturation, both connate (bound) and free (mobile), has been found to influence the oil recovery characteristics of many enhanced recovery processes (Dumore and Schols, 1974; Hagoort, 1980; Meszaros et al., 1990). From a gas injection point of view, oil recovery rates (and efficiency), especially during the injection of a water-soluble solvent (such as CO_2), have been found to be directly related to the free water saturation in the reservoir (Kulkarni and Rao, 2005). The bound and free water saturations influence the gas injection processes differently and their effects are summarized in the following sections, with the emphasis on gas gravity drainage.

Effect of Connate Water Saturation

In gas injection processes (especially secondary gravity-drainage process); three phases usually exist, even at initial (or connate) water saturation. Although the connate water saturation is generally considered to be immobile, micromodel studies (Sajadian and Tehrani, 1998) have demonstrated that this assumption may not always hold true. During gas gravity drainage, changes in the gravity – capillary force balances could result in saturation redistributions and / or connate water re-mobilization during the process.

There appears to be no consensus on the effects of connate water saturation on gravity drainage gas injection recoveries. Sparse experimental data available on the topic yielded a wide variety of conflicting conclusions (Dumore and Schols, 1974; Kantzas et al., 1988; Nahara et al., 1990; Skauge et al., 1994; Sajadian and Tehrani, 1998). Nahara et al.

(1990), based on centrifugal gas-oil displacements, report that gas-oil relative permeabilities are unaffected by the presence of water, as long as the water is immobile. On the other hand, Dumore and Schols (1974) showed that the presence of immobile connate water in Bentheim sandstones result in extremely low residual oil saturations during gravity drainage, irrespective of the gas/oil IFT values (that affect the gas-oil relative permeabilities).

Pavone et al.'s (1989) free gravity drainage experiments at low interfacial tensions with fractured reservoir cores suggested that the presence of immobile water reduces the oil relative permeability, and thereby the ultimate oil recovery. These findings appear to contradict the observations of Hagoort (1980) as well as Skauge et al. (1994), which showed that the presence of connate water helps to increase oil relative permeability and the maximum hydrocarbon pore volume (HCPV) oil recovery is possible at a connate water saturation of about 30%, in gravity drainage processes (Skauge et al., 1994).

Effect of Mobile Water Saturation

Presence of mobile water saturation in the reservoir has a strong influence on the gas-oil displacement process. Farouq Ali (2003) suggested that one of the main reasons for failures of miscible gas injection flood is its application in tertiary mode, wherein significant quantities of water need to be displaced and also the injected solvent, especially CO_2 is lost into the reservoir brine.

The mobile water 'shields' the oil from the injected gas resulting in delayed oil production, decreased gas injectivity and lower oil relative permeabilities (Kulkarni and Rao, 2005). Furthermore, the water-shielding phenomenon is a strong function of wettability, and hence more prominently observed in water-wet media than oil-wet media (Rao et al., 1992, Wylie and Mohanty, 1999). The water-shielding phenomenon leads to decreased oil recoveries in water-wet media, with similar oil trapping effects for either HC or CO_2, in both multiple contact miscibility (MCM) as well as first contact miscibility (FCM) displacements (Tiffin et al., 1991).

3.3.6 Fluid Dynamics of Gas Injection EOR Projects

Although the multiphase mechanisms (discussed previously) are translatable to (and participate in) any of the gas injection processes applied for light oil EOR, evaluation of the macroscopic fluid dynamics characterize the individual processes. Multiphase flow behavior (fluid dynamics) strongly influences the macroscopic displacement process and ultimately affects the performance of gas injection processes. These fluid dynamic effects are primarily influenced by the relative magnitude of the dominant reservoir forces (namely, gravity, capillary and viscosity) and are displayed through effects of relative permeability, oil recovery / injectivity patterns and water-to-oil ratios (in WAG processes).

This section identifies and summarizes the various multiphase fluid dynamics operational during any gas injection EOR process, with a special emphasis on gravity stable gas injection (consequently the GAGD process). The relevant multiphase fluid dynamics identified relevant for this study are: (i) gas injection mode, (ii) gravity / capillary / viscous force ratio effects, (iii) relative permeability and oil recovery characteristics and (iv) reservoir heterogeneity. However, this review is restricted to investigating the effects of gas injection mode and reservoir heterogeneity, since these parameters have been identified for further experimental investigation in this study (discussed in following sections).

3.3.6.1 Effect of Gas Injection Mode

Literature review discussed earlier (Section 3.2 and 3.3), demonstrates that the gas gravity drainage processes have been applied in both secondary as well as tertiary modes. This section summarizes the relevant multiphase fluid dynamics relevant to these two modes of gas injection. It is interesting to note the significant dynamic changes associated with the tertiary gas injection processes that are attributable only to the presence of mobile water saturation in the reservoir.

Secondary Mode Gas Gravity Drainage

Multiphase fluid dynamic considerations for gas injection under secondary conditions, generally assumes the connate water saturation to be immobile. Injection under secondary conditions, especially in an unsaturated oil reservoir (without gas cap), firstly results in an initial single-phase oil displacement followed by secondary gas-oil gravity drainage in the gas-invaded zone (Saidi and Sakthikumar, 1993). The secondary gravity drainage is controlled by the spreading coefficient (discussed in Section 3.5.3) and this secondary oil film flow (under positive spreading coefficients) is important for high gravity drainage oil recoveries in water-wet and mixed wet reservoirs. The influence of spreading coefficient (therefore film flow) on gravity drainage performance is not well understood in oil wet reservoirs.

For secondary mode gas gravity drainage under immiscible injection conditions, the threshold entry capillary pressure of the pore is the parameter that controls the extent of gas invasion. This capillary retention phenomenon, primarily responsible for trapping the reservoir oil (as well as wetting phase films), can be abated by lowering of the interfacial tension and / or increasing the viscous forces. Note that the capillary retention phenomenon is not a consideration for miscible gas gravity drainage floods, due to the absence of IFT between injected gas and reservoir oil thus negating the capillary effects.
Although the above results are generally applicable to wide range of gas gravity drainage applications, one of the major assumptions employed in the above analysis may not always hold true. As discussed in Section 3.5.5 (part a), the connate water does not

necessarily remain immobile during gravity drainage, thus violating the major assumption in the analysis, thereby resulting in saturation mobilization and redistribution attributable to the dynamics of the balance between gravity and capillary forces. Sajadian and Tehrani's (1998) micromodel studies also show that during gas gravity drainage, horizontal movement of the gas-oil contacts are not initially possible since the buoyancy forces overshadow the viscous forces, early in the life of the flood. However, in the latter stages of gas injection, liquid film flow becomes critical for gravity drainage oil production, both before and after the gas breakthrough at the production well.

Tertiary Mode Gas Gravity Drainage

Application of the gas gravity drainage process in the tertiary mode has been proven to be a viable and profitable commercial concept since the early 1980's. In gravity assisted tertiary gas injection processes, the carrying capacity of the oil films (transmissibility) is critical and determines the extent of possible reduction of the residual oil saturation (Ren et al., 2003). In watered-out reservoirs, the oil distribution could be continuous (oil-wet rocks) or as disconnected ganglia (other wetting states). In the presence of a third phase (namely injected gas), in non oil-wet systems, the oil can spread between the gas and water films under positive spreading conditions (see Section 3.5.3). However under negative spreading conditions, continuous oil films may not develop substantially decreasing recoveries. Micromodel studies (Kantzas et al., 1988; Dawe, 1990; Oren et al., 1992) on water-wet media provide with the visual proof for this phenomenon.

Other pore-level experiments (Ren, 2003) to study the drainage rates during gravity assisted tertiary gas injection, provide with additional visual proof that the oil flow rates through oil films are dependent on both, weight of the oil ganglia as well as the incremental volume of gas injected till gas breakthrough. Even after gas breakthrough, the model's gas out-flow has been observed to be intermittent (Sajadian and Tehrani, 1998) and the film flow rates become primarily gravity driven; thereby resulting in low oil flow rates. To mitigate this problem another process 'Second Contact Water Displacement' (SCWD) process has been proposed (Lepski et al., 1996; 1998) that possesses the potential to improve the oil production rates after gas breakthrough. Micromodel studies (Ren, 2002) to assess the feasibility of this process have shown some incremental recoveries and saturation redistributions during this process. However, other possible controlling economic parameters such as increased water saturations, decreased oil relative permeabilities, increased water shielding effects and higher surface water-handling costs are yet to be addressed.

3.3.6.2 Effect of Reservoir Heterogeneity

Stratification and heterogeneities strongly influence the oil recovery process since they control the injection and sweep patterns in the flood. Heterogeneity plays havoc with

horizontal gas floods leading to early breakthroughs and poor reservoir sweeps (Jackson et al., 1985; Rao, 2001). On the contrary, in gravity stable (vertical) gas floods heterogeneous stratification can delay gas breakthrough due to physical dispersion, and reduced gas channeling through the horizontally deposited high permeability layer, thereby ultimately improving sweeps.

The vertical-to-horizontal permeability (k_v/k_h) ratio is a major factor that is generally used to represent the extent of heterogeneity in a reservoir. Higher k_v/k_h ratios lead to increased cross flow in horizontal floods, perpendicular to the bulk flow direction, which are mainly influenced by viscous, capillary, gravity and dispersive forces (Rogers and Grigg, 2000). Although, the cross-flow phenomenon may increase the vertical sweep, it generally has detrimental effects on oil recovery, attributable to increased gravity segregation and decreased flow velocity, thereby leading to reduced frontal advancement in lower permeability layer(s) in horizontal (CGI or WAG) displacements. Higher k_v/k_h ratios and increased reservoir permeability contrasts not only adversely affect oil recovery in WAG process (Jackson et al., 1985), but also cause severe injection and conformance control problems (Gorell, 1990). Reservoir simulation studies (Jackson et al., 1985) conducted to examine the effects of k_v/k_h ratios on WAG oil recoveries also suggest that the higher values of k_v/k_h ratios adversely affect WAG oil recoveries.

In sharp contrast to the horizontal gas floods, the gravity stable gas injection seems largely immune to heterogeneity effects – instead the heterogeneity could be beneficial in improving injectivity and reservoir sweep. This statement is supported by comparable gravity stable injection recoveries demonstrated in sand-packs (Cardenas et al., 1981), laboratory corefloods (Catalan et al., 1994; Soroush and Saidi, 1999; Li et al., 2000), as well as commercial field injections in heterogeneous or fractured onshore / offshore reservoirs (Henriquez and Jourdan, 1996, Rao, 2001, Krijn et al., 2002, Sections 3.2 and 3.3), with widely varying reservoir and heterogeneity characteristics.

3.4 Experimental Design and Procedures

This section has been divided into two parts: (i) WAG experiments and (ii) GAGD experiments. The WAG experiments have been completed to provide with a base case scenario for the confident evaluation of the GAGD process. The bases cases were additionally designed to study the flooding characteristics of WAG and continuous injection processes in short and long Berea sandstone cores and to determine the effects of gas-oil miscibility and brine composition. Further details of the WAG experimental design are available elsewhere (Kulkarni, 2003).

3.4.1 WAG Experimental Procedure

Coreflood experiments to identify the multiphase flow characteristics of the fluids were central to this work. The corefloods of the project are of the dynamic displacement type.

Identification and separation of parameters to effectively study their effects on the process is required. Pure CO_2 gas has been used as an injectant in all the floods. n-Decane has been used as the 'Oleic' phase and two types of brine have been used as the aqueous phases to measure the effects of brine compositions (i.e. mono-valent vs. multi-valent brine).

Initially, base case flooding experiments have been conducted using Berea cores, 5% NaCl (mono-valent) brine and n-Decane. Because n-Decane is considered to be 'non-reactive' in terms of wettability effects, the data generated served as the base case for comparing water-wet system data. The base case experiments have been conducted in WAG and continuous gas injection corefloods in both miscible and immiscible modes using a horizontal Berea core system set up. Similar experiments have been conducted using n-Decane and multi-valent (Yates reservoir) brine so as to examine the results of brine composition and stability of clays. These experiments have provided the data on gas-oil displacements (both miscible and immiscible) in Berea sandstone cores for the 'non-reactive' system.

3.4.2 GAGD Experimental Design

The need for this section arises due to the pre-requisites of effective laboratory experimental design to facilitate the effective performance evaluation of the newly proposed Gas Assisted Gravity Drainage (GAGD) process, as an effective alternative to the industry-default WAG process. The GAGD process extends the highly successful gravity stable gas floods in pinnacle reefs and dipping reservoirs to horizontal type reservoirs. To allow for scalability of the laboratory experiments, the reproduction of the various multiphase mechanisms and fluid dynamics, which have been found to be influential in the success of the gravity stable gas floods is crucial. Literature reviews (Kulkarni, 2004; Section 3.3) of multiphase mechanics and fluid dynamics, suggests that dimensionless characterization of flood parameters to generate analogous field scale multiphase processes into the laboratory, is one of the most effective and preferred scaling tools.

This section examines the dimensionless reservoir characterization process and presents the protocols developed to achieve the goals of effective performance evaluation(s) of the GAGD process. This section also reinforces the relevance of dimensional analysis for development and optimization of the GAGD process, and also attempts to understand the individual effects of these dimensionless variables on multiphase mechanisms and fluid dynamics controlling gas gravity drainage.

3.4.1.1 Reservoir Characterization Requirements

To properly 'scale' and characterize a representative experiment or numerical model, several aspects pertaining to the spatial and / or physical mechanisms need to be

considered. Scaling is defined (Buckingham, 1914; Johnson, 1998; Novakovic, 2002) as a procedure of extrapolation of results obtained at one scale to another, e.g. from a small-scale laboratory observation to a large-scale process and vice versa.

A review of the various dimensionless groups traditionally employed in the literature as scaling tools are seen to be applicable to two distinct phase systems: single-phase and multi-phase. Intuitively, the dimensionless numbers applicable to single-phase systems are generally not relevant to model multiphase flow through porous media; however, they can sometimes be applicable to special scenarios wherein the fluid can be treated as single phase, e.g. pressure-transient analysis of under-saturated reservoirs (Novakovic, 2002). On the other hand, unlike the single-phase groups, the multi-phase dimensionless groups focus on the balance of the four major forces: viscous, gravity, capillary and dispersion; which also control gravity stable gas flow through porous media, and ultimately dictate breakthrough times, recoveries and dispersion.

In addition to the phase compatibility issues of dimensionless groups, the accurate numerical / experimental modeling require that the following five scaling issues also be addressed for upscaling, sensitivity analysis, stability analysis, reservoir characterization and numerical simulation (Novakovic, 2002): (i) scalability of physical effects, (ii) scalability of boundary conditions, (iii) scalability of reservoir shape, (iv) compatibility with existing reservoir simulation tools, and (v) numerical and physical dispersion.

Out these five scaling issues, only the first two are assessed to be pertinent to the laboratory experimental design for this work, wherein duplication of the multiphase mechanisms and fluid dynamics operational in the actual reservoir displacements to the laboratory is important. The remaining scaling issues also need to be addressed and should be considered for further development of the GAGD process.

3.4.1.2 Scalability of Physical Effects / Boundary Conditions

Scaling of the physical phenomenon as well as the imposed boundary conditions is critical in duplication of the multiphase mechanisms and fluid dynamics in the laboratory. Several dimensionless variables have been used in order to scale the flow behavior, with each variable representing a portion of reservoir fluid dynamics and multiphase mechanisms. Table 3.5 summarizes the basic dimensionless groups used for scaling of these phenomena from the laboratory to the field.

3.4.1.3 Dimensional Analysis of the Gravity Stable Gas Injection Process

Traditionally, the dimensional analysis has been an extremely useful tool for scaling of the laboratory experiments to field scale and vice versa. The fluid flow literature shows two distinct possible procedures for obtaining different dimensionless numbers for a given system. Basic fluid mechanics literature (Johnson, 1998; Fox and McDonald, 1998)

advocates the use of dimensional analysis (DA), while the porous media fluid mechanics studies (Shook et al., 1992) recommend the inspectional analysis (IA).

Table 3.5: Summary of Basic Multiphase Dimensionless Numbers (Novakovic, 2002)

Scaling Parameter	Variable	Formulation	Remarks
Boundary Conditions/ Response	Dimensionless Time	$t_D = \frac{V_{injected}}{V_{pore}}$	Imposed Injection Boundary Conditions
	Displacement Efficiency Factor	$E_D = \frac{V_{produced}}{V_{reference}}$	Dimensionless Production Response
Physical Effects Scaling	Mobility Ratio	$M = \frac{\lambda_{displaced}}{\lambda_{displacing}}$	Fluid-Fluid-Rock Interaction Effect on Flow Behavior
	Capillary Number	$N_C = \frac{F_{capillary}}{F_{viscous}}$	Fluid-Rock Interaction depicting entrapment at pore scale
	Gravity Number	$N_G = \frac{F_{gravity}}{F_{viscous}}$	Fluid-reservoir shape dependent, capturing the effect of buoyancy force

Dimensional and Inspectional Analysis

Buckingham (1914) developed the theory on physically similar systems that resulted in the development of a general analytical method, called the dimensional analysis. This dimensional analysis theory states that any equation that describes completely a relation among a number of physical quantities, is reducible to the form (Equation 3.13):

$\phi (\pi_1, \pi_2, ...etc.) = 0$ ..... (3.13)

In Equation 3.13, the π's are the independent dimensionless products of the form of the original quantities. The Buckingham (1914) theory thus helps characterize any physical phenomenon as an effect of various dimensionless groups, instead of individual variables. Furthermore the effects of these dimensionless groups could be experimentally investigated and universal equations could be derived for a set of variables representing different physical phenomena, thus eliminating the need for the experimental evaluation of numerous individual variables.

The term 'inspectional analysis', first coined by Ruark (1935), is generally regarded as a precursor to the dimensional analysis for improved understanding of the mechanistic behavior of a process. For the inspectional analysis of a physical phenomenon, it is necessary to write down the differential equations describing the physical process and the associating boundary or initial conditions to eventually derive various dimensionless groups governing the concerned process. Although dimensional analysis, based on

Buckingham's Pi theorem, generates complete and independent dimensionless groups for a process; this analysis generates a number of dimensionless group combinations which are non-unique solutions. Therefore, dimensionless analysis is seen to be best applicable in smaller physical systems. Inspite of the fact that inspectional analysis helps improved understanding of the underlying physical laws involved in the systems' flow behavior, the analysis is complex and cumbersome. On the other hand, although the dimensional analysis may result in non-unique solutions, it has been found to be sufficiently useful for processes involving similar flow behavior (Hagoort, 1990), thus making it more relevant to the GAGD experimental design.

Dimensional Analysis Literature Review

Dimensional analysis has been regarded to be a powerful tool that can be used to reduce the number of experimental variables required for the adequate description of the relationship among these variables. In many applications of science and engineering, especially experimental work, the mathematical relationship between the variables of a system is unknown (Chandler, 2003). The dimensional analysis of the process becomes almost indispensable since experimental evaluation and verification of all the process variables is not feasible or sometimes even impossible.

Inspite of the relevance of the dimensional analysis for improved understanding of any flow process, dimensional analysis and model studies for the gas gravity drainage applications are sparse. Geertsma et al.'s (1956) derivation of dimensionless groups using inspectional analysis is relevant to the GAGD experimental design since it not only describes dimensionless groups for solvent injection, but also helps identify the physical analogues of gravity drainage in other engineering sciences (such as Chemical and Mechanical engineering). Geertsma et al.'s correlation to the gravity drainage perspective has helped identify six commonly used dimensionless groups, namely Reynolds, Schmidt, Weber, Froude, Lewis and Grashoff groups, which could also be used for gravity drainage flow characterization.

Other gravity drainage studies (Edwards et al., 1998) show that two more dimensionless groups, the Dombrowski-Brownell number or microscopic Bond number (Equation 3.14) and macroscopic bond number (defined as Equation 3.15), need to be included to account for the gravity (buoyancy) forces relative to capillary forces during the gravity drainage process.

$$N_{DB} = \frac{\Delta\rho g k}{\sigma} \quad \text{..... (3.14)}$$

Where $\Delta\rho$ = fluid density difference, g is gravitational constant, k is permeability and σ is interfacial tension.

$$N_B = \frac{\Delta\rho g l^2}{\sigma\sqrt{\phi/k}} \quad \text{(3.15)}$$

Where l is the characteristic length (represented by the grain diameter), and ϕ is the porosity.

Grattoni et al.'s (2001) studies on gravity-dominated gas invasion with wettability and water saturation as variables show that in addition to the Bond and capillary numbers (Equation 3.16), the gravity number (Equation 3.17) plays a major role to improve the gravity drainage flow characterization along with a newly defined dimensionless group formed by combination of the effects of gravity and viscous to capillary forces.

The capillary number (Grattoni et al., 2001) describes the balance between viscous and capillary forces and is defined as Equation 16, while the Bond number measures the relative strength of gravity (buoyancy) and capillary forces (Grattoni et al., 2001) as described by Equation 15. The gravity number is defined by Equation 17 below.

$$N_C = \frac{v\mu}{P_C R_A} 2Cos\theta \quad \text{(3.16)}$$

$$N_G = \frac{\Delta\rho g k}{\Delta\mu v} \quad \text{(3.17)}$$

Where, v is the Darcy velocity, μ is the viscosity of the displacing phase, θ being the contact angle and R_A the average pore throat radius.

3.4.1.4 Identification of Key Variables through Dimensional Analysis

This section summarizes the results of the dimensional analysis of GAGD process, employed for the identification and characterization of the key operating variables, relevant dimensionless groups and their extension and comparison to field scale gravity stable gas injection applications.

Dimensional Analysis of the GAGD Process

Literature review shows that there has been limited work reported on the characterization or the dimensionless analysis for gravity drainage fluid flow; hence, dimensional analysis employing the Buckingham-Pi approach was conducted to facilitate effective GAGD experimental design.

Buckingham's Pi theorem (Buckingham, 1914) states that 'physical laws are independent of the form of the units, hence quantification and generalization of most mathematical relationships used to describe a physical phenomenon is best expressed in a dimensionless form'. This analysis becomes especially necessary for better understanding and performance prediction of novel – newer processes like the GAGD. The procedure of analysis has been documented and available elsewhere (Lui, 2003). The dependant and independent variables used in this analysis are shown in Table 3.6 along with their

fundamental dimensions. The nineteen dimensionless groups obtained after the analysis are summarized in Table 3.7.

Table 3.6: Dependant and Independent Variables used for Buckingham-Pi Analysis

Variable	Dimensions	Variable	Dimensions	Variable	Dimensions
Porosity (ϕ)	$[M^0.L^0.T^0]$	Length per Thickness (L/T) or Radius per Thickness (R/T)	$[M^0.L^0.T^0]$	Reservoir Absolute Permeability (k)	$[M^2.L^0.T^0]$
Reservoir Horizontal Permeability (k_h)	$[M^2.L^0.T^0]$	Ratio of Vertical to Horizontal Permeability (k_v/ k_h)	$[M^0.L^0.T^0]$	Gas Injection Pressure (P_{IG})	$[M^1.L^{-1}.T^{-2}]$
Reservoir Pressure (P_R)	$[M^1.L^{-1}.T^{-2}]$	Minimum Miscibility Pressure (MMP)	$[M^1.L^{-1}.T^{-2}]$	Gravity Force (g)	$[M^1.L^0.T^{-2}]$
Velocity (V)	$[M^1.L^0.T^{-1}]$	Injector Flow Rate (Q_I)	$[M^3.L^0.T^{-1}]$	Producer Flow Rate (Q_P)	$[M^3.L^0.T^{-1}]$
Gas Viscosity (μ_g)	$[M^1.L^{-5}.T^1]$	Oil Viscosity (μ_o)	$[M^1.L^{-5}.T^1]$	Capillary Pressure (P_C)	$[M^1.L^{-1}.T^{-2}]$
Oil-Water Interfacial Tension (σ_{OW})	$[M^1.L^1.T^{-2}]$	Water-Gas Interfacial Tension (σ_{WG})	$[M^1.L^1.T^{-2}]$	Oil-Gas Interfacial Tension (σ_{OG})	$[M^1.L^1.T^{-2}]$
Waterflood Residual Oil Saturation (S_{OR})	$[M^0.L^0.T^0]$	Connate Water Saturation (S_{WC})	$[M^0.L^0.T^0]$	Time (T)	$[M^0.L^0.T^1]$

It is important to note that the Buckingham-Pi analysis does not rank the dimensionless groups obtained in any order of relative importance as controlling variables of the process. Experimentation and inspectional analysis may be required to further characterize the controlling groups of variable(s) in gravity stable gas injection processes.

Dimensionless Numbers Governing the GAGD Process Performance

The literature review suggests that the most important dimensionless groups governing the gravity stable gas injection are the capillary number (N_C) and the Bond number (N_B), since these two numbers envelope majority of the reservoir forces active during gravity stable gas injection, namely the buoyancy, capillary and viscous forces. The microscopic Bond number, namely the Dombrowski – Brownell number (N_{DB}), could be a good parameter for microscopic displacement and film flow characterizations especially in gravity drainage applications where these phenomena are dominant, since it incorporates the pore size distribution as well as overall reservoir permeability in its definition. The microscopic Bond number (N_{DB}) would therefore help in improved characterizations of the governing forces in field as well as laboratory displacements.

The gravity number (N_G) and the New Group (N) by Grattoni et al. (2001) are different combinations of the capillary and Bond numbers incorporating a scaling

parameter for better displacement characterizations and appear to be good augmentations for scale-up and finer characterizations of the scaled GAGD experimental results.

Table 3.7: Dimensionless Groups Obtained Using Buckingham-Pi Analysis

No.	D. L. Group	No.	D. L. Group	No.	D. L. Group
1	ϕ	8	Q_P/Q_I	15	S_{OR}
2	L/R	9	$\frac{\mu_g.g^{(0.6)}}{Q_I^{(0.2)}.P_R}$	16	S_{WC}
3	k_v/k_h	10	P_C/P_R	17	$\frac{T.g^{(0.6)}}{Q_I^{(0.2)}.P_R}$
4	$\frac{k_h.g^{(0.4)}}{Q_I^{(0.8)}}$	11	$\frac{\mu_o.g^{(0.6)}}{Q_I^{(0.2)}.P_R}$	18	$(MMP)/P_R$
5	$\frac{k.g^{(0.4)}}{Q_I^{(0.8)}}$	12	$\frac{\sigma_{OW}.g^{(0.2)}}{Q_I^{(0.4)}.P_R}$	19	$\frac{\Delta\rho.g^{(0.8)}.Q_I^{(0.4)}}{P_R}$
6	P_{IG}/P_R	13	$\frac{\sigma_{WG}.g^{(0.2)}}{Q_I^{(0.4)}.P_R}$		
7	$\frac{V}{g^{(0.4)}.Q_I^{(0.2)}}$	14	$\frac{\sigma_{OG}.g^{(0.2)}}{Q_I^{(0.4)}.P_R}$		

GAGD Application in Miscible Mode and Highly Heterogeneous Reservoirs

Almost all the dimensionless numbers identified for the characterization of the gas gravity drainage process, involve gas-oil IFT and density and viscosity differences ($\Delta\rho$, $\Delta\mu$) in their definitions. These terms make the dimensionless groups inapplicable to miscible floods, since the gas-oil IFT as well as the density and viscosity differences, after miscibility development, is zero. To eliminate this redundancy, the following assumptions were made to facilitate the application of the same dimensional groups to miscible gas floods.

1. Miscibility is achieved when the value of interfacial tension (IFT) between injected gas and reservoir oil reaches 0.001 dynes/cm.
2. There are no density / viscosity contrasts between injected gas and reservoir oil in the 'mixing-zone' or the miscibility development zone. Hence the $\Delta\rho$ and $\Delta\mu$ terms can be replaced by ρ_{avg} and μ_{avg} respectively.

3. The characteristic length term for the concerned reservoir can be expressed as a square root of the ratio of absolute permeability to porosity.

These assumptions appear to be well justified, since they not only effectively eliminate the redundancy and provide a common comparison basis for both miscible and immiscible gas gravity drainage floods, but also truly reflect the prevalent reservoir physics during miscible gas injection.

3.4.1.5 Calculation of Dimensionless Numbers for the Field Projects

Ten commercial gas gravity drainage field applications were extensively studied and summarized (Section 3.4) for the identification and characterization of various multiphase mechanisms, fluid dynamics and calculation of the range of various dimensionless groups applicable to GAGD process. The detailed calculation protocol is included as Figure 3.10, while step-wise calculations for one commercial immiscible gravity drainage field project (West Hackberry Field, LA) is included as Appendix.

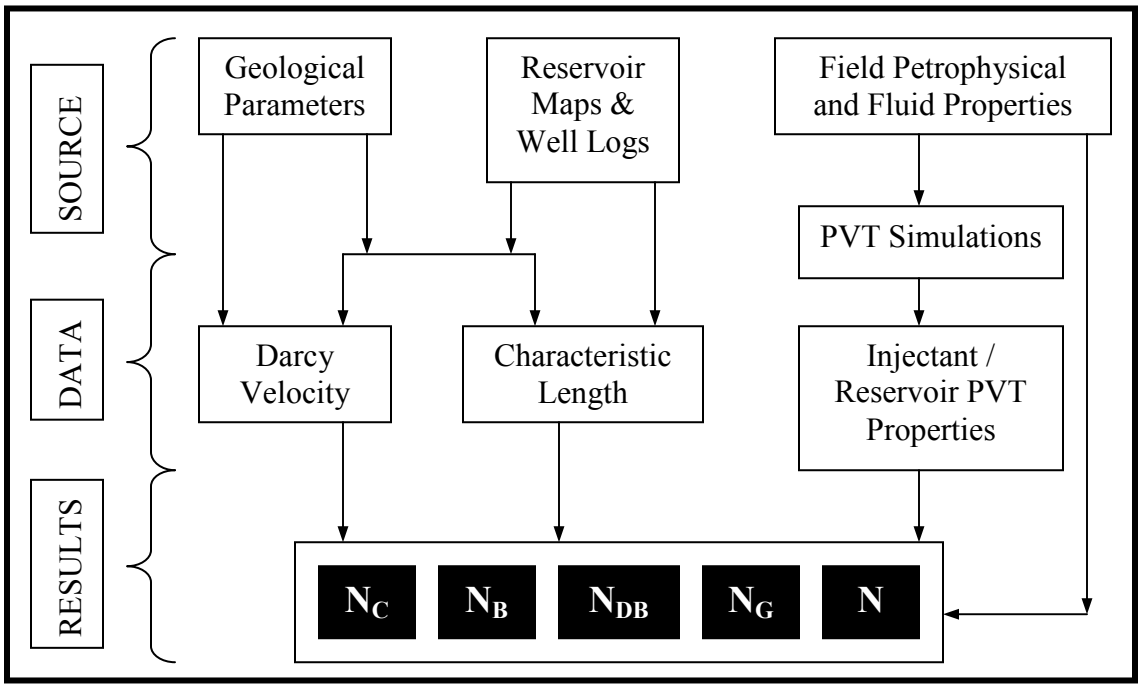

Figure 3.10: Protocol for Calculation of Dimensionless Groups for Field Cases (Where N_C = Capillary Number (Eqn. 16); N_B = Bond Number (Eqn. 15); N_{DB} = Dombrowski-Brownell Number (Eqn. 14); N_G = Gravity Number (Eqn. 17); N = New Group of Grattoni et al. (2001))

Calculation of these dimensionless numbers for field projects involved the use of various well logs (for thickness, net-to-gross values, OWC, GOC and grain size), field maps (for Darcy velocity), use of grain size classification systems (for Bond number), production / injection data (for New Grattoni et al. (2001) group), bottom hole pressure

survey plots (for PVT simulations), compositions of injected / produced fluids (for PVT simulations), and PVT compositional simulations (for fluid properties predictions).

It was noted earlier that these dimensionless groups are not applicable to miscible fluid injection mainly due to the absence of interfacial tension (IFT) and density / viscosity contrasts between displacing and displaced reservoir fluids. Definition of new dimensionless groups governing miscible flood behavior is necessary due to the increasing commercial trends toward miscible injections.

Hence to facilitate the calculation of various dimensionless groups in miscible field cases, appropriate modifications to the definition of dimensionless numbers to reflect the reservoir physics were also employed (see Section 4.4.3). The complete ranges of dimensionless groups for all the commercial gravity drainage projects is included as Table 3.8, and plotted as Figure 3.11.

Table 3.8: Dimensionless Number Ranges Obtained for Field Applications and Laboratory Studies

Dim. Groups		Field Range		Physical Model		Corefloods		
		IMM	*MIS*	*Para*	*nC10*	*Type*	*1-ft*	*6-ft*
N_C	*Min*	4.18E-08	1.84E-05			*IMM*	2.59E-06	2.59E-09
	Max	1.12E-09	1.83E-06	9.28E-09	6.92E-09	*MIS*	2.57E-04	2.57E-04
N_B	*Min*	1.21E-05	5.77E-02			*IMM*	1.64E-06	7.72E-07
	Max	2.84E-07	3.01E-03	1.48E-04	4.16E-05	*MIS*	1.70E-02	7.88E-03
N_{DB}	*Min*	3.14E-06	6.31E-03			*IMM*	3.09E-07	1.68E-07
	Max	1.50E-07	2.56E-04	1.23E+00	4.80E+01	*MIS*	3.15E-03	1.71E-03
N_G	*Min*	8.75E+02	2.96E+02			*IMM*	1.17E+01	6.38E+00
	Max	3.85E-01	1.62E+00	1.48E-04	3.90E-05	*MIS*	1.22E+01	6.66E+00
N	*Min*	-6.89E-05	-2.30E+00			*IMM*	-4.96E-04	-4.97E-04
	Max	-2.42E-03	-3.00E+00	6.17E-05	1.53E-05	*IMM*	-4.41E+00	-4.42E+00

Calculations of Dimensionless Numbers for Field Projects – A Case Study

Out of the ten field cases considered, calculation of dimensionless numbers for the West Hackberry tertiary air injection project is included here as an example case. The West Hackberry tertiary air injection project was a joint initiation by United States Department of Energy, Amoco Production Co. and Louisiana State University to demonstrate the feasibility of air injection in Gulf coast reservoirs with pronounced bed-dip using the Double Displacement Process (DDP) in 1993. The range of calculated dimensionless numbers for this project is included as Table 3.9. Further detailed calculations and methodology are included as elsewhere (Kulkarni, 2005).

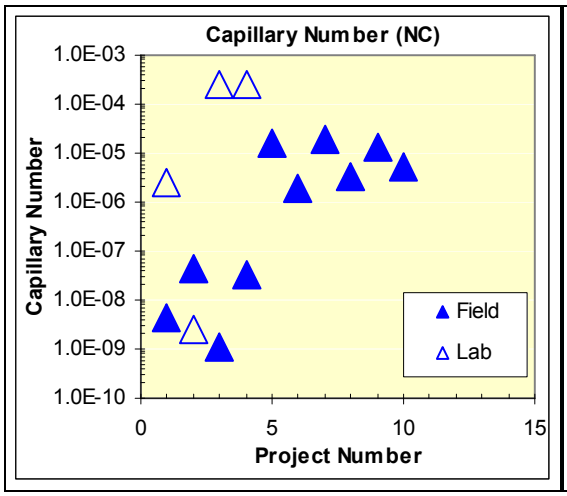

(a) Capillary Number Comparison

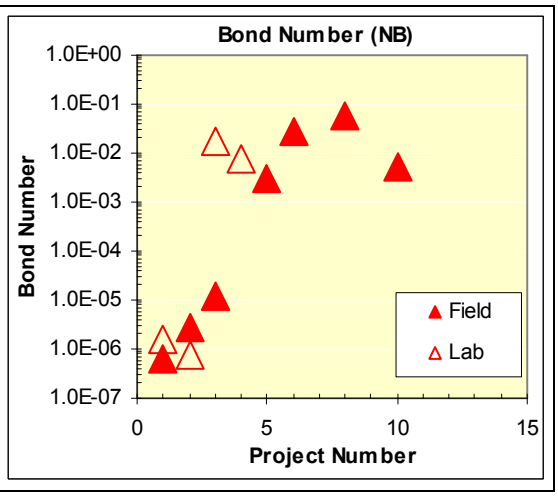

(b) Bond Number Comparison

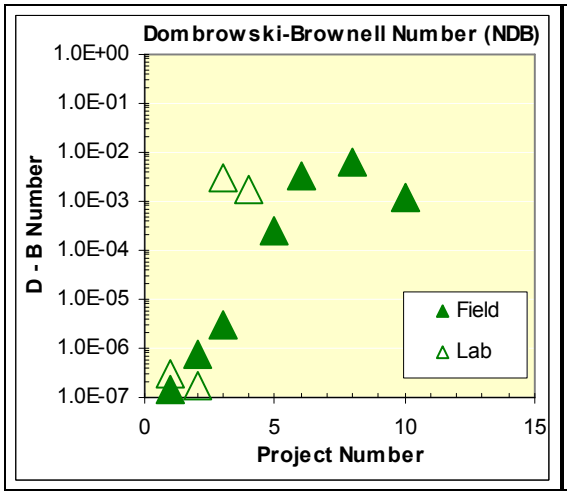

(c) D – B Number Comparison

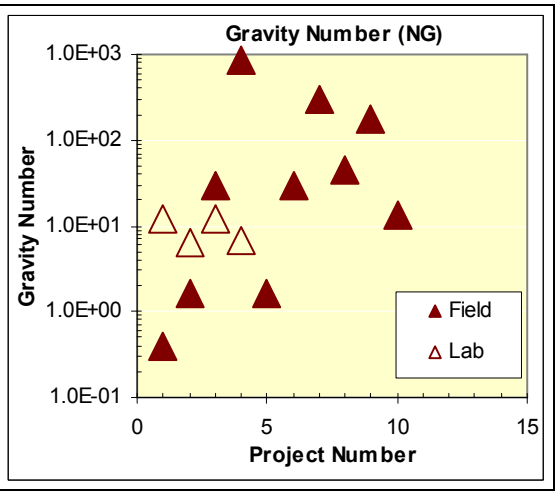

(d) Gravity Number Comparison

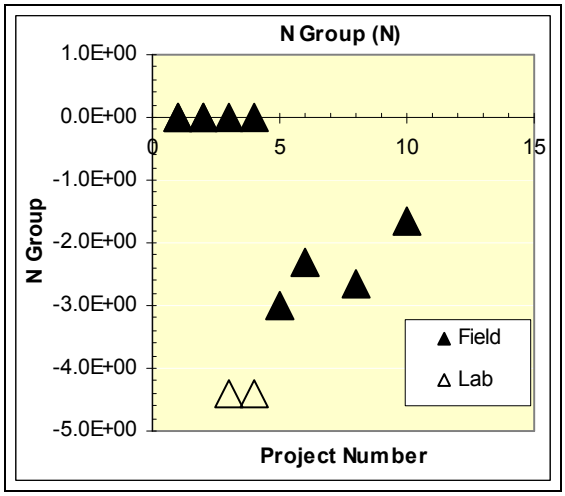

(e) N Group (Grattoni et al., 2001) Comparison

Figure 3.11: Graphical Comparison of Values of Dimensionless Groups Calculated for Field and Laboratory Cases

Important Conclusions from these Calculations – Example Case Study

The plots of operating Bond, capillary, Dombrowski-Brownell, Gravity and N groups for West Hackberry field are included in Figure 3.12 and 3.13. The ranges of operating bottom hole pressures (BHP) for West Hackberry field are 2400 psi – 3400 psi. For this range, the capillary number is observed to be a weak function of the reservoir Darcy velocity, but the Bond number shows a strong dependence of mean reservoir grain diameter. Hence, reservoir heterogeneity would become important parameter determining the overall displacement characteristics. The microscopic Bond number (that is the Dombrowski-Brownell number) and N group exhibit similar dependence on reservoir permeability and grain size distribution respectively. However, the Gravity number does not show significant dependence on grain size distribution and / or reservoir permeability. These groups are instead seen as strong functions of Darcy velocity.

The results indicate that these dimensionless numbers can be weakly characterized into two groups: (i) Petrophysical parameter(s) dependent groups – N_B, N and N_{DB} (which are characterized by reservoir permeability, porosity, grain size distribution and tortuosity) and (ii) Operational parameter(s) dependent groups – N_C, and N_G (which are characterized by injection pressures, rates, and other production parameters).

It is interesting to note that similar trends were observed for all other field studies, and the dimensionless number ranges are critical for effective GAGD experimental design. Furthermore this dimensional analysis suggests that the field project characterizations should be primarily based on the operating Bond, capillary, Dombrowski-Brownell, Gravity and N groups (by Grattoni et al. (2001)).

Table 3.9: Values of Dimensionless Groups Operating in West Hackberry Field

Number	Formula	Min. Value	Max. Value
Capillary Number	$N_C = \frac{V(m/s) * \mu(Pa.S)}{\sigma(N/m)}$	4.564E-09	4.1798E-08
Bond Number	$N_B = \frac{\Delta\rho(kg/m^3) * g(m/s^2) * l^2(m^2)}{\sigma(N/m)}$	0.03171	1.5932
Dombrowski-Brownell Number	$N_{DB} = \frac{\Delta\rho(kg/m^3).g(m/s^2).k(m^2)}{\sigma(N/m)}$	1.5024E-07	7.833E-07
Gravity Number	$N_G = \frac{\Delta\rho(kg/m^3).g(m/s^2).k(m^2)}{\Delta\mu(Pa.s).u(m/s)}$	0.3855	1.5932
New Group of Grattoni et al., (2001)	$N = N_B + A(\frac{\mu_D(Pa.s)}{\mu_G(Pa.s)}).N_C$	0.0361	1.627

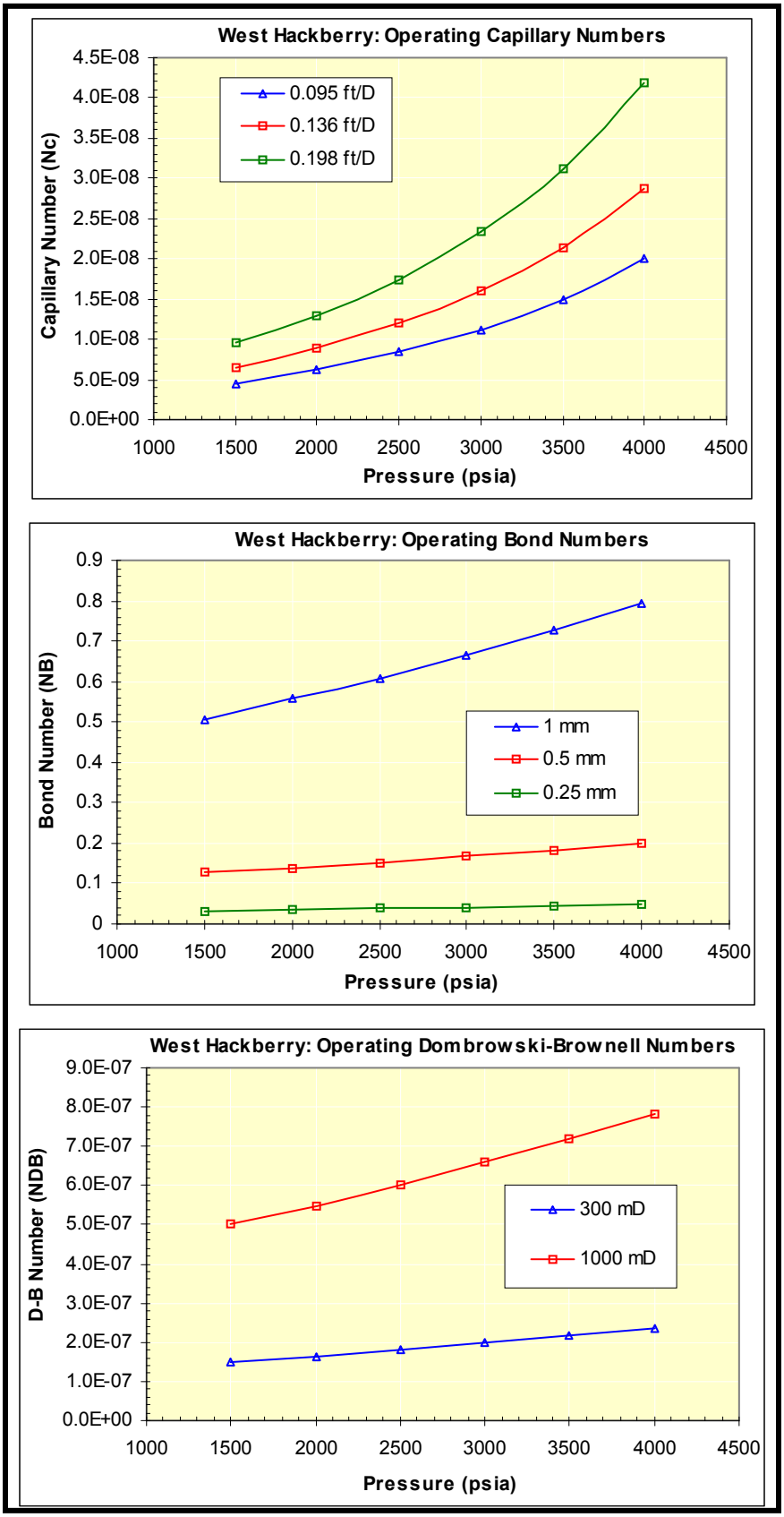

Figure 3.12: Calculated Operating Capillary, Bond and Dombrowski-Brownell Numbers

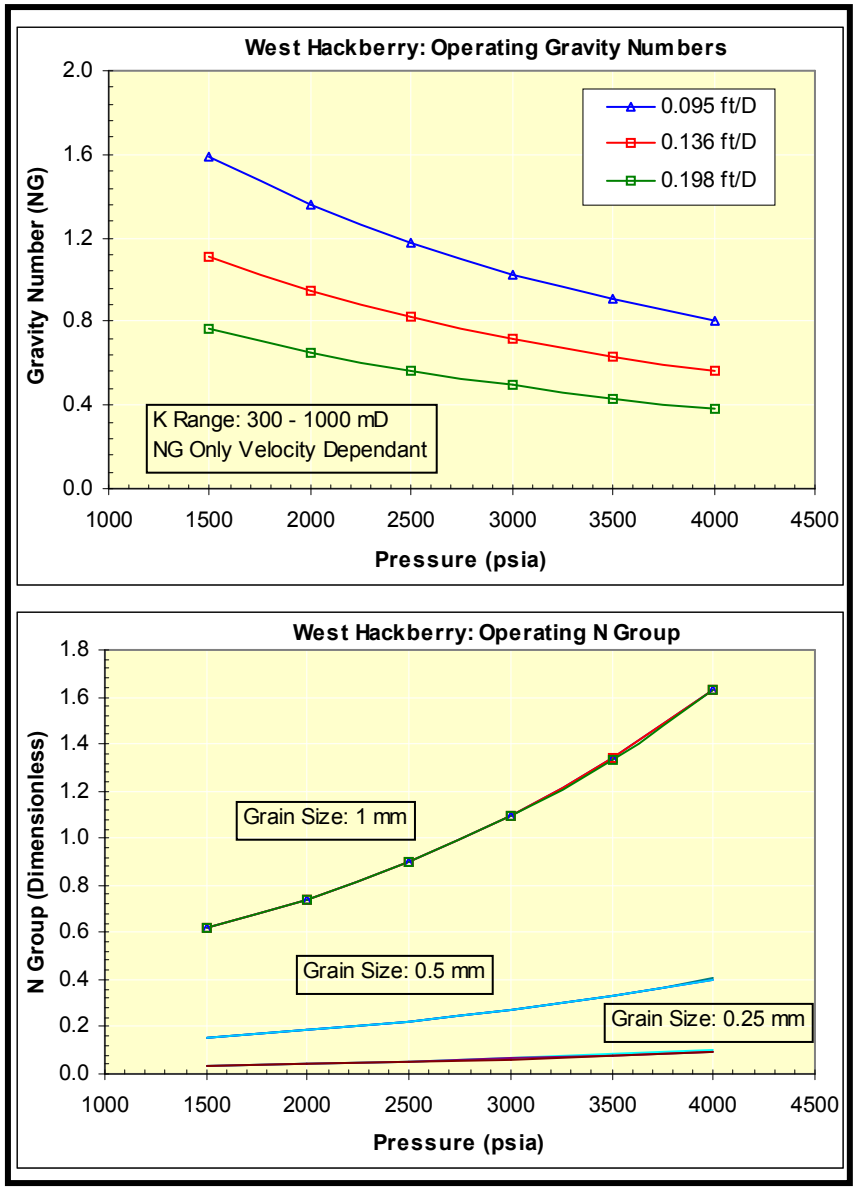

Figure 3.13: Calculated Operating Gravity and N Group Numbers

Lastly, it is important to note that none of the dimensionless groups governing the gravity drainage process contain the macroscopic length term i.e. displacement characteristics are independent of the length of the porous medium. Hence, scaled experimentation on shorter laboratory cores would be as effective and comparable to longer cores; thus de-emphasizing the need to conduct all the experiments on 6-ft Berea cores, which significantly reduces the experimentation time.

3.4.3 Dimensional Similarity Approach to GAGD Experimental Design

The literature review, summarized in previous sections, clearly shows that the five dimensionless numbers recommended for the characterization of the gravity drainage

field projects provide adequate reservoir mechanics information for gravity stable gas injection processes. Literature review and dimensional analysis further advocate the dimensional similarity based experimental design. To facilitate this design, the five dimensionless groups were calculated (see Section 4.5) for each of the gravity stable field projects studied (see Table 3.3). Attempts were made to duplicate the ranges obtained for these dimensionless groups in the laboratory by selecting proper fluids and operating conditions. This section details the calculation of dimensionless numbers for the laboratory experiments and summarizes the resulting experimental design.

3.4.3.1 Calculation of Dimensionless Numbers for Laboratory Core Displacements

The five dimensionless groups mentioned above were calculated for the GAGD corefloods conducted in this study. The ranges of the dimensionless numbers for both laboratory and field projects are tabulated as Table 3.8 and plotted as Figure 3.11.

It is observed that values of the dimensionless numbers for laboratory corefloods as well as the 2-D Hele-Shaw type visual physical model (Sharma, 2005) values lie within the field ranges. This clearly indicates that we are able to 'mimic' the various multiphase mechanisms and fluid dynamics operating in the field into the laboratory, and that the results of all the laboratory experiments completed in course of this work, are 'translatable' to the field.

This mechanistic scaling of the laboratory experiments not only helps regenerate field scale mechanics into the laboratory corefloods, but also provides with a realistic tool to study the effects of flood parameters on the processes' performance The following section details on the mechanistic and fluid dynamic experimental design of the 'scaled' laboratory experiments.

3.4.3.2 Flow Regime Characterization of the GAGD Process

Flow regime characterization is important for the elucidation of operating fluid mechanics during gravity drainage, and is also helpful in designing efficient gas injection programs in commercial floods. Localized variations in the capillary forces, due to pore scale heterogeneities, result in non piston-like (Buckley-Leverett type) displacements, called 'capillary fingering' (Aker, 1996). On the other hand, the viscous forces act across the fluids at all length scales, and combined with mobility ratio, are responsible for viscous fingering. In horizontal floods these displacement instabilities have a negative effect on the flood performance, and may lead to non-optimal recoveries in gravity stable gas injection processes.

Literature review (see Section 3.1) suggests the use of various stability criteria to assure the flood fronts' stability. The GAGD flood experimental design used three of the common stability criteria to assure the flood fronts' stability: Leas and Rappaport (1953)

criterion for horizontal injections and Dumore (1964) and Rutherford (1962; Mahaffey et al., 1966) criteria for gravity stable injections.

Experimental (Lenormand et al., 1987) and simulation model (Aker, 1996) studies for drainage flow characterizations in porous media are sparse, and rely on unrealistic horizontal type drainage floods conducted using either micromodels or Lattice-Boltzmann percolation flow simulation models. The Lenormand et al.'s (1988) 'phase-diagram' is the common gravity drainage flow regime identification plot (Aker, 1996; Sukop and Or, 2003). Dimensionless numbers calculated for both the miscible and immiscible GAGD laboratory coreflood experiments as well as the field gravity drainage applications were plotted on the digitized Lenormand et al.'s (1988) plot (Figure 3.14).

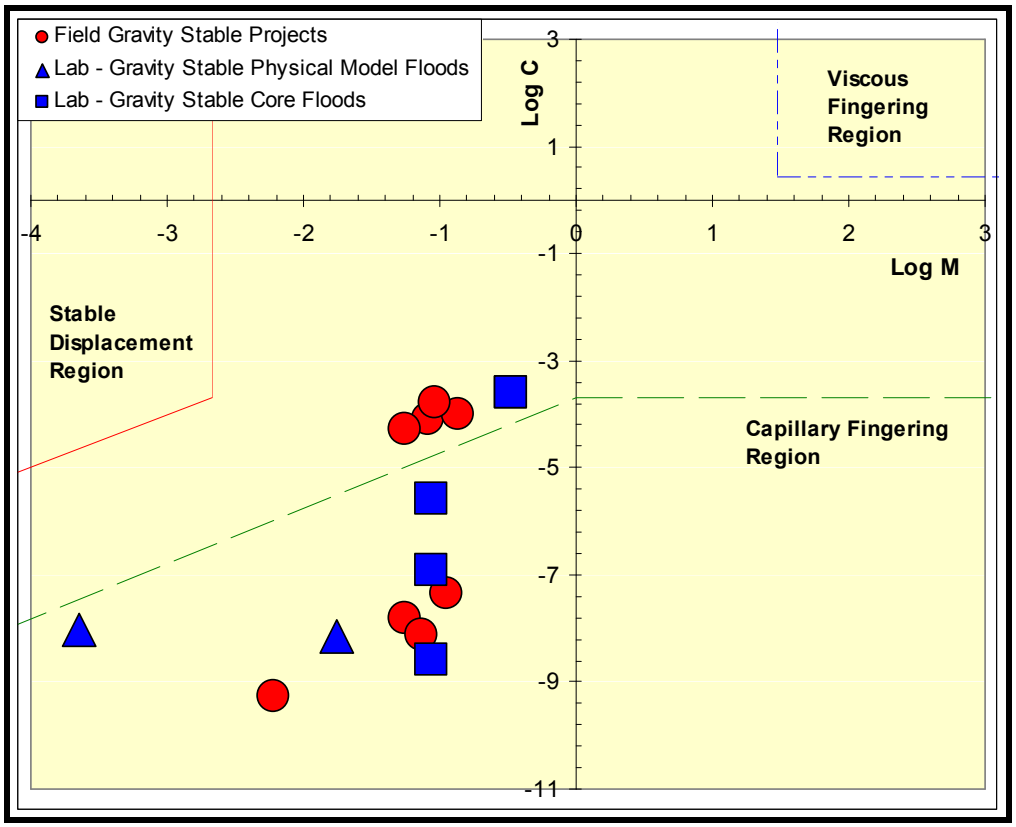

Figure 3.14: Digitized Lenormand et al's (1988) Horizontal Instability Plot Superimposed with Gravity Stable Field and Laboratory (Coreflood and Visual Model) Data

Since the Lenormand et al.'s (1988) plot was developed using horizontal micromodel displacement experiments, Figure 14 shows that the horizontal type injection at the respective capillary number and fluid property values would result in an unstable flood front (i.e. capillary fingering at the flood front would occur, resulting in non-optimal flood performance).

To assess the validity of the above hypothesis that the flood front during GAGD experiments conducted is stable, 2-D physical model experiments using Hele-Shaw type visual model were also conducted at various capillary number values and fluid viscosities (Sharma, 2005). Figure 3.15 compares the actual flood fronts (Sharma, 2005) observed during GAGD displacements and the flood front profile predicted by Lenormand et al.'s (1988) plot (reproduced by Sukop and Or, 2003).

In spite of the fact that Lenormand et al.'s plot predicts capillary fingering development during GAGD floods (Figure 3.14); Figure 3.15 clearly shows that during GAGD injection capillary fingering does not occur and that the GAGD flood fronts closely resemble the 'stable displacement' pattern predicted by Lenormand et al.'s (1988) plot (reproduced by Sukop and Or, 2003). This clearly suggests that satisfaction of the flood's frontal stability criteria is necessary and sufficient to ensure stable displacement in GAGD floods.

Incorporation of the Multiphase Mechanisms and Fluid Dynamics Operations in the Field Applications into Experimental Design

This section summarizes the isolation and characterization of various multiphase mechanisms and fluid dynamics duplicated from commercial gravity stable gas injection floods into the 'scaled' laboratory coreflood experiments.

The important parameters that were considered in the experimental design were: miscibility development, effect of spreading coefficient, reservoir heterogeneity, reservoir wettability (use of Yates Dolomite core) considerations, injectant type and mode(s) of injection.

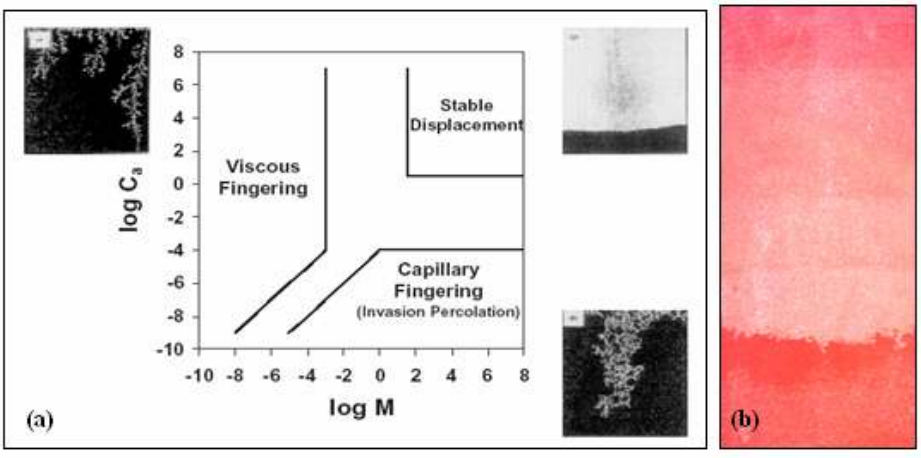

(a) Lenormand et al.'s (1988) Plot Superimposed with Lattice Boltzmann Percolation Model Photographs (Sukop and Or, 2003) **(b)** Observed GAGD Visual Model Stable Displacement Flood Front (Right) During GAGD Run (CR5) (Sharma, 2005)

Figure 3.15: Comparison of Actual GAGD Flood Front Profile (Sharma, 2005) with Flood Front Profile Predicted by Lenormand et al.' (1988) Phase Diagram

Miscibility Considerations

Important miscibility considerations during the optimization and development of the new GAGD process were addressed by conducting miscible and immiscible GAGD floods on 1-ft Berea cores using Yates reservoir brine, n-Decane and CO_2.

Effect of Spreading Coefficient

Laboratory and theoretical studies (Section 3.2) demonstrate that a positive spreading coefficient in strongly water-wet systems results in significantly high gravity drainage recoveries, while its effects on oil-wet media are not clear. Winprop® simulations for the n-Decane, Water, and CO_2 fluid triplets showed that a positive spreading coefficient results for the coreflood conditions being employed in this study. These values are summarized as Table 3.10.

To investigate the effects of a negative spreading on oil recovery in water-wet porous media, following three chemicals were considered as the 'oleic' phase: Aniline, Carbon Tetrachloride and Isopropyl Acetate. The various properties calculated for these three chemicals are included as Table 3.11 below.

Table 3.10: Simulated / Calculated Spreading Coefficients for n-Decane, Water, and CO_2 fluid triplets

$nC_{10}/H_2O/CO_2$	$\sigma_{G/W}$ (dy/cm)	$\sigma_{G/O}$ (dy/cm)	$\sigma_{W/O}$ (dy/cm)	Spreading Coeff.
500 psia / 76 °F	17.5074	8.7268	0.0044	(+) 8.78
2500 psia / 76 °F	0.3279	0.0000	0.0031	(+) 0.3248

Table 3.11: Calculated Aniline, Carbon Tetrachloride and Isopropyl Acetate Properties with CO_2 and Yates Reservoir Brine

Property / Chemical	Aniline	Carbon Tetrachloride	Isopropyl Acetate
P & T Conditions	500 psi & 76 °F	500 psi & 76 °F	500 psi & 76 °F
Chemical Formula	C_6H_7N	CCl_4	$C_5H_{10}O_2$
Molecular Weight	93.1	153.8	102.1
Normal Boiling pt	363.2 °F	169.7 °F	192.2 °F
Specific Gravity	1.02	1.59	0.88
Water Solubility	3.4 gm / 100 ml	0.1 gm / 100 ml	4.3 gm / 100 ml
$\sigma_{G/W}$ (dynes/cm)	17.5074	17.5074	17.5074
$\sigma_{G/O}$ (dynes/cm)	91.4017	4018.3194	36.8204
$\sigma_{W/O}$ (dynes/cm)	2.8867	1627.9867	0.1899
$S = \sigma_{G/W} - \sigma_{G/O} - \sigma_{W/O}$ (dynes/cm)	(-) 76.78	(-) 5628.7987	(-) 19.5029

It is interesting to note that Isopropyl Acetate has moderate solubility in brine and exhibits negative spreading coefficient at 500 psia and 76 ^{o}F. On the other hand, IPA exhibits first contact miscibility with CO_2 at pressures higher than 730 psia; and results in reversing the sign on the spreading coefficient value at miscible coreflood design conditions (spreading coefficient becomes positive at 2500 psia and 76 ^{o}F as shown in Equation 3.18 below). To investigate the effects of spreading coefficient on GAGD oil recoveries, GAGD type corefloods were conducted at 500 psia and 76 ^{o}F.

$S = \sigma_{G/W} - \sigma_{G/O} - \sigma_{W/O}$…….@ 2500 psia & 76 F……...……..(3.18)

S = (+) 0.0902 dynes/cm.

Effect of Reservoir Heterogeneity and Wettability

The GAGD corefloods conducted on homogeneous, strongly water-wet Berea sandstone cores for miscibility considerations (using n-Decane, Yates reservoir brine and CO_2), provided with a base case for the GAGD process performance evaluation against these two parameters. To investigate the effects of reservoir vertical fractures, the base case GAGD experiments were repeated on the same Berea core, but sliced in the center, resulting in a very high permeable vertical fracture connecting the injection and production fluid distributor plates.

On the other hand, to investigate the effects of reservoir wettability on GAGD flood performance, miscible as well as immiscible GAGD experiments were conducted using Yates reservoir fluids on Yates reservoir cores. Berea sandstone corefloods conducted previously also served as a base case to evaluate GAGD performance in highly fractured, heterogeneous and oil-wet to mixed-wet Yates reservoir cores.

Effect of Injectant Fluid Type

The recent spotlight on CO_2 sequestration makes CO_2 an ideal injectant in U.S. scenario (Kulkarni, 2003). Furthermore, the GAGD process using natural gas as injectant could possibly be very relevant to facilitate offshore EOR applications of the GAGD process. To evaluate the effect of gas injectant type on GAGD performance, miscible and immiscible GAGD floods were conducted using CO_2 injectant. However, discussion of the hydrocarbon GAGD floods is outside the scope of this dissertation. This is partly due to the complex mass-transfer effects involved in miscible HC slug design and displacement.

Effect of Injectant Fluid Mode

Gas injection literature review (see Chapters 1 and 3) suggests that gas injection has been applied in both secondary as well as tertiary injection modes in commercial gas injection projects. Although there is a difference of opinion as to whether gas injection be applied

in secondary or tertiary mode, it has been observed that project economics, reservoir wettability and gas availability are the critical decision parameters. Moreover, as the injection mode is generally reservoir specific, both of the gas injection modes were evaluated for GAGD experimental design. The other parameters of particular relevance to tertiary mode gas injection that need to be considered are: (i) reservoir mobile water saturation (Farouq Ali, 2003), (ii) reservoir residual oil saturation (Farouq Ali, 2003), (iii) solvent-brine solubility, especially in case of CO_2 injectant, and (iv) higher and preferential initial free water production in tertiary mode GAGD floods driven by gravity segregation and reservoir fluid saturations.

3.4.4 Experimental Details

3.4.4.1 Experimental Fluids

Analytic grade reagents were used in all the experiments. n-Decane, Isopropyl Acetate, various cleaning chemicals (Acetone, Methylene Chloride and Toluene) and the various salts used for synthetic Yates reservoir brine (default brine used for all experiments) preparation were obtained from Fisher Scientific with a purity of 99.9%. Brine was prepared by dissolving predetermined quantity of various salts (Table 3.12) in de-aerated deionized water from LSU's Water Quality Laboratory. The Berea sandstone (Liver Rock type) used in the experiments was obtained from Cleveland Quarries, Ohio, while the Yates reservoir rock and fluids were obtained from Marathon Oil Company.

3.4.4.2 Experimental Setup

The vertical coreflooding system schematic that was used for unsteady state GAGD experimentation is shown below as Figure 3.16. It consists of a high-pressure Ruska pump injecting fresh (tap) water at desired flow rate and pressure to the bottom part of the floating piston transfer vessel. The transfer vessel is filled with the fluid to be injected into the core.

High-pressure steel piping (1/8" ID) carries the fluid and is injected into the core with the assistance of a liquid re-distributor plate. The produced fluids were carried through the backpressure regulator into a measuring cylinder / electronic balance to determine fluids production as a function of run time. A parallel set of piping was constructed to facilitate the circulation of core clean-up fluids using a centrifugal pump. The inlet, outlet, differential, back and annulus pressures were measured using electronic pressure transducers (previously calibrated against a standard dead-weight tester) mounted on the coreflood apparatus.

The vital components of the core-flooding apparatus are labeled from 'A' to 'J'. Individual pictures of the equipment are shown in Figures 3.17 – 24 (not pictured: Parts G, H and J). The cores were coated with a single coating of epoxy, to prevent damage during handling and processing of the core such as end facing, polishing and cutting.

Table 3.12: Composition of Yates Reservoir Brine of pH 7.39 (Vijapurapu and Rao, 2002)

Parameter	Concentration (mg/L)
Total Dissolved Solids	9200
Calcium	425
Magnesium	224
Potassium	50.5
Sodium	1540
Hardness as $CaCO_3$	1500
Hardness as Carbonate	810
Hardness as Non-Carbonate	730
Bicarbonate	800
Alkalinity	810
Sulfate	660
Chloride	3700

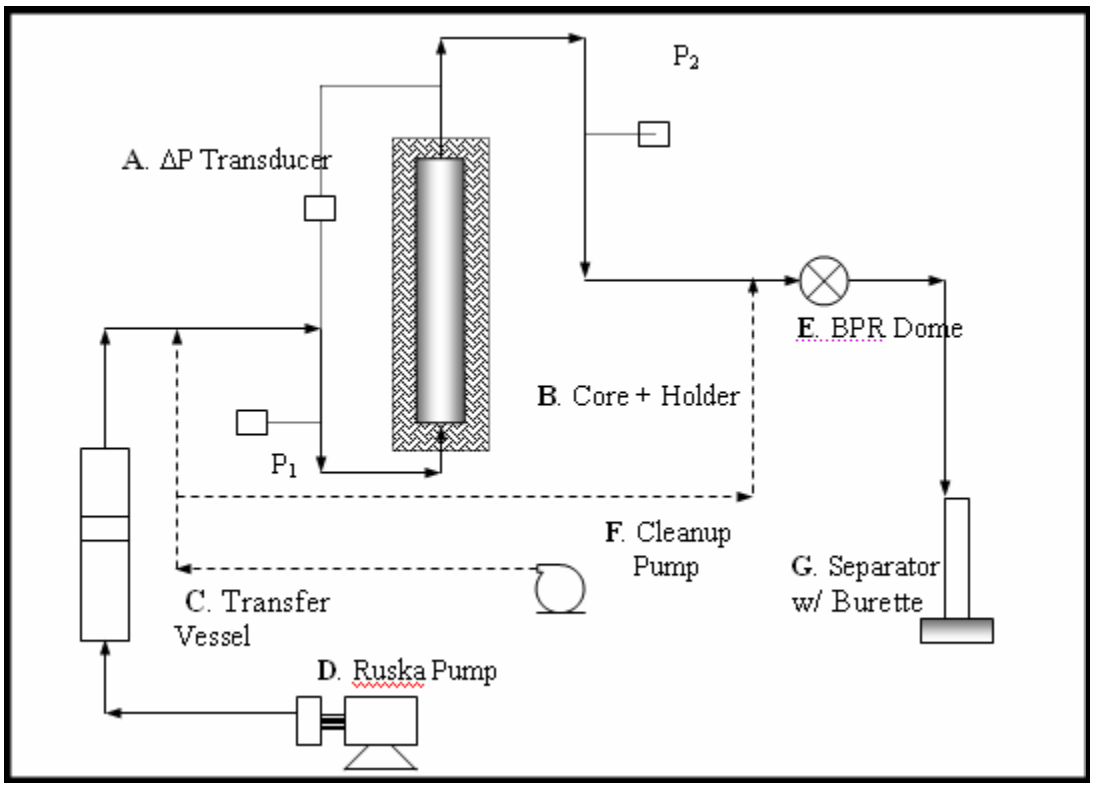

Figure 3.16: Vertical Core Flooding System Schematic

Legend for the above schematic:

..... : Electrical Lines

——— : 1/8" High Pressure Piping

– · – · – : Instrumentation Lines

– – – – – : Cleanup / Accessories Lines

Figure 3.17: Differential Pressure Transducer (Part A)

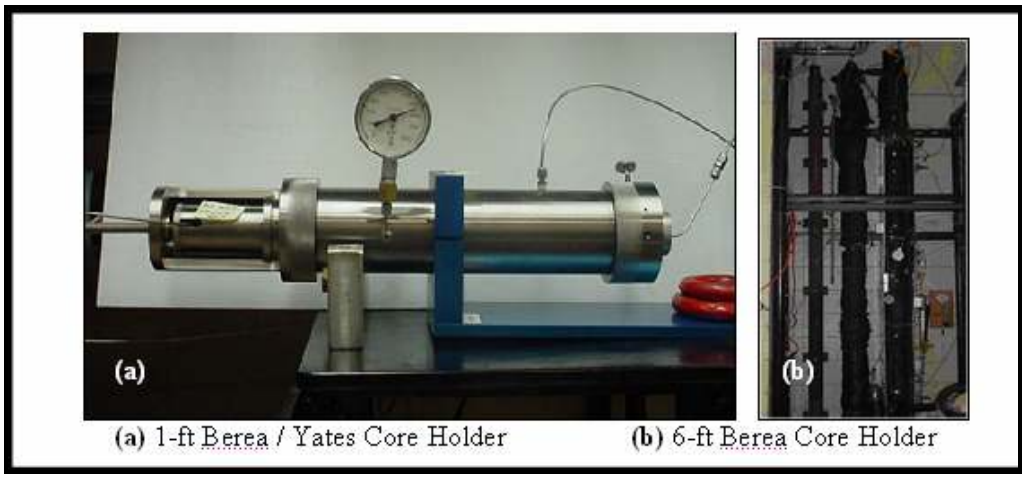

Figure 3.18: Core Holders used for GAGD Experiments (Part B)

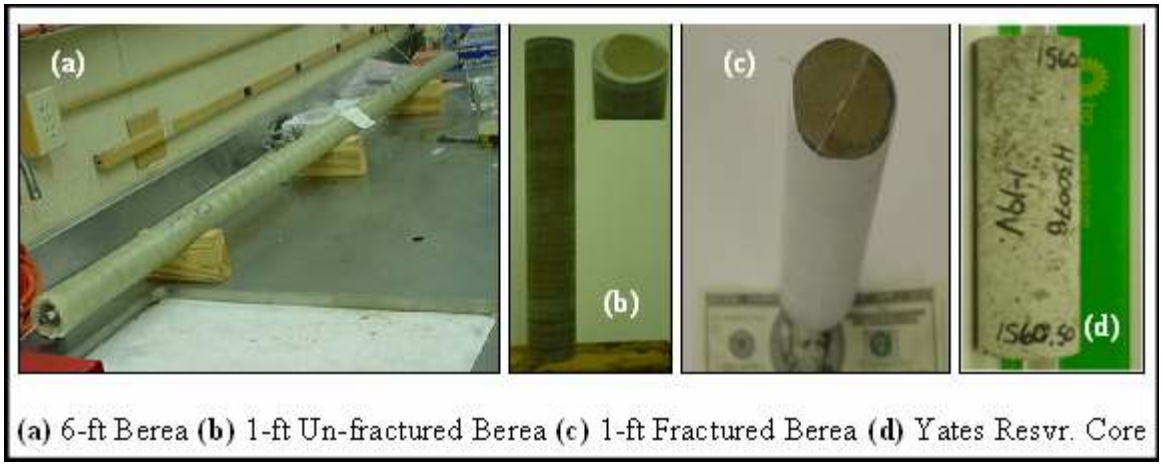

Figure 3.19: The Suite of Cores Employed for GAGD Experimental Design (Part B)

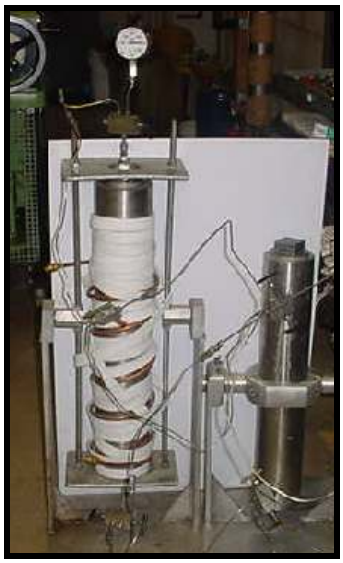

Figure 3.20: Fluid Transfer Vessel (Part C)

Figure 3.21: Ruska Positive Displacement Pump (Part D)

Figure 3.22: Back Pressure Regulator (Part E)

Figure 3.23: Centrifugal Pump used for Cleanup (Part F)

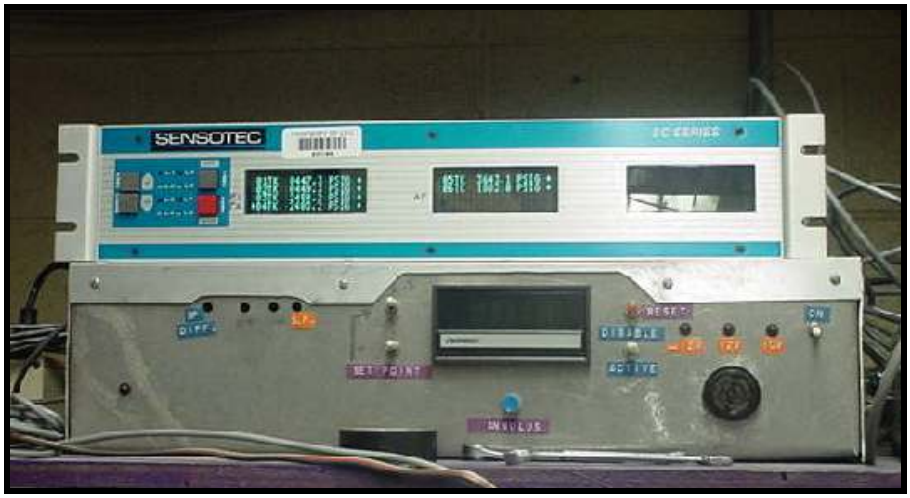

Figure 3.24: Injection, Production and Annulus Pressure Readout (Part I)

3.4.4.3 Experimental Flowchart

The complete suite of 'scaled' experiments that were designed for individual investigation of the various controlling parameters (discussed in previous sections) on the GAGD process performance evaluation has been summarized in Figure 3.25.

3.4.4.4 Experimental Procedure

There were two distinct experimental procedures (sets) that were followed for optimizing the gas injection process. First set comprised of the continued investigation of the recommendations and hypothesis provided in the M.S. thesis of Kulkarni (2003). This section involved all horizontal mode injections for: CGI, WAG and the 'happy-medium' between CGI and WAG identified in course of these experiments. The experimental protocol that was followed during this experimentation is documented elsewhere (Kulkarni, 2003; Kulkarni and Rao, 2004; Kulkarni and Rao, 2005). The first experimental set also provided with a base case scenario for the second suite of

corefloods designed for the further development and optimization of the newly proposed GAGD process (Rao, 2001).

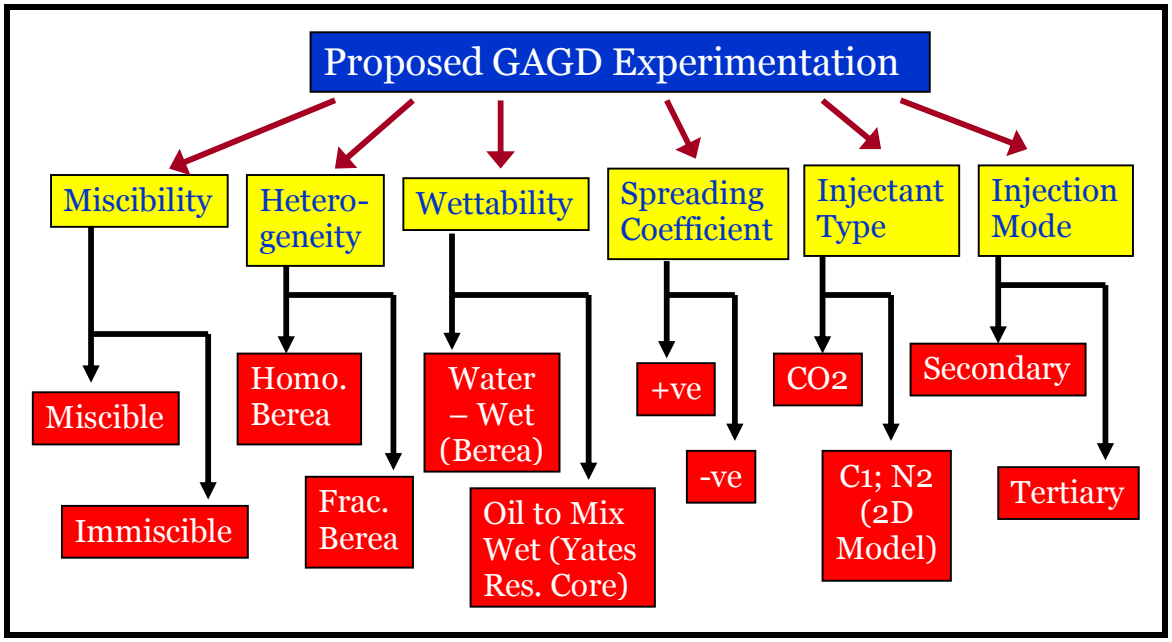

Figure 3.25: Experimental Flow Chart Designed for GAGD Process Evaluation

For the GAGD experimentation, apart from the employment of various experimental fluids and conditions (elucidated during the individual discussion of the experimental results), two discrete flood protocols were employed: Gravity Stable Displacement History (GSDH) GAGD floods and Non-Gravity Stable Displacement History (NSDH) GAGD floods. In GSDH GAGD floods, all the experimental steps, namely oil injection to connate water saturation (oil flood), water injection to residual oil saturation (water flood – where applicable), and gas injection in the GAGD mode, were conducted in a gravity stable mode. In GSDH GAGD floods, oil was injected into a fully brine saturated vertically oriented core from top to bottom, water was injected into a vertically oriented core at connate water saturation from the bottom (optional step), while the gas injection step was gravity stable, i.e. gas injection into a vertically oriented from the top. On the other hand, the NSDH GAGD floods conducted the oil and water injection steps on a horizontally oriented core were as only the gas injection was conducted in a gravity stable manner (vertically oriented core, with gas injection from the top). The GSDH floods, although unrealistic from a commercial gas injection point of view and purely of academic interest, provided with an 'upper-limit' estimate of the GAGD process performance.

In spite of the fact that CGI, WAG, Hybrid-WAG and GAGD coreflood experiments required significantly different gas injection protocols, the steps common to all the

experiments conducted were: Saturation of the core with Yates reservoir brine, determination of core pore volume and absolute permeability, oil injection (either in the horizontal or gravity stable mode) into the core to achieve connate water saturation, end-point oil-permeability, Yates reservoir brine injection (either in the horizontal or gravity stable mode) into the core to achieve waterflood residual oil saturation (for tertiary gas floods only), and end-point water-permeability measurement followed by the gas injection step in either CGI, WAG, Hybrid-WAG or GAGD mode.

The detailed experimental protocol that was employed for core cleaning, pore volume determination, absolute permeability determination, oil flooding, brine flooding and gas injection in CGI, WAG, Hybrid-WAG mode is available elsewhere (Kulkarni, 2003; Kulkarni and Rao, 2004; Kulkarni and Rao, 2005). For the GAGD experimentation the following changes were made:

1. The fluid injection rates during horizontal mode floods are determined by the Leas and Rappaport (1953), while the gravity stable gas injection rates are determined using the Dumore (1964) and Rutherford (1962; Mahaffey et al., 1966) flood front stability criterion.
2. The GAGD flood protocol was very similar to the CGI floods, with the exception that the gas injection step during GAGD floods was gravity-stable.

During the NSDH GAGD Yates core injections, the n-Decane is replaced with Yates stocktank crude oil in the oil flooding step.

3.4.4.5 Scope of Research

The scope of this study was limited to the experimental flow chart depicted in Figure 3.25. Majority of the experimentation was conducted by employing Yates reservoir fluids, n-Decane, with 1-ft Berea cores as the porous media. Moreover, as the dimensional scaling of the experiments helps eliminate the dependency of experimental results on the length of the porous media, only selected experiments were conducted on 6-ft Berea sandstone cores due to significantly higher run time requirements. Reservoir condition scaled experiments using Yates reservoir fluid and Yates field cores were also conducted to identify and characterize the influence of design parameters on realistic fluid systems. Lastly, all the GAGD experiments were conducted using pure CO_2 as injectant.

3.4.4.6 Base Case CGI and WAG Experimental Results

The base case CGI and WAG experiments were conducted with the objective of evaluating miscible and immiscible modes of gas injection, the effect of brine composition and core length on gas-oil displacements in porous media. Berea sandstone was chosen because of its wide acceptance as a relatively homogeneous porous medium well suited for controlled experiments.

Ten sets of experiments – eight with 1-ft Berea cores and two with 6-ft Berea cores were conducted. Two different brines, one a commonly used 5% NaCl solution and the other actual reservoir brine were used to examine the effects of rock fluid interactions. n-Decane was used as the oleic phase and pure Carbon dioxide as the injected gas. The 6-ft coreflood experiments were conducted using only 5% NaCl brine. Both miscible and immiscible displacements of n-Decane and Carbon dioxide gas were conducted. Miscible floods were performed at 2515 psia and the immiscible ones at 515 psia. Two modes of gas injection were used: Continuous Gas Injection (CGI) and Water-Alternating-Gas (WAG) injection.

Conventional plots of waterflood residual oil recovery vs. pore volume injected were found to yield misleading conclusions. Hence a new factor, namely Tertiary Recovery Factor (TRF) was defined to normalize by pore volume of CO_2 injected the oil recovery. Comparison of the results in terms of TRF enabled the evaluation of the performance of tertiary gas floods on the same basis.

The main conclusions from this study were:

1. The performance evaluation of the gas floods solely on the basis of oil recovery, could lead to misleading conclusions. Recoveries should be normalized by the amount of gas injected to enable direct comparisons.
2. Miscible gas floods were found to recover over 60 to 70% more of the waterflood residual oil than immiscible gas floods. While the recoveries in immiscible floods (both CGI and WAG) were about 23%, the miscible floods yielded 84.5% recovery for the WAG flood and 93.7% recovery for the CGI flood. This is not a surprising result, since laboratory 1D corefloods where sweep efficiency effects were minimal; miscibility has significant impact on oil recovery.
3. Based on oil recovery (as %ROIP), the CGI flood appeared to be better in performance than WAG flood. However, on the basis of the Tertiary Recovery Factor (TRF), where the recoveries were normalized by the volume of CO_2 injected, the WAG flood clearly out-performed the CGI flood. Furthermore, the performance of the CGI miscible flood approaches that of the immiscible gas floods, in terms of TRF, indicating deteriorating economics of the CGI compared to that of miscible WAG flood.
4. The definition of TRF enabled the identification of a process for optimizing tertiary recovery in gas floods. This consists of injecting a continuous gas slug of 0.7 PV (where the CGI flood showed maximum TRF value) followed by 1:1 WAG. This was found to be similar to the patented ‘Hybrid WAG’ and ‘DUWAG’ processes employed in the oil industry.
5. Miscible CGI floods showed negligible sensitivity to brine composition variations. Recoveries of 96.7% and 97.6% where obtained with 5% NaCl brine and Yates reservoir brine, respectively. As against this, the miscible WAG recoveries exhibited

significant dependence on brine composition. The miscible WAG recoveries showed a significant decrease (12%) in oil recovery when the connate brine was changed from 5% NaCl solution to Yates reservoir brine. While the recoveries for the miscible 5% NaCl brine were 84.5%, the recovery decreased to 72.5% for Yates reservoir brine. This is attributable to the higher solubility of CO_2 in natural multi-component brines than solutions of pure salts like NaCl, which results in higher volumes of CO_2 being available for oil recovery in 5% NaCl brine floods.

6. Both CGI and WAG (with 5% NaCl brine) immiscible experiments showed comparable oil recoveries of 21.9% and 23.7% in 1-ft Berea corefloods, respectively. However, significant differences (~ 21%) in the final oil recoveries of CGI and WAG were seen in 6-ft Berea cores, although the test conditions were identical. The CGI recovery increased from 21.9% in 1-ft Core to 33.5% in the 6-ft corefloods, whereas the WAG recovery showed a higher increase in recoveries, from 23.7% in 1-ft core to 54.4% in 6-ft core. Thus, it was seen that the gravity segregation phenomenon was amplified in long cores, thus making 6-ft corefloods more appropriate and useful to examine the WAG process performance.

The detailed results of these experiments are available elsewhere (Kulkarni, 2003); and only the recommendations summarized below:

1. 1-ft Berea core experiments should be used to identify important parameters affecting gas-oil displacements. The effect of these parameters should then be further examined using the 6-ft coreflood apparatus, as they are time consuming.
2. Berea cores previously exposed to crude oils should not be reused in other displacement experiments due to interfering wettability effects. Use of fresh Berea cores for each fluid pair is recommended.
3. Coreflood test conditions (namely pressure and temperature) should be chosen to avoid the two envelope of the injected gas in order to avoid liquefaction during the tests and to facilitate single-phase fluid transport through the apparatus.
4. The effect of CO_2 solubility in brine on gas-oil displacement should be minimized by using mutually saturated fluids.
5. “Hybrid-WAG” type corefloods should be conducted on long cores to determine the optimum mode for gas floods and to compare their effectiveness against gravity-stable gas floods.
6. Corefloods should be conducted with live reservoir fluids and formation rock samples an at reservoir conditions in order to enable collection of data for field-scale reservoir simulation studies and to facilitate field implementation of promising concepts and processes.

3.5 Experimental Results and Discussion

As suggested earlier, the experimental investigations for the development and characterization of the GAGD process can be divided into two parts: (i) further investigations of the recommendations of the M.S. Thesis (Kulkarni, 2003) and (ii) 'scaled' GAGD experimentation to elucidate the multiphase mechanisms and fluid dynamics of the newly proposed GAGD process. This division was necessary to provide with a common and effective performance evaluation of the GAGD process as well as to provide with a methodology to extend the laboratory observations to the field scale. This chapter limits the details to the results and inferences obtained from the experimental work.

3.5.1 Conventional Gas Injection Processes

This section reports the further investigation of the recommendations and hypotheses resulting from the previous tertiary coreflood work of the M.S. Thesis (Kulkarni, 2003). This work also extends the previous work on evaluation of the multiphase displacement characteristics of reservoir (Berea) rocks, and extends it to 'Hybrid' WAG type multi-phase displacements in the laboratory using Berea sandstone cores.

3.5.1.1 Research Focus

The research objective of this extended work was to further investigate the recommendations of the previous horizontal gas injection coreflood (CGI and WAG) results. The major objectives of this experimental investigation are summarized below:

1. Investigation of the delayed breakthrough observed in the previous coreflood studies by studying the system behavior with mutually saturated fluids.
2. To conduct high-pressure corefloods (CGI / WAG / Hybrid-WAG modes of gas injection) in immiscible and / or miscible modes with Berea cores at selected operating conditions under both secondary and tertiary injection strategies.
3. Further investigation of the predicted optimum 'Hybrid WAG' type injection by conducting 'Hybrid WAG' type corefloods using both CO_2 saturated as well as unsaturated brine.

3.5.1.2 Experimental Design

This section details the experimental design used to achieve the extended research objectives.

1. Literature review (Kulkarni, 2003) suggests that the water-shielding and solvent solubility effects are especially important during CO_2-WAG injection processes in the tertiary mode, wherein significant quantities of free water exist in the reservoir. To facilitate the characterization and quantification of these critical reservoir mechanics

in tertiary CGI and WAG processes; miscible WAG corefloods using mutually saturated fluids were conducted.

2. During tertiary mode CGI injection, significant delays in the oil breakthrough times (accompanied with only free water production) were observed (Kulkarni, 2003). It was hypothesized (Kulkarni, 2003) that in tertiary floods, the unsaturated nature of the brine results in dissolution of the injected CO_2 gas in brine, and CO_2 is unavailable for tertiary recovery till the core-fluids become saturated. To experimentally verify the validity of this assumption, tertiary mode immiscible CGI floods were conducted using mutually saturated (CO_2-saturated) coreflood fluids.
3. WAG literature review (Kulkarni, 2003) suggests that secondary mode gas injection is another popular methodology for commercial CGI and WAG applications. Since the immiscible horizontal CGI and WAG corefloods did not demonstrate significant variations in oil recovery characteristics, in the tertiary mode; only secondary mode miscible CGI and WAG corefloods were conducted using -Decane, Yates reservoir brine and pure CO_2. These corefloods thus effectively encompass the entire spectrum of the various modes of commercial CGI and WAG applications.
4. A new factor 'tertiary recovery factor' (TRF) was defined to facilitate the fair evaluation of the various CGI and WAG corefloods conducted (Kulkarni, 2003) to provide a base case for further evaluation of the GAGD process. TRF analysis of the miscible and immiscible CGI and WAG tertiary gas injection corefloods suggest that for optimum CO_2 utilization during horizontal mode gas injection a 'combination process' comprising of both CGI and WAG modes of injection should be employed. Two conceptually similar processes, termed as the 'Hybrid-WAG' (Huang and Holm, 1986) and 'DUWAG' (Tanner et al., 1992) were found to be previously patented and implemented in the industry by UNOCAL and Shell respectively. To experimentally verify this 'optimum' process, Hybrid-WAG type tertiary miscible corefloods were conducted using previously determined TRF maxima obtained from CGI and WAG flood analyses using n-Decane, Yates reservoir brine and pure CO_2.

3.5.1.3 Effect of CO_2 Solubility on Oil Recovery Characteristics

To achieve the research objectives 1 and 2, two horizontal mode tertiary coreflood experiments, namely immiscible CGI (termed experiment # 11) and miscible WAG experiments (termed experiment # 12) were conducted using CO_2-saturated Yates reservoir brine. Since there is no water injection in CGI flood, the secondary waterflood was conducted using saturated brine, and the drainage (oil flood) and EOR (immiscible CGI) floods were conducted at conditions similar to experiment 7 of the M.S. Thesis (Kulkarni, 2003). On the other hand, for the miscible WAG experiment, CO_2-saturated brine was used in the tertiary (EOR) mode while conducting the drainage (oil flood) and imbibition (Yates reservoir brine flood) steps at conditions similar to experiment 10 of

the M.S. Thesis (Kulkarni, 2003). The CO_2-saturated brine was hypothesized to saturate the core-brine and eliminate the CO_2 solubility effects during tertiary mode gas injection. The results of these two experiments are detailed in the following sections. The detailed analysis of the experimental results requires precise CO_2 solubility data with Yates reservoir brine, the simulation and analytical procedures employed for the CO_2-brine solubility determination are also included in this section.

Determination of Solubility of CO_2 in Yates Reservoir Brine

CMGL's Winprop® was used to determine the solubility of pure CO_2 gas in Yates reservoir brine. The solubility of CO_2 in water was studied as a function of temperature, pressure and salinity. The solubility of CO_2 in fresh water increases with increasing pressure, decreasing temperature (Crawford et al., 1963, Holm, 1963, Jarell, 2002) and the values of CO_2 solubility in fresh water obtained from different experimental studies (Crawford et al., 1963, Holm, 1963, Jarell, 2002) can be adjusted based on the salinity of the brine (at given pressure and temperature) as a percent of solubility retained (Jarell, 2002, Johnson et al., 1952, Martin, 1951, Chang et al., 1996).

The plots obtained from these references were digitized and are plotted below. To facilitate simpler computing procedures, a 6-order polynomial curve was fitted to the experimental data curve used to predict the effect of brine salinity on CO_2 solubility. The experimental data are included as Figure 3.26.

To evaluate and calibrate the simulator with the experimental values, the CO_2 solubility's were calculated at 70 ^oF, 100 ^oF, 130 ^oF and 190 ^oF using CMGL Winprop®; using two equations of state, namely, Peng Robinson (PR EOS) and Soave Redlich Kwong (SRK EOS) with two viscosity models for water, namely, Jossi-Thiel-Thodos (J-S-T) Correlation and Pedersen Corresponding States Model. The predicted values of solubility at desired conditions (82 ^oF and at 500 or 2500 psi) are summarized in Tables 3.13 and 3.14.

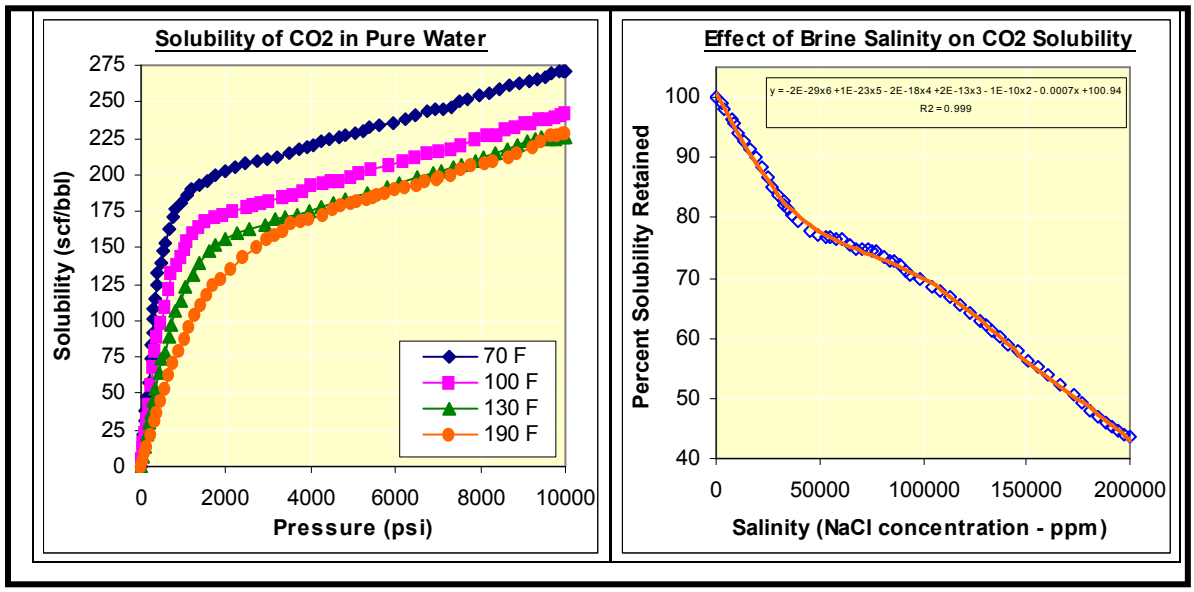

Figure 3.26: Experimental Solubility Data from Literature (Crawford et al., 1963, Holm, 1963, Jarell, 2002, Johnson et al., 1952, Martin, 1951, Chang et al., 1996).

Table 3.13: Predicted CO_2 solubility values in Yates Reservoir Brine at 500 psi and 82 ^{o}F

Solubility (mol %)	Data Source
1.89	PR EOS: Adjusted for salinity from pure water simulated value
1.93	SRK EOS: Adjusted for salinity from pure water simulated value
2.27	PR EOS: Brine simulated value
2.29	SRK EOS: Brine simulated value
1.89	Average of 70 ^{o}F and 100 ^{o}F data (85 ^{o}F)

Table 3.14: Predicted CO_2 solubility values in Yates Reservoir Brine at 2500 psi and 82 ^oF

Solubility (mol %)	Data Source
3.12	PR EOS: Adjusted for salinity from pure water simulated value
3.32	SRK EOS: Adjusted for salinity from pure water simulated value
3.64	PR EOS: Brine simulated value
3.64	SRK EOS: Brine simulated value
2.84	Avg. of 70 ^oF and 100 ^oF data (85 ^oF)

Results for 500 psi

The predicted values from simulation for both the EOS show higher solubility values as compared to those predicted by the experimentally averaged 85 ^oF data, as well as that predicted by the adjusted pure water solubility value. The experimental averaged value at 85 ^oF is 1.89 mol %, which is close to the prediction of PR EOS (adjusted value). As solubility increases with decreasing temperature, the solubility should be slightly higher than 1.89 mol %. Hence the value of 1.92 mol % predicted by the SRK EOS seems more realistic.

Results for 2500 psi

Solubility increases with decreasing temperature. Hence, the lower predicted solubility value by the 85 ^oF data seems appropriate. Comparison of the simulation data with experimental averaged data (at 85 ^oF) shows that the solubility of 3.64 mol %, as predicted by the PR and SRK simulations, is achievable at pressure > 8500 psi. Hence the simulated value of 3.64 mol % seems unrealistic in this case. The averaged data shows that solubility of approx. 3 mol % is obtained at 4000 psi and 85 ^oF range. Therefore, the PR EOS simulated value of 3.12 mol % solubility predicted from adjusting for salinity from pure water data is a good approximation of solubility of CO_2 in Yates reservoir brine.

Immiscible CGI Flood with CO_2 Saturated Brine in Secondary Mode

The flooding sequence for this coreflood consisted of an oil flood (primary drainage), a secondary waterflood (secondary imbibition with CO_2-saturated Yates reservoir brine), and a tertiary immiscible CGI injection. Rappaport and Leas (1953) stability criterion was satisfied in all the floods to avoid flow rate effects. The step-wise results of the

immiscible CGI coreflood experiment using CO_2 saturated Yates reservoir brine in secondary step is shown in Figure 3.27.

The experimental observations during this flood for the oil injection step (drainage) were similar to those previously observed in other horizontal corefloods. On the other hand, the results of the secondary waterflood with saturated Yates reservoir brine were markedly different, and showed significant pressure fluctuations till water breakthrough.

However these pressure fluctuations were stabilized immediately after a sharp water breakthrough. Even after water breakthrough, a significant delay (until 1.59 PVI) in gas (dissolved in brine) breakthrough times was observed along with continually increasing flood pressure-drops.

These pressure drop fluctuations during secondary CO_2-saturated brine injection are hypothesized to be attributable to the miscible displacement (consequently replacement) of the connate (unsaturated) core brine by the saturated injection brine. This replacement of the unsaturated core brine with saturated brine, helps significantly decrease the oil and gas breakthrough times for the tertiary CO_2 CGI flood and markedly improve the flood's gas utilization (TRF) factors (Figure 3.27(a) & 3.28(b)).

Miscible WAG Flood with CO_2 Saturated Brine in Tertiary Mode

The flooding sequence for this coreflood consisted of an oil flood (primary drainage), a secondary waterflood (secondary imbibition), and a tertiary miscible WAG (CO_2 gas alternating with CO_2-saturated Yates reservoir brine) injection. The step-wise results of the immiscible CGI coreflood experiment using CO_2 saturated Yates reservoir brine in secondary step is shown in Figure 3.29. For this miscible CO_2 WAG flood, the drainage and imbibition steps were similar to the previously conducted WAG corefloods, however significant improvement in the oil production rate was observed when the saturated brine was alternated with CO_2 instead of the non-saturated brine. Another characteristic flood feature observed during the employment of CO_2 saturated brine for the WAG flood, was the increased flood pressure drops. The increased pressure drops, and hence decreased gas injectivities compared to the previous normal brine WAG floods, could be attributable to the increased 3-phase relative permeability effects (Figure 3.30(b)).

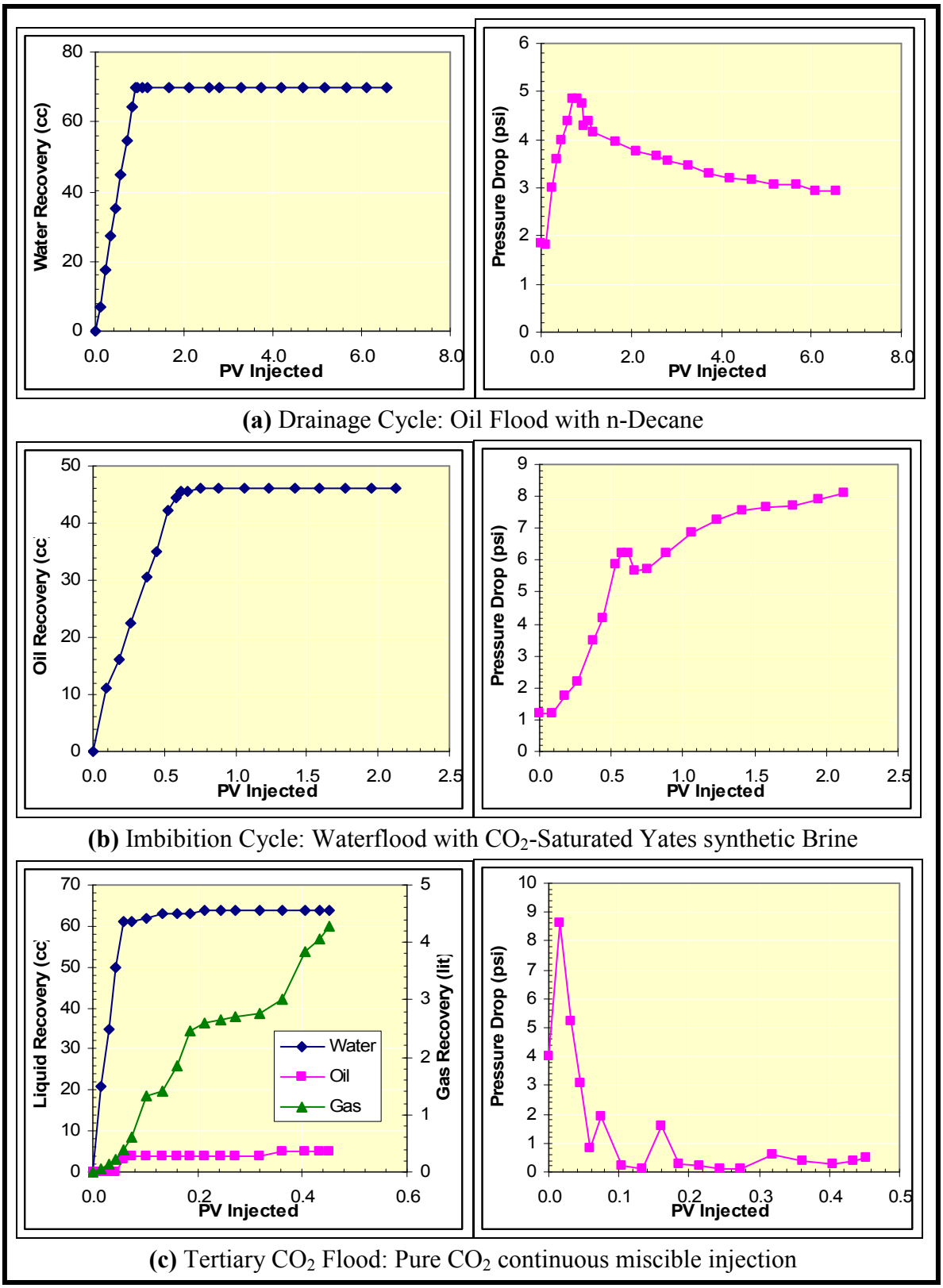

(a) Drainage Cycle: Oil Flood with n-Decane

(b) Imbibition Cycle: Waterflood with CO_2-Saturated Yates synthetic Brine

(c) Tertiary CO_2 Flood: Pure CO_2 continuous miscible injection

Figure 3.27: Data for Immiscible CGI flood: 1-ft Berea core + n-Decane + CO_2-Saturated Yates Reservoir Brine with Tertiary Continuous CO_2 Immiscible Injection.

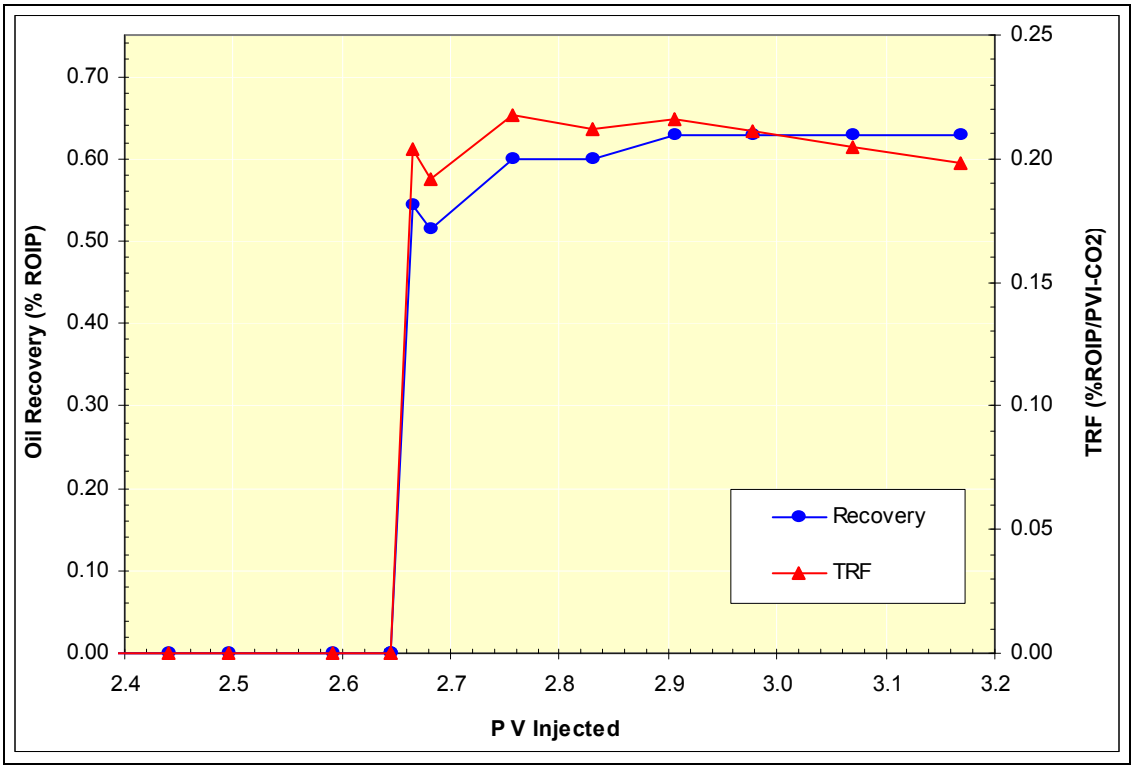

(a) Oil Recovery and TRF for CGI Flood with Unsaturated Brine Secondary Waterflood

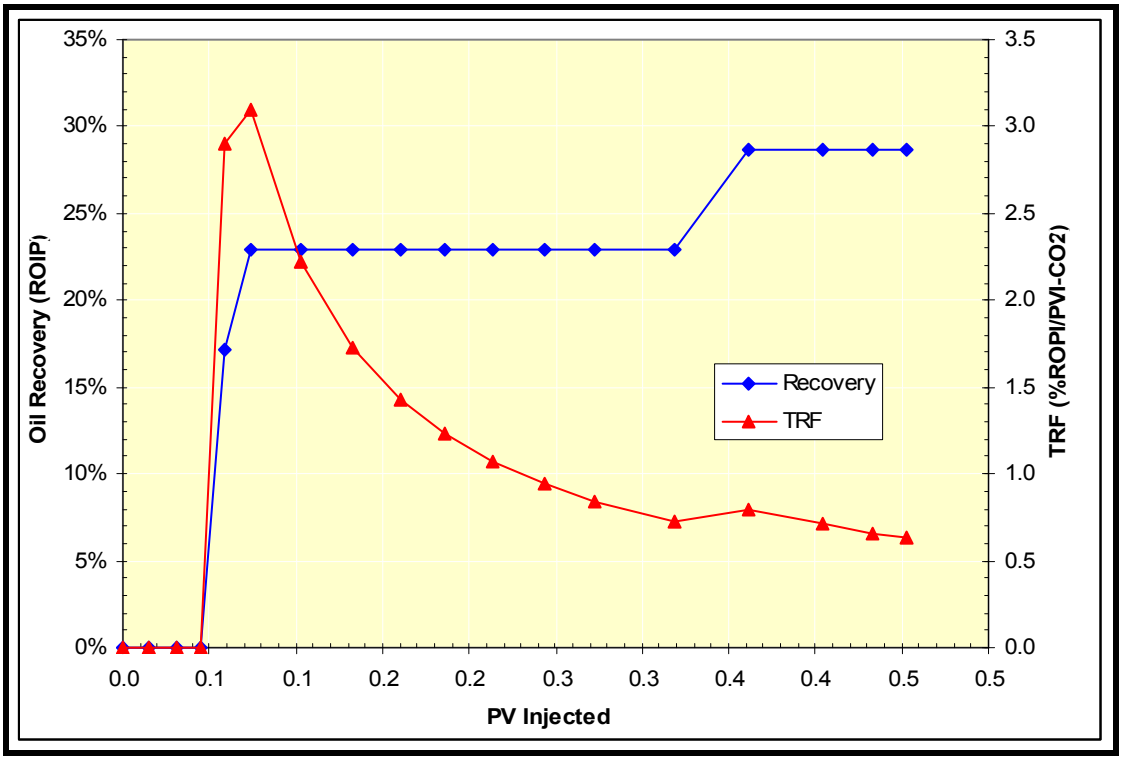

(b) Oil Recovery and TRF for CGI Flood with Saturated Brine Secondary Waterflood

Figure 3.28: Effect of Saturation of Brine with CO_2 on Immiscible CGI Recovery

The major observations obtained from the comparison of the normal (unsaturated) and saturated brine WAG floods (Figure 3.30) are:

1. Liquid and water productions for both the corefloods are identical.
2. The miscible WAG coreflood using CO_2-saturated brine recovered significantly higher oil (89.2% ROIP) compared to miscible WAG flood with normal brine (72.5% ROIP). This could be attributable to the decreased solubilization tendency of CO_2 in brine (due to previous saturation) and consequently resulting in higher gas volumes being available for oil recovery.
3. The improved oil recovery can also be partially attributed to the decreased viscosity contrasts (Figure 3.30(c)) between the injected and produced core fluids, thus leading to improved volumetric sweeps.
4. The TRF maxima (Figure 3.30(d)) were achieved at almost identical pore volume injections (0.84 for normal brine WAG (labeled experiment 10) and 0.82 for CO_2 saturated brine WAG (labeled experiment 12)).
5. The use of CO_2 saturated brine shows markedly decreased breakthrough times as well as increased gas productions (Figure 3.30(a) and 3.31(d)).

The analyses of these experimental results need all the data from previously completed horizontal mode CGI and WAG corefloods. The ten coreflood experiments completed prior to this analysis are available elsewhere (Kulkarni, 2003) and only relevant data is included here for sake of completeness.

The peak TRF values calculated for each of the twelve corefloods conducted are summarized in Figure 3.32. It is interesting to note that the peak TRF values, as observed from Figure 3.32, for the 5% NaCl brine miscible floods (both CGI and WAG) are higher than the Yates brine miscible floods. However, this effect has been reversed for the immiscible floods. This indicates that although the Yates brine has a higher CO_2 solubility than 5% NaCl brine at 500 psi; this effect is offset at 2500 psi (miscible) flooding conditions.

The highest TRF factor value for CGI floods was obtained by the use of saturated brine in secondary mode as expected. This data further fortifies the earlier assumption of relatively higher CO_2 solubility rate in brine at lower pressures and that this effect is mitigated at miscible flooding conditions (experiment 12). Consequently incremental benefits of the brine-CO_2 solubility reduction (by prior saturation) are more than offset by miscibility development.

The recoveries, residual oil saturations and gas utilization factors for the corefloods conducted are summarized in the Tables 3.15, 3.16 and 3.18 (Part (C)). The utilization factor, defined earlier, is a good indicator of the overall efficiency of the process, and is a useful augmentation, along with the TRF, for the analysis of the data. The utilization factor is a measure of the CO_2 design requirements for the field gas injection projects.

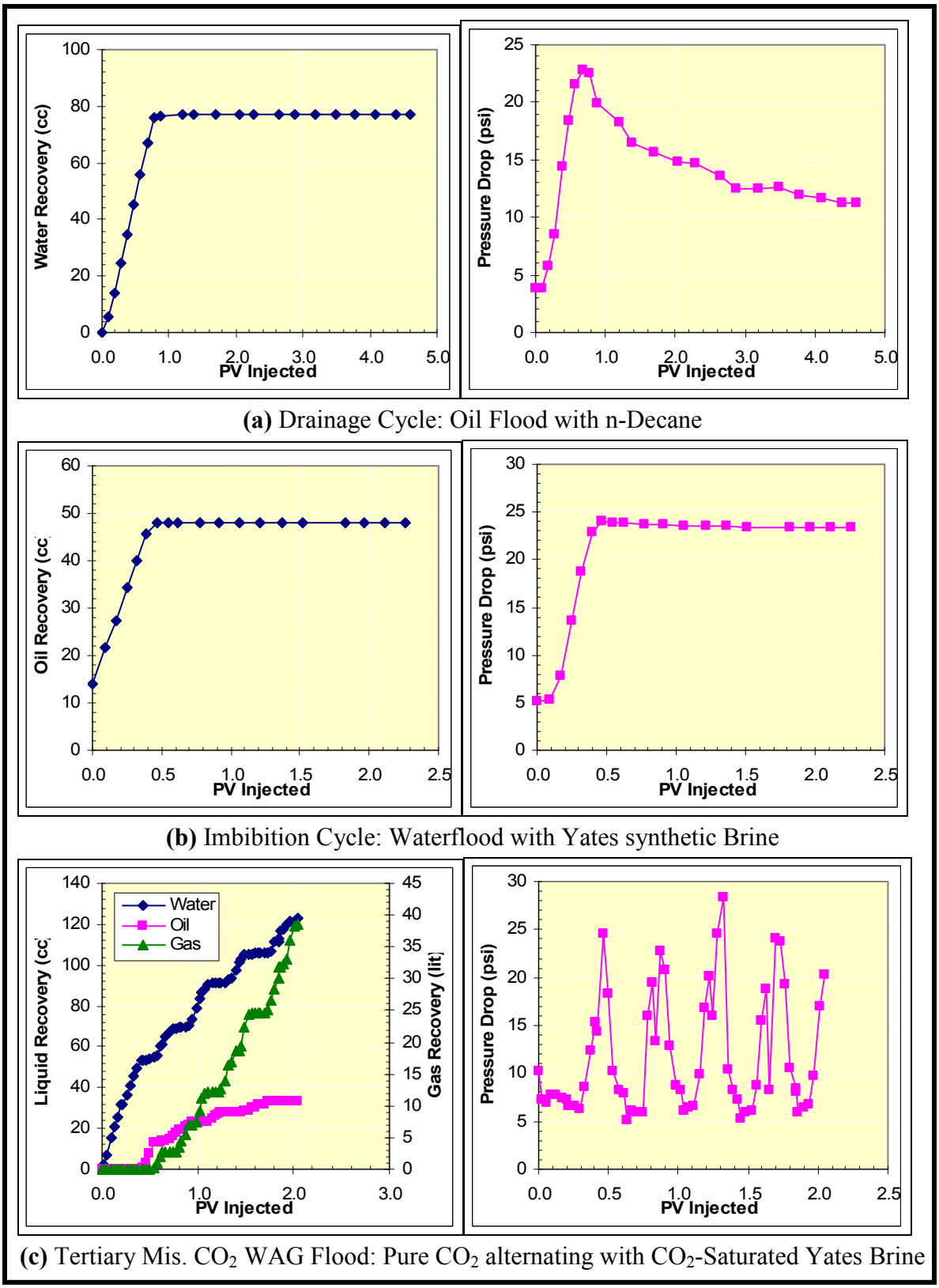

(a) Drainage Cycle: Oil Flood with n-Decane

(b) Imbibition Cycle: Waterflood with Yates synthetic Brine

(c) Tertiary Mis. CO_2 WAG Flood: Pure CO_2 alternating with CO_2-Saturated Yates Brine

Figure 3.29: Data for Tertiary Miscible CO_2 WAG Flood: 1-ft Berea core + n-Decane + CO_2-Saturated Yates Reservoir Brine with Tertiary WAG Miscible Injection.

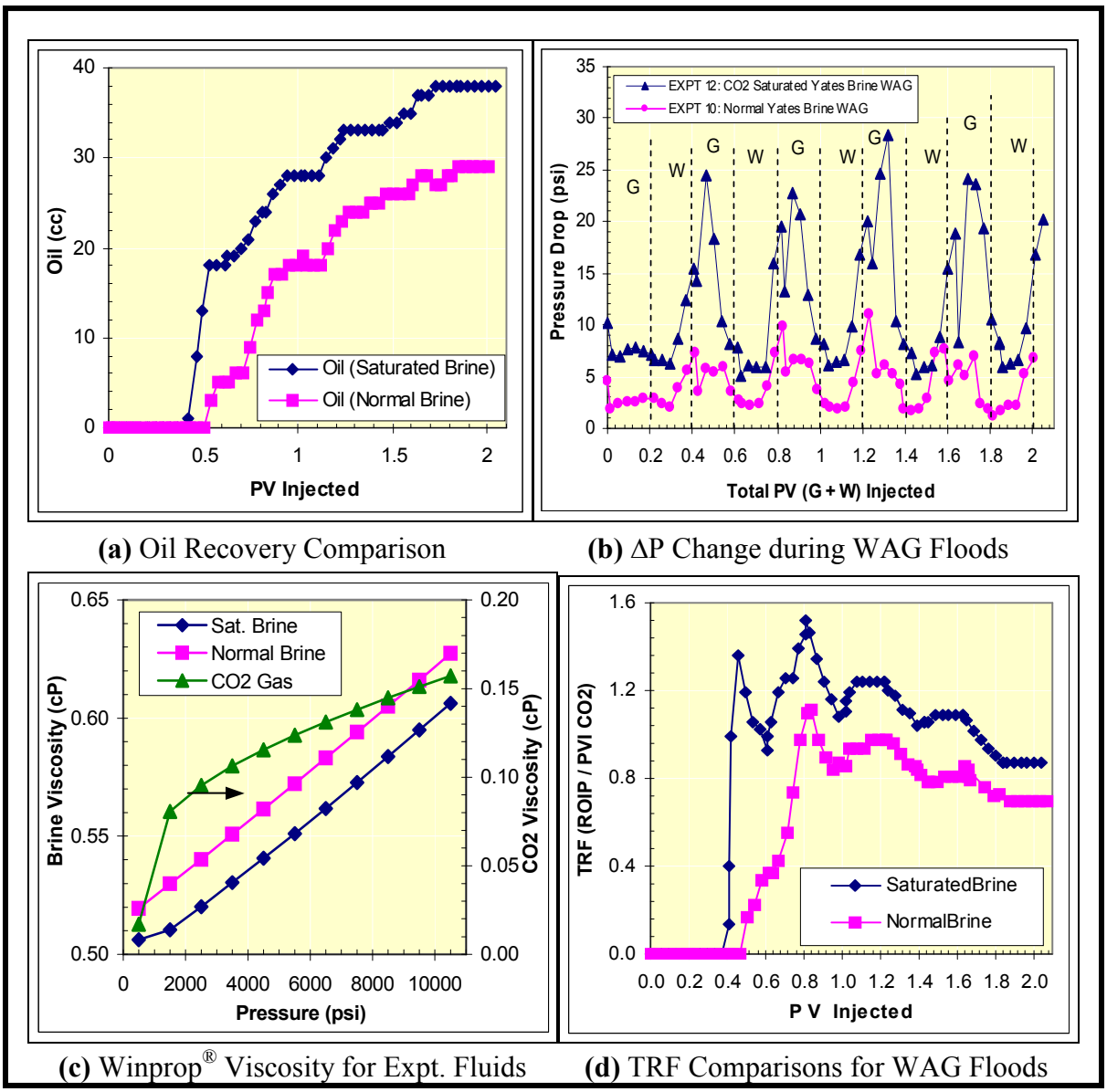

(a) Oil Recovery Comparison **(b)** ΔP Change during WAG Floods

(c) Winprop® Viscosity for Expt. Fluids **(d)** TRF Comparisons for WAG Floods

Figure 3.30: Effect of Saturation of Yates Reservoir Brine with CO_2 on Miscible WAG Recovery using n-Decane and CO_2

Explanation of the Observed Delayed Breakthroughs in Tertiary Immiscible Corefloods based on CO_2-Brine Solubility Concepts

One of the common features of the immiscible CGI Experiments 1 and 7 (Kulkarni, 2003) are the significant delays in oil production inspite of continuous gas injection. This delay was further investigated by plotting volumetric injection / production plots versus pore volume injection. Mass balance calculations showed that the water production till oil breakthrough matched the volume of cumulative CO_2 injection. The difference between injection and production observed in Figure 3.31 is attributable to the significant density differences between the injected CO_2 (4.86 lbm/ft^3) and reservoir brine (62.38 lbm/ft^3).

Table 3.15: Coreflood Results for 5% NaCl Brine + n-Decane + Berea Core System (for detailed experimental results see Kulkarni, 2003 and Kulkarni and Rao, 2005)

System: 5 % NaCl Brine + n-Decane + Berea Core	**P_{TEST} (psi)**	**Abs. Perm (D)**		**S_{WC}**	**S_{OI}**	**End Point Rel-Perms**
(A) Drainage (n-Decane) Step						
Experiment # 1	500	0.2526		12.5	87.5 %	34.5 %
Experiment # 2	500	0.3435		21.3	78.7 %	39.9 %
Experiment # 3	2500	0.2895		13.3	86.7 %	42.0 %
Experiment # 4	2500	0.1825		15.1	84.9 %	47.0 %
(B) Imbibition (5% NaCl brine) Step						
Experiment Title	P_{TEST} (psi)	S_{OR}		S_W	Recovery %OOIP	End Point Rel-Perms
Experiment # 1	500	35.0		65.0	60.0 %	08.01 %
Experiment # 2	500	27.7		72.3	64.8 %	08.09 %
Experiment # 3	2500	32.8		67.2	62.2%	08.05 %
Experiment # 4	2500	35.4		64.7	58.1%	08.72 %
(C) Tertiary Gas (EOR) Step						
Experiment Title	P_{TEST} (psi)	S_L	S_G	Rvry (cc)	Recovery %OOIP	Utilz. Ftr. (MCF/bbl)
Experiment # 1 (CGI – Immiscible)	500	47.9	52.1	10.5	8.8%	7.5
Experiment # 2 (WAG – Immiscible)	500	--	--	9	8.3%	4.5
Experiment # 3 (CGI – Miscible)	2500	26.4	73.6	43.5	36.6%	20.2
Experiment # 4 (WAG – Miscible)	2500	--	--	41	35.0%	9.0

Longer delays in oil production are observed for the Yates brine immiscible CGI flood (Figure 3.31(a)) compared to that of the 5% NaCl brine (Figure 3.31(b)). This is mainly due to the significantly higher solubility of CO_2 gas in multi-component brines than monovalent brines. Also the water-shielding and solubility requirements are higher in experiment # 7 than experiment # 1 due to higher water saturation (+10%) in the core (Figure 3.31). These results may have serious implications in the field projects, in that higher costs may be incurred due to delayed oil productions and increased CO_2 requirements in immiscible mode.

This phenomenon of delayed oil breakthrough is not observed for miscible floods since CO_2 has significantly higher density (51.15 lbm/ft^3) at 2500 psi injection pressures resulting in lower density contrasts between field brine and injected gas. Furthermore the differences between CGI and WAG oil breakthroughs are significantly reduced for the miscible floods compared to the immiscible floods where this difference could be as high as 1.8 PVI.

Table 3.16: Coreflood Results for Yates Reservoir Brine + n-Decane + Berea Core System (for detailed experimental results see Kulkarni, 2003 and Kulkarni and Rao, 2005)

System: Yates Reservoir Brine + n-Decane + Berea Core	P_{TEST} (psi)	Abs. Perm (D)	S_{WC}	S_{OI}	End Point Rel-Perms
(A) Drainage (n-Decane) Step					
Experiment # 7	500	0.1311	21.3	78.7	65.5 %
Experiment # 8	500	0.1869	19.1	80.9	58.3 %
Experiment # 9	2500	0.1443	18.4	81.6	59.1 %
Experiment # 10	2500	0.1906	16.9	83.1	66.8 %
(B) Imbibition (Yates reservoir brine) Step					
Experiment Title	P_{TEST} (psi)	S_{OR}	S_W	Recovery %OOIP	End Point Rel-Perms
Experiment # 7	500	25.5	74.5	67.6 %	11.80 %
Experiment # 8	500	27.7	72.3	65.8 %	07.51 %
Experiment # 9	2500	29.9	70.1	63.4%	11.56 %
Experiment # 10	2500	27.0	73.0	64.9%	09.39 %
(C) Tertiary Gas (EOR) Step					
Experiment Title	P_{TEST} (psi)	S_L	S_G	Rvry (cc)	Recovery %OOIP	Utilz. Ftr. (MCF/bbl)
Experiment # 7 (CGI – Immiscible)	500	27.8	72.2	22	20.4%	4.7
Experiment # 8 (WAG – Immiscible)	500	--	--	11	9.9%	3.1
Experiment # 9 (CGI – Miscible)	2500	19.8	80.2	40	35.7%	19.4
Experiment # 10 (WAG – Miscible)	2500	--	--	29	25.4%	12.9

Hence for miscible floods the added benefit of hastened oil breakthroughs by WAG employment is not available, and the CO_2-brine dissolution effect, favoring WAG application in immiscible mode, is not as pronounced for miscible floods.

3.5.1.4 Secondary Miscible CGI and WAG Corefloods

As noted earlier, commercial gas injection literature review indicates that secondary gas injection was another common application methodology. To achieve the research objective 3 (see Section 5.1.2), two horizontal mode miscible corefloods, namely secondary CGI and secondary WAG were conducted on 1-ft Berea sandstone core using n-Decane, Yates reservoir brine and pure CO_2.

Secondary Miscible CGI Flood

The results of the secondary mode miscible CGI flood (using n-Decane, Yates reservoir brine and CO_2) completed are summarized in Figure 3.33. As expected, the miscible CGI

recoveries were excellent (94.4%) and the TRF plot shifted to the left indicating higher and faster oil recoveries per unit volume of injectant, compared to those of tertiary floods. Furthermore, no delays in oil breakthrough were observed, and no free water was produced during the entire flood, indicating the connate water to be essentially immobile and the water shielding effect to be minimal.

Secondary Miscible WAG Flood

To isolate and quantify the effects of water-shielding and three-phase relative permeability on oil recovery, a miscible secondary WAG coreflood was required. Therefore a miscible WAG flood was conducted using n-Decane, Yates reservoir brine and CO_2; whose results are included as Figure 3.33. Note that each division on the X-axis in Figure 3.33(b) depicts one fluid slug, with the first slug being gas (CO_2).

Table 3.17: Coreflood Results for Yates Reservoir Brine + n-Decane + Berea Core System using CO_2 Saturated Yates reservoir brine for specified steps

System: Yates Reservoir Brine + n-Decane + Berea Core	P_{TEST} (psi)	Abs. Perm (D)	S_{WC}	S_{OI}	End Point Rel-Perms
(A) Drainage (n-Decane) Step					
Experiment # 11	500	0.4503	40.1	59.9	69.07%
Experiment # 12	2500	0.1361	27.2	72.8	58.25%
(B) Imbibition (Yates reservoir brine) Step					
Experiment Title	P_{TEST} (psi)	S_{OR}	S_W	Recovery %OOIP	End Point Rel-Perms
Experiment # 11 (Yates reservoir brine saturated with CO_2 Gas Flood)	500	14.9%	85.1%	65.79%	9.64%
Experiment # 12 (Unsaturated Yates reservoir brine Flood)	2500	20.9%	79.2%	56.46%	10.26%
(C) Tertiary Gas (EOR) Step					
Experiment Title	P_{TEST} (psi)	S_L	S_G	Recovery (%OOIP)	Utilz. Ftr. (MCF/bbl)
Experiment # 11 (CGI – Immiscible)	500	40.7%	59.3%	5 cc (4.80% OOIP)	2.5
Experiment # 12 (WAG – Miscible – Yates reservoir brine saturated with CO_2 Gas alternating with CO_2 Flood)	2500	--	--	33 cc (27.7% OOIP)	11.2

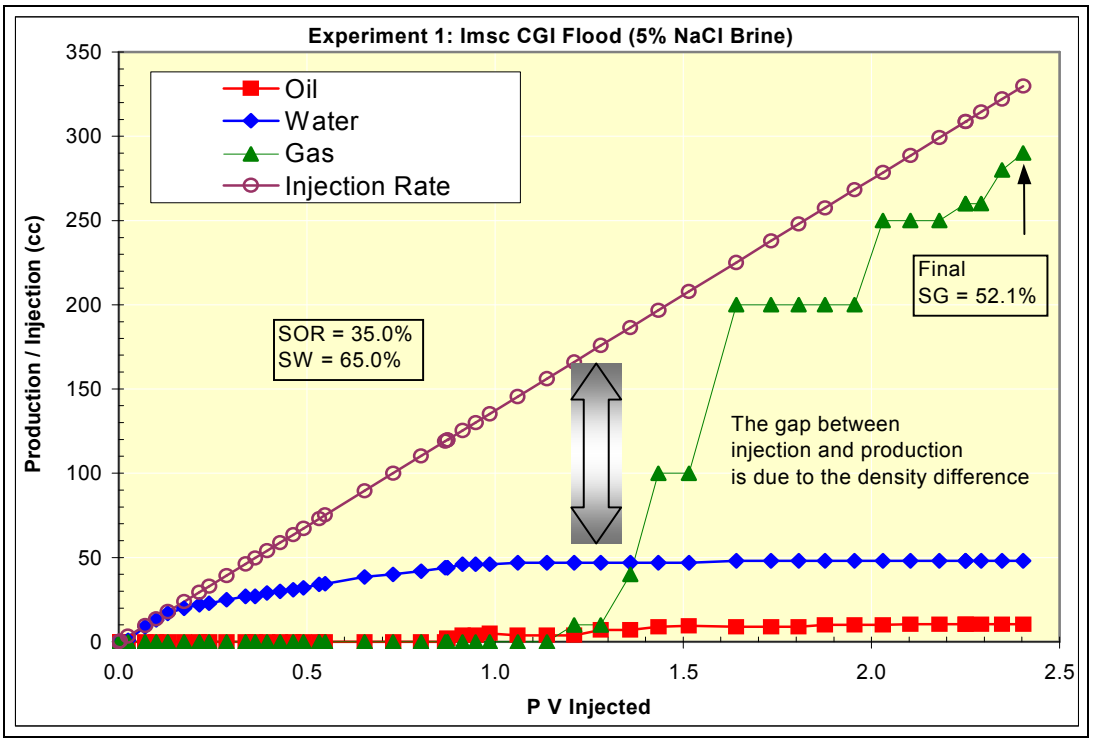

(a) Oil-Water-Gas-Injection Volumetric Plot: 5% NaCl Brine Immiscible CGI Flood

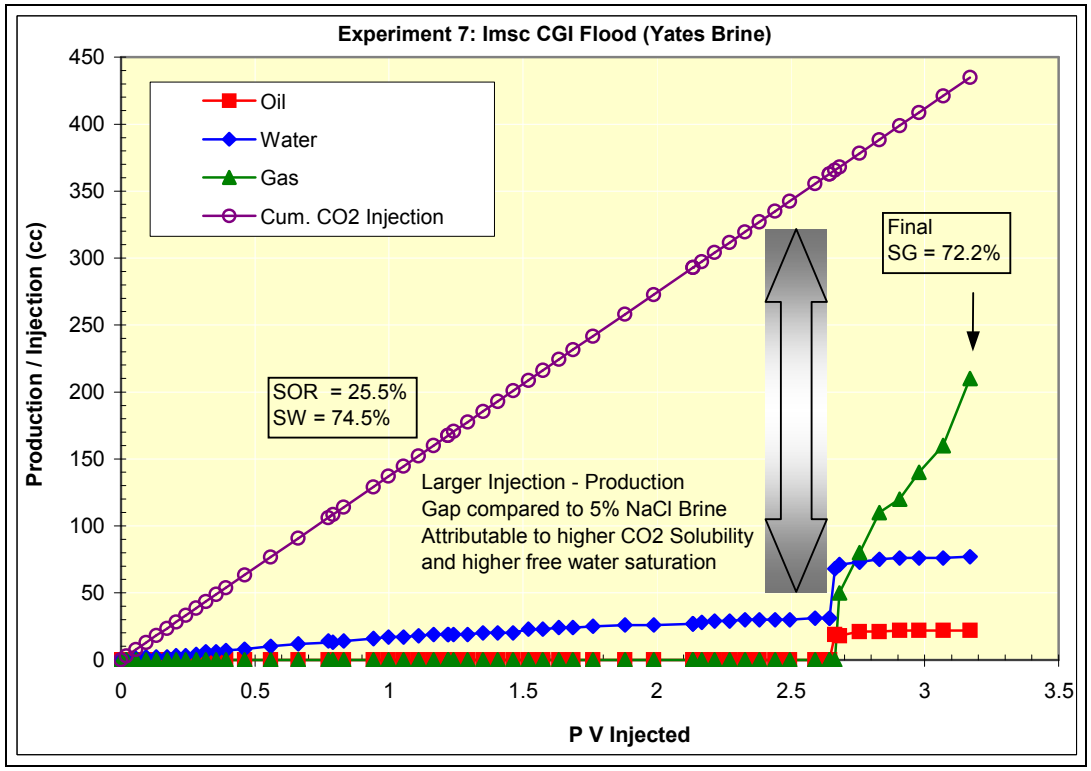

(b) Oil-Water-Gas-Injection Volumetric Plot: Yates Brine Immiscible CGI Flood

Figure 3.31: Investigation of the Delayed Oil Production for Immiscible CGI Floods using both 5% NaCl Brine and Yates Reservoir Brine

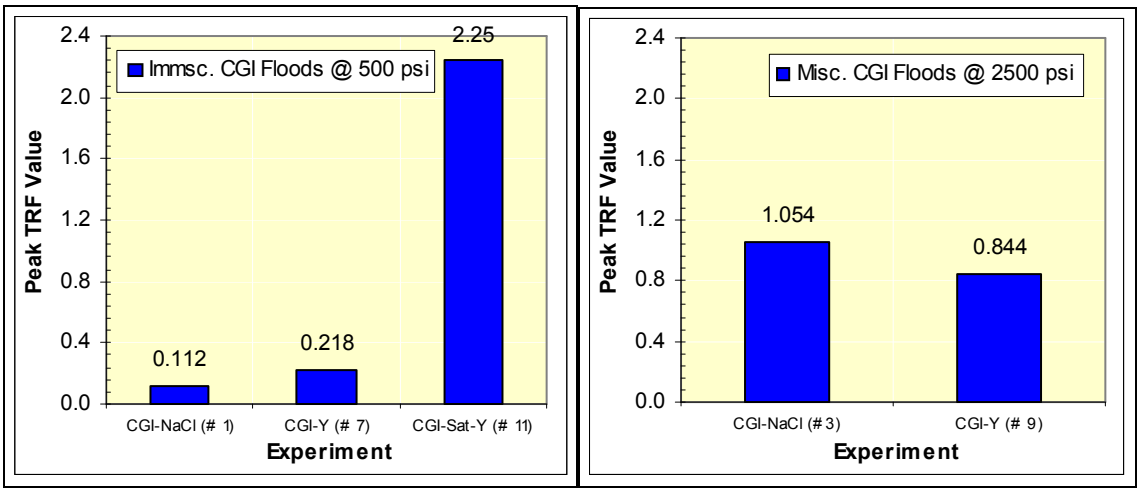

(a) Peak TRF Value Comparisons for Immiscible and Miscible CGI Floods

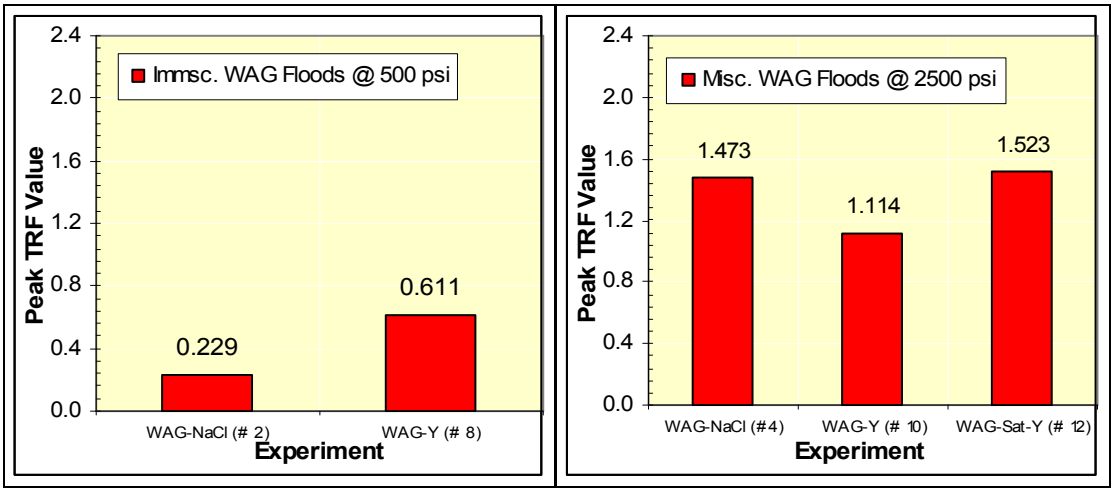

(b) Peak TRF Value Comparisons for Immiscible and Miscible WAG Floods

Figure 3.32: Comparison of Peak TRF Values for CGI and WAG Experiments For 5% NaCl Brine and Yates Reservoir Brine

3.5.1.5 Miscible Hybrid-WAG Coreflood

To achieve the research objective 4, miscible Hybrid-WAG type coreflood was conducted using n-Decane, Yates reservoir brine and pure CO_2 to asses the validity of the conclusions of the previous work that optimum performance may be obtained by the employment of the combination of CGI and WAG floods. The comparison of the results of the miscible CGI, WAG and Hybrid-WAG floods conducted in the laboratory are included as Figure 3.34.

Figure 3.34(a) depicts the conventional oil recovery (as % ROIP) plot for miscible CGI, WAG and Hybrid-WAG floods; while Figure 3.34(b) summarizes the TRF behavior for these corefloods.

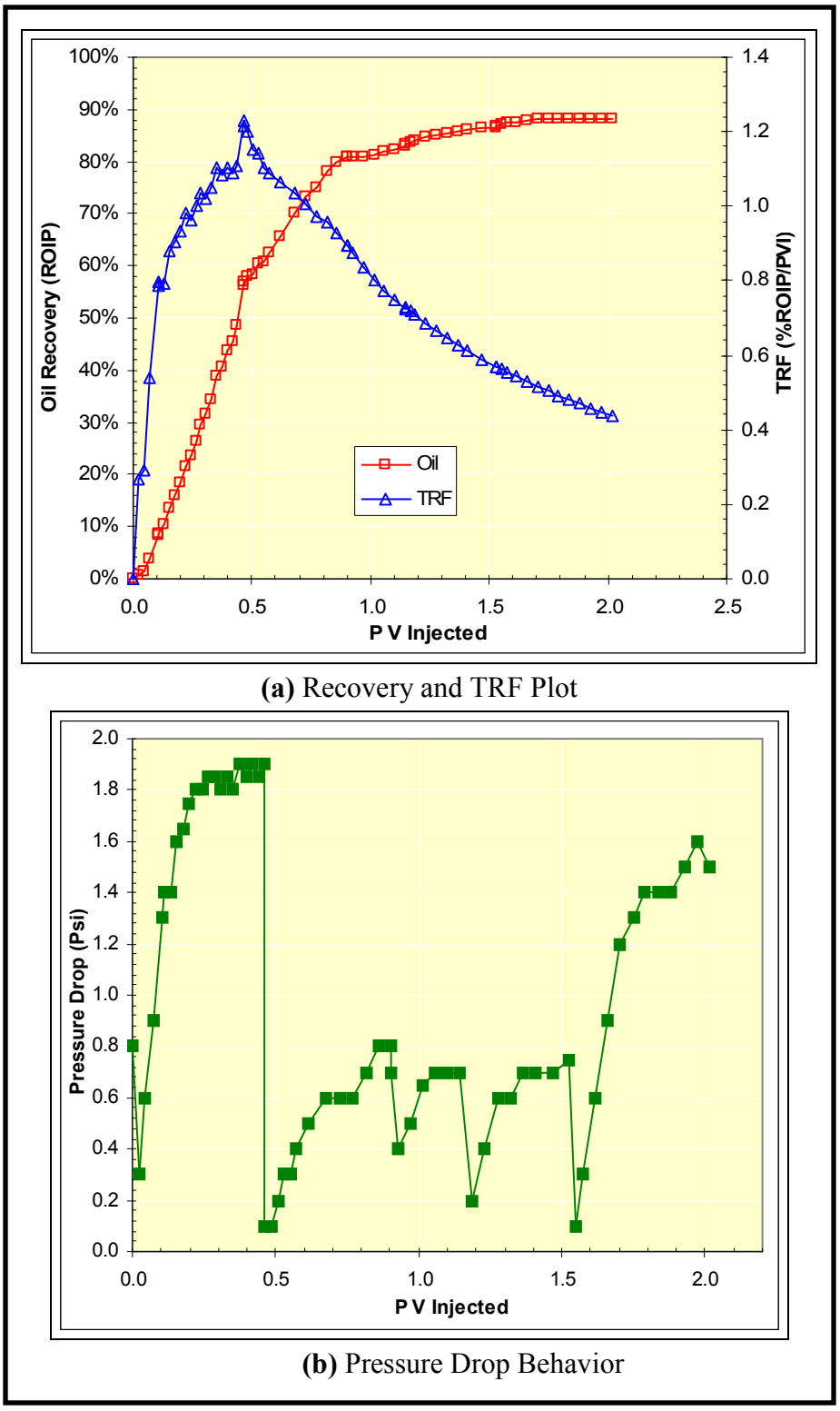

(a) Recovery and TRF Plot

(b) Pressure Drop Behavior

Figure 3.33: Recovery, TRF and Pressure Drop Behavior in Secondary Miscible CO_2 CGI Flood in n-Decane, Yates Reservoir Brine, 1-ft Berea System at 2500 psi and 72 ^{o}F

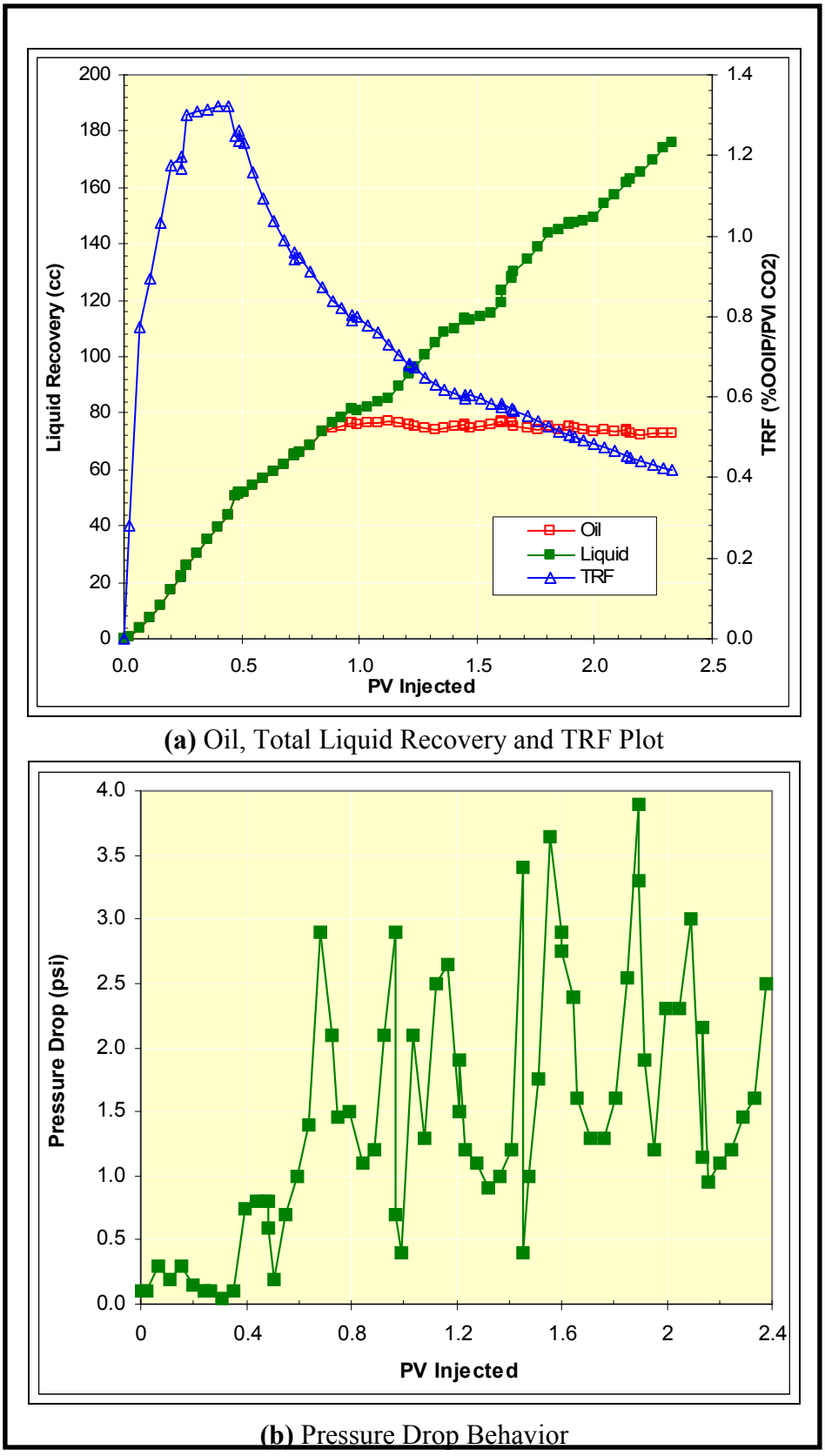

(a) Oil, Total Liquid Recovery and TRF Plot

(b) Pressure Drop Behavior

Figure 3.34: Recovery, TRF and Pressure Drop Behavior in Secondary Miscible CO_2 WAG Flood in n-Decane, Yates Reservoir Brine, 1-ft Berea System at 2500 psi and 72 ^{o}F

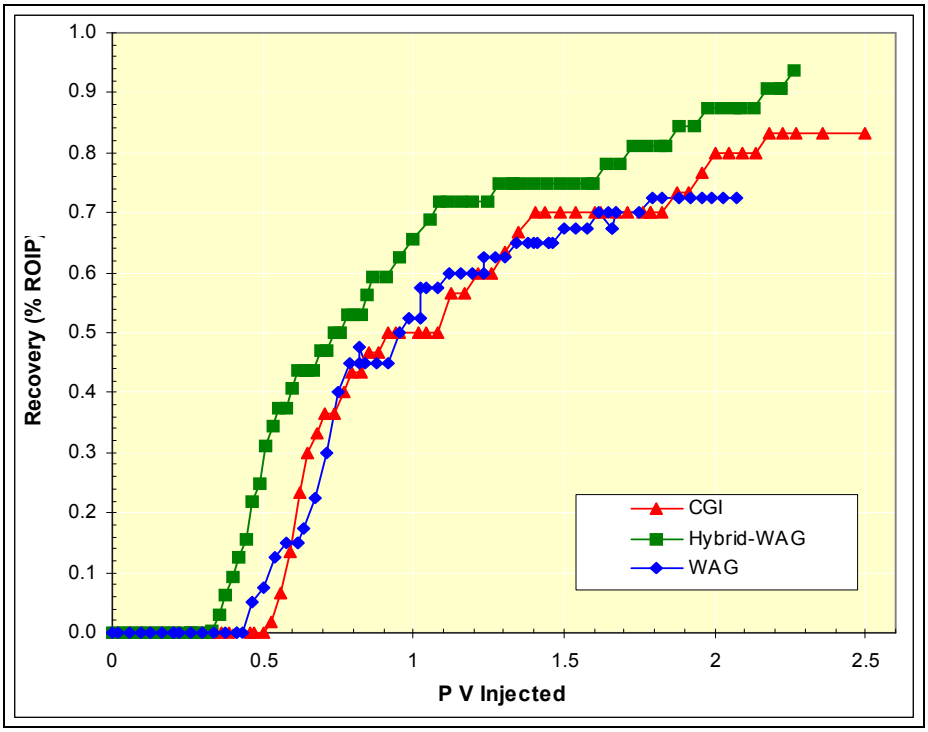

(a): Recovery as Percent Residual Oil in Place

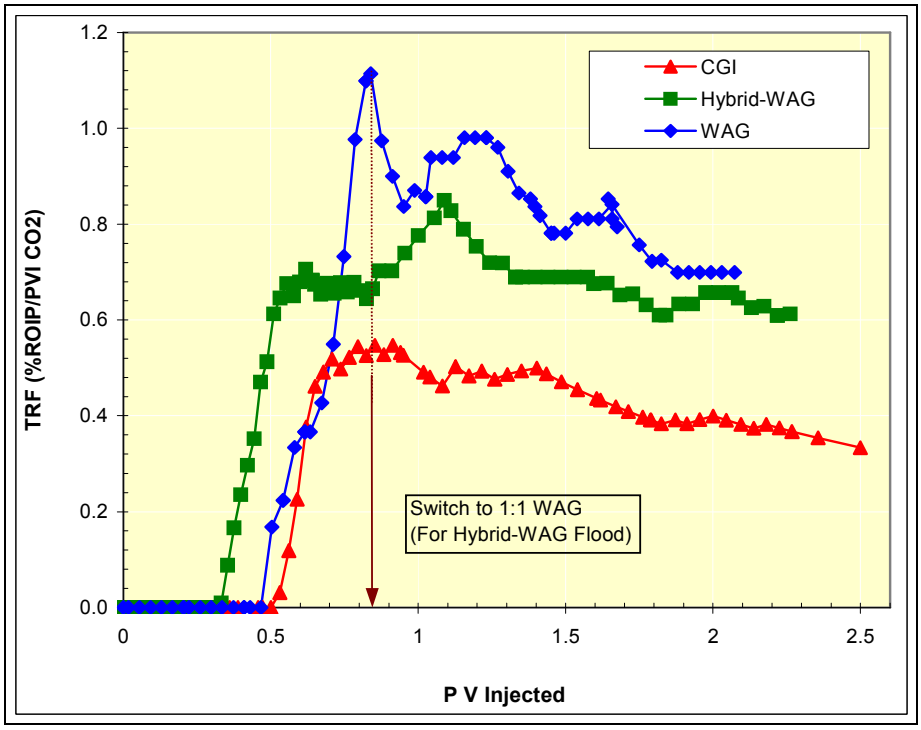

(b): Recovery as Fraction of Residual Oil in Place per PV of CO_2 Injected

Figure 3.35: Comparison of Miscible Hybrid-WAG, WAG and CGI Floods on 1-ft Berea in n-Decane, Yates Reservoir Brine, 1-ft Berea System at 2500 psi and 72 ^{o}F

The miscible 'Hybrid-WAG' experiment was conducted using Yates reservoir brine, n-Decane and pure CO_2. Figure 3.35(a) shows the conventional oil recovery (as % ROIP) plot for miscible CGI, WAG and Hybrid-WAG floods. As expected, the Hybrid-WAG type injection clearly out performs both the CGI as well as WAG floods from an oil recovery point of view. This data strengthens the initial speculation that optimum mode of injection is a 'combination' of CGI and WAG floods.

Important Operational Differences between the Optimum Processes Identified by this Work and 'Hybrid-WAG' / DUWAG

In this experimental work, all CGI experiments showed a TRF peak after about 0.6 – 0.8 PV injection, and that the TRF values of CGI floods till this peak are higher than the respective WAG floods (Kulkarni and Rao, 2005). However, after this peak, the CGI flood performance exponentially deteriorates. On the other hand, the WAG employment prevents this exponential TRF decline (after reaching a peak TRF value) (see Figures 3(b), 4(b) and 6(b) of Kulkarni and Rao, 2005) indicating improved gas utilization factors in both miscible and immiscible modes. Therefore to optimize gas utilization (and therefore flood economics), it is recommended that gas be injected in CGI mode till 0.7 PV injection (or at the TRF peak), followed by 1:1 WAG injection.

Conceptually the 'optimum' process (the combination of CGI and WAG) recommended by this work, is similar to the patented Hybrid-WAG and DUWAG processes implemented in the field previously. However, there are significant differences between these patented processes and the optimum process suggested by this experimental work, which is identified below.

The Hybrid-WAG and DUWAG were mainly the result of field dependant parameters such as market conditions (Bellavance, 1996) (namely, reduce the early peak CO_2 demands, maximize utilization of recycled CO_2, minimize manpower requirements and provide flexibility to accelerate or decelerate project development), and flooding conditions (Bellavance, 1996; Tanner et al., 1992) (namely WAG implementation only under the circumstances of premature gas breakthroughs or "Gassing Out" of wells).

Another striking feature of the 'optimum' process described in this paper, is that the reservoir heterogeneity factor has been effectively eliminated in these experiments by conducting all the CGI, WAG and Hybrid-WAG corefloods on one Berea core. This is not the case in the patented processes. For example, in the Wasson Denver Unit (Tanner et al., 1992) east-west anisotropy in the continuous CO_2 pilot area resulted in "non-radial flood fronts". Although the initial response of the continuous CO_2 pilot was encouraging; the "gassing-out" of production wells suggested subsequent WAG employment to control premature gas breakthroughs.

The main difference between the patented processes and this 'optimum' process is the slug-size. Hybrid-WAG process calls (Bellavance, 1996) for a 9% pore volume CGI

followed by 21% 1:1 WAG flood; whereas the DUWAG process (Tanner et al., 1992) requires 4 – 6 years of CGI flood (at the pilot rates of 2 – 7 MMCF/D) followed by 1:1 WAG till a 40% HCPV injection is achieved (although simulation studies (Tanner et al., 1992) suggest a higher HCPV injection (~ 60% PV) for higher recoveries).

The 'optimum' process suggested by this experimental work is: approx 60 – 80% pore volume CGI injection followed by 1:1 WAG, which conceptually agrees with the speculation of Tanner et al. (1992) that "…predict that a larger slug size (60% HCPV) could result in additional EOR recovery…without increasing peak gas production rates".

3.5.1.6 Comparison between Secondary and Tertiary CGI / WAG Corefloods

There are two important performance comparison parameters from the horizontal CGI/WAG floods completed that are critical to commercial gas injection projects and need to be analyzed: (i) Secondary floods – Injection Mode (CGI and WAG) and (ii) Effect of intermediate waterflood in gas flood oil recovery – Injection Type (Secondary and Tertiary). The collective comparisons are discussed below.

Both of the miscible secondary floods (2500-psi backpressure) completed, show high oil recoveries (> 95% OOIP) in both CGI and WAG modes of injection. The oil recovery trends (both volumes of oil produced as well as %OOIP recovery) are almost identical in both injection modes (Figure 3.36 (a) and (b) respectively).

The secondary gas flood oil recoveries (> 95% OOIP) are significantly higher than the waterflood recoveries (~ 60% OOIP) obtained at similar flooding conditions (Kulkarni, 2003), and are mainly attributable to the lower IFT values (miscibility development - consequently high capillary numbers) obtained in gas injection floods.

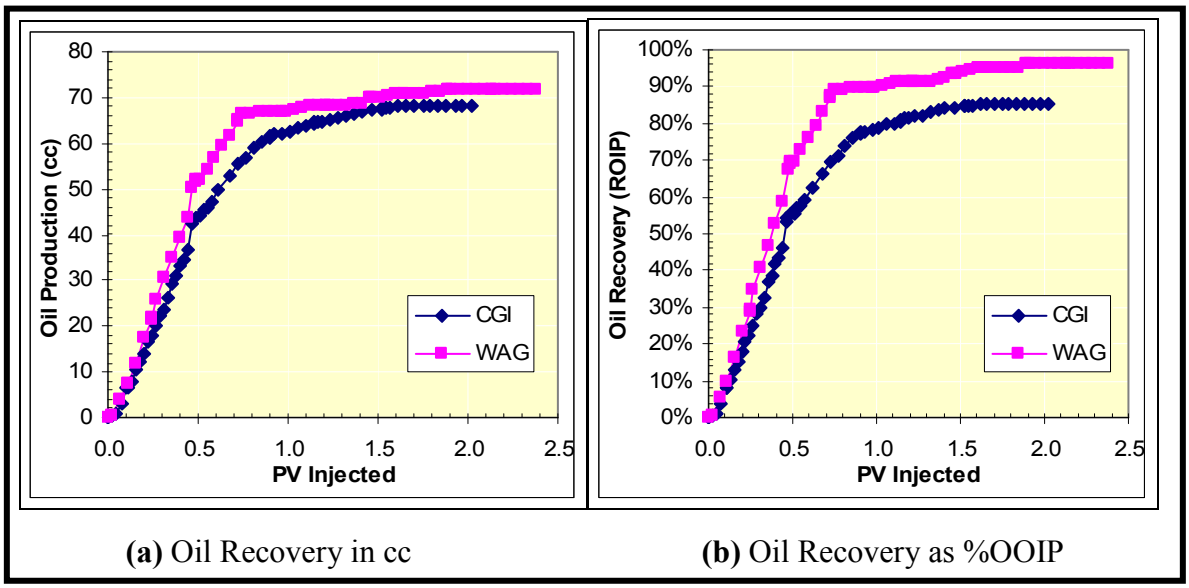

(a) Oil Recovery in cc **(b)** Oil Recovery as %OOIP

Figure 3.36: Oil Recovery Patterns in Secondary Miscible CGI and WAG Floods In n-Decane, Yates Reservoir Brine, 1-ft Berea System at 2500 psi and 72 ^{o}F

Furthermore, as expected, the TRF values for the secondary WAG floods are higher than those of the secondary CGI (Figure 3.36(a)). It is important to note that no free water production (Figure 3.36(b)) was observed during the secondary miscible CGI, affirming the assumption that the connate water saturation at the start of the experiment is essentially immobile, although saturation re-distributions are a possibility – as observed from the unstable pressure drops throughout the experimental run (Figure 3.33(b)).

Figure 3.37 summarizes the oil recovery characteristics obtained in miscible secondary and tertiary CGI and WAG floods. It should be noted that the oil recovery is expressed as percent initial oil in place (%IOIP) in both secondary and tertiary floods. The initial oil corresponds to the oil saturation existing at the start of each gas flood. It is seen that the secondary floods and the tertiary CGI flood oil recoveries are high (> 95%). The tertiary CGI flood was extremely successful in recovering residual oil even after a secondary waterflood and in the presence of high free-water saturations. However, the tertiary WAG flood recoveries are only marginal, demonstrating that the free-water injection (to improve conformance) results in increased water shielding effects – consequently deteriorating WAG performance with time. The important feature of this plot is the immediate oil production in secondary mode, in contrast to the delayed oil production (after ~ 0.5 PV injection) observed in tertiary floods.

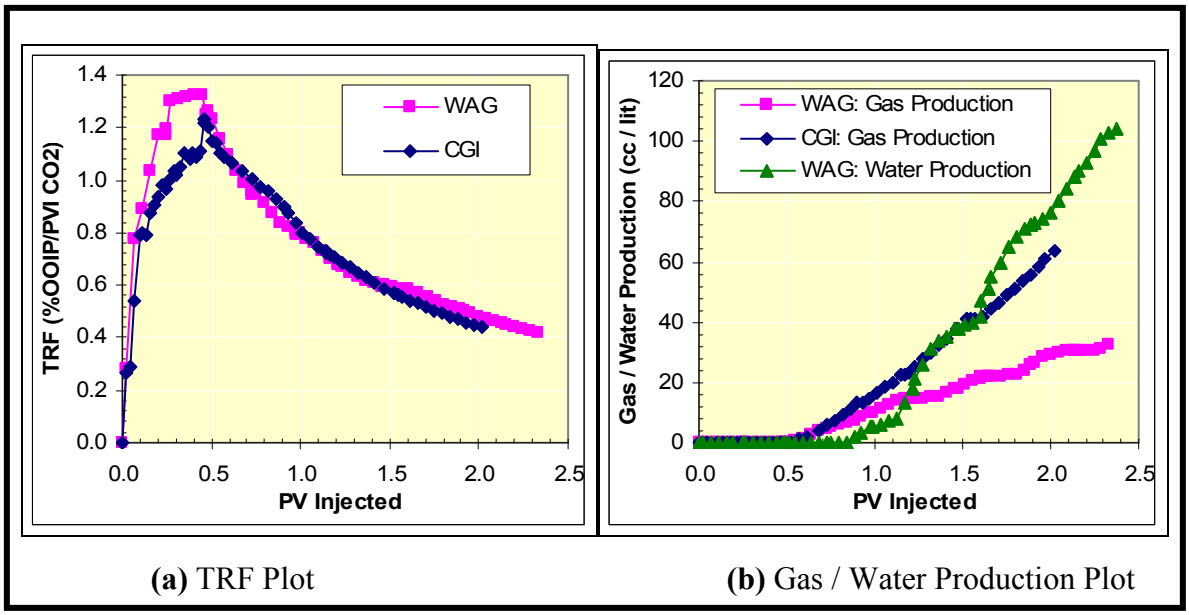

(a) TRF Plot **(b)** Gas / Water Production Plot

Figure 3.37: TRF and Gas / Water Production Plots for Secondary CGI / WAG Floods In n-Decane, Yates Reservoir Brine, 1-ft Berea System at 2500 psi and 72 ^{o}F

Figure 3.38 summarizes the TRF characteristics of the miscible secondary and tertiary CGI and WAG floods. The TRF plot clearly demonstrates the improved economics by virtue of secondary injection by hastened oil production and vastly improved CO_2 utilization factors. The striking feature(s) of Figure 3.38 are the first TRF peak obtained

by WAG employment, shift of the CGI TRF line to the left (in secondary mode compared to tertiary) and the near perfect duplication of oil recovery mechanisms (as seen from the near similar re-traces of the TRF plots) in both secondary and tertiary mode CGI and WAG miscible floods. Another interesting feature of Figure 3.38 is that the TRF trends of both secondary and tertiary floods are similar after ~ 0.8 (or 0.9) PV injections. The gas and water handling requirements in CGI and WAG secondary floods show that the CGI flood have higher cumulative gas recycling and handling requirements.

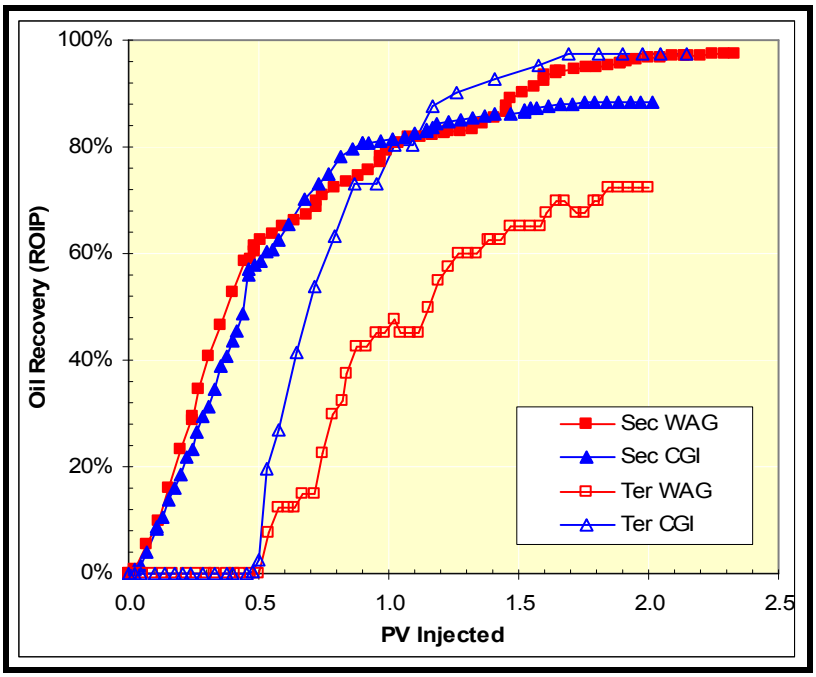

Figure 3.38: Oil Recovery Characteristics in Secondary and Tertiary Miscible Floods In n-Decane, Yates Reservoir Brine, 1-ft Berea System at 2500 psi and 72 ^{o}F

On the other hand, in the WAG flood, water breakthroughs are observed at about ~ 0.84 PVI, and the gas productions are comparable to the CGI up to that extent. After about 0.8 PVI injection, the gas production in CGI increased rapidly, whereas the WAG employment controls gas breakthrough (Figure 3.40(b)).

Figure 3.39 summarizes the pressure drop behavior of the miscible secondary and tertiary CGI and WAG floods. The highest pressure-drops are observed under tertiary mode WAG injection, followed by secondary mode WAG injection, while the miscible CGI floods demonstrate comparable pressure-drop characteristics. Figure 3.39 underscores the importance of injectivity problems, common to most WAG commercial field applications, and suggests that injectivity problems in WAG are probable even under secondary mode injections. The injectivity problems can lead to pressure surges, and could also be partially responsible for the loss of miscibility at the flood displacement front, which can be exaggerated by reservoir heterogeneity. This plot also suggests that

minimal operational problems, especially related to injectivity are probable in CGI mode injections (in both secondary as well as tertiary modes).

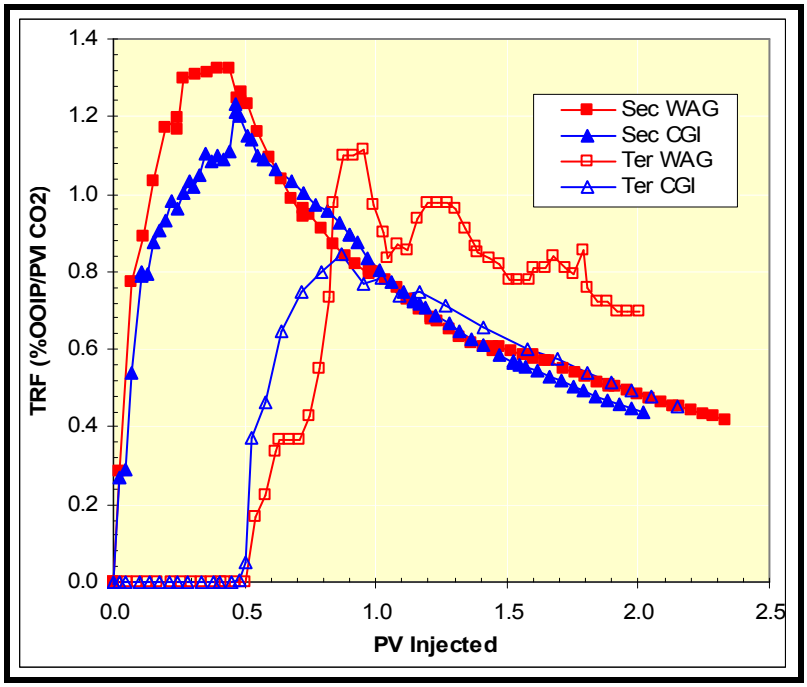

Figure 3.39: TRF Characteristics in Secondary and Tertiary Miscible Floods in n-Decane, Yates Reservoir Brine, 1-ft Berea System at 2500 psi and 72 ^{o}F

Figure 3.40 summarizes water and gas production characteristics in secondary as well as tertiary miscible floods. Figure 3.40(a) shows that tertiary floods start producing water right from the beginning of the flood whereas the water production and handling problems are almost non-existent in secondary floods until later life of the secondary CGI and WAG floods and that the secondary CGI flood does not produce any free-water.

Summary

The miscible secondary floods (conducted at 2500 psi backpressure) demonstrate high oil recoveries (> 95%) in both CGI and WAG mode of injection. The oil recovery trends (both volumes of oil produced as well as %OOIP recovery) are almost identical in both injection modes. The secondary gas flood recoveries (> 95% OOIP) are significantly higher than the waterflood recoveries (~ 60% OOIP) obtained at similar flooding conditions, mainly attributable to the lower interfacial tension (IFT) values (miscibility development - consequently high capillary numbers) obtained during gas injection.

As expected, the TRF values for the WAG floods are higher than those of the CGI. The TRF values for CGI and WAG peak at nearly the same PV injections (0.46 and 0.49 PVI respectively), but are markedly lower than the TRF peaks in tertiary floods (0.7 – 0.8 PVI), thus demonstrating the beneficial effects of early gas injection (in secondary mode)

by hastened oil recovery and improved CO_2 utilization factors. The water shielding effect, responsible for delayed oil production in tertiary floods, was almost non-existent in the secondary floods – even in WAG mode of injection.

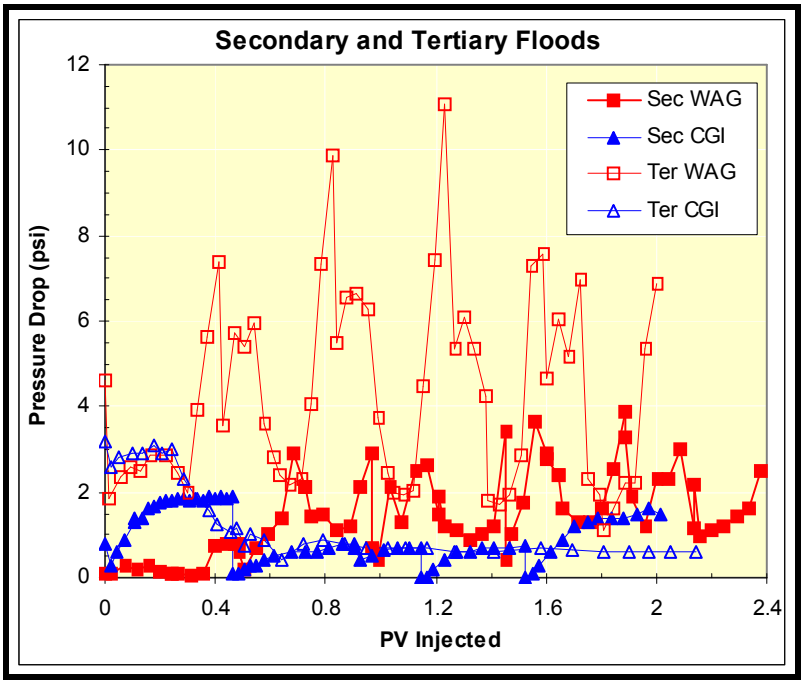

Figure 3.40: Pressure Drop Characteristics in Secondary and Tertiary Miscible Floods In n-Decane, Yates Reservoir Brine, 1-ft Berea System at 2500 psi and 72 ^{o}F

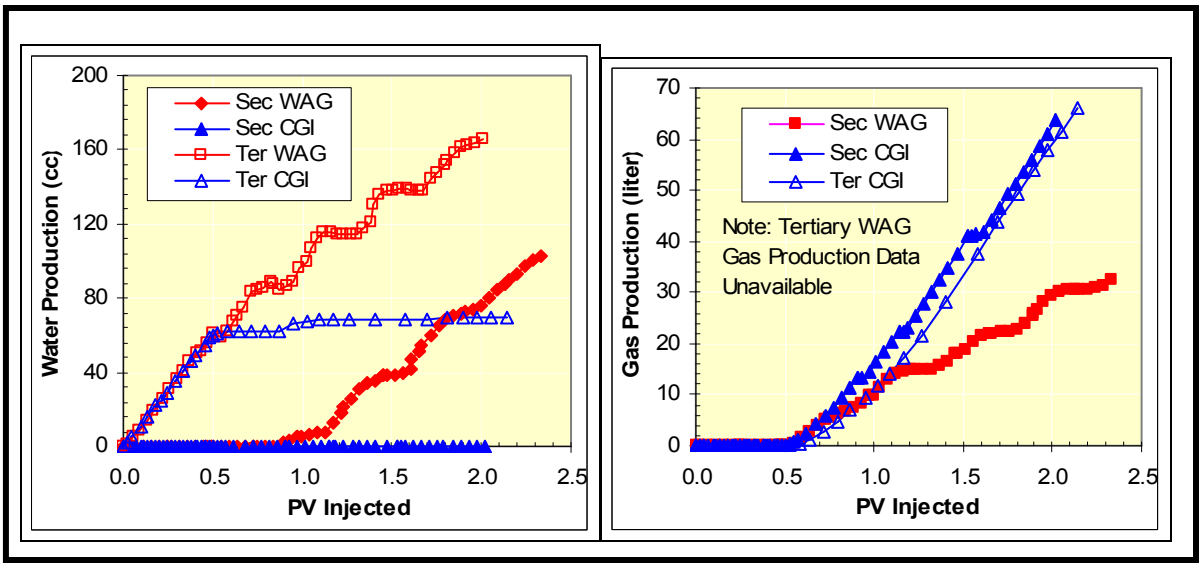

(a) Water Production **(b)** Gas Production

Figure 3.41: Water and Gas Production Plots for Secondary and Tertiary Miscible Floods In n-Decane, Yates Reservoir Brine, 1-ft Berea System at 2500 psi and 72 ^{o}F

The TRF trends (Figure 3.38) and the gas and water production trends indicate that it could be economical to inject in CGI mode up to about 0.7 to 0.9 pore volumes, and then switch over to 1:1 WAG for controlling gas and water productions, to improve efficiency. Hence, the 'happy-medium' of Hybrid-WAG, which was demonstrated to be relevant to tertiary gas floods in previous reports, could also be applicable to the secondary floods, and may be employed for optimum economics.

3.5.1.7 Preliminary Conclusions from Horizontal Corefloods

1. Based on oil recovery, the CGI flood appeared to be better in performance than WAG flood. However, on the basis of the overall Tertiary Recovery Factor (TRF), where the recoveries were normalized by the volume of CO_2 injected, the WAG floods clearly out-performed the CGI floods. Furthermore, the TRF performance of the CGI miscible flood approaches the relatively low recoveries obtained in the immiscible gas floods, indicating deteriorating returns from the CGI with time.
2. Miscible gas floods were found to recover over 60 to 70% more of the waterflood residual oil than immiscible gas floods. While the recoveries in immiscible 5% NaCl brine floods (both CGI and WAG) were about 23%, the miscible floods yielded 84.5% recovery for the 5% NaCl brine WAG flood (for 1.02 PV of CO_2 injected) and 96.7% recovery for the 5% NaCl brine CGI flood (for 2.44 PV of CO_2 injected). However, about 94% of the oil is produced in ~ 1.02 PV of CO_2 injected compared to 84.5% for WAG.
3. Miscible CGI floods showed negligible sensitivity to brine composition variations. Recoveries of 96.7% and 97.6% where obtained with 5% NaCl brine and Yates reservoir brine, respectively. In contrast, the miscible WAG recoveries exhibited significant dependence on brine composition. The miscible WAG recoveries showed a significant decrease (12%) in oil recovery when the connate brine was changed from 5% NaCl solution to Yates reservoir brine. While the recovery for the miscible 5% NaCl brine was 84.5%, it decreased to 72.5% for Yates reservoir brine. This is attributable to the higher solubility of CO_2 in natural multi-component brines than solutions of pure salts like NaCl, which results in higher volumes of CO_2 being available for oil recovery in 5% NaCl brine floods.
4. Solubility of CO_2 in reservoir brine (at lower pressures) may have serious implications in the reservoir projects, in that the costs may increase due to delayed oil productions and increased CO_2 requirements for injection in immiscible mode.
5. Unlike immiscible floods, where WAG employment hastens oil breakthroughs, the miscible WAG and CGI floods' oil breakthroughs occur at near identical pore volume injections. The delayed oil breakthroughs in immiscible floods are attributable to CO_2 solubility effects in core-brine. However, miscibility development offsets these brine

solubility effects and the need for pre-saturation of injection brine with CO_2 appears to be effectively eliminated.

6. Secondary gas floods demonstrate faster as well as higher oil recoveries and gas utilization factors indicating the beneficial effects of gas injection earlier in the life of the flood.
7. Experimental results show that for optimization of tertiary recovery in gas floods, a continuous gas slug of 0.7 PV (where the CGI flood showed maximum TRF value) followed by 1:1 WAG needs to be injected. This optimized method indicated by our results was found to be similar to the patented 'Hybrid WAG' and 'DUWAG' processes employed in the oil industry.
8. The 'Happy-Medium' between single slug and WAG processes has been conceptually identified and experimentally demonstrated.
9. In addition to sweep improvement, if the purpose of the employment of the WAG process to decrease the quantities of CO_2 injected, then the environmental benefit of CO_2 sequestration would be minimal.
10. Watered out reservoirs containing high water saturations serve as good candidates for CO_2 sequestration through CO_2 dissolution in brine.

3.5.2 Gravity Stable Displacement History (GSDH) GAGD Floods (On 1-ft Berea, n-Decane, Yates Reservoir Brine and CO_2)

The GAGD experimental design suggested two possible GAGD experimental protocols: all the coreflood steps such as oil flood, water flood (if applicable) and gas flood, be conducted either in a gravity stable manner (GSDH) or only the gas flood be gravity stable (NSDH). This section details the results of the scaled GSDH GAGD experiments completed; while the scaled NSDH GAGD experiments are discussed in Section 5.3 later. Five GSDH GAGD experiments, three immiscible and two miscible, were completed using n-Decane (oleic phase), Yates reservoir brine (water) and CO_2 on 1-ft Berea sandstone core. As dictated by the experimental design, all the experimental steps conducted during these experiments were in a gravity stable mode, i.e. the oil flood, water flood (secondary, if applicable) as well as the tertiary gas injection flood. The oil flood was completed by injecting n-Decane into a previously brine saturated core from the top, and the displacement was from top to bottom. The water flood was completed by injecting Yates reservoir brine from the bottom, and finally gas was injected (at 10 cc/hr) from the top. Inspite that these experiments are not realistic from a field perspective, they provided with an approximation of the upper limit for GAGD recovery characteristics.

3.5.2.1 Immiscible GSDH GAGD Floods

The three scaled immiscible GSDH GAGD experiments were conducted to evaluate: (i) the effect(s) of injection mode on GAGD recovery characteristics in an immiscible mode

and (ii) the effect(s) of injection rate on GAGD recovery characteristics in an immiscible mode. Figures 3.42 – 44 summarize the data obtained from these GSDH GAGD floods.

Part (a) of the figures provides the data for water recovery and pressure drop during the drainage cycle when n-Decane was injected into the brine saturated core. Part (b) provides the data for oil recovery and pressure drop when Yates reservoir brine was injected into the core at connate water saturations. Part (c) provides the data for water, and oil recoveries as well as pressure drop during the gravity stable GAGD tertiary recovery process, where in pure CO_2 was injected into the core at residual oil saturation.

3.5.2.2 Miscible GSDH GAGD Floods

Two scaled GSDH GAGD coreflood experiments using n-Decane, Yates reservoir brine and pure CO_2 on 1-ft Berea core in the miscible mode, were also completed. The objectives of these experiments were: (i) to evaluate the effect of injection mode on GAGD recovery characteristics in a miscible mode and (ii) to study the effect of miscibility development on GAGD recovery characteristics. Figures 3.45 and 3.46 summarize the data obtained from these GSDH GAGD miscible floods.

Similar to Figures 3.42 to 3.54, part (a) of the figures provide the data for water recovery and pressure drop during the drainage cycle when n-Decane was injected into the brine saturated core. Similarly, part (b) provides the data for oil recovery and pressure drop when Yates reservoir brine was injected into the core at connate water saturations. Finally, part (c) provides the data for water, and oil recoveries as well as pressure drop during the gravity stable GAGD tertiary recovery process, where in pure CO_2 was injected into the core at residual oil saturation.

3.5.2.3 Comparison of Immiscible and Miscible GSDH GAGD Floods

There are five major comparisons that can be made from the GSDH GAGD experiments completed: (i) effect of injection rate (10 cc/hr versus 40 cc/hr) on GAGD secondary immiscible floods, (ii) effect of injection mode (secondary versus tertiary) on GAGD immiscible floods, (iii) effect of injection mode (secondary versus tertiary) on GAGD miscible floods, (iv) effect of miscibility development (miscible versus immiscible) on GAGD floods, and (v) comparison of oil recovery characteristics of GAGD versus horizontal mode WAG floods. This sub-sections details this comparison for GSDH mode GAGD experiments.

Effect of Injection Rate on Secondary Immiscible GSDH GAGD Floods

The effect of injection rate on secondary immiscible GSDH GAGD floods is shown in Figure 3.47. In course of the dimensional analysis of the gravity stable field projects followed by the laboratory coreflood experimental design, various models were used to calculate the limiting 'Critical Injection Rate' (CIR) for the coreflood displacement

(flood interface) to be stable. During experimentation, the lowest value of the CIR predicted (which was – 43 cc/hr) from model calculations was used as the maximum injection rate. However, as the entire previous horizontal mode CGI / WAG corefloods were conducted at 10 cc/hr rates (as dictated by the Leas and Rappaport stability criterion); the GAGD corefloods were also conducted at the same injection rates. This assured normalization of viscous / capillary / dispersive forces in all the corefloods to provide with an effective comparison based on buoyancy forces only.

However, for the validation and experimental verification of the CIR's relevance to GAGD experimentation, two secondary immiscible gravity stable GAGD floods were conducted at different injection rates (both below the limiting CIR), namely 10 cc/hr and 40 cc/hr, using n-Decane, Yates reservoir brine and CO_2.

Figure 3.47(a) clearly shows that the effects of injection rate on the gravity stable GAGD floods are minimal. On the other hand, near perfect duplication of the tertiary recovery factors (TRF) for the two corefloods (Figure 3.47(b)) suggest that the gas utilization efficiencies too are independent of the injection rates, provided the injection rates are below the CIR. The pressure drop behavior suggests that in secondary floods, the pressure drops tend to stabilize near the absolute permeability pressure drop value (Figure 3.47(c)), indicating near perfect gas sweep efficiencies.

Effect of Injection Mode on Immiscible GSDH GAGD Floods

The effect of injection mode (secondary versus tertiary) on immiscible gravity stable GAGD floods is shown in Figure 3.48. The literature review suggests that the commercial gravity stable gas injection processes have be employed in both secondary as well as tertiary modes. To provide with effective comparisons and performance review between horizontal WAG / CGI floods and GAGD, all these experiments were completed in both secondary and tertiary modes. The secondary and tertiary mode CGI / WAG corefloods data are available elsewhere (Kulkarni, 2003; Rao et al., 2004).

To isolate the effects of injection mode on gravity stable immiscible GAGD floods, two immiscible gravity stable GAGD floods were conducted in secondary and tertiary modes of injection using n-Decane, Yates reservoir brine and CO_2.

Figure 3.48(a) shows that the gravity stable GAGD recovery efficiencies (average incremental recovery: 61.95% ROIP) are significantly higher than horizontal CGI / WAG floods (average incremental recovery: 34.34% ROIP), even under immiscible modes of injection. These oil recovery numbers show that the GAGD mode of injection clearly outperforms the WAG floods. Also it is important to note that the mode of injection (secondary or tertiary) significantly affects the GAGD performance under immiscible mode. Tertiary immiscible GAGD flood recovery (59.06%) is significantly lower than the secondary immiscible GAGD flood recovery (64.83%), thus suggesting higher incremental benefits of GAGD application in secondary mode.

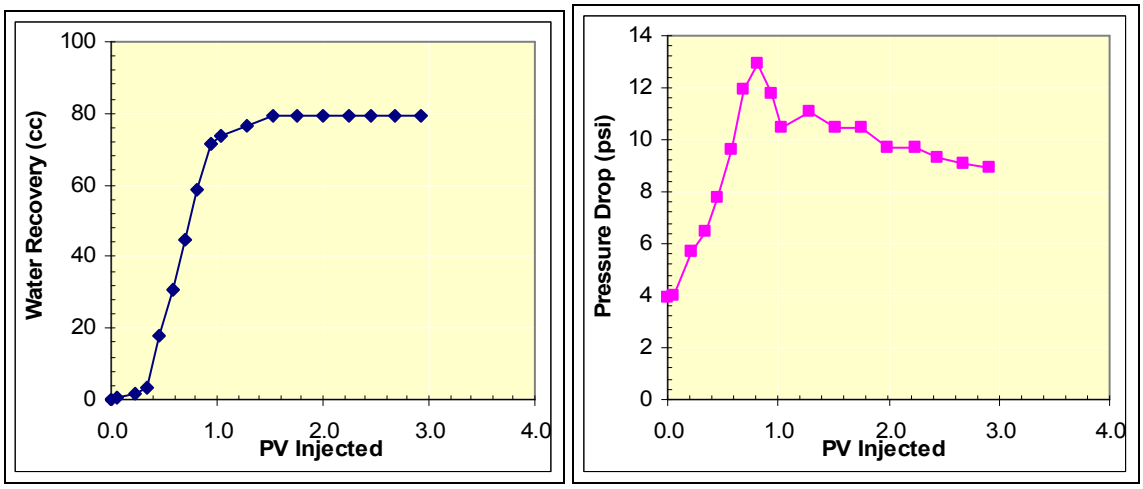

(a) Gravity Stable Drainage Cycle: Oil Flood with n-Decane

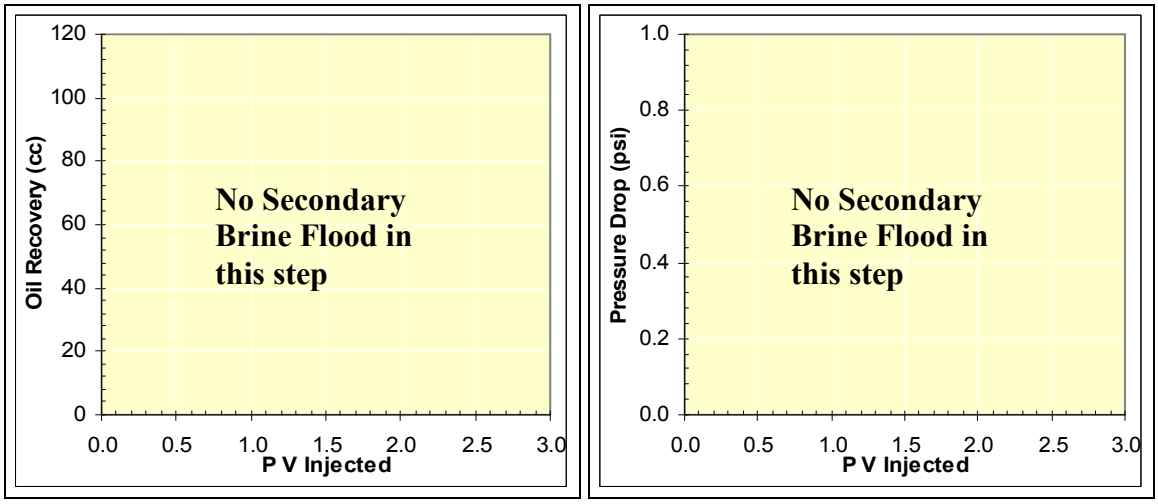

(b) Gravity Stable Imbibition Cycle: Brine Flood with Yates Reservoir Brine

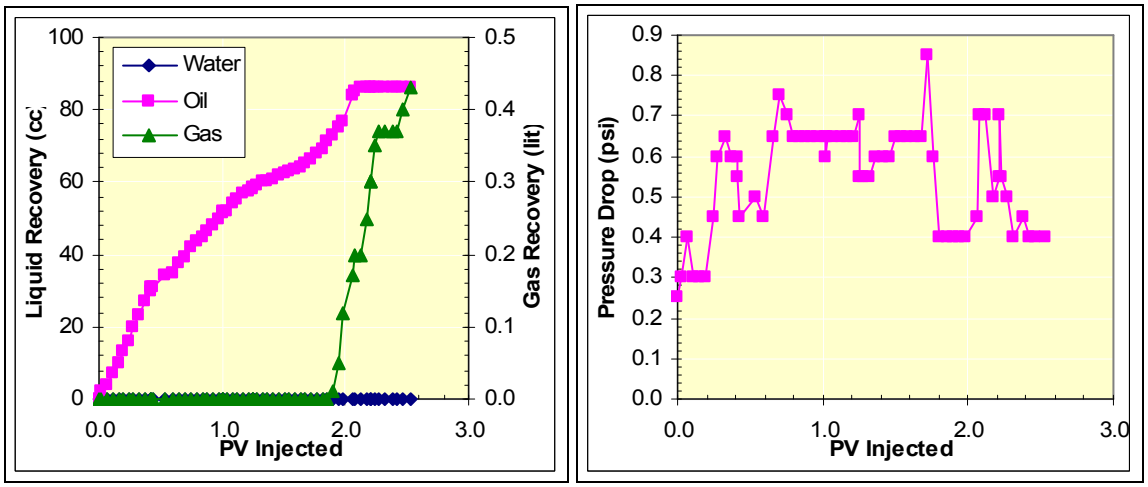

(c) Gravity Stable GAGD Cycle: Gas Flood with Pure CO_2

Figure 3.42: Data for Experiment GAGD GSDH # 1: 1-ft Berea Core + Yates Reservoir Brine with Gravity Stable Immiscible Secondary GAGD CO_2 Injection @ 10 cc/hr

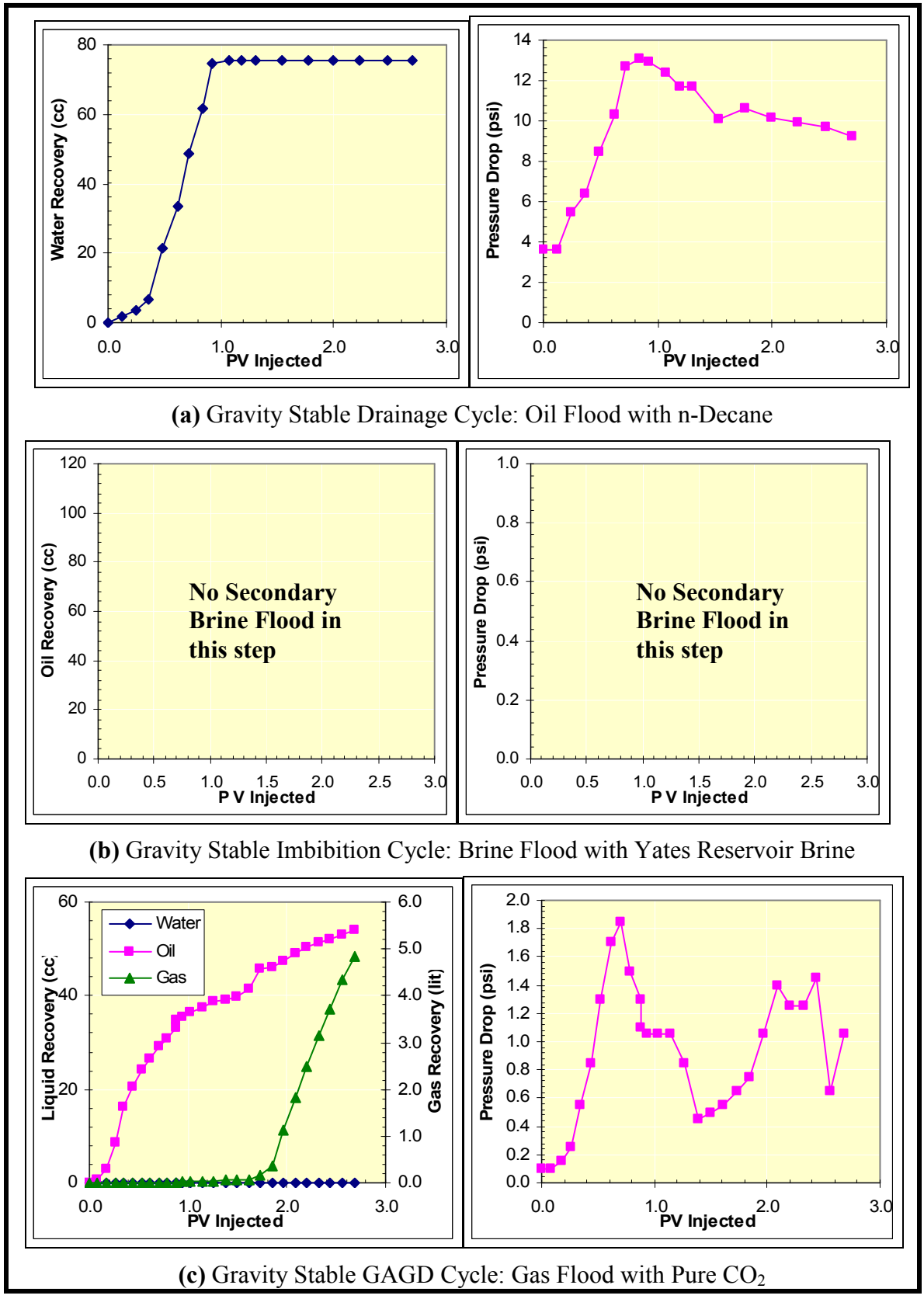

Figure 3.43: Data for Experiment GAGD GSDH # 1(A): 1-ft Berea Core + Yates Reservoir Brine with Immiscible Secondary GAGD CO_2 Injection @ 40 cc/hr

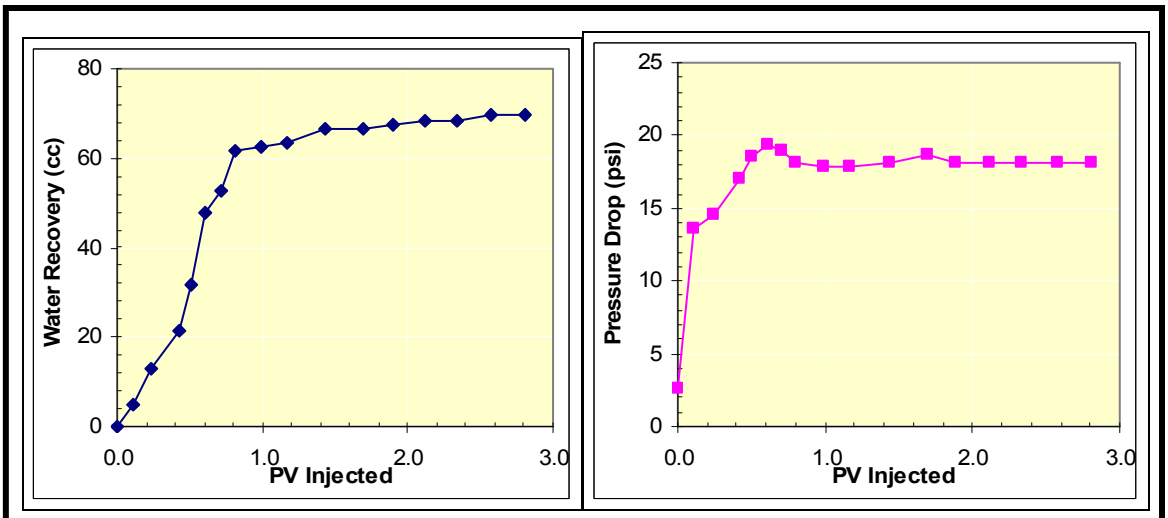

(a) Gravity Stable Drainage Cycle: Oil Flood with n-Decane

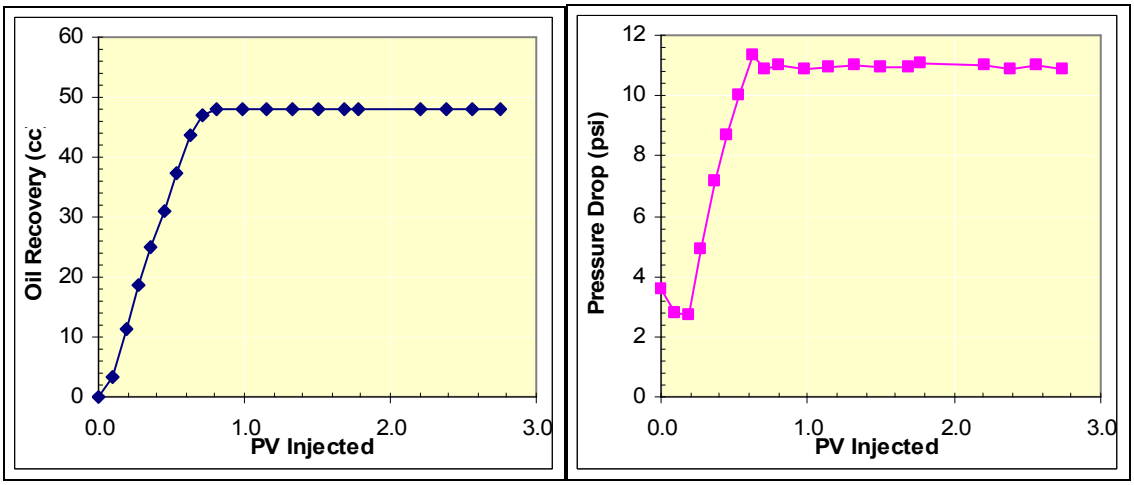

(b) Gravity Stable Imbibition Cycle: Brine Flood with Yates Reservoir Brine

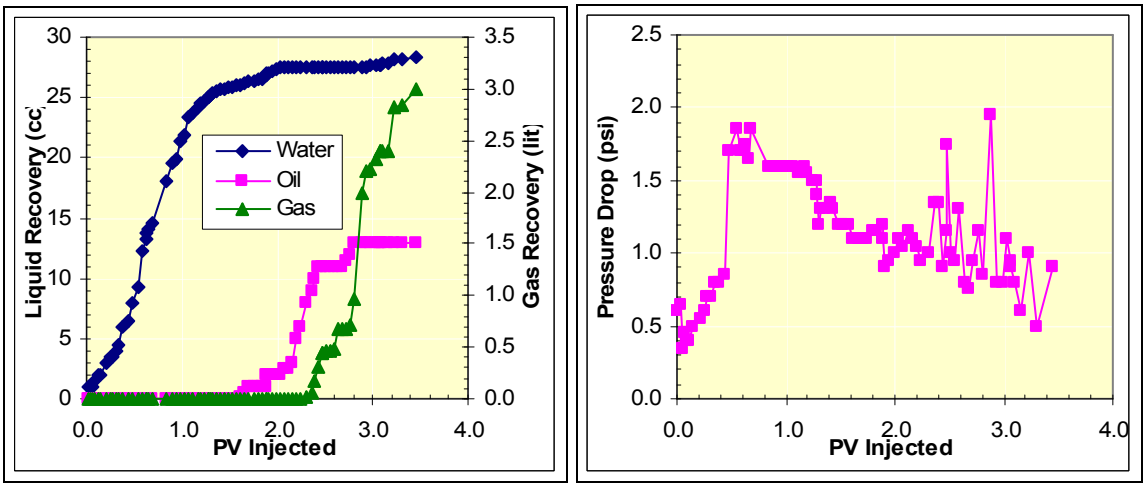

(c) Gravity Stable GAGD Cycle: Gas Flood with Pure CO_2

Figure 3.44: Data for Experiment GAGD GSDH # 2: 1-ft Berea Core + Yates Reservoir Brine with Gravity Stable Immiscible Tertiary GAGD CO_2 Injection @ 10 cc/hr

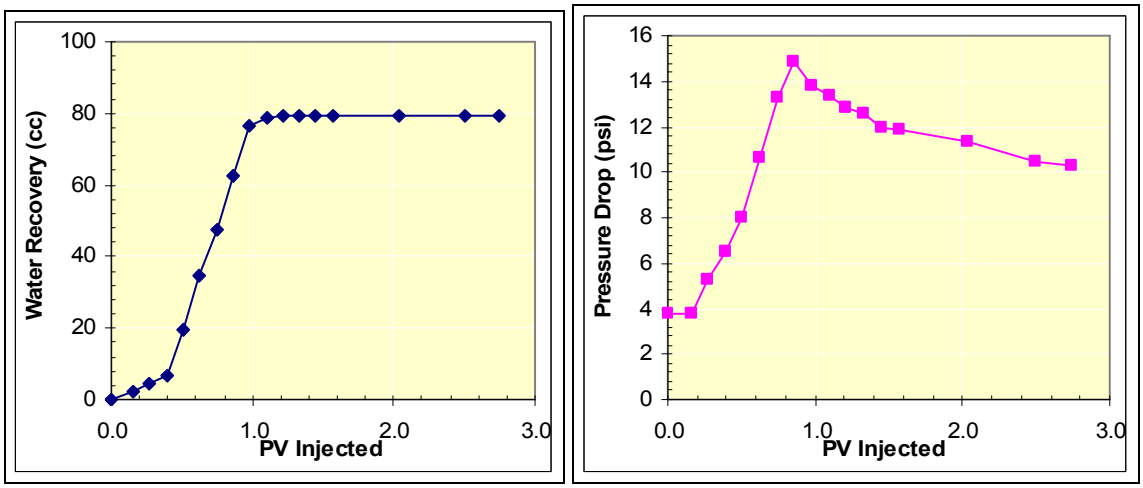

(a) Gravity Stable Drainage Cycle: Oil Flood with n-Decane

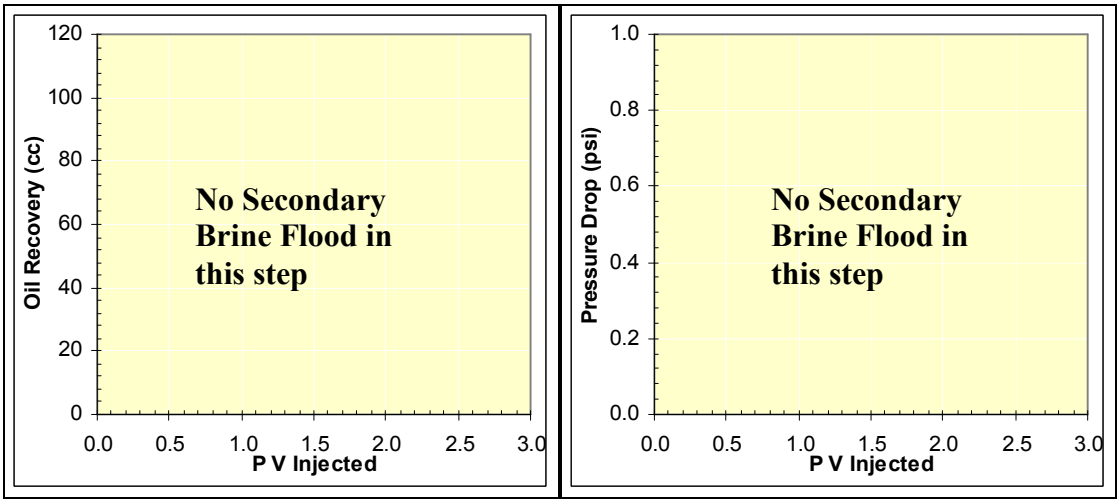

(b) Gravity Stable Imbibition Cycle: Brine Flood with Yates Reservoir Brine

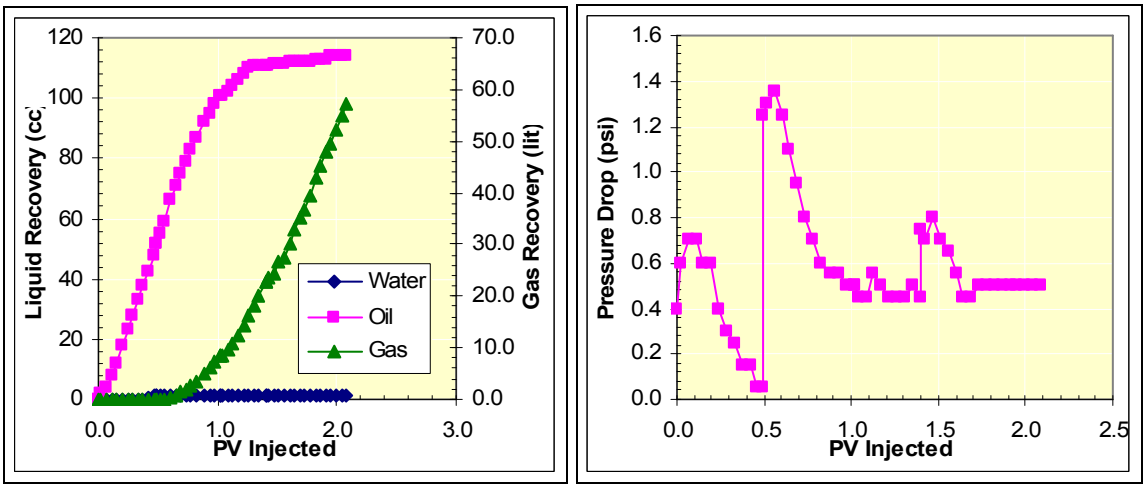

(c) Gravity Stable GAGD Cycle: Gas Flood with Pure CO_2

Figure 3.45: Data for Experiment GAGD GSDH # 3: 1-ft Berea Core + Yates Reservoir Brine with Gravity Stable Miscible Secondary GAGD CO_2 Injection @ 10 cc/hr

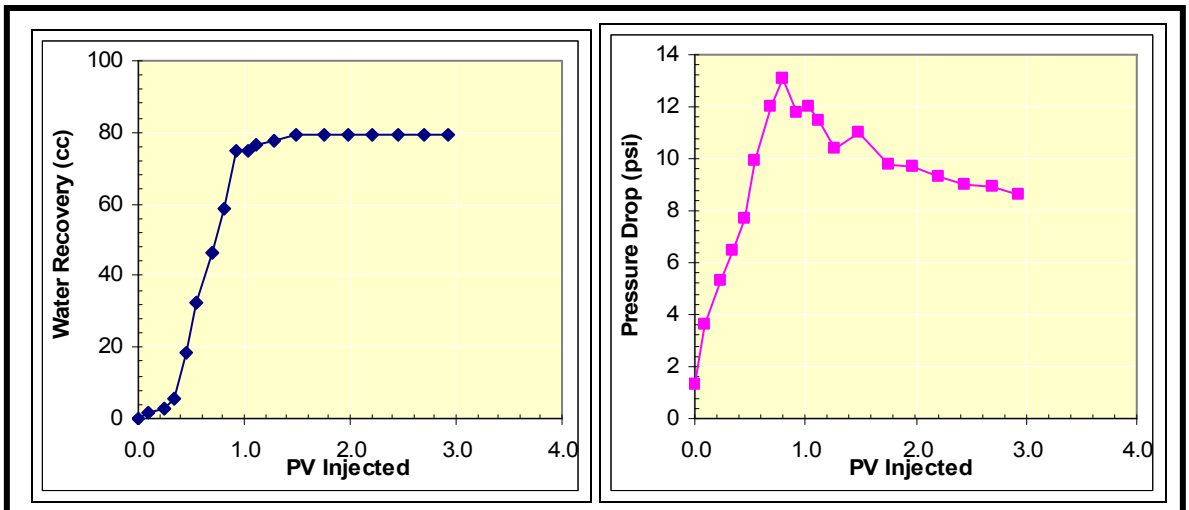

(a) Gravity Stable Drainage Cycle: Oil Flood with n-Decane

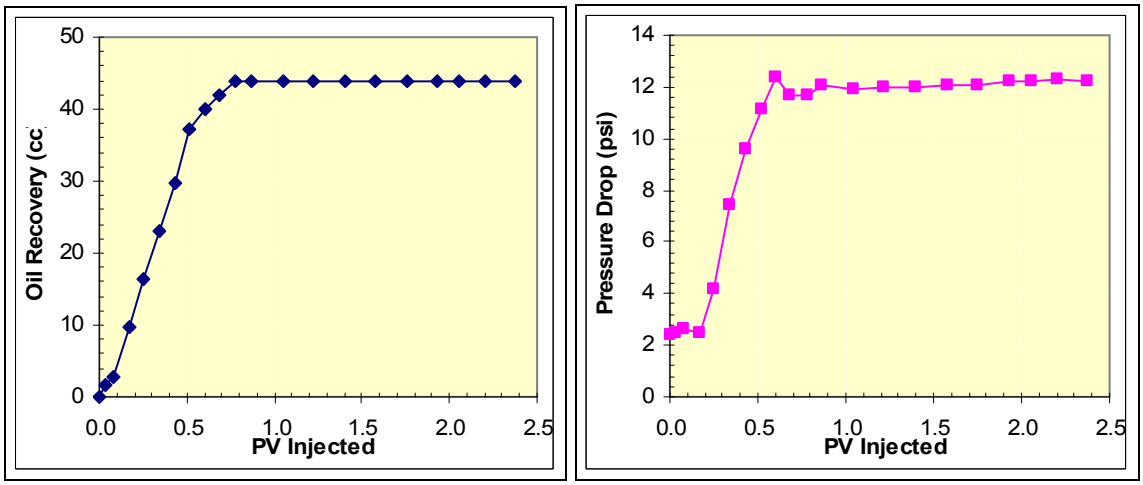

(b) Gravity Stable Imbibition Cycle: Brine Flood with Yates Reservoir Brine

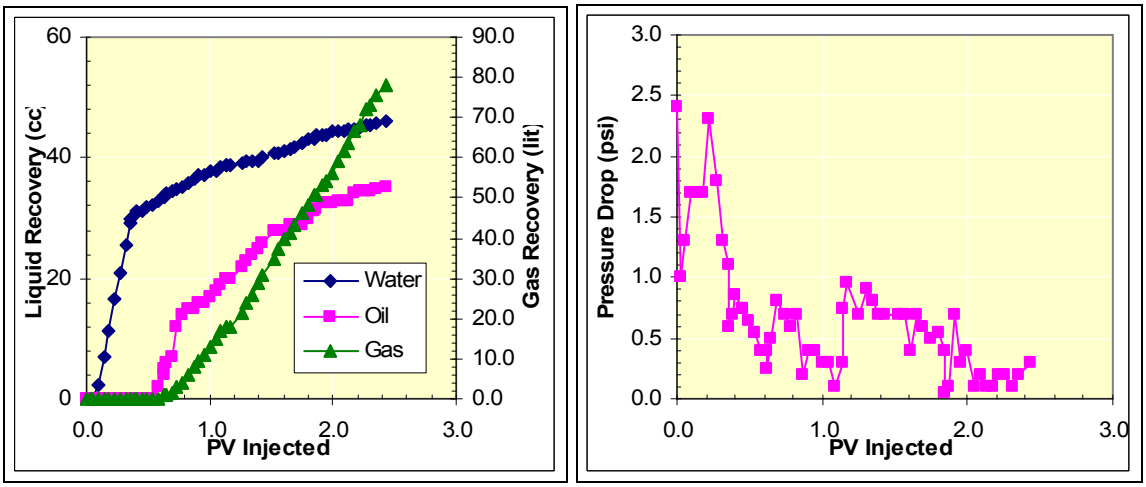

(c) Gravity Stable GAGD Cycle: Gas Flood with Pure CO_2

Figure 3.46: Data for Experiment GAGD GSDH # 4: 1-ft Berea Core + Yates Reservoir Brine with Gravity Stable Miscible Tertiary GAGD CO_2 Injection @ 10 cc/hr

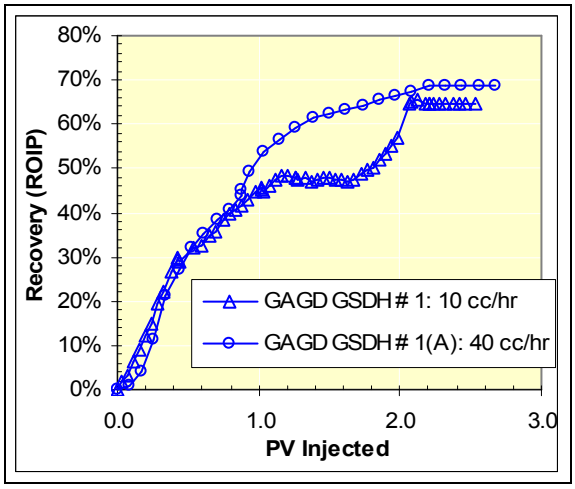

(a) Oil Recovery Characteristics versus PV CO_2 Injection

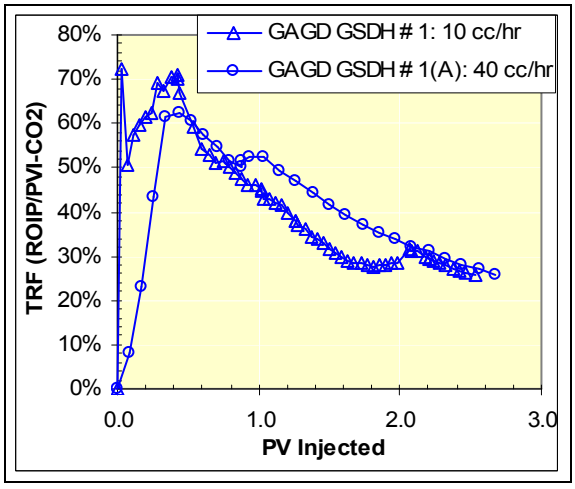

(b) TRF (%ROIP / PVI CO_2) Characteristics versus PV CO_2 Injection

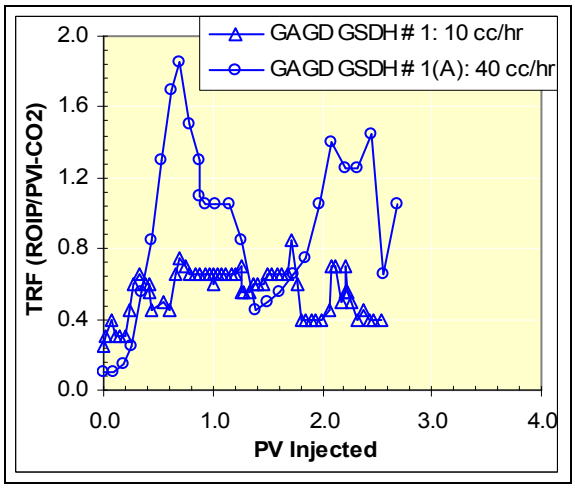

(c) Pressure Drop Characteristics versus Pore Volume CO_2 Injection

Figure 3.47: Effect of Injection Rate on Secondary Immiscible GSDH GAGD Floods in n-Decane, Yates Reservoir Brine and Pure CO^2 System

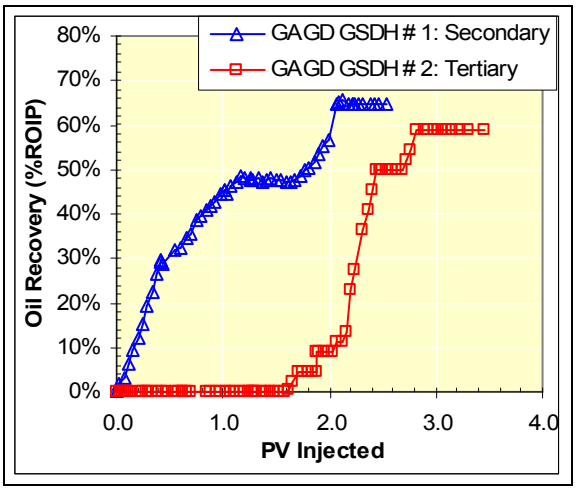

(a) Oil Recovery Characteristics versus PV CO_2 Injection

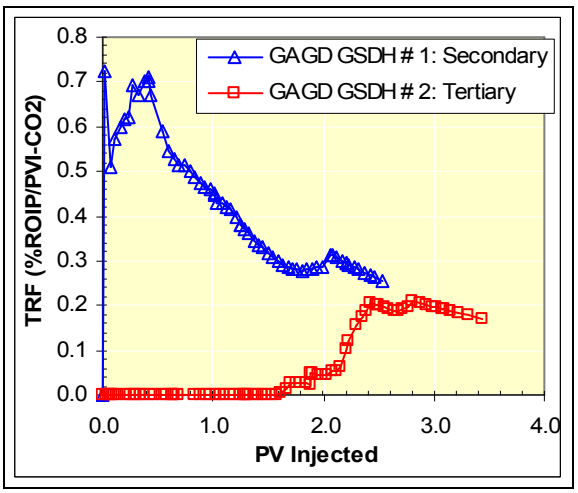

(b) TRF (%ROIP / PVI CO_2) Characteristics versus PV CO_2 Injection

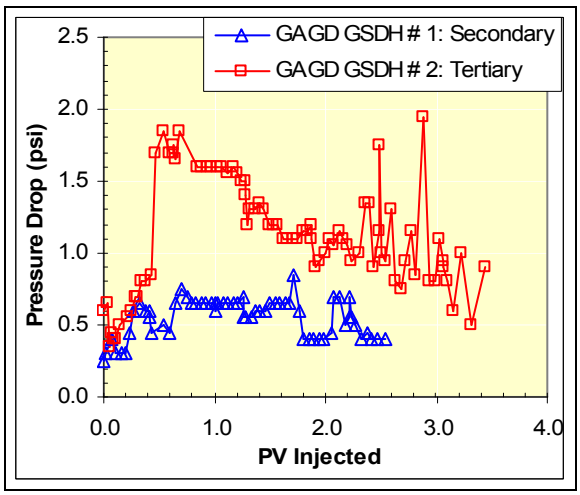

(c) Pressure Drop Characteristics versus PV CO_2 Injection

Figure 3.48: Effect of Injection Mode (Secondary versus Tertiary) on Immiscible GSDH GAGD Floods in n-Decane, Yates Reservoir Brine and Pure CO_2 System

The utilization factors pertaining to secondary floods show high TRF values till 1.0 pore volume injection (PVI), followed by a decline. However this decline is not exponential, as was observed in immiscible horizontal secondary CGI corefloods, suggesting sustained higher gas utilization factors for gravity stable GAGD corefloods. Furthermore, as observed in Figure 3.48(c), the pressure drop behavior tends to reach a plateau, although the approach could be asymptotic in tertiary gravity stable GAGD floods, suggesting high sweep efficiencies during these corefloods.

Effect of Injection Mode on Miscible GSDH GAGD Floods

The effect of injection mode (secondary versus tertiary) on miscible GSDH GAGD floods is shown in Figure 3.49. The literature review suggests that the commercial gravity stable gas injection processes have been employed in both secondary as well as tertiary modes, and that the miscible mode of injection is highly popular in commercial gas injection processes.

As previously practiced in immiscible GSDH GAGD floods, the miscible GSDH GAGD corefloods were also completed in both secondary and tertiary modes. Furthermore, to isolate the effects of injection mode on miscible GSDH GAGD floods, these two miscible GSDH GAGD floods were conducted in both secondary as well as tertiary modes of injection using n-Decane, Yates reservoir brine and CO_2.

Figure 3.49(a) shows that in the miscible gravity stable GAGD floods, near perfect sweep efficiencies were observed, and are significantly higher than the CGI / WAG miscible flood recoveries. It is important to note that excepting the delay in oil production for tertiary floods, there are minimal effects of injection mode on miscible GAGD recovery. The average incremental recovery in gravity stable GAGD floods was ~ 100% ROIP while the average incremental recoveries in horizontal mode CGI and WAG floods were 97.12% ROIP and 78.52% ROIP only. These oil recovery numbers show that the GAGD mode of injection far outperforms the WAG floods; while maintaining better gas utilization efficiencies as compared to the CGI floods (Figure 3.49(b)), by achieving hastened TRF peaks and asymptotic decreases in TRF values throughout the life of the flood. Furthermore, on a macroscopic scale, advantages of injecting in the GAGD mode far outweigh the CGI floods due to the favorable gravity force effects during GAGD (Rao et al., 2004). Consistent with the observations of immiscible GSDH GAGD floods, the pressure drop behavior in miscible gravity stable GAGD floods, also tend to reach a plateau, although the approach could be asymptotic in tertiary gravity stable GAGD floods (Figure 3.49(c)), suggesting high sweep efficiencies during these corefloods.

Effect of Miscibility Development on GSDH GAGD Corefloods

Comparison of Figures 3.48 and 3.49 clearly demonstrate the benefits of miscibility development during GAGD applications.

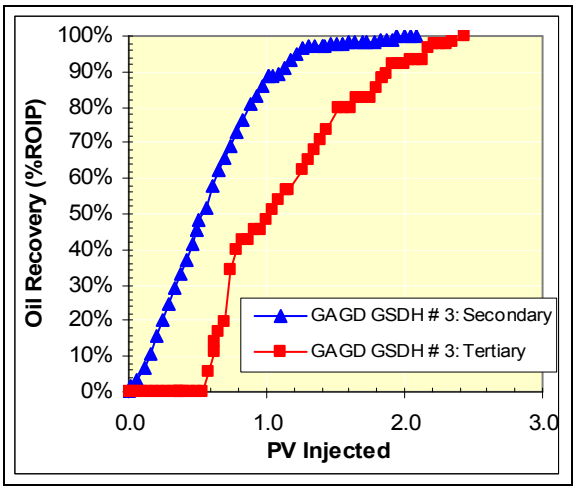

(a) Oil Recovery Characteristics versus PV CO_2 Injection

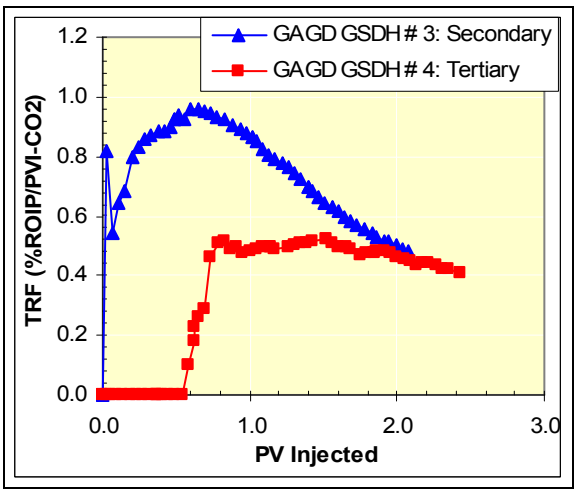

(b) TRF (%ROIP / PVI CO_2) Characteristics versus PV CO_2 Injection

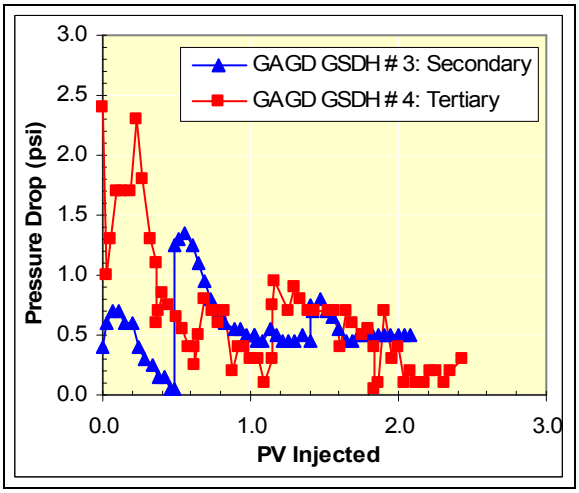

(c) Pressure Drop Characteristics versus PV CO_2 Injection

Figure 3.49: Effect of Injection Mode (Secondary versus Tertiary) on Miscible GSDH GAGD Floods in n-Decane, Yates Reservoir Brine and Pure CO_2 System

The average incremental oil recovery for miscible gravity stable GAGD floods is ~ 100% ROIP while average incremental oil recovery for immiscible gravity stable GAGD floods is 61.95% ROIP, thus attributing a clear 38.06% ROIP incremental recovery only to miscibility development. The trend to more efficient commercial miscible gas injection projects (EOR Survey, 2004) is comprehendible from the high recovery efficiencies observed in these vertical as well as horizontal gas injection coreflood experiments.

However, it is important to note that the GSDH GAGD floods fared well even in the immiscible mode of injection, in both secondary as well as tertiary application modes. The high gas utilization efficiencies coupled with the good oil recovery characteristics could therefore also help make the immiscible GAGD process desirable in low pressure and depleted oil reservoirs.

Preliminary Conclusions from GSDH GAGD Corefloods

Some of the characteristics features and preliminary conclusions obtained from the GSDH GAGD experimentation are:

Oil Recovery Characteristics:

1. Minimal effects of rate on oil recovery.
2. Excellent recovery characteristics even under immiscible injection mode.
3. Near perfect microscopic as well as microscopic sweep efficiencies during miscible injection.

Tertiary Recovery Factor (TRF) Characteristics:

1. Hastened TRF peaks for all secondary injections, followed by a rapid TRF (or gas utilization) decline after about 1.0 pore volume injection.
2. TRF peaks during tertiary injections, although lower and later in the flood's life, exponential performance (TRF) decline as observed in horizontal mode CGI / WAG injections was not observed.
3. Near-perfect TRF characteristics' reproduction clearly indicates the repeatability and the mechanistic duplication of the flood parameters.

Pressure Drop Characteristics:

1. Exponential approach to absolute permeability pressure drop measurement values of the secondary GSDH GAGD floods' pressure drop data (for both immiscible and miscible), demonstrates excellent reservoir sweep efficiencies.
2. Tertiary GAGD floods demonstrate pressure drop characteristics similar to the secondary GAGD floods, although in tertiary floods, the approach to the absolute permeability pressure drop value is asymptotic.
3. Higher initial free water saturation (tertiary mode GAGD injection), also seem to be affected by microscopic multiphase mechanisms such as CO_2-brine solubility effects, higher startup pressure drops (thus decreased gas injectivity), and three-phase relative permeability effects.

3.5.3 Non-Gravity Stable Displacement History (NSDH) GAGD Floods (On 1-ft Berea, n-Decane, Yates Reservoir Brine and CO_2)

Four scaled non-gravity stable displacement history (NSDH) GAGD experiments (two immiscible and two miscible) were completed in addition to the scaled GSDH GAGD experiments. For these scaled NSDH GAGD experiments, the oil (n-Decane) flood and the water (Yates reservoir brine) flood (only in tertiary mode gas floods) were conducted in a non-gravity stable (horizontal) mode. The oil flood was completed by horizontally injecting n-Decane into a previously brine saturated core, and the displacement was from left to right. The water flood was also completed in a similar manner by horizontally injecting Yates reservoir brine. The core was then positioned vertically and allowed to reach equilibrium for 24 hours. Pure CO_2 was injected (at 10 cc/hr) into this core from the top in a gravity stable manner, to represent the actual field GAGD implementation and provide with realistic and scalable recovery characteristics.

3.5.3.1 Immiscible NSDH GAGD Floods

The objectives of these scaled NSDH GAGD immiscible coreflood experiments were: (i) to evaluate the effect of injection strategy on GAGD recovery characteristics in an immiscible mode and (ii) to study the effect of the previous non-gravity stable waterflood (in tertiary mode floods only) on GAGD recovery characteristics in an immiscible mode. The results of these experiments are summarized in Figures 3.50 and 3.59.

In these Figures, Part (a) provides the data for water recovery and pressure drop during the drainage cycle when n-Decane was injected into the brine saturated core. Part (b) provides the data for oil recovery and pressure drop when Yates reservoir brine was injected into the core at connate water saturations. Part (c) provides the data for water, and oil recoveries as well as pressure drop during the gravity stable GAGD tertiary recovery process, where in pure CO_2 was injected into the core at residual oil saturation.

3.5.3.2 Miscible NSDH GAGD Floods

In addition to the scaled NSDH GAGD immiscible coreflood experiments, two NSDH GAGD miscible coreflood experiments using n-Decane, Yates reservoir brine and pure CO_2 were also conducted. The operating conditions of these miscible NSDH GAGD experiments were identical to those of immiscible NSDH GAGD floods, except for the higher operating pressures for miscible injections. The objectives of these scaled NSDH GAGD miscible coreflood experiments were: (i) to evaluate the effect of injection strategy on GAGD recovery characteristics in a miscible mode and (ii) to study the effect of miscibility development on GAGD recovery characteristics. The results of these experiments are summarized in Figures 3.52 and 3.53.

Similar to the data in Figures 3.50 and 3.51, Part (a) of the Figure provides the data for water recovery and pressure drop during the drainage cycle when n-Decane was

injected into the brine saturated core. Secondly, part (b) provides the data for oil recovery and pressure drop when Yates reservoir brine was injected into the core at connate water saturations. Finally, part (c) provides the data for water, and oil recoveries as well as pressure drop during the gravity stable GAGD tertiary recovery process, where in pure CO_2 was injected into the core at residual oil saturation.

3.5.3.3 Comparison of Immiscible and Miscible NSDH GAGD Floods

Similar to the scaled GSDH GAGD floods discussed in Section 5.2.3, there are three major comparisons that can be made from the scaled NSDH GAGD experiments completed till date: (i) effect of injection mode (secondary versus tertiary) on NSDH GAGD immiscible floods, (ii) effect of injection mode (secondary versus tertiary) on NSDH GAGD miscible floods, and (iii) effect of miscibility development (miscible versus immiscible) on NSDH GAGD floods.

Effect of Injection Mode on Immiscible NSDH GAGD Floods

To isolate the effects of injection mode on NSDH immiscible GAGD floods, two immiscible NSDH GAGD floods were conducted in secondary and tertiary injection modes using n-Decane and Yates reservoir brine.

The secondary and tertiary recovery characteristics of immiscible NSDH GAGD floods are included as Figure 3.54. Figure 3.54(a) shows that the NSDH GAGD recovery efficiencies (average incremental recovery: 54.79% ROIP) are significantly higher than horizontal CGI / WAG floods (average incremental recovery: 34.34% ROIP), even under immiscible modes of injection. These observations are consistent with the all gravity stable (GSDH GAGD) floods reported earlier, and that the GAGD mode of injection clearly outperforms the WAG floods.

Also it is important to note that the mode of injection (secondary or tertiary) significantly affects the NSDH GAGD performance under immiscible mode. Tertiary immiscible GAGD flood recovery (47.27%) is significantly lower than the secondary immiscible GAGD flood recovery (62.31%), thus reconfirming the previous inference that the incremental benefits of GAGD process are higher during secondary mode application.

The utilization factors (Figure 3.54(b)) pertaining to secondary floods show high TRF values till 1.4 PVI, followed by a non-exponential decline, suggesting sustained higher gas utilization factors for NSDH GAGD corefloods.

As observed in Figure 3.54(c), the pressure drop behavior tends to reach a plateau, although the approach could be asymptotic, similar to the tertiary GSDH GAGD floods, suggesting high sweep efficiencies during these NSDH GAGD corefloods.

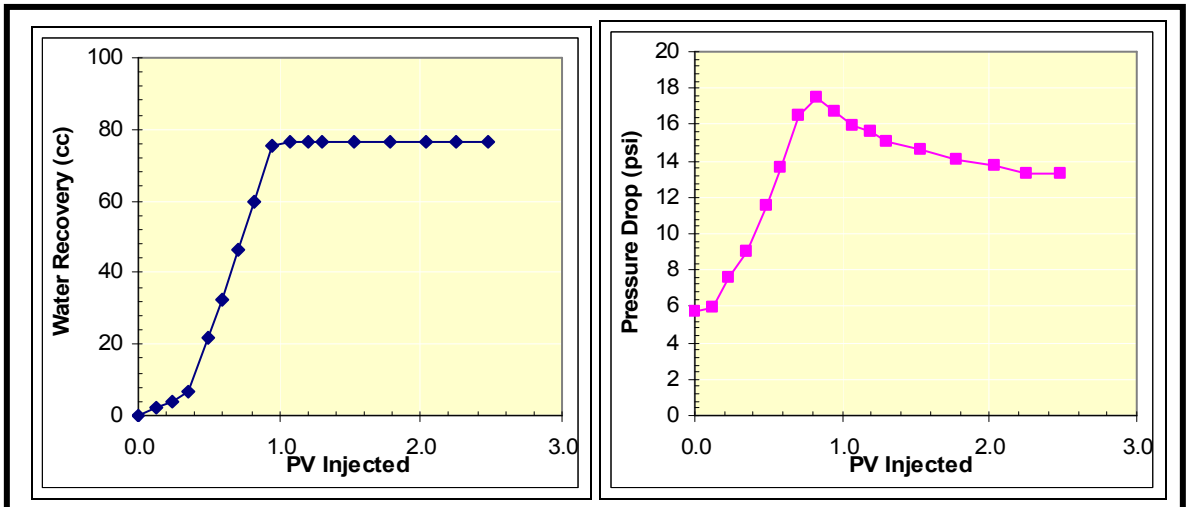

(a) Non-Gravity Stable Drainage Cycle: Oil Flood with n-Decane

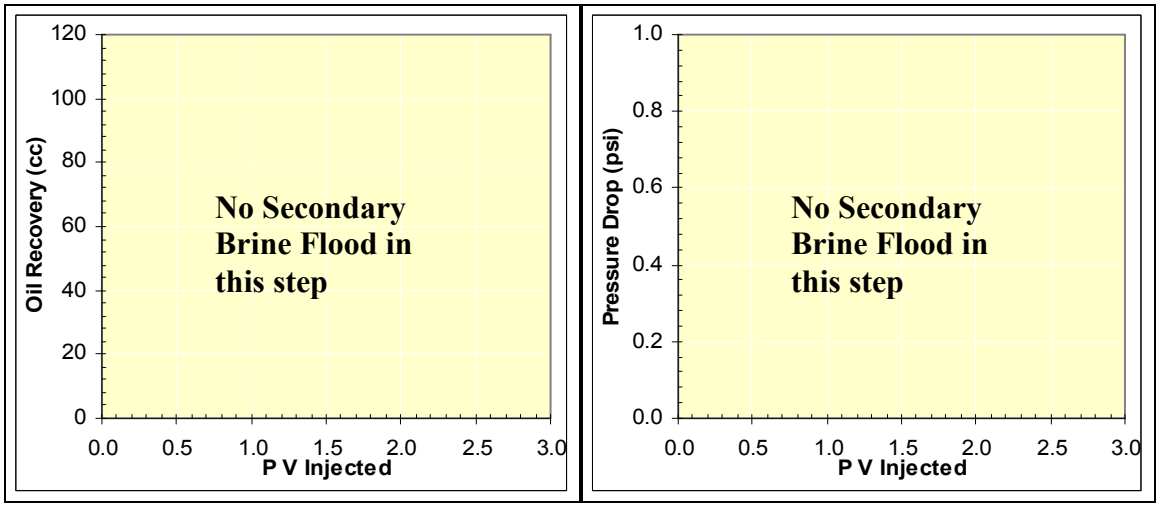

(b) Non-Gravity Stable Imbibition Cycle: Brine Flood with Yates Reservoir Brine

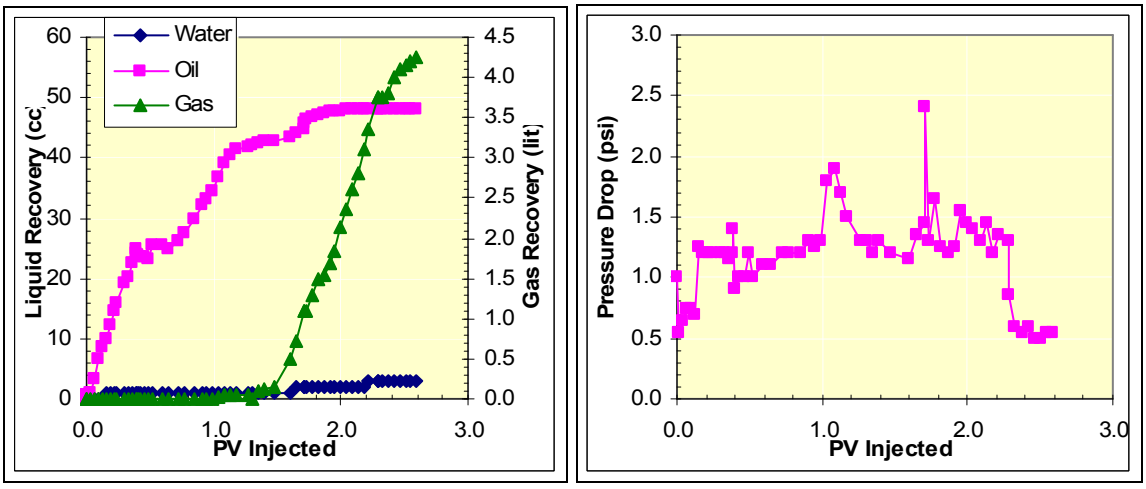

(c) Gravity Stable GAGD Cycle: Gas Flood with Pure CO_2

Figure 3.50: Data for Experiment GAGD NSDH # 1: 1-ft Berea Core + Yates Reservoir Brine with Gravity Stable Immiscible Secondary GAGD CO_2 Injection @ 10 cc/hr

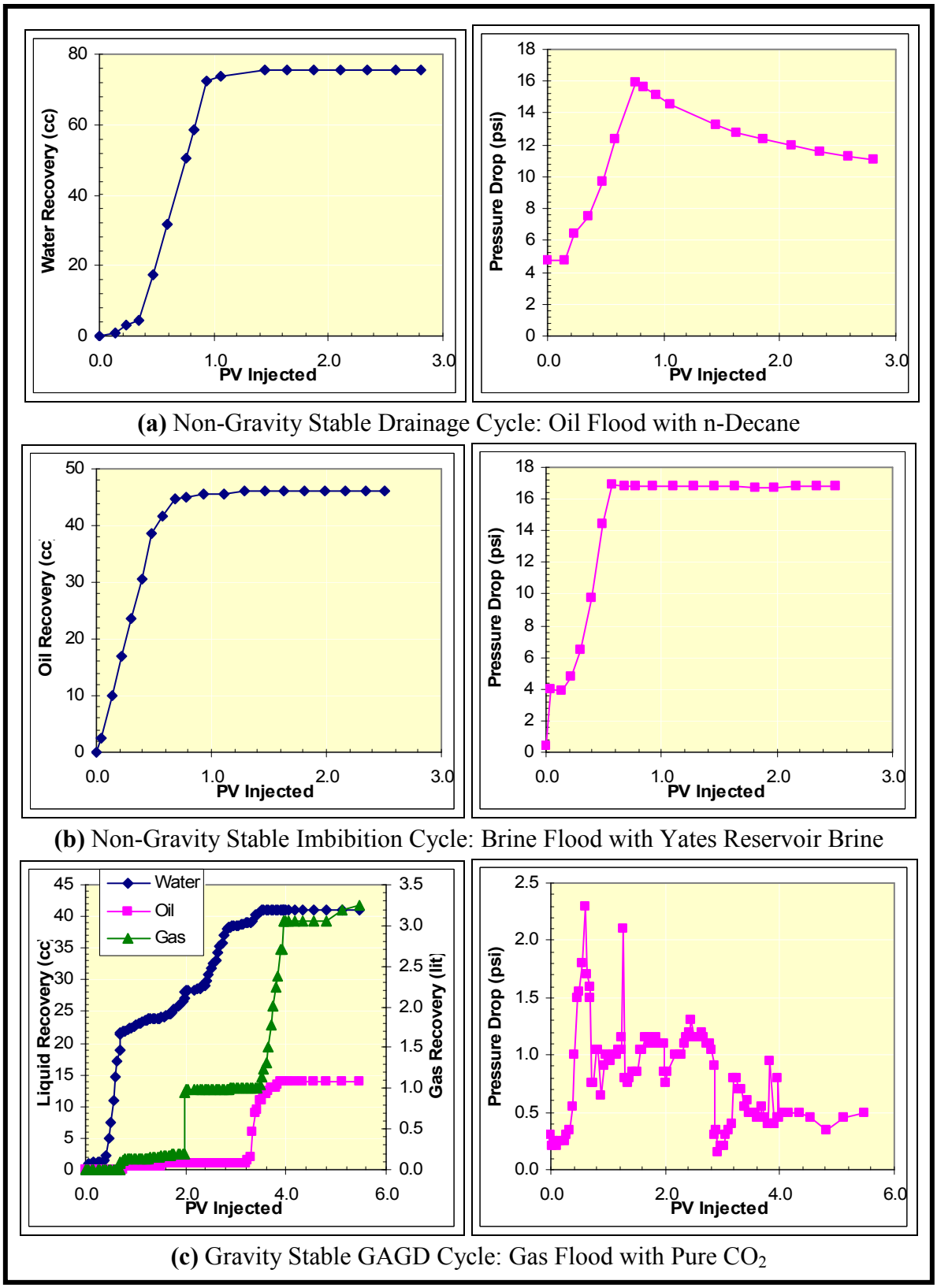

(a) Non-Gravity Stable Drainage Cycle: Oil Flood with n-Decane

(b) Non-Gravity Stable Imbibition Cycle: Brine Flood with Yates Reservoir Brine

(c) Gravity Stable GAGD Cycle: Gas Flood with Pure CO_2

Figure 3.51: Data for Experiment GAGD NSDH # 2: 1-ft Berea Core + Yates Reservoir Brine with Gravity Stable Immiscible Tertiary GAGD CO_2 Injection @ 10 cc/hr

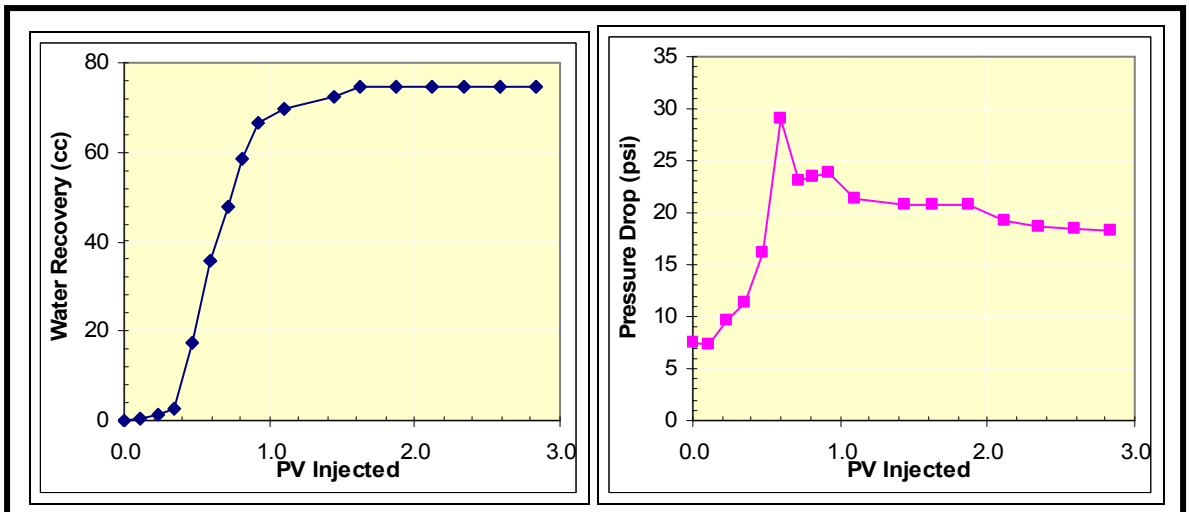

(a) Non-Gravity Stable Drainage Cycle: Oil Flood with n-Decane

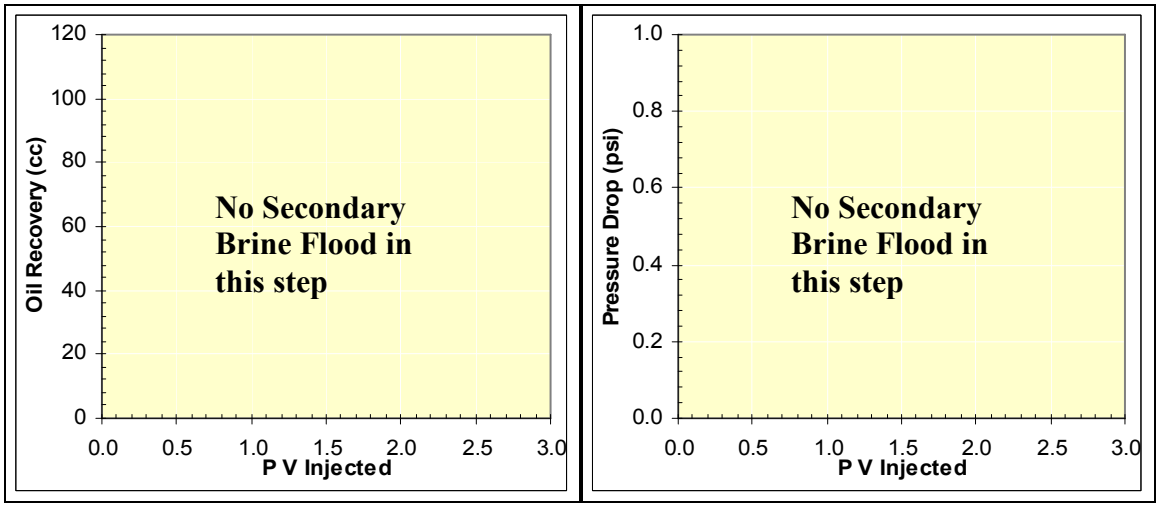

(b) Non-Gravity Stable Imbibition Cycle: Brine Flood with Yates Reservoir Brine

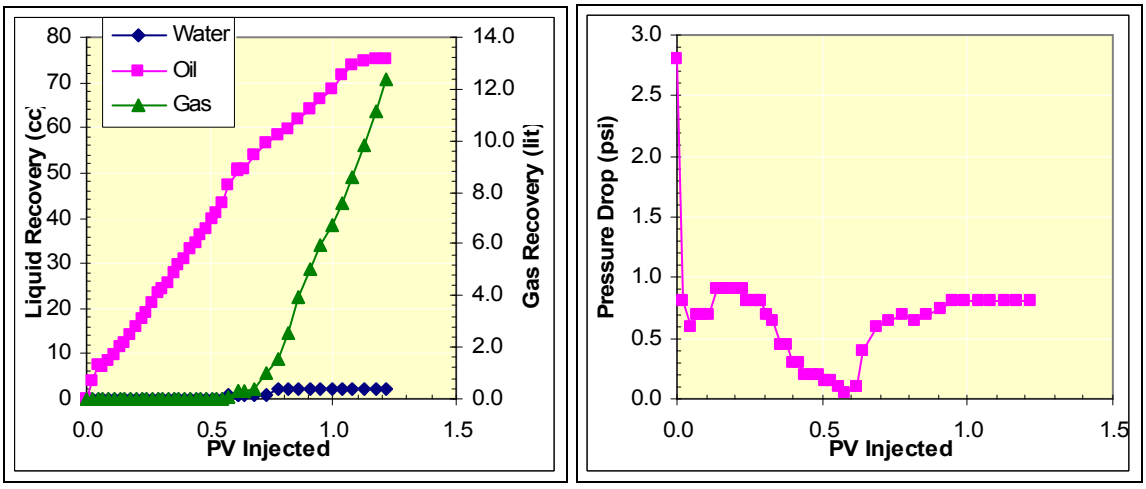

(c) Gravity Stable GAGD Cycle: Gas Flood with Pure CO_2

Figure 3.52: Data for Experiment GAGD NSDH # 3: 1-ft Berea Core + Yates Reservoir Brine with Gravity Stable Miscible Secondary GAGD CO_2 Injection @ 10 cc/hr

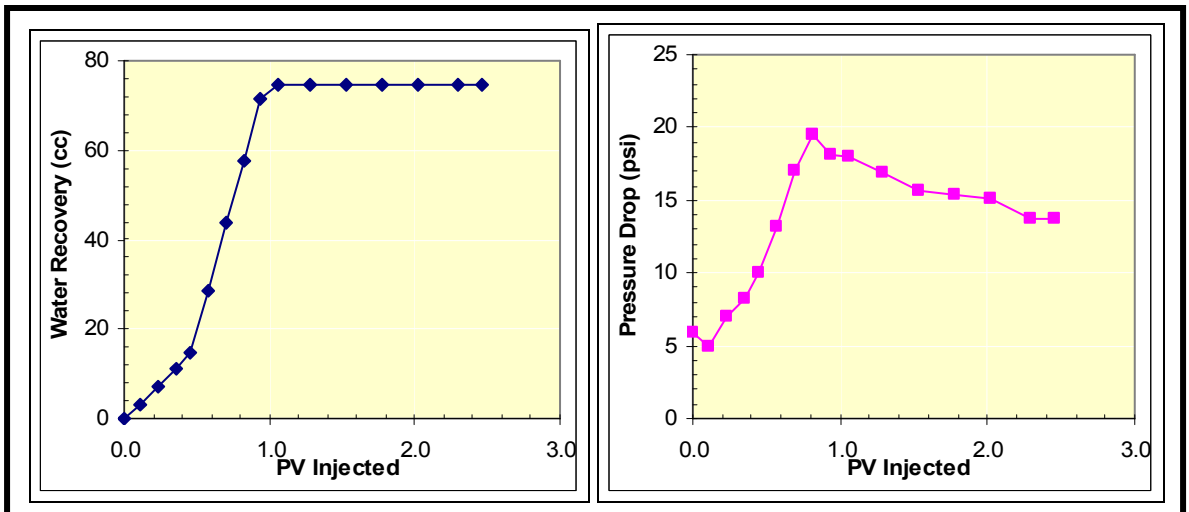

(a) Non-Gravity Stable Drainage Cycle: Oil Flood with n-Decane

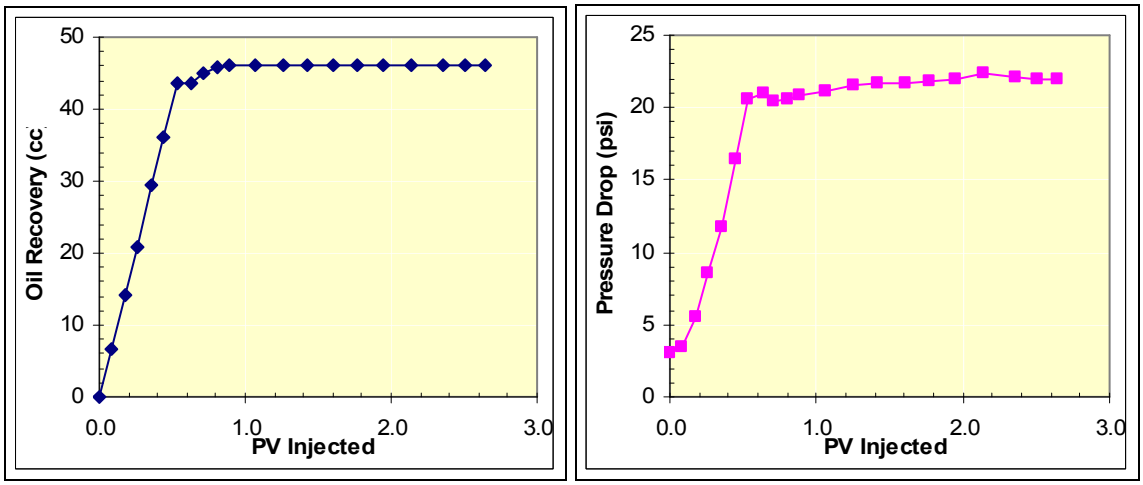

(b) Non-Gravity Stable Imbibition Cycle: Brine Flood with Yates Reservoir Brine

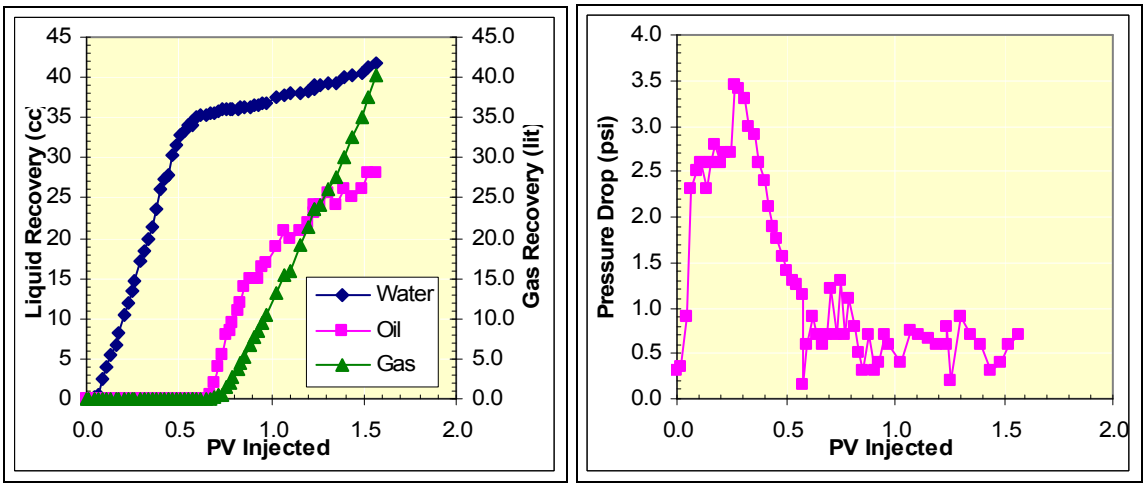

(c) Gravity Stable GAGD Cycle: Gas Flood with Pure CO_2

Figure 3.53: Data for Experiment GAGD NSDH # 4: 1-ft Berea Core + Yates Reservoir Brine with Gravity Stable Miscible Tertiary GAGD CO_2 Injection @ 10 cc/hr

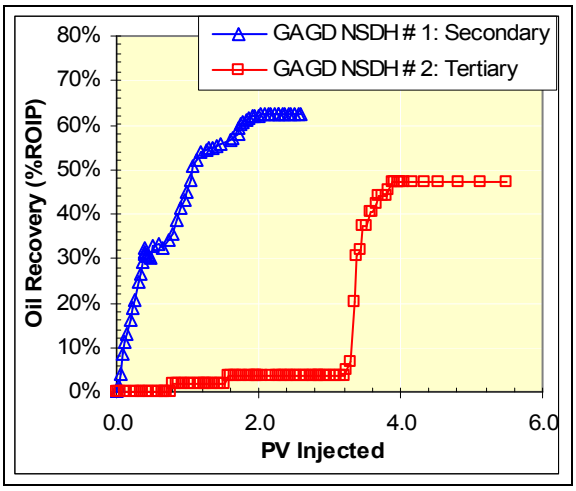

(a) Oil Recovery Characteristics versus PV CO_2 Injection

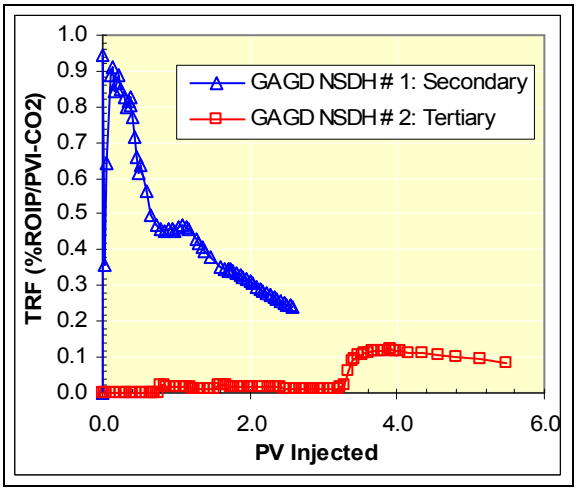

(b) TRF (%ROIP / PVI CO_2) Characteristics versus PV CO_2 Injection

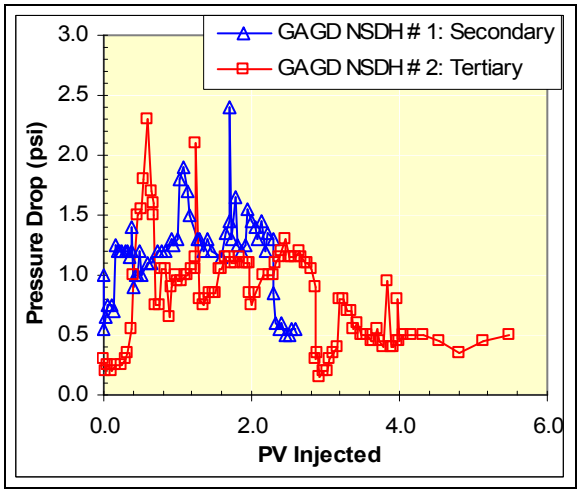

(c) Pressure Drop Characteristics versus PV CO_2 Injection

Figure 3.54: Effect of Injection Mode (Secondary versus Tertiary) on Immiscible NSDH GAGD Floods in n-Decane, Yates Reservoir Brine and Pure CO_2 SystemEffect of Injection Mode on Miscible NSDH GAGD Floods

Similar to the experimental protocol followed during scaled immiscible NSDH GAGD experimentation, the scaled miscible NSDH GAGD floods were also completed in both secondary and tertiary modes using n-Decane and Yates reservoir brine and pure CO_2. The effect of injection mode (secondary versus tertiary) on miscible gravity stable GAGD floods is summarized in Figure 3.55.

Figure 3.55(a) shows that in the miscible NSDH GAGD floods, near perfect sweep efficiencies were obtained, and hence significantly higher oil recoveries were obtained as compared to the CGI or WAG miscible floods. These results are consistent with the all GSDH GAGD floods discussed earlier. As observed in GSDH GAGD floods, except for the delay in oil breakthrough for tertiary floods, the effects of injection mode on miscible NSDH GAGD recovery are also minimal. The average incremental recovery in NGS GAGD floods was close to 100% ROIP, which was found to be significantly higher than the horizontal mode CGI (97.12% ROIP) and WAG (78.52% ROIP) floods.

The NSDH GAGD flood TRF behavior demonstrated superlative gas utilization factors (Figure 3.55(b)), which is observed from the hastened TRF peaks and asymptotic (non-exponential) decrease in TRF values throughout the life of the NSDH GAGD flood.

As observed in immiscible GSDH GAGD floods, the pressure drop behavior, in miscible gravity stable GAGD floods, also tend to reach a plateau, although the approach could be asymptotic in tertiary gravity stable GAGD floods (Figure 3.55(c)), also suggesting high sweep efficiencies during these corefloods.

Effect of Miscibility Development on NSDH GAGD Floods

Comparison of Figures 3.54 and 3.55 clearly demonstrate similar benefits of miscibility development in NSDH GAGD floods, as observed in GSDH GAGD floods. The average incremental oil recovery for miscible NSDH GAGD floods is 100% ROIP while average incremental oil recovery for immiscible NSDH GAGD floods is 54.79% ROIP, thus attributing a clear 45.21% ROIP incremental recovery to miscibility development in the NSDH injection mode. These observations are consistent with the GSDH GAGD floods discussed earlier.

These experimental results are in-line with the oil-industry's inclination towards more efficient commercial miscible gas injection projects (EOR Survey, 2004) in the vertical as well as horizontal gas injection modes. Furthermore, it is important to note that the worst GAGD flood performances are significantly better than the presently used WAG or CGI floods (Table 3.18), thereby making the GAGD process a better alternative to the WAG process even in low pressure and depleted oil reservoirs.

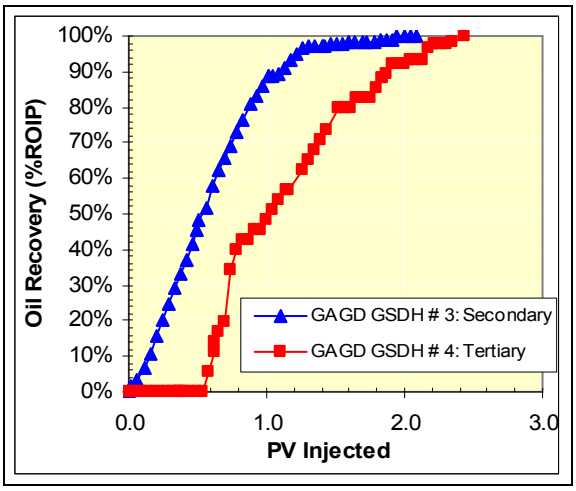

(a) Oil Recovery Characteristics versus PV CO_2 Injection

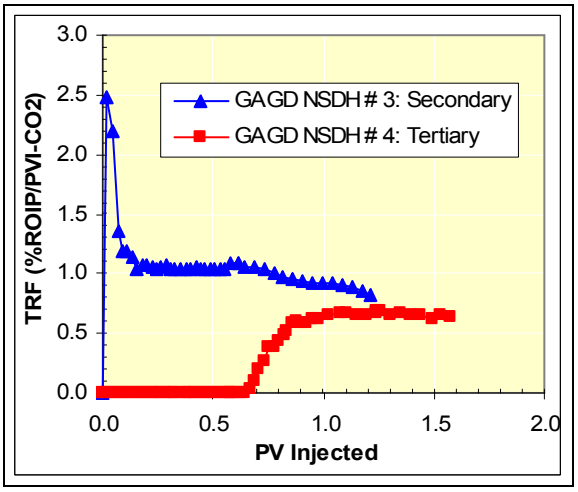

(b) TRF (%ROIP / PVI CO_2) Characteristics versus PV CO_2 Injection

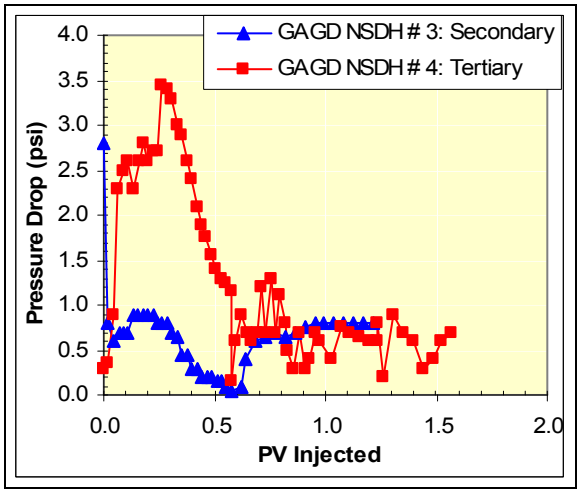

(c) Pressure Drop Characteristics versus PV CO_2 Injection

Figure 3.55: Effect of Injection Mode (Secondary versus Tertiary) on Miscible NSDH GAGD Floods in n-Decane, Yates Reservoir Brine and Pure CO_2 System

3.5.4 Comparison of GSDH and NSDH GAGD Performance

As suggested earlier, the GSDH mode GAGD floods were completed to provide with an upper performance limit of the GAGD floods. The NSDH (or only gas gravity stable) mode GAGD floods were repeated at similar operating conditions, for duplication of the realistic recovery sequences practiced in the oil field. The major comparison parameters between the all gravity stable (GSDH) and NSDH GAGD floods are: (i) Oil recovery characteristics, (ii) TRF behavior, and (iii) pressure drop behavior. Figures 3.56 and 3.57 summarize these comparisons between GSDH and NSDH GAGD floods.

Table 3.18: Comparison between the Best Case Scenarios with CGI, WAG, Hybrid-WAG and GAGD Processes as observed in the Scaled Laboratory Corefloods using n-Decane, Yates Reservoir Brine and Pure CO_2.

Process Description	Type of Flood	Recovery (%ROIP)	PVI Reqd.
Continuous Gas Injection (CGI)	Miscible – Secondary	97.56%	1.69
Water Alternating Gas (WAG)	Miscible – Secondary	72.50%	1.75
Hybrid-WAG	Miscible – Hybrid	93.75%	2.26
All Gravity Stable (GSDH) GAGD (Hypothetical Limiting Scenario)	Secondary or Tertiary (Miscible Flood)	Close to 100%	1.95
Gas Only Gravity Stable (NSDH) GAGD – (Realistic GAGD Application)	Secondary or Tertiary (Miscible Flood)	Close to 100%	1.12

3.5.4.1 Comparison of GSDH and NSDH GAGD Flood Oil Characteristics

The comparison is characterized as miscible and immiscible floods, discussed below.

Immiscible GAGD Floods

Figure 3.56(a) shows that the oil recovery characteristic patterns for the immiscible GAGD floods are similar. However, the NSDH secondary immiscible floods demonstrate hastened oil recoveries as compared to GSDH secondary immiscible floods, attributable to the lower efficiencies of the previous non-gravity stable floods. On the other hand, in case of tertiary floods, although the recovery patterns are similar, the NSDH GAGD floods demonstrate significantly slower oil recovery rates. This decreased rate appears to be due to the higher mobile water saturations in the upper core portions (from previous horizontal waterflood), resulting in higher water-shielding effects and hence decreased oil recovery rates during the tertiary NSDH GAGD floods.

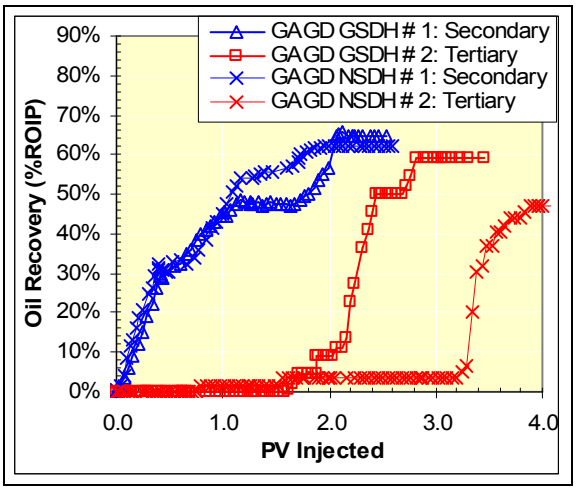

(a) Oil Recovery Characteristics versus PV CO_2 Injection

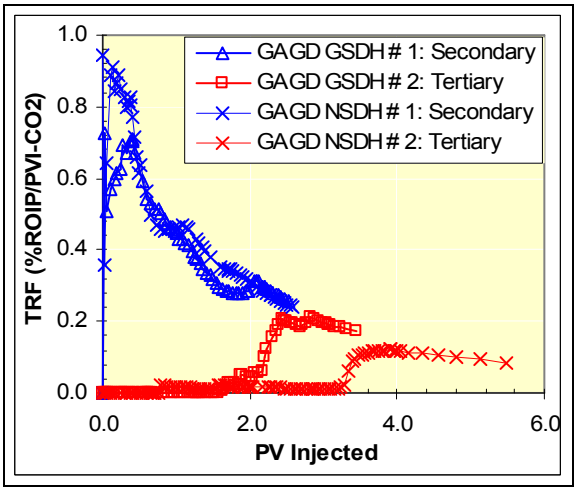

(b) TRF (%ROIP / PVI CO_2) Characteristics versus PV CO_2 Injection

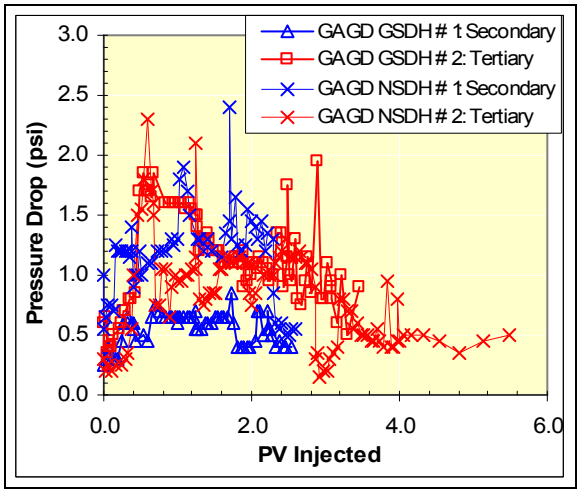

(c) Pressure Drop Characteristics versus PV CO_2 Injection

Figure 3.56: Effect of Injection Mode (Secondary versus Tertiary) on Immiscible GAGD Floods (GSDH and NSDH) in n-Decane, Yates Reservoir Brine and Pure CO_2 System

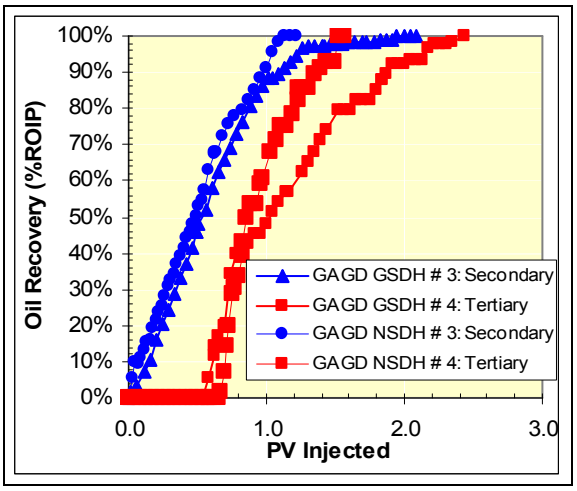

(a) Oil Recovery Characteristics versus PV CO_2 Injection

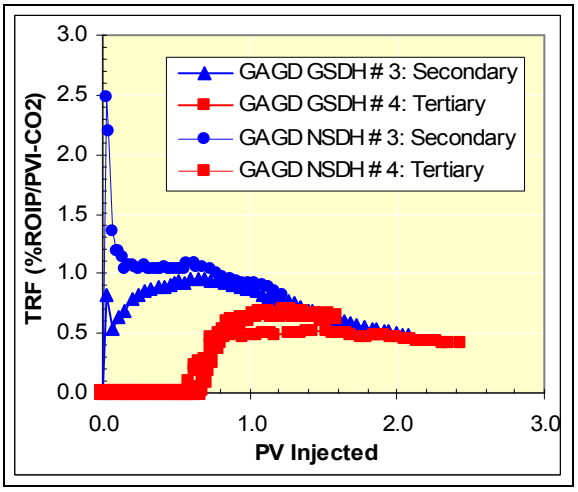

(b) TRF (%ROIP / PVI CO_2) Characteristics versus PV CO_2 Injection

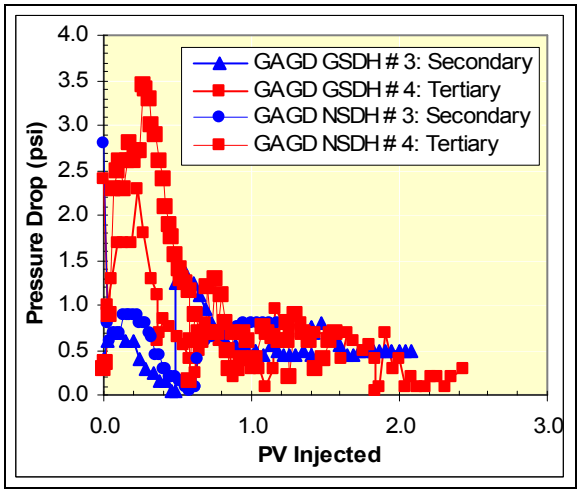

(c) Pressure Drop Characteristics versus PV CO_2 Injection

Figure 3.57: Effect of Injection Mode (Secondary versus Tertiary) on Miscible GAGD Floods (GSDH and NSDH) in n-Decane, Yates Reservoir Brine and Pure CO_2 System

Miscible GAGD Floods

Figure 3.57(a) summarizes the oil recovery characteristics of the miscible GAGD floods completed. The NSDH GAGD floods fare better than the GSDH GAGD floods, recovering 100% of the residual oil in both secondary and tertiary injection modes, compared to 98.89% recoveries in GSDH GAGD floods. The NSDH floods demonstrate hastened recoveries than their GSDH counterparts, affirming that the water-shielding effects, gas (CO_2) solubility effects, and the effect of previous non-gravity stable waterflood (in case of tertiary floods) is significantly lower.

3.5.4.2 Comparison of GSDH and NSDH GAGD Flood TRF Characteristics

Figure 3.56(b) and 3.57(b) summarize the TRF behavior of the immiscible and miscible TRF characteristics of the GAGD floods completed. Similar TRF patterns are observed for both GSDH and NSDH GAGD floods when each corresponding pair of floods is considered. This reconfirms that the mechanistic and dynamic characteristics of these corefloods are similar. It is important to note that, all the NSDH floods, except tertiary immiscible GAGD floods, demonstrate higher TRF values, consequently higher gas utilization efficiencies, as compared to the GSDH GAGD corefloods.

3.5.4.3 Comparison of GSDH and NSDH GAGD Flood Pressure Drop Characteristics

Figure 3.56(c) and 3.57(c) summarize the pressure drop behavior of the immiscible and miscible of the GAGD floods completed. As observed from the TRF characteristics previously, similar pressure drop patterns suggest similar mechanistic and dynamic characteristics of these corefloods.

Higher pressure drops observed in NSDH floods as compared to GSDH floods, for both miscible and immiscible modes of injection, appear to be due to the previous non-gravity stable steps as well as the relatively higher water saturations in the upper-portion of the core during these NSDH GAGD displacements.

3.5.4.4 Preliminary Conclusions from GSDH and NSDH Mode GAGD Corefloods

1. GAGD experimentation (in an all gravity stable as well as only gas gravity stable mode of injection) clearly shows that the GAGD process can potentially outperform all the commercial modes of gas injection, namely CGI, WAG and Hybrid-WAG as demonstrated by scaled laboratory corefloods.
2. Similar patterns obtained for oil recovery, TRF and pressure drop characteristics as observed in both GSDH and NSDH GAGD floods suggest that we are able to duplicate the multiphase mechanisms as well as fluid dynamics operational in the field into the laboratory.

3. Minimal injectivity and operational problems would be encountered during the GAGD process applications, as observed from pressure drop characteristics of GAGD floods completed.
4. GAGD application in secondary mode is beneficial from a recovery as well as gas utilization point of view.
5. Although miscibility development is beneficial in some cases, immiscible GAGD employment could generate comparable oil recovery characteristics. Consequently, miscibility development may not be a controlling economic decision for the application of the GAGD process, especially under secondary injection modes.
6. Both miscible and immiscible GAGD processes demonstrate excellent recovery characteristics.

3.5.5 Evaluation of Various Modes of Gas Injection with GSDH GAGD Performance (on 6-ft Berea, n-Decane, 5% NaCl Brine and CO_2)

The immiscible gas assisted gravity drainage (GAGD) flood was conducted in a 6-ft Berea core using 5% NaCl brine and n-Decane. Initially floods with long cores have been conducted with n-Decane, 5% NaCl brine prior to exposing the cores to crude oils. Immiscible CGI and WAG floods were conducted at similar conditions for comparison with GAGD floods. Results of these floods are included as Figure 3.58. Figure 3.58 shows amplification of the difference in the recoveries between CGI and WAG, which were not obvious in 1-ft immiscible corefloods. This shows that gravity segregation would be more pronounced in the longer cores; hence long core tests are not only appropriate and useful but also essential for performance assessment of floods involving gravity segregation effects. Figure 3.58 shows that the GAGD process has the highest recovery efficiency compared to WAG and CGI. The GAGD process produces nearly 8.6% higher tertiary EOR oil than WAG and 31.3% over CGI even in the immiscible mode.

3.5.6 NSDH Mode GAGD Experimentation on Real Reservoir Systems (On Yates Reservoir Core, Yates Reservoir Fluids and CO_2)

Antecedently, all the scaled laboratory experimentation was limited to using model fluid systems and porous media for the performance evaluation of the GAGD process. To include realistic reservoir systems into the GAGD process evaluation(s), scaled GAGD corefloods were conducted using Yates reservoir rock-fluid systems at reservoir conditions. The GAGD experiments (two miscible and two immiscible) completed using Yates reservoir cores (Figure 3.59), Yates reservoir fluids and CO_2 are:

1. Immiscible NSDH secondary GAGD Yates flood using Yates reservoir core, Yates crude oil, Yates reservoir brine and CO_2.

2. Immiscible NSDH tertiary GAGD Yates flood using Yates reservoir core, Yates crude oil, Yates reservoir brine and CO_2.
3. Miscible NSDH secondary GAGD Yates flood using Yates reservoir core, Yates crude oil, Yates reservoir brine and CO_2.
4. Miscible NSDH tertiary GAGD Yates flood using Yates reservoir core, Yates crude oil, Yates reservoir brine and CO_2.

For these four NSDH GAGD experiments, the oil (Yates crude oil) flood as well as the water (Yates reservoir brine) flood (only in tertiary mode gas floods) was conducted in a non-gravity stable (horizontal) mode. The oil flood was completed by injecting Yates crude oil into a previously brine saturated core mounted horizontally. The brine flood was also completed in a similar manner by mounting the core horizontally. The core was then positioned vertically and allowed to attain reach equilibrium of fluids distribution over 24 hours. Pure CO_2 was injected into this core (at 20 cc/hr) from the top in a gravity stable manner to duplicate actual GAGD implementation in the field.

3.5.6.1 Immiscible NSDH GAGD Yates Floods

The experimental objectives of the two immiscible NSDH GAGD Yates corefloods (Figures 3.60 and 3.61) were: (i) to evaluate the effect of injection strategy on GAGD recovery characteristics in an immiscible mode, (ii) to study the effect of the previous non-gravity stable waterflood (in tertiary mode floods only) on GAGD recovery characteristics in an immiscible mode, (iii) to study the effects of rock mineralogy (dolomite versus Berea sandstone) on GAGD recovery characteristics in an immiscible mode, and (iv) to characterize and identify the positive or negative effects of natural fractures (Yates cores are naturally fractured) on immiscible GAGD flood performance.

3.5.6.2 Miscible NSDH GAGD Yates Floods

Two NSDH GAGD miscible coreflood experiments with Yates reservoir core, Yates crude oil, Yates reservoir brine and pure CO_2 were also completed for the GAGD process performance evaluation on real reservoir systems. The operating conditions of these experiments were identical to those of immiscible NSDH GAGD Yates floods except for the higher operating pressures in miscible NSDH GAGD Yates floods. The experimental objectives of the two miscible NSDH GAGD Yates corefloods (Figures 3.62 and 3.63) were: (i) to evaluate the effect of injection strategy on GAGD recovery characteristics in a miscible mode, (ii) to study the effect of miscibility on GAGD recovery characteristics, (iii) to study the effect of the previous non-gravity stable waterflood (in tertiary mode floods only) on GAGD recovery characteristics in miscible mode, (iv) to study the effects of rock mineralogy (dolomite versus Berea sandstone) on GAGD recovery characteristics in miscible mode, and (iv) to characterize and identify the positive or negative effects of

natural fractures (Yates cores are naturally fractured) on miscible GAGD flood performance.

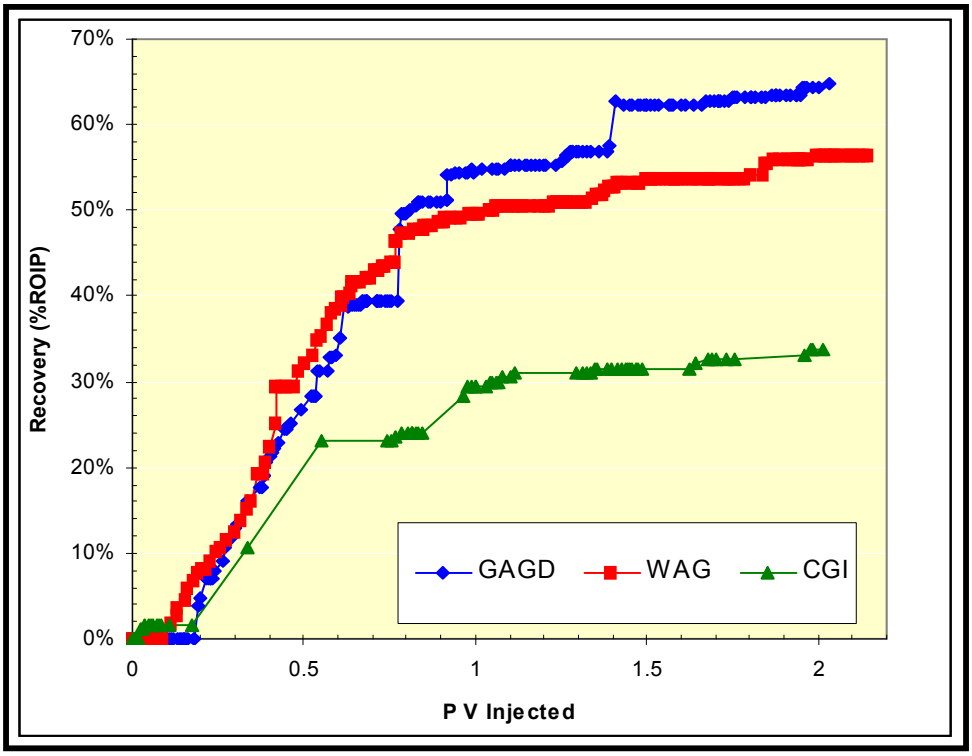

Figure 3.58: Comparison of GAGD floods with WAG and CGI in Immiscible Mode in 6-ft Long Berea Cores with n-Decane, 5% NaCl Brine with Gravity Stable Immiscible GAGD CO_2 Injection @ 10 cc/hr

5.6.3 Comparison of Model and Realistic Fluid NSDH GAGD Floods

The important inferences obtained by performance evaluation of the previously completed GAGD floods on Berea corefloods using model fluid systems and GAGD floods using real reservoir fluid systems are summarized:

1. GAGD experimentation (in all gravity stable as well as gas only gravity stable mode of injection) clearly shows that the superlative GAGD process performance is consistent in both model fluid systems as well as real reservoir fluid systems (Table 3.19). These results further underscore the benefits of working in tune with nature by employing the GAGD process for improved oil recovery.
2. It is interesting to note that the miscible GAGD flood performance is comparable in both model and real reservoir fluid systems. This re-confirms the previous inference that we are able to duplicate multiphase mechanisms and fluid dynamics using dimensional analysis in a consistent manner.
3. In immiscible GAGD floods, the gas utilization factor (TRF) in Yates immiscible GAGD corefloods is significantly lower compared to model fluid GAGD

experiments. This effect was not observed in miscible corefloods. The incremental gas requirements are mainly attributable to: (i) changes in the rock mineralogy, (ii) presence of natural fractures in the core, resulting in higher gas requirements to facilitate fracture-matrix mass transfer, (iii) significant difference in the wettability characteristics of the Yates reservoir core compared to Berea sandstone, and (iv) severe water-shielding and CO_2 solubility effects in tertiary mode Yates GAGD corefloods.

4. GAGD application in secondary mode not only hastens oil recovery, but also is beneficial from an overall recovery and gas utilization point of view (Figures 64 and 65).

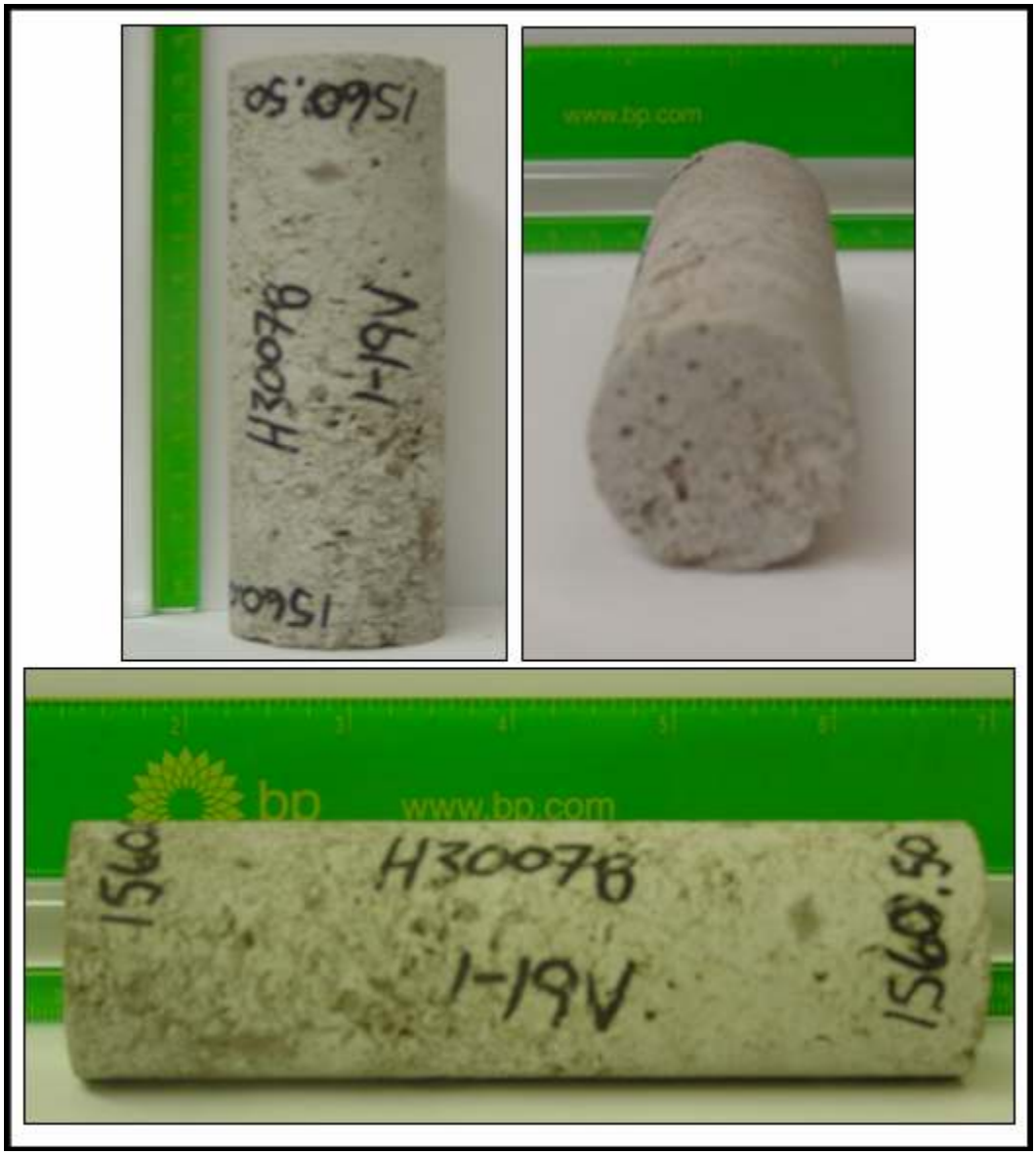

Figure 3.59: Various Views of the Actual Yates Reservoir Core Used for the Scaled NSDH GAGD Yates Experimentation Depicting the Natural Fractures and Heterogeneity

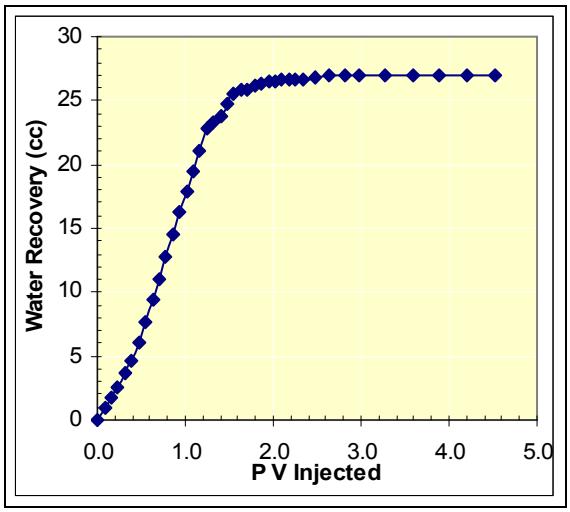

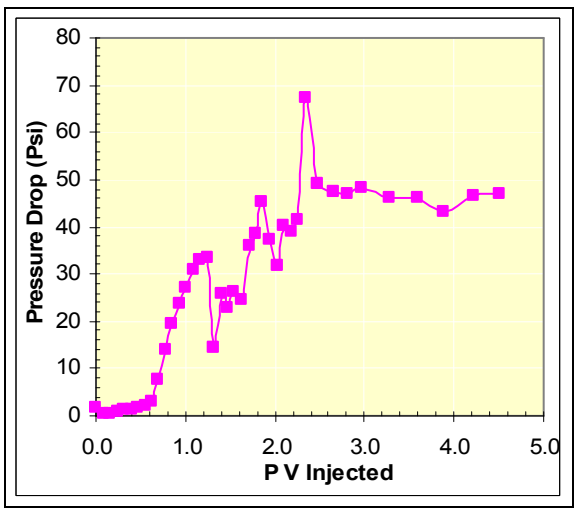

(a) Non-Gravity Stable Drainage Cycle: Oil Flood with Yates Crude Oil

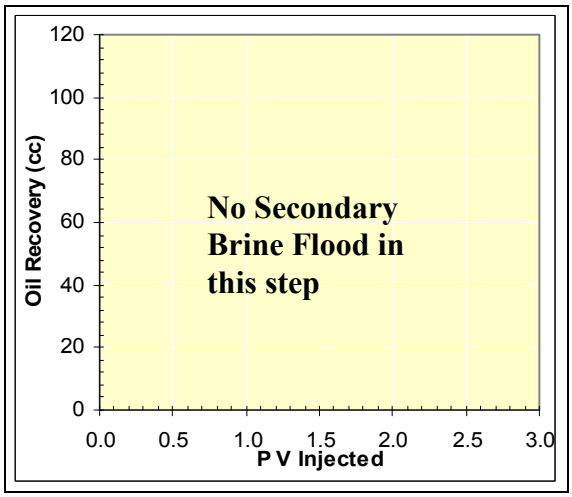

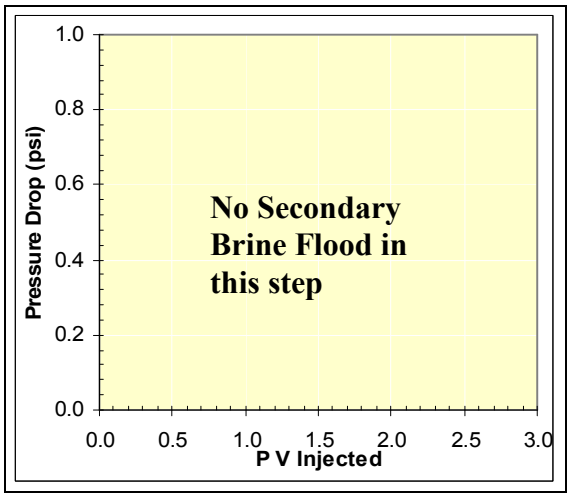

(b) Non-Gravity Stable Imbibition Cycle: Brine Flood with Yates Reservoir Brine

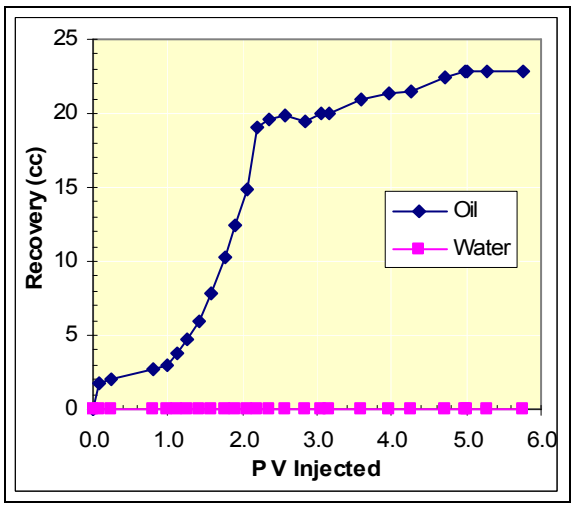

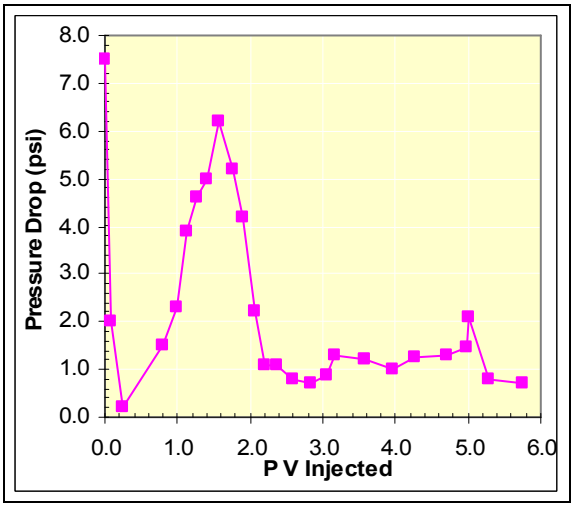

(c) Gravity Stable GAGD Cycle: Gas Flood with Pure CO_2

Figure 3.60: Data for Experiment GAGD Yates # 1: Yates Reservoir Rock-Fluid System with Gravity Stable Immiscible Secondary GAGD CO_2 Injection @ 20 cc/hr

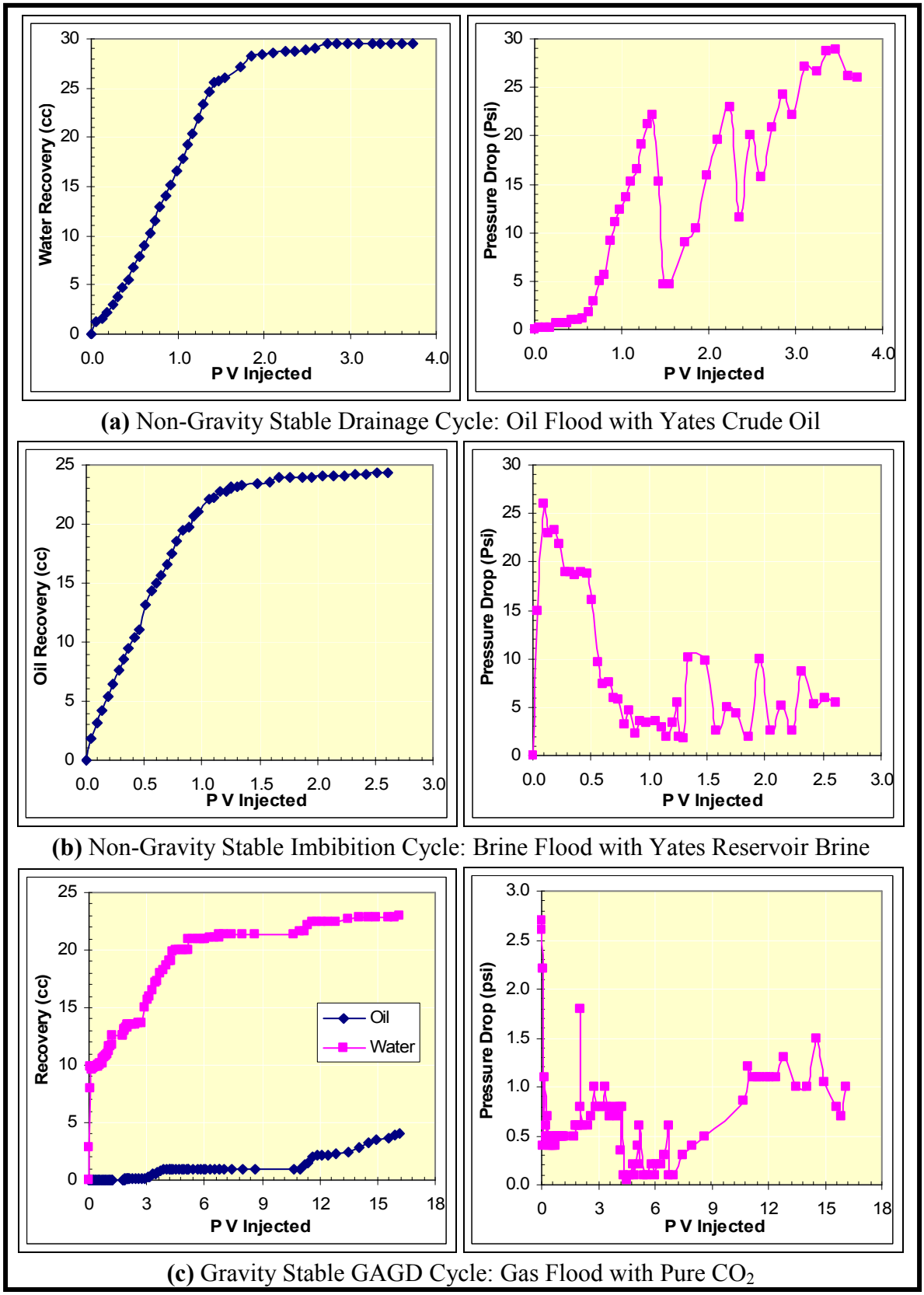

Figure 3.61: Data for Experiment GAGD Yates # 2: Yates Reservoir Rock-Fluid System with Gravity Stable Immiscible Tertiary GAGD CO_2 Injection @ 20 cc/hr

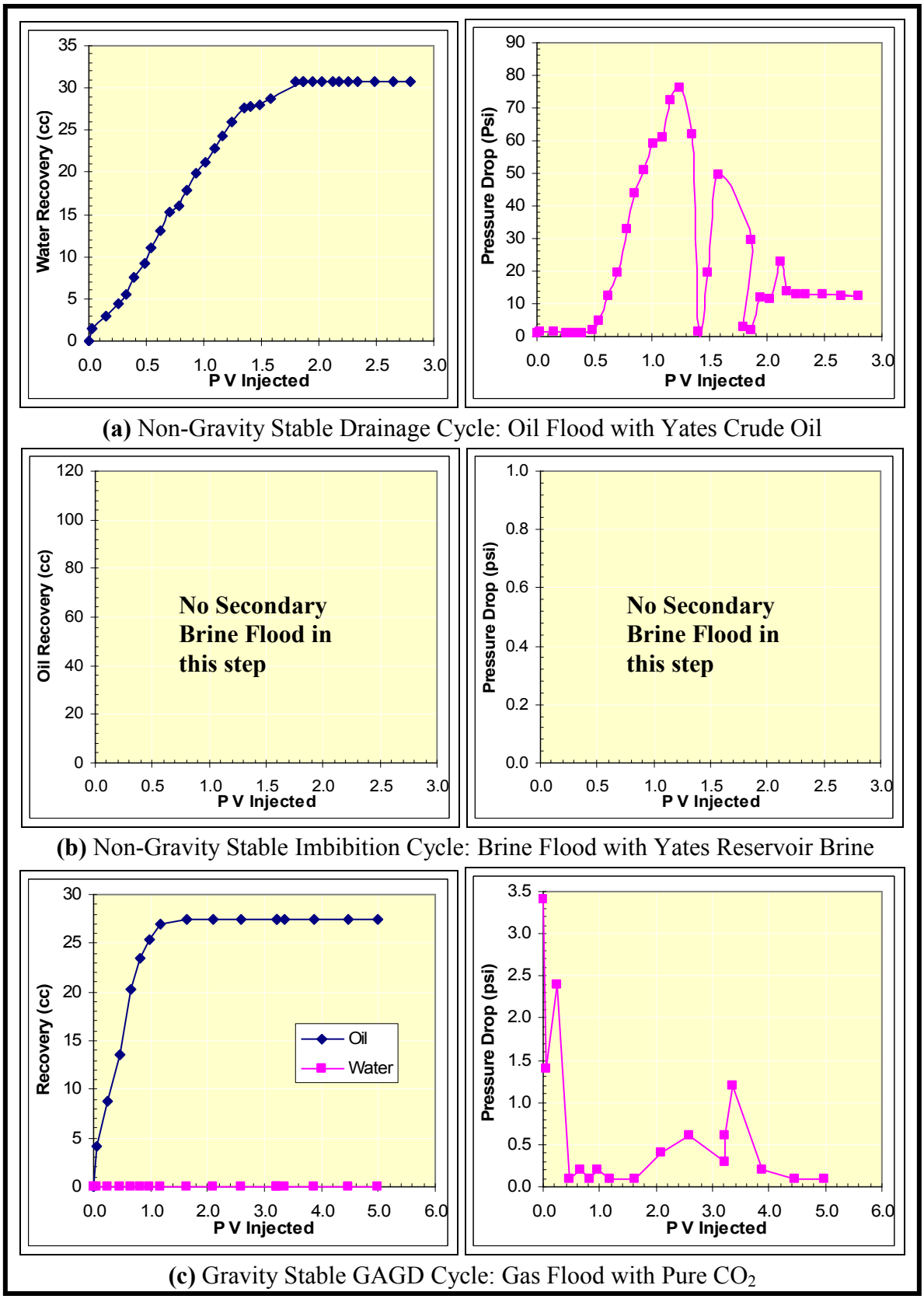

Figure 3.62: Data for Experiment GAGD Yates # 3: Yates Reservoir Rock-Fluid System with Gravity Stable Miscible Secondary GAGD CO_2 Injection @ 20 cc/hr

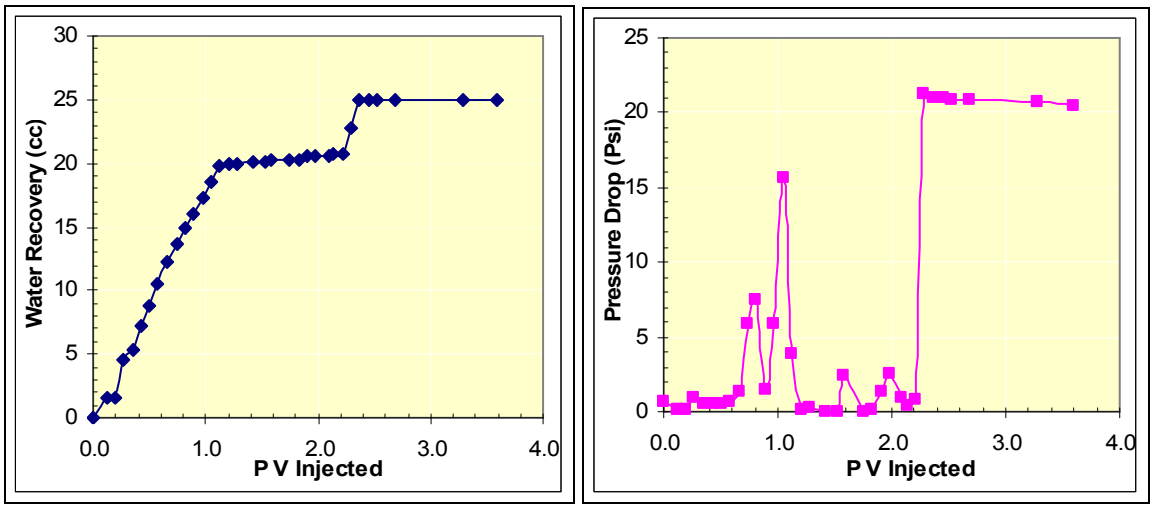

(a) Non-Gravity Stable Drainage Cycle: Oil Flood with Yates Crude Oil

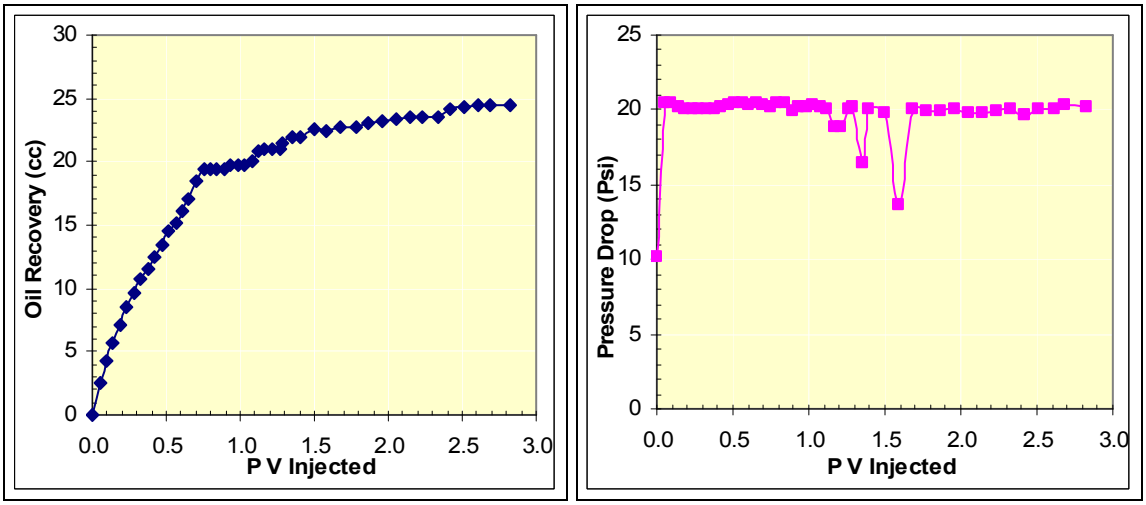

(b) Non-Gravity Stable Imbibition Cycle: Brine Flood with Yates Reservoir Brine

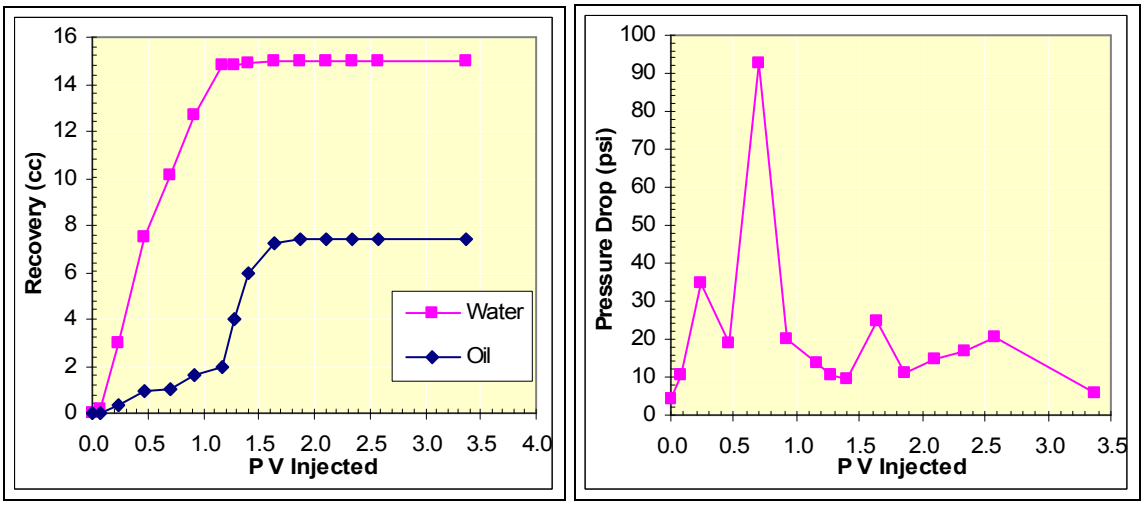

(c) Gravity Stable GAGD Cycle: Gas Flood with Pure CO_2

Figure 3.63: Data for Experiment GAGD Yates # 4: Yates Reservoir Rock-Fluid System with Gravity Stable Miscible Tertiary GAGD CO_2 Injection @ 20 cc/hr

Table 3.19: Performance Evaluation of the NSDH GAGD Floods in Model Fluid Systems and Real Reservoir Systems as observed in the Scaled Laboratory Corefloods using Pure CO_2 as Injectant

Process Description	Type of Flood	Recovery (%ROIP)	PVI Required.
Immiscible NSDH GAGD floods using model fluid systems	Secondary	62.31%	2.59
	Tertiary	47.27%	3.99
Miscible NSDH GAGD floods using model fluid systems	Secondary	~ 100%	1.27
	Tertiary	~ 100%	1.53
Immiscible NSDH GAGD floods using Yates reservoir fluid systems	Secondary	85.13%	4.985
	Tertiary	78.85%	16.124
Miscible NSDH GAGD floods using Yates reservoir fluid systems	Secondary	~ 100%	1.636
	Tertiary	~ 100%	2.105

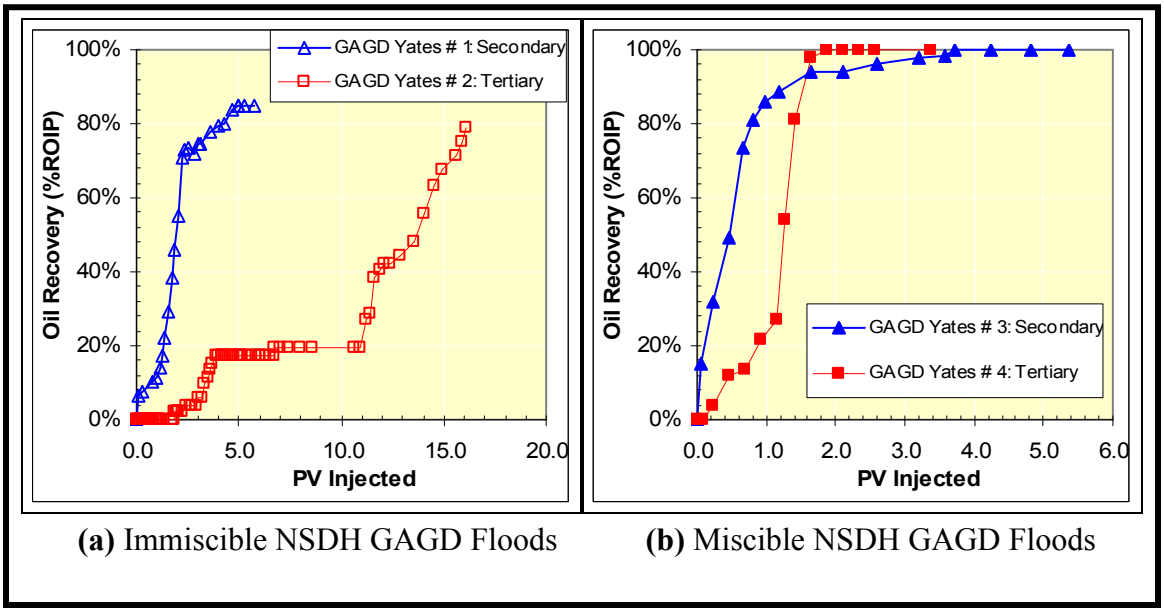

(a) Immiscible NSDH GAGD Floods **(b)** Miscible NSDH GAGD Floods

Figure 3.64: Comparison of Oil Recovery Characteristics between Immiscible and Miscible Gas Only Gravity Stable (NSDH) GAGD Yates Floods using Yates Reservoir Core, Yates crude oil, Yates reservoir brine and CO_2.

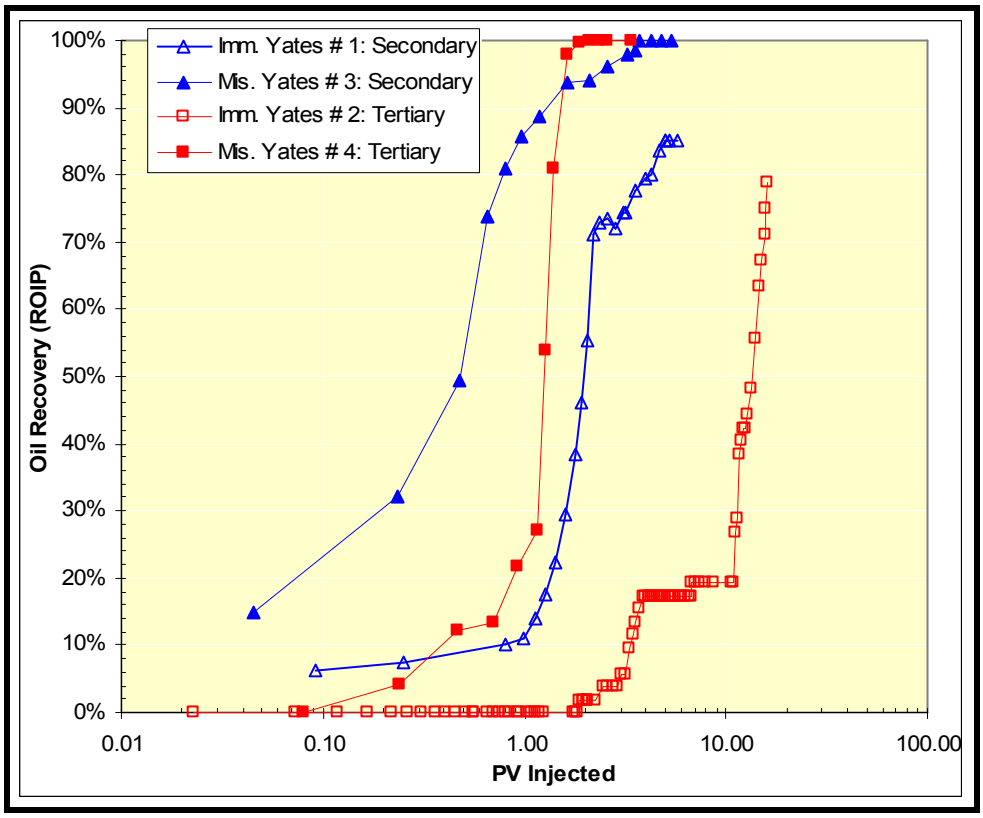

Figure 3.65: Comparison of Oil Recovery Characteristics between all NSDH GAGD Yates Floods using Real Reservoir Fluid Systems.

3.5.7 Effect of Reservoir (Core) Heterogeneity on GAGD Corefloods

During various presentations of this research work, many researchers have questioned the applicability of the GAGD process in such fractured systems and speculated that the presence of long, highly conductive vertical fractures in the reservoir would have a detrimental effect on the GAGD process performance. To examine the effects of vertical fractures on GAGD, two sets of miscible secondary GSDH GAGD coreflood experiments at similar operating conditions were conducted: one in using un-fractured Berea sandstone core, while the other in same Berea core sliced vertically along the axis.

The secondary mode miscible and immiscible GSDH GAGD corefloods conducted using un-fractured Berea sandstone core (summarized in Section 5.2) provide with the base case scenario for the performance evaluation of the GAGD process in presence of long, highly conductive vertical fractures.

The same Berea core used for the GSDH GAGD experiments was later sliced vertically in the middle and assembled using highly permeable sand (rounded glass beads) filling and Kim-wipes® for capillary contact (Figure 3.66), to generate an end-to-end vertical fracture with a fracture permeability of about 15 Darcy and matrix permeability of about 300 mD. The miscible and immiscible secondary GSDH GAGD

fractured floods (Figure 3.67 and 3.68) were repeated at similar operating conditions, using n-Decane, Yates reservoir brine and CO_2, on this high pressure fractured core assembly.

3.5.7.1 Effect of the Presence of Vertical Fractures on GAGD Performance

The GAGD process performance appears to be relatively insensitive to the detrimental effects of vertical, high permeability fractures. It is interesting to note that, in the immiscible GAGD flood (see Figure 3.69(a)), the presence of vertical fractures seem to 'hasten' the rate of oil recovery! This inference further seems to be supported by the force analysis of the dominant reservoir mechanics (Figure 3.70).

On the other hand, the miscible fractured GAGD flood demonstrated consistent performance when compared to the un-fractured coreflood till gas breakthrough. And although the fractured core system requires higher pore volume gas injection, the similarity in the ultimate oil recoveries (see Figure 3.69(b)), further substantiates the observations of the immiscible fractured corefloods, that the presence of fractures may not be completely detrimental to oil recovery in the GAGD process.

In an ultimate recovery equation, the reservoir properties are constants, whereas the improved recovery process selection is the primary variable. From an oil field and economics perspective, we have little or no control over the reservoir properties. For example, if we have a highly fractured reservoir, the WAG process yields very low oil recoveries. In this case, even the most conservative performance estimates of the GAGD process far out-perform even the highest known WAG recoveries.

3.5.8 Injection Rate Effects on GAGD Performance and Possibility of Regain of Floods' Conformance

One of the critical issues of horizontal mode gas injection projects is the premature gas breakthroughs, either due to reservoir heterogeneities, unfavorable gravity segregation of the injected and reservoir fluids, or very high injection rates resulting in injected gas shooting to the producer without effectively sweeping the reservoir, ultimately leading to an unfortunate and abrupt end of the flood's life. The reservoir heterogeneities particularly detrimental to horizontal injections (including waterfloods) have been identified to be the high permeability streaks or fractures (high permeability reservoir contrasts) between the injection and producing well. The effects of reservoir heterogeneities on GAGD floods were experimentally investigated in Section 5.7. This section details the experimental study conducted to investigate the rate effects on GAGD flood performance as well as to experimentally address the economically important question: Is premature gas breakthrough the end of the gas floods' life?

Literature review on gravity stable gas injection (see Section 3.1.2. and 3.1.3) suggests that to avoid viscous instabilities and improved flood conformance, the gas

injection rates should not exceed a 'critical' injection rate. Although there are many analytical models that could be used for the prediction of this 'critical' injection rate, the significant variations in the predicted rates inculcate doubt about the most relevant and accurate model for gravity stable gas injection applications. One of the possible solutions to this issue is to conduct a series of scaled experiments at various gas injection rates and correlate them to the gas breakthrough times and recoveries.

Figure 3.66: Pictures Showing Sliced Berea Core with Sand Pattie and Kim-wipes® for Capillary Contact (Top) and the final assembled core with a central 15-D perm fracture

Numerical experiments may not be useful to solve this problem, because of the limited correlation models available in simulator. However, the experimental verification of the various models used to characterize the 'critical' gas injection rates for gravity

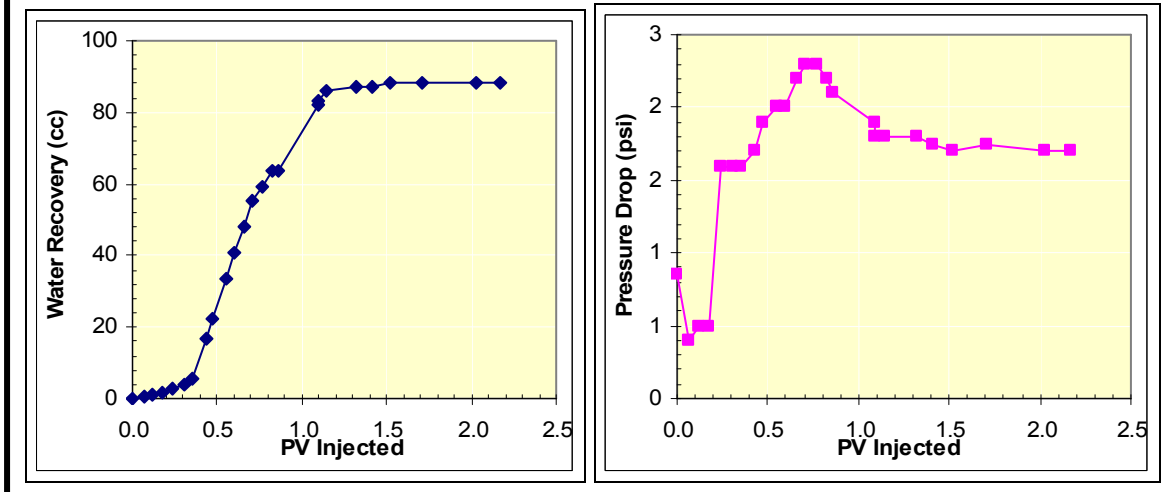

(a) Gravity Stable Drainage Cycle: Oil Flood with n-Decane

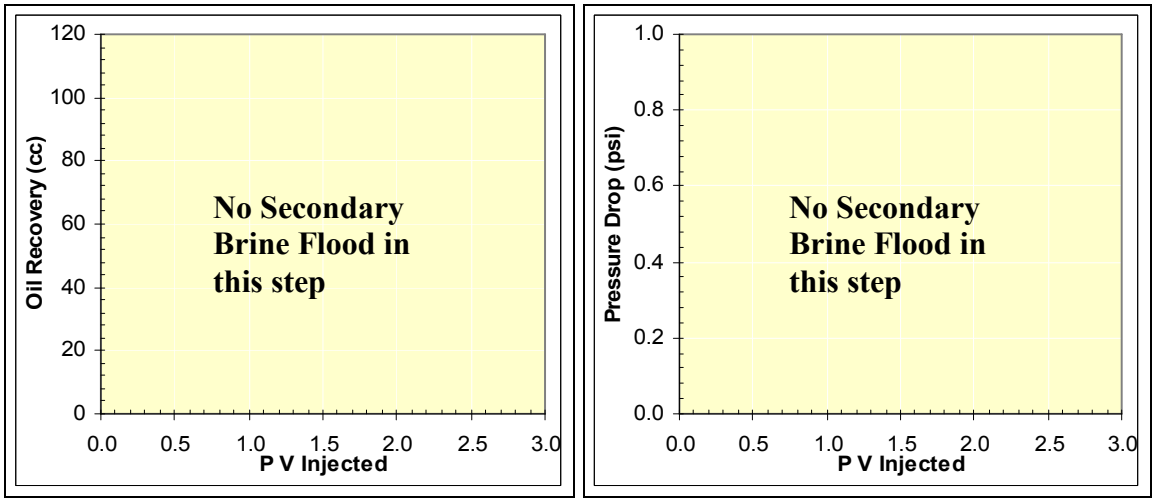

(b) Gravity Stable Imbibition Cycle: Brine Flood with Yates Reservoir Brine

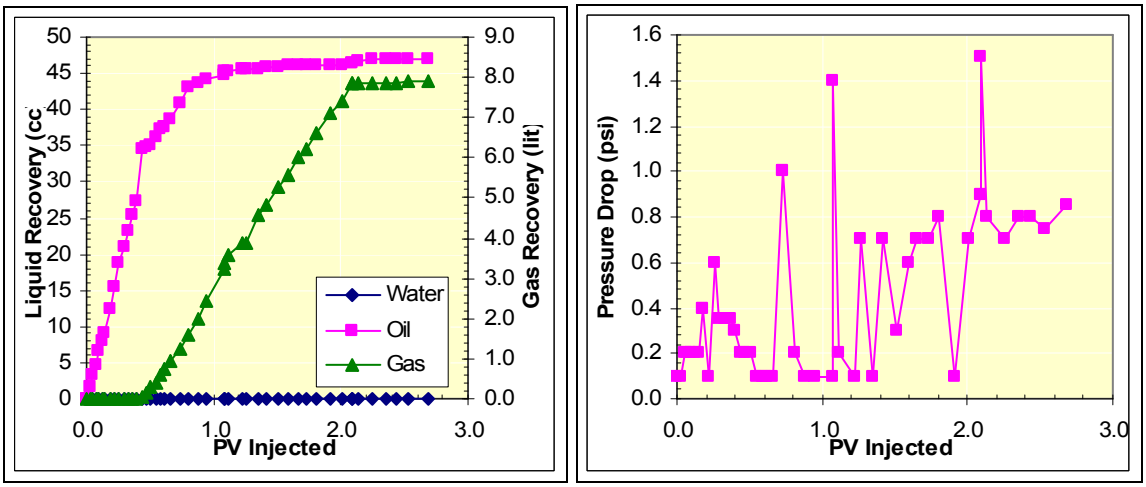

(c) Gravity Stable GAGD Cycle: Gas Flood with Pure CO_2

Figure 3.67: Data for Experiment GAGD Frac # 1: 1-ft Berea Core + Yates Reservoir Brine with Gravity Stable Immiscible Secondary GAGD CO_2 Injection @ 20 cc/hr

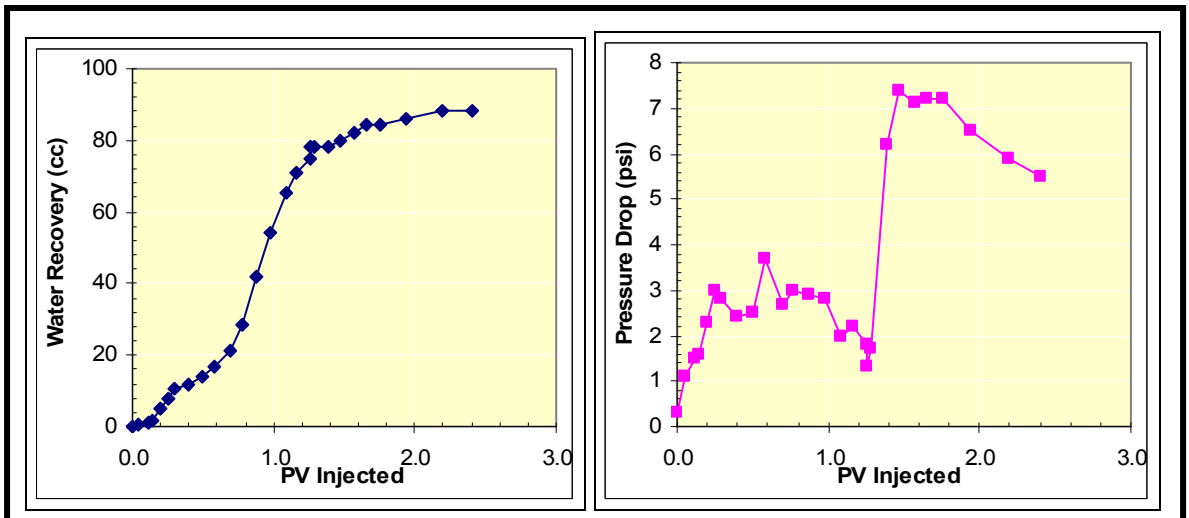

(a) Gravity Stable Drainage Cycle: Oil Flood with n-Decane

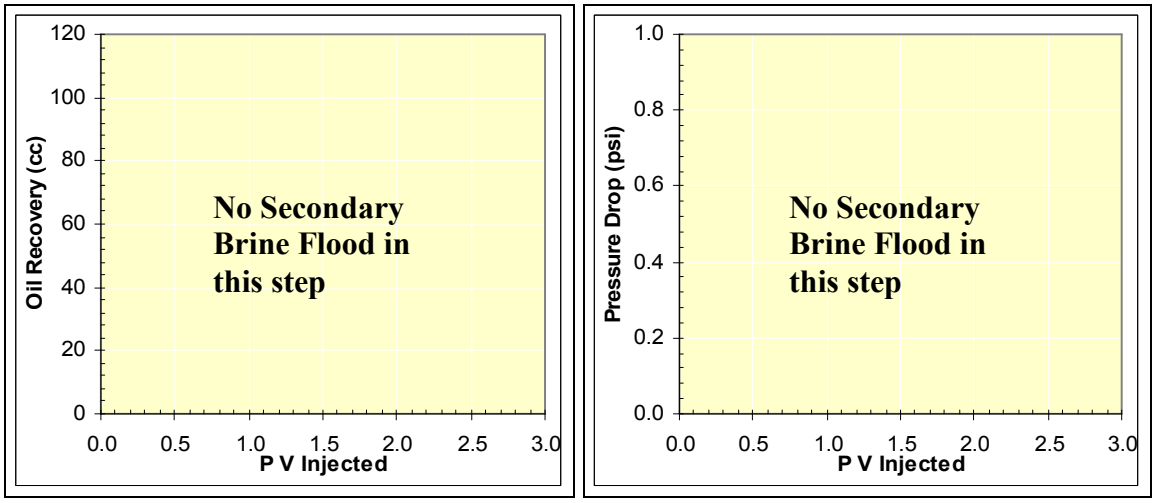

(b) Gravity Stable Imbibition Cycle: Brine Flood with Yates Reservoir Brine

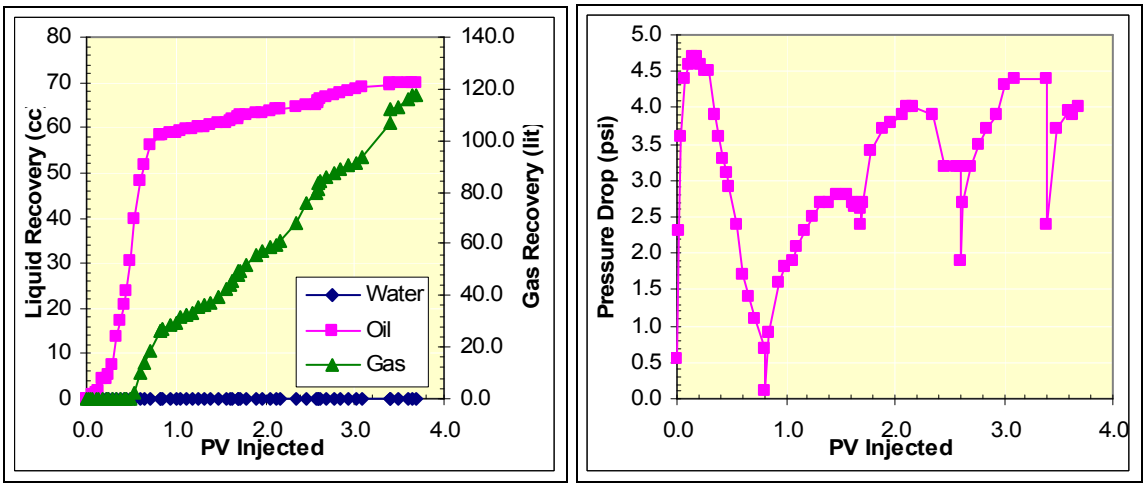

(c) Gravity Stable GAGD Cycle: Gas Flood with Pure CO_2

Figure 3.68: Data for Experiment GAGD Frac # 2: 1-ft Berea Core + Yates Reservoir Brine with Gravity Stable Miscible Secondary GAGD CO_2 Injection @ 20 cc/hr

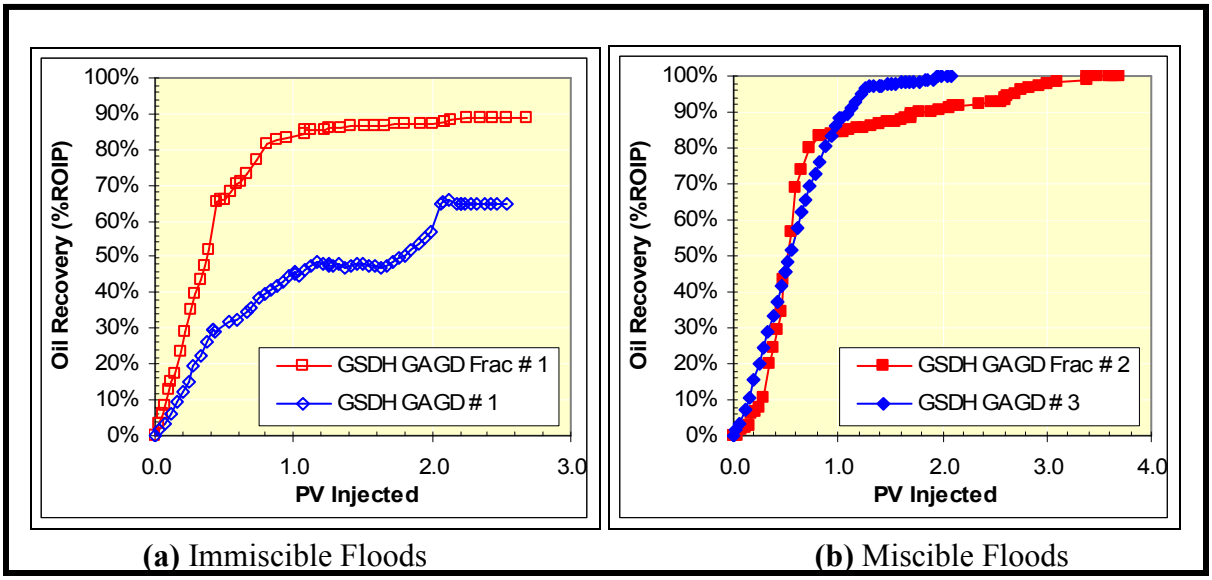

Figure 3.69: Immiscible and Miscible Oil Recovery Characteristic(s) Comparisons for Vertically Fractured and Non-Fractured NSDH GAGD Corefloods on Berea Core with Similar Matrix Heterogeneity

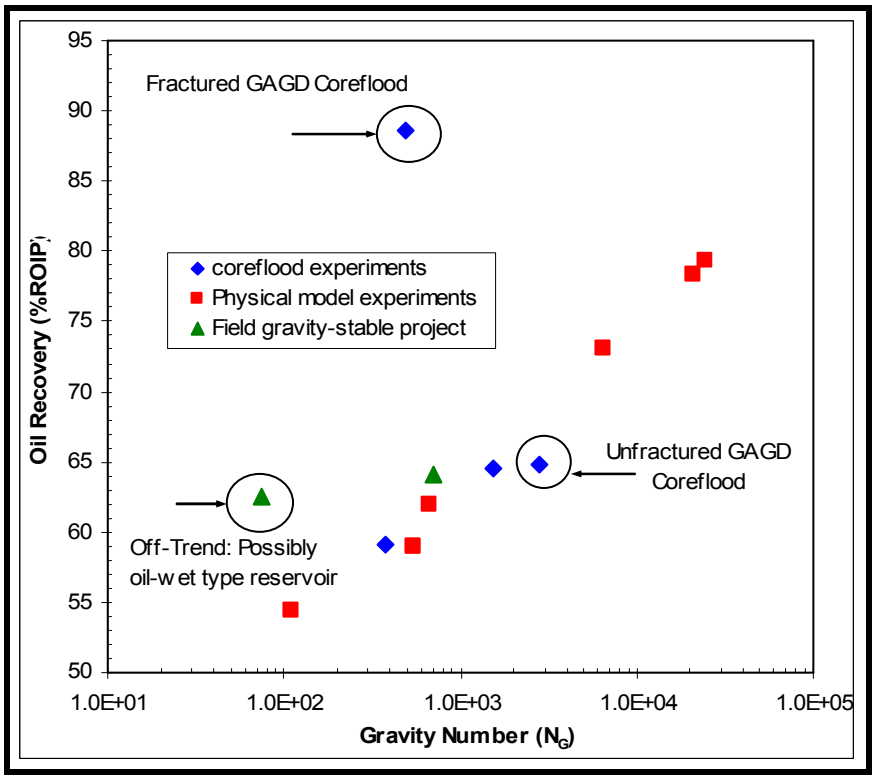

Figure 3.70: Dimensionless Force Analysis of the Dominant Reservoir Mechanics Corroborating the Observed Higher Fractured Core Immiscible GAGD Recoveries

stable gas injection applications is outside the scope of this dissertation. To study the effects of injection rate on flood performance and address the issue of the possibility of renewed flood control, a scaled three-stage secondary immiscible GSDH GAGD

experiment was conducted using n-Decane, Yates reservoir brine and CO_2 on 6-ft Berea sandstone core.

To facilitate ease of comparison, all the flood parameters, excepting gas injection rates, were kept similar to the previously conducted immiscible secondary GSDH GAGD floods. It is important to note that the dimensional scaling of the experiment helps eliminate the core length influences on the flood's performance. The vertically oriented core was brought to initial oil saturation by injecting n-Decane (at 320 cc/hr) from top. The secondary immiscible GSDH GAGD step was divided into three sub-steps: (i) injection of CO_2 at a very high rate (nearly 8 times the calculated critical rate) till gas breakthrough, (ii) stop gas injection and allow the system to come to equilibrium (till core pressure stabilizes or differential pressure gauge reads nearly zero), and finally (iii) gas injection at about 80% of the lowest calculated 'critical' injection rate, till no additional oil is produced. The data from this experiment is included as Figure 3.71.

The oil recovery and TRF data for the GSDH GAGD IRC # 1 Experiment is included in Figure 3.72. A picture of the collection burette, showing the initial premature gas breakthrough time and production has been also included in Figure 3.72, to provide with additional visual proof of the above described phenomenon. Additionally, since the oil recovery and pressure drop data plotted versus pore volume injected (Figure 3.71(c) and 3.72) masks the information about shut-in time(s), phase segregation and the system's pressure behavior, the same data has been plotted on cumulative injection time scale (Figure 3.73).

It is extremely encouraging to see that the premature gas breakthrough (due to very high injection rates) very early in the life of the GAGD flood does not negatively influence the ultimate oil recoveries achievable as well as the fact that the gas bubble developed in the reservoir during GAGD flood is definitely controllable via the rate of injection. Furthermore, this experiment provides a visual / physical proof of the benefits of working in tune with nature and that 'not all is lost' in the GAGD mode of injection after gas breakthrough, as compared to the horizontal mode WAG floods.

3.5.9 Analysis of GAGD Performance

In course of optimization of the GAGD process, various scaled experiments were conducted to isolate and identify the effects of specific parameters on GAGD process performance. To identify the effects of various flood parameters on GAGD ultimate recoveries and the oil production rates; all the GAGD experiments completed were classified as immiscible and miscible and were plotted as Figure 3.74 and 3.75 respectively. Figure 3.74 summarizes all the immiscible GAGD experiments conducted. It can be clearly seen that the secondary GAGD floods demonstrate faster oil recovery rates than their tertiary counterparts. However, the ultimate recoveries for all the immiscible floods can be comparable.

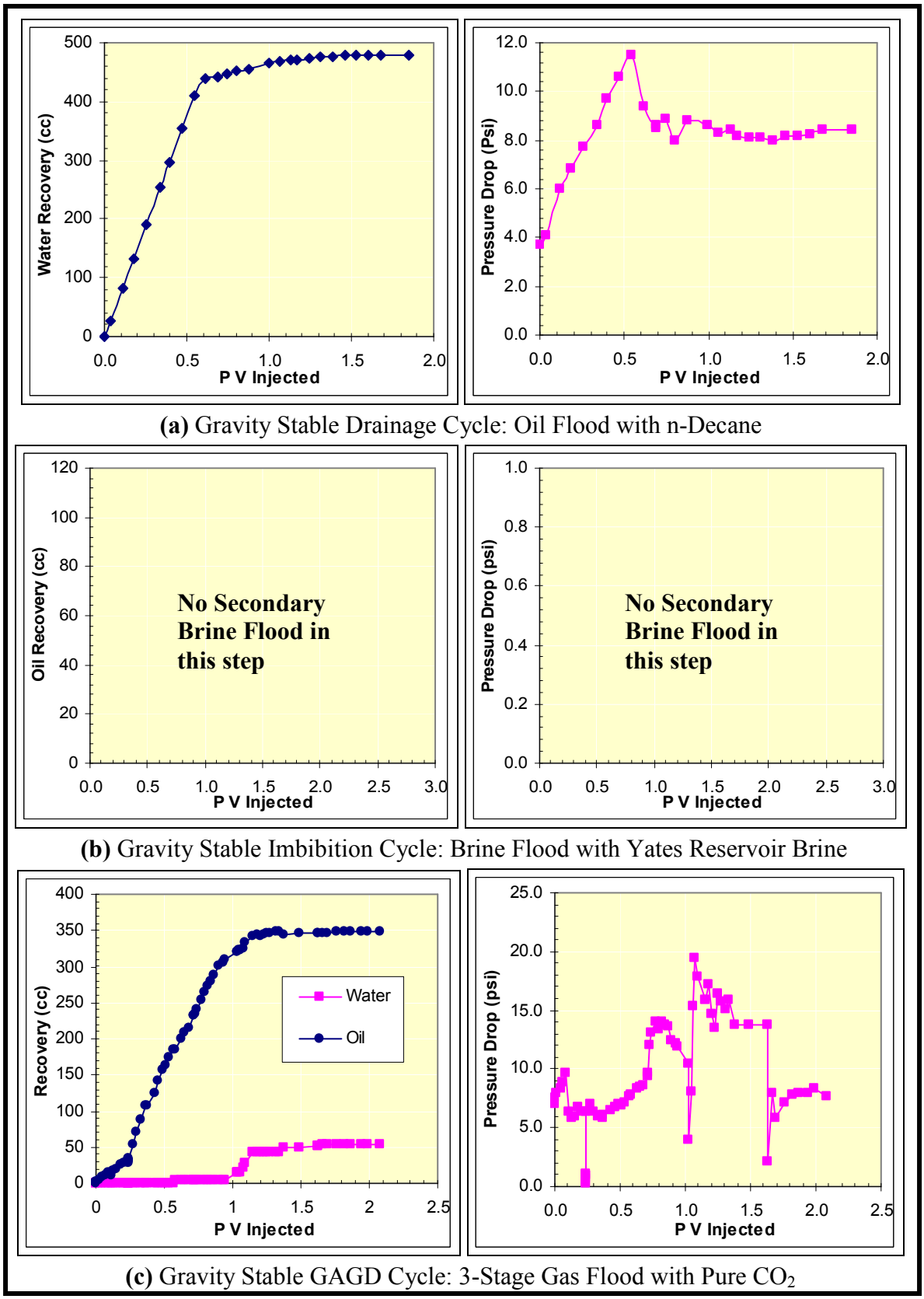

Figure 3.71: Data for Experiment GSDH GAGD IRC # 1: 6-ft Berea Core + Yates Reservoir Brine with Immiscible Secondary GAGD CO_2 Injection @ varied Rate

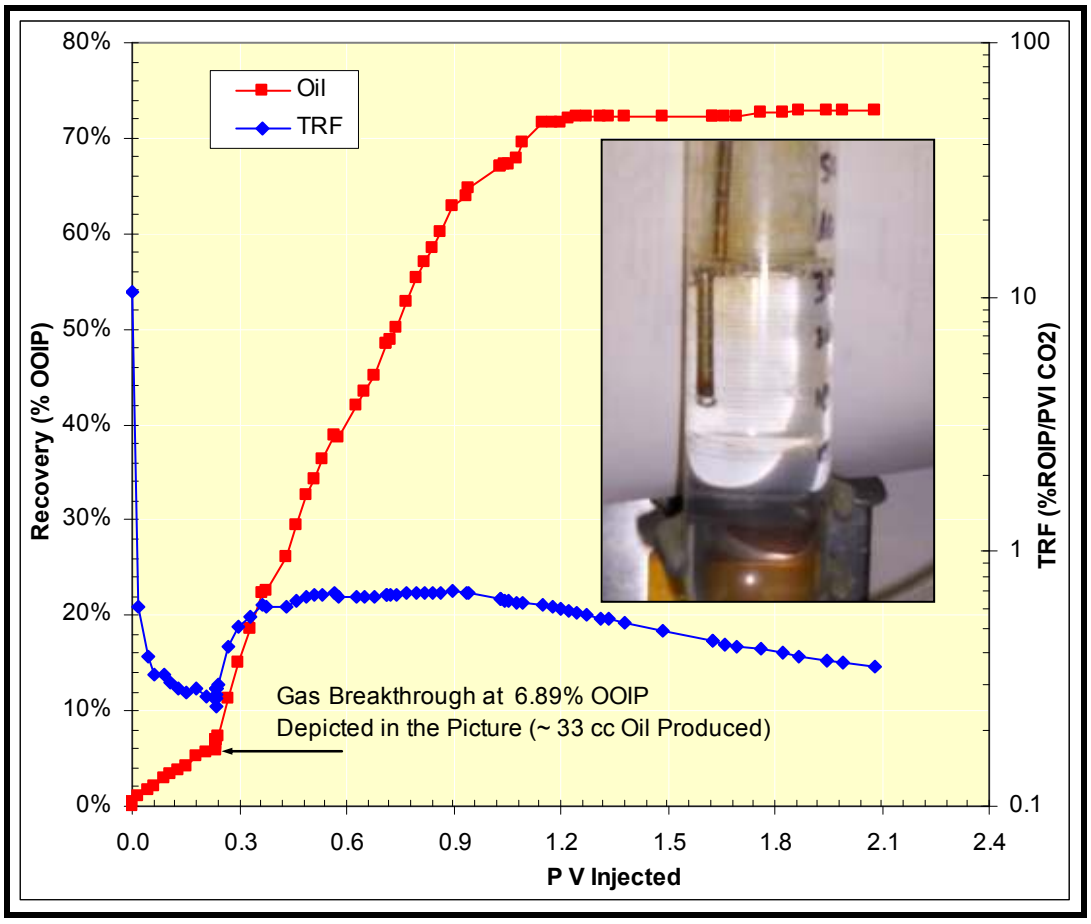

Figure 3.72: Oil Recovery and TRF Data for the GSDH GAGD IRC # 1 Experiment

It is interesting to note that the worst GAGD flood recovery (47.27% ROIP) is more than four times the best average miscible WAG flood recoveries. Surprisingly, all the GAGD miscible floods, irrespective of the flood characteristics, such as fractured core, GSDH or NSDH mode injection, reservoir or model fluid systems; recover almost all of the residual oil. This shows that the effect of various operating parameters on GAGD performance has little or no significance. Furthermore, the range of oil recovery rates (therefore process times) demonstrated by various floods is also similar and not as varied as their immiscible counterparts.

3.5.9.1 Mechanisms and Dynamics of the GAGD Process

In addition of better understand the fluid dynamics of displacement and drainage occurring during GAGD, the fluids production characteristics of each of the floods were plotted together as in Figures 3.76 to 3.78 (from Table 3.20). The two major factors affecting the oil, gas and water flow (injection rates as well as production and breakthrough times) during GAGD floods are: (i) CO_2 solubility effects in Yates

reservoir brine and the oleic phase (n-Decane or Yates stock tank oil) , and (ii) CO_2 phase behavior during immiscible flood pressure and temperature conditions.

The solubility effects of CO_2 in Yates reservoir brine are reported in Section 5.1.3. Solubility calculations suggest that the CO_2 solubility in the core brine delays the oil breakthrough times by nearly 0.5 pore volume. It has been hypothesized that the gas may not be available for CO_2 mobilization and recovery until nearly all the brine becomes saturated with the solvent.

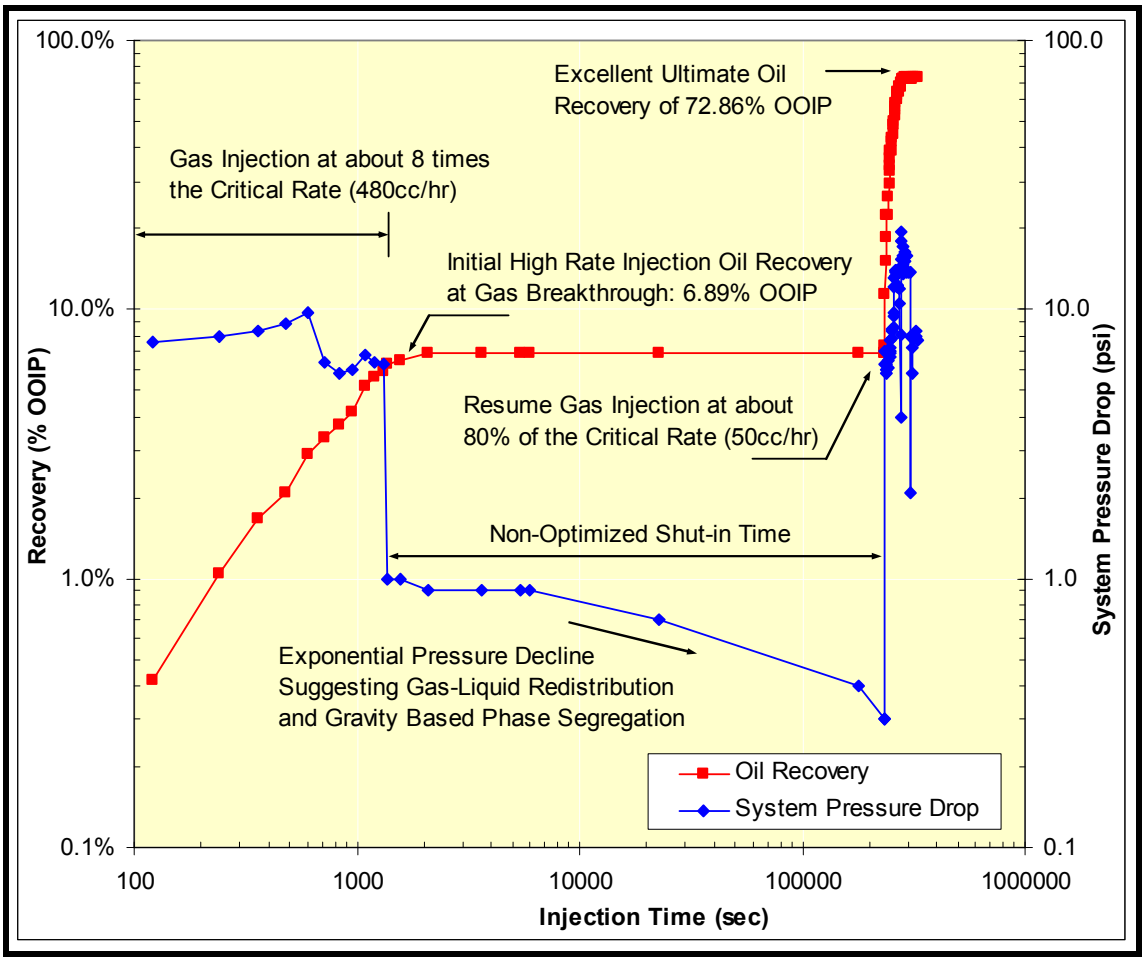

Figure 3.73: Oil Recovery and System Pressure Drop Data Plotted on a Time Scale for the GSDH GAGD IRC # 1 Experiment

Secondly, the temperature of the immiscible GAGD floods (82 ^{o}F) being slightly below the critical temperature of CO_2 (87.8 ^{o}F), influence the oil, water and gas production characteristics during the immiscible GAGD floods. This proximity of the experimental conditions to the CO_2 vapor pressure curve possibly resulted in the liquefaction of CO_2 in the transfer vessel (TV) and fluid lines during pumping due to variations (increases) in the system injection pressure. This liquefaction results in CO_2 being injected as a liquid phase (since the TV is at lower temperature (70 ^{o}F) than the

core (82 ^{o}F)) into the core. The produced gas volumes being measured by the gasometer at ambient conditions is about five times the injected liquid CO_2 volumes (based on the CO_2 pressure-volume diagram.

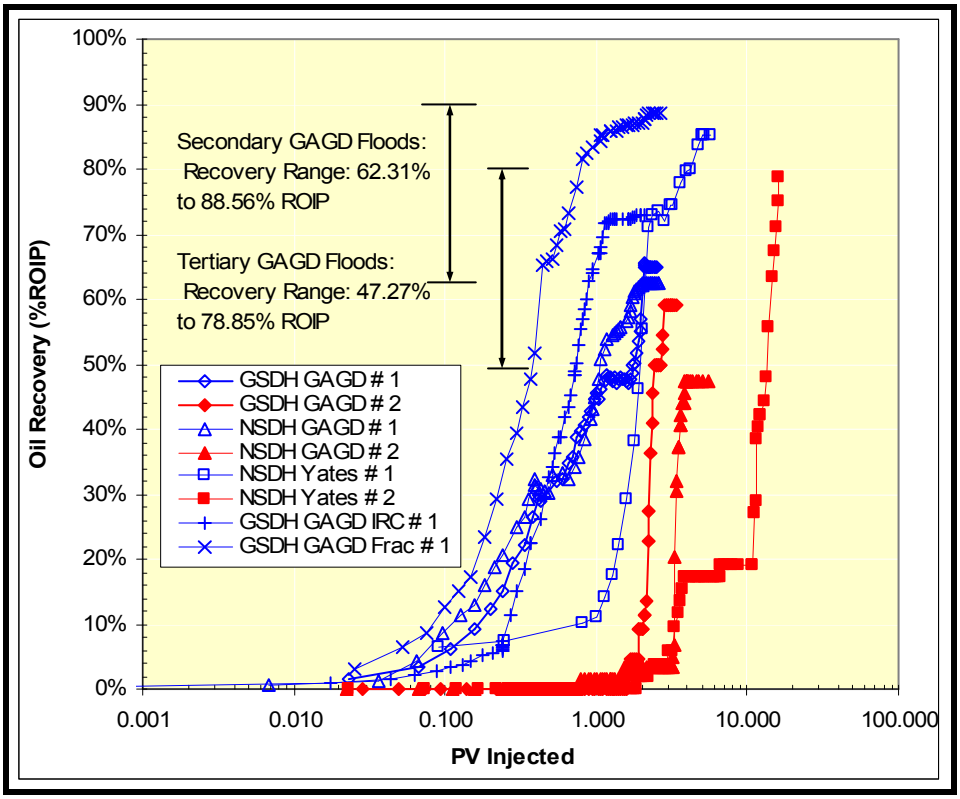

Figure 3.74: Performance Comparison of Various Immiscible GAGD Floods Completed

During secondary GAGD floods, majority of the oil gets produced before the gas breakthrough; whereas in tertiary GAGD floods, water constitutes the majority of the production before gas breakthrough. Since in the immiscible mode of injection during secondary gas floods, the water being essentially immobile, two-phase flow is expected; whereas in the tertiary floods three-phase flow is anticipated.

The GAGD secondary flood data support the former hypothesis for secondary mode floods; while during the immiscible tertiary floods, the data appear not to support the anticipated three phase flow. Experimental observations depicted in Figures 3.76 to 3.78, suggest that for the majority of the multiphase flow, even during tertiary floods, is of two phases; and limited (if any) three phase flow effects are encountered. For tertiary GAGD floods, the initial water production is through gas-water displacements, whereas most of the oil is produced by the gas-oil drainage process.

In secondary immiscible GAGD floods the oil production is found to decease to zero after gas breakthrough, whereas in immiscible tertiary mode GAGD floods, the oil

production continues even after gas breakthrough. The latter effect appears to be a commingled effect of the drainage and the displacement phenomena.

The high density difference existing between oil and gas during immiscible secondary mode GAGD floods also appears to contribute to the drainage of the oil from the gas zone to gas-oil interface. This drained oil accumulates ahead of the gas-oil front, thereby forming an oil bank, which is being continually displaced immiscibly by the expanding gas zone. The contribution of the displacement mechanism to oil production during secondary immiscible GAGD flood is evident from the fact that oil production begins immediately after gas injection (in both NSDH and GSDH modes of injection). This suggests that the displacement mechanism dominates early in the life of the flood, since sufficient time for the formation of a gas zone (essential for drainage mechanism to occur) has not elapsed.

Conversely, during miscible GAGD floods, single phase oil flow dominates during secondary injection modes. Therefore, the pressure drop characteristics approach absolute permeability values (Figures 3.49 and 3.57), and suggest that the second phase (CO_2) does not compete to flow with the oil. This results in higher production rates supported by non-compressible liquid CO_2 injection.

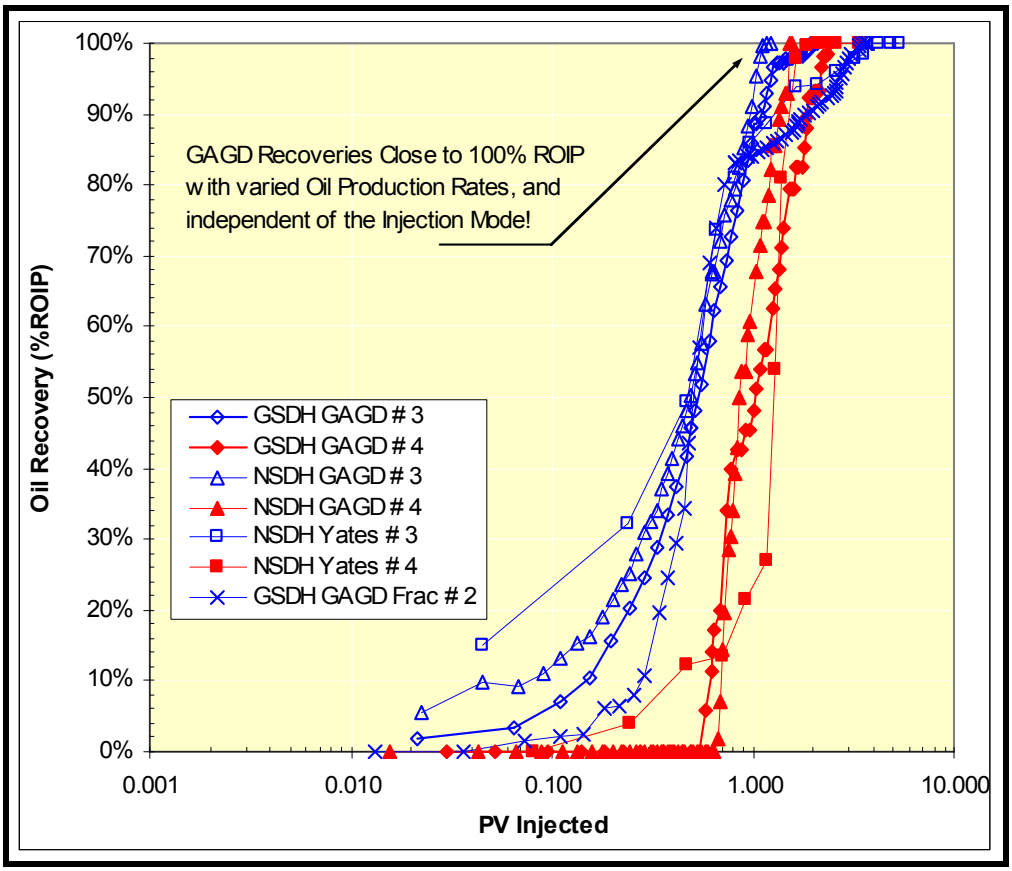

Figure 3.75: Performance Comparison of Various Miscible GAGD Floods Completed

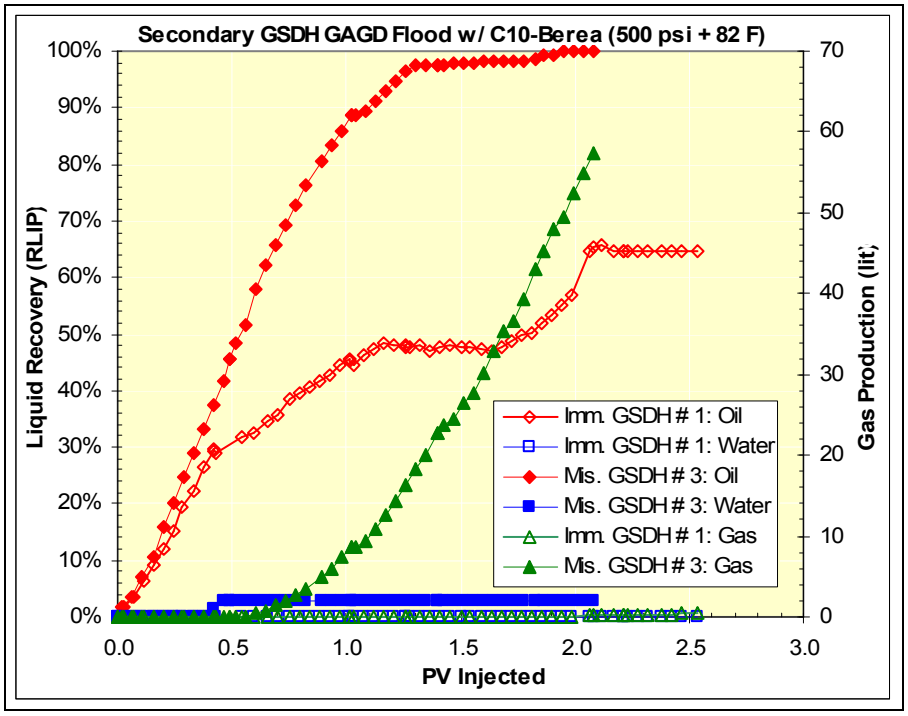

(a) Secondary GSDH GAGD Floods

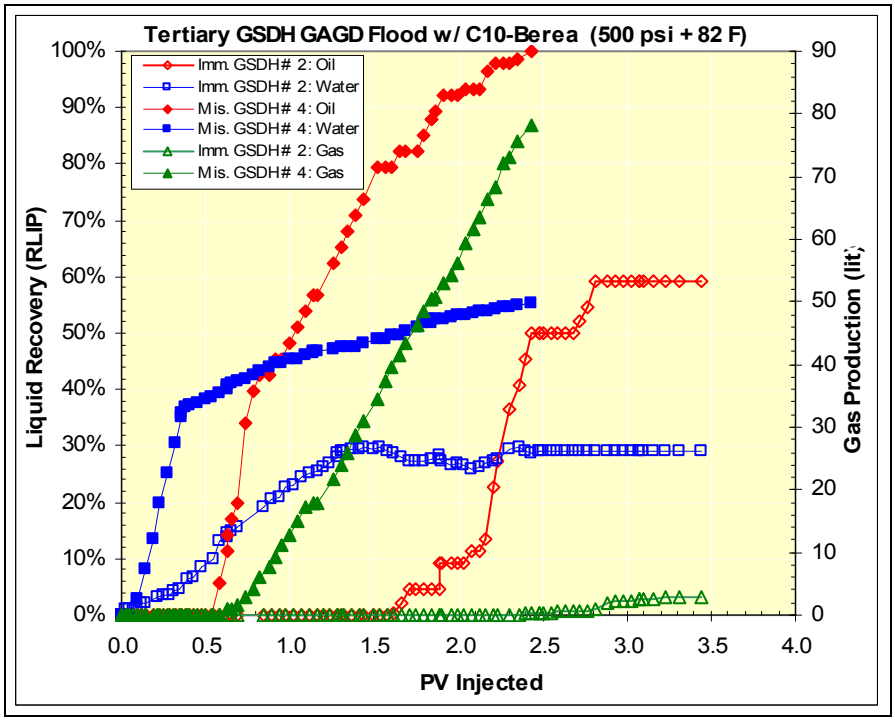

(b) Tertiary GSDH GAGD Floods

Figure 3.76: Normalized Oil, Water and Gas Recovery Characteristics for Immiscible and Miscible GSDH GAGD Experiments with 1-ft Berea, n-Decane and CO_2

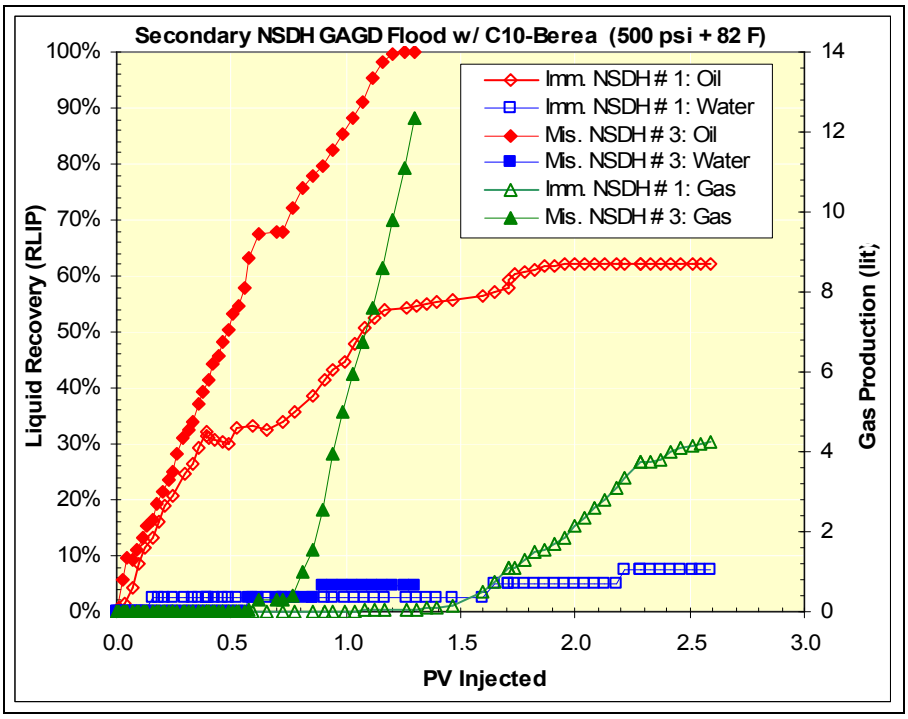

(a) Secondary NSDH GAGD Floods

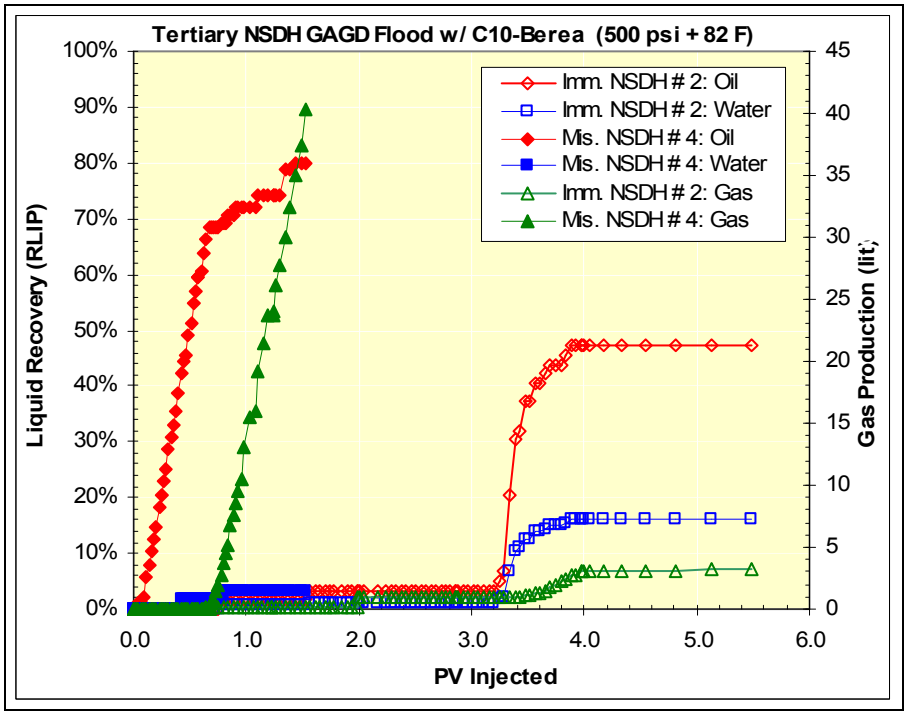

(b) Tertiary NSDH GAGD Floods

Figure 3.77: Normalized Oil, Water and Gas Recovery Characteristics for Immiscible and Miscible NSDH GAGD Experiments with 1-ft Berea, n-Decane and CO_2

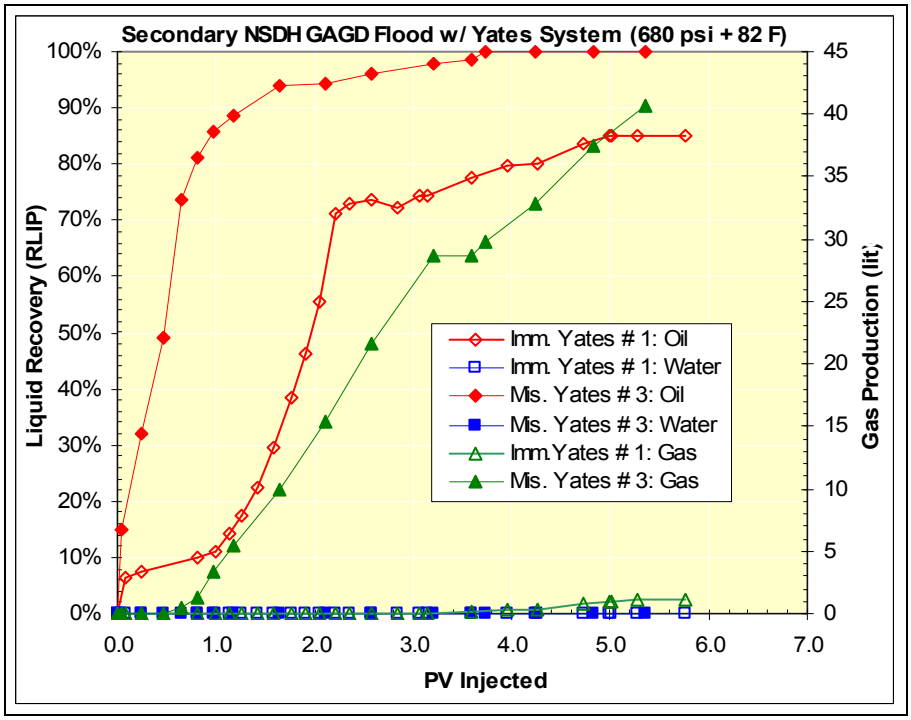

(a) Secondary NSDH GAGD Floods

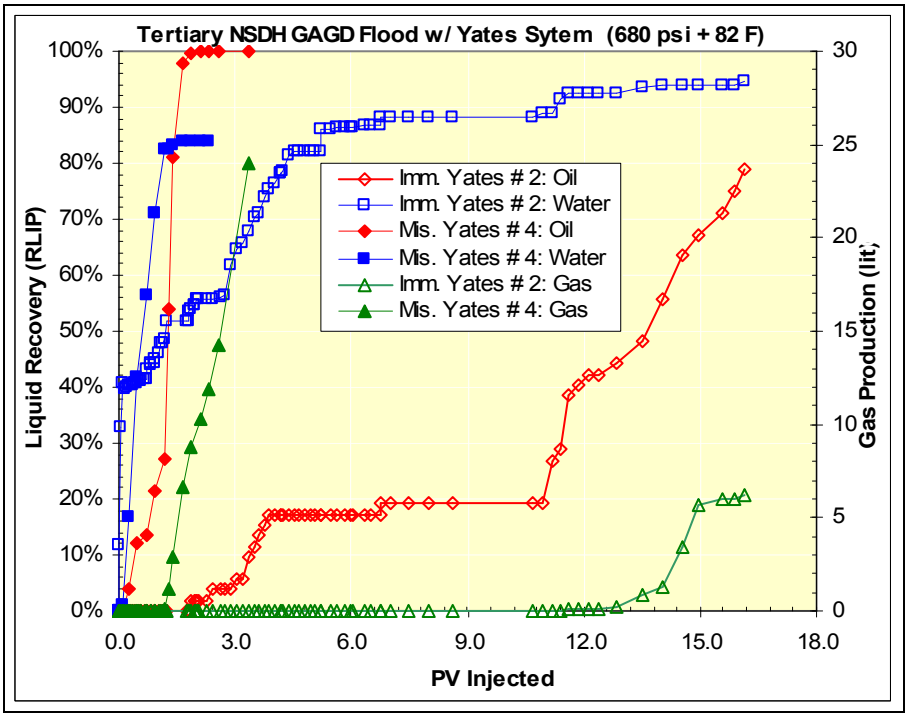

(b) Tertiary NSDH GAGD Floods

Figure 3.78: Normalized Oil, Water and Gas Recovery Characteristics for Immiscible and Miscible NSDH GAGD Experiments with Yates Reservoir System and CO_2

Table 3.20: Rock and Fluid Characteristics for all the GAGD Corefloods Conducted during this Study

Immiscible Floods: 500 psi **Miscible Floods: 2500 psi** **System Temperature: 82 ^{o}F**	**P_{TEST}** (psi)	**Abs. Perm** (D)	**Core PV** (cc)	**S_{WC}** (%)	**WF Recvry** (%OOIP)	**GF Recvry** (%ROIP)
(A) GSDH Corefloods						
Rock-Fluid System: Yates Reservoir Brine + n-Decane + 1-ft Berea Core						
GSDH GAGD # 1 (Secondary Immiscible)	500	0.2224	116.26	31.53	N/A	64.83
GSDH GAGD # 2 (Tertiary Immiscible)	500	0.3028	116.26	40.14	68.95	59.06
GSDH GAGD # 3 (Secondary Miscible)	2500	0.2440	116.26	31.53	N/A	~ 100
GSDH GAGD # 4 (Tertiary Miscible)	2500	0.3331	116.26	31.53	58.28	~ 100
GAGD Frac # 1 (Secondary Immiscible)	500	0.7790	141.26	37.56	N/A	88.56
GAGD Frac # 2 (Secondary Miscible)	2500	0.7932	141.26	37.56	N/A	~ 100
GAGD IRC # 1 (Secondary Immiscible)	500	3.0061	756.39	36.67	N/A	72.86
(B) NSDH Corefloods						
Rock-Fluid System: Yates Reservoir Brine + n-Decane + 1-ft Berea Core						
NSDH GAGD # 1 (Secondary Immiscible)	500	0.1426	116.26	34.12	N/A	62.31%
NSDH GAGD # 2 (Tertiary Immiscible)	500	0.1784	116.26	34.98	60.82	47.27
NSDH GAGD # 3 (Secondary Miscible)	2500	0.1176	116.26	35.84	N/A	~ 100
NSDH GAGD # 4 (Tertiary Miscible)	2500	0.1509	116.26	35.84	61.64	~ 100
Rock-Fluid System: Yates Reservoir Brine + Yates ST Crude + Yates Reservoir Core						
GAGD Yates # 1 (Secondary Immiscible)	680	0.2596	22	24.12	N/A	76.04
GAGD Yates # 2 (Tertiary Immiscible)	680	0.3858	22	27.36	67.46	78.85
GAGD Yates # 3 (Secondary Miscible)	2500	0.3574	22	21.91	N/A	~ 100
GAGD Yates # 4 (Tertiary Miscible)	2500	0.7797	22	31.94	72.66	~ 100

Until gas breakthrough, the gas production occurs primarily due to the displacement mechanism, coupled with the formation of a miscible zone behind the front. It appears that the GAGD fluid mechanics are characterized by two phenomena: single phase Darcy displacement of pure oil, followed by an oil-solvent mixed miscible zone. Gas breakthrough occurs when the leading edge of the miscible zone reaches the producer, when the entire core pore volume is occupied by the miscible zone. After gas breakthrough, the oil production rates decrease (as observed in all three miscible GAGD floods in Figures 3.76 to 3.78), attributable to the solvent dilution of the oil. It is important to note that the flow mechanics after gas breakthrough are the combined effects of displacement and drainage effects. During miscible gas injection, the Figures 3.76 to

3.78 suggest that about 60% to 65% of the oil production with n-Decane occurs due to the displacement mechanism at gas breakthrough. On the other hand, for the Yates reservoir rock-fluid systems (Figure 3.78), this contribution increases to 74% oil production at gas breakthrough. This appears to be the effect of high viscosity ratio of Yates crude-CO_2 (16.0/0.1) compared to n-Decane-CO_2 (0.92/0.1).

3.5.10 Comparison of Laboratory Experimental Results to Field Data

Dimensional analysis of various field studies on gravity stable gas injection (see Chapter 4) suggested the use of various dimensionless numbers to characterize and correlate GAGD oil recoveries. Literature review recommends the use two separate and equally important dimensionless groups: capillary (N_C) and Bond (N_B) numbers for GAGD characterization. Therefore these groups were employed as performance indicators and the results are detailed below.

3.5.10.1 Immiscible Scaled GAGD Floods

The results obtained from the physical model (Sharma, 2005) and immiscible core flood experiments were compared with data obtained from the gravity drainage field projects. Significant variations in the N_C and N_B values for individual floods were observed, making the performance evaluation difficult. To facilitate effective comparisons, as well as to account for the relative variations of the Bond and capillary numbers in each of these floods, a single comparison parameter was hence required.

The gravity number is a combination of Bond and capillary numbers, and incorporates the relative variations of the major reservoir forces, namely the gravity, capillary and viscous forces. Therefore, the Gravity number appeared to be more appropriate for the comparison of laboratory and field data. Therefore the results for all the laboratory experiments (both the physical model and corefloods) and the field recovery data were plotted against the gravity number in Figure 3.79.

From Figure 3.79, it can be seen that there is a good logarithmic relationship, with very low data dispersion, between the GAGD recovery characteristics and the Gravity number. This is very encouraging, since the data for this comparison are obtained from vastly varied sources, such as from the atmospheric pressure, homogeneous 2-D sand packs, to the highly heterogeneous and high-pressure field flood projects. These findings indicate that the performance of the GAGD process appears to be well characterized by the use of the gravity number. Additionally the correlation developed can also be used for pre-prediction of oil recoveries for field GAGD projects if the N_G value is known.

Figure 3.79 also suggests that there could be two logarithmic correlations between oil recovery and gravity number, based on the wettability characteristics of the porous medium. Although the oil-wet nature of the Yates corefloods has been confirmed from contact angle experiments (Xu, 2005), the reservoir mineral composition of the field

study suggests it to be an oil-wet type of porous medium. This plot suggests that the gas injection process performance is enhanced in oil-wet media, which also appears to be supported by the literature review.

3.5.10.2 Miscible Scaled GAGD Floods

The miscible GAGD flood results for the physical model were not available due to experimental limitations; hence characterization of these floods was completed using 1-D GAGD corefloods and field results. However, the N_G versus oil recovery plot did not yield a very good correlation, as it did for the immiscible floods. However, the individual plots of N_C and N_B versus recovery resulted in good correlations. Therefore, it was hypothesized that there is some other important mechanistic parameter that is not well represented in the gravity number, and a mathematical combination of the N_C, N_B and N_G groups with that mechanistic parameter should yield an improved correlation parameter. Literate review suggested the importance of two ratios: density and viscosity (gas to oil). The density ratio was factored into the newly defined group (Equation 3.19) below:

$$New - Group = NG + \left(\frac{\rho_G}{\rho_O} (N_C + N_B) \right) \quad \text{..... (3.19)}$$

When immiscible and miscible GAGD physical model (Figures 3.80 and 3.81), coreflood and field data were plotted against this correlation, excellent correlation was obtained for immiscible floods; while an acceptable (significantly improved fit over N_G vs. Recovery) correlation was obtained for miscible floods. Although this new number is significantly more complex than N_G, and its physical phenomena interpretation may be difficult; it is definitely a positive step toward confident and improved characterization of the GAGD process.

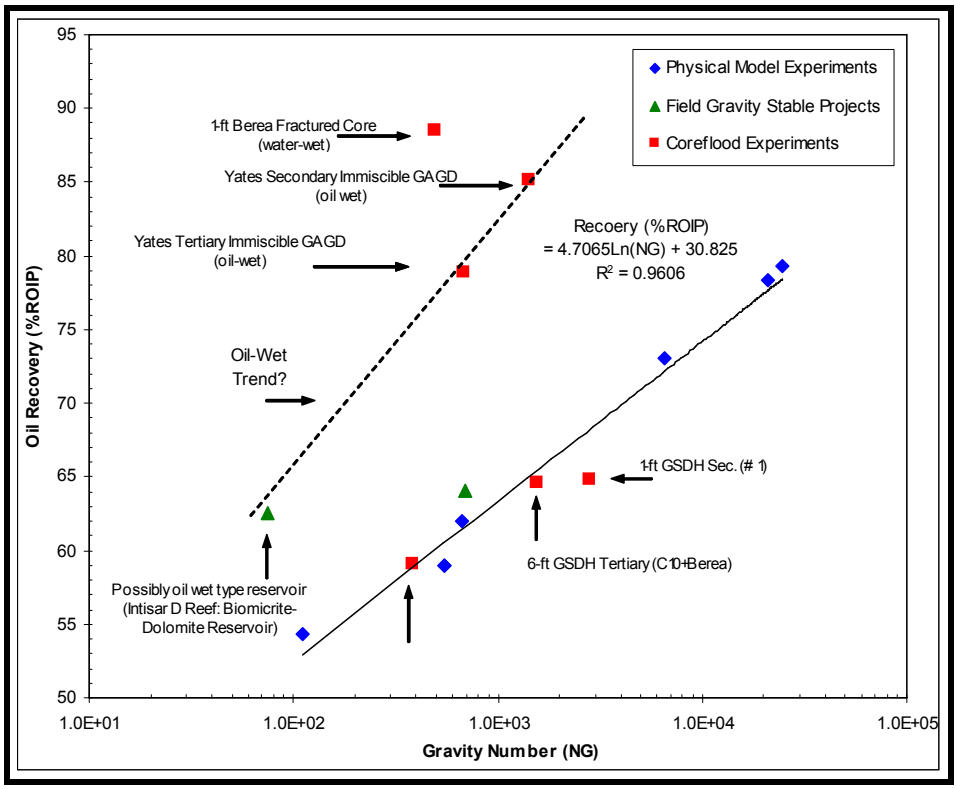

Figure 3.79: Comparison of Immiscible GAGD Laboratory Experimentation and Field Gravity Drainage Projects' Performance versus Flood Gravity Number

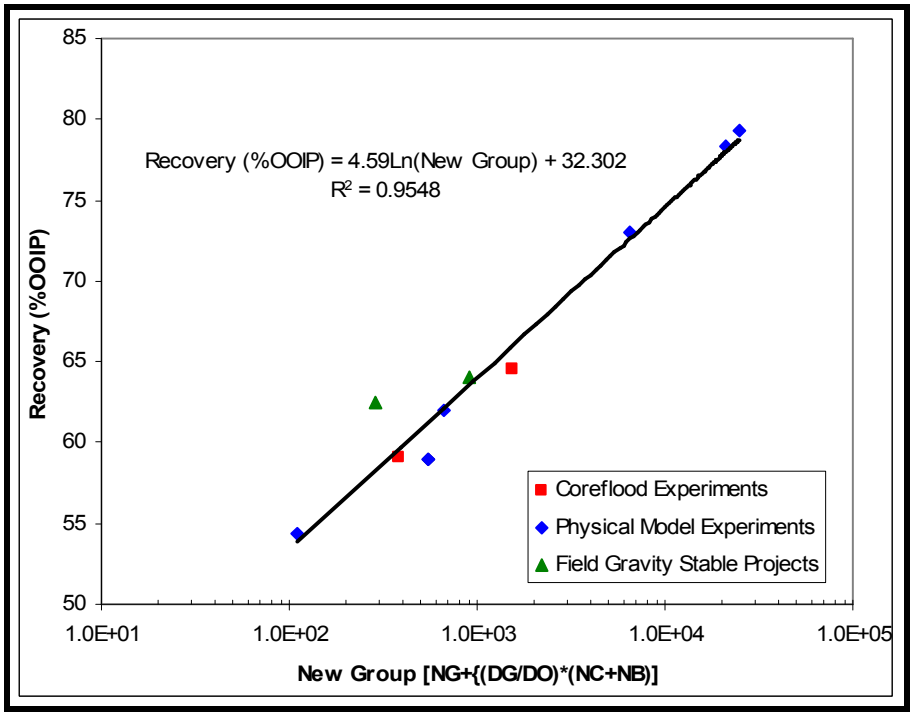

Figure 3.80: Comparison of Immiscible GAGD Laboratory Experimentation and Field Gravity Drainage Projects' Performance versus New Group

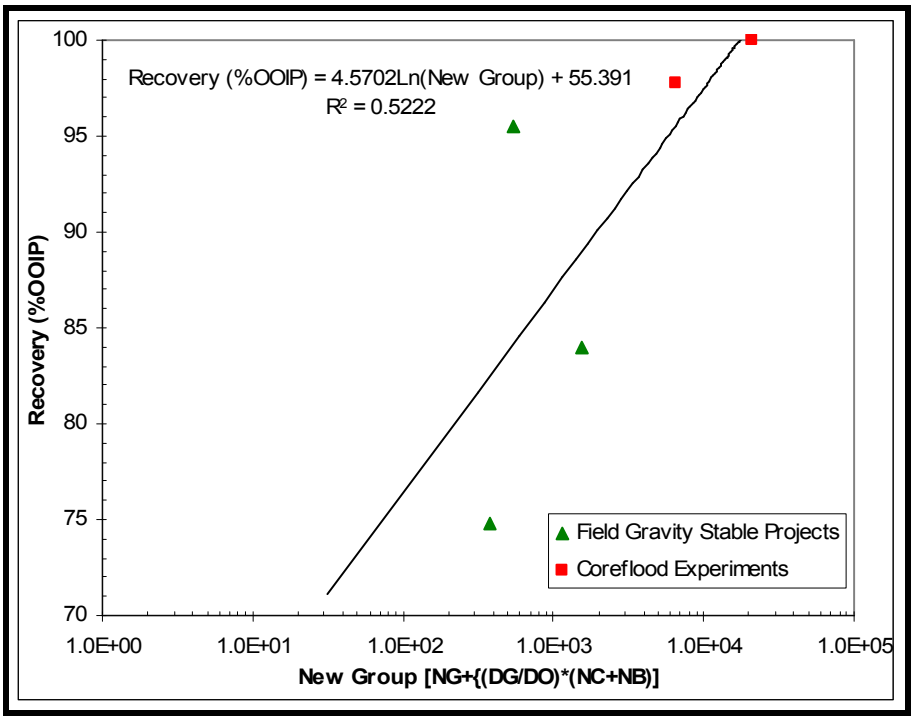

Figure 3.81: Comparison of Miscible GAGD Laboratory Experimentation and Field Gravity Drainage Projects' Performance versus New Group

3.6 Analytical and Conceptual GAGD Modeling

Forecasting the reservoir behavior and the oil recovery characteristics is one of the most important tasks of reservoir engineering. Since the GAGD process is new, its analytical and conceptual coupling with the existing knowledge base is essential for better understanding. The literature views on gravity drainage and gravity stable gas injection were summarized in Section 3.1. This chapter attempts to identify the gravity drainage flow mechanisms, and improve our understanding by using existing simple analytical models to predict the recovery patterns from GAGD applications.

3.6.1 Inferences from Gravity Drainage Literature

The inferences resulting from the detailed gravity drainage mechanistic review (see Section 3.1) relevant to GAGD modeling are summarized:

1. Literature seems to use the words 'gravity stable gas displacement' and 'drainage' interchangeably.
2. Although, the original Buckley-Leverett model was hypothesized to be applicable to gas floods as well, the two assumptions used by Buckley-Leverett model, no mass transfer between phases and incompressible phases, result in severely limiting its application to GAGD type (gravity drainage) floods.
3. Buckley and Leverett (1942) theory suggests that the gravity drainage phenomenon is "exceedingly slow".

4. Terwilliger et al.'s (1951) model result in two inferences that appear to be relevant for the mechanistic description of the GAGD process: (i) as oil production rate approaches zero, the oil drains under its own weight, in the gas swept zone, fast enough to maintain the "static capillary saturation distribution" in the gas-oil contact transition zone; and (ii) at very high production rates, oil drainage under its own weight is negligible and recoveries approach those of horizontal gas drives.
5. It is interesting to note that Grattoni et al.'s (2001) studies on gas invasion under gravity-dominated conditions, to study the effects of wettability and water saturation on three-phase flow; reconfirm the first inference of Terwilliger et al.'s (1951) model, which states that there exists a critical height in the porous medium above which the oil saturation is negligible. The second inference, more relevant to the GAGD process, also seems to be supported from the first part of the scaled GSDH GAGD IRC # 1 experiment (see Section 5.8) conducted to study the influence of injection rate on GAGD flood performance. Interestingly, the oil recovery (6.89% OOIP) obtained in the first part, wherein the gas injection rate far exceeded the critical injection rate, is very close to the average field scale horizontal mode immiscible CGI (or WAG) recoveries of about 6.4% OOIP (Christensen et al., 1998).

3.6.2 Application of Traditional Gravity Drainage Models to the GAGD Process

All the limited number of existing models of the gravity drainage process seems to be limited by the fact that "…capillary pressure is usually neglected or considered inappropriately (Li and Horne, 2003)". To assess the applicability of various traditional models to the new GAGD process, two models were chosen after careful review: Richardson and Blackwell (1971) and Li and Horne (2003).

3.6.2.1 Richardson and Blackwell (R&B) Model

The R&B model was selected because of its simplicity and versatility. This model was applied to the following secondary mode GAGD experiments: (i) gravity stable displacement history secondary immiscible GAGD flood (GSDH GAGD # 1), gravity stable displacement history secondary miscible GAGD flood (GSDH GAGD # 3), non-gravity stable displacement history secondary immiscible GAGD flood (NSDH GAGD # 1), and non-gravity stable displacement history secondary miscible GAGD flood (NSDH GAGD # 3). The step by step procedures for calculating the oil recovery rates are available in the Richardson and Blackwell (1971) reference. The model application required some data that was not measured during regular experimentation. Therefore CMGL's Winprop® PVT simulator was used to generate some of the missing data. The GAGD experiments conducted in the laboratory used a gas injection rate of 10 cc/hr. This rate is less than one-half of the Dietz's (1953) critical rates; hence the R&B model was found to be applicable to these floods. The R&B model application procedure also

requires the reservoir to be 'divided' into blocks of equal size. Since all the GAGD experiments were conducted on 1-ft Berea cores, six arbitrary divisions of 0.1667 ft each were used for the model prediction.

The data used for the prediction of oil production rates using the R&B model are included in Table 3.21. The calculated fractional flow of gas during GAGD experiments is summarized in Table 3.22. The calculated vertical drainage rates and gas interface height for each core block is plotted in Figure 3.82. Lastly the comparison between predicted and actual oil recoveries is summarized in Table 3.23.

The R&B model was validated against the Hawkins Dexter field data, and the model was found to under predict the ultimate oil recovery by 5.2% OOIP. From Table 3.23, it is clearly seen that the maximum error generated by this model's application to the GAGD floods is 6.4%. This makes the R&B model a good prediction tool for gravity drainage ultimate recoveries. However, since this model does not predict oil production rates, another model was required for this purpose. To facilitate prediction of production rates, another model by Li and Horne (2003) was employed, and the results are discussed in the following sections.

Table 3.21: Data Used for R&B Model Application

Experiment Number	Type	GSDH # 1	GSDH # 3	NSDH # 1	NSDH # 3
Pore Volume (Vp) (cubic ft)	Expt. Data	0.0041	0.0041	0.0041	0.0041
Cross-Sectional Area (A) (sq. ft)	Expt. Data	0.0218	0.0218	0.0218	0.0218
Permeability (Darcy)	Expt. Data	0.2224	0.2440	0.1426	0.1176
Density Difference (lbm/ft3)	Winprop	38.3655	44.8946	38.3655	44.8946
Oil Viscosity (cP)	Winprop	0.9250	0.9250	0.9250	0.9250
Gas Viscosity (cP)	Winprop	0.0165	0.1879	0.0165	0.1879
Relative Permeability to Oil (Fraction)	Expt. Data	0.1001	0.1001	0.1001	0.1001
Relative Permeability to Gas (Fraction)	Expt. Data	0.0018	0.0500	0.0018	0.0500
Recovery (%OOIP)	Expt. Data	0.7544	1.0000	0.7387	1.0000
Connate Water Saturation (Swc)	Expt. Data	0.0194	0.0194	0.0452	0.0624
Residual Oil Saturation to Gas (Sor)	Expt. Data	0.3516	0.0000	0.3804	0.0000
Critical Rate (Dietz's Model) (ft3/D)	Calculated	4.3674	0.0786	2.7998	0.0379
Critical Rate (Dietz's Model) (cc/hr)	Converted	5152.9055	92.6803	3303.4372	44.6689
Gas Fraction of Flowing Stream (Fg)	Calculated	0.5546	0.8064	0.5358	0.7570
Actual Rate of Frontal Movement (ft/D)	Calculated	0.0812	0.0559	0.0841	0.0595
Time to Breakthrough (Days)	Calculated	12.3096	17.8986	11.8912	16.8010

3.6.2.2 Li and Horne (L&H) Model

Since the R&B model did not predict the oil production rates, the Li and Horne (2003) empirical model was employed. The important feature of this model is the ability to incorporate capillary pressure data to improve gravity drainage recovery predictions. The capillary pressure data for the GAGD experiments and L&H model application was generated using the Brooks-Corey (1966) model.

To check the validity of this model as well as to calibrate the data, the L&H model was employed to predict free gravity drainage data generated from 2-D Hele Shaw physical model runs (Sharma, 2005). The experimental and predicted recovery data comparison for two free gravity drainage floods is summarized in Figure 3.83.

Table 3.22: Calculated Fractional Flow of Gas for GAGD Floods

Kor	Kgr	Fg1 (GSDH # 1)	Fg2 (GSDH # 3)	Fg3 (NSDH # 1)	Fg4 (NSDH # 3)
0.1001	0.0000	0.0000	0.0000	0.0000	0.0000
0.0900	0.0020	0.6069	0.1105	0.5882	0.1043
0.0800	0.0040	0.7987	0.2187	0.7766	0.2077
0.0700	0.0060	0.8883	0.3246	0.8666	0.3102
0.0600	0.0080	0.9373	0.4282	0.9175	0.4116
0.0500	0.0100	0.9661	0.5294	0.9489	0.5122
0.0400	0.0120	0.9833	0.6283	0.9692	0.6117
0.0300	0.0140	0.9934	0.7248	0.9825	0.7102
0.0200	0.0160	0.9986	0.8189	0.9913	0.8078
0.0100	0.0180	1.0005	0.9106	0.9968	0.9044
0.0000	0.0200	1.0000	1.0000	1.0000	1.0000

Table 3.23: Comparison of Experimental and Predicted Ultimate Oil Recovery for Various GAGD Floods

Experiment	Experimental Recovery	R&B Model	Model Error
	%OOIP	%OOIP	Avg. Error: 5.6%
GSDH # 1	64.8%	75.5%	-16.5%
GSDH # 4	100.0%	94.2%	5.8%
NSDH # 1	62.3%	73.5%	-17.9%
NSDH # 4	100.0%	93.6%	6.4%

It is important to note that the L&H model is applicable only to free gravity drainage floods. Application of this model to forced gravity drainage (FrGD) 1-D GAGD corefloods and 2-D physical models resulted in over-prediction of the oil production rates. This is intuitive, since the pure (or free) gravity drainage performance is usually better than the forced gravity drainage performance (Muskat, 1949).

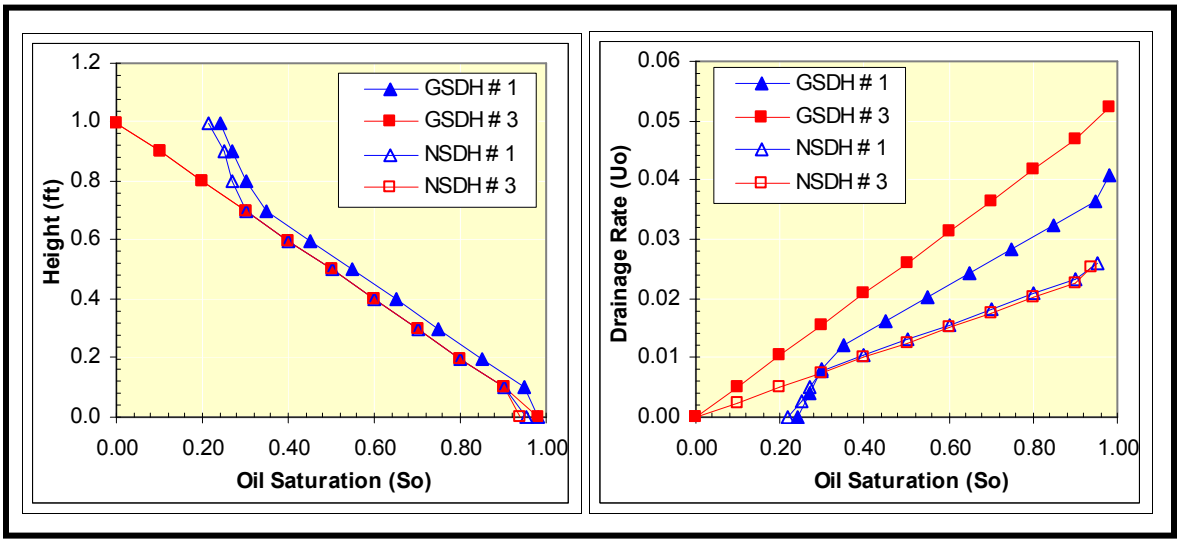

Figure 3.82: R&B Model Predicted Vertical Drainage Rates and Gas Interface Height for Each Core Block

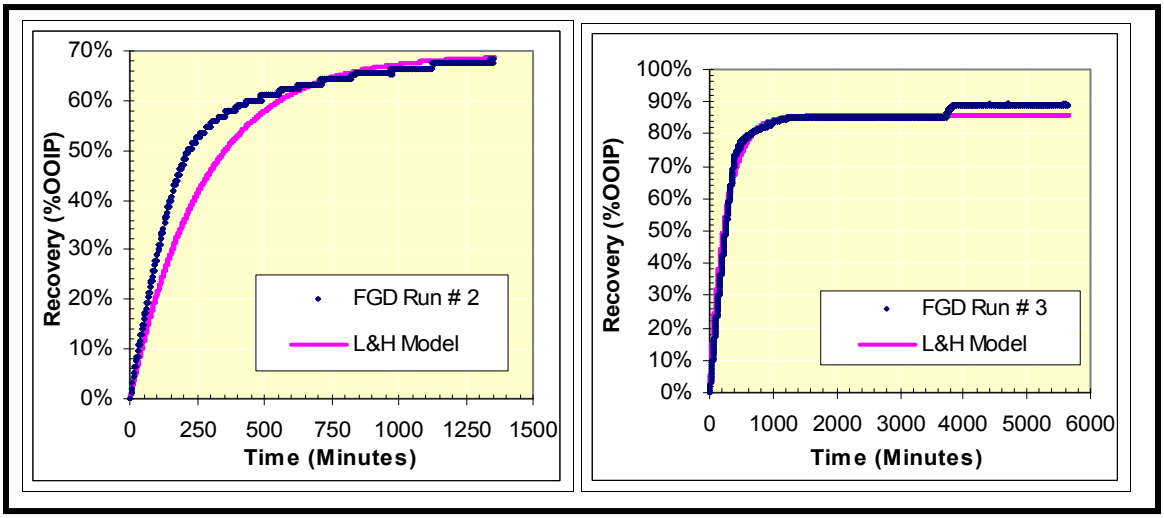

Figure 3.83: Comparison of Experimental and L&H Model Predicted Oil Production Rates for Two Selected Free Gravity Drainage Tests in a 2-D Physical Model

Proposed Modification to the Capillary Pressure Model Incorporated in the L&H Model to facilitate its application to Forced Gravity Drainage

Sensitivity analysis of the L&H model application to the forced gravity drainage 1-D and 2-D scaled GAGD experiments suggested the inadequacy of the Brooks-Corey model for capillary pressure modeling. Furthermore, the insensitivity of the pore size distribution

index (λ) as well as dimensionless length (Zc) of the model in production rate prediction; while the significant dependence on the depth corresponding to entry capillary pressure (Ze) data suggested the need for modification of the L&H model.

Further consideration of the 'demarcator' concept of Cardwell and Parsons (1948) to generate analytical models for gravity drainage in low IFT conditions and / or fractured reservoir systems as well as regression analysis of the GAGD data suggested that for improved GAGD recovery predictions, the Ze needs to be multiplied by a factor defined by Equation 3.20.

$$Ze^{*} = Ze\left(L - \frac{P_C^{(Entry)}}{PS^{(Injection)}} \right) \quad \text{..... (3.20)}$$

Where, Ze^{*} is the modified Ze, Ze is the original depth corresponding to entry capillary pressure (Li and Horne, 2003), L is the equivalent length of the porous medium, $P_C^{(Entry)}$ is the entry capillary pressure calculated by Brooks-Corey model, and $P_S^{(Injection)}$ is the average system injection pressure (recorded during experimentation).

This modification is very similar to the 'demarcator' concept proposed by Cardwell and Parsons (1948), and is also more representative of the multiphase mechanics operational in the flood. And although the employment of this equation sometimes generates negative dimensionless length (Zc) values; it does reflect the physical phenomenon operational in the flood. For example, for coreflood experiments, Equation 25 generates a negative Zc value, physically suggesting that the entry capillary pressure effects (or capillary end effects) are insignificant. On the other hand, this value is found be zero or positive in free or forced 2-D Hele Shaw physical model runs, suggesting stronger capillary end effects, which are also supported by visual inferences (Sharma, 2005). Finally, it is intended to make the capillary pressure modeling representative of the physical system as well as the improved performance prediction for the new GAGD scaled laboratory experiments.

Tables 3.24 and 3.25 summarize the data employed for the application of the modified L&H model to the GAGD process's coreflood and physical model experiments. Comparison of the modified L&H model predictions and the experimental results is graphically depicted in Figures 3.84 and 3.85. As can be observed from Figures 3.84 and 3.85, excellent match between the experimental and model results is obtained. Furthermore, this modified model appears to be more representative of the various multiphase flow phenomena (such as displacement, film flow and gravity drainage)

Table 3.24: Data Used for Modified L&H Model Application to 2-D GAGD Floods

Experiment Number	Type	FrGD # 1	FrGD # 2	FrGD # 3	FrGD # 4
Beta (β)	Calculated	0.016528	0.01552413	0.018871722	0.019756
Pore Volume (Vp)	Expt. Data	514.8	522	520	530
Recovery (%OOIP)	Expt. Data	0.675578	0.494708356	0.593096558	0.708109
Connate Water Saturation (Swc)	Expt. Data	0.203574	0.22605364	0.173076923	0.245283
Residual Oil Saturation to Gas (Sor)	Expt. Data	0.258378	0.391068629	0.336477847	0.220295
Initial Oil Production Rate (Qoi)	Calculated	4.578103	3.102686421	4.812883847	5.595865
Ultimate Oil Production by FGD (Npo Inf.)	Calculated	276.9869	199.8621759	255.0315198	283.2435
Average Residual Oil Saturation (Sor Avg.)	Calculated	0.258378	0.391068629	0.336477847	0.220295
Depth Corresponding to Entry Pc (Ze)	Expt. Data	0.35	0.35	0.35	0.35
Pore Size Distribution Index (λ)	Assumed	3	5	3	5
Dimensionless Length (Zc)	Calculated	0	0	0	0

Table 3.25: Data Used for Modified L&H Model Application to 2-D GAGD Floods

Experiment Number	Type	GSDH # 1	GSDH # 3	NSDH # 1	NSDH # 3
Beta (β)	Calculated	0.0010	0.0014	0.0016	0.0016
Pore Volume (Vp)	Expt. Data	116.2600	116.2600	116.2600	116.2600
Recovery (%OOIP)	Expt. Data	0.7544	1.0000	0.7387	1.0000
Connate Water Saturation (Swc)	Expt. Data	0.0194	0.0194	0.0452	0.0624
Residual Oil Saturation to Gas (Sor)	Expt. Data	0.2408	0.0000	0.2494	0.0000
Initial Oil Production Rate (Qoi)	Calculated	0.0881	0.1603	0.1304	0.1773
Ultimate Oil Production by FGD (Npo Inf.)	Calculated	86.0000	114.0000	82.0000	109.0000
Average Residual Oil Saturation (Sor Avg.)	Calculated	0.2408	0.0000	0.2494	0.0000
Depth Corresponding to Entry Pc (Ze)	Expt. Data	0.3500	0.3500	0.3200	0.3500
Pore Size Distribution Index (λ)	Assumed	3.0000	5.0000	3.0000	5.0000
Dimensionless Length (Zc)	Calculated	-0.1483	-0.1483	-0.0499	-0.1483

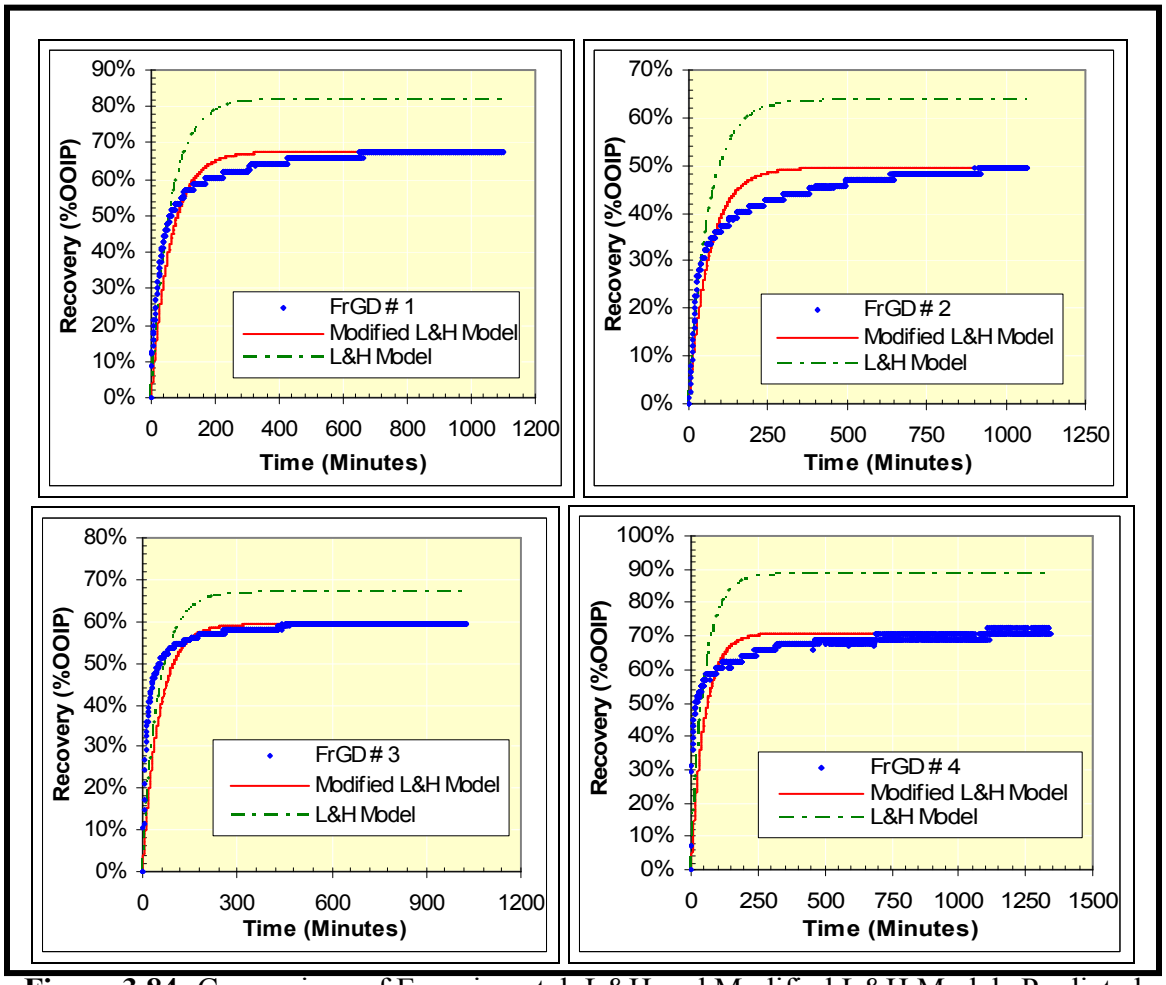

Figure 3.84: Comparison of Experimental, L&H and Modified L&H Models Predicted Oil Production Rates for Forced Gravity Drainage 2-D Physical Model GAGD Floods

3.6.3 Inferences and Recommendations for Future Modeling Work of the GAGD Process

The literature review on gravity drainage suggests that the fundamental understanding and modeling of the gravity drainage process is still a challenge to the reservoir engineer, mainly because of the limitations of the reservoir simulation tools to better include the physics of the process into improved reservoir management. This section summarizes the important mechanistic and dynamic characteristics of the gravity drainage process identified and also attempts to distinguish between displacement and drainage phenomena. Finally some recommendations for continued research on analytical modeling of the new GAGD process are also included.

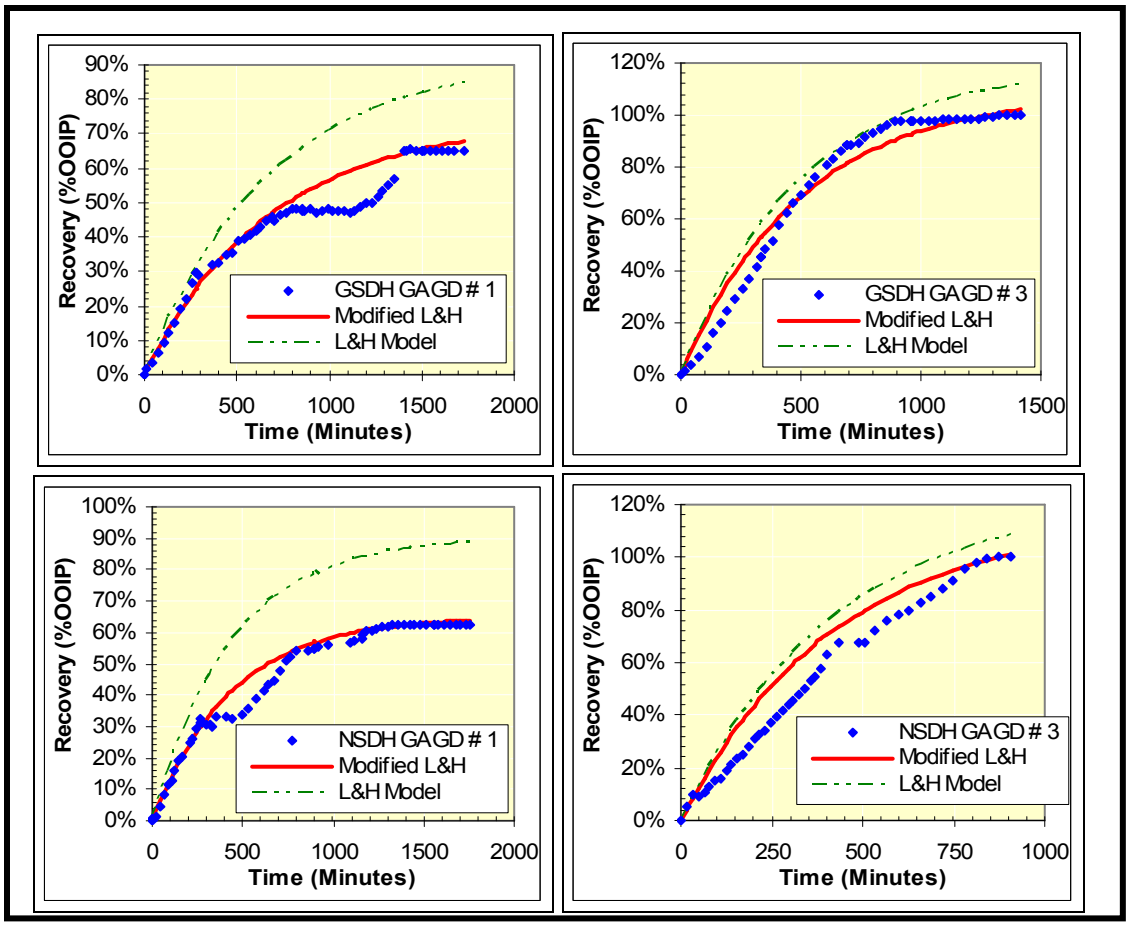

Figure 3.85: Comparison of Experimental and Modified L&H Model Predicted Oil Production Rates for Forced Gravity Drainage 1-D GAGD Corefloods

3.6.3.1 Hypothesized Gravity Drainage Mechanisms and its Possible Distinction from Buckley Leverett Type Displacements

The literature review (Schechter and Guo, 1996) suggests that there are three distinct categories of the gravity drainage processes: (i) forced gravity drainage by gas injection at controlled flow rates, (ii) centrifuge simulated gravity drainage (not occurring in natural systems), and (iii) free fall gravity drainage occurring in a variety of cases, such as pressure depleted fractured and volumetric reservoirs, and gas injection (or pressure maintenance) into highly fractured reservoirs.

It appears that the displacement (classical definition) is an indivisible characteristic of the forced gravity drainage (GAGD) phenomenon. However, the displacement phenomenon appears to be one of the several distinct phenomena occurring during the GAGD process. Nevertheless, almost all the models used to characterize forced gravity drainage (relevant to the GAGD process), employ the Buckley-Leverett approach. Inspite of the inherent limitations of the B-L theory (imparted due to unrealistic assumptions from gravity drainage injection view-point: see Section 6.1.2), its application to a wide variety of scenarios with fair results, suggest it to be relevant and important to forced

gravity drainage (therefore GAGD) applications. However, from a theoretical point of view, this argument appears to be valid only when there is little or no pressure variation within the gas chamber, which may be achievable for constant pressure type and low injection rate floods. Therefore, the B-L theory could be useful to model gravity drainage until gas breakthrough.

It is interesting to note that all the forced gravity drainage models that employ B-L approach appear to be valid only until gas breakthrough. This is a serious limitation, since the modified B-L theory (which includes the capillary pressure effects on oil recoveries and breakthrough times) suggests that in real reservoir systems (water-wet), the production rates decrease after breakthrough and this decrease is proportional to pore volume injection, residual saturation and the corresponding oil relative permeability; and therefore cannot be used to predict post breakthrough oil production rates. Furthermore, for pure piston-like displacements, in water-wet porous media (ignoring capillary pressure), 'clean' breakthroughs are observed, i.e. no oil production after water breakthrough. This statement is also supported by the scaled secondary waterflood data on realistic water-wet porous media (also reported in this study). GAGD experimental data (presented in Chapter 5) clearly demonstrate that GAGD oil production rates do not drop significantly even after gas breakthrough. This suggests that the spreading coefficient and oil film flow rates are important for GAGD oil recovery (especially after gas breakthrough) and must be incorporated into the GAGD analytical models. Gravity drainage literature review also seems to support this view.

It is hypothesized that the GAGD process operates in three distinct multiphase modes: (i) piston-like displacement (B-L theory, decline curve and continuity equation, and Darcy's law are valid), (ii) gravity drainage mechanisms (oil film flow under positive spreading coefficient conditions), and finally (iii) extraction mechanism. The lumped approach of Richardson and Blackwell (1971) and Pedrera et al. (2002) also seems to support this multi-level and multi-mechanistic approach.

The first multiphase mode is supported by many authors (Terwilliger et al., 1951; Hagoort, 1980; Li et al.; 2000) and is best depicted in Hagoort's (1980) schematic of the forced gravity drainage (gravity stable gas displacement) flood front (Figure 3.86). The second multiphase mechanism stems from the limitations of the B-L theory to accurately predict the oil production rates under forced gravity drainage (GAGD) floods. Scaled corefloods, physical model results as well as field reviews clearly demonstrate that oil production rates may not drop after gas breakthrough.

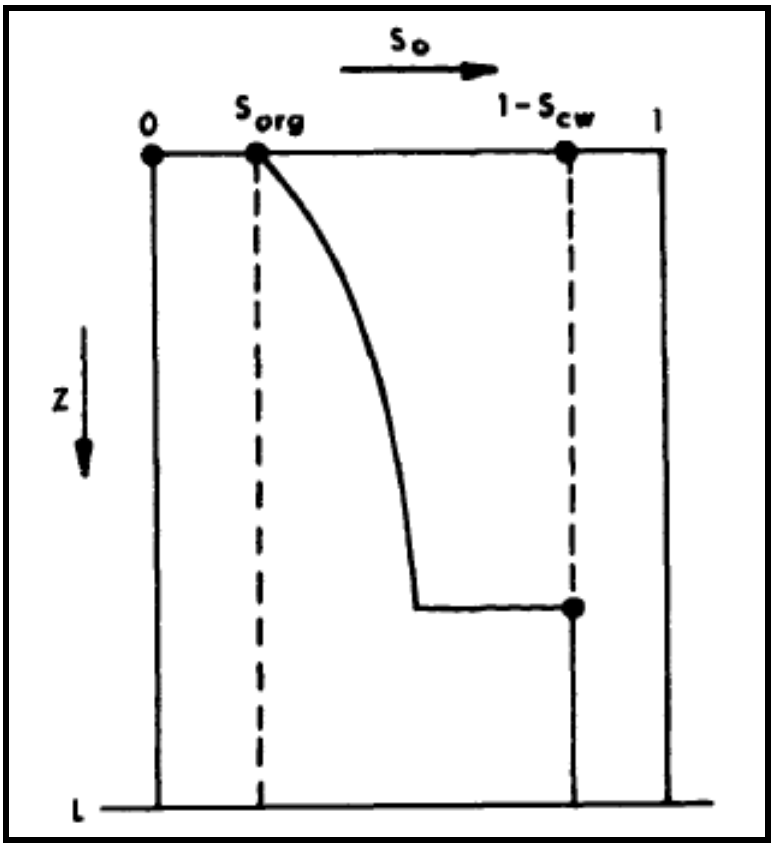

Figure 3.86: Buckley-Leverett Saturation Profile for Stable Downward Displacement (Hagoort, 1980)

Additionally, the B-L 'shock-front' concept does not appear to be applicable to the forced gravity drainage process. The saturation shock (from initial oil saturation ahead of the flood front to residual oil saturation immediately behind the front) does not appear to be representative of the reservoir mechanics during forced gravity drainage (GAGD), attributable to the presence of oil films, which act as high-speed conduits for oil production. The laboratory studies on gravity drainage (see section 3.1.3) appear to support this view since they stress the importance of thicker and continuous oil films to promote improved film flow and consequently higher gravity drainage recoveries.

The last multiphase mechanism was not apparent from 'model' laboratory fluids used for scaled GAGD floods. This phenomenon was noticed during GAGD Yates corefloods, wherein the color of the produced crude oil started fading towards the end of the flood. The pictorial representation of this phenomenon is shown in Figure 3.87.

The reduced color intensity of the produced oil suggested the possibility of the 'in-situ' oil up gradation and increased API gravity of the produced oil during the GAGD process. The possibility of dilution of the produced oil by the injected solvent was limited, since this oil sample was recovered after the backpressure regulator (at ambient

conditions. Since the injected solvent (CO_2) cannot exist in the liquid phase at ambient conditions, the dilution effect is probably not relevant in this scenario.

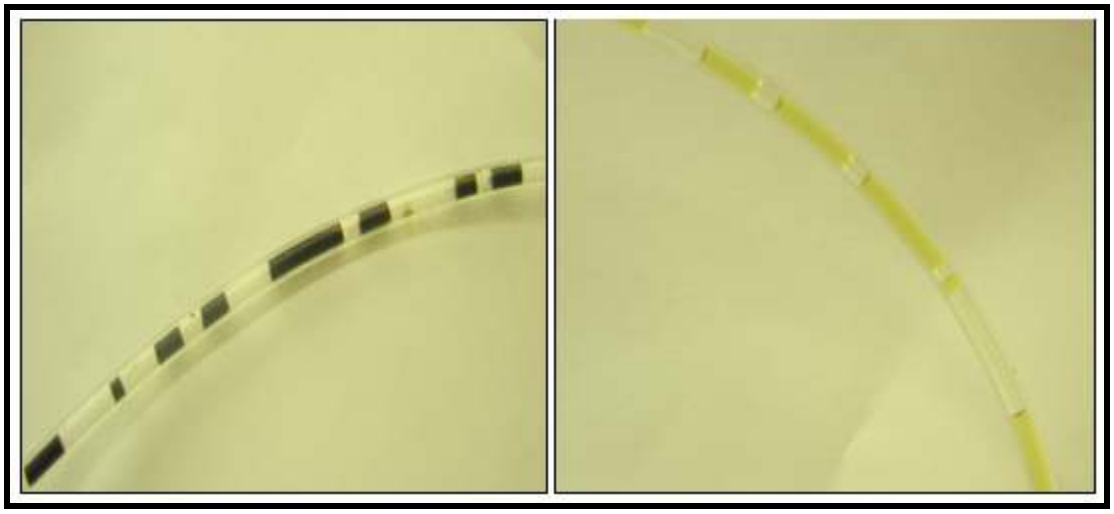

Figure 3.87: Gradual Color Fading of the Produced Oil for GAGD Yates Corefloods

A fully compositional numerical simulation model which included the effects of molecular diffusion and interfacial tension (Darvish et al., 2004: Figure 88) reconfirms the presence of the two mechanisms during forced gravity drainage, film flow gravity drainage and extraction mechanism, and also attests that the film flow gravity drainage phenomenon does not become active (at a given point in the porous medium) till that point comes at the trailing end of the gas front.

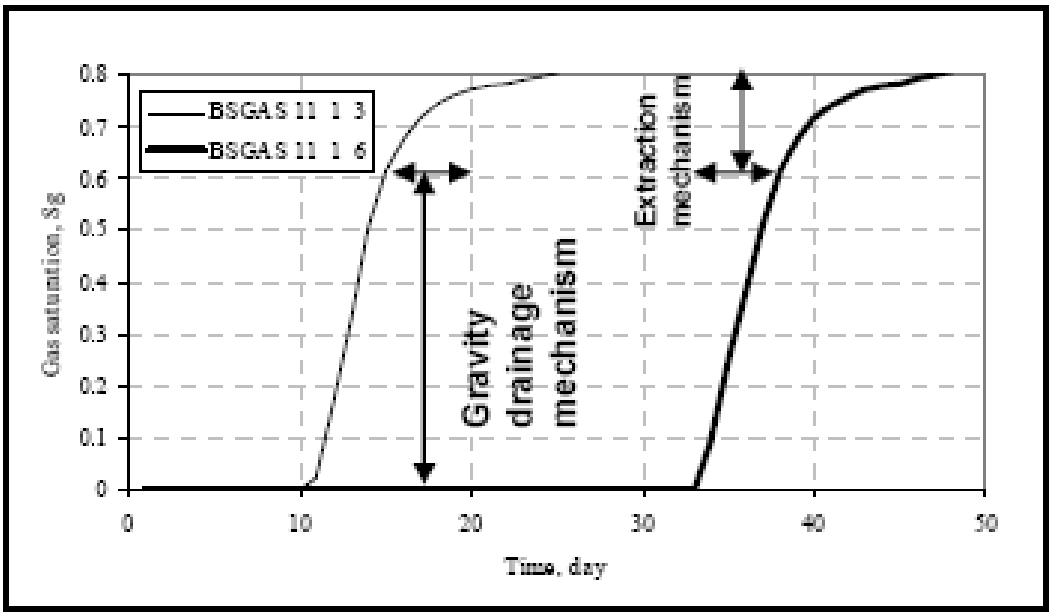

Figure 3.88: Numerical Simulations Demonstrating the Presence of Gravity Drainage Film Flow Mechanism and the Extraction Mechanism in Forced Gravity Drainage (GAGD) Type Flow (Darvish et al., 2004)

3.6.3.2 Inferences and Recommendations

The above discussion clearly suggests that the characterization and modeling GAGD process is a multi-mechanistic approach. The modified L&H model and the proposed multi-step explanation of the GAGD flood mechanism (consisting of Buckley-Leverett flooding till gas breakthrough, film flow phenomenon and extraction mechanism), appears to be well supported by previous work. One of the critical limitations of the modified L&H model is its empirical nature, which significantly limits its scope of application. Additionally, there appear to be many smaller multiphase mechanisms operational during the GAGD process using CO_2 such as: extraction, molecular diffusion, non-linear film flow, solvent (CO_2) dissolution, viscous displacement, capillary retention etc. which need to be better understood. The next step to this work would be the characterization of the contribution of these individual mechanisms in the gravity drainage process and development of an analytical model of the phenomena.

3.7 Conclusions and Recommendations

This section summarizes the conclusions resulting from this experimental study, and also attempts to detail the possibilities for continued research work into gas assisted gravity drainage.

3.7.1 Conclusions

3.7.1.1 Conclusions from Dimensional and Mechanistic Studies on GAGD Process

1. The critical multiphase mechanisms and fluid dynamics operational during gravity stable gas injection (consequently the GAGD process) have been identified and studied in detail in course of this study. The multiphase mechanisms identified to be relevant to the GAGD process are: (i) gravity segregation, (ii) wettability, (iii) spreading coefficient, (iii) miscibility, and (iv) connate and mobile water saturation. The fluid dynamics identified are: (i) gas injection mode and (ii) reservoir heterogeneity effects. Each of these multiphase mechanisms and fluid dynamics have been experimentally investigated in this study.

3.7.1.2 Conclusions from Scaled GAGD Experimentation

1. The GAGD process could potentially outperform all the presently practiced commercial modes of gas injection, namely CGI, WAG and Hybrid-WAG, as verified by scaled laboratory corefloods. While the recoveries in immiscible CGI and WAG scaled corefloods were 33.7% and 56.4% ROIP respectively, the immiscible GAGD coreflood recoveries were 58.37% ROIP. On the other hand, the miscible CGI, WAG Hybrid-WAG and GAGD coreflood recoveries, under miscible flooding conditions, were 97.6%, 72.5%, 93.6% and 100% ROIP respectively. It is important to note that the gas requirements to achieve these recoveries were lowest in the GAGD process.

2. Although miscibility development is beneficial in many GAGD applications, immiscible GAGD employment could generate comparable (in the range of 47.27% to 88.56% ROIP) oil recovery characteristics, which has also been found to be nearly 5 to 8 times miscible WAG performance (average incremental field scale oil recovery reported: 9.4% OOIP). Therefore, miscibility development may not be a controlling economic decision for the commercial GAGD process application.
3. However, it is important to note that all the miscible GAGD corefloods conducted in this study, eventually resulted in near perfect (near 100% ROIP) oil recoveries, irrespective of core properties or experimental conditions.
4. The GAGD flood tertiary recovery factor (TRF) behavior demonstrated significantly higher (nearly 2 to 3 times) gas utilization factors as compared to CGI, WAG and Hybrid-WAG floods. This hastened TRF peaks and asymptotic (non-exponential) decrease in TRF values throughout the life of the GAGD flood, as compared to steep declines in TRF for WAG floods, indicates sustained and superior gas utilization.
5. The exponential pressure drop decrease observed in GAGD corefloods, as against the sustained high pressure drops during CGI and WAG floods, suggests lower injectivity problems during field implementation of the GAGD process. The rapid approach of the flood pressure drop to absolute permeability pressure drop values is also indicative of the higher sweep efficiencies of the GAGD flood.
6. Comparable oil recovery patterns in widely varied experimentation systems, ranging from uniform porous media (Berea sandstone) to highly heterogeneous fractured cores (Yates reservoir cores (dolomite)), in both miscible and immiscible modes, clearly indicates that GAGD process appears to be immune to the effects of reservoir heterogeneity, a serious concern for horizontal mode gas injections. Additionally, the presence of vertical fractures in the reservoir could be beneficial to the GAGD process as observed from near perfect recoveries for miscible floods, and higher immiscible recoveries of 88.56% and 64.83% ROIP, respectively, for fractured and un-fractured GAGD coreflood experiments.
7. The long core experiment conducted to investigate the possibility of gas bubble control during the GAGD process suggests that: (i) the premature gas breakthrough (due to very high injection rates) very early in the life of the GAGD flood does not negatively influence the ultimate oil recoveries achievable, and that (ii) the gas bubble developed in the reservoir during GAGD flood is definitely controllable via the rate of injection. Furthermore comparable oil recoveries for the variable rate coreflood and constant rate coreflood experiment (72.86% and 64.83% ROIP respectively) suggest that the GAGD recoveries are independent of injection rate (provided they are below the critical injection rate)

3.7.1.3 Conclusions from Conceptual Studies on GAGD Process

1. Preliminary mechanistic and dynamic differences between the drainage and displacement phenomenon have been identified and a new mechanism to characterize the GAGD process fluid mechanics (consisting of Buckley-Leverett flooding till gas breakthrough, film flow phenomenon and extraction mechanism) has been proposed.
2. To incorporate the relative variation in the capillary, viscous and buoyancy forces into a single parameter and to provide with a common comparison and prediction tool, a new dimensionless number [$N_G + \{(\rho_G/\rho_O)*(N_C+N_B)\}$] has been identified. Good correlation between the newly proposed number and GAGD recoveries was observed. More importantly, the ability of this correlation to match immiscible as well as miscible GAGD flood performance makes it a useful tool for predicting GAGD oil recoveries.
3. The Richardson and Blackwell analytical model was successfully applied to predict the ultimate oil recoveries for the GAGD process, within 6.4% error.
4. Since the Richardson and Blackwell model could not predict the dynamic GAGD behavior, an empirical Li and Horne model (developed for free gravity drainage applications) was used. Although this model predicted the dynamic behavior of free GAGD process, it was found to over predict the forced GAGD oil recoveries.
5. A new parameter (Ze^*) was therefore introduced in the Li and Horne model for improved prediction of the dynamic GAGD flood behavior. The introduction of this parameter resulted in an accurate model (although empirical) to predict GAGD oil recoveries.

3.7.2 Recommendations for Future Work on GAGD Process

3.7.2.1 Recommendations for Conceptual and Analytical Development

1. Detailed study of drainage versus displacement characteristics.
2. Development of an analytical or computational GAGD performance prediction model using simple analytical models.
3. Development of GAGD screening criteria based on rock and fluid characteristics, to enable reservoir screenings prior to GAGD process application (e.g. defining the minimum vertical to horizontal permeability (k_v/k_h) ratio, porosity, oil API gravity, connate water saturation (S_{wc}) or residual oil saturation (S_{or})).
4. Investigation of single-well GAGD applications in reservoirs commonly found in the Gulf of Mexico: thin bedded, laminated sheet sands, shaly sands, highly faulted and complex reservoirs (e.g. a channel-levee complex).
5. Development of a flow regime characterization map for major flow regimes generated during GAGD displacements and their cross-characterization with observed oil recoveries.

6. Tools for pre-prognosis of possible operational and execution problems, such as gas compressibility issues possibly resulting in decreased injectivity during immiscible gas injections.

3.7.2.2 Recommendations for Further Laboratory Experimentation

1. Conducting scaled laboratory GAGD corefloods using different crude oils (with varying fingerprint characteristics such as high ashphaltenes content, high paraffin content, high resin content etc.) at respective reservoir conditions and with reservoir cores, to study the dependence (if any) of the GAGD process performance on crude oil characteristics and oil-gas interactions.
2. Investigation of possibly improved protocols for tertiary GAGD implementation (e.g. producing mobile water before gas injection through horizontal well to decrease the water-shielding effects and improved oil relative permeabilities, etc.)
3. GAGD studies using hydrocarbon and flue gas for offshore and CO_2 sequestration applications.
4. Investigation of reverse GAGD injection for gravity stable pressure and depletion management (PDM) in hydrocarbon gas reservoirs (e.g. injection of water using horizontal well and gravity stable gas production using vertical wells).

3.7.2.3 Recommendations for 2-D/3-D Simulation / Experimental Model Studies

1. Micromodel studies for visualization of oil film flows during GAGD floods.
2. Investigation of the effects of withdrawal rates on GAGD gas chamber characteristics and development.
3. Investigation of the effects of reservoir heterogeneity, shale barriers and poor cement job (channeling) on GAGD gas injectivity and oil recovery.
4. Characterization of reservoir wettability effects on GAGD oil recoveries.
5. Investigation of optimum injection well spacing as well as the true vertical span between injector and producer for GAGD applications.
6. Studies to improve production rates in GAGD process (e.g. by possible variation between the viscous / capillary / gravity force ratios).
7. Investigations of GAGD application in water drive reservoirs (e.g. strong bottom or edge water drives).
8. Investigation of possible improved GAGD oil recovery rates by employment of peripheral water injection in volumetric reservoirs, followed by the double displacement process (DDP) to maximize both microscopic and macroscopic sweep.

References

1. "Country Analysis Brief: United States of America", Short Term Energy Outlook, United States Energy Information Administration (USEIA), U.S. Department of Energy, Washington D.C., May 2005
2. 2000 worldwide EOR Survey Oil and Gas Journal, March 20, 2001.
3. Ahmed, T.: "A Generalized Methodology for Minimum Miscibility Pressure," SPE Paper 39034 presented at the 1997 Latin American and Caribbean Petroleum Engineering Conference and Exhibition, Rio de Janeiro, Brazil, Aug. 30-Sept.3.
4. Aker, E., "A Simulation Model for Two-Phase Flow in Porous Media", Thesis for the Degree of Candidatus Scientiarum, University of Physics, University of Oslo, Norway, Dec, 1996
5. Ali, J.K.: "Predictions of Parachors and Petroleum Cuts and Pseudo Components," Fluid Phase Equilibria, 95 (1994) 383-398.
6. American Standards for Testing and Materials: "Practice for Calculation of Gas Chromatographic Response Factors", method ASTM D4626, May 2005.
7. American Standards for Testing and Materials: "Standard Test Method for Boiling Range Distribution of Petroleum Fractions by Gas Chromatography", method ASTM D2887, July 2004.
8. Anderson, W.G., "Wettability Literature Survey – Part 2: Wettability Measurement," SPE Paper 13933, pp. 1246-62, 1986.
9. Anton Paar Instruction Manual, "DMA HP Density Measuring Cell for High Pressure and High Temperatures", GmbH, Graz, Austria, 2005.
10. Asar, H. and Handy, L.L.: "Influence of Interfacial Tension on Gas/Oil Relative Permeability in a Gas-Condensate System", paper SPE 11740 (1987), paper presented at the 1983 SPE California Regional Meeting, Ventura, March 23-25.
11. Audolfo, H, Jourdan, C A, "Management of Sweep-Efficiency by Gas-Based IOR Methods", SPE 36843, presented at the 1996 SPE European Petroleum Conference held in Milan, Italy, 22-24 October 1996.
12. Ayirala, S C, "Surfactant-induced Relative Permeability Modifications for Oil Recovery Enhancement", MS Thesis, The Craft and Hawkins Department Of Petroleum Engineering, Louisiana State University and A & M College, Baton Rouge, LA, Dec 2002.
13. Ayirala, S. C., "Measurement and Modeling of Fluid-Fluid Miscibility in Multicomponent Hydrocarbon Systems" Ph.D. Dissertation, The Craft & Hawkins Department of Petroleum Engineering, Louisiana State University and A & M College, Baton Rouge, LA 70803, Aug 2005
14. Ayirala, S.C., Xu, W. and Rao, D.N.: "Interfacial Behavior of Complex Hydrocarbons at Elevated Pressures and Temperatures", The Canadian Journal of Chemical Engineering, February 2006, volume 84.

15. Backmeyer, L. A., Guise, D. R., MacDonnell, P. E., Nute, A. J., "The Tertiary Extension of the Wizard Lake D-3A Pool Miscible Flood" SPE 13721, presented at the 1984 SPE 59th Annual Technical Conference and Exhibition held in Houston, Texas, September 16-19, 1984

16. Bangla, V K, Yau, F, Hendricks, G R, "Reservoir performance of a Gravity stable vertical CO_2 miscible flood: Wolfcamp reservoir, Wellman Unit", SPE 22898, presented at the 66th annual technical conference and exhibition of the Society of Petroleum Engineers, held in Dallas, TX, Oct 6-9, 1991.

17. Barkve, T., Firoozabadi, A., "Analysis of reinfiltration in fractured porous media" SPE 24900, presented at SPE 67th Annual Technical Conference and Exhibition, Washington, DC, Oct 4-7, 1992

18. Behbahaninia, A.R.: "A Universal Set of Weight Factors for Tuning Peng-Robinson Equation of State," paper presented at the Petroleum Society's Canadian International Petroleum Conference 2001, Calgary, Alberta, Canada, June 12-14, 2001.

19. Bellavance, J. F. R., "Dollarhide Devonian CO_2 Flood: Project Performance Review 10 Years Later" SPE 35190, presented at the SPE Permian Basin Oil and Gas Recovery Conference, Midland, TX, Mar 27 – 29, 1996

20. Benham, A.L., Dowden, W.E. and Kunzman, W.J.: "Miscible Fluid Displacement-Prediction of Miscibility," Petroleum Transactions Reprint Series No. 8, Society of Petroleum Engineers of AIME (1965) 123.

21. Benmekki, E H, and Mansoori, G. A., "Accurate vaporizing gas-drive minimum miscibility pressure prediction", SPE 15677, Presented at the 61st Annual Technical Conference and Exhibition of the Society of Petroleum Engineers held in New Orleans, LA October 5-8, 1986.

22. Blanco, A.M. and Ortega, J.: "Experimental Study of Miscibility, Density and Isobaric Vapor-Liquid Equilibrium Values for Mixtures of Methanol in Hydrocarbons (C5, C6)," Fluid Phase Equilibria, 122 (1996) 207-222.

23. Blunt, M., Zhou, D and Fenwick, D., "Three-Phase Flow and Gravity Drainage in Porous Media," Transport in Porous Media, 20, 77-103, 1995.

24. Blunt, M.J., "An Empirical Model for Three-Phase Relative Permeability, SPE 67950, revised for publication from paper SPE 56474, presented at the 1999 SPE Annual Technical Conference and Exhibition held in Houston, 3-6 October."

25. Brigham, W. E., "Mixing Equations in Short Laboratory Cores", SPE Journal, Feb 1974, pp. 91 – 99, Trans AMIE v. 257

26. Brock, H.L. and Bird, R.B.: "Surface Tension and Principle of Corresponding States," AIChE J., 1 (1955) 174-177.

27. Brooks, R. H., Corey, A. T., "Properties of Porous Media Affecting Fluid Flow", J. Irrig. Drain., Div., Am. Soc. Civ. Eng., 92(2), 1966

28. Buckingham, E., “Model Experiments and the Forms of Empirical Equations” Trans. A.S.M.E. 37, 1915, pp. 263-296

29. Buckingham, E., “On Physically Similar Systems: Illustrations of the Use of Dimensional Equations”, Phys. Review 4, 1914, pp. 345-376

30. Buckingham, E., “The Principle of Similitude”, Nature 96, 1915, pp. 396-397

31. Buckley, J S, Morrow, N R, “Characterization of Crude Oil-wetting Behavior by Adhesion Tests”, SPE 20263 presented at the 1990 SPE/DOE Enhanced Oil Recovery Symposium, Tulsa, OK, April 22-25, 1990.

32. Buckley, S. E., Leverett, M. C., “Mechanism of Fluid Displacement in Sands”, Petrol Trans AIME 146, 1942, pp. 107–116

33. Butler, R. M., “Gravity Drainage to Horizontal Wells”, JCPT – 92 – 04 – 02, presented at the 42nd Annual Technical Meeting, of the petroleum society, Apr 1992, vol.31, No.4

34. Campanelli, J.R. and Wang, X.: “Dynamic Interfacial Tension of Surfactant Mixtures at Liquid - Liquid Interfaces,” J. Colloid and Interface Sci., 213 (1999) 340-351.

35. Cardenas, R. L., Alston, R. B., Nute, A. J., Kokolis, G. P., “Laboratory Design of a Gravity Stable, Miscible CO2 Process,” SPE 10270, presented at the 56th Annual Fall Technical Conference and Exhibition of the SPE of AIME, held in San Antonio, TX, October 5-7, 1981

36. Cardwell, W. T., Parsons, R. L., “Gravity Drainage Theory,” Trans. AIME 179, 1949

37. Carey, B.S., “The Gradient Theory of Fluid Interfaces,” PhD Dissertation, University of Minnesota, Minneapolis, 1979.

38. Carlos Alvarez, Eduardo Manrique and Vladimir Alvarado, “WAG pilot at VLE field and IOR opportunities for mature fields at Maracaibo Lake”, SPE 72099, presented at the SPE Asia Pacific Improved Oil Recovery Conference held in Kuala Lumpur, Malaysia, 8-9 October 2001.

39. Carlson, L. O., “Performance of Hawkins Field Unit under Gas Drive-Pressure Maintenance Operations and Development of an Enhanced Oil Recovery Project,” SPE 17324, presented at the SPE/DOE Enhanced Oil Recovery Symposium held in Tulsa, Oklahoma, April 17-20, 1988

40. Catalan, L. J. J., Dullien, F. A. L., Chatzis, I., “The Effects of Wettability and Heterogeneities on the Recovery of Waterflood Residual Oil with Low Pressure Inert Gas Injection Assisted by Gravity Drainage”, SPE Advanced Technology Series, 2, No. 2, 1994

41. Caudle, B.H. and Dyes, A.B., “Improving Miscible Displacement by Gas-Water Injection”, Transactions of the American Institute of Mining, Metallurgical, and Petroleum Engineering, 213 (1958), pp. 281-284

42. Chalier, G., Giry, V., Madaoui, K., Sakthikumar, S., Maquignon, P. H., “Three Phase Oil Relative Permeability Determination As A Key Point In The Evaluation Of A Tertiary Gas Gravity Drainage Project”, SPE 30761, presented at the SPE

Annual technical conference and exhibition of the Society of Petroleum Engineers, held in Dallas, TX, Oct 22-25, 1995

43. Chandler, M., "Linear Algebra", Course Notes, University of Missouri, Rolla, Fall 2003

44. Chang, Y. B., Coat, B. K., Nolen, J. S., "A Compositional Model for CO2 Floods Including CO2 Solubility in Water", SPE 35164, Presented at the 1996 Permian Basin Oil and Gas Recovery Conference, Midland, Texas, 27-29 Mar1996

45. Chang, Y.C. and Moulton, R.W.: "Quaternary Liquid Systems with Two Immiscible Liquid Pairs," Industrial Engineering Chemistry, 45 (1953) 2350-2361.

46. Chatzis, I, Kantzas, A, Dullien, F A L, "On the investigation of gravity assisted inert gas injection using micro models, long Berea cores and computer assisted tomography", SPE 18284, presented at the 63rd annual technical conference and exhibition of the Society of Petroleum Engineers, held in Houston, TX, Oct, 2-5, 1988.

47. Chavepeyer, G., Platten, J.K., Ouazzani, M.T., Glinski, J. and Cornu, D., J. Colloid Interface Sci., 157 (1993) 278.

48. Christensen J.R., M. Larsen, H. Nicolaisen, "Compositional Simulation of Water-Alternating-Gas Processes, SPE 62999, presented at the 2000 SPE Annual Technical Conference and Exhibition held in Dallas, Texas, 1-4 October 2000."

49. Christensen, J R, Stenby, E H, Skauge, A, "Review of the WAG field experience", SPE 71203, revised paper 39883, presented at the 1998 SPE International petroleum conference and exhibition of Mexico, Villhermosa, March 3-5, 1998.

50. Clever, H.L. and Chase, W.E., Jr.: "Thermodynamics of Liquid Surfaces, Surface Tension of n-hexane-cyclohexane mixtures at 25, 30 and 35o C," J. Chem. Eng. Data, 8 (1963) 291-292.

51. Coats, K.H. and Smart, G.T.: "Application of a Regression-Based EOS PVT Program to laboratory Data," SPE Reservoir Engineering Journal, 1 (1986) 277-299.

52. Coats, K.H.: "Simulation of Gas Condensate Reservoir Performance," JPT, 40 (1988) 1870-1886.

53. Coll, C., Muggeridge, A. H., and Jing, X. D., "Regional Upscaling: A New Method to Upscale Waterflooding in Heterogeneous Reservoirs for a Range of Capillary and Gravity Effects", SPE 59337, presented at 2000 SPE/DOE Improved Oil Recovery Symposium, Tulsa, OK, Apr 3 – 5, 2000

54. Computer Modelling Group Ltd., Winprop Phase Property Program, Calgary, Canada, 2002.

55. Cornelisse, P.M.W., Peters, C.J. and de Swaan Arons, J.: "Application of the Peng-Robinson Equation of State to Calculate Interfacial Tensions and Profiles at Vapor-Liquid Interfaces," Fluid Phase Equilibria, 82 (1993) 119-129.

56. Craig Jr., F. F., "Reservoir Engineering Aspects of Waterflooding", Monograph Vol. 3, SPE Textbook Series, Richardson, TX, 1993.

57. Craig, F.F., Sanderlin, J.L., Moore, D.W and Geffen, T.M., "A Laboratory Study of Gravity Segregation in Frontal Drives," Trans. AIME, (1957) 210, 275-281.

58. Crawford H. R., Neill G. H., Bucy B. J., Crawford, P. B., "Carbon Dioxide A Multipurpose Additive for Effective Well Stimulation", Journal of Petroleum Technology, Mar 1963, pp. 237

59. Dake, L. P., "The Practice of Reservoir Engineering", Elsevier Science B.V., 1981

60. Danesh, A., Krinis, D., Harderson, G. D., Peden, J. M., "Pore-Level Visual Investigation of Miscible and Immiscible Displacements", J. of Pet. Sci. and Eng., vol. 2, no. 3, 1989

61. Danesh, A., PVT and Phase Behavior of Petroleum Reservoir Fluids, Elsevier Science B.V., Amsterdam (1998).

62. Danesh, A.S., Dandekar, A.Y., Todd, A.C. and Sarkar, R.: "A Modified Scaling Law and Parachor Method Approach for Improved Prediction of Interfacial Tension of Gas-Condensate Systems," SPE Paper 22710 presented at the 66th SPE Annual Technical Conference and Exhibition, Dallas, TX, October 6-9, 1991.

63. Darvish, G. R., Lindeberg, E., Kleppel, J., Torsaeter, O., "Numerical Simulations For Designing Oil/CO2 Gravity-Drainage Laboratory Experiments of A Naturally Fractured Reservoir", EOR-OG 320, presented at the 7th International Conference on Greenhouse Gas Control Technologies, Vancouver, Canada, Sep 5 – 9, 2004.

64. Da-Sle, W. J., Guo, D. S., "Assessment of a Vertical Hydrocarbon Miscible Flood in the Westpem Nisku D Reef," SPE Reservoir Engineering, May 1990, pp. 147-154

65. Dawe, R. A., "Reservoir Physics at the Pore Scale", Commemoration volume of 75 years of oil field science at the Royal School of Mines, Imperial College of Science and Technology, University of London, 1990

66. Dawe, R. A., Correspondence with Dr. D. N. Rao, Imperial College, Sept 1992

67. DesBrisay, C. L., Ghussein, F. E., Holst, P. H., "Review of Miscible Flood Performance, Intisar "D" field, Socialist People's Libyan Arab Jamahiriya," SPE 10245, presented at the 56th Annual Fall Technical Conference and Exhibition of the Society of Petroleum Engineers of AIME, held in San Antonio, TX, Oct 5 - 7, 1981

68. DesBrisay, C. L., Gray, J. W., Spivak, A., "Miscible Flood Performance of the Intisar "D" field, Libyan Arab Republic," SPE 5080, SPE - Journal of Petroleum Technology, August 1975, pp. 935 – 943

69. Diamant, H., Ariel, G. and Andelman, D.: "Kinetics of Surfactant Adsorption: the Free Energy Approach," Colloids and Surfaces A: Physicochemical and Eng. Aspects, 183-185 (2001) 259-276.

70. Dietz, D. N., "A Theoretical Approach to the Problem of Encroaching and Bypassing Edge Water," Proc., Koninklijke Nederlandsche Akad Wetenschap, Vol. B56, 1953, pp.83

71. Dijke, van, M.I.J., K.S. Sorbie, M. Sohrabi, D. Tehrani and A. Danesh, "Three-phase flow in WAG processes in mixed-wet porous media: pore-scale network simulations and comparison with micro model experiments" SPE 75192, at the SPE/DOE Thirteenth Improved Oil Recovery Symposium held in Tulsa, Oklahoma, 13-17 April 2002."

72. Donahue, D.J. and Bartell, F.F, J. Phys. Chem., 56 (1952) 480.

73. Dorshow, R.B.: "The Simultaneous Measurement of Interfacial Tension and Oil Viscosity at Reservoir Conditions for Prudhoe Bay Fluids by Surface Laser Light Scattering Spectroscopy," SPE Advanced Technology Series, 3 (1995) 120-128.

74. Dumore, J. M., "Stability Considerations in Downward Miscible Displacements", SPE Journal, Dec 1964, pp. 356 – 362, Trans AIME 231

75. Dumore, J. M., Schols, R. S., "Drainage Capillary Pressure Functions and the Influence of Connate Water", SPE Journal, Oct 1974

76. Dykstra, H., "The Prediction of Oil Recovery by Gravity Drainage", Journal of Petroleum Technology, May 1978

77. Edwards, J. T., Honarpour, M. M., Hazlett, M., Cohen, A., Membere, F., Pebdani, C., Clarton, R., Al-Hussainy, "Validation of Gravity-dominated relative permeability and residual oil saturation in a giant oil reservoir", SCA 9903, presented at the 1998 SPE ATCE at New Orleans, LA, Sept 27-30, 1998

78. Ekrann, S., "An Analysis of Gravity-Segregated Piston-Like Displacement in Stratified Reservoirs," SPE Reservoir Engineering, Feb 1992, pp. 143-148

79. Elsharkawy, A.M., Poettmann, F.H. and Christiansen, R.L.: "Measuring CO_2 Minimum Miscibility Pressure: Slim-Tube or Rising-Bubble Method?" Energy & Fuels, 10 (1996) 443-449.

80. Eng, J H, Bennion, D B, Strong, J B, "Velocity Profiles in perforated completions", Journal Of Canadian Petroleum Technology, Oct 1993, Vol. 32, No. 8, pp. 49 – 54.

81. Enick, R M, Beckman, E J, Shi, C, Huang, Z, Xu, J, Kilic, S, "Direct thickeners for CO_2", SPE 59325, presented at the 2000 SPE/DOE Improved oil recovery symposium held in Tulsa, OK, April, 3-5, 2000.

82. EOR Survey, Oil and Gas Journal, Apr 15, 2002

83. EOR Survey, Oil and Gas Journal, Apr 12, 2004

84. Fanchi, J.R.: "Calculation of Parachors for Compositional Simulation: An Update," SPE Reservoir Engineering, (1990) 433-436.

85. Farouq Ali, S. M., "The unfulfilled promise of EOR – What lies ahead?" SPE – Turkey Section, TPAO, National Oil and Natural Gas Company of Turkey, September 2003

86. Fawcett, M.J.: "Evaluation of Correlations and Parachors to Predict Low Interfacial Tension in Condensate Systems," SPE Paper 28611 presented at the 69th SPE

Annual Technical Conference and Exhibition, New Orleans, LA, September 25-28, 1994.

87. Fayers, F.J, and Lee, S: "Crossflow Mechanisms by Gas Drive in Heterogeneous Reservoirs," SPE Paper 24934 presented at the 67th SPE Annual Technical Conference and Exhibition, Washington, DC, October 4-7, 1992.

88. Filoco, P R, Sharma, M M, "Effect of brine salinity and crude-oil properties on oil recovery and residual oil saturations", SPE 65402, Presented at 1998 SPE Annual Technical Conference and Exhibition, held in New Orleans, LA 27-30 Sept 1998.

89. Firoozabadi, A. and Aziz, K.: "Analysis and Correlation of Nitrogen and Lean Gas Miscibility Pressure," SPE Reservoir Engineering Journal, 1 (1986) 575-582.

90. Fleming, P.D. and Vinatieri, J.E.: "The Role of Critical Phenomena in Oil Recovery Systems Employing Surfactants," J. Colloid Interface Sci. 81 (1981) 319.

91. Fox, R. W., and McDonald, T. A., "Introduction to Fluid Mechanics", J. Wiley, 1998

92. Geertsma, J., Croes, G. A., Schwarz, N., "Theory of Dimensionally Scaled Models of Petroleum Reservoirs," Pet. Tran. AIME, VOL. 207, 1956

93. Gillham, T., Cerveny, B., Turek, E., "West Hackberry Tertiary Project", Annual Report Sept 3, 1994 – Sept 2, 1995, DOE Contract # DE-FC22-93BC-14963, Report DOE/BC/14963-10, Amoco Production Co., Houston, TX, May 1996

94. Glaso, O.: "Miscible Displacement: Recovery Tests with Nitrogen," SPERE (Feb. 1990) 61-68.

95. Glinski, J., Chavepeyer, G. and Platten, J.K.: "An Empirical Relation between Mutual Solubilities and Interface Tension for Two Partially Miscible Liquids," Physica B, 193 (1994) 154.

96. Gorell, S B, "Implications of water alternate gas injection profile control and injectivity", SPE 20210, presented at the 1990 SPE/DOE symposium on Enhanced Oil Recovery held in Tulsa, OK, April 22-25, 1990.

97. Grattoni, C. A., Jing, X. D., Dawe, R. A., "Dimensionless Groups For Three Phase Gravity Drainage Flow In Porous Media", Journal of Petroleum Science and Engineering, 29 (2001), pp. 53 – 65

98. Graue, D.J. and Zana, E.T.: "Study of a Possible CO_2 Flood in Rangely Field," JPT (July 1981) 1312-1318.

99. Green, D W, Willhite, G P, "Enhanced oil recovery", SPE Textbook series, Volume 6, 1998.

100. Gunawan, S., Caie, D., "Handil Field: Three years of lean gas injection into water flooded reservoirs", SPE 57289, presented at the 1999 SPE Asia Pacific Improved Oil Recovery Conference held in Kuala Lumpur, Malaysia, Oct 25-26, 1999

101. Hadlow, R E, "Update of Industry experience with CO_2 Injection", SPE 24928, presented at 1992 SPE annual technical conference and exhibition, Washington D C, Oct 4-7,1992.

102. Hagen, S. and Kossack, C.A.: "Determination of Minimum Miscibility Pressure Using a High-Pressure Visual Sapphire Cell," paper SPE 14927 presented at the 1986 SPE/DOE Enhanced Oil Recovery Symposium, Tulsa, OK, April 20-23.

103. Hagoort, J., "Oil Recovery by Gravity Drainage," SPE 7424, June 1980, 139-150.

104. Hair, M.L., Leyden, D.E. (Ed.), "Silanes, Surfaces and Interfaces," (pp. 25-41). New York, USA: Gordon and Breach Science Publishers, 1986.

105. Henriquez, A., Jourdan, C. A., "Management of sweep efficiency by gas based IOR methods", SPE 36843, 1996 SPE European Petroleum Conference, Milan, Italy, October 22 – 24, 1996

106. Hill, D G, "Clay Stabilization – Criteria for best performance", SPE 10656, presented at the SPE formation damage control symposium, held in Lafayette, LA, Mar 24-25, 1982.

107. Hill, S., "Channeling in Packed Columns", Chemical Engineering Science, no. 6 - 1, 1952, pp. 247-253

108. Hinderaker, L., Utseth, R. H., Hustad, O. S., Kvanvik, B. A., and Paulsen, J. E., "RUTH – A comprehensive Norwegian R&D program on IOR", SPE 36844, Presented at the SPE European Petroleum Conference held in Milan, Italy, Oct 22-24, 1996.

109. Holm, L. W., "CO_2 Slug and Carbonated Water Oil Recovery Processes", Producers Monthly, Sept 6, 1963

110. Holm, L.W. and Josendal, V.A.: "Discussion of a Determination and Prediction of CO_2 Minimum Miscibility Pressure", J. Pet. Tech. (May 1980) 870-871.

111. Holm, L.W., and Josendal, V.A.: "Effect of Oil Composition on Miscible-Type Displacement by Carbon Dioxide", Soc. Pet. Eng. J. (February 1974) 87-88.

112. Holm, L.W., and Josendal, V.A.: "Mechanisms of Oil Displacement by Carbon Dioxide", J. Pet. Tech. (December 1974) 1427-1438.

113. Holm, L.W.: "Miscible Displacement," in H.B. Bradley (Ed.), Petroleum Engineering Hand Book, Society of Petroleum Engineers, Richardson, TX (1987) 1-45.

114. Hough, E.W. and Stegemeier, G.L.: "Correlation of Surface and Interfacial Tension of Light Hydrocarbons in the Critical Region," SPE Journal, 1 (1961) 259-263.

115. Howes, B. J., "Enhanced oil recovery in Canada: Success in progress", Journal of Canadian Petroleum Technology, November – December 80-88, 1988

116. Huang, E T S, Holm, L W, "Effect of WAG injection and wettability on oil recovery during carbon dioxide flooding", SPE 15491, presented at 1986 Annual technical conference and exhibition, New Orleans, LA, Oct 5-8, 1986.

117. Huang, E. T. S., Holm, L. W., “Effect of WAG injection and wettability on oil recovery during carbon dioxide flooding”, SPE 15491, presented at 1986 Annual technical conference and exhibition, New Orleans, LA, Oct 5-8, 1986

118. Huang, J.S. and Kim, M.W.: “Microemulsions near Critical Points,” in: V. Degiorgio, M. Corti (Eds.), Physics of Amphiphiles: Micelles. Vesicles and Microemulsions, North-Holland Physics Publishing, 1985, p. 864.

119. Hugill, J.A. and Van Welsenes, A.J.: “Surface Tension: A Simple Correlation for Natural Gas and Condensate Systems,” Fluid Phase Equilibria, 29 (1986) 383.

120. International Petroleum News and Technology: “Oil & Gas Journal”, PennWell, April, 2006.

121. Islam, M.R., “Emerging Technologies in Enhanced Oil Recovery,” Regional symposium on improved oil recovery in the gulf region 17-19 Dec. 1995.

122. Jackson, D D, Andrews, G L, Claridge, E L, “Optimum WAG ratio Vs Rock wettability in CO_2 flooding”, SPE 14303, presented at 60th Annual technical conference and exhibition of the Society of Petroleum engineers held in Las Vegas, NV, Sept 22-25,1985.

123. Jacobson, H.A.: “Acid Gases and Their Contributions to Miscibility,” JCPT (April-May 1972) 57-59.

124. Jacquin, C. H., Legait, B., Martin, J. M., Nectoux, A., Anterion, F., Rioche, M., “Gravity Drainage in a Fissured Reservoir with Fluids not in Equilibrium”, Journal of Petroleum Science and Engineering, vol. 2, 1989, pp. 217.

125. Jakupsstovu, S. I., Zhou, D., Kamath, J., Durlofsky, L., Stenby, E. H., “Upscaling of miscible displacement processes” Proceedings of the 6th Nordic Symposium on Petrophysics, May 15-16, 2001, Trondheim, Norway

126. Jarrell, P. M., Fox, C. E., Stein, M. H., Webb, S. L., “Practical Aspects of CO2 Flooding”, SPE Monograph, 2002 pp. 220

127. Jayasekera, A. J., Goodyear, S. G., “Improved hydrocarbon recovery in the United Kingdom continental shelf: past, present and future”, SPE 75171, Presented at the SPE/DOE Thirteenth Symposium on Improved Oil Recovery held in Tulsa, OK, Apr 13–17, 2002

128. Jennings, Jr., H.Y.: The Effect of Temperature and Pressure on the Interfacial Tension of Benzene-Water and Normal Decane-Water,” Journal of Colloid and Interface Science, 24 (1967) 323-329.

129. Jensen, T B, Harpole, K J, Osthus, A, “EOR Screening for Ekofisk”, SPE 65124, presented at the 2000 SPE European Petroleum Conference held in Paris, France, 24-25 October 2000.

130. Jessen, K., Michelsen, M.L. and Stenby, E.H.: “Effective Algorithm for Calculation of Minimum Miscibility Pressure,” paper SPE 50632 presented at the 1998 European Petroleum Conference, Hague, Netherlands, Oct. 20-22.

131. Johns, R.T., Fayers, F.J. and Orr Jr., F.M.: "Effect of Gas Enrichment and Dispersion on Nearly Miscible Displacements in Condensing Vaporizing Drives," SPE Advanced Technology Series, 2(2) (1993) 26-34.

132. Johns, R.T., Sah, P. and Solano, R.: "Effect of Dispersion on Local Displacement Efficiency for Multicomponent Enrichment Gas Floods above the MME, SPE Paper 64725 presented at the SPE International Oil and Gas Conference, Beijing, China, November 7-10, 2000.

133. Johnson, R. W., "The Handbook of Fluid Dynamics", CRC Press, 1998

134. Johnson, W. E., Macfarlane, R. M., Breston, J. N., "Changes in Physical Properties of Bradford Crude Oil When Contacted with CO_2 and Carbonated Water", Producers Monthly, Nov 16, 1952

135. Johnston, J. R., "Weeks Island Gravity Stable CO_2 Pilot," SPE 17351 presented at the SPE/DOE Enhanced Oil Recovery Symposium held in Tulsa, Oklahoma, Aril 17-20, 1988

136. Jones, F O, "Influence of Chemical Composition of Water on Clay Blocking of Permeability", SPE 631, Journal of Petroleum Technology (April 1964), 441-446.

137. Kalaydjian, F, Vizika, O, Moulu, J C, "Role of wettability and spreading on gas injection processes under secondary conditions", presented at the 7th European IOR symposium, held in Moscow, Russia, Oct 27-29, 1993.

138. Kantzas, A., Chatzis, I., Dullien, F. A. L., "Mechanisms of capillary displacement of residual oil by gravity assisted inert gas injection", SPE 17506, presented at presented at SPE rocky mountain regional meeting held in Casper, Wyoming, May 11-13, 1988

139. Karim, F, Berzins, T V, Schenewerk, P A, Bassiouni, Z A, Wolcott, J M, "Light oil recovery from cyclic injection: Influence of drive gas, injection rate and reservoir dip, SPE 24336, presented at SPE rocky mountain regional meeting held in Casper, Wyoming, May 18-21, 1992.

140. Kechut, N I, Zain, Z M, Ahmad, N, Anwar, D M, Ibrahim, R D M, "New experimental approaches in minimum miscibility pressure (MMP) determination", SPE 57286, presented at the 1999 SPE Asia Pacific Improved Oil Recovery Conference held in Kuala Lumpur, Malaysia, 25-26 October 1999.

141. Khilar, K C, Vaidya, R N, Fogler, H S, "Colloidally - Induced Fines Release in Porous Media", Journal of Petroleum Technology, July 1990, vol. 4, pp. 213 – 221.

142. King, R. L., Lee, W. J., "An engineering study of the Hawkins (Woodbine) field", SPE 5528, SPE Journal of Petroleum Technology, Feb 1976, pp. 123 – 128

143. Klins, M.A., "Carbon Dioxide Flooding – Basic Mechanisms and Project Design", International Human Resources Development Corporation, Boston, 1984.

144. Krijn, W., Clemens, T., Rijkels, L., "Simulation of Gas/Oil gravity drainage in a stack of interacting blocks: Pseudo relations for a limited number of grid blocks", SPE

77722, presented at the SPE Annual Technical Conference and Exhibition, San Antonio, Texas, September 29 – Oct 2, 2002

145. Kruss User's Manual, Drop Shape analysis, Kruss GmbH, Hamburg 2000.

146. Kulkarni, M. M., "Immiscible and Miscible Gas-Oil Displacements in Porous Media", M.S. Thesis, The Craft & Hawkins Department of Petroleum Engineering, Louisiana State University and A & M College, Baton Rouge, LA, Aug 2003

147. Kulkarni, M. M., "Multiphase Mechanisms and Fluid Dynamics in Gas Injection Enhanced Oil Recovery Processes", PhD Dissertation, The Craft & Hawkins Department of Petroleum Engineering, Louisiana State University, Baton Rouge, LA, Aug 2005

148. Kulkarni, M. M., and Rao, D. N., "Is Gravity Drainage an Effective Alternative to WAG?", American Institute of Chemical Engineers' 2004 Annual Meeting, Austin, TX, Nov 7 –12, 2004.

149. Kulkarni, M. M., and Rao, D. N., "Is there a 'Happy-Medium' between Single Slug and Water-Alternating-Gas (WAG) Processes?", 11th IORS, Mumbai, India, Sept 6 – 7, 2004

150. Kulkarni, M. M., Rao, D. N., "Experimental Investigation of Miscible and Immiscible Water-Alternating-Gas (WAG) Process Performance", PETROL 1277, Journal of Petroleum Science and Engineering, Being Published in 2005

151. Kuo, S.S.: "Prediction of Miscibility for the Enriched-Gas Drive Process," SPE Paper 14152 presented at the 1985 SPE Annual Technical Conference and Exhibition, Las Vegas, NV, Sept. 22-25.

152. Kwan, M Y, Cullen, M P, Jamieson, P R, Fortier, R A, "A Laboratory Study of Permeability Damage to Cold Lake Tar Sands Cores", Journal of Canadian Petroleum Technology, Vol. 28 (1), Jan-Feb 1989, pp. 56-62.

153. Lake, L.W., Enhanced Oil Recovery, Prentice-Hall Englewood Cliffs, NJ (1989) 234.

154. Larsen J.K., N. Bech, and A. Winter, " Three-Phase Immiscible WAG Injection: Micro model Experiments and Network Models, SPE 59324,presented at the 2000 SPE/DOE Improved Oil Recovery Symposium held in Tulsa, Oklahoma, 3-5 April 2000."

155. Larsen, J.A., and Skauge, A.: "Methodology for Numerical Simulation with Cycle-dependent Relative Permeabilities," SPEJ, 163- 73, June 1998 (11).

156. Lee, J.I. and Reitzel, G.A.: "High Pressure, Dry Gas Miscible Flood - Brazeau River Nisku Oil Pools," JPT, 34 (1982) 2503-2509.

157. Lee, L.H.: "Relevance of Film Pressures to Interfacial Tension, Miscibility of Liquids, and Lewis Acid – Base Approach," Journal of Colloid and Interface Science, 214 (1999) 64-78.

158. Lee, S.T. and Chien, M.C.H.: "A New Multicomponent Surface Tension Correlation Based on Scaling Theory," SPE Paper 12643 presented at the SPE/DOE Fourth Symposium on Enhanced Oil Recovery, Tulsa, OK, April 15-18, 1984.

159. Lenormand, R., Touboul, E., Zarcone, C., "Numerical Models and Experiments of Immiscible Displacements in Porous Media", Journal of Fluid Mechanics, Vol. 189, 1988, pp. 165

160. Lepski, B., Bassiouni, Z. A., "Screening of oil reservoirs for gravity assisted gas injection", SPE 39659, presented at 1998 SPE/DOE Improved Oil Recovery Symposium held in Tulsa, OK, April 19-22,1998

161. Lepski, B., Bassiouni, Z., and Wolcott, J., "Second-Contact Water Displacement Oil Recovery Process", SPE 35360, presented at the SPE/DOE Symposium on Enhanced Oil Recovery, Tulsa, OK, Apr 21 – 24, 1996

162. Leverett, M. C., "Capillary Pressure Behavior in Porous Solids", Trans. Soc. Pet. Eng. of AMIE, 142, 1941, pp. 152-169

163. Lewis, O.J., "Gravity Drainage in Oil Fields," Trans. AIME, volume 155, pp. 133, 1944.

164. Li, D., Lake, L. W., "Scaling Fluid Flow Through Heterogeneous Permeable Media", SPE 26648, SPE Advanced Technology Series, Vol. 3. No. 1, 1993

165. Li, H., Putra, E., Schechter, D. S., Grigg, R. B., "Experimental Investigation of CO2 Gravity Drainage in a Fractured System" SPE 64510, presented at the SPE Asia Pacific Oil and Gas Conference and Exhibition held in Brisbane, Australia, Oct 16 – 18, 2000

166. Li, K., Horne, R. N., "Prediction of Oil by Gravity Drainage", SPE 84184, presented at the SPE ATCE, Denver, CO, Oct 5 – 8, 2003

167. Longeron, D. G., Kalaydjian, F., Bardon, C., Desremaux, L. M., "Gas/oil capillary pressure: Measurements and reservoir conditions and effect on gas-gravity drainage", SPE 28612, presented at the SPE Annual technical conference and exhibition of the Society of Petroleum Engineers, held in New Orleans, LA, Sept 25-28, 1994

168. Luan, Z., "Some Theoretical Aspects of Gravity Drainage in Naturally Fractured Reservoirs", SPE 28641, presented at the SPE ATCE, New Orleans, LA Sep 25-28, 1994

169. Lui, C., "Dimensional Analysis", Course Notes ME503 Viscous Fluid Flow, Rose-Hulman Institute of Technology, Fall 2003

170. Macleod, D.B.: "On a Relation between Surface Tension and Density," Trans. Faraday Soc., 19 (1923) 38-42.

171. Mahaffey, J. L., Rutherford, W. M., Matthews, C. S., "Sweep Efficiency by Miscible Displacement in a Five-Spot", SPE 1233, SPE Journal, Mar 1966

172. Mannhardt, K., The Measurement of Interfacial Tension by the Spinning Drop Apparatus, Technical Report Submitted to Petroleum Recovery Institute, Calgary, Canada, Mar. 13 (1987).

173. Martin David, F. and Taber, J.J: "Carbon Dioxide Flooding", paper SPE 23564, JPT (April 1992).

174. Martin, J. W., "Additional Oil Production through Flooding with Carbonated Water", Producers Monthly, Jul 18, 1951

175. Matthews, C.S. and Lefkovits, H.C.: "Gravity Drainage Performance of Depletion-Type Reservoirs in the Stripper Stage," Trans., AIME, 207 (1956), 265-274.

176. McCain, W.D., Jr., "The Properties of Petroleum Fluids," PennWell Publishing Company, Tulsa, Oklahoma, 1990.

177. McCoy, T F, Reese, D E, Johnson, PG, "Depletion Performance of Poorly Stimulated Layered Reservoirs without Crossflow", SPE 59757, presented at the 2000 SPE/CERI Gas Technology Symposium held in Calgary, Alberta Canada, 3-5 April 2000.

178. McGuire, P.L. and Moritz Jr., A.L.: "Compositional Simulation and Performance Analysis of the Prudhoe Bay Miscible Gas Project," SPE Reservoir Eng., 7 (1992) 329.

179. McKean, T A M, Thomas, A H, Chesher, J R, Weggeland, M C, "Schrader bluff CO_2 EOR evaluation", SPE 54619, presented at the 1999 SPE western region meeting held in Anchorage, Alaska, 26-26 May 1999.

180. Meszaros, G., Chakma, A and Islam, M.R., "Scaled Model Studies and Numerical Simulation of Inert Gas Injection with Horizontal Wells", SPE 2059, Presented at the annual technical conference and exhibition of the SPE, New Orleans, LA, September 23-26, 1990.

181. Meszaros, G., Chakma, A., Zha, K. N., Islam, M. R., "Scaled model studies and numerical simulation of inert gas injection with horizontal wells", SPE 20529, presented at the 65th SPE annual technical conference and exhibition, held in New Orleans, LA, Sept 23-26, 1990

182. Metcalfe, R.S. and Yarborough, L.: "The Effect of Phase Equilibria of CO_2 Displacement Mechanism", Soc. Pet. Eng. J. (August 1979) 242-252; Trans., AIME, 267.

183. Moissis, D. E., Miller, C. A., Wheeler, M. F., "A parametric study of viscous fingering in miscible displacement by numerical simulation", Technical report 87-18, Rice University, Houston TX, June 1987, Available: Numerical Simulation in Oil Recovery, Minneapolis, Minn., 1986, pp. 227-247, Springer, New York, 1988

184. Monroe, W.W., Silva, M.K., Larsen, L.L. and Orr F.M., Jr.: "Composition Paths in Four-Component Systems: Effect of Dissolved Methane on 1D CO_2 Flooding Performance," SPE Reservoir Engineering Journal (Aug. 1990) 423-432.

185. Moritis G (2000). EOR Survey: EOR weathers low oil prices. Oil and Gas Journal, March 20, 2000.

186. Moritis, G, "Impact of production and development RD&D ranked", Production Editor, Oil and Gas Journal, Oct. 30, 1995.Vol 93, Issue 44.

187. Moritis, G., "Special Report: EOR Survey", Oil and Gas Journal, Volume 102.14, Apr 12, 2004

188. Moritis, G.: "CO_2 Injection Gains Momentum," Oil and Gas Journal, 104 (14), 2006.

189. Moritis, G.: "EOR Continues to Unlock Oil Resources," Oil and Gas Journal, 102 (2004) 45-65.

190. Morrow, N.R., "Wettability and Its Effect on Oil Recovery," SPE Paper 21621, pp.1476-84, 1990.

191. Moulu, O. Vizika, P. Egermann and F. Kalaydjian, "A New Three-Phase Relative Permeability Model For Various Wettability Conditions, SPE 56477,presented at the 1999 SPE Annual Technical Conference and Exhibition held in Houston, Texas, 3-6 October 1999."

192. Muggeridge, A. H., Jackson, M. D., Agbehi, O., Al-Shuraiqi, H., Grattoni, C. A., "Quantifying Bypassed Oil in the Vicinity of Discontinuous Shales during Gravity-Dominated Flow", SPE 94134, presented at SPE Europec / EAGE Annual Conference, Madrid Spain, Jun 13-14, 2005

193. Mungan, N, "An evaluation of carbon dioxide flooding", SPE 21762, presented at the SPE Western regional meeting held in Long Beach, CA, March 20-22, 1991.

194. Mungan, N.: "Permeability Reduction through Changes in pH and Salinity", SPE 1283, Journal of Petroleum Technology, December 1965, pp. 1449-1453.

195. Muskat, M., "Physical Principals of Oil Production", McGraw-Hill Book Company, New York, 1949

196. Nahara, G. M., Pozzi, A. L., Blackshear, T. H., "Effect of Connate Water on Gas / Oil Relative Permeabilities for Water-Wet and Mixed-Wet Berea Rock", SPE 20503, presented at the SPE Annual Technical Conference and Exhibition, New Orleans, LA, Sep 1990

197. Nenniger, E., Storrow, J A., "Drainage of Packed Beads in Gravitational and Centrifugal-force Fields", AIChE (1958), 4, No 3, pp. 305

198. Nghiem, L.X. and Heidemann, R.A.: "General Acceleration Procedure for Multiphase Flash Calculations with Application to Oil-Gas-Water Systems," paper presented at the 2nd European Symposium on Enhanced Oil Recovery, Paris, France, November 8-10, 1982.

199. Novakovic, D., "Numerical Reservoir Characterization Using Dimensionless Scale Numbers with Application in Upscaling", Ph.D. Dissertation, The Craft and Hawkins Department of Petroleum Engineering, Louisiana State University and Agricultural & Mechanical College, Aug 2002

200. Nummedal, D., Towler, B., Mason, C., and Allen, M., "Enhanced Oil Recovery in Wyoming: Prospects and Challenges", Prepared for Governor Dave Freudenthal, University of Wyoming, June 15, 2003

201. Nute, A. J., "Design and evaluation of a gravity stable, miscible CO_2 solvent flood, Bay St. Elaine field", SPE 11506, presented at the Middle East Oil technical conference of the Society of Petroleum Engineers, held in Manama, Bahrain, March 14-17, 1983

202. Odd Steve Hustad, "A Coupled Model for Three-Phase Capillary Pressure and Relative Permeability, SPE 63150, presented at the 2000 SPE Annual Technical Conference and Exhibition held in Dallas, Texas, 1-4 October 2000."

203. Office of Technology Assessment (OTA), "Enhanced Oil Recovery Potential in the United States" Congress of the United States, NTIS Order # PB-276594, 1978, 12 Volumes

204. Oren, P. E., Billiotte, J., Pinczewski, W. V., "Mobilization of waterflood residual oil by gas injection for water wet conditions", SPE 20185, SPE Formation Evaluation, March 1992, pp. 70-78

205. Oren, P. E., Pinczewski, W. V., "Effect of Wettability and Spreading on Recovery of Waterflood Residual Oil by Immiscible Gas Flooding", SPE Formation Evaluation, 9 (2), 1994, pp. 149 – 156

206. Orr, F M, Jensen, C M, "Interpretation of Pressure-Composition phase diagrams for CO2/Crude-oil systems", SPE 11125, SPE-J, 1984.

207. Orr, F M, Johns, R T, Dindoruk, B, "Development of Miscibility in Four-Component Vaporizing Gas Drives", SPE 22637, Presented at the 66th Annual Technical Conference and Exhibition of the Society of Petroleum Engineers held in Dallas, TX, October 6-9, 1991.

208. Orr, F M, Silva, M K, "Equilibrium Phase compositions of CO2/Hydrocarbon Mixtures – Part 1: Measurement by continuous multiple – contact experiment", SPE 10726, SPE-J, April 1983.

209. Orr, F.M., Jr., Johns, R.T. and Dindoruk, B.: "Development of Miscibility in Four Component CO2 Floods," SPE Reservoir Engineering Journal (May 1993) 135-142.

210. Oss, van, C.J., Chaudhury, M.K. and Good, R.J.: "Monopolar Surfaces," Adv. Colloid Interface Sci., 28 (1987) 35.

211. Oyno, L., Uleberg, K., Whitson, C. H., "Dry Gas Injection Fractured Chalk Reservoirs – An Experimental Approach", SCA 9527, presented at the 1995 SCA Conference, San Francisco, CA, Aug 20 – 22, 1995

212. Padilla, R. S., Camacho, R. V., "Reservoir Performance under Solution Gas Drive and Gravity Drainage", SPE 92186, presented at the SPE IPC in Mexico, Puebla, Mexico, Nov 8 – 9, 2004

213. Paidin, W.R.: "Physical Model Study of the Effects of Wettability and Fractures on Gas-Assisted Gravity Drainage (GAGD) Performance"; Louisiana State University, Baton Rouge, M.S. Thesis.

214. Pavone, D., Bruzzi, P., Verre, R., "Gravity Drainage at Low Interfacial Tensions", Fifth European Symposium on Improved Oil Recovery, Apr 1989

215. Pederson, K.S. and Fredenslund, A.A.: "An Improved Corresponding States Model for Prediction of Oil and Gas Viscosities and Thermal Conductivities," Chem. Eng. Sci., 42 (1987) 182-186.

216. Pederson, K.S., Thomassen, P. and Fredenslund, A.: "On the Dangers of Tuning Equation of State Parameters," Chemical Engineering Science, 43 (1988) 269-278.

217. Pedrera, B., Bertin, H, Hamon, G., Augustin, A., "Wettability Effect on Oil Relative Permeability During a Gravity Drainage", SPE 77542, presented at the SPE/DOE 13th Symposium on Improved Oil Recovery, Tulsa, OK, Apr 13 – 17, 2002

218. Peng, D.Y. and Robinson, D.B.: "A New Two-Constant Equation of State," Ind. Eng. Chem. Fundam., 15 (1976) 59-64.

219. Perkins, T. K., Johnston O. C., "A Review of Diffusion and Dispersion in Porous Media", SPE Journal, Mar 1963, pp. 70 – 84, Trans AMIE v. 228

220. Petroleum Engineering International, 1995, Figure Reproduced from: Rao, D. N., "An Overview of Gas Injection EOR", Presented at the Graduate Seminar, The Craft & Hawkins Department of Petroleum Engineering, Louisiana State University and A & M College, Baton Rouge, LA, Mar 25, 2004

221. Piper, L. D., Morse, R. A., "Criteria for Displacement by Gas Versus Water in Oil Reservoirs", SPE 10870, SPE Unsolicited Paper, 1982

222. Platt's Oil Guide to Specifications, "Crude Oil Specifications – United States", Energy Market Information Resource, Standard & Poor's Platt's, Official Website, 2005

223. Pozzi, A. L., Blackwell, R. J., "Design of Laboratory Models for Study of Miscible Displacement", SPE 445, presented at the 37th Annual Fall Meeting, Los Angeles, CA, Oct 7 – 10, 1963

224. Prieditis, J., Wolle, C.R., Notz, P.K., "A Laboratory and Field Injectivity Study: CO_2 WAG in the San Andres Formation of West Texas" SPE 22653, presented at the 66th Annual Technical Conference and Exhibition of the Society of Petroleum Engineers held in Dallas, TX, October 6-9, 1991.

225. Quale, O.R.: "The Parachors of Organic Compounds," Chem. Review, 53 (1953) 439-586.

226. Rao, D N, "Gas Injection EOR – A new meaning in the new millennium" Invited article for the Distinguished Author Series, Journal of Canadian Petroleum Technology, Vol. 40, No. 2, pp. 11-18, Feb 2001.

227. Rao, D. N., “Rutherford Stability Criterion”, The Craft & Hawkins Department of Petroleum Engineering, Louisiana State University and A & M College, Baton Rouge, LA

228. Rao, D. N., “The Concept, Characterization, Concerns and Consequences of Contact Angles in Solid-Liquid-Liquid Systems”, Invited paper presented at the Third International Symposium on Contact Angle, Wettability and Adhesion, Providence, Rhode Island, May 20-23, 2002

229. Rao, D. N., Ayirala, S. C., Kulkarni, M. M., and Sharma, A. P., “Development of the Gas Assisted Gravity Drainage (GAGD) Process for Improved Light Oil Recovery”, SPE 89357, Presented at the 2004 SPE/DOE Fourteenth Symposium on Improved Oil Recovery, Tulsa, OK, Apr 17 – 21, 2004

230. Rao, D. N., Girard, M. G., Sayegh, S. G., “The influence of reservoir wettability on waterflood and miscible flood performance”, Journal of Canadian Petroleum Technology, Vol. 31, No. 6, June 1992

231. Rao, D. N., United States Department of Energy Research Proposal, Application 2137, Volume II – Technical Application, Program Solicitation No. DE-PS26-01NT41048 for “Development of Technologies and capabilities for development of Coal, Oil and Gas energy resources” Project titled – “Development and Optimization of Gas Assisted Gravity Drainage (GAGD) process for improved light oil recovery”, Jun 2001

232. Rao, D.N. and Ayirala, S.C.: “Authors’ Response to Comments on A New Mechanistic Parachor Model to Predict Dynamic Interfacial Tension and Miscibility in Multicomponent Hydrocarbon Systems by F.M. Orr and K. Jessen, Article in Press, Journal of Colloid and Interface Science, 2006.

233. Rao, D.N. and Lee, J.I.: “Application of the new Vanishing Interfacial Tension Technique to Evaluate Miscibility Conditions for the Terra Nova Offshore Project”, Elsevier, Journal of Petroleum Science and Engineering 35 (2002) 247-262.

234. Rao, D.N. and Lee, J.I.: “Determination of Gas-Oil Miscibility Conditions by Interfacial Tension Measurements,” Journal of Colloid and Interface Science, 262 (2003) 474-482.

235. Rao, D.N., Mcintyre, F.J., and Fong D.K.: “Application of a New Technique to Optimize Injection Gas Composition for the Rainbow Keg River F Pool Miscible Flood,” JCPT, 38 (1999) 1-10.

236. Rao, D.N.: “A New Technique of Vanishing interfacial Tension for Miscibility Determination,” Fluid Phase Equilibria, 139 (1997) 311-324.

237. Rao, D.N.: “A New Vanishing Interfacial Technique for Miscibility Determination”, Elsevier, Fluid Phase Equilibria (1997), volume 127-139.

238. Rapoport, L.A., “Scaling Laws for Use in Design and Operation of Water-Oil Flow Models,” Trans. AIME, (1954) 204, 143-150.

239. Rappaport, L A, Leas, W J, "Properties of Linear Waterfloods", Trans. AIME, (1953) 198, pp. 139.

240. Rappaport, L. A., Leas, W. J., "Properties of Linear Waterfloods", Trans. AIME, (1953) 198, pp. 139

241. Rathmell, J.J., Stalkup, F.I., and Hassinger, R.C.: "A Laboratory Investigation of Miscible Displacement by Carbon Dioxide", paper SPE 3483 presented at the 1971 SPE Annual Fall Meeting, New Orleans, October 3-6.

242. Ray, M. R., "An Evaluation of known remaining oil resources in the State of Louisiana", Project on Advanced Oil Recovery and the States, Volume III, DOE/BC/14431-1 (Vol. 3), Distribution Category UC-122, Office of Scientific and Technical Information, DOE Information Bridge, Oak Ridge, Tennessee, November 1994

243. Redlich, O. and Kwong, J.N.S., Chem. Rev., 44 (1949) 233.

244. Ren, W., "Application of the Gravity Assisted Tertiary Gas Injection Process", M.Sc. Thesis, University of Alberta, Edmonton, Canada, 2002

245. Ren, W., Cunha, L. B., Bentsen, R., "Numerical Simulation and Screening of Oil Reservoirs for Gravity Assisted Tertiary Gas-Injection Processes", SPE 81006, presented at the SPE Latin American and Caribbean Petroleum Engineering Conference held in Port-of-Spain, Trinidad, West Indies, April 27 – 30, 2003

246. Richardson, J. G., Blackwell, R. J., "Use of Simple Mathematical Models for Predicting Reservoir Behavior", SPE 2928, Journal of Petroleum Technology, Sep 1971

247. Rogers, J. D., Grigg, R. B., "A literature analysis of the WAG injectivity abnormalities in the CO_2 process", SPE 59329, presented at the 2000 review SPE/DOE Improved Oil Recovery symposium on held in Tulsa, OK, April 3-5, 2000

248. Rojas, G., and Farouq Ali, S.M., "Scaled Model Studies of Carbon Dioxide/Brine Injection Strategies for Heavy Oil Recovery from Thin Formations," JCPT, 86-01-07, 1986.

249. Rosen, M.J. and Gao, T.: "Dynamic Surface Tension of Aqueous Surfactant Solutions 5. Mixtures of Different Charge Type Surfactants," J. Colloid and Interface Sci., 173 (1995) 42- 48.

250. Rosenbauer, R J, Koksalan, T, "Experimental determination of the solubility of CO_2 in electrolytes: Application to CO_2 sequestration in deep-saline aquifers", Paper 135-2, presented at the 2002 Denver Annual Meeting, The Geological Society of America, Denver, CO Oct 29, 2002.

251. Ruark, A.E., "Inspectional Analysis: A Method which Supplements Dimensional Analysis," J. of the Mitchell Society, August 1935.

252. Rutherford, W. M., "Miscibility Relationships in the Displacement of Oil by Light Hydrocarbons", SPE 449, SPE Journal, Dec 1962

253. Saidi, A. M., Sakthikumar, S., "Gas Gravity Drainage under Secondary and Tertiary Conditions in Fractured Reservoirs", SPE 25614, SPE Journal, 1993

254. Sajadian, V. A., Tehrani, D. H., "Displacement Visualization of Gravity Drainage by Micromodel", SPE 49557, presented at the 8th Abu Dhabi International Petroleum Exhibition and Conference, Abu Dhabi, UAE, Oct 11-14, 1998

255. Sajadian, V. A., Tehrani, D. H., "Displacement Visualization of Gravity Drainage by Micromodel", SPE 49557, presented at the 8th Abu Dhabi International Petroleum Exhibition and Conference, Abu Dhabi, UAE, Oct 11-14, 1998

256. Sanchez, N L, "Management of Water Alternating Gas (WAG) Injection Projects", presented at the 1999 SPE Latin American and Caribbean Petroleum Engineering Conference held in Caracas, Venezuela, 21-23 April 1999.

257. Schechter, D.S. and Guo, B.: "Parachors Based on Modern Physics and Their Uses in IFT Prediction of Reservoir Fluids," SPE Reservoir Evaluation & Engineering, (1998) 207-217.

258. Scheuerman, R F, Bergersen, B M, "Injection Water Salinity, Formation Pretreatment, and Well operations Fluid Selection Guidelines", Journal of Petroleum Technology, July 1990, pp. 836 – 845.

259. Schramm, L L, Isaacs, E, Singhal, A K, Hawkins, B, Shulmeister, B, Wassmuth, F, Randall, L, Turta, A. Zhou, J, Tremblay, B, Lillico, D, Wagg, B, "Technology Development For Conventional Petroleum Reservoirs", Journal Of Canadian Petroleum Technology, Canadian Advantage 2000, pp. 31 – 46.

260. Sharma, A. P., "Physical Model Experiments of Gas Assisted Gravity Drainage", M.S. Thesis, Louisiana State University and A & M College, Baton Rouge, LA, Aug 2005

261. Sharma, A.P., "Physical Model Experiments of the Gas-Assisted Gravity Drainage Process," M.S. Thesis, LSU - Petroleum Engineering, August 2005.

262. Shook, M., Li, D., and Lake, L. W., "Scaling Immiscible Flow through Permeable Media by Inspectional Analysis", In-Situ 4, 1992, pp. 311 – 349

263. Sidgwick, N.V. and Spurrel, W.J.: "The System Benzene-Ethyl Alcohol-Water between +25o and –5o," Journal of Chemical Society, 117 (1920) 1397-1404.

264. Sigmund, P.M.: "Prediction of Molecular Diffusion at Reservoir Conditions. Part II – Estimating the Effects of Molecular Diffusion and Convective Mixing in Multicomponent Systems," JCPT (July-September 1976) 53-62.

265. Simon, R., Rosman, A. and Zana, E.: "Phase-Behavior Properties of CO_2-Reservoir Oil Systems," SPEJ (Feb. 1978) 20-26.

266. Skauge, A., Eleri, O. O., Graue, A., Monstad, P., "Influence of Connate Water on Oil Recovery by Gravity Drainage", SPE/DOE 27817, presented at the SPE/DOE Ninth Symposium on Improved Oil Recovery, Tulsa, OK Apr 17 – 20, 1994

267. Skauge, A., Paulsen, S., "Rate Effects on Centrifuge Drainage Relative Permeability", SPE 63145, presented at the SPE ATCE, Dallas, TX Oct 1 - 4, 2000

268. Slobod, R. L., Howlett, W. E., "The effects of gravity segregation in studies of miscible displacement in vertical unconsolidated porous media", SPE Journal, March 1964, pp. 1-8

269. Soave, G., Chem. Eng. Sci., 27 (1972)1197.

270. Soroush, H., Saidi, A. M., "Vertical gas oil displacements in low permeability long core at different rates and pressure below MMP", SPE 53221, Presented at the 1999 SPE Middle East Show, Bahrain, February 20 – 23, 1999

271. Spence, A.P. and Ostrander, J.F.: "Comparison of WAG and Continuous Enriched-Gas Injection as Miscible Processes in Sadlerochit Core," SPE Paper 11962 presented at the SPE 58th Annual Technical Conference and Exhibition, San Francisco, CA, USA, Oct. 1983.

272. Stalkup Jr., F I, "Miscible Displacement", Monograph Volume 8, Society of Petroleum Engineers, Henry L Doherty Series, 1985

273. Statement of Mark Maddox, Acting Assistant Secretary for Fossil Energy to the Subcommittee on Energy Policy, Natural Resources and Regulatory Affairs, Committee of Government Reform, U.S. House of Representatives, July 7, 2004

274. Stegemeier, G.L., Laumbach, D.D and Volek, C.W., "Representing Steam Process with Vacuum Models," SPE 6787, SPEJ, 151-174, June 1980.

275. Sternling, C.V. and Scriven, L.E.: "Interfacial Turbulence: Hydrodynamic Instability and Marangoni Effect," AIChE J., 5 (1959) 514-523.

276. Sudgen, S.: "The Variation of Surface Tension with Temperature and Some Related Functions," Journal of Chemical Society, (1924) 32-41.

277. Sukop, M. C., and Or, D., "Invasion Percolation of Single Component, Multi-phase Fluids with Lattice Boltzmann Models", Physica B 338, pp. 298 – 303

278. Supranowicz, R., Butler, R. M., "Vertical confined water drive to horizontal well: Part I: Water and oil of equal densities", Paper # 2, presented at the third technical meeting of the south Saskatchewan section, the petroleum society of CIM, held in Regina, Sept 25 – 27, 1989

279. Taber, J. J., Martin, F. D., Seright, R. S., "EOR screening criteria revisited", SPE/DOE 35385, Presented at SPE/DOE 10th symposium on Improved Oil Recovery, Tulsa, OK, 21-24 Apr 1996

280. Tang, G, Morrow, N R, "Oil recovery by waterflooding and imbibition – invading brine cation valency and salinity", SCA 9911 proceedings of the international symposium of the Society Of Core Analysts, Golden, CO, August 1999.

281. Tanner, C S, Baxley, P T, Crump III, J C, Miller, W C, "Production performance of the Wasson Denver Unit CO2 flood", SPE/DOE 24156, presented at the

SPE/DOE eighth symposium on Enhanced Oil Recovery held in Tulsa, OK, Aug 22-23, 1992.

282. Taylor, K.C. and Nasr-EI-Din, H.A.: "The Effect of Synthetic Surfactants on the Interfacial Behavior of Crude Oil/Alkali/Polymer Systems," Colloids and Surfaces A: Physicochemical and Eng. Aspects, 108 (1996) 49-72.

283. Terwilliger, P. L., Wilsey, L. E., Hall, H. N., Bridges, P. M., Morse, R. A., "An Experimental and Theoretical Investigation of Gravity Drainage Performance," Trans., AIME 192, 1951, pp. 285-296

284. Thomas, F B, Erain, A, Zhou, X, Bennion, D B, Bennion, D W, Okazawa, T, "Does miscibility matter in gas injection?" Journal of Canadian Petroleum Technology, 95-51, Presented at the 46th Annual technical meeting of the Petroleum Society of CIM, in Banff, Alberta, Canada, May 14-17, 1995.

285. Thomas, J, Berzins, T V, Monger, T G, Bassiouni, Z A, "Light oil recovery from cyclic CO2 injection: Influence of gravity segregation and remaining oil", SPE 20531, presented at the 65th Annual technical conference and exhibition of the Society of Petroleum Engineers, held in New Orleans, LA, Sept 23-26, 1990.

286. Tiab, D. & Donaldson, E.C., "Petrophysics – The Theory and Practice of Measuring Reservoir Rock and Fluid Transport Properties," Houston, USA: Gulf Publishing Company, 1996.

287. Tiffin, D. L., Kremesec, V. J., "A mechanistic study of gravity-assisted flooding", SPE/DOE 14895, presented at the SPE/DOE fifth symposium on Enhanced oil recovery of the Society of Petroleum Engineers and the Department of Energy, held in Tulsa, OK, April 20-23, 1986

288. U.S. Geological Survey (USGS), United States Department of the Interior, USGS Fact Sheet FS – 115 – 00, October 2000

289. US Department of Energy website: http://www.energy.gov/

290. Varian Operator's Manual, "CP-3800 GC and CP-8410", Varian Inc., Walnut Creek, CA, 2000-2004.

291. Vijapurapu, C.S. and Rao, D.N.: "The Effect of Rock Surface Characteristics on Reservoir Wettability," in K.L. Mittal (Ed.), Contact Angle, Wettability and Adhesion, Vol.3, VSP International Science Publishers, 2003, pp. 407-426.

292. Vijapurapu, Chandra S, "The Effects Of Rock And Fluids Characteristics On Reservoir Wettability", MS Thesis, The Craft and Hawkins Department Of Petroleum Engineering, Louisiana State University and A & M College, Baton Rouge, LA, Dec 2002.

293. Virnovsky, G. A., Helset, H. M., Skjaveland, S. M., "Stability of Displacement Fronts in WAG Operations," SPE Journal, Dec 1996, pp. 383-394

294. Walsh, B.W. and Orr Jr., F.M.: "Prediction of Miscible Flood Performance, the Effect of Dispersion on Composition Paths in Ternary Systems," In Situ, 14(1) (1990) 19-47.

295. Wang, Y. and Orr, F.M., Jr.: "Calculation of Minimum Miscibility Pressure," paper SPE 39683 presented at the 1998 SPE/DOE Improved Oil Recovery Symposium, Tulsa, OK, April 19-22.

296. Wang, Y. and Peck, D.G.: "Analytical Calculation of Minimum Miscibility Pressure: Comprehensive Testing and Its Application in a Quantitative Analysis of the Effect of Numerical Dispersion for Different Miscibility Development Mechanisms," paper SPE 59378 presented at the 2000 SPE/DOE Improved Oil Recovery Symposium, Tulsa, OK, April 3-5.

297. Weinaug, C.F. and Katz, D.L.: "Surface Tensions of Methane-Propane Mixtures," Industrial Engineering Chemistry, 35 (1943) 239-246.

298. Welge, H. J., "A simplified method for computing oil recovery by gas or water drive", Petrol Trans AIME 195, 1952

299. Whitson, C.H. and Brule, M.R.: Phase Behavior, SPE Henry L. Doherty series, Richardson, TX (2000) 72-73.

300. Wide Range Cryoscope Instruction Manual, "Cryette WRTM", Model 5009, Precision System Inc., Natick, MA, 2004.

301. Wilke, C.R. and Chang, P.: "Correlation of Diffusion Coefficients in Dilute Solutions," AIChE J., 1 (1955) 264-270.

302. Wilke, C.R.: "Diffusional Properties of Multicomponent Gases," Chem. Eng. Progress, 46 (1950) 95-104.

303. Wilke, C.R.: "Estimation of Liquid Diffusion Coefficients," Chem. Eng. Progress, 45 (1949) 218-224.

304. Wylie, P. L., Mohanty, K. K., "Effect of Wettability on Oil Recovery by Near Miscible Gas Injection", SPE 59476, SPE Reservoir Evaluation and Engineering 2(6), Dec 1999

305. Xu, Wei, "Experimental Investigation of Dynamic Interfacial Interactions at Reservoir Conditions", M.S. Thesis, Louisiana State University, Mar 2005

306. Yeh, S W, Ehrilch, Robert, Emanuel, A S, "Miscible-Gas-Flood-induced wettability alteration: Experimental observation and oil recovery implications", SPE 20186, SPE Formation Evaluation, 1992, pp. 167-172.

307. Yildiz, H O, Valat, M, Morrow, N R, "Effect of Brine Composition on Recovery of an Alaskan Crude Oil by Waterflooding", Journal of Canadian Petroleum Technology, 1999, Vol. 38, pp. 26-31.

308. Zick, A.A.: "A Combined Condensing/Vaporizing Mechanism in the Displacement of Oil by Enriched Gases", paper SPE 15493, presented at the 1986 Annual Technical Conference and Exhibition of the SPE, New Orleans, October 5-8.

309. Zuiderweg, F.J. and Harmens, A.: "The Influence of Surface Phenomena on the Performance of Distillation Columns," Chem. Eng. Sci., 9 (1958) 89-103.

310. Zurita, R.A.A. and McCain, Jr., W.D.: "An Efficient Tuning Strategy to Calibrate Cubic EOS for Compositional Simulation," SPE 77382 (Sept., 2002).

4. Technology Transfer Efforts

Numerous technology transfer efforts were undertaken by the LSU-EOR Research Group during this project period from Oct 2002 to date. This project research has yielded 2 doctoral dissertations, 5 master's theses, 16 reviewed journal publications, 20 full-length papers published in international conference proceedings, and 7 presentations in international symposiums.

Additionally, invited presentations were held at:

- The Independent's Day Session at the SPE/DOE IOR Symposium in April 2006.
- The Desk and Derrick Club of Baton Rouge on September 21st, 2006.
- LSU's Saturday Science program on October 7th, 2006.

A two-hour course was also given at the Oil and Natural Gas Corporation Limited (ONGC) in Ahmedabad, India.

This work also helped arrange for a half-day workshop at the Petroleum Club of Shreveport, LA, hosted by the Petroleum Technology Transfer Council (PTTC).

Finally, the technology transfer efforts have resulted in two patent applications and one commercial license of the GAGD process.

4.1 Technical Progress Reports

Eleven Quarterly Technical Progress Reports, 3 Annual Reports, and one Final Technical Report have been prepared and submitted to US-DOE during the project period from October 2002 to December 2006.

4.2 Ph.D. Dissertations

1. Ayirala, S.C., "Measurement and Modeling of Fluid-Fluid Miscibility in Multicomponent Hydrocarbon Systems," Craft and Hawkins Department of Petroleum Eng., Louisiana State University, Baton Rouge, LA 70803, Aug 2005.
2. Kulkarni, M.M., "Multiphase Mechanisms and Fluid Dynamics in Gas Injection Enhanced Oil Recovery Processes", Craft and Hawkins Department of Petroleum Eng., Louisiana State University, Baton Rouge, LA 70803, Aug 2005.
3. Paidin, W.R, Craft and Hawkins Department of Petroleum Eng., Louisiana State University, Baton Rouge, LA 70803, In progress.

4.3 M.S. Theses

1. Mahmoud, T. N. N., "Demonstration and Performance Characterization of the Gas Assisted Gravity Drainage (GAGD) Process using a Visual Model," Craft and Hawkins Department of Petroleum Eng., Louisiana State University, Baton Rouge, LA 70803, August 2006.

2. Paidin, W. R., "Physical Model Study of the Effects of Wettability and Fractures on Gas-Assisted Gravity Drainage (GAGD) Performance," Craft and Hawkins Department of Petroleum Eng., Louisiana State University, Baton Rouge, LA 70803, May 2006.
3. Sharma, A. P., "Physical Model Experiments of the Gas-Assisted Gravity Drainage Process," Craft and Hawkins Department of Petroleum Eng., Louisiana State University, Baton Rouge, LA 70803, August 2005.
4. Xu, W., "Experimental Investigation of Dynamic Interfacial Interactions at Reservoir Conditions," Craft and Hawkins Department of Petroleum Eng., Louisiana State University, Baton Rouge, LA 70803, May 2005.
5. Kulkarni, M.M., "Immiscible and Miscible Gas-Oil Displacements in Porous Media", Craft and Hawkins Department of Petroleum Eng., Louisiana State University, Baton Rouge, LA 70803, Aug 2003.

4.4 Reviewed Journal Publications

1. Rao, D.N., and Ayirala, S.C.: "Authors' Response to the Comments on A New Mechanistic Parachor Model to Predict Interfacial Tension and Miscibility in Multicomponent Hydrocarbon Systems by F.M. Orr and K. Jessen," Article in Press, Journal of Colloid and Interface Science, 2006.
2. Ayirala, S.C. and Rao, D.N.: "A New Mechanistic Parachor Model to Predict Dynamic Interfacial Tension and Miscibility in Multicomponent Hydrocarbon Systems," Journal of Colloid and Interface Science, 299 (2006) 321-331.
3. Ayirala, S.C. and Rao, D.N.: "Application of Parachor Model to the Prediction of Miscibility in Multi-Component Hydrocarbon Systems," Journal of Physics: Condensed Matter, 16 (2004) S2177- S2186.
4. Ayirala, S.C. and Rao, D.N.: "Dew Point Pressure Prediction of Gas Condensate Reservoirs," Oil Asia Journal, September-October 2005.
5. Ayirala, S.C. and Rao, D.N.: "Miscibility Determination from Gas-Oil Interfacial Tension and P-R Equation of State," Manuscript Accepted for Publication in Canadian Journal of Chemical Engineering, 2006.
6. Ayirala, S.C. and Rao, D.N.: "Solubility, Miscibility and their Relation to Interfacial Tension in Ternary Liquid Systems," Fluid Phase Equilibria Journal, 249 (2006) 82-91.
7. Ayirala, S.C., and Rao, D.N.: "A New Mechanistic Parachor Model to Predict Dynamic Interfacial Tension and Miscibility in Multicomponent Hydrocarbon Systems," Journal of Colloid and Interface Science, 299 (2006) 321-331.
8. Ayirala, S.C., and Rao, D.N.: "Comparative Evaluation of a New MMP Determination Technique," Manuscript under Review for Publication in SPE Journal, 2006.

9. Ayirala, S.C., and Rao, D.N.: "Miscibility Determination from Gas-Oil Interfacial Tension and P-R Equation of State," Manuscript under Review for Publication in Canadian Journal of Chemical Engineering, 2006.
10. Ayirala, S.C., and Rao, D.N.: "Solubility, Miscibility and their Relation to Interfacial Tension in Multicomponent Hydrocarbon Systems," Manuscript under Review for Publication in Fluid Phase Equilibria Journal, 2006.
11. Ayirala, S.C., Xu, W. and Rao, D.N.: "Interfacial Behavior of Complex Hydrocarbon Fluids at Elevated Pressures and Temperatures," Canadian Journal of Chemical Engineering, 84 (Feb. 2006) 22-32.
12. Rao, D.N. and Ayirala, S.C.: "The Multiple Roles of Interfacial Tension in Fluid Phase Equilibria and Fluid-Solid Interactions," Journal of Adhesion Science and Technology, 20 (Feb. 2006) 125-142.
13. Rao, D.N., and Ayirala, S.C.: "Mechanistic Modeling of Dynamic Vapor-Liquid Interfacial Tension in Complex Petroleum Fluids," Manuscript under Review for Publication in Contact Angle, Wettability and Adhesion, Vol. 5, Ed. K.L. Mittal, 2006.
14. Kulkarni, M. M., and Rao, D. N., "Experimental Investigation of Miscible and Immiscible Water-Alternating-Gas (WAG) Process Performance", Journal of Petroleum Science and Engineering, 48 (2005), 1 – 20.
15. Kulkarni, M. M., and Rao, D. N., "Experimental Investigation of Miscible and Immiscible Water-Alternating-Gas (WAG) Process Performance", PETROL 1277, J. of Pet. Sci. and Eng, 2005.

4.5 Manuscripts under Review for Journal Publication

1. Rao, D.N. and Ayirala, S.C.: "Mechanistic Modeling of Dynamic Vapor-Liquid Interfacial Tension in Complex Petroleum Fluids," Manuscript under Review for Publication in *Contact Angle, Wettability and Adhesion*, Vol. 5, Ed. K.L. Mittal, 2006.

4.6 Full-Length Papers Published in International Conference Proceedings

1. Ayirala, S.C. and Rao, D.N.: 'Measurement and Modeling of Gas-Oil Miscibility for Improved Oil Recovery," Paper presented at the 20th International Symposium of the Society of Core Analysts, Trondheim, Norway, Sept. 12-16, 2006.
2. Rao, D.N. and Ayirala, S.C.: "Mechanistic Modeling of Dynamic Vapor-Liquid Interfacial Tension in Complex Petroleum Fluids," Invited paper presented at Fifth International Symposium on Contact Angle, Wettability and Adhesion, 21-23 June 2006, Toronto, Canada.

3. Ayirala, S.C. and Rao, D.N.: "Comparative Evaluation of a New MMP Determination Technique," SPE Paper 99606 presented at 2006 SPE Symposium on Improved Oil Recovery, April 22-26, Tulsa, U.S.A.
4. Ayirala, S.C., Xu, W. and Rao, D.N.: "Interfacial Behavior of Complex Hydrocarbon Fluids at Elevated Pressures and Temperatures," Paper presented at the 2005 International Conference on MEMS, Nano and Smart Systems, July 24-27, Banff, Alberta, Canada.
5. Ayirala, S.C. and Rao, D.N.: "Dew Point Pressure Prediction of Gas Condensate Reservoirs," Paper No. 470 presented at the 6th International Petroleum Conference and Exhibition, Petrotech-2005, New Delhi, India, January 16-19, 2005.
6. Ayirala, S.C. and Rao, D.N.: "Solubility, Miscibility and their Relation to Interfacial Tension for Application in Reservoir Gas-Oil Systems," SPE Paper 91918 presented at the SPE International Petroleum Conference, Puebla, Pue., Mexico, Nov. 7-9, 2004.
7. Ayirala, S.C. and Rao, D.N.: "Application of a New Mechanistic Parachor Model to Predict Dynamic Gas-Oil Miscibility in Reservoir Crude Oil-Solvent Systems," SPE Paper 91920 presented at the SPE International Petroleum Conference, Puebla, Pue., Mexico, Nov. 7-9, 2004.
8. Rao, D.N. and Ayirala, S.C.: "The Multiple Roles of Interfacial Tension in Fluid Phase Equilibria and Fluid-Solid Interactions," Invited paper presented at Fourth International Symposium on Contact Angle, Wettability and Adhesion, Philadelphia, PA, June 14-16, 2004.
9. Rao, D.N., Ayirala, S.C., Kulkarni, M.M. and Sharma, A.P.: "Development of Gas Assisted Gravity Drainage (GAGD) Process for Improved Light Oil Recovery," SPE Paper 89357 presented at the SPE/DOE 14th Symposium on Improved Oil Recovery, Tulsa, OK, April 17-21, 2004.
10. Ayirala, S.C., Rao, D.N. and Casteel, J.: "Comparison of Minimum Miscibility Pressures Determined from Gas/Oil Interfacial Tension Measurements with Equations of State Calculations", SPE Paper 84187 presented at the 2003 SPE Annual Technical Conference and Exhibition, Denver, Colorado, October 5-8, 2003.
11. Ayirala, S.C. and Rao, D.N.: "Validation of New Experimental Approach of Vanishing Interfacial Tension (VIT) for Minimum Miscibility Pressure (MMP) Determination Using Equation of State", Paper Presented at the Astatphys-Mex 2003 Petroleomics Symposium, Puerto Vallarta, Mexico, August 22-25, 2003.
12. Kulkarni, M. M., and Rao, D. N., "Experimental Investigation of Various Methods of Tertiary Gas Injection", SPE 90589, Presented at the 80th SPE ATCE, Houston, TX, Sept 26 – 29, 2004

13. Kulkarni, M. M., and Rao, D. N., "Analysis of the Novel Toe-To-Heel Air Injection (THAI) Process using Analytical Models", AIChE 2004 Annual Meeting, Austin, TX, Nov 7 –12, 2004
14. Kulkarni, M. M., and Rao, D. N., "Is Gravity Drainage an Effective Alternative to WAG?", AIChE 2004 Annual Meeting, Austin, TX, Nov 7 –12, 2004
15. Kulkarni, M. M., and Rao, D. N., "Analytical Prediction of In-Situ Combustion (ISC) Process Performance – Applicability to Indian EOR Scene", 11th Annual India Oil and Gas Review Symposium and International Exhibition (IORS), Mumbai, India, Sept 6 – 7, 2004
16. Kulkarni, M. M., and Rao, D. N., "Is there a 'Happy-Medium' between Single Slug and Water-Alternating-Gas (WAG) Processes?", 11th IORS, Mumbai, India, Sept 6 – 7, 2004
17. Kulkarni, M. M., Sharma, A. P., and Rao, D. N., "Use of Dimensional Analysis for Scaling Immiscible Gas Assisted Gravity Drainage (GAGD) Experiments", SCA P064,19th International Symposium of the Society of Core Analysts, Toronto, Canada, Aug 2005
18. Kulkarni, M. M., and Rao, D. N., "Experimental Investigation of Miscible Secondary Gas Injection", SPE 95975, 81st Society of Petroleum Engineers' ATCE, Dallas, TX, Oct 2005
19. Kulkarni, M. M., and Rao, D. N., "Characterization of Operative Mechanisms in Gravity Drainage Field Projects Through Dimensional Analysis", SPE 103230, Society of Petroleum Engineers' ATCE, San Antonio, TX, Sept 24-27, 2006.
20. Kulkarni, M. M., "Analytical Modeling of the Forced Gravity Drainage GAGD Process", American Inst. of Chemical Engineers Annual Meeting, San Francisco, CA, Nov 12 –17, 2006.

4.7 Technical Paper Presentations in National/International Symposiums

1. Ayirala, S.C., Kulkarni, M.M. and Rao, D.N.: "Application of GAGD Process in a Louisiana Oil Field – Reservoir Characterization and Simulation," Paper presented at the PPTC Workshop, Shreveport, Sept.13, 2006.
2. Ayirala, S.C. and Rao, D.N.: "Mass Transfer Effects in Fluid-Fluid Miscibility Determination," Paper presented in the 230th ACS National Meeting, Washington, DC, USA, Aug. 28-Sept.1, 2005.
3. Rao, D.N. and Ayirala, S.C.: "Influence of Solid-Liquid-Liquid Interactions on Multiphase Transport Behavior in Porous Media," Paper presented at the 2005 International Conference on MEMS, Nano and Smart Systems, July 24-27, Banff, Alberta, Canada.

4. Ayirala, S.C.: "A New Quantitative Technique for Quick and Cost-Effective Determination of Gas-Oil Miscibility," Paper presented at the SPE 2005 Gulf Coast Regional Student Paper Contest, March 11-12, Lafayette, LA.
5. Rao, D.N. and Ayirala, S.C.: "Measurement and Modeling of Gas-Oil Interfacial Tension at Reservoir Conditions," Paper presented at the 2004 SPE ATW-Gas Condensate Reservoir Development and Management Work Shop, Houston, TX, May 19-20, 2004.
6. Ayirala, S.C. and Rao, D.N.: "Modified Parachor Model for Prediction of Interfacial Tension in Multi-Component Hydrocarbon Systems," Paper presented at the 227th National ACS Meeting, Anaheim, CA, March 28-April 1, 2004.
7. Ayirala, S.C. and Rao, D.N.: "Solubility, Miscibility and their Relation to Interfacial Tension for Ternary Fluid Systems," Paper presented at the 227th National ACS Meeting, Anaheim, CA, March 28-April 1, 2004.